The Behaviour of Multi-storey Composite Steel Framed Structures in Response to Compartment Fires

Susan Lamont

Doctor of Philosophy
University of Edinburgh
2001

Declaration

This thesis and the research described and reported within has been completed solely by Susan Lamont under the supervision of Dr A.S. Usmani, Prof. D.D. Drysdale and Dr B. Lane.

Where other sources are quoted full references are given.

Susan Lamont

February 2002

Abstract

For many years the ability of highly redundant composite framed structures to resist the effects of fire has been undervalued and largely misunderstood. This was first realised when, after a number of real fires in multi-storey composite steel framed structures, structural failure did not occur. The Broadgate Phase 8 fire is probably the most notable. This accidental fire happened during the construction phase when the steel frame was only partially fire protected. Despite very high temperatures during the fully developed phase of the fire and considerable deflections in the composite slab there was no collapse. This initiated construction of an 8-storey composite steel frame at Building Research Establishment's (BRE's) large scale test facility in Cardington. Six fire tests were conducted, of varying size and configuration, to observe and ultimately explain why composite steel-framed structures adopt very large deflections during a fire but do not collapse.

Computer modelling of the tests by a number of research groups, including the University of Edinburgh, followed. Finite element modelling of these tests provided a wealth of information about the behaviour of whole frame structures in fire. However despite extensive dissemination of the available information, improvements in design guidance have been hindered by the wide scope it was required to cover and the large number of variables involved, when the new knowledge was based on analysis of only six tests all conducted on the same structure.

The purpose of this research has been to confirm and extend the conclusions of the Cardington frame fire tests and the subsequent numerical modelling. Two generic composite steel frames were designed in accordance with EC4 Part 1.1. Their shape and size in plan were chosen to be significantly different from the Cardington frame.

An investigation of the methods available to model compartment fires was carried out. Comparisons were made between predicted natural fires and atmosphere temperatures measured during experimental compartment fires. Heat transfer models were also tested against steel and concrete temperatures recorded during the Cardington tests. Using these design tools, natural fire curves were assumed and heat transfer calculations were made, to obtain steel and concrete temperature histories as inputs to structural anal-

yses.

A series of parametric studies was conducted on the two generic frames to investigate the response of the structure if the fire exposure or location changed. The fire scenarios included compartment fires on the whole floor, at the edge and corners of the structures. By altering the size and location of the compartment, the level of restraint to thermal expansion and thermal bowing of the structural elements changed.

A further set of studies varied the number of beam members with applied fire protection. Three scenarios were tested. Primary and edge beams protected, only edge beams protected and all beams unprotected. In all studies secondary beams were unprotected and columns were protected to their full height. The behaviour observed in the Cardington frame tests has been confirmed in both generic frames and new phenomena have been highlighted.

The temperature history of a natural fire depends upon the available ventilation, fire load, room geometry and thermal properties of the boundary wall materials. Many fire scenarios exist leading to a range of thermal responses in the structural elements, which are manifested in various combinations of deflections and forces. In composite floor slabs fires of short post-flashover duration result in low concrete temperatures but high temperatures in the steel beams. High gradients exist over the depth of the composite causing thermal bowing behaviour. Fires of longer duration allow the concrete to reach much greater temperatures therefore, thermal expansion of the composite is the more dominant behaviour.

Differences in compartment fire size and location provide various degrees of restraint to an expanding structure. The level and location of restraint is a contributing factor to the patterns of deflections and forces.

Removing applied fire protection from all steel beams leads to greater deflections of the composite floor. However, relative displacements between an unprotected edge beam and the centre of the fire compartment may be reduced causing a reduction in the tensions experienced by the slab at high deflections. Providing applied fire protection to steel beams in composite structures may not be necessary although the impact of large deflections on compartment breach should be considered.

Overall the generic frame structures behaved well under all scenarios tested.

Publications

The following papers and reports have been produced as a result of this research:

Journal Papers

S. Lamont, A.S. Usmani and D.D. Drysdale. Heat transfer analysis of the composite slab in the Cardington frame fire tests. Fire Safety Journal Vol. 36, No. 8, 2001.

A.M. Sanad, S. Lamont, A.S. Usmani and J.M. Rotter. Structural behaviour in fire compartment under different heating regimes-Part 1 (slab thermal gradients). Fire Safety Journal, Vol. 35, 2000.

A.M. Sanad, S. Lamont, A.S. Usmani and J.M. Rotter. Structural behaviour in fire compartment under different heating regimes-Part 2 (slab mean temperatures). Fire Safety Journal, Vol. 35, 2000.

A.S. Usmani, J.M. Rotter, S. Lamont, A.M. Sanad and M. Gillie. Fundamental principles of structural behaviour under thermal effects. Fire Safety Journal Vol. 36, No. 8, 2001.

S. Lamont, B. Lane, A.S. Usmani and D.D. Drysdale. The fire resistance test in the context of real beams. (submitted to AISC Engineering Journal June 2001).

Conference Papers

S. Lamont, A.S. Usmani, J.M. Rotter and B. Lane. New concepts in structural strength assessment for large buildings in fire. In Proceedings of the 2001 Structures Congress and Exposition, ASCE, SEI.

S. Lamont, A.S. Usmani and D.D. Drysdale. Fire protection of steel beams in composite framed structures. In proceedings of the 9^{th} Fire science and Engineering Conference, Interflam 2001.

Presentations to STIFF

S. Lamont and A. Usmani. A comparison of structural behaviour in response to a well-ventilated and an under-ventilated fire. Presented at STIFF (STeel in Fire Forum) 23rd April 2001. www.shef.ac.uk/fire-research/steelinfire.

S. Lamont and A. Usmani. A comparison of structural behaviour in response to a "short-hot" and a "long-cool" fire. Presented at STIFF (STeel in Fire Forum) 12th September 2001. www.shef.ac.uk/fire-research/steelinfire.

Other publications

S. Lamont and D.D. Drysdale. Evaluation of the software O Zone. In Development of the UK and European fire design codes-Natural fires and the response of structural steel. CORUS Publication, 2001.

Acknowledgements

A special thank you to my supervisors Dr A.S. Usmani, Prof. D.D. Drysdale and Dr B. Lane for their support and expert advice.

Thank you to my family, friends and most of all to Max for their faith and support throughout the last three years.

This research was funded by an EPSRC Case award through Ove Arup and is gratefully acknowledged.

Contents

List of Figures

List of Tables

Abbreviations

SCI = Steel Construction Institute

BRE = Building Research Establishment

DETR = Department of the Environment Transport and Regions

PiT = Partners in Technology

EC = Eurocode

BS = British Standard

ASTM = American Society for Testing and Materials

ISO = International Standards Organisation

CIB = Conseil Internaionale du Bâtiment

NFSC = Natural Fire Safety Concept

NRCC = National Research Council Canada

NFPA = Natioanl Fire Protection Association

SFPE = Society of Fire Protection Engineers

NIST = National Institute for Standards and Technology

LWC = Lightweight concrete

NWC = Normal weight concrete

FEAST = Finite Element Analysis of Shells at high Temperatures

SRAS = Stress Resultant Analysis of Shells

FEAI = Finite Element Analysis Interface

Chapter 1

Introduction

1.1 Background to the project

Fire safety engineers are concerned first and foremost with life safety not only of the occupants of a building but also the fire service. The aim of structural fire engineering design is to ensure that structures do not collapse when subjected to high temperatures in fire. Traditional prescriptive methods of design based on fire resistance testing, require steel elements of construction to stay below a critical temperature, typically 550^{o}C, for the fire resistance period of the structure. This has led to extensive use of passive fire protection to limit the heating of the structural elements (boards, sprays and intumescents) at considerable cost (up to 20% of the total construction cost[142]).

It has been acknowledged for many years that the failure of determinate structures in the fire resistance furnace bears little resemblance to the failure of similar elements as part of a highly redundant frame. However the fire resistance test has a history of safety albeit not based on scientific reasoning.

Design of structures for fire still relies on single element behaviour in the fire resistance test. The future of structural fire design has to be evaluated in terms of the whole performance based design of structures for fire. This should include natural fire exposures, heat transfer calculations and whole frame structural behaviour, recognising the interaction of all elements of the structure in the region of the fire and any cooler elements outside the boundary of the compartment.

The beginnings of change started after evidence from real fires suggested that the contributions of modern steel deck composite floor systems were under utilised when designing for the fire limit state.

On the 23rd June 1990 a fire developed in the partly completed fourteen storey building in the Broadgate development.[116] The fire began in a large contractors hut on the first floor and smoke spread undetected throughout the building. The fire detection and sprinkler system were not yet operational out of working hours.

The fire lasted 4.5 hours including 2 hours where the fire exceeded 1000^{o}C. The direct fire loss was in excess of £25million however, only a fraction of the cost (£2million) represented structural frame and floor damage. The major damage was to the building fabric as a result of smoke. Moreover, the structural repairs after the fire took only 30 days. The structure of the building was a steel frame with composite steel deck concrete floors and was only partially protected at this stage of construction. During and after the fire, despite large deflections in the elements exposed to fire, the structure behaved well and there was no collapse of any of the columns, beams or floors.[116] The Broadgate phase 8 fire was the first opportunity to examine the influence of fire on the structural behaviour of a modern fast track steel framed building with composite construction.

Prompted by the evidence from Broadgate, Building Research Establishment (BRE) built an 8-storey composite steel and lightweight concrete frame at their large scale test facility at Cardington. The frame was subjected to six full-scale fire tests (2 by BRE and 4 by British Steel (now CORUS)) enabling the behaviour of the structure during fire to be observed and recorded. The outputs from these tests were introduced to the public domain. Edinburgh University in collaboration with British Steel and Imperial College carried out a research project (funded by the Department of Environment, Transport and Regions "Partners in Technology" scheme) to model the structural behaviour of the 4 British Steel tests using finite element codes. One aim of the research programme was to develop numerical models capable of predicting the structural behaviour of a modern, multi-storey composite steel frame building during a real compartment fire. The most important outcome however was the explanation and understanding of the structural behaviour in response to fire.
The computer package ABAQUS[102] was used by Edinburgh University and British Steel to develop numerical models of the four tests. ABAQUS is a powerful commercial code capable of modelling the geometric and material nonlinear behaviour of a structure during fire. The models have captured the global structural behaviour and agree with measured data from the tests. The results and understanding gained through the models have highlighted complex behaviour.

1.2 Aims of this research

This PhD project has evolved as a direct result of the modelling of the Cardington frame fire tests. Both the test data and the modelling provided a wealth of new information about whole frame structural behaviour in fire. However the tests were carried out on one building. As a result of the Cardington frame tests and theoretical work by Bailey[23] SCI (Steel Construction Institute) have produced a simple conservative design guide in the form of look-up tables for composite frame structures in fire. The tables are applicable to common buildings. This level one design guide is as a major step forward for structural fire engineering in the UK. However, for detailed design guidance to be produced different buildings of various sizes and configurations should be investigated under contrasting fire scenarios. The primary aim of this project was to use the modelling approach developed and checked against real test data to create generic composite steel frames and fire scenarios. Parametric studies and sensitivity analyses were conducted on the generic frames. *"What-if"* scenarios considered included, *what-if*,

- there is a fire in a corner or edge compartment or over a whole floor level?
- only the columns are protected?

- the fire severity changes?

The key parameters investigated were the temperature distributions in the structural elements for various compartment fires and the restraint provided by the edge beams (protected or unprotected) or the surrounding cooler structure to the fire compartment. A clear understanding of compartment fire dynamics and heat transfer was necessary to create design fires and compute the heat transfer to the structural elements. Thus a detailed review of the tools available to fire engineers to calculate compartment fire exposures and heat transfer was conducted.
Output from these analyses adds to the information collected as a result of modelling the Cardington frame tests and will help the development of performance based design guidance for fire.

1.3 Outline of thesis chapters

Chapter 2
An overview of structural fire safety design and research
Traditional and performance based design methods and the history of this field of research will be outlined. Research into the behaviour of single elements of construction in fire and studies of steel frames before the Cardington frame tests will be presented. A summary of the factors affecting structures in fire, for instance degradation of mechanical properties and restraint conditions, will also be given.

Chapter 3
Thermal response of structures to real fires
Prescriptive fire gradings and design methods based on heating single elements in the fire resistance test over-simplify the whole fire design process. The real problem can be addressed by performance based design methods where possible fire scenarios are investigated and fire temperatures are calculated based on the compartment size, shape, ventilation, assumed fire load and thermal properties of the compartment boundaries. The temperatures achieved by the connected structure can then be determined by heat transfer analysis. This chapter describes and tests some of the methods available to engineers and designers to predict fire temperatures and heat transfer to the structure.

Chapter 4
Whole frame composite steel structures in fire: Research and design developments
This chapter will review recent experimental work and numerical modelling of whole

frame composite steel structures in fire. Design methods developed as a direct result of this research will also be discussed.

Chapter 5

Heat transfer analysis of the Cardington frame fire tests using HADAPT

This chapter describes heat transfer analysis of the Cardington frame tests. Using the finite element code HADAPT the temperatures achieved by the composite slab and the edge beams were predicted. The results of these analyses are given and discussed. This work was carried out for two reasons. One to supplement the existing Cardington frame data and two to have a reliable method of modelling heat transfer to structural elements for any compartment fire scenario.

Chapter 6

Analytical and numerical analysis of simple beam models in fire

This chapter describes analytical and numerical analyses on a simple beam to aid our understanding of the behaviour of structures in fire. Thermal bowing and thermal expansion effects were analysed on a simple beam, first individually and then combined. The effect of the beam end restraint conditions were also studied to explain why runaway occurs much earlier in axially unrestrained beams, as tested in the fire resistance test, when compared with axially restrained beams, typical of beams in real structures.

Chapter 7

Structural behaviour in British Steel Test 1 under different heating regimes

Following the simple studies and understanding of thermal bowing and thermal expansion effects in Chapter 6. A parametric study was conducted on an ABAQUS grillage model of British Steel Test 1 (restrained beam test) to understand the effects on the structure, of systematically changing the temperature regime in the slab. The parametric study and the results are outlined in this chapter.

Chapter 8

Parametric studies on a small generic composite steel frame

Two generic composite steel frames, different in plan and size from Cardington, were designed in accordance with Eurocode 4 Part 1.1.[78] This chapter describes the structural response of a small frame (2x2 bays in plan) to whole floor compartment fires with different ventilation characteristics. Changing the available ventilation and fuel in a compartment leads to fires of short or prolonged post-flashover duration and different thermal responses in the steel and concrete.

The Cardington frame survived several fire tests where all the steel beams were un-

protected. The structural behaviour of the small generic frame to three fire protection configurations, 1) the edge and primary beams were protected, 2) only the edge beams were protected and 3) all beams were left unprotected, is also described. In each case the columns were always protected to their full height.

Chapter 9

Parametric studies on a large generic composite steel frame

This chapter describes results from a series of parametric studies on a 9x9 bay generic composite frame. Compartment fire scenarios in the corner and on the side of the building were analysed. The locations provided different boundary restraint conditions to the expanding compartment floor and different deflection and force patterns in the beams and slab. The effect of protecting the edge beams on the structural behaviour of the large frame is also described.

Chapter 10

Conclusions and Further work

Chapter 2

An overview of structural fire safety design and research

2.1 Introduction

This overview of structural fire safety design and research includes three main topics.

1. Traditional and Performance Based Design Methods
2. Factors affecting structures in fire
3. Literature review of single element behaviour in fire and steel frame analysis before the Cardington frame fire tests.

Traditionally steel fire design has been based upon fire resistance testing although fire resistance by calculation has also been implemented for many years. The fire resistance test and its shortcomings are discussed and fire resistance by calculation is introduced. Methods given in BS 5950 Part 8, EC3 and EC4 are described. The history of performance based design for steel is then outlined.

Factors affecting structural behaviour in fire are described, such as material degradation at elevated temperatures, restrained thermal expansion, thermal bowing and the degree of redundancy available when the structure acts as a whole. Each factor is addressed separately but in an integrated structure exposed to fire they will all interact to generate more complex structural behaviour.

This chapter also reviews research into the fire resistance of single elements of structure and early analysis of frames prior to the Broadgate Phase 8 fire and the Cardington frame fire tests. Chapter 4 looks at whole frame composite steel structures in fire and the new understanding developed over the last 10 years.

2.2 Traditional Design

The term fire resistance is associated with the ability of an element of building construction to continue to perform its function as a barrier or structural component during the course of a fire. Traditionally the fire resistance of a building element (beam, column etc.) has been determined by testing a full scale sample (under load if necessary) to failure while subjected to a standard fire.

2.2.1 The fire resistance test

Fire resistance testing of construction was formalised over 80 years ago although testing had been going on prior to that in an unplanned and informal manner.[157] The main

reason for testing was that insurance companies needed to have some comparative evaluation between different types of construction. The earliest recorded tests were in the UK, Germany and the USA. The Associated Architects in the UK tested a floor in the 1790s. The Technical High School in Munich tested a column in 1884 and in the Denver Equitable Building in the USA a floor was tested in 1890.

Early tests were carried out in brick huts using wood as a fuel where the floor or wall under test was part of the hut itself. Early testing was very simple, construction was tested and observations made of its behaviour, primarily with reference to collapse and to the transfer of fire to the unexposed side of the wall or floor. The main test station in the UK at Borehamwood was opened in 1935.[157]

It can be said that the fire resistance test assesses the behaviour of components and structures in the post-flashover stage of a fully developed fire. Techniques for conducting fire resistance tests have not changed significantly in the last 60 years.[16,17] Fire resistance testing consists of subjecting a prototype sample of the construction to prescribed heating conditions in a furnace and judging its performance based on specified criteria. The standard tests enable elements of construction such as walls, floors, columns and beams to be assessed according to their ability to: retain their stability; offer resistance to the passage of flame and hot gases and/or provide resistance to heat transmission. The failure criteria for load-bearing horizontal elements of construction is either when a deflection of L/20 is achieved or the rate of deflection (mm/min) calculated over 1 minute intervals exceeds $\frac{L^2}{9000d}$. However the latter limit should only be applied beyond a deflection of L/30. The time to failure in the fire resistance furnace determines the fire resistance rating of the element under test.

Standard fire tests are conducted worldwide and are defined by the International Standards Organisation in ISO 834. Standard fire tests in the United Kingdom are defined in BS 476: Parts 20-23 Fire tests on building materials and structures.[40]

- Part 20: Method for determination of the fire resistance of elements of construction (general principles)
- Part 21: Method for determination of the fire resistance of loadbearing elements of construction
- Part 22: Method for determination of the fire resistance of non-loadbearing elements of construction

- Part 23: Methods for determination of the contribution of components to the fire resistance of a structure

The heating conditions in the furnace are described by a standard temperature-time curve. The British Standard temperature-time curve is given by Equation 2.1, first published in 1932.[16,17,157] The temperature of the furnace is programmed by controlling the rate of supply of fuel. Traditionally fire resistance design in the UK has assumed fire exposure to equal the British Standard standard fire curve.

$$T = T_0 + 345 \log(0.133t + 1) \tag{2.1}$$

t = time (sec)
T = temperature of the furnace atmosphere next to the specimen (^{o}C)

During the British Standards tests on load bearing elements the support conditions provided can be similar to that which would apply in service. However, when the service conditions are unknown the test beam or slab is installed as simply supported i.e axially unrestrained to thermal expansion.

The first ASTM standard for fire resistance testing, C19 (now E119[8]), was published in 1918.[157] The standard fire curve is prescribed by a series of points rather than an equation but is almost identical to the British Standard curve. Both the British Standard temperature-time curve and the ASTM curve are illustrated in Figure 2.1.

Several differences exist between the American and British tests. In terms of beams and floor slabs failure criteria for stability is based on deflections in the BS test but limiting temperatures in the ASTM test. The American standard also includes a restrained beam test, a restrained assembly test and a hose test.

E 119 allows restrained floor assemblies with fire endurance classifications greater than 1 hour to have half the fire protection of an unrestrained assembly for specific temperature criteria. Therefore savings in fire protection can be made for longer fire resistance periods if the building element can be classified as restrained. ASTM E119 recognises the positive effects of restraint to thermal expansion of beams and floors but there is confusion in some parts of the USA about the application of restrained and unrestrained fire resistance ratings.[87] Gewain and Troup[87] have tried to address this confusion. Key conclusions of their paper are that a restrained assembly fire resistance rating is appropriate for steel beam floor and roof assemblies. The least stiff connection used in steel

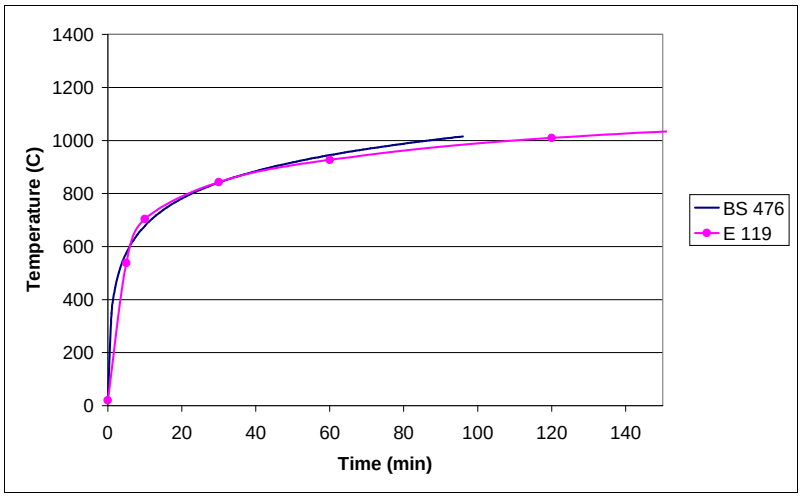

Figure 2.1: Standard Temperature-time curves

frame construction is adequate to develop restrained performance. Also unrestrained fire resistance tests of beam floor and roof systems have no relevance to the behaviour of these systems under fires in real buildings.

During the hose test, elements heated by the standard fire are subjected to the impact and cooling effects of a hose stream.

2.2.2 Critical steel temperature

Until recently 550^{o}C has been classified as the upper limit for steel temperatures in fire. Steel loses 40% of its room temperature strength by 550^{o}C. For this reason protection has traditionally been applied to reduce the heating rate of steel so that it retains sufficient strength and stiffness during its prescribed period of fire resistance.[160]

2.2.3 Fire protection

Fire protection of steel can be achieved by three methods 1) insulating the element with spray material or board type protection, 2) shielding or 3) hollow sections can be filled with concrete or liquid to form a heat sink.

2.2.3.1 Traditional fire protection materials

Traditional fire protection materials have included concrete, blockwork and plasterboard. Until the late 1970's concrete was the most common form of fire protection for

steelwork.[65] The major disadvantages are cost, the increase in weight to the structure and the time it takes to apply on site. Nowadays modern lightweight sprays and boards have replaced these.

2.2.3.2 Modern fire protection materials

Passive fire protection materials insulate the structure from high temperatures. The insulation materials can be classified as non-reactive (e.g. boards and sprays) or reactive (e.g. intumescent coatings).

Boards are fixed dry usually to columns. Beams are more commonly protected with spray materials. The main advantages of spray coverings are, they are cheap and they easily cover complex details. However application is wet and may delay other work on site.

Site applied intumescent coatings are paint like substances or mastics. Paints are stable at low temperatures but swell at around 200^oC to provide a charred layer of low conductivity material to insulate the steel. Mastics are applied using a trowel or as a heavy duty spray. They form a thick protective coating which is impervious at ambient and at high temperatures. They can be hard and ceramic in appearance or soft and tar like. The main advantage of intumescents paints over other protection products are their appearance. However they are more expensive than sprays and boards, application is wet and there is a limit to the fire resistance periods they can achieve typically 30 and 60 minutes.[189] A limited number provide longer fire resistance periods but the cost increases considerably. Paints are also applied off-site.

2.2.3.3 Partially exposed steelwork[65]

Standard fire tests on partially exposed steel have shown that structural members not fully exposed to the fire exhibit increased levels of fire resistance.[65, 189, 204] 30 and 60 minutes fire resistance can be achieved using this approach and higher levels of fire resistance can be achieved with reduced fire protection thicknesses. The most common methods of achieving partially exposed steel are listed below.

1. Web in-filled columns: Normal weight concrete is poured between the flanges of the column. The load carrying capacity of the concrete is ignored in the design of the column but during a fire as the steel weakens the load carried by the flanges is transferred to the concrete providing up to 60 minutes fire resistance.

2. Block in-filled columns: Concrete blocks are cemented between the flanges and tied to the web achieving 30 minutes fire resistance. Longer periods can be reached by protecting only the exposed flanges.

3. Shelf angle floor beams: Shelf angle floor beams are beams with angles bolted to the web to support the floor slab thus shielding the upper part of the beam from the fire leaving only the bottom of the beam exposed. 60 minutes fire resistance can be achieved using this method.

4. Slim floor beams: There are two types of slim floor in the UK (SLIMFLOR and SLIMDEK). Essentially the profiled concrete slab has a deep deck incorporating the beams within the floor slab system thus the slab protects almost the whole beam section.

5. Filled hollow sections: Hollow columns can gain enhanced fire resistance (up to 2 hours) by filling them with concrete. During a fire heat flows through the steel to the low conductivity concrete. As the steel loses its yield strength with increasing temperature the load is transferred to the concrete. Adding fibre or bar reinforcement to the concrete can attain enhanced periods of fire resistance.[65]

6. Water-filled sections: Hollow sections may be filled with water to reduce heating in fire. This method is expensive and infrequently used.[43]

2.2.4 Shortcomings of the fire resistance test

The fire resistance test has been criticised by many researchers over many years. One major criticism is that the temperature of the furnace gases do not represent the fire exposure to the element under test because the fire exposure is dependent on the physical properties of the furnace. The construction shape influences the degree of turbulence and thus convective heat transfer. However most significantly the thermal inertia of the wall linings affect the radiative heat transfer to the element under test.[158] Indeed Drysdale[67] suggests that no two furnaces will give the same fire exposure. Furnaces also differ in the fuel adopted. They may be gas or oil fired.

Another criticism of the standard temperature-time curve is that it bears little resemblance to a real fire temperature-time history. It has no decay phase and as such does not represent any real fire although Malhotra[157] reports that it is designed to typify temperatures experienced during the post-flashover phase of most fires. Figure 2.2 illustrates the temperature-time histories of "real" fires, of varying fire load and ventilation, together with the standard curve. This highlights that the standard curve

does not represent many real fires in the post-flashover phase or otherwise.

Several criticisms can be made with regard to the tests ability to represent real structural behaviour in fire. A major limitation of furnace tests is that the elements of construction are tested in isolation or as part of small assemblies none of which can expect to represent the behaviour of an integrated structural frame exposed to a real fire. The end restraint conditions applied during the tests are unrealistic. The code recommends that restraint conditions should represent those met in practise. This is difficult to achieve in test conditions as restraint is difficult to measure and is likely to change throughout the test. Very often elements are tested unrestrained. In a real building during a compartment fire the rest of the structure would restrain the heated elements from expanding and the behaviour of the element in terms of deflections and failure would be quite different from that in an unrestrained standard test. Large deflections or "runaway" in unrestrained steel beams at high temperatures are as a direct result of imposed loading on a weakened structure. Large deflections in restrained members are often present primarily because of thermal expansion and thermal bowing effects. Columns are only subjected to axial loads yet in real structures they carry axial load and bending moments.

Although the shortcomings of the fire resistance test are significant, standard fire resistance tests are the only universally recognised method of determining the fire resistance of elements of construction.

2.2.5 Equivalent fire exposure

Ingberg[114] proposed a solution to the problem of standard fire curves not representing real fires in the 1920s. Analysis of a small number of room fire tests revealed that fire load was an important factor in determining fire severity. He suggested that fire severity could be related to the fire load of a room and expressed as an area under the temperature-time curve. The severity of two fires were equal if the area under the temperature-time curves were equal (above a base line of 300^oC). Thus any fire temperature-time history could be compared to the standard curve. Ingberg related fire load to an equivalent time in the standard furnace and produced Table 2.1. This approach was based on limited information of fire load densities thus has limited applicability. Drysdale[67] highlights that direct scaling between the heating effect of real fires and a standard fire is impossible because heat transfer when dominated by radiation depends upon radiative heat flux on T^4, i.e 10 minutes at 900^oC will not have the same effect as 20 minutes at 600^oC.

Combustible content (wood equivalent)		Equivalent	Standard fire duration
(lb/ft^2)	(kg/m^2)	($kJ/m^2 \times 10^{-6}$)	(h)
10	49	0.90	1
15	73	1.34	1.5
20	98	1.80	2
30	146	2.69	3
40	195	3.59	4.5
50	244	4.49	6
60	293	5.39	7.5

Table 2.1: Ingberg's fuel load fire severity relationship[67]

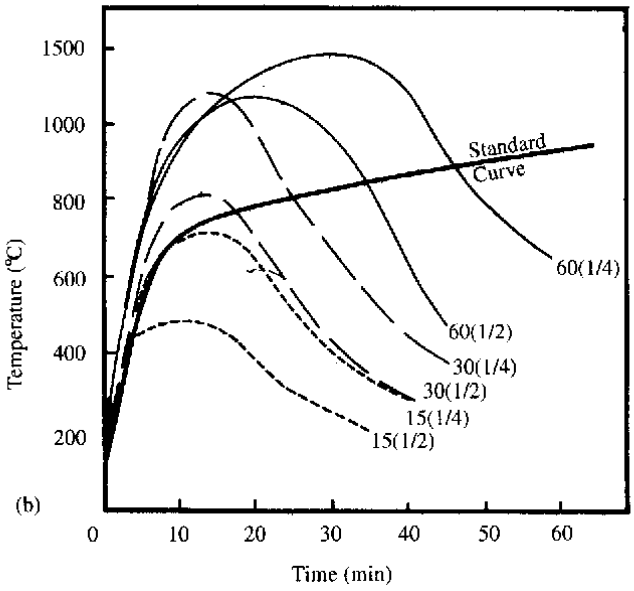

Figure 2.2: Comparison of the standard fire curve and real temperature-time histories. The fire load is in kg/m^2 and the ventilation is a fraction of one wall e.g 15(1/2) corresponds to a fire load of $15kg/m^2$ and ventilation equal to half of one wall[67]

Most regulatory bodies accepted Ingberg's fire severity approach and fire resistance testing to the standard temperature-time curve continued. Ingberg's approach was used in the UK to define equivalent fire severities in the post-war building studies report No.20-Fire Grading of Buildings.[104] The requirements for fire resistance were related to the assumed levels of fire loads in different occupancies. This approach was inappropriate because it took no account of the factors which dictate the severity of a compartment fire namely, ventilation, compartment dimensions and the properties of the boundary wall linings.[67]

Since Ingberg's early attempt at relating the severity of the standard fire to a real compartment fire many researchers have developed similar but more sophisticated time equivalent relationships.

The time equivalent concept makes use of the fire load and ventilation data in a real compartment fire to produce a value, which would be "equivalent" to the exposure time in the standard test. Law[139] defines t-equivalence as "the exposure time in the standard fire resistance test which gives the same heating effect on a structure as a given compartment fire". Formulating equivalent fire exposures has traditionally been achieved by gathering data from room-burn experiments where protected steel temperatures were recorded and variables relating to the fire severity were systematically changed (e.g. ventilation, fire load, compartment shape). The concept is illustrated in Figure 2.3.

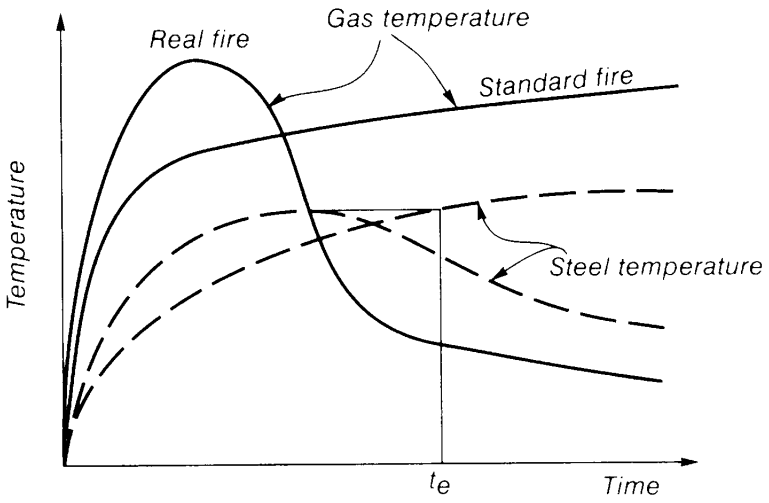

Figure 2.3: Equivalent fire severity on a temperature basis[43]

Law[139] developed a time equivalence relationship to include the effect of ventilation using data gathered from a CIB study of fully developed compartment fires.[241] This relationship is described by Equation 2.2. The floors (A_F) were very well insulated so were not included in the total surface area of the compartment (A_t).

Law's t-equivalence formula

$$\tau_e = 0.022 \frac{A_F L}{\sqrt{(A_v (A_t - A_F - A_v))}} \tag{2.2}$$

where,
τ_e = Equivalent fire resistance (h)
A_F = floor area (m^2)
A_t = total area of the compartment boundaries including the compartment opening (m^2)
A_v = Area of the ventilation opening (m^2)
L = Fire load (kg/m^2)

Pettersson and co workers,[195] adopted Law's method of t-equivalence but developed a new expression using the family of calculated temperature-time curves for particular compartments derived by Magnusson and Thelandersson.[155] Pettersson's t-equivalence approach takes into consideration the effect of the thermal inertia of the compartment wall lining (see Equation 2.3).

Pettersson's t-equivalence formula

$$\tau_e = 0.31 C \frac{A_F L}{(A_t A_v \sqrt{h_v})^{\frac{1}{2}}} \tag{2.3}$$

where,
C = factor depending on the thermal absorptivity of the compartment boundaries ($hm^{3/4}kg^{-1}$)
h_v = height of ventilation opening (m)

The normalised heat load concept is one of the most recent developments in this area and was introduced by Harmathy[99] although it has not been readily adopted. The normalised heat load, H_N ($s^{1/2}K$), is defined as the heat absorbed by the element per unit surface area during fire exposure. Harmathy's t-equivalence relationship is given by Equation 2.4.

Harmathy's t-equivalence formula

$$t_e = 6.6 + 9.6 \times 10^{-4} H_N + 7.8 \times 10^{-9} H_N^2 \tag{2.4}$$

for,

$$0 < H_N < 9 \times 10^4$$

$$H_N = 10^6 (11.0\delta + 1.6) L \frac{A_F}{[A_t (k\rho c)^{1/2} + 1810 (A_v \sqrt{h_v} L A_F)^{1/2}]} \tag{2.5}$$

where,

$\delta = 0.41 \left(\frac{H^3}{A_v \sqrt{h_v}} \right)^{1/2}$ or 1 whichever is less
k = thermal conductivity of the compartment boundaries (W/mK)
ρ = density of the compartment boundaries (kg/m^3)
c = heat capacity of the compartment boundaries (J/kgK)
H = compartment height (m)

Eurocode 1 Part 1.2[75] gives another approach to t-equivalence (Equation 2.6). The Equation is based on work by Schneider *et al* using the German multi-room fire code (MFRC) to calculate the fire behaviour, as cited by Law.[140]

EC1 Part 1.2 t-equivalence formula

$$t_{e,d} = q_{f,d} k_b w_f \tag{2.6}$$

where,
$t_{e,d}$ =equivalent time of fire exposure (minutes)
$q_{f,d}$ =design fire load density (MJ/m^2)
k_b =conversion factor for thermal properties of enclosure
w_f =ventilation factor (m$^{-1/2}$)

Characteristic fire load densities ($q_{\mathrm{f,d}}$) are listed in the Draft Eurocode or the actual fire load density can be calculated (method given in DD 240[115]). The factor k_b is

related to the thermal inertia of the compartment boundaries ($b = (\rho c \lambda)^{\frac{1}{2}}$). The values range from 0.04 to 0.07 with the latter as default if no detailed information is known.

The ventilation factor (w_f) considers the height of the fire compartment, the floor area and the areas of vertical openings. It also takes account of horizontal openings in the roof.

For no horizontal openings and $k_b = 0.07$,

$$t_e = 1.26 \frac{L}{A_F} w_f \tag{2.7}$$

$$w_f = \left(\frac{6.0}{H}\right)^{0.3} \left[0.62 + 90(0.4 - \frac{A_v}{A_F})^4\right] \tag{2.8}$$

Restrictions placed on the Eurocode t-equivalence relationship are given by relationships 2.9-2.12.

$$b_v = 12.5 \left(1 + 10\alpha_v - \alpha_v^2\right) \tag{2.9}$$

$$\left(\frac{6.0}{H}\right) \left[\frac{0.62 + 90(0.4 - \alpha_v)^4}{(1 + b_v \alpha_h)}\right] > 0.5 \tag{2.10}$$

$$b_v \geq 10 \tag{2.11}$$

$$0.025 \leq \alpha_v \leq 0.25 \tag{2.12}$$

where,
$\alpha_v = \frac{A_v}{A_F}$
$\alpha_h = \frac{A_h}{A_F}$

A_h =the area of horizontal openings in the roof

The main difference between EC1 and Pettersson's t-equivalent formula is that EC1 is independent of opening height but depends on ceiling height. Thus similar results are obtained in small compartments with tall windows but EC1 gives lower fire severities in large compartments where ceilings are tall and window heights low. However, neither formula has been tested for large or tall compartments.[43]

Law[140] compares the different t-equivalence formulae with experimental data for compartment fires. Pettersson's formula and the approach by Law provide better results than EC1 for the data considered. Law[140] also highlights the problems with t-equivalence as a design tool. Although it gives an indication of the total heating effect of a compartment fire it does not differentiate between a short, hot post-flashover fire and a long, cooler post-flashover fire. Thus the impact on the heated structure of these fires is not considered. Long cooler fires allow protected steel and concrete to achieve much higher temperatures. Similarly, Thomas *et al*[234] in their review of the role of t-equivalence in structural fire design conclude that t-equivalent may be very inaccurate out with the range of data for which it was tested. In general t-equivalence is only applicable to protected steel members although EC1 allows it to be used with all construction materials.[75]

The concept of t-equivalence was innovative when the only fire exposure considered in structural fire design was the standard curve. In performance based design natural fire exposures should be used to give the design a rigorous, scientific basis.

2.2.6 Natural Fire method

With the t-equivalence approach the heating effect in a compartment is calculated based on real compartment fire behaviour and that heating is related back to the standard furnace test. In more recent times however, the energy and mass balance equations for the fire compartment are used to determine the actual thermal exposure and fire duration. This is known as the natural fire method. This method means the combustion characteristics of the fire load, the ventilation effects and the thermal properties of the compartment enclosure are considered. It is the most rigorous means of determining fire duration. This is not related in any way to the standard fire resistance test and therefore represents the real fire duration, once flashover has occurred. The standard fire curve, t-equivalence and natural fire curves can all be used to determine the behaviour of structures in fire. The standard fire resistance method being the most conservative

and the natural fire method the most rigorous. Estimating natural fire exposures is discussed in Chapter 3.

2.2.7 Fire resistance by calculation

Fire resistance has traditionally been based upon the fire resistance test. However fire resistance of single elements or frames by calculation is becoming more common.
The fire resistance of a structure or element must be greater than the fire severity. Fire resistance design can be in terms of time, temperature or strength:

- Time to failure in the fire resistance furnace (or equivalent time) must be greater than the fire duration as calculated or specified by code
- Temperature to cause failure must be greater than the maximum temperature reached in the fire duration
- Strength or load bearing capacity at elevated temperatures must be greater than the applied load during the fire

A typical fire resistance calculation involves estimating an expected natural fire exposure, conducting a heat transfer analysis to calculate the temperature of the structural elements and then calculating the load capacity taking into account material degradation at high temperatures.

A design guide for structural fire safety was developed on behalf of the CIB (Conseil International du Batiment) in workshop CIB W14. Figure 2.4 forms the basis of this guide. It summarises the different methods for design of load bearing structures and structural elements under fire exposure conditions. Thermal exposure H_1 is the standard fire, H_2 is the t-equivalence concept and H_3 are natural fire exposures. Similar degrees of sophistication exist for the structural model adopted. S_1 considers a single element, S_2 a sub-frame and S_3 the complete structure. S_1-H_1 is the simplest design approach and is still very commonly used. S_3-H_3 is restricted to research although there are some examples of real structures designed this way.[91,93,203]

2.2.7.1 Methods of calculating the fire protection requirements

In prescriptive guidance such as Approved Document B, the level of fire resistance for a particular building is related to the fire load available and the size or height of the building.[62] If the temperature of the steel structure exceeds the critical temperature in a period of time less than the fire resistance specified by Approved Document B then

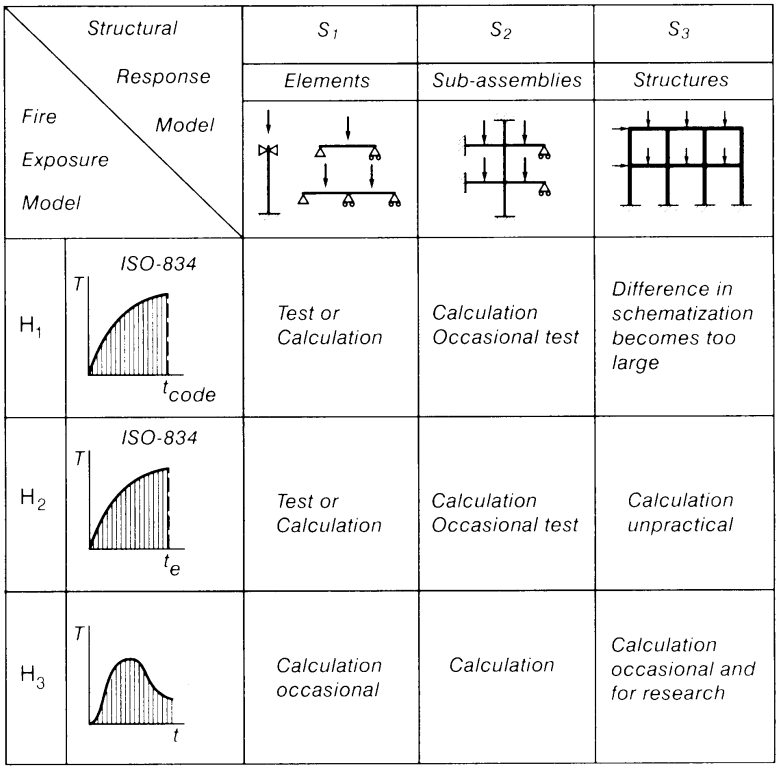

Figure 2.4: Fire and structural response models[238]

the fire protection thickness is prescribed using the "yellow book[7]" or can be calculated using BS5950 Part 8 or EC3 part1.2 or EC4 Part 1.2. All three methods only consider single elements of structure.

2.2.7.1.1 The Yellow Book[7] The "yellow book" approach uses fire test data in accordance with BS 476 Part 21. All approved fire protection materials have been tested in accordance with BS 476 and the required thickness of each product has been evaluated with regard to fire resistance period and section factor (ratio of heated perimeter to cross-sectional area of a steel section). The performance requirements for fire protection are expressed in well defined steps of 30 minutes up to 240 minutes. These results are all based on a limiting steel temperature of 550^{o}C. Table 2.2 shows a typical extract from a look-up table in the "yellow book". The section factor or Hp/A concept is the ratio of the heated perimeter, Hp (m) to the cross sectional area, A (m^2) of the structural element. Figure 2.5 illustrates the Hp/A concept.

2.2.7.1.2 BS 5950: Part 8[41] BS 5950 Part 8 is the British Standard code of practice for fire resistance design. It details fire resistance derived by tests. It also

	Dry thickness in mm to provide fire resistance of			
Hp/A up to	$\frac{1}{2}$ hour	1 hour	$1\frac{1}{2}$ hour	2 hour
30	10	10	10	11
110	10	10	18	25
250	10	13	24	34

Table 2.2: Extracts from a typical table in the " Yellow Book" for Fendolite M11

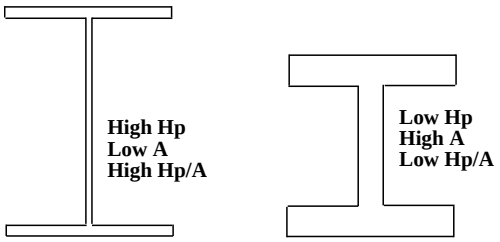

Figure 2.5: The Hp/A concept

allows fire resistance by calculation using the *Limiting Temperature Method* or *Moment capacity method*. The engineer calculates the load ratio of the beam (Equation 2.13). If this value is low i.e. the load capacity at 20^oC is high compared to the applied load at the fire limit state, then the upper limit of the steel temperature may be greater than 550^oC. The limiting temperature method allows the designer to compare the temperature at which the member will fail with the member temperature at the required fire resistance time. The code details limiting temperatures for various load ratios.

$$\text{Load ratio} = \frac{\text{The load at the fire limit state}}{\text{The load capacity at } 20^oC} \tag{2.13}$$

The moment capacity method allows the designer to calculate the moment capacity using the temperature profile at the required fire resistance time. If the applied moment is less than the moment capacity, the section can be left unprotected. The moment capacity method can only be applied to beams with webs which are plastic or compact sections.

2.2.7.1.3 The Eurocodes Methods described in EC3 Part1.2 or EC4 Part 1.2 are very similar to BS 5950 Part 8.

The Eurocodes are a collection of the most recent methodologies for design. Eurocode

3: Design of Steel Structures, Part 1.2: Structural fire design and Eurocode 4: Design of steel and composite structures, Part 1.2: Structural fire design were formally approved in 1993. Each Eurocode is supplemented by a National Application Document (NAD) appropriate to the country. It details safety factors and other issues specific to that country. SCI have published a guide comparing EC3 and EC4 with BS 5950[143] to aid the transition for designers in the UK. All Eurocodes are presented in a limit state format where partial safety factors are used to modify loads and material strengths. EC3 and EC4 are very similar to BS 5950 Part 8 although some of the terminology differs. EC3 and EC4 Parts 1.2 and BS 5950 Part 8 are only concerned with calculating the fire resistance of steel or composite sections. Three levels of calculation are described in EC3 and 4. Tabular methods, simple calculation models and advanced calculation models (similar to figure 2.4). Tabular methods are look up tables for direct design based on parameters such as loading, geometry and reinforcement. They relate to most common designs. Simple calculations are based on principles such as plastic analysis taking into account reduction in material strength with temperature. These are more accurate than tabular methods. Advanced calculation methods relate to computer analyses and are not used in general design.

2.3 The Swedish Design Guide

Pettersson and co workers[195] published one of the most innovative design guides for fire safety design of structures over 25 years ago. The methodology and principles outlined in the guide are still applicable today and in many respects are an improvement on prescriptive design. The guide advocates the use of natural fire curves and heat transfer calculations to obtain protected and unprotected steel temperatures in fire. This aspect of the guide is described in more detail in Chapter 3.

Pettersson developed a series of calculation methods based on structural engineering principles for steel members in fire. Through experimental and theoretical studies an empirical equation for the critical deflection of beams was derived (Equation 2.14).

$$y_{\mathrm{cr}} = \frac{L^2}{800d} \tag{2.14}$$

where,
y_{cr} = Critical deflection at mid-span (m)
L = the beam (m)

d = depth of the beam (m)

From this, the critical load to cause a mid-span deflection y_{cr} was derived and is described by Equation 2.15.

$$P_{\mathrm{cr}} = \beta \frac{C \sigma_s W}{L} \tag{2.15}$$

where,
σ_s = yield stress at ambient (kN/m^2)
W = section modulus (m^3)
C = constant dependent on the loading and end conditions of the beam

β is the ratio of load that causes y_{cr} under fire conditions to load that produces σ_s at ambient. The ratio β is very similar to the load ratio in BS 5950 Part 8.

Pettersson plotted β for a number of loading and beam configurations against temperature for different heating rates, thus allowing for creep effects. The steel temperature and heating rate could be calculated from heat transfer.

Pettersson also includes an approach to the design of steel columns calculating the critical buckling stress σ_k taking into consideration the slenderness of the column, material degradation with temperature and the degree of restraint to thermal expansion. The results are plotted in design charts for various degrees of restraint, slenderness and temperature.

The Swedish design Guide like BS 5950 Part 8, EC3 and EC4 is relevant to single element behaviour but the approach is based on engineering logic taking into account all aspects of the elements behaviour in fire.

2.4 Performance based design

Building codes worldwide are moving from prescriptive to performance-based approaches. Performance based codes establish fire safety objectives and leave the means for achieving those objectives to the designer.[258] One of the main advantages of this is that the most recent models and fire research can be used by practising engineers inevitably leading to innovative and cost effective design. Prescriptive codes are easy to use and

building officials can quickly determine if a design follows code requirements. However they are too onerous for many modern designs. This is especially true of modern steel framed buildings. The fire resistance ratings in building codes were not made for these types of structure. By assuming a worst case but realistic natural fire scenario and calculating the heat transfer to the steel, the load carrying capacity of the steel members can be checked at high temperatures and requirements for fire protection, if any, can be judged in a rational manner.

Performance based design has been documented in the literature extensively over the past 10 years.[31,42–44,81,91,95,119,159,193,202,244,258] Custer and Meacham[202] report that by 1996 there were 13 countries (Australia, Canada, Finland, France, England, Wales, Japan, The Netherlands, New Zealand, Norway, Poland Spain, Sweden and the USA) and 2 organisations (ISO and CIB) actively developing or using performance based design codes for fire safety.

Buchanan[42,43] in a description of the fire code development in New Zealand summarises the basic elements of performance based codes,

1. State objectives clearly
2. Specify performance requirements clearly
3. Allow any solution which meets these requirements. Also allow the use of new knowledge as it becomes available

Buchanan also states that performance goals should specify a level of safety that is independent of prescriptive building codes. Very often requirements are descriptive rather than quantitative which causes problems in determining whether performance criteria have been met. This is one of the major reasons why prescriptive codes are still in use. Figure 2.6 is an outline of the New Zealand Performance Based Fire engineering design procedure.[43] It essentially requires a number of possible worst case scenarios to be analysed. For instance the worst fire load and ventilation condition to produce the most severe fire.

New Zealand had a performance based code and regulations by 1992 but they kept prescriptive codes as an alternative solution.[44] The code, in a similar manner to other performance based regulations encourages the use of engineering calculations based on a thorough understanding of fire behaviour. Computer based fire growth tools like FPETool and HAZARD1 are being widely used, for instance to model natural fires,

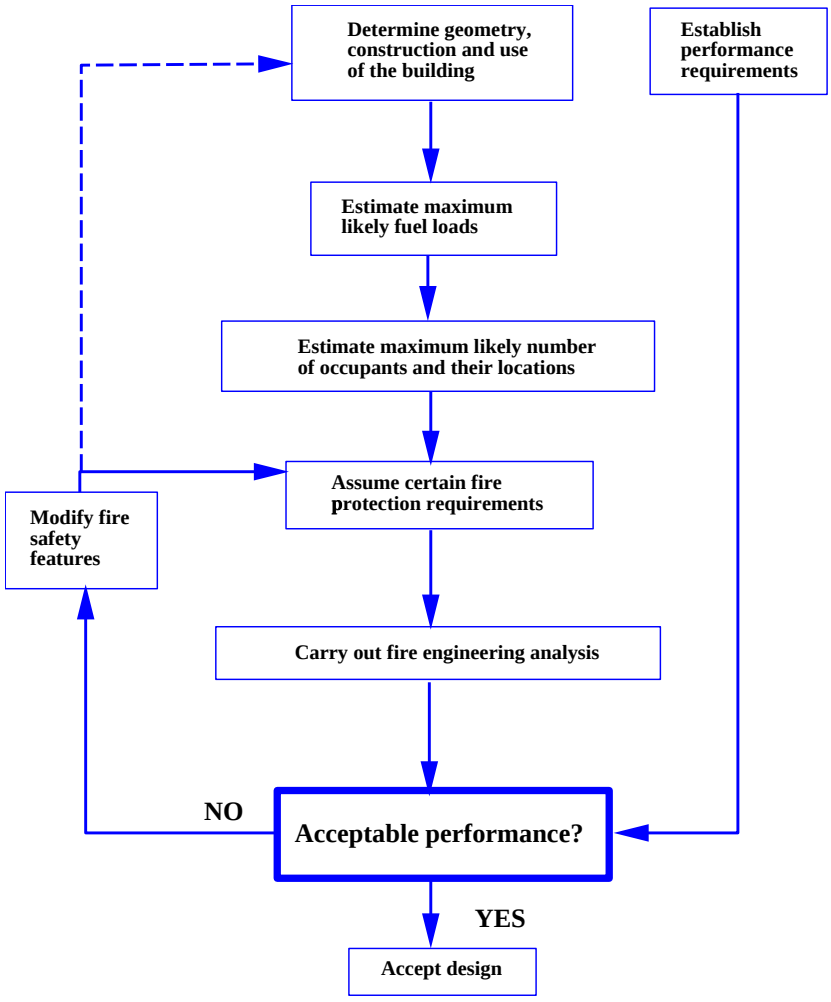

Figure 2.6: Outline of the New Zealand fire engineering design procedure

smoke movement and sprinkler response. New Zealand is also in the process of reviewing a design guide prepared by The Heavy Engineering Research Association (HERA)[55] on the behaviour of composite multi-storey steel framed structures in fire. The aim of the guide is to reduce the number of beams with applied fire protection.

In England and Wales building regulations were published as a performance based document in 1985.[202] Britain produced a Draft British Standard Code of Practice for the Application of Fire Safety Engineering Principles to Fire Safety in Buildings, DD 240[115] in 1992. This is to be shortly replaced by a new standard BS 7974 and a series of published documents.[53] Also a new set of standards are being developed in the UK, BS9999 to replace BS 5588: Fire precautions in the design construction and use of buildings. The new standard is prescriptive but fire safety engineering methodologies are being used in their development.[92,230]

The Cardington frame fire tests and subsequent numerical modelling has shown that multi-storey steel-frame structures survive compartment fires when all the steel beams are unprotected, despite temperatures in the steel of $> 1000^{o}$C. The SCI design guide "Fire safe design: A new approach to multi-storey steel framed buildings[170] " was published in 2000. It is based on theoretical work by Bailey[23] and presents a performance Based Design approach to composite steel frames enabling fire protection to be omitted from secondary steel beams.

Australia produced a draft performance based code in 1995. Quantifiable performance based codes rely on risk assessment modelling. The Australian draft is an attempt to produce a probabilistic code. The Australians were among the first to move towards a performance based approach. The Warren centre conference and reports were a major influence.[30, 44, 119]

In Canada Harmathy published a Performance based guide "Design approach to fire safety in buildings" 25 years ago. More recently the NRCC (National Research Council of Canada) collaborated with Victoria University of Technology in Australia to establish fire risk assessment models.[202] As a result the NRCC fire lab have developed FIRECAM[32] (A FIRE risk Cost Assessment Model) a key element of their performance based code.

NFPA (National Fire Protection Association)[171] and SFPE (Society of Fire Protection Engineers) are key players in the establishment of performance based Codes in the USA. The SFPE Guide[63] and NFPA 10 now have performance based solutions. However legal responsibility for building and fire codes lies within 50 states.

Performance based fire safety engineering design is now implemented and accepted in many countries. The design methodology has key advantages over prescriptive based design.

2.5 Factors affecting the behaviour of structures in fire

Structural behaviour in fire depends upon a number of variables. These include material degradation at elevated temperature and restraint stiffness of the structure around the fire compartment. High temperatures and gradients in structural elements are the driving force behind large deflections and axial forces. This section analyses each

factor on an individual basis. In buildings exposed to fire they all interact to define the structural behaviour.

2.5.1 Mechanical properties of steel at elevated temperatures

2.5.1.1 Thermal expansion

Thermal expansion is a measure of a materials ability to expand (or contract) in response to temperature changes. The coefficient of thermal expansion, α is defined as the expansion of a unit length of material when it is raised by 1^oC,[144] see Equation 2.16.

$$\alpha = \frac{\epsilon_{\text{thermal}}}{\Delta T} \tag{2.16}$$

where,
$\epsilon_{\text{thermal}}$ = thermal strain
ΔT = Temperature change

Figure 2.7 shows the influence of temperature on the coefficient of thermal expansion for steel. Thermal expansion increases linearly up to 700^oC when there is a temporary sudden shrinkage with any further increase in temperature. This is caused by the phase transformation from pearlite to austentite and a rearrangement of the crystal structure. The shrinkage is about 15% of the expansion from 20-700^oC. The type and strength of steel seem to have little impact on the thermal expansion.[4,56,144] However, the temperature associated with phase transformation does depend upon the carbon content.[56] For design purposes an average thermal expansion is assumed. BS 5950 Part 8 assumes 14×10^{-6}.[41]

2.5.1.2 Poisson ratio

Poisson ratio is defined as the ratio of lateral strain to longitudinal strain. When a body is pulled it becomes longer and thinner when it is squashed it becomes shorter and thicker. There is very little data on the variation of Poisson ratio, ν, with increasing temperature. Values are also dependent on measured elastic and shear moduli ($\nu = \frac{E}{2G}$). Errors in either value can cause large errors in ν.[56] Reported test data indicate values of 0.27 at ambient and 0.30 at 600^oC.[56] There is very little variation with increasing temperature.

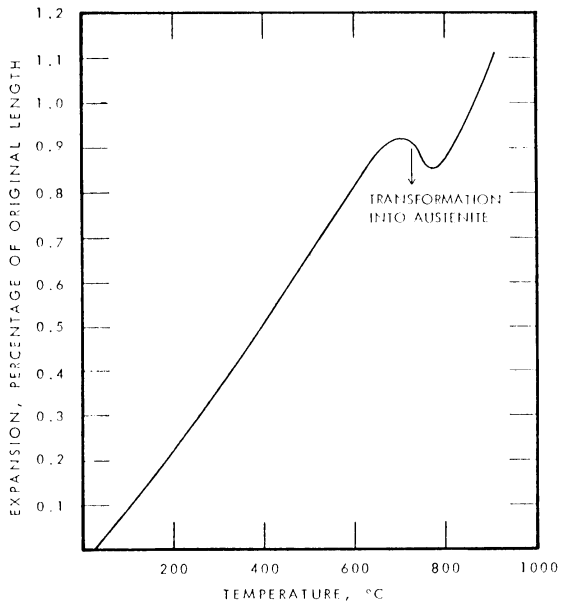

Figure 2.7: Thermal expansion of steel with increasing temperature[144]

2.5.1.3 Creep

Creep is the deformation with time as a result of a constant load. At normal stress and ambient conditions creep is negligible. At higher stresses and temperatures creep can be significant.[144] The chemical composition and the degree of processing strongly influence creep behaviour, thus a common description for every type of steel is difficult to define. Creep strain can only be measured under steady-state conditions where the creep strain can be separated from thermal and stress induced strains. However, Anderberg[4] describes a method of coupling transient (load and temperature varying) creep with the steady state measurements. Eurocode 3 includes creep in its stress-strain curves implicitly.[138,245]

2.5.1.4 Stress-strain relationships

Figure 2.8 shows stress strain relationships for hot rolled steel with increasing temperature. At ambient there is a well defined yield between the elastic and plastic portions of the curve. With increasing temperature this form is lost. The $\sigma - \epsilon$ behaviour becomes highly non-linear with increasing temperature, with both strength and stiffness decreasing. At higher temperatures the concept of 1% proof stress is typically adopted. The stress is measured at a strain equal to 1% permanent deformation of its original length (see Figure 2.9). When calculating the structural performance of a steel member to BS 5950 Part 8 strains between 0.5 and 2% are considered. The level depends on whether

the beam is acting compositely with a slab or whether it has any applied protection. For instance composite members protected with a material which has demonstrated its ability to remain intact at 2% strain in a fire resistance test can be designed to 2% proof stress. Non-composite members protected or unprotected are designed to 1.5% proof stress.

The strains induced in a structural elements are described by Equation 2.17.

$$\Delta\epsilon = \epsilon_\sigma(\sigma, T) + \epsilon_{\mathrm{Th}}(T) + \epsilon_{\mathrm{cr}}(\sigma, T, t) + \epsilon_{\mathrm{tr}}(\sigma, T) \tag{2.17}$$

where,
ϵ =Total strain
ϵ_σ =Mechanical strain
ϵ_{Th} =Thermal strain
ϵ_{cr} =Creep strain
ϵ_{tr} =Transient strain

Thermal strains depend on the temperature and thermal expansion of the material. Mechanical strains are a result of applied loading or restrained thermal strains. Creep strain is the long term deformation of material under constant load. Creep is more important at high temperatures but fires are of short duration so has less relevance. Transient strain is associated with the expansion of cement paste when concrete is heated for the first time under load. In fire the components of thermal and mechanical strains are of fundamental importance. Rotter *et al*[207, 249] have used this relationship (Equation2.17 less creep and transient strains) to understand structural behaviour in fire to fully explain the Cardington frame fire tests.

The strength properties of steel are generally determined by tensile testing. A test bar is stretched at constant rate and the loading and elongation are recorded. Tests at elevated temperatures are conducted in many ways. The two most common approaches are 1) Isothermal and 2) Anisothermal. Isothermal testing is steady state. The specimen is subject to constant temperature and strain is applied at a constant rate. In a transient anisothermal test the sample is loaded and then heated at a uniform rate 5-50^{o}C/min until failure. Strain measurements are taken throughout. A zero load test is conducted to measure thermal strains which need to be subtracted from the loaded strain measurements. The test is repeated for several loads and σ-ϵ diagrams drawn.[4, 143]

Neither test method is realistic of fire conditions. Isothermal tests are not transient and the loading on a structure is effected by restrained thermal expansion and bowing effects therefore the load is not constant as in an anisothermal test.

There is variability in test data primarily due to the quality and dimensions of the different test specimens and the accuracy of testing.

2.5.1.4.1 Stress-strain behaviour in design A bilinear representation of the σ-ϵ behaviour is used for design at ambient. The steel behaves in a linear-elastic manner up to yield at which point it is allowed to strain infinitely with constant stress. A bi-linear model of steel does not adequately represent the highly non-linear relationship at higher temperatures.[56, 126]

EC3[77] behaviour of steel includes strain hardening below 400^oC. EC3 curves are based on reduction factors for steel σ-ϵ behaviour at high temperatures (Figure 2.10). Twilt and Both[246] compared EC3 steel properties and those derived by Anderberg[4] showing the Anderberg model to be 1.3-1.5 times stronger at elevated temperatures.
The stress-strain temperature data in BS 5950 Part 8 was derived experimentally by Kirby.[127]
Modified Ramberg-Osgood stress-strain relationships are quoted in the literature as a means of calculating σ-ϵ-T relationships in numerical modelling techniques.[20, 210] The original Ramberg-Osgood correlation was a simple power-law equation to approximate stress-strain behaviour up to yield.[138]

2.5.2 Mechanical properties of concrete at elevated temperature

2.5.2.1 Thermal Expansion

Thermal expansion like all other properties of concrete is complicated by the the complex nature of the composite material. α is dependent upon stress level, type of aggregate, % volume of cement paste and rate of heating.[124, 158, 227] Cement paste expands up to 150^oC but contracts between $150 - 400^oC$ (see Figure 2.11). This is associated with water evaporation and chemical changes. However the aggregates may still expand.[228] Figure 2.11 shows thermal expansion for different aggregate types. The figure shows that thermal expansion is non-linear with increasing temperature and that the main factor affecting the thermal strain is the type of aggregate. At very high temperatures

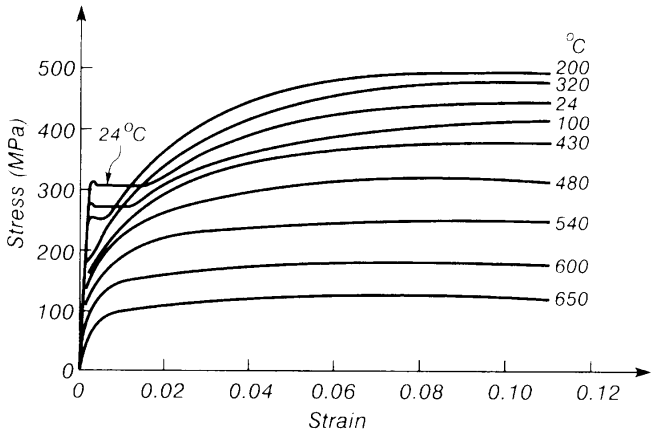

Figure 2.8: Stress-strain curves for typical-hot rolled steel at elevated temperatures[100]

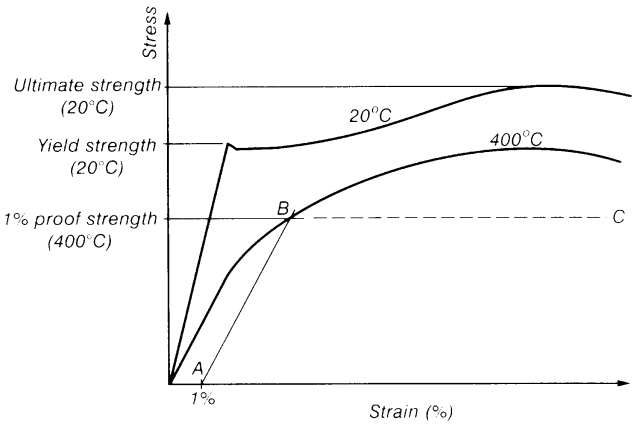

Figure 2.9: Stress-strain curves for steel illustrating yield strength and proof strength[43]

(600-800^{o}C) thermal expansion remains constant or decreases.[228]

Eurocode 2 Design of concrete structures, Part 1.2: Structural fire design[76] assumes $\alpha(\theta) = 8 \times 10^{-6}$ for $20 \leq \theta \leq 1000^o$C.

2.5.2.2 Poisson ratio

Just as data on Poisson ratio for steel was limited it is also very rare for concrete. Figure 2.12 shows the results of Ehm (1985) as cited by Schneider.[228] At 20^{o}C ν is constant until 70% of the ultimate stress. At 450^{o}C ν is only constant until 20%. In cases where $\nu > 0.5$ these indicate material effects far beyond the elastic range.[228]

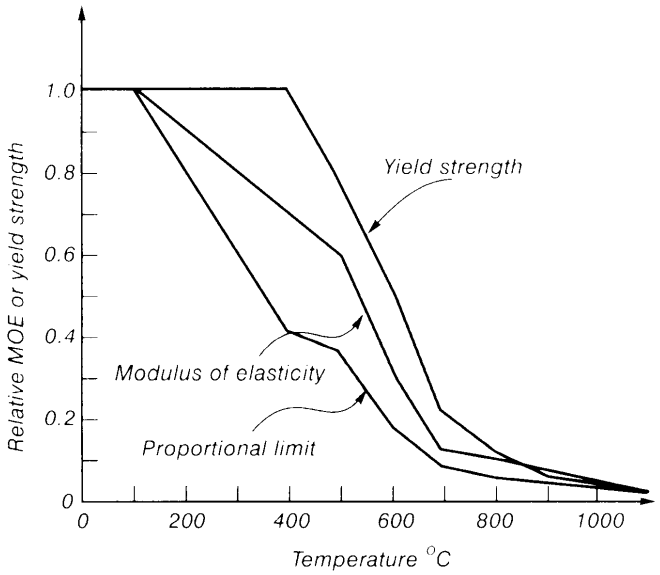

Figure 2.10: Reduction in yield strength and modulus of elasticity of steel with temperature (EC3 1995)[43]

2.5.2.3 Creep

Creep is more significant in concrete than steel. Concrete creep consists of the creep of the cement paste and the creep of the aggregate. The reason concrete does not disintegrate at high temperatures as a result of differential thermal expansion between the cement paste and the aggregate is the ability of the paste to creep.[123]

Conventional creep test data have little application to the behaviour of concrete structures under fire conditions. Specimens are heated to constant temperature and a constant load is applied for days to get constant strain. Fires last a few hours and temperatures are transient. However short duration transient creep tests are useful.[158] Figure 2.13 show tests on gravel aggregate concrete on preloaded specimens. It shows that up to a temperature of 400^oC creep is not significant for short duration heating but it is affected by preload and becomes significant at higher temperatures. Concrete elements exposed to fire on all four sides could reach very high temperatures despite its low conductivity especially if the fire has a long duration. However, concrete slabs exposed to fire on one side will only achieve high temperatures through a small depth of the concrete. In the latter case the mean temperature is not likely to exceed 200^oC and creep effects will be less important.

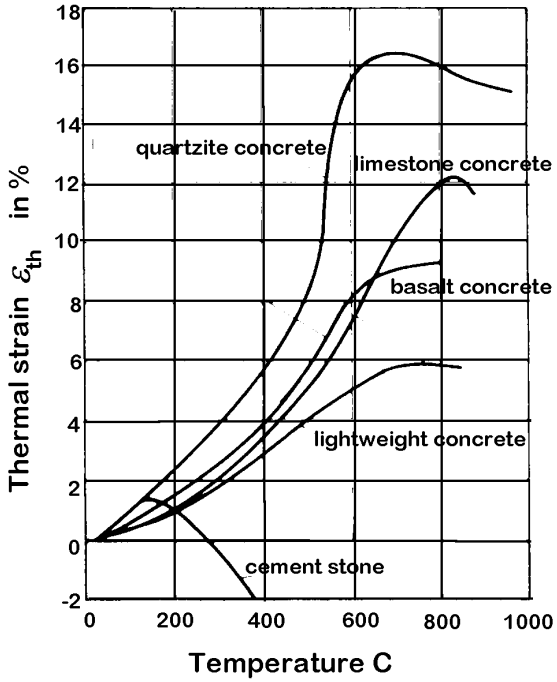

Figure 2.11: Thermal expansion of concretes[228]

2.5.2.4 Stress-strain relationships

Stress-strain behaviour of concrete is radically different in compression and tension. In tension concrete is often assumed to have zero tensile strength. Schneider[228] reports tensile strengths of about 10% of the compression strength. Strength is affected by type and size of aggregate, % cement paste and water/cement ratio at ambient and at elevated temperatures. Loading of a specimen is beneficial to its compressive strength.[144]

There can be large variation in test results[144] these are attributed to a large number of factors including the method of testing, rate of heating, duration of heating, size and shape of specimen and loaded or unloaded conditions.

2.5.2.4.1 Design stress-strain curves The stress-strain behaviour of concrete can be described by a set of equations in EC2.[76] Figure 2.14 shows compressive stress-strain data for concrete at elevated temperatures according to EC2. High temperature creep is included implicitly. Concrete stiffness reduces much more than steel with increasing temperature resulting in greater strains. This can lead to large deflections in concrete members exposed to fire.
The Eurocode provides guidelines on the tensile capacity of concrete but also allows

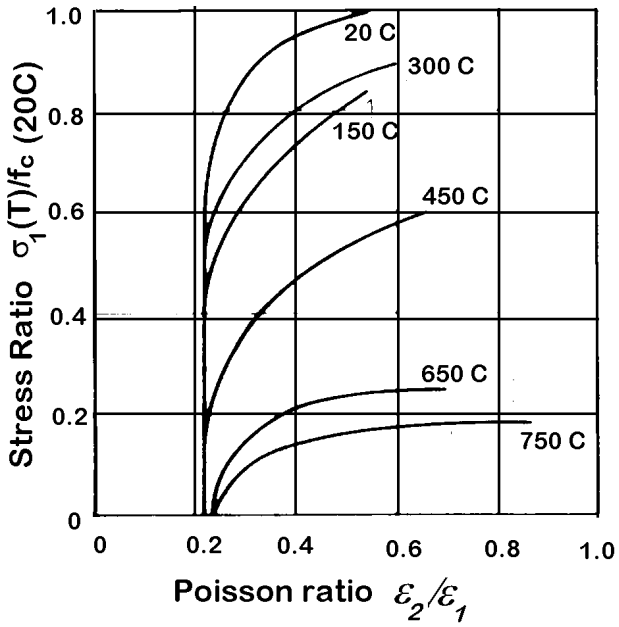

Figure 2.12: Poisson ratio[228]

designers to consider it to be negligible. Figure 2.16 shows design values from BS 8110 for the reduction of modulus of elasticity with temperature. Figure 2.15 gives design values for compressive strength with temperature. The dotted line in Figure 2.16 was introduced to correct for the fact that in Figures 2.15 and 2.16 the modulus of elasticity and compressive strength reach zero at different temperatures.[43]

2.5.2.5 Spalling[158]

Spalling is the loss of surface material from a concrete element and is dependent on aggregate, moisture content, stress level and temperature. Aggregate splitting is the splitting and bursting of silica containing aggregates due to physical changes in the crystalline structure at high temperatures. This is a surface effect and as such has little effect on the structural performance. Explosive spalling is characterised by large or small pieces of concrete being violently expelled from the surface often exposing reinforcement thus reducing the load bearing capacity of the structure. Normal weight concrete is much more susceptible to spalling than light weight concrete. Spalling is associated with differential expansion and thus can occur under heating or cooling.

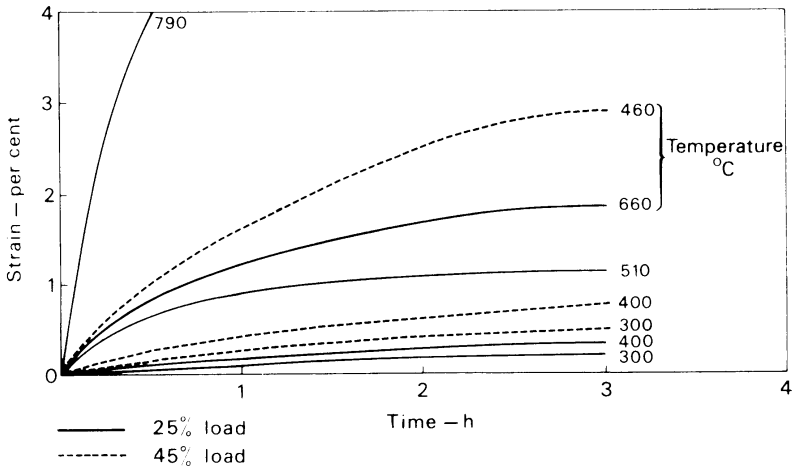

Figure 2.13: Concrete creep[158]

2.5.3 Thermal Bowing and Thermal Expansion

Increasing temperature causes thermal expansion of structural elements and differential heating results in thermal bowing. In buildings experiencing real fires these two phenomena act together and are very often restrained leading to thermally induced stresses and large deflections.

Both effects can be illustrated by considering a single beam element. If the temperature of a beam of length l is increasing uniformly along its length and over its depth such that the whole beam is at the same temperature at any given time, the beam will expand with an increase in temperature ΔT according to Equation 2.18.

$$\Delta l = \alpha \Delta T l \tag{2.18}$$

Where α equals the thermal expansion coefficient of the constituent material. If the beam is axially unrestrained then it will simply increase in length. If the beam is restrained from expanding at its ends then an equal but opposite compressive force will develop reacting against the expansion. This may result in the beam buckling at a critical compressive force accommodating expansions in downwards deflection or extensive elastic and plastic straining until the material yields.

Thermal gradients exist through the cross-section of elements of structure because of differences in the thermal diffusivity of materials and as a direct result of differential heating. If members are heated from one side such as edge beams or heated from

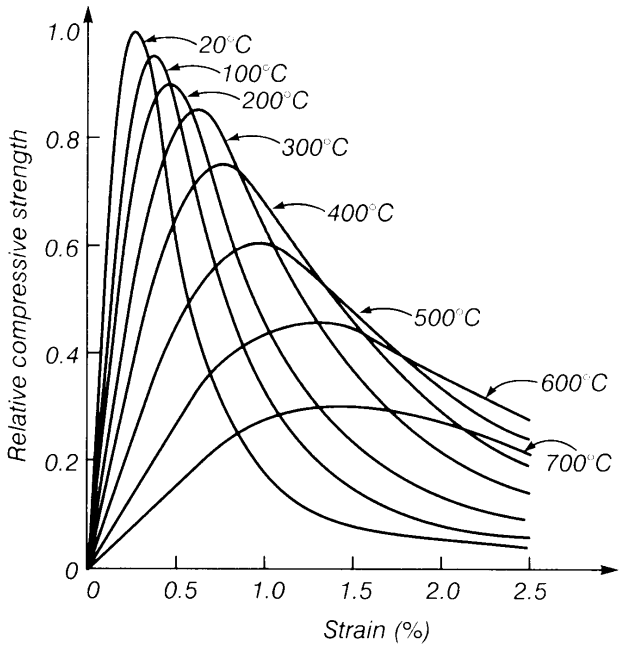

Figure 2.14: Stress strain relationships for concrete at elevated temperatures (EC2 1993)[43]

underneath such as floor slabs gradients will develop across the section or through their depth.

Steel has a very high value of thermal conductivity so steel beams and columns subject to fire on all sides achieve uniform temperatures quickly and very low gradients exist. Beams supporting floor slabs will achieve higher temperatures in their lower flange than their top flange. This is due to less direct heat being applied to the top flange and the heat sink effect of the cooler slab. Differences between the top and bottom flange can be up to 100-200^{o}C.[195] Concrete has a much lower thermal conductivity so slabs heated on one side for instance, achieve very high gradients. Composite slabs develop large gradients between the steel beam and the concrete slab. This is magnified if the fire is very hot but of short duration because the steel reaches high temperatures quickly and the concrete has little time to respond to heating.

Increasing temperatures cause materials to expand. Gradients through the depth of an element cause one side to expand more than the other, creating greater thermal strains on one side than the other. This results in the element trying to bow towards the source of heat. If the ends are axially and rotationally restrained from bowing this will result in the development of a moment along the element. If the ends are rotationally free the beam will deflect (or bow) towards the heat. The thermal curvature ϕ associated

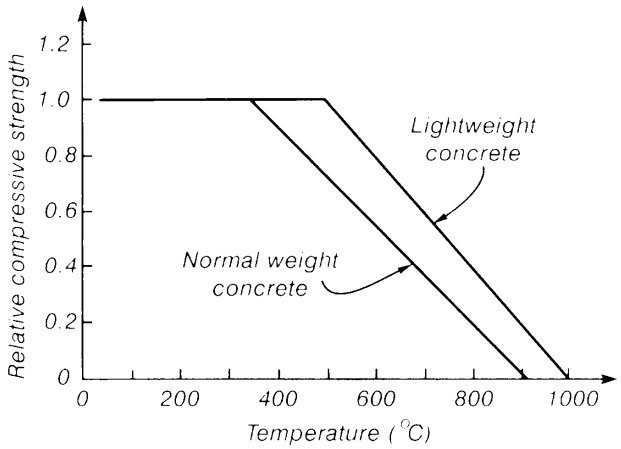

Figure 2.15: Design values for reduction in compressive strength with temperature[43]

with a linear gradient, $T_{,\mathrm{y}}$, through the depth of an element is given by Equation 2.19.

$$\phi = \alpha T_{,\mathrm{y}} \tag{2.19}$$

α equals the thermal expansion coefficient of the constituent material.

Thermal gradients also exist along elements of structure. Columns invariably attain greater temperatures near the top of a compartment than near the floor. Beams and slabs may also experience gradients along their length as a result of localised heating. In beams, temperatures near the connections are very often cooler that at the centre. Pettersson[195] reports on early work by Thor which shows that there is an increase in the load carrying capacity compared with beams which have uniform temperatures along their length. In statically indeterminate beams Thor found the rise in load bearing capacity could be considerable.

Rotter *et al*[207] and Usmani *et al*[249] have considered the effects of thermal bowing and thermal expansion from first principles on the behaviour of restrained steel and composite beams. This work is summarised in Chapter 6 of this thesis alongside numerical calculations to verify the theory.

The effects of restrained thermal expansion and bowing have been observed in tests and analytical studies previously.[57, 83, 112, 158, 195] Cooke[57] reports a programme of tests

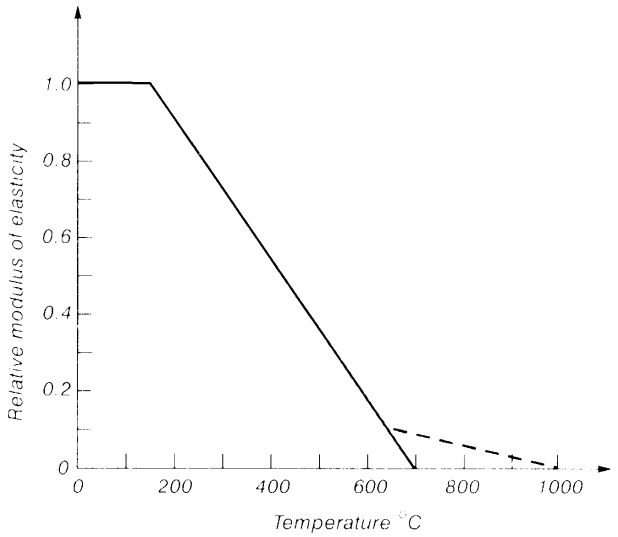

Figure 2.16: Design values for reduction of modulus of elasticity[43]

carried out at the Warrington Fire Research Centre on simply supported reinforced concrete floor slabs of 4.5m span. Mid-span deflections and longitudinal deflections caused by thermal bowing were measured for slabs of 150mm and 250mm thickness made of normal weight and lightweight concrete. The slabs were exposed to one of two heating regimes the standard curve in BS476:Part 8:1972 (now superseded by BS 476 Parts 20-23) or the more severe standard curve proposed for hydrocarbon fires by the Norwegian Petroleum Directorate. Results of the parametric study showed that the imposed load is responsible for only a small part of the deflection. This is in agreement with modelling of the Cardington tests.[187] The thermal bowing deflections of lightweight concrete slabs were significantly lower than the deflections experienced in similar normal weight concrete slabs. Cooke[57] attributed this to the different thermal expansion values of the respective aggregates. The more severe hydrocarbon fire produced higher deflections overall especially in the earlier stages of the test. Cooke does not explain this but the nominal curve for hydrocarbon fires reaches much higher temperatures (almost immediately in excess of 800^{o}C) and would result in much higher gradients over the depth of the section.

The significance of restrained thermal expansion is acknowledged in design codes but little information is provided on how to include the effects in design thus is very often ignored.

2.5.4 Redundancy

Single determinate elements tested in the fire resistance furnace can only form one load path determined by equilibrium of the forces. Indeterminate or redundant structures are capable of transferring load through many alternate load paths and as a result the pattern of forces and stresses is determined by the relative stiffness of the elements of the structure as well as equilibrium and compatibility conditions. Redundant structures allow load transfer to stiffer parts of the structure when one or more elements fail allowing the structure to survive. The benefits of redundancy rely on ductility of the connected structure and the ability to form new load paths. The Broadgate building and the Cardington 8-storey composite steel test frame have shown considerable redundancy in fire.

2.5.5 Loading

In fire design the applied loads are assumed to be lower because the imposed loads are reduced by evacuation and contents burning. Design codes allow lower partial safety factors for loading in fire. Safety factors for loading in BS 5950 Part 8 and EC1/EC3 are given in Table 2.3. It has been proposed that in the next version of BS 5950 Part 8 the safety factor for imposed loading for fire design should be reduced from 0.8 to 0.5. This would mean a reduction in load ratio of the individual structural elements and a corresponding increase in limiting temperature according to BS 5950 Part 8, inevitably leading to a reduction in passive fire protection and savings for steel design. However, in large structures where phased evacuation is adopted i.e. parts of the building are evacuated whilst others remain occupied in areas protected by compartmentation measures, the imposed loading may still be high. Also loading on the floors above the fire compartment (the load carried by the fire exposed weaker elements) will only be reduced by evacuation not by combustion of the contents. However, work at Edinburgh has shown that loading under fire conditions, where the elements of structure are axially restrained against thermal expansion, has little impact on the deflection response until near impending runaway failure.[136,187] Moreover, experience at Cardington has shown that it is very difficult to achieve imposed loads representative of those assumed in design. Covering the Cardington frame floors in sand bags[197] only achieved an imposed load of 0.83kN/m^2 during the tests. On this basis reducing the safety factor on imposed loads for fire seems reasonable, providing characteristic imposed loads assumed in ambient design are not excessively reduced in the future.

	γ_f	
Load	BS 5950 Part 8	EC1/EC3
Dead load	1.0	1.0
Imposed Loads:		
(a) permanent	1.0	1.0
(b) non-permanent	0.8	0.5 to 0.9
Wind loads	0.33	0 or 0.5

Table 2.3: Load factors for fire limit state[41, 75, 77]

2.6 Research into the behaviour of single elements of structure in fire

Most analytical methods for determining the fire resistance of structures centred on single elements. The response of columns and beams under fire conditions has been investigated over many years but with increased intensity in the 80s.[133] At this time extensive testing was conducted in Europe in the UK, Germany, Netherlands, France and Belgium.[5, 118] These test results have been extensively used for comparison with numerical models. The response of a whole building under fire has received less attention.

2.6.1 Computer models for structures

There are a number of numerical computer programs developed in research centres to calculate the behaviour of structures in fire. Some of the well known codes used for fire research include CEFICOSS[225] (ProfilARBED-Recherches, Luxembourg), DIANA (TNO Delft), VULCAN[109] (University of Sheffield), SAFIR (the next generation of CEFICOSS developed at the University of Liege, Belgium) and SISMEF (CTICM, France). CEFICOSS, DIANA and SAFIR include thermal analysis as well as structural analysis. All except CEFICOSS model 3D behaviour, CEFICOSS models 2D. VULCAN is based on the code INSTAF.[210]
General finite element codes like ANSYS and ABAQUS[102] have also been used to analyse fire. ABAQUS is used at the University of Edinburgh, by CORUS and the University of Manchester. Imperial College have developed a research code ADAPTIC capable of modelling structural fire behaviour.[74]

2.6.2 Columns

The research described in this thesis is primarily concerned with the response of composite floor slabs in whole frame structures but the effect of restrained thermal expansion

has been analysed more in columns than beams and slabs. Thus a review of column research aided understanding of restrained thermal expansion and thermal bowing. Columns and beams both experience restrained thermal expansion in fire conditions but columns are further complicated by axial forces as a result of live loading, initial out of straightness, eccentric loading and bending moments as a result of expanding beams.

The European Convention for Constructional Steelwork (ECCS) proposed buckling curves for columns at ambient in the late 70s as cited by Lane.[138] There are 5 basic buckling curves (classified a_0,a,b,c,d) which are applicable to cross-sections of different shapes. Beam-column connections are considered by including a factor to account for moment and eccentricity.
Janss and Minne[118] presented a method to calculate the buckling of steel columns under concentric and eccentric loading in fire conditions. They simply included temperature dependent material properties in the ECCS ambient buckling curves and calibrated the results against experiments from Belgium, Denmark and Germany. A correction factor was introduced to get better agreement with the experimental results. Only type 'c' cross sections were considered because of limited test data on other sections.
In the 80s, Lie[147] described work carried out at NRCC (National Research Centre of Canada) on developing mathematical models for calculating the fire resistance of compression members. Rubert[209] analysed the effects of load level (utilisation factor) and slenderness on the critical temperatures of steel columns. Also Anderberg *et al*[5] compared analytical predictions of the mechanical behaviour of fire exposed steel structures with experimental data on axially free and restrained columns tested in Norway and France. Results from the materially and geometrically non-linear finite element model Steelfire, developed by Forsen, are compared. Results from Steelfire agree well with the test data. The authors add that full axial restraint is very difficult to achieve in practise therefore test conditions are difficult to define especially at high restraint, thus some results may be fortuitous.

In 1990 Corradi[58] carried out a parametric study on the interaction diagrams of steel columns in fire conditions to study the influence of the slope of the hardening branch in steel stress-strain plots. Corradi found that a bi-linear approach was not adequate because it consistently overestimated the load carrying capacity even for small axial forces. Also in a tri-linear model the interaction curves were very sensitive to change in the slope of the hardening zone.

Wang and Moore[256] developed a simple analytical relationship for restrained thermal expansion in axially loaded columns assuming axial expansion could be explained by

Figure 2.17. ΔP is the additional compressive load generated in the column as a result of restraining the expansion $\Delta\epsilon_{\text{th}} L_c$. The equation is compared with parametric studies on a numerical model. The failure temperature of the column in the frame with stiffer beams (higher restraint to expansion) was generally lower. However, by increasing the applied load the reduction in failure temperature slowed. Wang and Moore concluded that the effect of restrained thermal expansion in columns generally increases the axial compression force and was particularly detrimental to slender columns. The magnitude of the additional axial forces depends on the column stiffness, restraining stiffness, column slenderness and applied axial load. The simple calculation was also tested against the squashing of columns at Broadgate. The failure temperature was found to coincide with the predicted failure temperature after the fire.

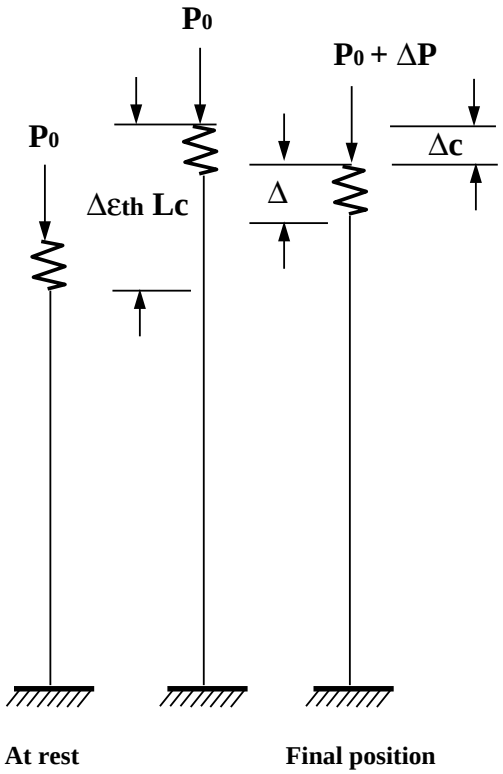

Figure 2.17: Column expansion in fire

Baker *et al*[26] studied analytical and experimental results to determine the significance of local buckling, the post-buckled response and high temperature creep effects. Stocky (stub) columns were analysed and in all cases the columns exhibited local buckling and a stable post-buckling load-deflection response. ABAQUS non-linear shell elements were used to model the local buckling. Localised deflections were found in the hottest areas of the column (high temperature variations of up to (196^{o}C)) initially and after

local buckling. The material properties were determined by a series of tensile coupon tests at various temperatures and strain rates. There was good agreement with the analytical and experimental results. Conclusions state that rate dependent material properties are accurate enough to predict the behaviour of steel columns at elevated temperatures for a short time and at lower temperatures (below 400^oC) for a long time.

Janss[117] highlights that discrepancies arise when the fire resistance is determined by test and by calculation. He attributes this to assuming characteristic material properties, uniform temperature distribution and design yield strength when carrying out a calculation. In tests there may be a considerable distribution in temperature leading to an increase in the failure temperature. By adopting a unified statistical evaluation procedure put in place to verify EC equations, adaptation factors are proposed to modify the design assumptions so that critical temperatures are found which are at the same level as standard tests.

Ali *et al*[2] reports on an experimental program designed to investigate the effects of imposing axial restraint on steel columns in fire. The work was carried out at the University of Ulster. 45 fire test and 10 pilot studies were conducted on a rig capable of applying axial load and restraint. They defined the restraint stiffness (α_k) as the ratio of the stiffness of the restraining element (K_s) to the axial stiffness of the expanding column (K_cT). By studying two previously recorded load tests α_k was found to be in the region 0.1-0.55 in practice. Tests were carried out to ensure uniform temperature over the height of the column. The tests were conducted under constant load and a heating rate of 10^oC/min until failure. Preliminary reports of the pilot study concluded that imposing restraint reduces the fire resistance of the column. In unloaded columns increasing α_k from 0.04 to 0.32 almost doubled the value of axial force induced in the column and reduced the failure temperature from 518^oC to 223^oC. This is in agreement with Wang and Moore.[256] When the columns were loaded to 64% of their capacity and for the same increase in α_k the failure temperature reduced to 185^oC.

Baker and Xie[27] studied elasto-plastic creep of steel columns exposed to fire. The research was carried out because it was thought at higher temperatures and loads in unexposed columns, creep and local buckling may become important. These were very often ignored by other researchers. They were not concerned with creep in protected columns over the length of a fire. Stub columns were heated locally mirroring the hottest layer of gases in a compartment near the top of the column. Gradients were ignored and only axial deflections were allowed. There was plastic shortening and local buckling within 0.3m of the top connection. This is very similar to the response of

the columns in the Broadgate building and in British Steel Test 2[197] at Cardington. The columns in the Cardington test were only protected to 0.5m below the underside of the slab. Further analysis showed creep to dominate at high load levels beyond 600^{o}C.

Researchers in Australia[52] have shown that the column effective length concept is valid at both ambient and elevated temperatures. They found that the time to collapse of unprotected steel columns was less for higher loads, medium slenderness ratios and lighter (less compact) column sections.

Franssen *et al*[85] reports on a comparison between five structural fire codes. CEFICOSS, DIANA, SAFIR, SISMEF and LENAS-MT developed jointly by CTICM and Takenaka in Tokyo. The five codes were to be used in an ECSC research project to determine the buckling curves of hot rolled H steel sections in fire for EC 3 Part 10 (now EC3 Part 1.2). The comparison was conducted to check the consistency of the results from all five codes. Eight tests including Lee's frame, an eccentrically loaded column and an axially loaded column at ambient and elevated temperatures were analysed. The conclusions state that if bending is the predominant behaviour all five codes give very similar results. If axial loads dominate, slight differences occur although the greatest difference between any two codes was 6%.

In 1995 Franssen[83] *et al* proposed a simple model to determine the fire resistance of axially loaded members, similar to the ambient form in EC3 Part 1.1 (based on ECCS buckling curves). Thus the ultimate load of columns at elevated temperatures could be determined on a calculator. The initial relationship is for simply supported , axially loaded, symmetrically heated H columns. The extent of the analyses was considerable. 200,000 numerical tests were conducted analysing 2 yield strengths, 339 hot rolled H sections, 2 buckling axes, 10 slendernesses, 12 applied loads and two thermal regimes (constant temperature and the standard fire). These were matched with 80 experiments.

Recently Correia[205] has studied the critical temperatures of compressed steel elements with restrained thermal elongation. 168 tests on hinged bars with 4 slendernesses, 2 eccentricities and 6 levels of restraint were carried out. Test and computer simulation have shown that neglecting the effects of thermal axial restraint may result in overestimating the fire resistance of columns. The research found that restrained thermal elongation of centrally compressed elements with slenderness greater than 80 lead to reductions of T_{crit} of 200^{o}C. However if eccentricity was high there was no significant

variation in critical temperature.

Bailey[19] analyses the assumption that columns designed to current design procedures are adequate when composite frames are designed to the new SCI guide i.e passive fire protection is removed from secondary beams. The results do not concur that columns are stable. P-δ effects caused by expanding beams could cause column instability. The analyses showed that column instability was effected by beam-column heating rates, beam cross-section size, span of the beams, end rigidity of the heated column and column axial load. Nominal effects were column cross-section size, beam-column connection rigidity and horizontal restraint to the heated beams (provided realistic values were chosen).

It has been shown that axial restraint and its effect on thermally expanding columns has been researched for many years. Most of the research has been on single elements. Restrained thermal expansion of columns leads to increased axial forces and early failure of the elements.
In composite floor slabs buckling of the steel beams as a result of large compressions induced by restrained thermal expansions is a positive event. The buckle allows the increase in length as a result of thermal expansion to be accommodated in downward deflections relieving axial compressions. This is discussed in this thesis.

2.6.3 Beams

Burgess *et al*[48] developed a secant stiffness approach to fire analysis of steel beams with non-linear material behaviour. The moment-curvature-temperature relationships were derived using a Ramberg-Osgood Equation. Initially only uniform temperatures could be described, through the depth of the section and along its length. The secant stiffness approach was adopted because there were no limitations on the shape of the stress-strain curves and the model was stable at zero tangent stiffness (pure yield). Later modelling of non-uniform temperatures was incorporated in the model.[46] The effect of this was twofold. The neutral-axis depth changes and additional deformations due to non-uniform thermal expansion (bowing) had to be modelled. Thermal bowing was included by an equivalent moment at the ends of each beam element. The scope of the analysis did not include axial thrusts or semi-rigid connection behaviour. The secant approach was also used to study the connection stiffness and the behaviour of steel beams in fire.[72] There are significant increases in failure temperature when the rotational stiffness is increased from simply supported conditions. They conclude that

the influence of the connection temperature is not critical.

In 1991 El-Rimawi *et al*[47] reported a series of numerical studies on the fire resistance of steel beams in fire. FIRES T2, originally developed at the University of California Berkeley, was used to calculate the thermal regime. They highlighted the increased fire resistance of beams exposed to fire on three sides (supporting a concrete slab) over 4-sided exposure. In this instance deflections were dominated by thermal bowing as a result of the gradient between the top and bottom flanges. By exploiting this phenomenon increased fire resistance was obtained in asymmetric sections. The effect of support conditions, span:depth ratio and design stress were also investigated. Some benefit was derived from partial heating over the length of a beam.
Liu[149] developed a 3D shell model using a tangential stiffness approach to analyse the behaviour of steel beams and connections in fire. The code was written in Fortran 77. The model is geometrically and materially non-linear. Non-uniform temperatures can also be modelled. Numerical results were compared with real fire test data on steel beams and beam-column connections. Good agreement with fire resistance ratings and deflection-time histories were obtained.

Bailey *et al*[22] considers the lateral torsional buckling of uniformly heated, unrestrained steel beams. Different sections, spans and load cases are considered. Failure is by lateral torsional buckling in all cases. When compared with limiting temperatures in BS 5950 Part 8 and EC3 Part 1.2 the model predicted lower temperatures than the code. In conclusion the authors recognise that beams in real structures are restrained therefore failure is unlikely to occur .

More recently Becker[35] has considered the heat sink effects of slabs in continuous construction on connection temperatures. A standard fire is assumed and a thermal analysis of insulated and non-insulated continuous construction conducted. The structural significance is tested with SAFIR. The temperature drop in bare steel is insignificant for practical purposes after 30-60 minutes standard fire exposure. However for insulated steel the effect of the heat sink on the non-uniformity of longitudinal temperature differences is much more significant. A one bay frame example is given in the paper and the structural model predicts a 16% increase in the fire resistance from 60-70 minutes when uniform and non-uniform temperatures are considered. Natural fires were not considered.

2.6.4 Slabs

The most important phenomena in slabs with regards to their behaviour in fire is membrane action. Compressive and tensile membrane action provide reserves of strength allowing whole frame structures to survive fire.[6, 111, 187, 197] Traditionally slab designs are based on yield line theory with no consideration of membrane effects.

Compressive membrane forces only occur if the edges of the slab are fixed. They are induced when deflections cause the slab edges to move outward and react against the lateral restraint, producing arching action of the slab between the boundaries. Compressive membrane forces in the slab result in an increase of the flexural strength.[54]

At large deflections the slab edges tend to move inwards and if the edges are suitably laterally restrained tensile membrane forces are induced which may enable the slab to carry significant load by catenary action of the reinforcing steel. Compressive membrane action relies on in-plane restraint from the boundaries therefore can only occur in fixed boundary conditions. Tensile membrane action can occur in fixed or simply supported conditions.[252]

Figure 2.18 shows the classic load-deflection response for a clamped and simply supported slab. Initially a restrained slab will arch from boundary to boundary inducing compressive membrane action. As deflection increases, load increases. Point B is the maximum compressive force, several times greater than the strength according to yield-line theory. As deflections increase further the depth of the cracked slab increases therefore composite strength diminishes. At point C the slab has cracked over its whole depth and tensile membrane action has developed (Figure 2.19). The load is supported by the mesh anchored at the supports. As the deflection increases further, load carrying capacity increases until rupture at point D. In a simply supported slab compressive membrane action is limited. However at large deflections slabs can develop an in-plane ring beam in compression[254] to support the tensile membrane action (Figure 2.20). In a simply supported slab there is a smooth transition from flexural behaviour to tensile membrane action.

Compressive membrane action is not stable and realistic support conditions are seldom completely restrained which explains why designers will not rely on its benefits. Tensile membrane action is stable but occurs at large deflections which would exceed serviceability conditions. This is less of problem in fire conditions. When considering membrane action the yield-line pattern, yield condition, geometric compatibility, force equilibrium and the work method of plastic analysis must all be considered.[254]

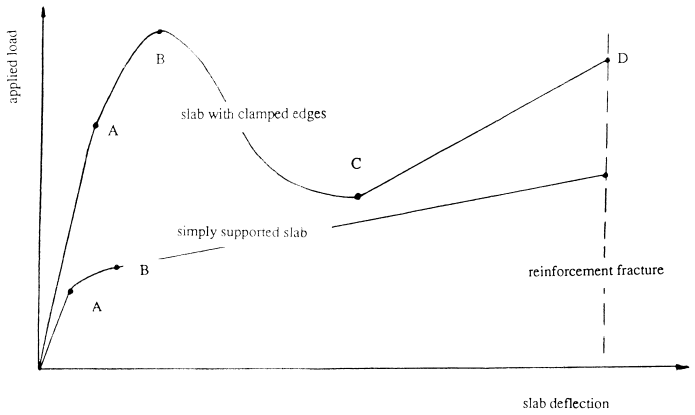

Figure 2.18: Complete load-deflection curve for a reinforced concrete slab[252]

2.6.4.1 Membrane action at ambient

In 1952 a series of tests were carried out on a reinforced concrete building in Johannesberg. From two tests to destruction on interior slab panels in both tests the collapse load was more than twice that predicted by the yield line method.[173] Ockleston who was responsible for the tests later showed that the result can be explained by the arching action due to the development of compressive membrane stresses in the concrete slab.[174]

Park was actively researching membrane actions in slabs in the 60s[191,192] experimentally and analytically. He derived expressions for the ultimate strength of uniformly loaded, axially restrained, two-way concrete slabs with and without reinforcement including compressive membrane action.

Park also developed an analytical solution for slabs in tensile membrane action with clamped edges.[190] Wood developed a solution for tensile membrane action in simply supported circular plates and Kemp for simply supported square slabs as cited by Christiansen.[54] Later Wang[254] adopted Kemp's approach modifying it for rectangular slabs.

In recent years Eyre and Kemp[80] have analysed the various methods of predicting the ultimate load capacity of reinforced concrete slabs including compressive membrane action and discuss the implications associated with the assumed stiffness of the slab itself. They found when very rigid supports are used the theory predicts an overly stiff load-deflection response.

Guice[94] report tests on one-way reinforced concrete strips with partial lateral and rotational restraint. The tests were carried out because in reality idealised boundaries do not exist and there is little data on partial restraint. They found lateral restraint is

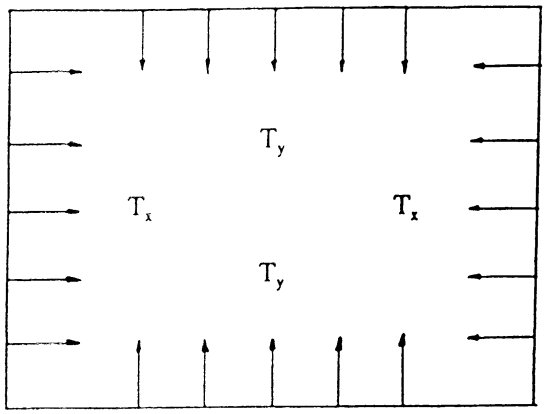

Figure 2.19: Tensile membrane load carrying mechanism in a slab with clamped edges[252]

essential in developing both compressive and tensile actions. Small rotational freedoms significantly enhance tensile membrane capacity. Increasing the area of steel and slab thickness also enhances the compressive membrane capacity and sufficient ductility in the steel reinforcement must be provided to ensure tensile membrane resistance.

2.6.4.2 Membrane action at elevated temperatures

Tensile membrane action played an important role in the survival of the Cardington frame fire tests. This was highlighted in the numerical modelling.[88,112,187,252] Test data to support the theory was not conclusive. A major concern was that there were no measurements to prove a compressive membrane ring had developed at the edge of the compartments to support tensile membrane action at the centre. Consequently Bailey[25] *et al* conducted a large scale ambient test (additional deflections as a result of thermal gradients were not considered) to understand and record tensile membrane action. They conducted the large scale test on a profiled composite slab similar to that used at Cardington. The test slab measured 9.5m x 6.5m in plan. It was supported on composite edge beams with shear stud connectors around the slabs perimeter. During the Cardington tests the metal deck de-bonded from the slab so this was removed for the test. Tensile membrane action was observed and the failure load was double that predicted by classic yield-line theory.

Wang[252–254] has conducted the most recent analytical work on tensile membrane action in fire. He developed a procedure for rectangular slabs based on Kemp's methodology for square slabs and predicted the final deflection after cooling in the BRE corner test. Huang[112] has reported a series of analyses using linear and non-linear slab elements

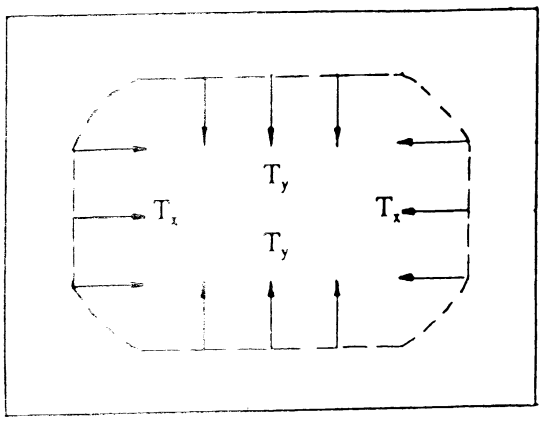

Figure 2.20: Tensile membrane load carrying mechanism in a simply supported slab[252]

in VULCAN. A comparison is made between the different levels of restraint in all the Cardington frame fire tests and the effect on the slab. Conclusions include that tensile membrane action is minimised if the floor slab is only in single curvature, observed in the half floor test.

2.7 Frame Analysis

The increased benefit in fire resistance of studying frames has been realised for some time. Frame analysis has concentrated on developing numerical models. Unfortunately whole frame experiments are expensive and the models are very often tested on experimental data from single elements or sub-frames.

Saab and Nethercot[210] developed a non-linear analysis of 2D steel frames under fire conditions by extending the finite element model INSTAF. Non-linear stress-strain-temperature relationships are based on the Ramberg-Osgood equation and creep is included implicitly. The solver is an incremental Newton-Raphson method. The model allows variation of temperature distribution both along and across each member. It was verified against test results on frames and columns. In 1996 Najjar[166] reports on further development of INSTAF, to model 3D steel frames in fire. Bailey[18] extended INSTAF considerably to include continuous concrete floor slabs, semi-rigid connections, lateral torsional buckling and strain reversal in steel.

Modelling strain reversal is important for cooling. El-Rimawi[71] included unloading of the steel stress-strain curve in the model NARR2 with a bi-linear unloading curve. The approach adopted by Bailey was curvi-linear based on the Ramberg-Osgood stress-strain relationship.[20] Bailey assumed the loading and unloading paths separate in the inelastic range and the upper bound of the elastic limit is 0.1% proof stress at elevated temperatures. A comparison between a spreading fire and simultaneous heating of a whole compartment was conducted. The authors acknowledge the limited study but preliminary conclusions included that there were higher deflections in the source bays of the spreading fire studies than with simultaneous heating of the same member. Extra compressions and deflections were induced in cooling beams adjacent to beams heating up.

In two papers Wang[255,257] describes the development and verification of a finite element program at BRE to study the structural response of steel frames at elevated temperatures. Two and three dimensional frames can be modelled. The model can also include concrete.

Franssen[83] analysed a 2D unprotected steel frame tested at Cardington. The application of 1D, 2D and 3D heat flow models was discussed. The effects of restraint, frame continuity and thermal expansion were highlighted. The calculation of frame stability was compared with the draft EC3.[83] A possible outcome of the research was the ability to test scenarios where it was safe to use the simplified EC3 approach. Conclusions included that the yield stress at ambient has an influence on the fire resistance and the variation of lateral in-plane restraint has a major effect on the fire resistance. Also the calculated fire resistance of a single beam has a much lower value than the frame. Finally the influence of thermal expansion cannot be ignored.

El-Rimawi *et al*[70] developed the secant stiffness method for beams to include thermal degradation characteristics of the connection between members and the effects of axial force. It highlights that survival can be significantly enhanced by connection characteristics. In a further paper[73] the same method was adopted to analyse a "rugby-frame" model of an external bay in the bottom storey of a building.

There was significant research in Japan in the late 80s and early 90s into the behaviour of whole steel frames in fire. In two papers Hirota *et al*[103] and Nakamura *et al*[167] describe the results of 50 experiments on 2D, 2 storey and 3D, 3 storey steel frames. In each study a column or girder or column and girder were heated by an electric furnace. The results were compared with analytical theory derived in the 60s by Saito. The

theory is based on the stiffness method and takes into account the effects of restrained thermal expansion. They found that the structural behaviour was influenced more by a heated girder than a heated column. Nakamura *et al*[167] also conducted tests on a 6 storey full-scale steel frame. Again single columns were heated. Local buckling of a column influenced the whole structure.
A method of calculating the stress and deformation behaviour of a high rise steel structure exposed to a compartment fire is studied by Saito *et al.*[213] The structure is split into 3 sections. The first is the structure exposed to fire (local substructure), second is the adjacent substructure and the third comprises the remainder of the cool structure. The structure exposed directly to fire is analysed in the elasto-plastic range. The adjacent substructure is analysed in the elastic range. The calculation is for the restrained forces acting on the local substructure (fire compartment) as a result of restrained thermal expansion and the deflections of the adjacent substructure. The calculation method was carried out on 48 buildings.

Lane[138] studied column collapse in a series of pairs of laboratory-scale five storey, two bay, plane steel frames. The pairs of frames were designed to show restrained column collapse in one frame and column collapse due to hinges forming in the restraining beams in the other. The tests were conducted at ambient and at elevated temperature. At ambient the pairs of frames collapsed under the same load but by the two different collapse mechanisms showing the design was reliable at ambient. Elevated temperature tests involved heating various combinations of columns and/or beams. The various tests showed the importance of restrained thermal expansion. Although full restraint could not be achieved in any of the tests. The experiments were compared with an elastic frame analysis based on the slope-deflection method and the simple column design method in EC3. The thesis overall highlights the need for a more intelligent approach to fire resistance design moving away from single element behaviour in the fire resistance test. This work was conducted after the Broadgate fire and at the same time as the Cardington tests.

After the Broadgate Phase 8 fire and the Cardington frame tests there were benchmarks to test composite frame models. Research intensified because almost all the tests had unprotected steel beams but collapse was not seen. This research is discussed in Chapter 4.

2.8 Conclusion

A detailed definition of fire resistance has been given and methods of calculating fire resistance of structural elements has been outlined. The fire resistance test is inadequate in a number of respects not least because the fire exposure is not representative of real fires or that single elements are tested to failure and the results used in the design of whole frames.

The history and development of performance based design in fire safety has been described.

Factors influencing the behaviour of steel and composite structures in fire have been analysed. Each factor was discussed separately although in a real structure they would interact to define the behaviour. Early research into the behaviour of structures in fire centred around single elements of structure. Columns and beams have been analysed for many years. More recently research into membrane behaviour of slabs in fire has been investigated although membrane action at ambient has been researched since the 60s. Large deflections in slabs during a fire allow tensile membrane action to develop. This enhances the strength thus the fire resistance of the slab. Many computer codes have been developed to model steel frames in fire. Later the inclusion of slab models enabled composite frame response to be modelled. This was the state of the art before the Cardington frame fire tests.

Chapter 3

Thermal response of structures to real fires

3.1 Introduction

Reliable structural analysis for fire requires the atmosphere temperatures during the compartment fire and the subsequent heat transfer to the structural elements to be known with reasonable accuracy. The validity of the standard fire curve as a fire exposure has already been described in Chapter 2. The curve bears little resemblance to any natural fire curves and is not representative of many. Researchers tried to resolve this problem with the concept of t-equivalence. However the most accurate method for fire design is to model the actual expected fire curve given a compartment of specific dimensions, fire load and ventilation characteristics. In structural fire engineering reliable natural fire models can provide a sound basis for realistic heat transfer analysis and thus temperature histories of the connected structure. This chapter reviews methods of determining natural fires. The advantages and disadvantages of complex mathematical models, computer models and simple empirical and parametric relationships are considered.

Just as there are many approaches to calculating natural fire curves there are also many models (with varying degrees of sophistication) for calculating heat transfer. Methods developed and available to the designer will be reviewed. The basis of any heat transfer analysis are the input data. The heating regime is essential but the thermal characteristics of the material are also important. Published information on the thermal properties of steel and concrete will also be reviewed.

3.2 Natural Fire Curves

The standard fire curve describes the variation of the temperature of the fire gases within a standard furnace but bears little resemblance to any natural fire curve. It takes no account of the different thermal exposures which result from different compartment geometries, ventilation conditions, fire loads and compartment boundary materials.[120] With the t-equivalence approach the heating effect in a compartment is calculated based on real compartment fire behaviour and that heating is related back to the standard furnace test. However, the energy and mass balance equations for the fire compartment can be used to determine the actual thermal exposure and fire duration. This is known as the natural fire method. This method allows the combustion characteristics of the fire load, the ventilation effects and the thermal properties of the compartment enclosure to be considered. It is the most rigorous means of determining fire duration. This is not related in any way to the standard fire resistance test and represents the real fire duration, once flashover has occurred. Local fires can only be determined by natural fire curves.

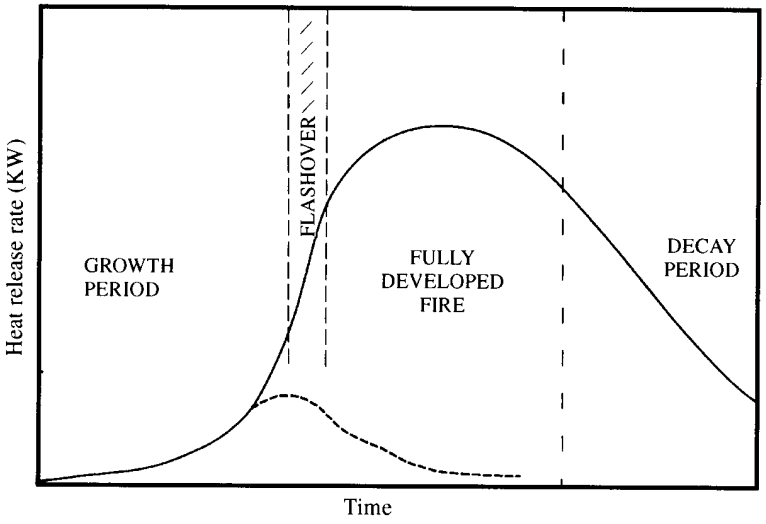

Figure 3.1: The course of a well-ventilated compartment fire[67]

3.3 Compartment Fires

The compartment fire process can be described by three distinct phases, the pre-flashover fire, the fully-developed fire (or post-flashover fire) and the cooling phase. There is a rapid transition stage called flashover between the pre-flashover and fully developed fire. This is shown in Figure 3.1[67] which illustrates the whole process in terms of heat released against time. While still small (during the growth phase) the compartment fire will behave as it would in the open. As it grows the confinement of the compartment begins to influence its behaviour (Figure 3.2). If there is sufficient fuel and ventilation the fire will develop to flashover and its maximum intensity, when all combustible surfaces are burning. If the fire is extinguished before flashover or if the fuel or ventilation is insufficient there will only be localised damage. Post-flashover the whole enclosure and its contents will be devastated. Structural damage and fire spread beyond the compartment of origin is also likely unless the fire is in a fire rated enclosure. Structural fire engineers are concerned with elements of structure subjected to high temperatures for a prolonged period of time. Post-flashover fires provide the worst case scenario. However localised heating of key elements of structure must also be considered.

Flashover is defined as the "relatively rapid transition between the primary fire which is essentially localised around the item first ignited, and the general conflagration when all surfaces within the compartment are burning.[66]" It is a transition period as a result

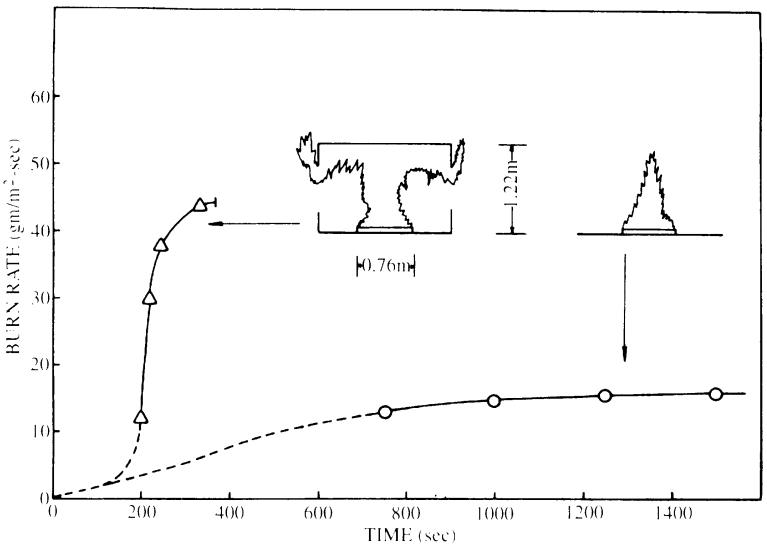

Figure 3.2: The effect of enclosure on the rate of burning of a slab of polymethylmethacrylate (Friedman 1975 as cited by Drysdale[67])

of several mechanisms each one contributing to the growth of the fire to a size at which *flashover* becomes inevitable. If there is insufficient fuel, ventilation or propensity for fire spread then a compartment fire may not achieve a rate of heat release sufficient for flashover to occur. The fire will remain small around the items first ignited (represented by the broken line in Figure 3.1).

Many researchers have investigated the *flashover* process. Several attempts have been made at predicting the onset of flashover associated with the compartment fire reaching a critical size in terms of its rate of heat release. The onset of flashover has been linked with radiant heat fluxes at floor level in excess of 20kW/m^2 and temperatures of 600^oC under the ceiling (for typical ceiling heights of 2.5-3m).[67,120,237] The onset of continuous flaming out through the openings is an indication that flashover has occurred. The rate of heat release and so the onset of flashover depends on the size of the compartment, the thermal characteristics of the boundaries, the amount and type of fuel and the available ventilation. Thomas[251] developed a criterion for flashover based on the size of the ventilation openings. Analysis of a large number of compartment fires showed that flashover would only occur if the heat release from the fire reached a certain level. Thomas's flashover criterion is described by Equation 3.1.

$$Q_{\text{fo}} = 0.0078A_t + 0.378A_v\sqrt{H_v} \tag{3.1}$$

where,
Q_{fo} =Critical value of heat release for flashover (MW)
A_t =the total internal surface area of the compartment (m^2)
$A_v\sqrt{H_v}$ =opening factor ($m^{5/2}$)

3.3.1 The Pre-flashover Fire

During the growth phase of any fire the flames form a buoyant plume above the items first ignited. In a compartment, if the fire grows to a size where the plume impinges upon the ceiling a ceiling jet will develop radiating outwards from the central axis of the plume. When the flow of hot gases meet the walls of the enclosure a hot smokey layer builds up under the ceiling, radiating heat back down towards the lower compartment and the fuel below. The development of the smoke layer is important for flashover. The radiative heat feedback from the dense, hot smoke results in the ignition of many more items in the room which in turn increases the level of hot gases near the ceiling. An understanding of pre-flashover fires is very important for life safety. The prime objective of the fire safety engineer is to prevent or delay flashover providing adequate time for the occupants of the building to escape. In multi-storey structures this is achieved by designing early detection and sprinkler systems. Activation times of sprinklers and detectors need to be calculated. Thus a design rate of fire growth has to be predicted based on the type, orientation and amount of fuel and available ventilation. Other calculations may include the depth and temperature of the smoke layer. These calculations are often performed by 2 zone computer models (discussed in Section 3.6.2.1). Hand calculations are described by Walton and Thomas.[251]

Several empirical correlations exist for the fire plume and ceiling jet (Equations 3.2 and 3.3). They estimate the temperature (T) or velocity (U) of the flames at a particular height (H) in the plume or radius (r) along a ceiling jet. They are used in design to predict the activation times of sprinklers and detectors. Alpert[3] developed the original correlations from large scale quasi-steady fire experiments although others exist.[36,165] In general the relationships are only applicable to large spaces with flat unobstructed ceilings.[36]

$$\Delta T = k_T \frac{Q^{2/3}}{H^{5/3}} \tag{3.2}$$

Growth rate	Typical scenario	α (kW/s^2)
Slow	Densely packed paper products	0.00293
Medium	Traditional mattress or armchair	0.01172
Fast	PU mattress (horizontal) or PE pallets stacked 1m high	0.0469
Ultra fast	High rack storage, PE rigid foam stacked 5m high	0.1876

Table 3.1: Parameters used for t^2 fires (Evans 1995 as cited by Drysdale 1998)[67]

$$U = k_u \left(\frac{Q}{H}\right)^{1/3} \tag{3.3}$$

3.3.1.1 t^2 Fires

Power law fires are commonly used to define fire growth rates. t^2 fires are the most common (Equation 3.4, Figure 3.3 and Table 3.1). They describe the growth rate of a design fire such that the rate of heat release is directly proportional to the time squared. DD240 gives the growth parameters listed in Table 3.2 and guidance on the building occupancy associated with each growth rate. For instance an office is associated with a medium growth rate and industrial storage an ultrafast growth rate.[115] The t^2 relationship fits well with measured test data but only after ignition is well established. A time t_0 is specified as the period between ignition and initial flaming.[120]

Temperature and velocity relationships have also been devised for power law fires. Heskestad *et al* (as cited by Mowrer[165]) developed non-dimensional correlations for temperature rise and velocity using t^2 fire data.

$$\dot{Q} = \alpha(t - t_0)^2 \tag{3.4}$$

where,
$\dot{Q}$ =heat release rate (kW)
α =fire growth constant see Table 3.1
t_0 = delay between ignition and initial flaming (s)
t= time (s)

Fire Growth rate	Fire growth parameter α (kW/s^2)	Time for Q_g=1000kW (s)
Slow	0.0029	600
Medium	0.012	300
Fast	0.047	150
Ultra fast	0.188	75

Table 3.2: Fire growth parameters and time to reach the rate of heat release Q_g =1000kW for t^2 fires in DD 240[115]

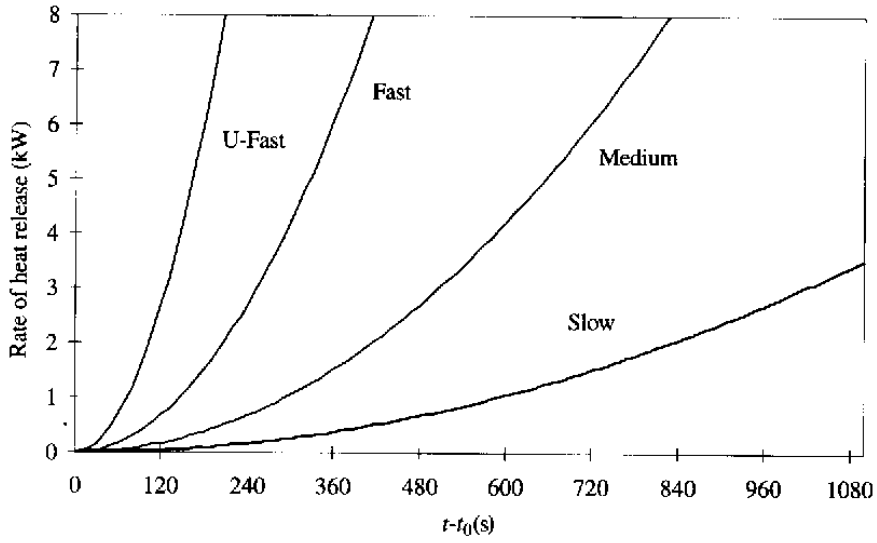

Figure 3.3: t^2 fire growth according to Equation 3.4[67]

3.3.1.2 Heat Release data

Burning rates are often given as mass loss rates ($\dot{m}$) in kg/s or Rates of Heat Release (RHR) , $\dot{q}$ in kW. Mass loss data is less useful. The advent of oxygen consumption calorimetry provided an accurate method of measuring RHR in the open. RHR data from tests on pool fires, wood cribs and in furniture calorimeters provide some information on growth rates. Items tested include upholstered chairs, mattresses, pillows and televisions.[10]

3.3.1.3 Calculating Rate of Heat Release (RHR) to Eurocode 1

Eurocode 1[75] presents a method for calculating the maximum, constant rate of burning in a fully developed fire. The rate of burning is equated to a RHR by multiplying the rate of burning by the effective heat of combustion of wood.

$$R = \min\left[\frac{L}{\tau_F}, (0.18(1 - e^{-0.036\eta})A_w\sqrt{h_a W/D})\right] \tag{3.5}$$

where,

R =rate of burning (kg of wood/s)
L =total fire load (kg of wood)
τ_F =free burning fire duration (assumed to be 1200s)
A_w =sum of window area on all walls (m^2)
h_a =weighted average of window heights on all walls (m)
W =width of wall containing window/s (m)
D =depth of fire compartment (m)
$\eta = \frac{A_T}{(A_w\sqrt{h})}$ ($m^{-1/2}$)
A_T=area of all surfaces minus the area of windows (m^2)

The two terms in Equation 3.5 indicate whether the fire is ventilation controlled (burning is controlled by the rate of air in-flow) or fuel controlled (dependent on the surface area and burning characteristics of the fuel). The first term determines the RHR under fuel bed controlled conditions and the second term under ventilation controlled conditions. Neither growth or decay RHR are calculated. The free burning fire duration τ_F is always assumed to equal 1200 seconds.

3.3.2 The Post-flashover fire

After flashover high temperatures are sustained until the fuel is almost completely consumed. The compartment is engulfed with hot gases and products of combustion. RHR is at its highest. External flaming through the windows will also occur as the unburnt pyrolysis products in the fuel rich atmosphere flow out of the window and burn in the presence of air. Intensive research into compartment fires has centred around the post-flashover fire because the fire is most severe in this period but also because the compartment can be treated as one volume of uniform temperature and composition, simplifying modelling. Many compartment fire models only consider this stage.[122,195] Growth and decay are not easily treated theoretically.[97]

3.3.3 The decay period

The rate of decay of a compartment fire depends on the shape and material of the fuel, the size of the openings and the thermal properties of the wall linings. It is not easy to predict. Large openings allow heat to escape very quickly. Walls of low thermal inertia store less heat so decay rates are more rapid. However walls of low thermal inertia also have low thermal conductivity which insulates the compartment, retaining heat if there is any further burning.[43]

The decay period is assumed to start after the average temperature has dropped by 80% of the maximum value.[67] In design if considerable knowledge of the contents is known and a limited amount of fuel can burn then measured RHR data may provide information to the designer on decay rates.[120]

3.4 The burning regime: Ventilation vs. Fuel controlled fires

The influence of ventilation on compartment fires was first realised by Kawagoe in the late 50s.[121] Kawagoe was one of the first researchers to try and understand compartment fires using scaled experimental models. By studying the burning of wood cribs in enclosures he found that the rate of burning was independent of the amount of fuel but highly dependent on the ventilation particularly the height of the opening. He correlated the rate of mass loss R (kg/s) with the area (A_w) and height (H) of the opening semi-empirically (Equation 3.6).

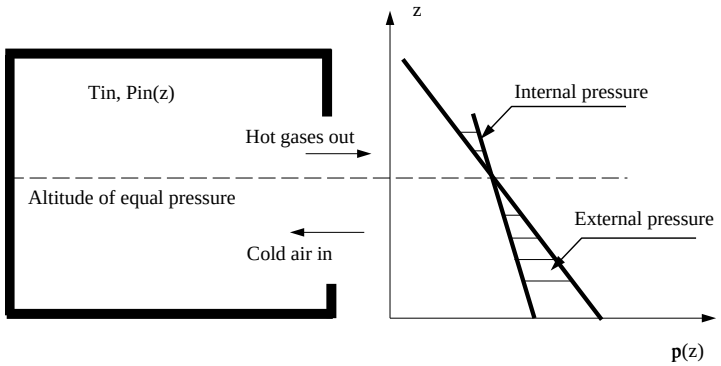

Figure 3.4: Pressure profile over the opening in a compartment resulting in cold air flowing in and hot gases flowing out

$$R = 0.092 A_w H^{1/2} \tag{3.6}$$

The relationship fits very well with the data analysed. However, Thomas *et al*[241] have shown that the relationship breaks down at high ventilation rates. Kawagoe's experiments were all ventilation controlled i.e the rate of burning equals the rate of ingress of air.

The empirical relationship can also be derived theoretically by analysing the flow of gases in and out of the compartment. Drysdale[67] describes this. Several assumptions are made,

- The gases are uniform throughout the compartment
- There is no net flow by buoyancy in the compartment
- Hot gases leave the compartment through the opening above a neutral plane and cold air enters below the neutral plane (See Figure 3.4)
- The flow in and out of the opening is driven by buoyancy
- There is no interaction between the in flowing and out flowing gases

The horizontal flow out of the compartment above the neutral plane can be calculated using Bernoulli's theorem. Thus the mass flow rates in and out can also be quantified. Assuming a general chemical equation and correlating this with the ratio of mass flowrates in and out of the compartment, Equation 3.6 for the burning rate can be derived.

The empirical and theoretical equations are exactly the same. Drysdale regards the emergence of exactly the same constant of proportionality as fortuitous when all the assumptions are considered but the emergence of the combined term, $A_w\sqrt{H}$, as significant.[67] The combination of $A_w\sqrt{H}$ is called the *ventilation factor*.

3.4.1 Opening factor

The opening factor is defined as the ventilation factor divided by the total surface area A_t of the enclosure (Equation 3.7). Magnusson and Thelandersson[155] were the first to use the opening factor. It was derived to reduce the number of independent variables when describing different compartment fire curves. Magnusson and Thelandersson divided the fire load and the ventilation factor by the total enclosure surface area (A_t) thus three variables affecting the development of compartment fires were reduced to two.[120] Both the ventilation factor and the opening factor are a method of expressing the available ventilation to a compartment and are highly dependent on the height of the opening, H.

$$OF = \frac{A_w\sqrt{H}}{A_t} \tag{3.7}$$

In rooms where there are more than one opening a weighted value of $A\sqrt{H}$ is calculated based on Figure 3.5.

3.4.2 Differentiating between fuel and ventilation controlled fires

Differentiating between a fuel controlled and a ventilation controlled fire is an important part of predicting the behaviour of a compartment fire. In the ventilation controlled regime there is insufficient air in the room thus the burning rate is dependent on the air supply. Duration of the fire is dependent on the total fire load.[239] A fuel-controlled fire exists if the supply of air is large and the burning rate depends on the surface area and the burning characteristics of the fuel.

Harmathy[96,97] developed a semi-empirical equation based on experimental data to define whether a fire is fuel or ventilation controlled.

Bullen and Thomas[45] showed that beyond a certain value of $A_w\sqrt{H}$ the rate of burning became independent of the ventilation. Shown by a rapid drop in burning rate in Figure

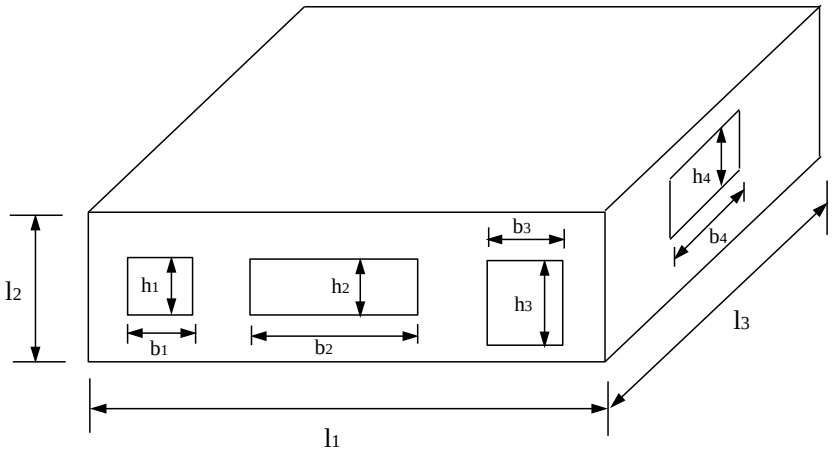

$A_w = A_1 + A_2 + ... A_4 = b_1h_1 + b_2h_2 + ... + b_4h_4$

$H = (A_1h_1 + A_2h_2 + ... + A_4h_4)/A$

$A_t = 2(l_1l_2 + l_1l_3 + l_2l_3)$

Figure 3.5: Determination of a weighted value of $A_w\sqrt{H}$ for enclosures with more than one opening[195]

3.6. Figure 3.6 also shows that as the area of the fuel surface increases the transition between the two regimes occurs at larger values of $A_w\sqrt{H}$.

Most fires in buildings are ventilation controlled, although in modern buildings with large windows and small fuel surface areas, fuel controlled burning may result. The duration of the fire in both regimes depends on the absolute fire load available.[239]

3.4.3 Fuel controlled fire

Calculating the rate of burning in a fuel controlled fire is not simple. However it is known that fuel controlled fires are normally less severe[241] (See Figure 3.7). This can be attributed to the excess air cooling the fire. Harmathy[97] suggested designing buildings to ensure fuel-controlled fires because they are less severe thus reducing the need for fire protection. This is not practical because it is almost impossible to restrict the fuel load over the lifetime of a building. Moreover, designing for a ventilation controlled fire is conservative.

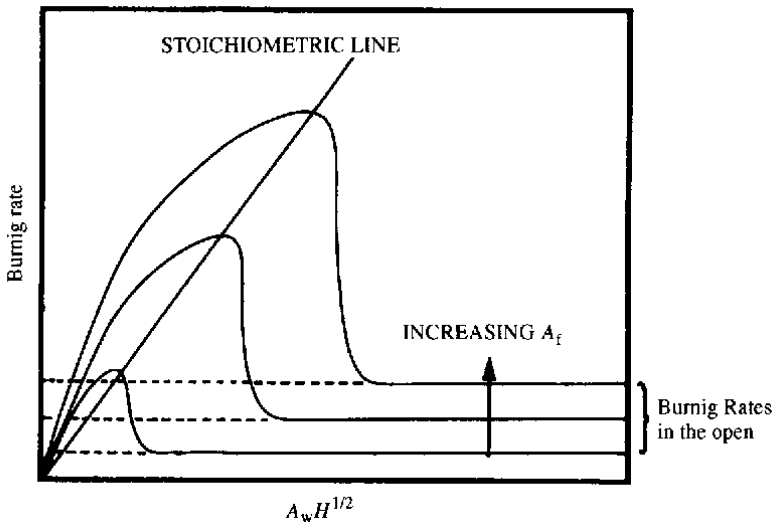

Figure 3.6: Schematic diagram showing the variation of mass burning rate with ventilation parameter $A_w H^{1/2}$ and fuel bed area A_f[45]

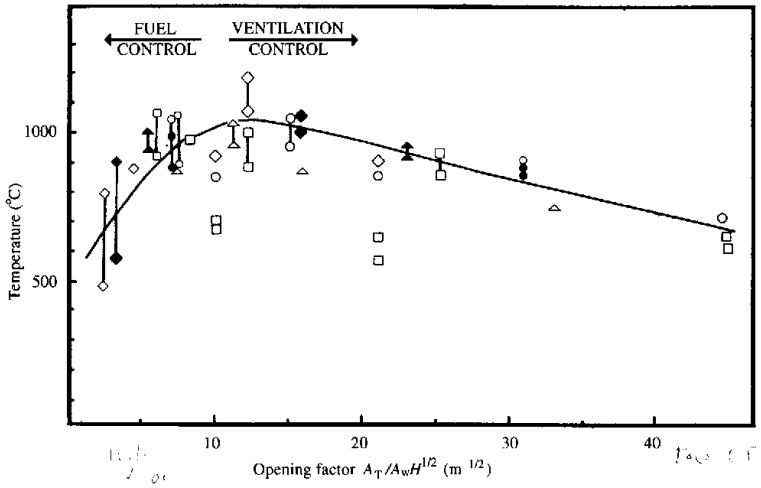

Figure 3.7: Average compartment temperatures during the steady burning period for wood crib fires in model enclosures as a function of the 'opening factor'. Symbols refer to different compartment shapes.[241]

3.5 CIB compartment fire experiments

In the 1960s eight countries collaborated under the CIB (Conseil Internationale du Bâtiment) in a major experimental programme to improve understanding of the behaviour of fully developed compartment fires. Over 400 experiments were conducted in small-scale compartments 0.5m, 1.0m and 1.5m high of various shapes, areas of ventilation and fuel load (in the form of wood cribs). The effect of wind was also treated. Thomas and Heselden[241] report on this work. Several conclusions were reached. They found that $\dot{m}/A_w H^{1/2}$ is not a constant as Kawagoe suggests in Equation 3.6 but depends on compartment shape and A_t (in this case the surface area of the enclosure minus the area of the openings and the floor area). The intensity of radiation correlated with the rate of burning except for small ventilation openings and the maximum temperature in a given compartment fire occurred just inside the ventilation controlled regime. Law used these data in determining a t-equivalence model for fire resistance[139] as discussed in Chapter 2. Law related the CIB fires to the fire resistance time in a standard furnace in terms of failure of a protected steel column at 400^oC and 550^oC. Law[139] wanted to understand the effect on structural temperatures of the rate of burning. By reducing the rate of burning, the fire duration increased but the atmosphere temperatures decreased thus the effect on structural temperature may have been small. The main factor affecting t-equivalence was $\frac{L}{\sqrt{A_w A_T}}$. She found that scale and stick thickness of the wood cribs had negligible effects on t-equivalence. Closer stick spacing gave longer values of t-equivalence because of increased fire duration.
Thomas and Law[242] also used the CIB data to study the behaviour of flames outside ventilation openings. This work formed the basis for the SCI design guide *Fire Safety of Bare External Structural Steel*.[141]

3.6 Compartment fire modelling

The development of a temperature-time curve to be able to describe the temperature history of a compartment fire has been researched for decades. The earliest significant work was carried out by Kawagoe and Sekine[122] in the 60s.

3.6.1 Model types

Compartment fire models can be split into three categories,

1. Mathematical models

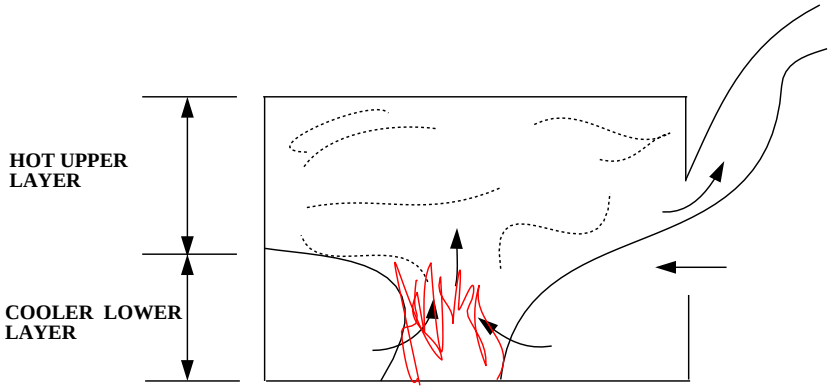

Figure 3.8: 2 zones in a compartment fire model

- Deterministic
- Probabilistic

2. Empirical or parametric models
3. Computer models
   - Zone
   - Field

3.6.1.1 Zone modelling

Zone modelling is a simple representation of the compartment fire process and the basis for almost all compartment fire modelling so is discussed first. The approach emerged in the 1970s.[200] During the pre-flashover fire the compartment can be described by 2 zones and the fire plume. There is a hot upper volume representing the smoke layer under the ceiling and a cooler lower volume as a result of thermal stratification due to buoyancy (See Figure 3.8) near the floor. Each layer is of relatively uniform temperature and composition. Post-flashover, turbulent gases completely fill the compartment and the enclosure can be represented by one well-mixed volume of uniform temperature and gas concentration.[237]

3.6.1.2 Mathematical models

Mathematical fire models are separated into two types, deterministic and probabilistic. Probabilistic models rely on probability data. They describe a building fire as a series of events.[120] The transition from one event to the next defines the development of the

Authors	Years	Type
Kawagoe and Sekine[122]	1958-1963	Transient
Odeen[186]	1963-1970	Transient
Magnusson and Thelandersson[155, 156]	1970-1974	Transient
Tsuchiya and Sumi[243]	1971	Transient
Harmathy[96, 97]	1972	Steady
Thomas and Nilsson[236]	1973	Steady
Bullen and Thomas[45]	1977-1980	Transient
Bohm[37]	1977-1982	Transient
Babrauskas and Williamson[13, 14]	1978-1981	Transient
Babrauskas and Wickstrom[12]	1979	Transient
Schneider and Haksever as cited by[11]	1980	Transient
Babrauskas[9]	1981	Steady
Nakaya and Akita[168]	1983	Transient

Table 3.3: List of major deterministic post-flashover models[11]

fire. Each transition has a probability of occurrence associated with it. However due to the lack of reliable probability data these models are very restricted.

Deterministic models are based on scientific algorithms of the important physical phenomena in a compartment fire. Deterministic models encompass simple one zone models where the whole compartment is one volume to field models where the compartment may be split into hundreds of thousands of 3D elements. A numerical solution for the equations of conservation of mass, species, momentum and energy is required for each volume.

Many deterministic models of post-flashover fires have been developed starting in the early 60s.[122] All post-flashover models are based on the assumption that the gas temperature in the compartment is uniform. The major models are listed in Table 3.3 adapted from Janssens.[11] Most of the models described as transient i.e varying with time, are *quasi-steady* because transients are normally ignored in the gas phase.[11]

Computer zone models are based on deterministic modelling and are developing all the time. These will be reviewed in Section 3.6.2.1. OZone,[50] a one zone compartment fire model is the most recent model of its type in Europe and is currently being developed in Belgium at the University of Liege.

In terms of the basic concepts all the models listed in Table 3.3 are very similar. To be able to determine the temperature course of a fire it is necessary to know at each moment in time the rate at which heat is produced and the rate at which heat is lost to exposed materials and surroundings i.e The Heat Balance for the enclosure.

Kawagoe and Sekine[122] developed the earliest Heat Balance model. The compartment was rectangular with one opening and walls of single thickness and material. The model only allowed temperatures in the post-flashover regime to be estimated. Independently Odeen[186] derived the same relationship for opening factor as Kawagoe. He also derived a method to estimate the cooling phase. Magnusson and Thelandersson[155] modelled the post-flashover fire and the cooling phase. They considered ventilation controlled fires as a conservative approach using Kawagoe's relationship (Equation 3.6) for the post-flashover phase and developed a new relationship for the cooling phase because Equation 3.6 is not valid during cooling. Tsuchiya and Sumi[243] considered the composition and geometrical shape of fuel in their heat balance calculation.

3.6.1.3 Heat balance equation for an enclosure (Pettersson et al, 1976[195])

Pettersson and co workers published a detailed description of their work in defining T-t curves for compartment fires in the Swedish design guide.[195] The curves are often referred to as Pettersson curves but the model was developed by Magnusson and Thelandersson.[155] Pettersson used their curves to check steel temperatures for design. The solution of the heat balance allows the T-t history in the post-flashover and the decay phase of the fire to be defined. The full heat balance relationship is described by Equation 3.8 and illustrated in Figure 3.9.

$$\dot{q}_C = \dot{q}_L + \dot{q}_W + \dot{q}_R + \dot{q}_B \tag{3.8}$$

where,
$\dot{q}_C$ =the heat released during combustion (W),
$\dot{q}_L$ =the heat removed due to the replacement of the hot gases by cold air (W),
$\dot{q}_W$ =the heat dissipated to and through the wall, ceiling and floor structures (W),
$\dot{q}_R$ =the heat dissipated by radiation through openings in the fire compartment (W)
$\dot{q}_B$ =the quantity of heat stored in the gas volume in the fire compartment per unit time (W).

A series of assumptions were made in order to solve the heat balance,[195]

1. combustion is complete and takes place exclusively inside the fire compartment
2. at every instant the temperature is uniformly distributed within the entire fire compartment

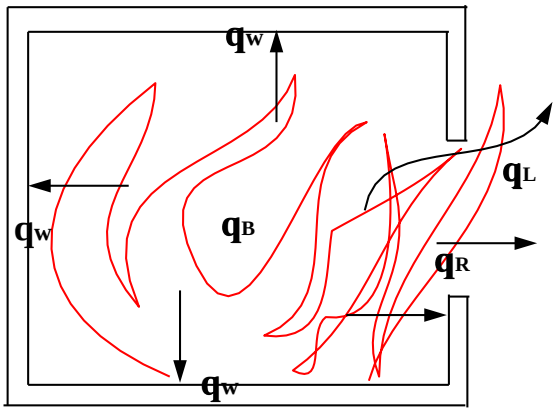

Figure 3.9: Illustration of the heat balance in a fire compartment (Pettersson, 1976[195])

3. at every instant the surface coefficient of heat transfer for the internal enclosing surface of the fire compartment is uniformly distributed

4. The heat flow to and through the enclosing structures is unidimensional and with the exception of any door and window openings, is uniformly distributed for each type of enclosing structure

Pettersson[195] describes the treatment of each term in Equation 3.8 separately.

3.6.1.3.1 $\dot{q}_C$ The term $\dot{q}_C$ representing the heat released during combustion can be written as

$$\dot{q}_C = 0.09 A_w H^{1/2} \Delta H_c \tag{3.9}$$

where,
ΔH_c= Heat of combustion of wood (J/kg)

The fire is assumed to be ventilation controlled throughout the post-flashover phase with the mean rate of combustion described by Equation 3.9 (Kawagoe's relationship, Equation 3.6). If the fire is in the fuel-controlled regime Equation 3.6 will overestimate the rate of burning.[67] $\dot{q}_C$ is assumed to remain constant immediately after flashover until all the fuel has been consumed.

3.6.1.3.2 $\dot{q}_L$ Heat losses by convective flow through the openings ($\dot{q}_L$) are governed by the fact that there is a linear pressure distribution in the vertical direction over the

opening (Figure 3.4 illustrated this) and a neutral layer where there is no difference between the static pressure outside and inside. Assuming a neutral layer and the whole fire compartment is at the same temperature (the compartment gases are well mixed) the quantity of gas flowing out and the quantity of cool air flowing inwards can be calculated using Bernouilli's theorem.

3.6.1.3.3 $\dot{q}_W$ To calculate the dissipation of heat through the walls ($\dot{q}_W$) the equations of conduction have to be solved numerically considering the changing thermal properties of the wall material with increasing temperature. The enclosing boundary is divided into n layers each of thickness Δx. A series of first order difference equations describing conduction can then be solved for each layer, over time intervals Δt.

3.6.1.3.4 $\dot{q}_R$ The quantity of heat which is lost by radiation through the openings in the fire compartment can be calculated using the Stefan-Boltzman Law.

$$\dot{q}_R = A_W \epsilon_F \sigma (T_g^4 - T_0^4) \tag{3.10}$$

where,
A_W =the total area of the openings (m^2)
ϵ_F =effective emissivity of the gases within the compartment
σ =Stefan-Boltzmann constant (W/m^2K^4)
T_g =is the gas temperature inside the fire compartment (K)
T_0 =is the outside ambient temperature (K)

3.6.1.3.5 $\dot{q}_B$ The final component of Equation (3.8) is the term $\dot{q}_B$ which can safely be ignored because the quantity of heat stored in the gas volume is insignificant in comparison with the other heat quantities.[195]

3.6.1.3.6 Solution to the heat balance Equation 3.11 is the solution to the heat balance for any post-flashover, ventilation controlled fire. The Equation is solved by numerical integration. Graphical (Figure 3.10) and tabulated values of the solution are available.[195]

$$T_g = \frac{\dot{q}_C + 0.09 c_p A_w H^{1/2} T_0 + (A_T - A_w)\left[\frac{1}{\gamma_i} + \frac{\Delta x}{2k}\right]^{-1}(T_g - T_1) - \dot{q}_R}{0.09 c_p A_w H^{1/2} + (A_T - A_w)\left[\frac{1}{\gamma_i} + \frac{\Delta x}{2k}\right]^{-1}} \tag{3.11}$$

where

$$\gamma_i = \frac{\epsilon_r \sigma}{T_g - T_i}(T_g^4 - T_i^4) + 0.023 \tag{3.12}$$

Figure 3.11 shows the T-t histories of many compartment fire tests with one of the theoretical curves. Good agreement is found.

The effects of different boundary materials on the fire temperature can also be included. Compartments are split into 8 categories (A-H). Compartment type A is the base case and has thermal properties corresponding to average values for brick, concrete and lightweight concrete. A conversion factor is applied to the base case for compartments with different boundary materials. Figure 3.12 illustrates this. Compartment type C is made from highly insulating lightweight concrete thus resulting in the highest temperatures. The lowest temperatures are in compartment type F of 80% uninsulated steel sheeting and 20% concrete.

Magnusson and Thelandersson's heat balance approach is based on ventilation controlled conditions. If the fire load is low and there are large openings in the compartment fuel controlled conditions may persist. Determining the rate of combustion is difficult in these fires because the combustion process is determined by the method of storage and the degree of distribution of the fuel (fuel surface area). In fire compartments with large openings the assumption that gas flow out and airflow in only has a horizontal velocity component (as in Figure 3.4) weakens. The horizontal pressure difference is reduced and the flow of hot gases out and air in reduces. Pettersson[195] reports on work by Magnusson and Thelandersson on increasing the openings in fire compartments. They calculated natural fire curves based on 60% of the rate of combustion in the ventilation controlled regime. They also assumed a decrease in the gas interchange through the opening. When q_L was equal to 80% of the value under ventilation controlled conditions the agreement with experimental data was good. If only 60% of the fuel is burning in fuel controlled conditions this implies the compartment is supplied with excess cool air, cooling the fire and making it less severe.

Slightly later Babrauskas and Williamson[15] developed a theoretical model which enables

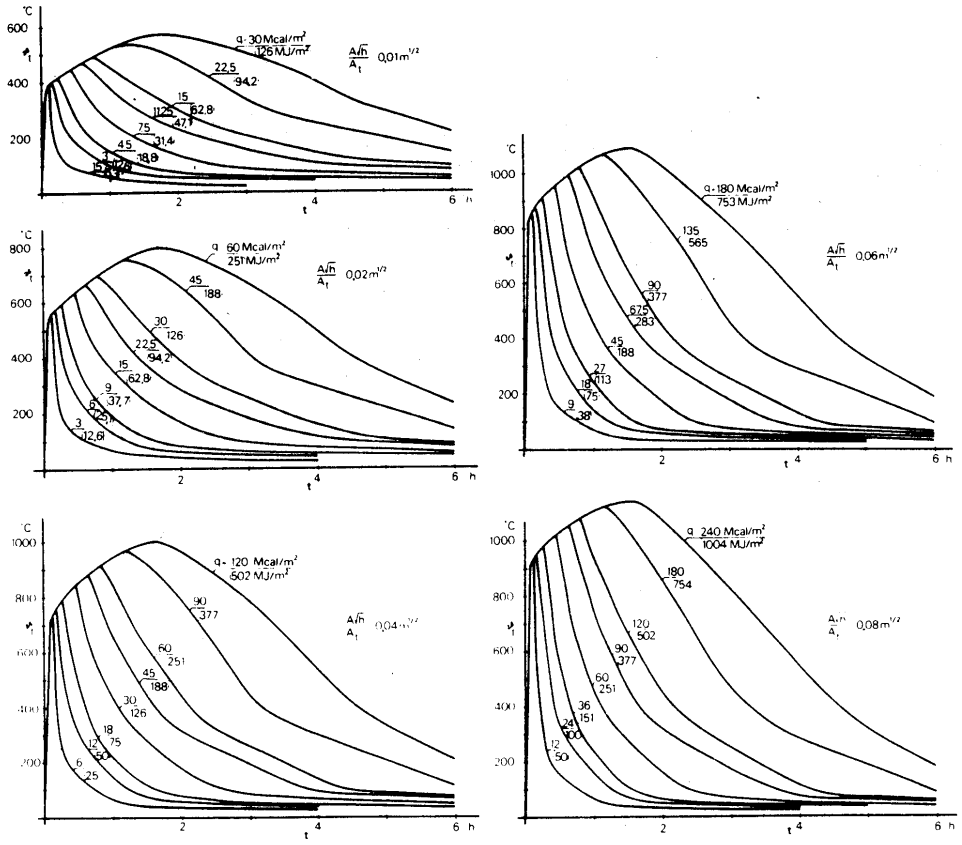

Figure 3.10: Theoretical temperature-time curves for compartment fires with different fire load densities and opening factors (Pettersson, 1976[195])

the calculation to assume fuel or ventilation controlled conditions at every stage in the analysis. This is more sophisticated than Pettersson's model which assumes ventilation controlled conditions throughout the fully developed fire. Their model requires details of the fuel nature and distribution. Babrauskas[9] also developed a hand calculation "*a closed form approximation*" to calculate approximate post-flashover temperatures. The approach can be used for any fire providing the fuel release rate is known or can be estimated.

3.6.1.4 Empirical/Characteristic temperature curves

In parallel to the mathematical modelling many research groups have analysed experimental data and arrived at simple empirical relationships. In Figure 3.13[145] curve (a) illustrates a fire temperature time curve derived theoretically for a certain building while curve (b) is for the same scenario but it is assumed that the rate of burning remains constant until all combustible materials are consumed then the fire temperature

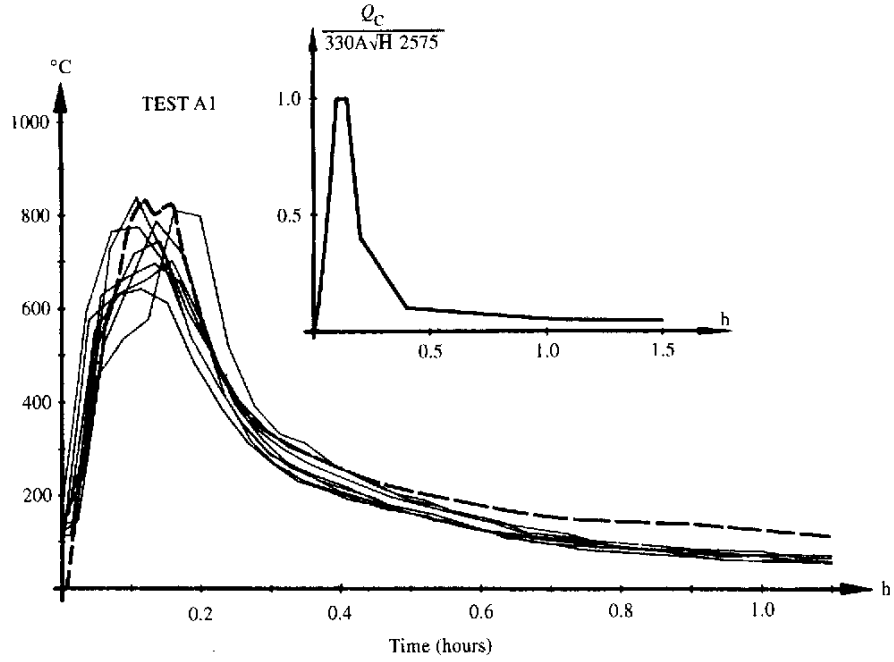

Figure 3.11: Gas temperature-time curves in full-scale fire. Solid lines represent experimental data for a fire load density of 96MJ/m^2 and an opening factor, $\frac{A_w\sqrt{H}}{A_t} = 0.068m^{1/2}$. The dashed line is the calculated temperature-time curve using the measured rate of burning (Pettersson, 1976[195])

drops linearly to room temperature. Curve (b) is slightly different to (a) but it is much easier to define. Lie[146] suggests that the lengthy computation involved in calculating the temperature-time curve from the heat balance equation is excessive especially when you consider the assumptions and possible causes of error in the compartment fire model. A characteristic T-t curve *"whose effect, with reasonable probability will not be exceeded during the use of the building"* is simpler.

Lie[146] analysed two compartments with very different boundary materials (Table 3.4). Using Kawagoe's heat balance approach he calculated curves in the post-flashover phase for several opening factors. The curves could be reasonably described by an exponential function in terms of opening factor, time and a constant taking into account the properties of the boundaries (see Equation 3.13). Similar exponential relationships are used for the EC1[75] parametric T-t curve and in the Swedish Design Codes referenced by Pettersson *et al.*[195] Lie also derived an expression for the decay period based on observations made by other researchers.[96,97,121,155] In general the longer the post-flashover phase the lower the rate of decrease in temperature in the decay phase.

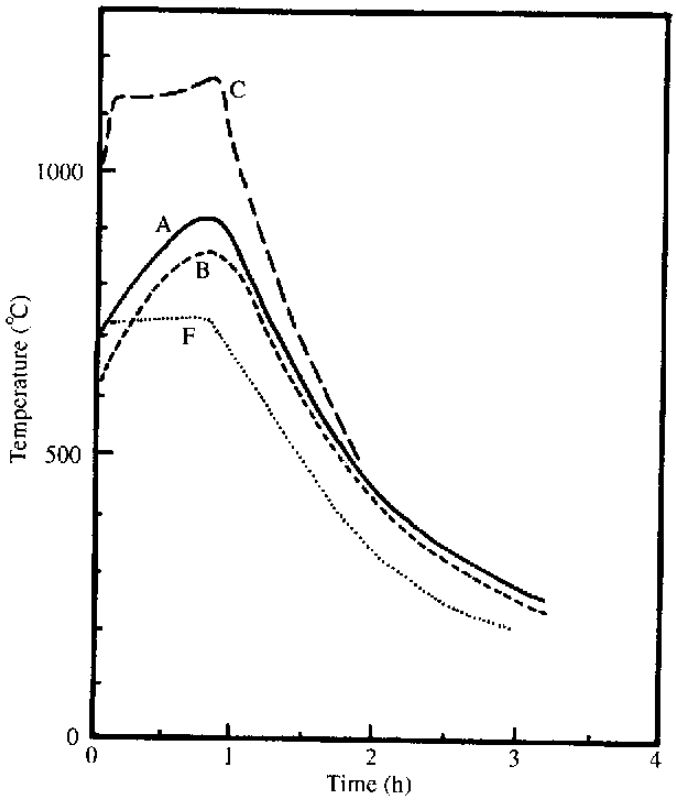

Figure 3.12: Theoretical temperature-time curves for fully developed fires in compartments of different boundaries: A, materials with thermal properties corresponding to the average values for concrete, brick and lightweight concrete; B, concrete (500kg/m^3); F, 80% uninsulated steel sheeting, 20% concrete. In all cases the fire load and ventilation factor were consistent(Pettersson, 1976[195])

$$T = 250(10O)^{\frac{0.1}{O^{0.3}}} e^{-O2t} \left[3(1 - e^{-0.6t}) - (1 - e^{-3t}) + 4(1 - e^{-12t})\right] + C\left(\frac{600}{O}\right)^{0.5} \tag{3.13}$$

where,

T =the fire temperature (^{o}C)

t =time (h)

O =opening factor (m$^{1/2}$)

C =a constant taking into account the properties of the boundary material (C=0 for heavy materials and C=1 for light materials)

The Equation is valid for

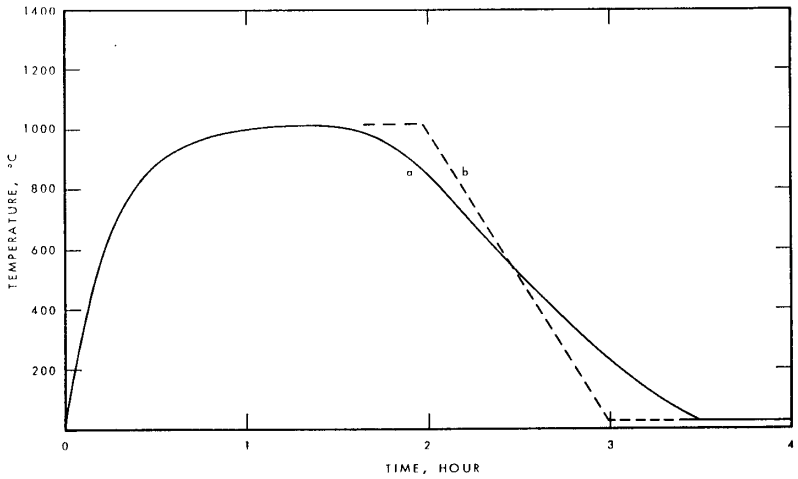

Figure 3.13: A comparison of Temperature-time curves (Lie, 1974[145])

Thermal properties	Heavy material	Light material
	($\rho \geq 1600 kg/m^2$)	($\rho < 1600 kg/m^2$)
K(W/mK)	1.16	0.58
ρc (J/m^3K)	2150×10^3	1075×10^3
Thickness of the bounding material (m)	0.15	0.15

Table 3.4: The thermal properties of compartment boundary materials

$$t \leq \frac{0.08}{O} + 1 \tag{3.14}$$

A comparison of the curves calculated using Equation 3.13 and the heat balance method can be seen in Figures 3.14 and 3.15. These show that temperature-time curves can be developed for fires with mainly cellulosic fuels that reasonably describe the curves derived from solving the heat balance. The study also highlights the importance of including the properties of the boundary materials even if it is only in a simple manner.

3.6.1.5 Parametric T-t curves

Parametric temperature-time curves[75, 154, 195] are relatively simple relationships relating fire load, ventilation and properties of the wall lining materials. They assume the temperature within the compartment is uniform thus only predict post-flashover fires. They are easy to use and can be solved using a spreadsheet.

3.6.1.5.1 The Parametric T-t curve in EC1[75] The parametric T-t curve in EC1[75] is designed to predict the T-t history of post-flashover compartment fires for

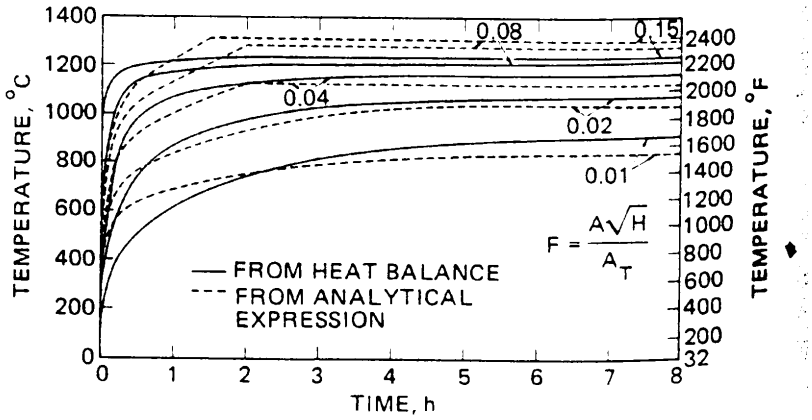

Figure 3.14: Comparison between T-t curves obtained by solving a heat balance and those described by an analytical expression for ventilation-controlled fires in enclosures bounded by dominantly heavy materials ($\rho \geq 1600 kg/m^3$). (Lie, 1995[146])

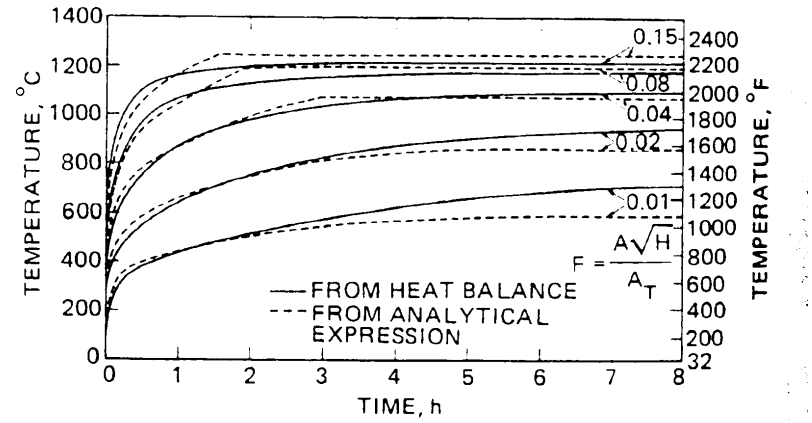

Figure 3.15: Comparison between T-t curves obtained by solving a heat balance and those described by an analytical expression for ventilation-controlled fires in enclosures bounded by dominantly light materials ($\rho \leq 1600 kg/m^3$) (Lie,1995[146])

any combination of fuel load, ventilation and wall lining materials. The origins of the curve are unknown but it seems to be based on the standardised curve in the Swedish building regulations. Equation 3.15 describes the parametric T-t curve as described in the proposed Eurocode. The parametric curve is valid for compartments up to a floor area of $100m^2$ and compartment height of 4.5m.

$$\theta_g = 1325(1 - 0.324e^{-0.2t^*} - 0.204e^{-1.7t^*} - 0.472e^{-19t^*}) \tag{3.15}$$

where,
θ_g = temperature in the fire compartment (^oC)
$t^* = t\Gamma$ (h)
t =time (h)

$$\Gamma = \frac{\left[\frac{O}{b}\right]^2}{\left[\frac{0.04}{1160}\right]^2} \tag{3.16}$$

$b = \sqrt{\rho ck}$ and $1000 \leq b \leq 2000$
O =opening factor:$\frac{A_v\sqrt{h}}{A_t}$ and $0.02 \leq O \leq 0.20$ ($m^{1/2}$)
A_v =Area of vertical openings (m^2)
A_t =Area of enclosure (walls, ceiling, floor and openings) (m^2)
ρ =density of the boundary of the enclosure (kg/m^3)
c =specific heat of the boundary of the enclosure (J/kgK)
k =thermal conductivity of the boundary of the enclosure (W/mK)

Franssen[84] has shown that when $O = 0.04$ and $b = 1160$ i.e. $\Gamma = 1$ and $t^* = t$ the parametric curve is almost identical to the ISO standard fire curve for the duration of the post-flashover phase.

The duration of the fire is determined by the fire load in Equation 3.17.

$$t_d^* = 0.13 \times 10^{-3} q_{t,d} \Gamma / O \tag{3.17}$$

where,

$$q_{\mathrm{t,d}} = q_{\mathrm{f,d}} \frac{A_f}{A_t} \tag{3.18}$$

and

$$50 \leq q_{\mathrm{t,d}} \leq 1000$$

$q_{\mathrm{t,d}}$ =design value of the fire load density (MJ/m^2) related to the surface area A_t (m^2) of the enclosure

$q_{\mathrm{f,d}}$ =design value of the fire load density related to the surface area of the floor (MJ/m^2).

The temperature-time curves in the cooling phase are given by:

$$\theta_g = \theta_{\max} - 625(t^* - t_d^*) \tag{3.19}$$

$$\theta_g = \theta_{\max} - 250(3 - t_d^*)(t^* - t_d^*) \tag{3.20}$$

$$\theta_g = \theta_{\max} - 250(t^* - t_d^*) \tag{3.21}$$

where,

$\theta_{\max}$ =maximum temperature in the heating phase (^{o}C) for $t^* = t_d^*$

The standard fire curve of the Swedish design codes is described by Equation 3.22. The obvious difference between the two curves is the introduction of the thermal properties (thermal inertia) of the compartment boundaries in Equation 3.15. The cooling phase in the Swedish building regulations is a linear reduction in temperature (10^oC/min) whereas the cooling phase in the new parametric T-t curve is given by Equations 3.19, 3.20 and 3.21. Equations 3.19-3.21 are dependent on the design fire load related to the surface area of the floor and the compartment.

$$\theta_t - \theta_0 = 1325 - 430e^{-0.2t} - 270e^{-1.7t} - 625e^{-19t} \tag{3.22}$$

where,
θ_t =gas temperature at time, t (^{o}C)
θ_0 =gas temperature at time, t=0 (^{o}C)
t =time (h).

3.6.1.5.2 Comparison with compartment fire test data As part of the research conducted for this thesis, Edinburgh University in collaboration with British Steel through the DETR PiT project "*Development of the UK and European design codes-Natural fires and the response of structural steel*[150]" investigated the validity of the parametric equations given in Eurocode 1. The parametric curve was compared directly with measured compartment fire test temperatures. The data were gathered from experiments carried out in America, France and UK. However the experiments carried out by Kirby and Wainman[131] in Britain were the most comprehensive. The tests were originally conducted to record unloaded, unprotected steel temperatures but atmosphere temperatures were also taken. The report can be found in Appendix A. Conclusions of the report included:

1. Parametric temperature-time curves overestimate the temperatures achieved in wood fires although they are "better" for higher fire load densities and low opening factors.

2. There is good correlation for wood/plastic fires although there is a possibility that the parametric T-t curve will underestimate the real fire.

Feasey and Buchanan[43] have shown that the temperatures from the Eurocode formula are often too low and recommend increasing the reference value of b from 1160 to 1900 W^2s/m^4K^2.

Franssen[84] analysed the validity of the curve against data from 48 fire tests. A comparison of the air temperature was made for each test. Also a comparison of the maximum temperatures calculated in 2 hypothetical steel sections (one protected and one unprotected). The agreement is poor for the air and unprotected steel. Better agreement is found with the protected steel. Improvements are suggested based on modifying the consideration of multiple wall layers. In EC1 the wall model is not realistic. For example it assumes a 2 layer wall with a thick layer of concrete on the outside and light insulation on the inside is the same as a 2 layer wall with thick concrete on the inside and insulation on the outside. The material on the inside nearest the fire has the greatest influence on the fire development. Franssen also makes suggestions to improve the predicted temperatures in fuel-controlled fires. The parametric model is based on

post-flashover ventilation controlled fires so this is not valid.
Pettersson (as cited by Karlsson[120]) compared the Eurocode parametric curves with Magnusson and Thelandersson's model for an opening factor of $0.04m^{1/2}$ and found very poor agreement with the cooling phase. .

3.6.2 Compartment fire models for computers

Fire models enable us to make an assessment of the fire risk, to assess the likely severity and extent of the fire, to estimate the influence of suppression systems, model evacuation of people (egress models), improve research and understanding of fire development and in some situations resolve litigation issues. In general fire models can compute temperatures (atmosphere and surface), flow rates of gas through openings, heat fluxes, smoke movement, toxic gas production, activation times for sprinklers and detectors.

3.6.2.1 Zone models for computers

Computer based compartment fire models can be classified as zone models or field models. A zone model is normally made up of a small number of (2-5) zones. However, in post-flashover models a one zone model is acceptable. These assume the whole compartment is at a uniform temperature and gas concentration.
Some of the more complex zone models allow radiation calculations between the upper layer and room objects. They may also allow multiple fire plumes and multiple compartment analysis with mass exchange between each compartment. Zone models use numerical methods to evaluate the temperature of the gases during the development of a compartment fire.

A number of authors have reviewed computer based fire models for design.[86,202,250] Friedman has carried out an extensive survey of fire and smoke models 31 of which were zone models. Most of the models are very similar. Some go further by calculating the consequences of the fire for instance HAZARD1, one of the many models developed at the Building and Fire Research Laboratory (bfrl) at the National Institute for Standards and Technology (NIST).

The bfrl at NIST formally the Centre for Fire Research at the National Bureau of Standards have produced a series of compartment fire zone models.[172] FPETool is an early model, it is made up of a set of routines including FIREFORM which is a collection of individual calculations such as Thomas's correlation for flashover. FIREFORM also estimates smoke temperatures, detector or sprinkler response and a very simplistic

model for egress time. MAKEFIRE is another routine of FPETool used to generate RHR data. FIRE SIMULATOR is the 2 zone model within FPETool and can generate the effects of a pre-flashover and a post-flashover fire including the amount of CO, CO_2 and O_2 in the smoke, the temperature-time history of the environment and a prediction of the heat transfer through the walls and ceiling.

CFAST, also developed at NIST is a zone model capable of predicting fire spread to many compartments (the most recent version allows up to 15 compartments). Output includes RHR data, temperatures of the upper and lower layers and smoke toxicity. The radiant heat feedback from the upper layer to objects in the room below is also estimated allowing ignition calculations.

FASTLite[198] is the most recent hybrid of FPETool introduced in 1996. It builds upon the routine FIREFORM in FPETool and a simplified version of CFAST (modelling 3 rooms only).

The programs ASET and FIRST reviewed by Walton[250] were also developed at the National Bureau of Standards. ASET (available safe egress time) calculates the temperature and position of the hot smoke layer in a single room with closed windows. ASET-B is a compact version of ASET for personal computers. FIRST is a descendant of the HARVARD[163] programs and is able to predict the development of a fire (ignition of up to three targets) and the resulting conditions.

One of the most recent computer zone models, OZone is being developed at the University of Liege, Belgium. OZone[50] was originally developed as part of a European Coal and Steel Community project entitled the Natural Fire Safety Concept.[224] It created considerable interest in Europe and it was suggested that it could replace the parametric temperature-time relationship in Eurocode 1. As part of the DETR PIT project "*Development of the UK and European design codes-Natural fires and the response of structural steel*[150]" the first version of OZone was evaluated in detail by Lamont *et al.*[135] The full report can be found in Appendix B. OZone was tested against experimental data from fire tests conducted by CORUS Research, Development and Technology, Swinden Technology Centre.[131,132] In general the correlation between the measured and predicted results was found to be poor. Moreover using the software proved to be confusing and it was possible to set the model running using input files that were clearly nonsensical. While some of these aspects could be addressed by improving the software there were concerns about the theoretical background to the model. One ma-

jor concern was the use of a *"design"* rate of Heat Release (RHR) curve based on a t^2 growth phase, a constant release phase and a linear descending branch after 70% of the fire load has been consumed. A one zone model can only be used to predict post-flashover temperatures and should not contain a growth phase. Further developments in the software are being made which could solve the problems associated with using the code. However dissimilarities between measured and predicted temperatures may still exist.

3.6.2.1.1 Limitations of zone models The zones within the models assume uniform temperatures therefore localised heating/cooling effects near the fire plume or near openings are not accounted for. Flow regimes within the space are not predicted and plume interactions are not modelled because the zone model assumes only one plume in the space.

3.6.2.2 CFD models[86,120,196,233]

Field models are fire adaptations of Computational fluid dynamics (CFD) computer programs. CFD computer codes solve the Navier Stokes Equations for fluid flow. The domain is divided into 3-dimensional cells or control volumes and the equations describing the conservation of heat, mass, momentum and species are solved for each cell. This type of model is computationally demanding, time consuming and difficult to use. Zone models can model the fire compartment with very few zones whereas a typical field model will need thousands of cells to model the same space. Codes include CFX, a general purpose CFD code developed by AEA Technology Engineering Software, JASMINE a fire specific CFD program developed at Fire Research Station, SOFIE and SMARTFIRE also both fire specific, developed at the University of Cranfield and the University of Greenwich respectively.

NIST have recently developed a new CFD type model called Fire Dynamics Simulator (FDS).[188] FDS simulates smoke and or air flow movement caused by fire. The results are viewed in Smokeview. The equations solved in FDS differ from those in CFD codes. Most CFD models to date adopt the k-ϵ turbulence model which is a time-averaged approximation to the conservation equations of fluid dynamics. This smoothes the results of the model and hinders modelling of the evolution of large eddy structures in fire plumes and local transient events. FDS uses an approximate form of the Navier-Stokes equations to be used with low Mach number applications suitable for the low speed motion of gas driven by chemical heat release and buoyancy forces. FDS can

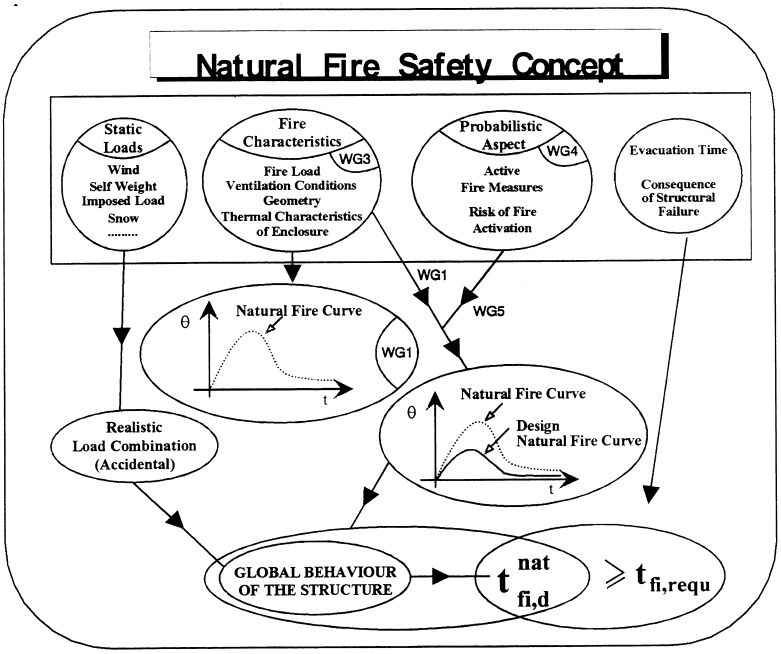

Figure 3.16: Scope of the Natural Fire Safety Concept Research[224]

conduct Large Eddy Simulations (LES) to model building fires for instance or Direct Numerical Simulations (DNS) which could model small-scale combustion experiments.

3.6.3 The Natural Fire Safety Concept[224]

The research project "Competitive steel buildings through natural fire safety concept" was undertaken by 11 European partners co-ordinated by PROFIL-ARBED-Research, starting in June 1994 and running until December 1998. The scope of the research is illustrated in Figure 3.16.

There were 5 working groups (WG) each contributing to a different aspect of the project.

- WG1- Natural fire models
- WG2- Equivalent ISO time methods
- WG3- Fire characteristics for use in a natural fire design of building structures
- WG4- Statistics
- WG5- Methodology to deduce from the probability data the "Design Natural Fire Curve"

Working group 1 lead by Franssen at the University of Liege analysed the parametric temperature-time curve in the Eurocode and reviewed existing CFD and zone models for computers. Their review of the parametric T-t curve has already been reported in Section 3.6.1.5.2. A database of natural fire tests was also collated from experiments conducted in France, UK, Netherlands and Australia. The main outcome of WG 1 was the one zone compartment fire model OZone.[50]

Working group 2 reviewed t-equivalence relationships from the literature and design codes. These methods were analysed at an early stage in the project but are not relevant to the Natural Fire Safety Concept because they relate to the standard T-t curve. This was acknowledged by the authors.

Working group 3 was responsible for supplying ready to use data and guidance on the input data for natural fire design for those with no expert knowledge of compartment fire dynamics. General information is given on various types of compartment fire model. Methods of calculating fire load and RHR are reviewed. RHR from t^2 fires and experimental data are discussed. The calculation method in EC1 for determining the maximum RHR is also reviewed. A proposed RHR curve for the NFSC is given. The curve includes a t^2 growth phase, a steady state phase equal to that given in EC1 and a linear decay phase after 70% of the fire load has been consumed. This is illustrated in Figure 3.17. This approach forms the basis of the OZone model. The OZone model is based on post-flashover fire theory where it is assumed that the whole compartment is always at uniform temperature. These assumptions are not true pre-flashover and invalidates the growth phase used in the OZone model. The flashover criteria in Figure 3.17 is also not present in the OZone model. The shortcomings of OZone are discussed later in this chapter and in Appendix B.

Working groups 4 and 5 consisted of the same team members. Statistics from real fires in Switzerland, France, Finland and the UK over the period 1986-1995 were gathered into a single database covering 40,000 losses. Probabilities deduced from the database formed the basis for a risk analysis of fire start considering the influence of active fire fighting measures (fire fighters and sprinkler systems) and occupancy type. This information was quantified in terms of factors on the fire load. The factors consider compartment size, building type and active fire protection measures. The characteristic fire load is multiplied by all factors to obtain the design fire load. The design fire load is then input to OZone to calculate the natural fire curve.

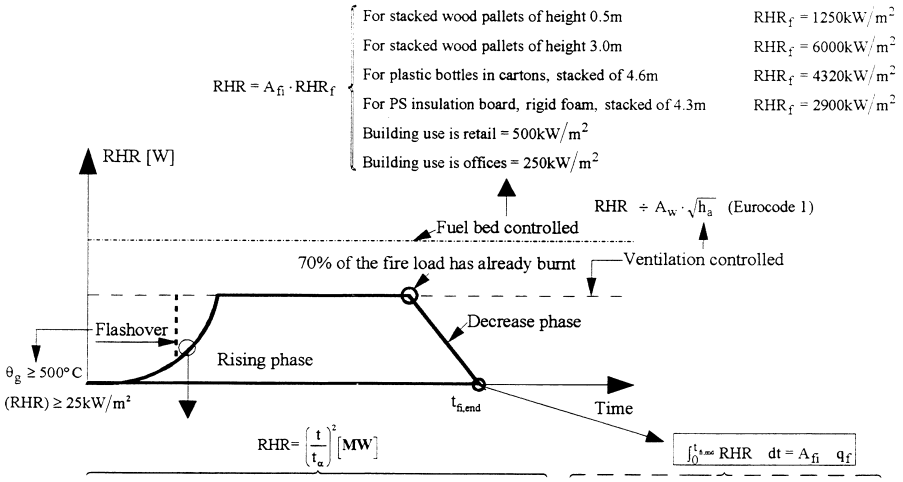

Fire growth rate	Typical equivalent materials	t_α: Time [s] for RHR = 1 MW	Occupancy
Slow	no uniform fire load	600	Picture gallery
Medium	Cotton/polyester sprung mattress	300	Dwelling Hotel reception Office Hotel bedroom
Fast	Full mail bags, plastic foam, stacked timber pallets	150	Shop
Ultra-fast	Methyl alcohol pool fire, faster burning upholstered furniture	75	Chemical Plant

OCCUPANCY	Fire load (80 % fractile) $q_{k,f}$ [MJ/m^2]
Dwelling	948
Hospital	280
Hotel (room)	377
Library	1824
Office (standard)	511
School	347
Shopping centre	730
Theatre (cinema)	365
Transport (public space)	122

Figure 3.17: Scope of the Natural Fire Safety Concept Research[224]

The NFSC project has gathered together a considerable amount of information available to designers to calculate natural fire curves. The statistical analysis was significant. However OZone needs to be fully validated as a reliable design tool. This is discussed in greater detail in later sections.

3.7 Other factors influencing the rate of heat release in a compartment fire

3.7.1 Vent location

The opening factor is applicable to vertical openings but horizontal openings may also exist. Openings in the ceiling result in hot gases escaping through the roof while cool air enters from the windows on the wall.[239] Smoke extraction techniques use this principle to remove hot products of combustion from the smoke layer thus reducing the likelihood of flashover. Pettersson *et al*[195] address openings in the roof with a modified ventilation parameter. $\frac{A\sqrt{h}}{A_T}$ is multiplied by a correction coefficient f_k determined from a nomogram in the Swedish design guide. The nomogram assumes flow through the horizontal openings is not dominant. An upper bound is imposed on the model above

which the flow conditions are no longer relevant. This upper bound is achieved when the neutral axis depth coincides with the top of the vertical opening. i.e all combustion gases are vented through the horizontal opening.

Cross ventilation resulting from windows present in opposite walls causes a high intake of air and cooling effects. Law[141] reports that in compartments without cross ventilation air is entrained into a compartment through the same window as the flames emerge. The flames occupy the upper two thirds and the air enters through the lower third. However, in through draft conditions with windows on the opposite sides of the compartment the flames will emerge from the whole area of the window.[141]

If the window area is large in relation to the cross-sectional area of the compartment the pressure differences between the room and ambient air may be quite small. Air may be entrained into the compartment by the turbulence of the flames.[96,239] Compartment fire models calculate air intake on the basis of a pressure difference between inside and outside the compartment and cannot predict air being entrained by turbulent flames.

3.7.2 Fuel load

The fire load for an enclosure is a measure of the total energy released by combustion of all combustible materials in the enclosure.[120] Traditionally the fuel load has been expressed in equivalent kilograms of wood. The characteristics of fire loads in buildings evolve as the nature of building contents change. A modern office may contain lots of plastics, yet many compartment fire models are based on data from experiments with wood crib fires bringing their validity into question.

The results of several extensive fuel load surveys are detailed in the CIB guide.[238] Eurocode 1 gives five classes of fire load ranging from 250-2000MJ/m^2 floor area. Buchanan[43] states that for safe fire design the fire load should have less than a 10% probability of being exceeded in the 50 year life of the building.

3.7.2.1 Fuel shape

Smaller fuel packages with increased surface area produce higher maximum temperatures but large fuel packages result in longer decay periods.[243] Decay periods vary with the size of the fuel rather than opening factor or wall material properties.

Tall fuel loads and combustible wall linings tend to decrease the time to flashover. Flame spread over vertical surfaces is much faster than over horizontal fuel beds. Flames hugging the vertical surface raise the temperature of the fuel in front of the flame front thus fire spread is more rapid. Flames and hot products of combustion collect under the ceiling much more rapidly leading to early flashover.[67]

3.7.3 Compartment dimensions

Most models for compartment fires are tested on regular shaped compartments with small openings. Buchanan[43] states that compartments with floor areas up to $6m \times 6m$ can be modelled with confidence. This seems conservative although researchers have always recognised that the validity of compartment models to large, long or tall compartments is questionable. Law recognised the need for an understanding of deep compartments in the 70s.[139]

3.7.3.1 Long compartments

The most comprehensive analysis of compartment fires in long enclosures has been conducted by Thomas and Bennetts.[235] They conducted an experimental program designed to investigate the enclosure shape and opening width and their effect on the burning rate. Fire tests were conducted on enclosures 1500mm by 600mm by 300mm high with vents of several widths. The main conclusions were that the fuel mass loss rates of fires in long and wide enclosures differ markedly if the width of the ventilation opening is less than the full width of the enclosure.

Kirby *et al*[132] conducted a series of 6 experiments on long compartments. The ventilation was provided by a window at one end of the compartment (short elevation). Tests were conducted with each of the four ventilation levels, 1, 1/2, 1/4 and 1/8 of the end wall. The wood cribs were situated in lines over the depth of the compartment. The cribs furthest from the ventilation were lit first. The fire moved towards the ventilation igniting each line of cribs. At the same time the cribs at the back of the compartment ceased burning. The cribs near the vents burned until there was no fuel left then the fire moved back over the cribs again towards the rear of the compartment. Figure 3.18 shows the recorded atmosphere temperatures in test 6 of the British Steel long compartment tests. This pattern of behaviour was observed in all six tests. It was also observed by Thomas and Bennetts.[235] The behaviour of compartment fires in long compartments is still not well understood however it is clear the behaviour is quite different from our understanding of "regular" compartment fire dynamics.

The importance of the compartment fire temperatures are their impact on structural elements. Deep compartments may exhibit different temperatures over the depth of

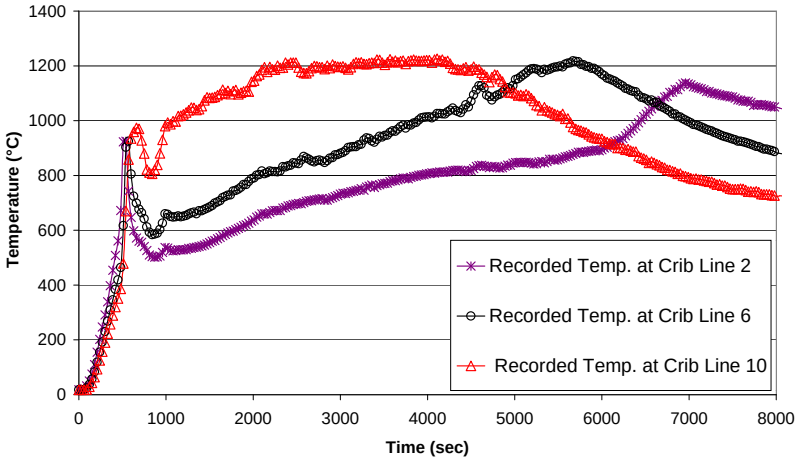

Figure 3.18: Plot of the recorded atmosphere temperatures in British Steel long compartment test 6

the compartment but is this more detrimental to the structure than a uniform temperature? Kirby *et al*[132] included protected steel sections in their long compartments. Six 254x146x43UBs and six 203x203x52UCs were fixed to the insulated roof slabs at each measuring station over the depth of the compartment. Maximum temperature differences of 100^{o}C were recorded. However in Test 6 (atmosphere temperatures shown in Figure 3.18) the maximum difference between any two recorded steel temperatures was only 50^{o}C. Test 6 had the smallest ventilation at only 1/8 of the end wall. Overall the greatest steel temperatures were recorded midway back through the compartment when the ventilation equalled the area of one end wall. For ventilation of 1/2 and 1/4 of one end wall the greatest steel were recorded at gridline 10 near the vent. Unprotected steel is very fast to react to temperature changes in the atmosphere therefore greater differences may have existed if the steel was unprotected. Research into temperature gradients along steel beams has shown that there is increased load carrying capacity when the steel beams are cooler near the connections.[195] However Bailey[20] has shown that extra deflections and forces are induced in cooling beams during a spreading fire than when the whole structure is heated to the one temperature. This is probably a much more severe situation than the cooling and heating in the deep compartment tests. Further research is needed into the effect of deep compartment fires on steel temperatures.

3.7.4 Thermal inertia of the compartment boundaries, $k\rho c$

The inclusion of $k\rho c$ in the parametric T-t curve is one of the major differences between EC1 and the Swedish building regulations. It has long been recognised that the

combination of the thermal properties k, ρ and c where, k is the thermal conductivity, ρ is the density and c the thermal capacity, of a material has an important role to play in the time constant of heating materials and the growth of fires.[195, 240] Thomas and Bullen[240] compared the time to flashover for a compartment with two different lining materials. For high values of kρc where the compartment boundaries (walls, ceiling, floor) have been treated as a semi-infinite slab kρc affects the time to flashover as $(k\rho c)^{\frac{1}{2}}$ or a lesser power. At low values of kρc the flashover times become dependent on other physical processes notably the convective flow.[240]

3.8 Heat Transfer

Once the rate of heat release or temperature history of a compartment fire is known the temperature of the structure can be calculated by heat transfer analysis.

Heat energy travels from areas of high temperature to areas of lower temperature by three means, conduction, convection and radiation.

Conduction occurs in solids and involves hot energetic molecules within the solid passing energy to adjacent less energetic molecules. These molecules in turn become hot and pass energy to further adjacent molecules. This process continues along the solid. The greater the thermal conductivity of a material the faster heat will dissipate through it.

Convection occurs in fluids. As a region of hot fluid increases in temperature it expands and decreases in density. The less dense hot fluid rises and colder fluid take its place resulting in a convection current. Convective flow is important in the early stages of a fire.

Thermal radiation is a type of electro-magnetic radiation and requires no substance to transfer heat. Radiation in all parts of the electro-magnetic spectrum can be absorbed transmitted or reflected at a surface. It becomes the dominant mode of heat transfer in the later stages of a fire and determines the growth and spread of fires in a compartment.[67]

3.8.1 The Heat Transfer Equations

3.8.1.1 Conduction

Fourier's Law states that heat is transferred in proportion to the temperature gradient and can be expressed by Equation 3.23.

$$\dot{q}''_x = -k\frac{\Delta T}{\Delta x} \tag{3.23}$$

where ΔT is the temperature difference over a distance Δx, k is thermal conductivity (W/mK) and $\dot{q}''_x$ is the heat flux or amount of heat penetrating a unit area of the surface per unit time. The negative sign indicates the heat flow is from higher temperatures to lower temperatures. Equation 3.24 describes Fourier's Law in differential form.

$$\dot{q}''_x = -k\frac{dT}{dx} \tag{3.24}$$

Equations 3.23 and 3.24 describe steady state conduction and do not consider the heat required to change the temperature of material being heated or cooled.[43] Equations for non-steady state conduction also exist.

3.8.1.2 Convection

Newton recognised that convective heat transfer is a function of the temperature difference between the solid (T_s) and the temperature of the surrounding fluid or gas (T_f). The empirical relationship by Newton is described by Equation 3.25,

$$\dot{q}''_x = h(T_s - T_f) \tag{3.25}$$

h (W/m^2K) is the convective heat transfer coefficient. Convection heat transfer also depends on the characteristics of the system, the geometry of the solid and the properties of the fluid including the flow parameters. Typical values of h for a fire exposed structural element are in the range 20-25 W/m^2K.[43,67,126,161,195] In the compartment fire hot gases are transferring heat to a solid structural element therefore convection can be treated as a boundary condition. However in porous materials convection will also occur inside the pores of the material.

3.8.1.3 Radiation

Thermal radiation is heat transferred by electro-magnetic waves. An ideal thermal radiator (a black body) will emit energy at a rate proportional to the 4th power at the absolute temperature of the body (Equation 3.26),

$$\dot{q}_x'' = \epsilon\sigma T^4 \tag{3.26}$$

where σ = Stefan Boltzman Constant ($5.669 \times 10^{-8} W/m^2K^4$) and ϵ= emissivity. $\epsilon = 1$ for a blackbody and $\epsilon < 1$ for all other surfaces. Thermal radiation is the main mode of heat transfer in compartments from flames and smoke to the fuel and the surrounding structure. It also a major factor in fire spread from building to building.

The intensity of the radiation falling on a surface remote from the emitter can be found by using the appropriate "configuration factor" (ϕ) which takes into account the geometrical relationship between the emitter and the receiver,

$$\dot{q}_x'' = \phi\epsilon\sigma T^4 \tag{3.27}$$

where,
ϵ =resultant emissivity of the emitting and receiving surfaces.

3.8.2 Solving the heat transfer Equations

3.8.2.1 Analytically

Only the simplest heat transfer calculations can be solved analytically, e.g. steady state analyses where the geometry and boundary conditions are well known. Lumped heat capacity methods are used where the material can be assumed to be at constant temperature. A semi-infinite slab approximation is assumed where the heat transfer is essentially 1D and the heat is absorbed before reaching the unexposed side.
Simple lumped mass, heat transfer expressions are used in design to calculate the temperatures of protected and unprotected steel under quasi-steady conditions. These can be solved using an iterative spreadsheet calculation.[67,161,195]

3.8.2.2 Numerically

The most powerful tools for calculating heat transfer are numerical methods using finite difference or finite element formulations. These provide solutions for transient heat transfer problems where the materials' thermal properties are complex. A typical example is heat transfer to concrete where the effects of moisture make modelling difficult. Finite element models specific to fire design include CEFICOSS,[226] FIRES-T3,[201] TASEF[232] and THELMA (developed at BRE). General finite element codes will also calculate heat transfer. For instance the commercial code ABAQUS.[102] A criticism of computer codes is that they are often non-user friendly.

A reliable heat transfer model relies on accurate input data including material properties and boundary conditions. The finite element model must have adequate mesh and time discretisation. It must also be validated by testing against benchmarks of known solution or by comparison with experimental data. Wickstrom[259] highlights three issues to be considered when using a computer code,

1. validity of the calculation method
2. accuracy of the material properties
3. accuracy and reliability of the computer code.

Point one is important because effects such as spalling, phase change and water migration in concrete cannot be determined by a model based on heat transfer alone. Coupled heat and stress analyses needs to be conducted for spalling. Most building materials are not stable through the range 20^oC to 700^oC. They undergo reactions accompanied by transformations in their micro-structure and changes in their properties. Phase changes need to be incorporated to model water evaporation and chemical transformations. Accurate material properties are very important although they are not always readily available especially at high temperatures.[194]

3.9 Thermal properties of materials

Mechanical, physical, chemical and thermal properties of materials can all be affected by fire.[4,82,98,100,101,125,144,148,158,161,169,199,228] The mechanical properties of steel and concrete and how they alter under heating were discussed in Chapter 2 in the context of the structural behaviour. In this context we are concerned with the thermal properties (conductivity, k and specific heat, c) and how they change with increasing

temperature. Material density and moisture content (free and chemically bound) with changing temperature are also important.

Heat transmission solely by conduction can only occur in poreless non-transparent solids. In most building materials the mechanism of heat transfer is by conduction, convection and radiation. However if the pore size is less than 5mm the contribution of the pores to convective heat transmission is negligible.[101] Radiation becomes the dominant mode of heat transfer at high temperatures in fire because of the T^4 dependence.

Thermal properties influence the rate of heat transfer into the construction. The thermal inertia $k\rho c$, of the material affects the surface temperature in the early stages of fire exposure. Thermal inertia is normally associated with low density insulating materials and has been primarily considered in the design of the exposed surface linings of furnaces but may have some relevance for aerated lightweight concretes.[158] Under transient heating the thermal conductivity of the material and the specific heat capacity are related in terms of the thermal diffusivity in m^2/h (Equation 3.28),

$$\alpha = \frac{k}{\rho c} \tag{3.28}$$

k = thermal conductivity (J/sm^{o}C)
ρ = density (kg/m^3)
c = specific heat (J/kg^{o}C)

The thermal diffusivity is a measure of the rate of heat transport from the exposed surface to the inside and of the temperature rise at a depth in the material. The larger the diffusivity the larger the temperature rise.[144]

The properties of materials at high temperatures are difficult to measure experimentally and are not readily available. During the mid forties the Building Research Station provided some data on the high temperature properties of concrete and steel as part of the notes on repair to damaged buildings.[158] However most of the work on material properties at high temperatures has been carried out since the mid-fifties.[158]

Due to the increasing application of numerical methods in fire engineering the International Organisation on Testing and Research on Materials and Structures (RILEM) set up a committee in 1979, under the chairmanship of Malhotra,[158] to consolidate data

on material properties at high temperatures. One of the major outcomes of this committee was to identify the differences in data caused by different testing techniques. A definite distinction has to be made between the studies conducted under steady state conditions and those under transient conditions. Data on the properties of building materials are found throughout the literature. One of the most extensive references is by Harmathy[100] where the properties of steel, concrete and other building materials are reviewed.

3.9.1 Steel

Steel is an exceptionally good conductor thus reaches uniform temperatures when exposed to fire. At ambient steel has a thermal conductivity, k of 54W/mK which decreases to half this value by 800^{o}C. Beyond 800^{o}C it remains constant (Figure 3.19(a)). The specific heat of steel at 20^{o}C is about 450J/kgK increasing to 700J/kgK at around 600^{o}C. At 730^{o}C steel undergoes a chemical transformation from ferrite-pearlite to austentite. This is associated with a huge increase in specific heat, shown in Figure 3.19(b). The specific heat of steel seems to be independent of the grade of the steel.[158] The density of steel is approximately 7850kg/m^3 decreasing slightly with increasing temperature.

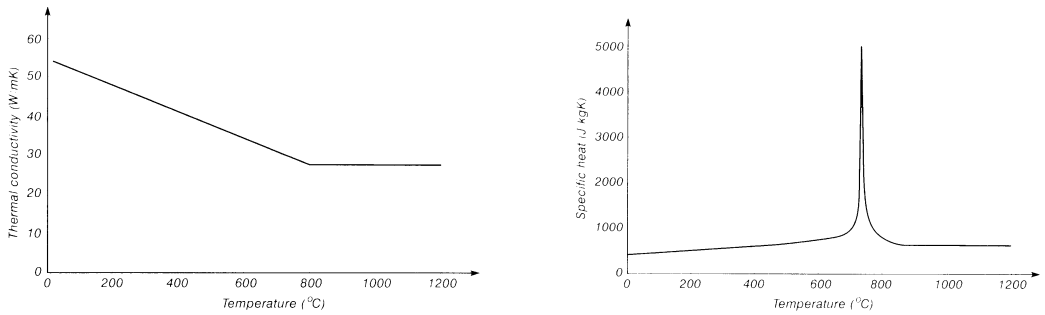

(a) Conductivity

(b) Specific heat

Figure 3.19: Thermal properties of steel[43]

3.9.2 Concrete

Concrete covers a vast array of different materials all of which are formed by the hydration of Portland cement. The hydrated cement paste accounts for only about 24-43 volume percent of the materials present so that the aggregate used has a significant effect on the properties.[101] Three common aggregates are siliceous aggregates (gravel, granite and flint), calcareous aggregates (limestones) and lightweight aggregates made

from sintered fuel ash.[169] Concrete has excellent fire resisting properties. Compared with steel it has a very low conductivity, thus low thermal diffusivity. A major disadvantage of concrete is spalling, the loss of surface material as a result of high temperatures (Chapter 2).

Lightweight concretes (LWC) have the best thermal properties with half the thermal conductivity of normal weight concrete (NWC). Typical densities of LWC range 1200-1900kg/m^3 but they can be as low as 1000kg/m^3. NWC is in the range 2000-2900kg/m^3. Densities show only a slight temperature dependence, mostly due to moisture losses. Limestone concretes are an exception. They show a significant drop in density at about 800^{o}C due to the decomposition of the aggregate[228] (Figure 3.20).

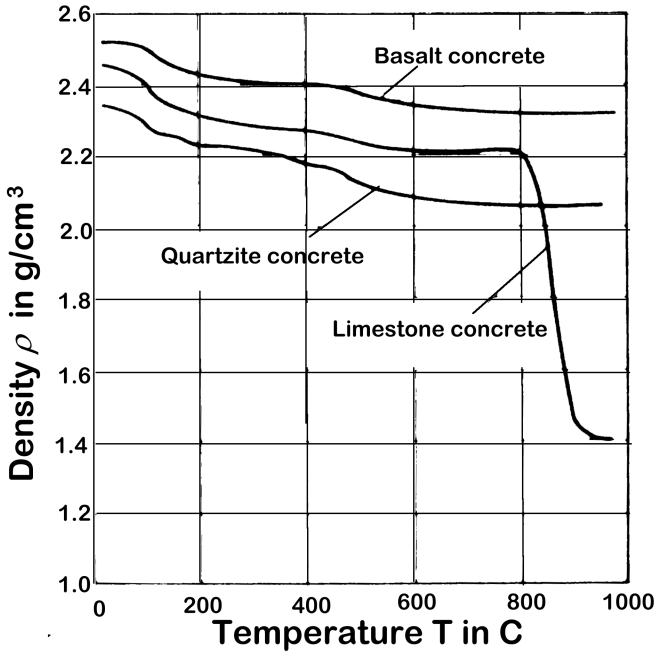

Figure 3.20: Density of structural concrete at high temperatures[228]

Thermal conductivity of concrete depends upon the nature of the aggregate, the porosity of the concrete and, until dry, the moisture content. The conductivity of most concretes vary linearly with moisture content. Up to 100^{o}C conductivity of NWC increases with temperature after which there is a reduction. LWCs tend to be more constant[228] (See Figure 3.21)(a).

In fire, water is driven out therefore the conductivity of dry concrete is also an issue. A general picture of concrete conductivity with increasing temperature is given by Figure 3.22(a). At 800^oC the value is about 50% of the value at 20^oC.
Specific heat of NWC increases with temperature and LWC is almost constant. All concretes with free water experience a sudden rise in specific heat as water evaporates around 100^oC (See Figures3.21(b) and 3.22(b)).

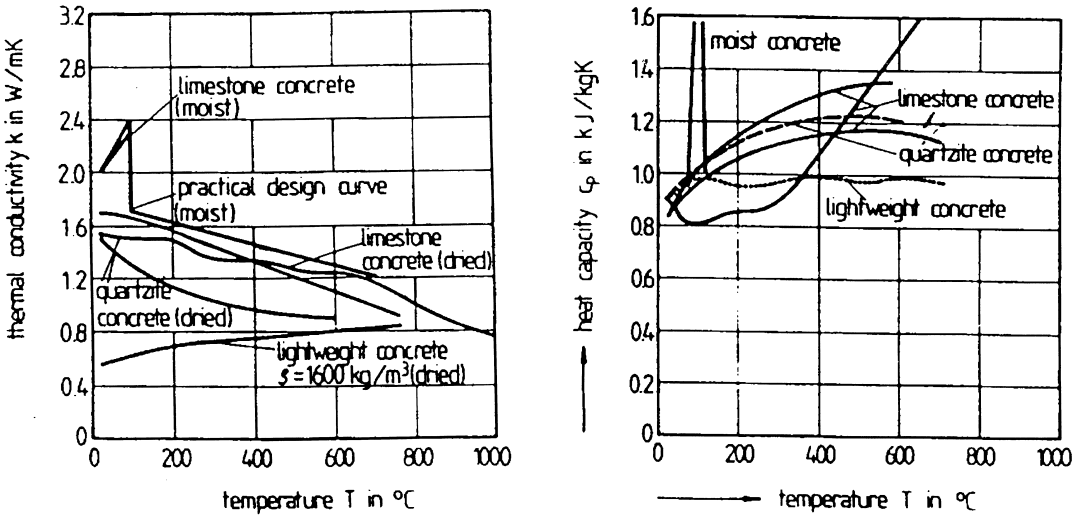

(a) Conductivity

(b) Specific heat

Figure 3.21: Thermal properties of different structural concretes[228]

3.9.2.1 Moisture in Concrete

Concrete like most building materials contains two phases a solid phase and a gaseous phase in the solid matrix. The pores of a solid may be interconnected or non-interconnected. Fluids can only move through the pores if they are interconnected. Vapour migrates through the capillaries to the outer surfaces turning to steam on the hot side and condensing on the cool side, termed "weeping". The loss of moisture will reduce the density by a small amount but for practical purposes this can be ignored.[158] However wet concretes show specific heat values nearly twice as high as oven-dried concretes.[228]

Free water evaporates from concrete at $100 - 150^oC$ whilst chemically bound water remains until temperatures of 450^oC.[228] Moisture absorbed by the concrete significantly increases its thermal conductivity because the conductivity of air is lower than water.

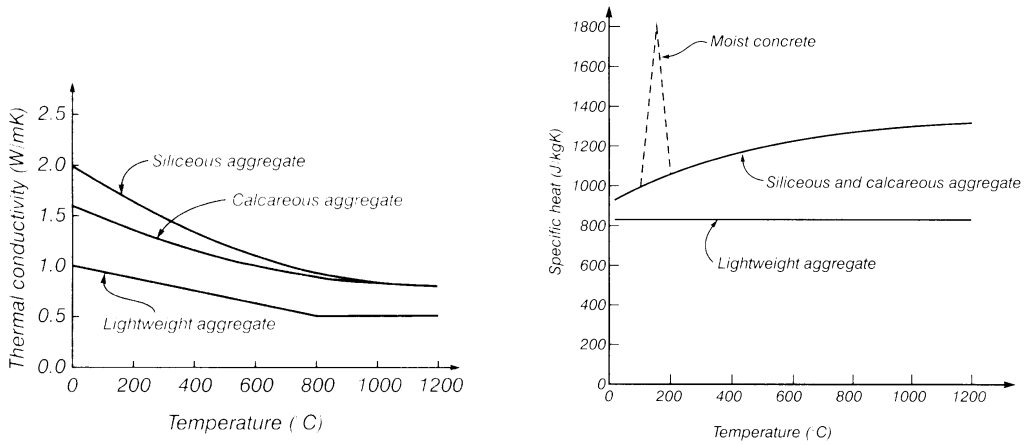

(a) Conductivity

(b) Specific heat

Figure 3.22: Thermal properties of concrete[43]

In lightweight concrete an increase in moisture content of 10% increases the conductivity by 50%. However the conductivity of the water is less than half that of the hydrated cement paste so the lower the water content of the mix the higher the conductivity of the hardened concrete.[228]

In materials with large effective pore space or high permeabilities the moisture can retreat to the cooler surface (unexposed face of the element) ahead of the heat flow.

3.10 Predicting steel temperatures

Predicting steel temperatures for design is achieved by heat transfer analysis using simple quasi-steady lumped mass models[75,158,161,195] or sophisticated numerical tools. Nomograms are also available in the literature and design guides.
The heating rate of a steel section is dependent on the size, shape and the location of the member in the compartment and the thickness and nature of any protection applied. The steel location in relation to the flames is very important. Typical locations which can give widely varying heating rates include,

1. A column placed inside a compartment and exposed to flames on four sides
2. A column placed outside a building
3. A beam which is either protected by a suspended ceiling or is high enough above the fire so that the upper limit of the flames is below the bottom flange. The latter is only possible during localised pre-flashover fires.

4. A beam supporting a floor slab in which the flames reach the underside of the slab

5. Embedded columns and beams

6. Cross-sectional shapes e.g. circular or H-section

3.10.1 $\frac{H_p}{A}$ Concept

The heating rate of a steel section in a fire depends upon, the perimeter of steel exposed to flames and , the cross-sectional area of the section. The Hp/A ratio sometimes called the section factor is the ratio used to quantify the heating rate of steel in a fire. Hp is the heated perimeter of the section and A the cross-sectional area of the steel section. The Hp value varies according to the size of the element and where it is located in the building e.g if the same section was in the wall or in the middle of the room. Tables are available presenting $\frac{Hp}{A}$ values for the standard steel section sizes.[7]

The position of the steel member is taken into account by calculating a resultant emissivity value which has values in the range 0.3-0.7, 0.7 being associated with a member totally engulfed in flames and 0.3 relating to a member which is remote from direct flame impingement.[126]

3.10.2 Simple heat transfer models

3.10.3 Uninsulated steel[161]

Equation 3.29 is a typical example of a quasi-steady lumped mass model for estimating unprotected steel heating rates. It calculates the net heat transferred per unit length of steel in time Δt. The assumptions are that at all times the temperature of the steel is uniform and the heat flow is unidimensional (corners and edges ignored).[67]

$$\Delta T_s = \frac{\alpha}{\rho_s c_s} \frac{A_s}{V_s} (T_t - T_s) \Delta t \tag{3.29}$$

where,

$$\alpha = \alpha_c + \alpha_r \tag{3.30}$$

α = surface heat transfer coefficient (kW/m^{2}K)
α_c = Convective portion of heat transfer (kW/m^{2}K)
α_r = Radiative portion of heat transfer (kW/m^{2}K)

$$\alpha = 0.023 + \frac{56.7 \times 10^{-12}}{(T_t - T_s)} \epsilon_r \left(T_t^4 - T_s^4\right) \tag{3.31}$$

where,

ρ_s = density of the steel (kg/m^3)
c_s = heat capacity of the steel (kJ/kg)
A_s = Area of the steel per unit length (m^2/m)
V_s = Volume of the steel per unit length (m^3/m)
T_t = Temperature of the compartment gases (atmosphere) (K)
T_s = Temperature of the steel (K)
Δt = Time increment (s)
Q = Heat transferred to the steel (kJ/m)
ϵ_r = Resultant emissivity

Equation 3.29 was tested against measured steel temperatures (see Appendix A). The correlation was very good.

3.10.4 Insulated steel

Similar but more complex relationships exist for protected steel.[126, 158]

Net heat transferred to the steel in time Δt:

$$Q = \frac{1}{\frac{1}{\alpha} + \frac{d_i}{k_i}} A_i (T_t - T_s) \Delta t \tag{3.32}$$

where,

$$Q = \rho_s c_s V_s \Delta T_s \tag{3.33}$$

thus,

$$\Delta T_s = \frac{A_i}{\left(\frac{1}{\alpha} + \frac{d_i}{k_i}\right) \rho_s c_s V_s} (T_t - T_s) \Delta t \tag{3.34}$$

Equation 3.34 assumes the temperature gradient in the insulation is linear at all times i.e. the thermal capacity of the insulation is negligible. This approximation cannot be assumed for thick, dense insulating materials.
In fire $\frac{1}{\alpha} << \frac{d_i}{k_i}$, so

$$\Delta T_s = \frac{k_i}{d_i \rho_s c_s} \frac{A_i}{V_s} (T_t - T_s) \Delta t \tag{3.35}$$

where,

A_i = Cross-sectional area of insulation per unit length of column (m^2/m)
k_i = thermal conductivity of the insulation (W/mK)
d_i = thickness of insulation (m)

As a simple rule the thermal capacity of a material can be considered low if,

$$c_s \rho_s A_s > 2 c_i \rho_i d_i H p_i \tag{3.36}$$

If the thermal capacity must be accounted for then,

$$\Delta T_s = \frac{\frac{\lambda_i}{d_i}}{c_s \rho_s} \frac{H p_i}{A} \left[\frac{1}{1+\xi}\right] (T_t - T_s) \Delta t - \frac{\Delta T_t}{1 + \frac{1}{\xi}} \tag{3.37}$$

where,

$$\xi = \frac{c_i d_i \rho_i H p_i}{2 c_s \rho s A} \tag{3.38}$$

Hp_i = Internal surface area of insulation per unit length of column (m^2/m)
c_i = specific heat of the insulation (J/kgK)

The heat transfer to unprotected and protected steel can be calculated using the Equations in Eurocode 3 Design of steel structures, Part 1.2: General rules (Structural Fire Design).[77] They are very similar to Equations 3.29 and 3.37.

3.10.5 Nomograms

Nomograms for critical steel temperatures exposed to the standard fire curve are given in the literature.[161] Pettersson[195] gives nomograms for natural fires assuming the set of natural fire curves given by Magnusson and Thelandersson.[155]

More recently nomograms for unprotected steel temperatures were developed by Kirby and Tomlinson[130] as part of a DETR PIT project.[150] They plot design fire load density against maximum steel temperature for various steel "Element factors" and properties of the compartment boundaries b. Element factors were introduced by Kirby.[130] They are similar in concept to the section factor $\frac{H_p}{A}$ but the element factor considers only the critical part of the steel member exposed to fire. It is defined as the ratio of the surface area of a flange or web of a section exposed to fire to the cross section area of that part of the section. $\frac{H_p}{A}$ considers the whole cross-section. Nomograms exist for a number of opening factors. The data were obtained by using the parametric curve in EC1: Part 2.2 to describe the various fire exposures and the heat transfer equation for unprotected steel in EC3. Maximum steel temperatures were calculated for the critical "element" of the steel member. An example of one of the nomograms is given in Figure 3.23.

3.11 Modelling heat transfer in concrete

Heat transfer to steel is reasonably easy and accurate to calculate. Concrete is considerably more complex. Moisture evaporation, water migration, reinforcing steel and radiation and convection heat transfer in the pores are a few of the problems associated with modelling concrete.

Nomograms based on the standard fire test have been produced for concrete sections (Figure 3.24). To calculate the heating effect of natural fires numerical heat transfer analysis using computer software is necessary. There was considerable progress in this field in terms of concrete temperatures throughout the 70s and early 80s[28,29,33,60,61,212] particularly by the nuclear industry. The development of performance based design codes in fire engineering has rekindled interest in this subject.

Modelling heat transfer into concrete is complicated by the presence of moisture within

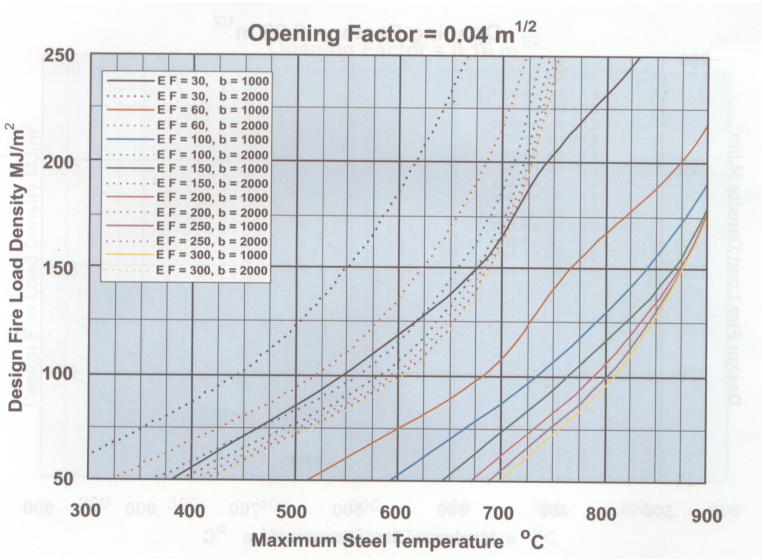

Figure 3.23: Typical nomogram for estimating maximum steel temperatures using the "Element factor"[130]

the free pores of the material. An increase in temperature causes an increase in pore pressure which in turn causes migration of water vapour, and eventually drying of the concrete. This is gradual and develops as the interface between the "dry" and "wet" concrete moves into the material (see Figure 3.25). This Figure also shows that the water vapour can either escape towards the heated surface or recondense on the cool side of the interface. This has been recognised by researchers[60,61,212] and is illustrated in Figure 3.25.

Many researchers have looked at the problem of moisture migration caused by temperature differences in porous media.[59,68,105,212] Others have investigated the specific problem with respect to concrete nuclear reactors[28,29,60] and the thermal response and integrity of a concrete building during and after a fire.[1,28,113,211] Some examples of specific research are highlighted now.

Siang *et al*[107] developed differential equations and numerical solutions for simultaneous heat and mass transfer of naturally drying cement paste in concrete slabs. They also reviewed contemporaneous theories about moisture migration. More recently Ahmed *et al*[106] developed and numerically solved a mathematical model to predict heat and mass transfer in concrete structures subjected to fire. The model simulates changes in pore pressure, temperature and moisture with corresponding changes in concrete properties and has also been able to predict "moisture clog" and the spalling of concrete. Ahmed *et al*[1] modelled pore pressure, moisture and temperature in high-strength con-

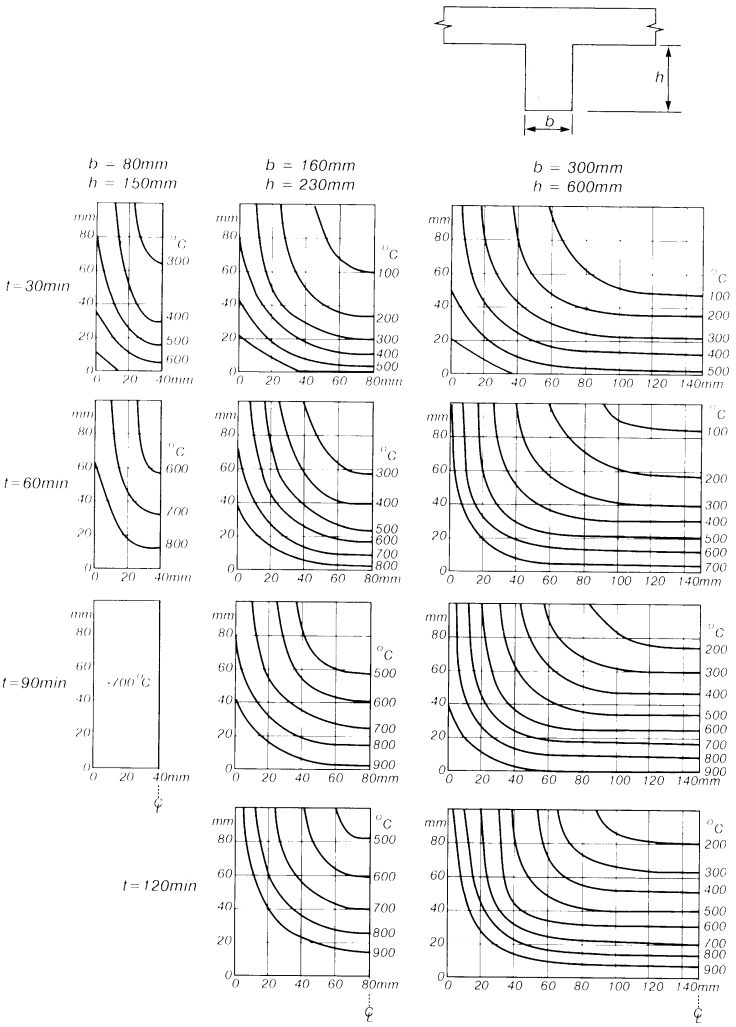

Figure 3.24: Temperature contours in concrete beams exposed to the standard fire from EC2[43]

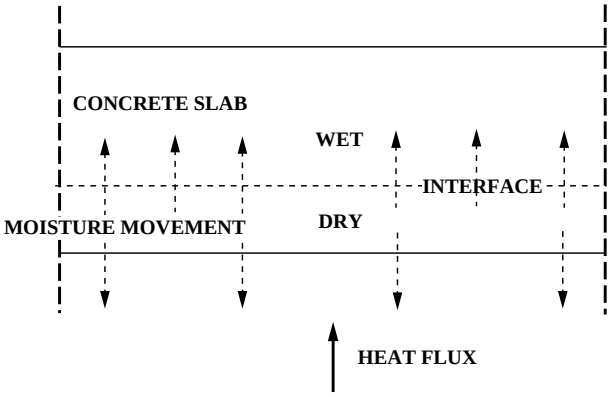

Figure 3.25: A slab heated on one face showing the dry-wet interface

crete columns. Model predictions agreed well with test data.

Although there are now models which are capable of predicting moisture concentrations and pore pressures these are complex and expensive to process. Very often the use of simpler, faster models capable of predicting temperatures with reasonable accuracy is valid. This is especially true if spalling of the concrete is unlikely and the moisture can migrate to an unheated surface and escape. In terms of obtaining temperature data as input for a structural analysis a simple approach including moisture evaporation but ignoring moisture migration may be all that is required. A slightly conservative estimate of the real temperatures will be achieved because the high localised moisture concentrations, experienced near the dry-wet interface are not modelled.

There are various heat transfer programs available for determining the temperature of structural elements exposed to fire. One of the earliest computer codes developed was FIRES-T[33,34] at the University of California. This has since been superseded by FIRES-T3.[201] Milke[162] gives a review of FIRES-T3 and another similar code TASEF.[232] When modelling concrete both programs include moisture evaporation but ignore moisture migration. Selih *et al*[229] compares a model which includes moisture migration and calculates pore pressures with two simpler models where all liquid water evaporates at 100^oC and moisture migration is ignored. CEFICOSS[226] is a code capable of dealing with the thermal and structural response during a fire. THERMIN, developed by Luyckx *et al*[151] is designed to deal with composite sections and internal voids within structural elements. The aim of this code is to overcome the problem of modelling sections where one material has a very high conductivity and is thermally thin and one material has a low conductivity and is considerably thicker as is common in modern steel and concrete composite sections.

3.12 Conclusions

There are a whole range of design tools available to the engineer to calculate first the compartment fire history and secondly the heat transfer to the elements of construction.

The advent of reliable and powerful computers has enabled very sophisticated modelling of fires and heat transfer. The level of sophistication necessary depends on the fire engineering design. In most cases a simple parametric calculation of the post-flashover fire is all that is required. Detailed examination of two compartment fire models has

highlighted the shortcomings of these tools however in general, they over predict compartment fire temperatures leading to safe designs. These were reported in Appendix A and B.

Heat transfer to steel can be calculated by hand or spreadsheet because its high conductivity and homogeneity make simple calculations accurate. Concrete temperatures are more difficult to predict and require finite element models to get accurate data. However simple nomograms for concrete sections exposed to standard fires also exist.

Chapter 4

Composite steel frame structures in fire: Research and design developments

4.1 Introduction

Since the Broadgate phase 8 fire in the late 80s and the realisation that composite steel deck floor systems are under utilised when designing for the fire limit state, research into the behaviour of whole frame, composite steel structures in fire has increased considerably. The most notable work in the UK are the Cardington frame fire tests on an 8-storey composite steel frame. Researchers in the UK and Europe have studied and simulated these tests numerically.[21, 109, 187] Subsequently, new design guidance for composite steel structures in fire has been developed. SCI have produced a design guide[170] based on a theoretical analysis by Bailey.[23] New Zealand have also produced a draft design guide[55] based on the Cardington Frame fire tests and work by Wang.[252] The most recent developments in this field will be reviewed in this chapter.

4.2 Case studies

4.2.1 Broadgate Phase 8

The Broadgate fire was introduced in Chapter 1 of this thesis. Structural damage caused by the fire included distortion of a number of trusses and universal beams and axial shortening of five columns by 100mm. The deflection of the trusses produced dishing of the floor of up to 600mm relative to the columns. The concrete floor slab separated from its metal decking in some areas but generally followed the level of its deflected supporting members. Despite large deflections, the structure behaved well and there was no collapse of any of the columns, beams or floors.[116]

The behaviour of the structure and the floor members showed that a steel frame designed to BS 5950 : Part 8 is structurally safe when exposed to a severe fire. The study[116] carried out after the Broadgate fire showed that when fire affects only part of a structure (compartmentation) and when the framework acts as a total entity structural stability is improved.
Detailed studies of the material properties at high temperatures were carried out and it was concluded that apart from the concrete to the first floor no material showed significant loss of strength due to the fire. Detailed metallurgical investigations were carried out to asses the temperatures reached by the quenched and tempered bolts recovered from several of the beam to column connections in the areas of the fire which showed most damage. These indicated that the most severe temperatures achieved by the bolts during the fire or during manufacture were limited to 540^oC. Similar evidence from a truss indicated that the member had been heated to around 600^oC. The principles of

BS5950 Part 8 would suggest that these members would transfer load to cooler parts of the structure until temperatures of about 700-800^{o}C but the investigations suggest that the temperatures achieved did not exceed 600^{o}C so an alternative explanation for the deformations observed was needed.

4.2.2 Churchill Plaza building, Basingstoke

In 1991 a fire took hold in the Mercantile Credit Insurance building in Basingstoke.[197] The twelve storey high building was constructed in 1988 and was of composite steel and concrete construction. The columns and the composite floor beams had applied fire protection but the soffit of the floor slab was unprotected. The fire rating of the building was 90 minutes.

The fire started on the 8th floor and spread to the tenth floor as external glazing failed. The protection materials performed well and there was no permanent deformation of the steel frame or damage to the protected connections. Similar to Broadgate the metal deck showed signs of debonding from the concrete floor slab probably due to the steam from the concrete. Load tests on the most damaged parts of the slab showed it had adequate strength to be used unrepaired. No structural repair was required on the protected steel. The cost of repair to the building was £5million but most of this was repairing smoke damage.

4.3 Fire tests

4.3.1 BHP William Street fire tests, Melbourne[197]

Built in 1971 in the centre of Melbourne, 140 William street at 41 storeys high was the tallest building in Australia. This building is also of composite construction similar to Broadgate and Mercantile centre, with a square plan and central square inner core. The steelwork around the inner core and the external columns were protected with concrete whereas the beams and the soffit of the composite steel deck floors were protected with asbestos based material. In 1990 during a refurbishment programme the decision was made to remove the hazardous asbestos material. Prior to the refurbishment the fire resistance rating of the building was 120 minutes. To maintain this level after refurbishment the regulations at the time required fire protection to the steel beams and the soffit of the lightly reinforced concrete slab. The light hazard sprinkler system would also have had to be upgraded. In the 1990s the fire resistance of buildings was a matter for debate in Australia and the refurbishment of the William street building provided an opportunity to determine whether these measures were really necessary.

Two risk assessments were conducted. The second was the most interesting. It assumed no protection to the beams or the soffit of the slab and use of the existing sprinkler system.

A series of four fire tests were carried out on a purpose built test building at BHP Research Melbourne Laboratories. The test simulated a 12m x 12m corner bay of the real building and was furnished to resemble a typical office with a 4m x 4m small office constructed near the perimeter of the building. Water tanks provided the imposed loading. The first two tests were concerned with testing the performance of the existing light hazard sprinkler system. Test 3 was designed to test the composite slab. The soffit of the slab was left unprotected although a non-fire-rated suspended ceiling was in place. The supporting beams were partially protected. The fire was started in the open plan area and allowed to develop fully. A maximum atmosphere temperature of 1254^oC was achieved. The ceiling remained intact during the tests and was beneficial in protecting the slab. In test 4 the ability of the steel beams to withstand a fire without protection was assessed. The fire was started in the small office but unfortunately did not spread to the rest of the compartment and another fire was set in the open plan area. The atmosphere temperature reached 1228^oC whilst the steel beams reached temperatures of 632^oC. Deflections of 120mm were recorded in one of the beams during the test. The steel beams and slab were shielded by the ceiling resulting in relatively low steel temperatures and small deflections in comparison with Broadgate. The results of the various fire tests concluded that the William street building did not need fire protection on the beams or the underside of the slab and the existing sprinkler system was adequate.

4.3.2 Stuttgart-Vaihingen University fire tests, Germany

In 1985 a fire test was undertaken on a four storey steel-framed demonstration building at the Stuttgart-Vaihingen University in Germany.[197] The building was a test building and as such was constructed from many different types of composite elements including various types of composite floors. The main fire test was conducted on the third floor in a compartment covering approximately one third of the building. The fire load was provided by wooden cribs. The atmosphere temperature exceeded 1000^oC whilst the steel temperatures reached 650^oC. Investigation of the beams after the test showed spalling of the infilled webs but the behaviour of the beams was very good with no significant permanent deformations after the fire. The composite floor reached deflections of 60mm and retained its integrity.

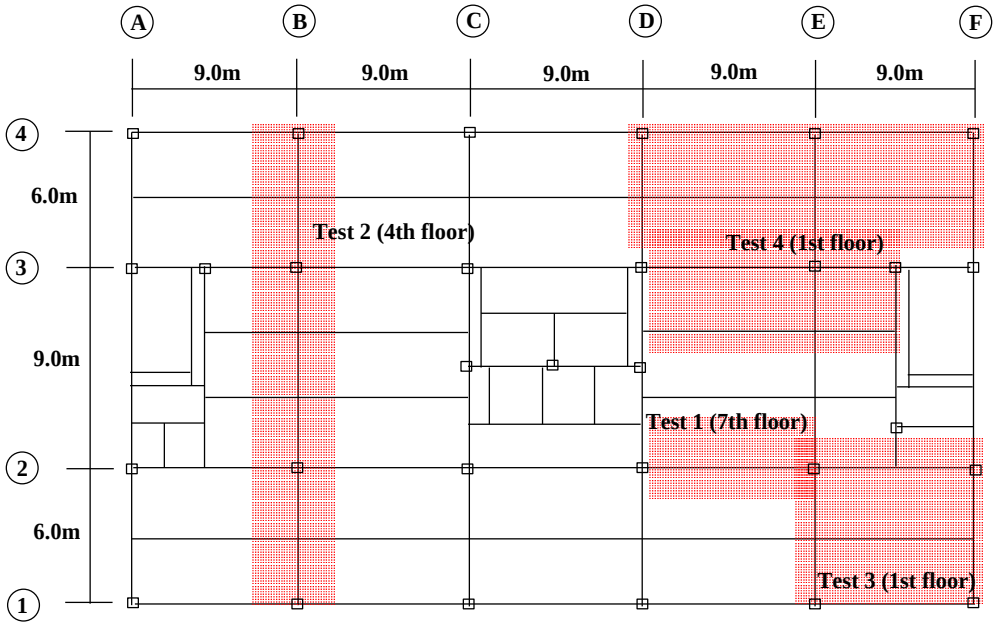

Figure 4.1: Plan view of the Cardington 8-storey frame showing the 4 British Steel Tests

4.3.3 Cardington frame fire tests

The Broadgate fire provided the greatest insight into the ability of composite structures to resist fire. In all the other case studies and tests there was some form of protection to the steel. In the Chuchill Plaza building the steel frame was completely protected. The tests in Australia provided protection to the slab and beams with an unrated suspended ceiling and in Germany all the steel sections were protected by heat sinks of concrete. The tests at Cardington were much closer to the Broadgate scenario thus fully testing the capacity of the frame.

Over a period of September 1995-June 1996 British Steel (now CORUS) conducted 4 fire tests on the 8-storey composite steel frame structure at BRE's (Building Research Establishment) large scale test facility at Cardington. BRE carried out two further complementary tests around the same period. Figures 4.1 and 4.2 show the 4 tests conducted by CORUS and the two further tests carried out by BRE respectively.[128,197]

4.3.3.1 Physical aspects of the tests

4.3.3.1.1 British Steel Test 1: Restrained Beam Test 1 illustrated in Figure 4.1 was carried out on the 7th floor of the 8-storey frame and involved a single 305 x 165 mm beam and the surrounding concrete floor spanning 9m between a pair of 254 x 254

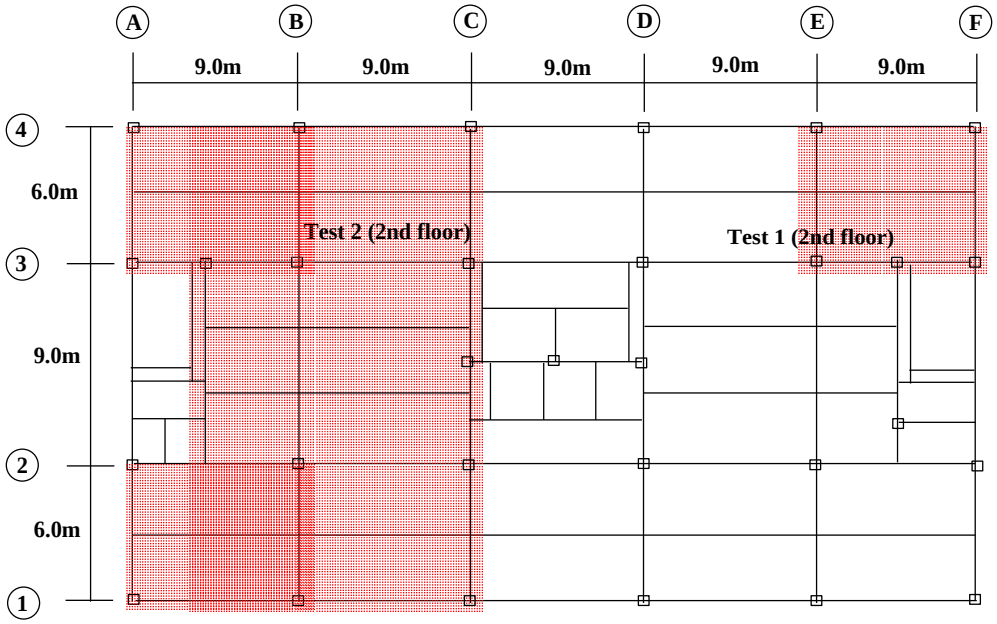

Figure 4.2: Plan view of the Cardington 8-storey frame showing the 2 BRE Tests

mm columns. The beam was surrounded by a gas fired furnace but the columns and connections were left outside. The furnace was 8m long x 3m wide x 2m high; insulated with mineral wool and ceramic fibre.[38] During the test the beam was heated at between 3-10^{o}C/min until temperatures of 800-900^{o}C were achieved.[129] The test beam and surrounding structure were extensively instrumented to measure temperatures, strains, deflections and rotations. The temperatures in the steel beam were recorded at many points along its length and through the depth. The temperatures through the slabs depth were only recorded at four points on plan (at two points between the beam and furnace wall and two locations over the tested joist). Maximum deflections of 232mm were recorded at 887^{o}C.[6, 197]

The aftermath of the test is shown in Figure 4.3. Local buckles in the flange near the connections and folds in the web can be observed. The local buckles are caused by a combination of the high compressions in the highly restrained expanding hot beam and the additional compressions as a result of the high gradient in the composite. The gradient causes a hogging moment, thus increased compressions in the lower part of the beam. The folds in the web may have occurred during cooling. On cooling the beam tries to retract into its original shape. However not all of the deflected shape can be recovered because of plastic straining thus the beam is effectively shorter. Tension folds probably develop in the web as the beam is pulled back into position. This phenomena can be seen in all the British Steel tests. In most cases some bolts or part of the plates forming the connections have failed releasing the tension forces developed during

Figure 4.3: British Steel Test 1: Restrained beam test

cooling (Figure 4.5).

4.3.3.1.2 British Steel Test 2: Plane frame The second test involved heating a series of beams and columns across the full 21m width of the building on the fourth floor using a gas furnace. A furnace 21m long x 3m wide x 4m high was constructed using 190mm lightweight concrete blockwork. It was lined with 50mm thick ceramic fibre blanket to reduce heat losses.[38,129,197] Natural gas was supplied to eight industrial burners installed along one side of the furnace. Maximum atmosphere temperatures of 750^{o}C were achieved. The primary and secondary beams were unprotected. The top 800mm of the columns including the connections were also unprotected. The supporting columns were squashed by 180mm (pictured in Figure 4.4) at unprotected column temperatures of 670^{o}C.[197] As a direct result of this squashing all further tests had protected columns to the underside of the slab.[38,128,129,197]

4.3.3.1.3 British Steel Test 3: Corner fire Test 3 was carried out in the South East corner of the 8-storey frame on the first floor in a compartment 10m x 7.5m x 4.0m high. The fire load comprised wood cribs giving a total fire load density of

Figure 4.4: Column squashing in British Steel Test 2: Plane frame test

Figure 4.5: Connection failure in British Steel Test 2: Plane frame test

Figure 4.6: Local buckling of beams in British Steel Test 3: Corner test

45kg/m^2. The fire was designed using the parametric Equations in EC1 Part 2.2 to achieve atmosphere temperatures greater than 1000^{o}C. The edge beams and columns were protected in this test.[6, 38, 128, 129] The greatest steel temperature (935^{o}C) and deflection (428mm) were recorded in beam EF between gridlines 1 and 2 (See Figure 4.1). The deflection recovered to 296mm after cooling.[197] Protected steel members were placed in the compartment in order to compare protected steel temperatures measured in the test with the time to achieve these temperatures in a standard ISO 834 test. The equivalent time in the fire resistance test was 86 minutes.[197]

4.3.3.1.4 British Steel Test 4: Office Demonstration The office fire demonstration was the largest British Steel compartment fire test incorporating a floor space 18m wide and up to 10m deep (135m^2). It was conducted on the first floor in the North East corner and simulated a typical open plan office with real office equipment (and some wood cribs) providing a total fire load density of 46kg/m^2. The area of ventilation was equal to 20% of the floor area.[197] The height of the compartment was 4.0m. In this test only the columns were protected. The unprotected beams achieved temperatures of up to 1150^{o}C. Maximum deflections reached 640mm. Figure 4.7 is a picture of the test in progress. Figures 4.8 and 4.9 show the structure after the fire. As in other tests the flanges of the beams experienced extensive buckling and there were signs of tensions developed during cooling (Figure 4.9). The equivalent time of

Figure 4.7: Compartment fire in progress in British Steel Test 4: Office demonstration test

fire exposure in the standard test was shorter than test 3, 74 minutes. No concrete temperatures were measured during this test, hindering accurate numerical modelling of the structural behaviour.

4.3.3.1.5 BRE Test 1: Corner test The BRE corner test was conducted on the 2nd floor over an area 54m^2. The internal compartment boundaries were steel stud fire resistant board partitions (120 minutes fire resistance with a displacement head of 15mm). All structural steelwork excluding the columns were left unprotected. Twelve timber cribs provided 40kg/m^2 fire load. At the start of the test all windows and doors were closed, the fires development was strongly influenced by the lack of oxygen. Atmosphere temperatures of 1051^{o}C were recorded after 102 minutes but in the initial stages the fire died down very quickly and smoldered until after 55 minutes. The fire brigade intervened twice breaking windows to feed the fire with oxygen. The temperature-time history of the fire atmosphere is shown in Figure 4.11 The bottom flange of the central secondary beam achieved a maximum temperature of 903^{o}C after 114 minutes. The maximum recorded slab deflection (269mm) occurred after 130mins recovering to 160mm after cooling. Unlike the British Steel corner test the compartment walls were directly below the axis of the beams on column lines thus the edge beams experienced high gradients across the width of the cross-section. One of the edge

Figure 4.8: Aftermath of the British Steel Test 4: Office demonstration test

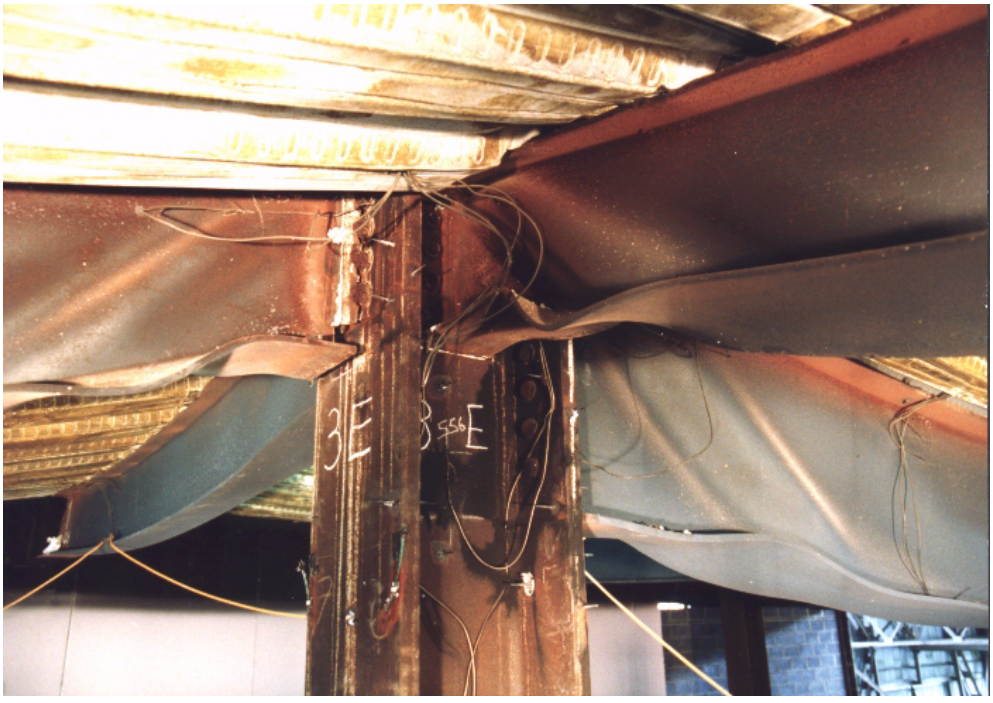

Figure 4.9: Local buckling of the lower flange and folding of the webs in British Steel Test 4: Office demonstration test

beams distortionally buckled over its length as a result of these gradients and restraint to thermal expansion. Unlike all the other Cardington frame fire tests there was no local buckling of the beams and no evidence of cooling in the form of failed connections or folds in the web.[197]

4.3.3.1.6 BRE Test 2: Large Compartment The large compartment test was constructed on the second floor extending over the full width of the building, between gridline A and 0.5m from gridline C see Figure 4.2. The total floor area of the compartment was 340m^2. 40kg/m^2 fire load was placed in the form of 42 wooden cribs. The compartment was formed by constructing a fire resistant stud partition wall across the width of the building and around the vertical access shafts. Double-glazing was installed on two sides of the building along gridlines 1 and 4. The middle third of the glazing was left open on both sides to allow sufficient ventilation for the fire to develop. All steel beams including the edge beams were left unprotected but the columns were protected.
Rapid ignition resulted in the windows breaking during the early part of the test but the maximum temperature achieved was fairly low at 763^{o}C. The steel reached a maximum temperature of 691^{o}C and a maximum displacement of 557mm was recorded halfway between gridlines 2 to 3 and B to C. The residual displacement after the structure had cooled was 481mm. Overall the structure behaved very well and there were no signs of collapse. Most internal beams showed evidence of local buckling in the lower flange and the web near the connections. In some of the partial depth end plates the plate had fractured down one side and in one instance the web had fractured. The deflection of the slab caused integrity failure of the compartment wall because it was greater than the 15mm allowance.

4.3.3.1.7 Atmosphere temperatures The atmosphere temperatures recorded in all six tests are illustrated in Figures 4.10-4.12 for comparison. British Steel test 1 and 2 have very similar heating rates. British Steel test 4 was the shortest duration fire. The BRE corner test achieved the highest temperatures but for a very short time while the BRE large compartment barely reached an average of 700^{o}C during the most intense phase of the fire.

4.4 The PIT Project

In 1995 Edinburgh University in collaboration with CORUS and Imperial College proposed a project to model the 4 British Steel fire tests on the Cardington frame. It was funded by the DETR "Partners in Technology" scheme. The title of the project was

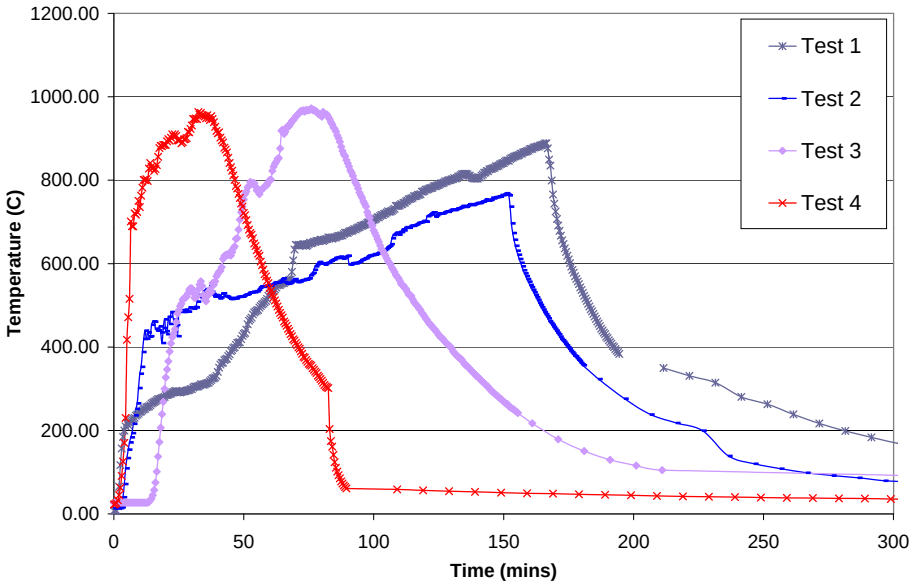

Figure 4.10: Average atmosphere temperatures recorded in the British Steel tests

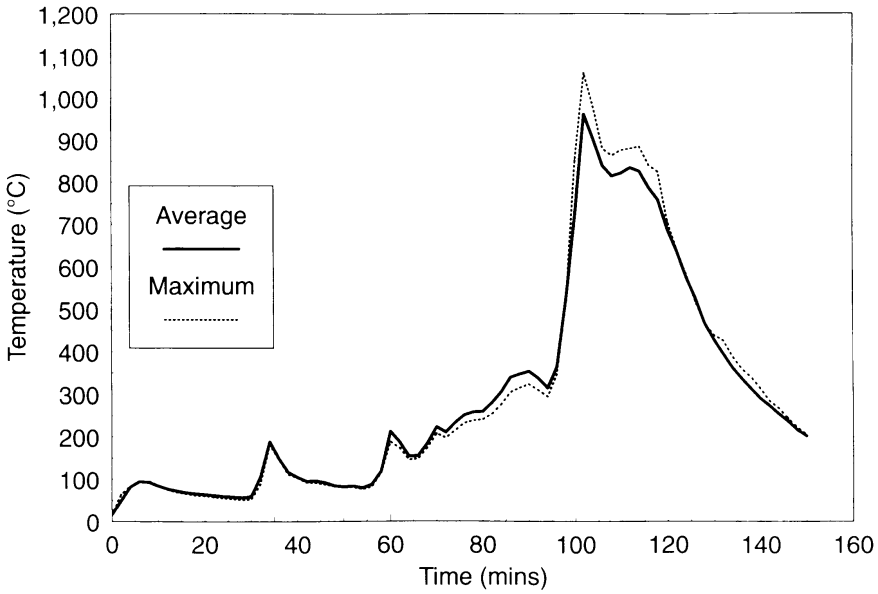

Figure 4.11: Average atmosphere temperatures recorded in the BRE corner test[197]

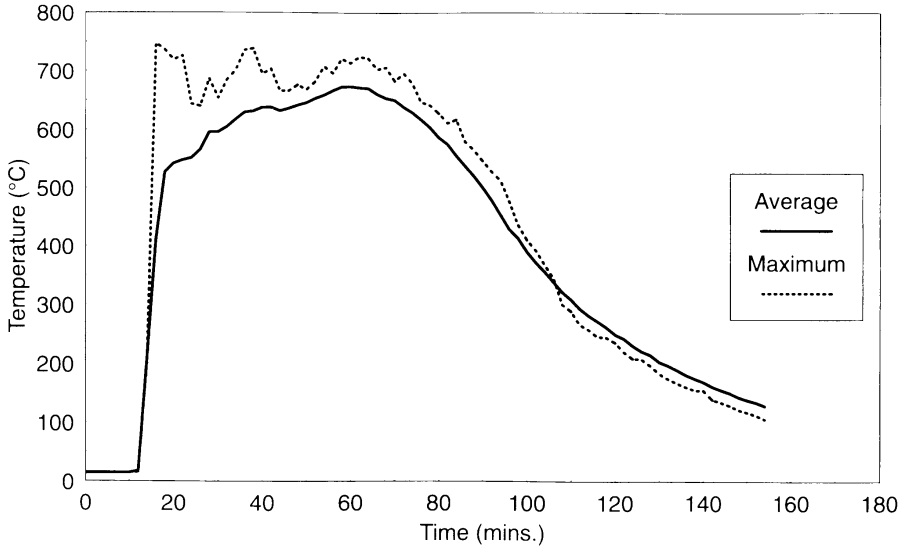

Figure 4.12: Average atmosphere temperatures recorded in the BRE large compartment test (1/2 floor)[197]

"The behaviour of steel framed structures under fire conditions" and the main objective was described as,

"*To understand and exploit the results of the large scale fire tests at Cardington so that rational design can be developed for composite steel frameworks at the fire limit state*[187]"

The PiT project started in March 1996 running for four years ending in March 2000. Although the main research team consisted of Edinburgh University, CORUS and Imperial College, BRE and SCI also provided valuable input. SCI was primarily responsible for the design output from the project. Sheffield University were part of the steering committee.

The numerical models of the tests ranged in complexity from very simple grillage models to detailed shell representations of the beams and slab. The University of Edinburgh and CORUS used the commercial code ABAQUS whilst Imperial College made use of their in-house finite element code ADAPTIC. The output from all the models were comparable and agreed with the measured test data. Conclusions of the project were,

- The Cardington composite steel framed building exhibited very stable behaviour under the various fire scenarios tested because of the nature of its highly redundant structural form.
- The thermo-mechanical phenomena observed (a combination of restrained thermal expansion and thermal bowing) defines the structural behaviour and depends

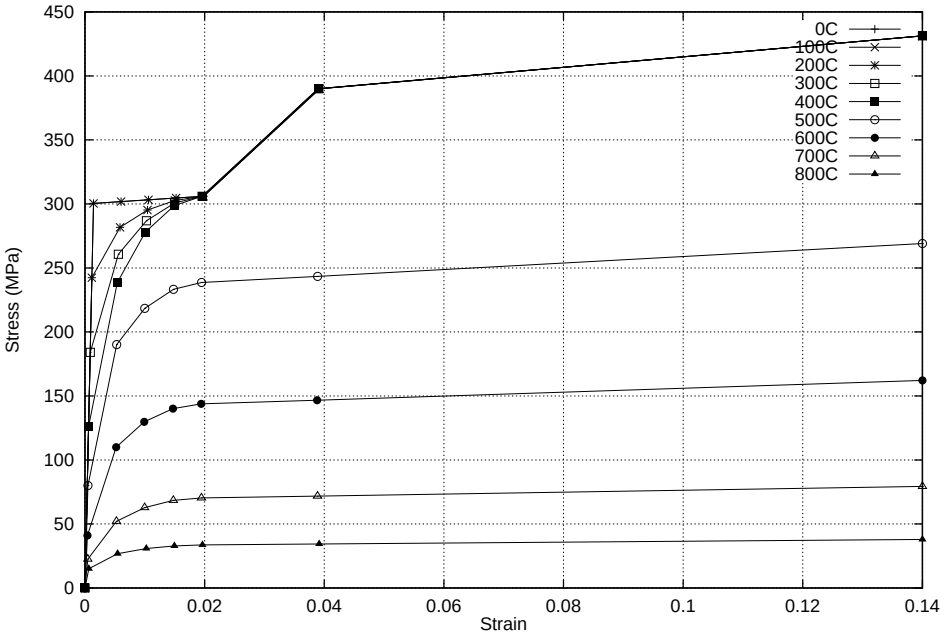

Figure 4.13: Steel material behaviour in Eurocode 3 Part 1.2[77]

upon the frame layout and the thermal regime of the fire compartment

4.4.1 The numerical models

Rigorous finite element models were developed by all of the three main contributors. The ability to reliably model material and geometrical non-linearities was a key factor in choosing the finite element codes. ABAQUS is a commercially available well accepted package tested rigorously by multiple users modelling a variety of problems. ADAPTIC has been developed over many years and is also a very reliable research code. All models were thoroughly checked against real test data. The results from corresponding models showed the same structural behaviour reinforcing the individual models results.

4.4.1.1 Material models

The stress-strain material definitions in EC2 Part 1.2 and EC3 Part 1.2 were assumed for concrete and steel respectively. The steel material model is elasto-platic and includes enhancement from strain hardening above 400^{o}C. The steel model may be conservative as was discussed in Chapter 2. Both sets of properties include degradation with increasing temperature and are illustrated in Figures 4.13 and 4.14.

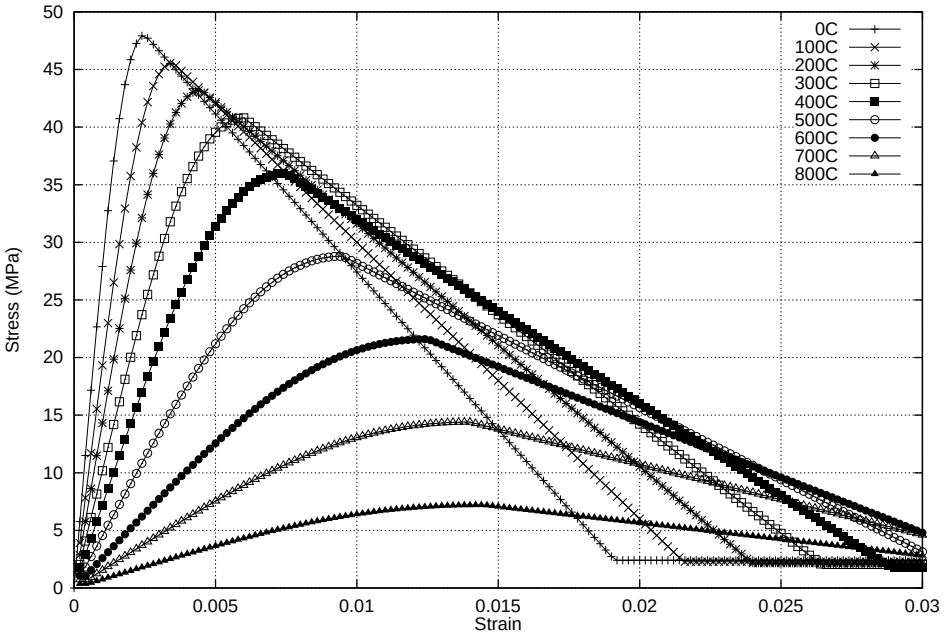

Figure 4.14: Compressive concrete material behaviour in Eurocode 2 Part 1.2[76]

4.4.1.2 The University of Edinburgh Numerical Models

The University of Edinburgh modelled British Steel test 1 and test 3 using ABAQUS. Both grillage[223] and shell models were developed.[88] Depth integration techniques are normally used to model materially non-linear plate structures using plate or shell finite elements. Stresses are calculated at integration points through the depth of the elements and section forces are obtained by integration of these stresses.

Several attempts were made to model the Cardington tests using the ABAQUS concrete model and this approach. Convergence of the problem was never achieved. Thus a Stress-resultant approach was tried. Stress-resultants enable the geometry of the plate and the material behaviour to be described by one set of equations. Forces and moments per unit width of the plate are calculated based on the strain, curvature and temperature of the plates reference surface. Gradients can also be incorporated. However results are in terms of stress resultants only so the variation of stress over the depth of the plate is not given. Both the grillage and shell representations developed by Edinburgh adopt a stress-resultant approach.

For ABAQUS to model plates using a stress resultant approach an additional user defined sub-routine is required. Hence Gillie[88] developed a suite of programs called FEAST. FEAST is used in the research presented in this thesis to model generic composite steel frames. Therefore an understanding of the code and its assumptions are stated here.

4.4.1.2.1 Development of FEAST[88] FEAST (**F**inite **E**lement **A**nalysis of **S**hells at High **T**emperatures) enables analysis of generic composite plates like the Cardington floor slab at high temperatures.
The FEAST suite consists of 3 programs,

1. SRAS - Stress Resultant Analysis of Shells. The program defines the force-strain and moment-curvature relationship for user defined plates over a given range of stress-strain-temperature states
2. FEAI - Finite Element Analysis Interface. This program allows stress resultant based calculations for user defined plates to be undertaken by ABAQUS
3. MFDU - Moment-Force Diagram Utility. This program produces moment-force interaction diagrams for plates analysed by SRAS

All three programs are described in detail by Gillie.[88] The first two will be described briefly here. The code was written in FORTRAN 77 for any general plate. There are no limitations on the number of layers modelled or the number of materials incorporated. SRAS needs an input file which splits the plates cross-section into a number of layers. Each layer is defined by its area, material and distance from the plates reference surface. The file also contains user defined information about the range of reference surface strain, curvature and temperature values over which the stress resultants are to be calculated and also the intervals between these values. Stress-strain-temperature data files are read for each material. The strain in a given layer is calculated by Equation 4.1 assuming plane sections remain plane after bending.

$$\epsilon_l = \epsilon_r + z_1 \phi \tag{4.1}$$

where,
ϵ_l = average strain in the layer
ϵ_r = reference surface strain
z_l = distance of the centre of a layer from the reference surface
ϕ = curvature of the reference surface

The temperature in the layer depends upon the reference surface T and the thermal gradient through the depth of the plate.

SRAS allows polynomials to describe the gradient through the depth, over a number of reference surface temperature ranges. The layers of the plate may also be separated into groups and separate gradients defined.
Once the strain and temperature are defined the stress in each layer is calculated from the stress-strain relationship of the relevant material. Thus the forces can be obtained by integration over the area of the section. Moments are derived in a similar manner. Figures 4.15 and 4.16 illustrate the calculations conducted by SRAS in the form of a flowchart.

The shell elements in ABAQUS are defined by force-strain and moment-curvature relationships calculated by the program SRAS. FEAI is the user defined sub-routine required by ABAQUS to use the shell elements. FEAI calculates curvatures and thermal strains based on the linear gradient and the reference surface temperature given directly in the ABAQUS input file. The gradient given in the input file is linear through the depth of the section and increases linearly with time to the end of the analysis. The reference temperature however increases with time according to a user defined amplitude curve and can follow the history of the fire. The thermal expansion coefficient for the plate, the final thermal gradient and the Poisson ratio of the plate is transferred directly from the ABAQUS input file to FEAI.
ABAQUS calls FEAI at the start of each load increment and passes information to it about the state of the plate section. This includes the reference temperature, a vector of the stress resultants, a vector of the total strains and a vector of the total strain increments for the current iteration of the load increment. FEAI updates the stress resultants and re-calculates a section stiffness matrix. The stress resultants in FEAI are computed in a similar manner to the stress resultants in SRAS. The only difference being that strains and curvatures are obtained from an ABAQUS analysis.

4.4.1.2.2 Assumptions made during the modelling of the Cardington Slab using FEAST

1. There is no coupling between shear forces and membrane forces and twisting moments and bending moments.

2. The shear stiffness was taken as half of the lesser of two membrane stiffnesses. This was assumed because outside the elastic range the shear modulus is ill defined particularly at elevated temperatures. Also geometrically orthotropic plates make it difficult to assume an area for integrating shear strains. Similarly the twisting stiffness was assumed to be half of the lesser of two bending stiffnesses. Gillie supports these assumptions by stating that the shear modulus is given by Equation 4.2 which means it is always less than half of the elastic modulus.

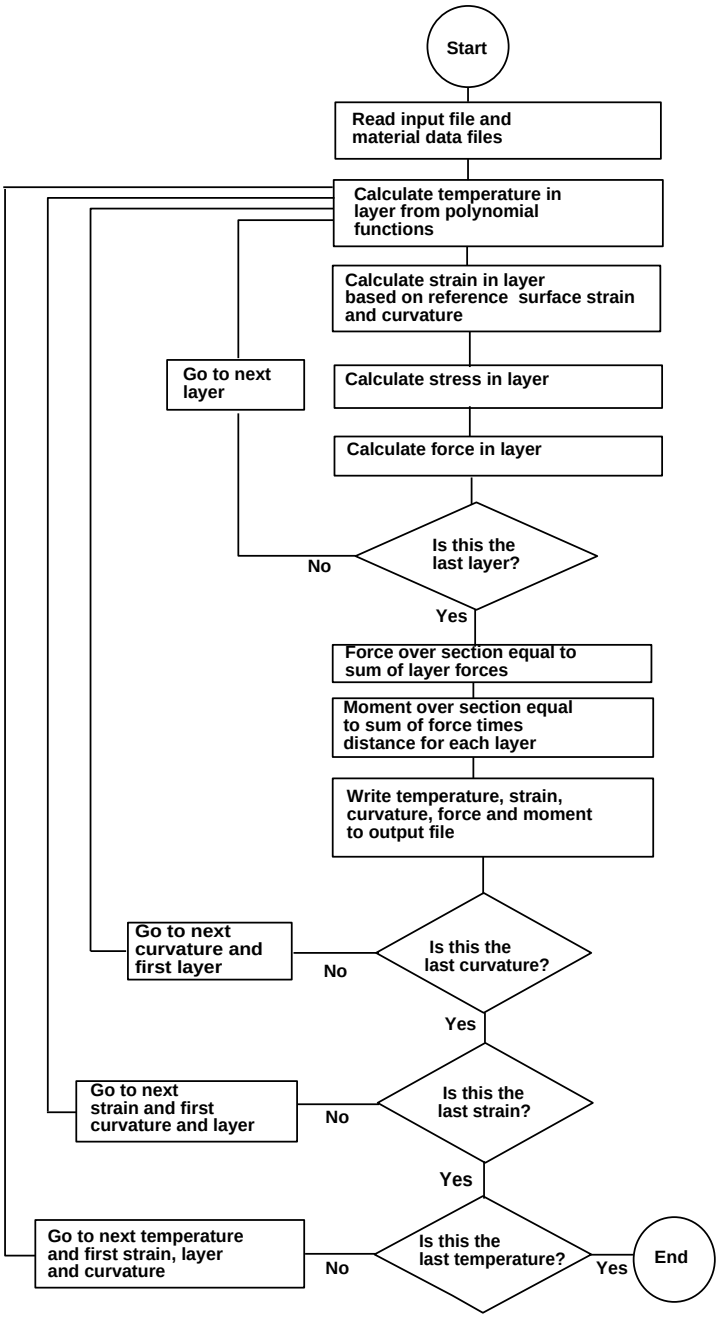

Figure 4.15: Flowchart describing the program SRAS[88]

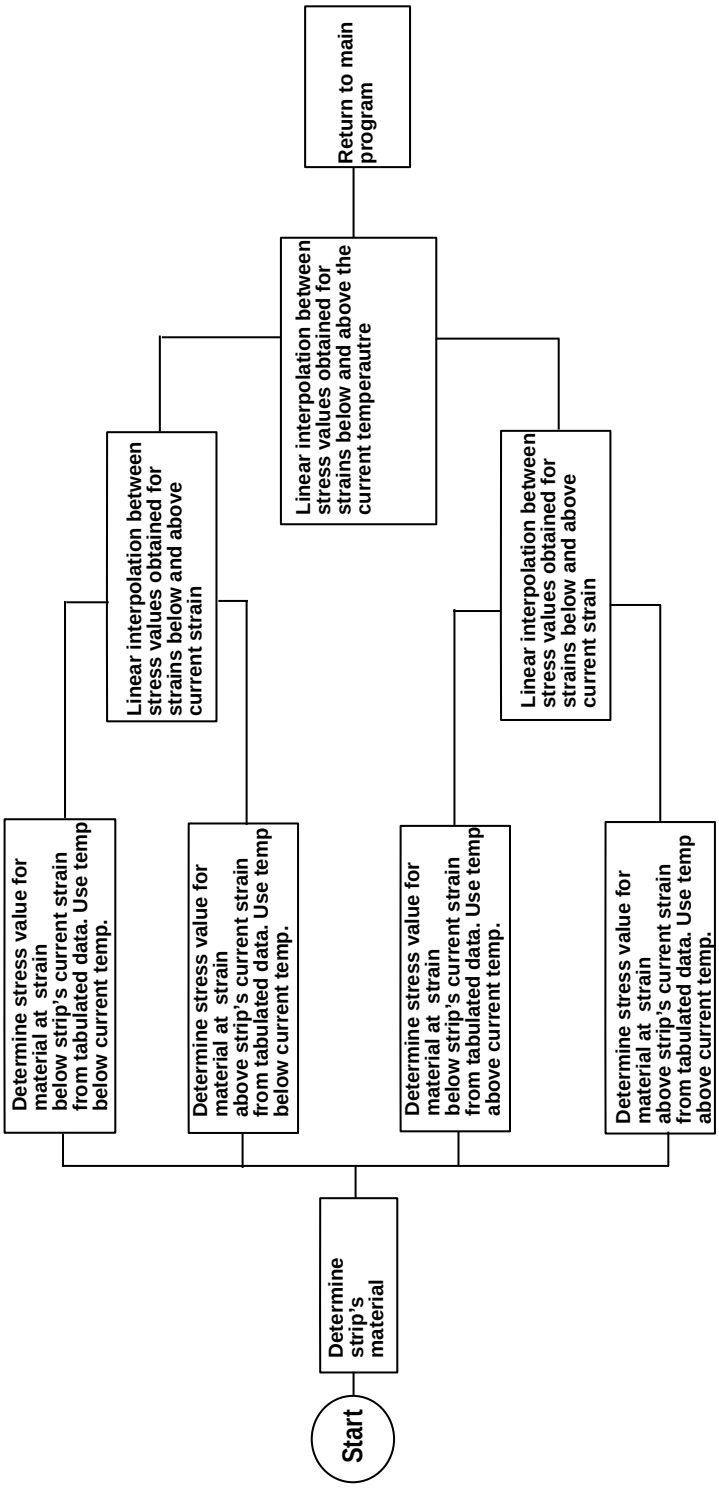

Figure 4.16: Flowchart describing the details of stress calculation within SRAS[88]

$$G = \frac{E}{1(1+\nu)} \tag{4.2}$$

These first two assumptions are inherent in FEAST. The following four assumptions were made about the Cardington slab.

1. The stress-strain relationships for concrete and steel were unique.
2. The material behaviour was uniaxial.
3. The Cardington slab had uniform thickness and material properties throughout the building.
4. The transverse shear stiffness remained constant for all strain and temperature states.

Assumption 1 means the materials follow the same stress-strain path during loading and unloading. This is not true in the post-elastic range but can be justified because the models run to the end of the post-flashover fire and do not attempt to model cooling of the structure. This assumption also implies that creep strains are not present or in this case present in the constitutive relationships. In Chapter 2 it was stated that the Eurocode models implicitly include creep effects thus the Cardington slab model includes "long term" loading effects. This is unrealistic because fires last for a few hours. Gillie justifies the assumption by citing Twilt.[245] Twilt reports that creep strains are a small part of the behaviour of engineering materials and not likely to effect the overall structural behaviour except immediately prior to failure.

A uniaxial material model for the steel elements is justified because all the steel elements were stressed uniaxially. Biaxial concrete properties are stronger than uniaxial properties by up to 20%. In effect the model of the Cardington slab is slightly weaker than the real slab. Gillie concludes that this may be offset by assuming the design thickness of the floor. The real slab is thicker due to inaccuracies in pouring concrete on site.[109,206]

The third assumption is the only practical approach for a model. Gillie assumed the concrete strength was 48kN/m^2 based on measurements taken from the slab and the steel strength was given in the building design notes.[38]

The final assumption is a restriction placed by ABAQUS. Gillie demonstrates that this limitation would not have a large effect on the analysis. He quotes an example of a linear elastic cantilever under transverse loading from Case *et al*[51] and shows that shearing deflections are only significant for deep cantilevers. Thus not important for

the shallow Cardington slab. The model assumes very high transverse shear stiffnesses so that any predicted transverse shear deflections would be close to zero.
The slab model was divided into layers as required by FEAST. The ribs were divided into trough and rib sections to allow different temperature profiles in the two areas. The temperature profiles were derived from the experimental data. Very few concrete temperatures were measured therefore the slab was assumed to have a uniform gradient over the floor but varying with time. The reinforcing mesh was modelled as a layer of steel equal to the cross-sectional area of the reinforcement. Perpendicular to the ribs the slab model ignored the strength of the ribs and the metal deck. The slab gradients perpendicular to the ribs were complicated because the profile depended on whether the slab was over a rib or a trough. The hottest profiles were those over the troughs. Since the slab behaviour would be governed by the weakest part of the cross-section Gillie assumed the profiles over the trough for the whole slab perpendicular to the ribs. The material properties based on the Eurocode models have already been discussed. Steel was assumed to behave in the same manner in tension and compression and concrete had a tensile strength equal to one tenth of its compressive strength. In FEAI the same properties were used for the ascending branches of the stress-strain curves but the materials were assumed to be infinitely ductile. This is because the Newton Raphson type solver (that must be used for thermo-mechanical analyses in ABAQUS) is unable to solve structures with negative stiffnesses. This means local failures like rupture cannot be modelled but global runaway failures can.

4.4.1.3 British Steel Numerical Models

Researchers at British Steel (now CORUS) also used ABAQUS. A number of models were developed of half the Cardington floor[177–185] assuming one symmetry boundary condition. These include,

1. Grillage model using ABAQUS beam elements for the beams and beam general section elements for the slab in tests 1, 2 and 3.

2. Shell elements for the beam and beam general section for the slab in tests 1 and 2. Representing the beams in a 3D manner with shells allowed the local buckles observed near the connections in all the tests to be modelled.

3. ABAQUS beam elements for the beams and elastic shell elements for the slab in tests 1, 2, 3 and 4. The orthotropic behaviour of the slab in the direction of the ribs was modelled by adding downstand beam elements to the underside of the elastic shells.

4. Models of the floor slab using linear elastic shell elements with discrete hinges where yield lines were expected to develop for tests 1, 2 and 4.

The various levels of sophistication adopted by British Steel allowed the important features of the tests in terms of the overall behaviour to be highlighted. For instance the very detailed representation of the beams with shell elements allowed local buckling to be modelled but the overall structural response was unaffected by this level of modelling detail.

4.4.1.4 Imperial College Numerical Models

ADAPTIC[231] supports the use of beam elements only, therefore all Imperial College models were of the grillage type. All four tests were modelled and good agreement with the test results and ABAQUS models were obtained. The results have been reported by Elghazouli *et al.*[74]

4.4.1.5 Results from and verification of the Numerical Models

Figures 4.17-4.19 plot results from the Edinburgh University grillage and FEAST analyses of British Steel test 1 beside deflections and strains measured in the test. For both models the predicted deflected shapes match the real test data very well. Figure 4.19 shows strains measured in the beam alongside the grillage model predictions. Although the magnitudes are not identical the pattern of behaviour has been captured. As well as verifying the models against test data the results were cross checked with other models from the rest of the project group.

The finite element calculations match the tests deflections and strains reasonably well but the key issue is the ability of the numerical models to provide information on results which could not be measured in the real test. Bending moments in beams under high temperatures with severe yielding and axial forces developed in the slab cannot be measured in a test. Sanad *et al*[222,223] have produced a detailed description of the behaviour of British Steel test 1 based on a grillage model. The papers illustrate and explain the changing load paths as the composite beam responds to increasing temperatures by expanding and bowing. The importance of $P-\Delta$ effects are realised. Similar detail is given for test 3.[215]

4.4.2 Theoretical analyses

In parallel to the numerical modelling a theoretical understanding of the thermal effects based on fundamental principles of structural mechanics has been developed.[208,248,249]

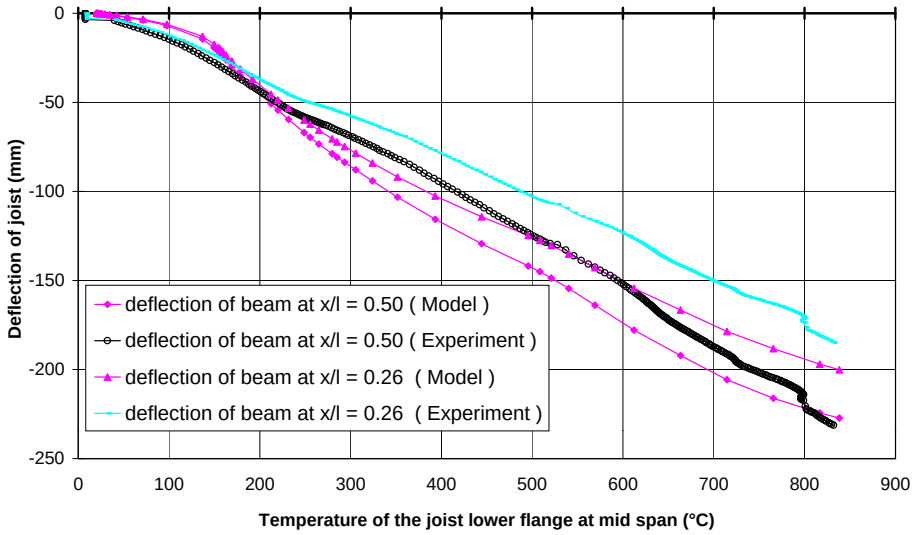

Figure 4.17: Deflection against beam lower flange temperature measured and predicted by the Edinburgh University grillage model of test 1

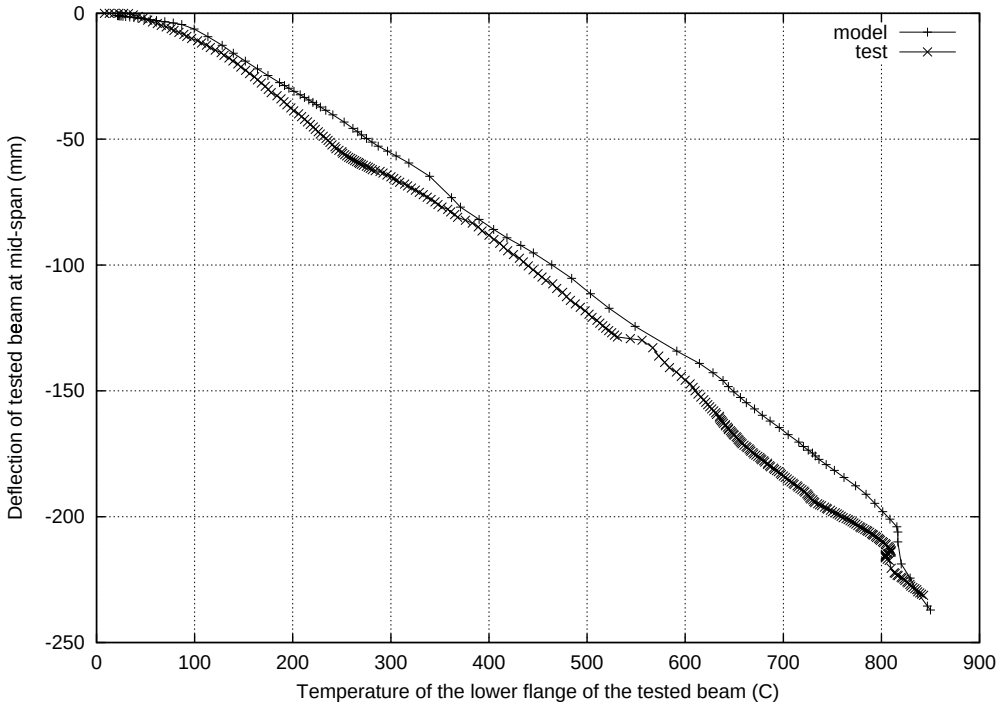

Figure 4.18: Deflection against beam lower flange temperature measured and predicted by the Edinburgh University FEAST model of test 1

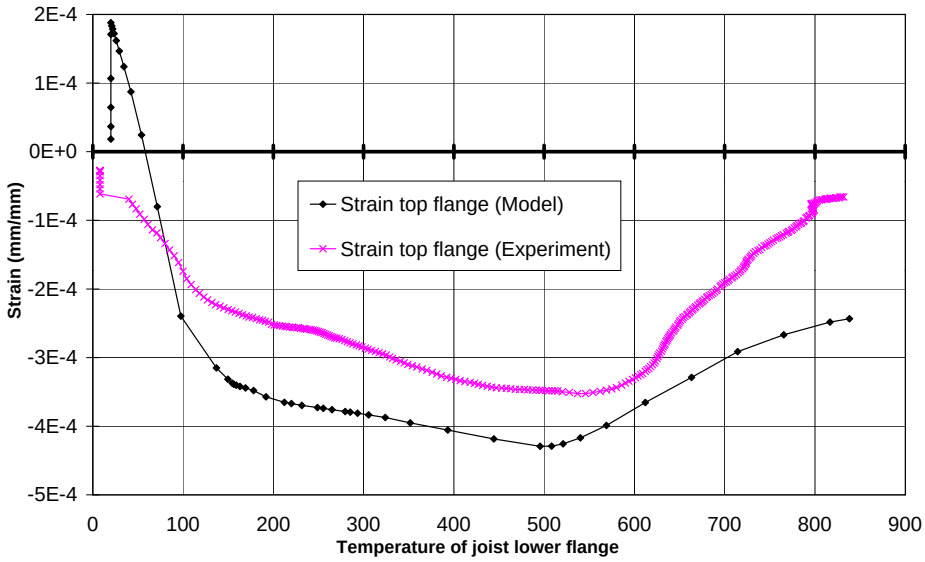

Figure 4.19: Strains measured and predicted by the Edinburgh University Grillage model of British Steel test 1

This is summarised in Chapter 6 where theory developed by Usmani *et al*[249] is validated against simple numerical beam models as part of this research. This fundamental level of understanding was necessary to decipher the complex output from the test models. Conclusions of the work were,

- Restraint to lateral translation (expansion) produces compression forces.
- Through depth thermal gradients impose curvature (bowing).
- In fixed-ended members curvature causes uniform moment.
- In pin-ended restrained members curvature leads to tension.
- Higher restraint leads to greater deflections.
- Very little restraint is required to cause buckling of the steel beams and high deflections.
- Combinations of thermal expansion and bowing with various restraint conditions can produce a large range of deflection and internal force patterns
- In slabs and other 2D members compatibility of displacements in the two directions may govern internal forces and displacements.

4.4.3 Parametric studies

After extensive verification and testing of the models several parametric studies were undertaken by all three modelling groups. These were mostly conducted on grillage type models of test 1 because the time for the analysis to run was short.
Parametric studies included,

1. Effects of increasing the live loads on British Steel Test1.[74,218]
2. Effect of changing steel section in the British Steel Test 1 composite beam.[217]
3. Effect of changing boundary restraints on British Steel Test1.[216]
4. Effect of changing slab temperature evolution on British Steel Test 1.[219–221]

Very little change in deflection was observed when the live loads were doubled which confirms that deflections under fire conditions are dominated by thermal bowing and thermal expansion effects. Studies on a simple beam model have shown that the level of live load only becomes important at impending runaway failure.[136]
Changing the section size by varying the area of the tested beam by plus or minus 50% has little impact on the deflection response. This study also highlights that the strength of the section is less important while thermal actions dominate.
Restraint conditions have a major effect on the deflection and internal forces in any member subject to heating. During the tests at Cardington the restraint conditions changed as beams buckled.
The effect of altering the temperature evolution in the slab was studied in detail. It involved changing the mean temperature or the gradient in the slab in the direction of the ribs or the direction of the tested beam. Each variable was tested separately. This study is reported in Chapter 7 and elsewhere.[208,220,221]

4.4.4 Analysis of the raw test data by British Steel

British Steel conducted a comprehensive study of all the test data recorded during the 4 British Steel tests. Trends of behaviour were sought and reported.[176] In some instances the test data alone was insufficient but supplemented with output from numerical modelling the structural behaviour could be explained.
Measured deflections, rotations and lateral displacements were studied and compared. For each test the report summarises the key events at critical beam temperatures giving an explanation based on experimental evidence and numerical modelling.

4.4.5 Conclusions of the PIT project

In general the main conclusions of the PiT project were that composite framed structures possess great reserves of strength by adopting large deflection configurations. Thermal expansion and thermal bowing of the structural elements as a result of the heating regime define the structures behaviour. Material degradation plays a secondary role and loading only governs the response near impending failure. Previous perceptions recognised the reserves of strength. However the importance of thermal expansion and thermal bowing causing large deflections without mechanical straining was not fully appreciated or explained.

4.5 Numerical Modelling at Sheffield University

The University of Sheffield have been researching the effect of fire on structures for over 12 years. Early work was on steel beams, columns and frames.[20, 49, 70, 166] More recently the group was involved in the planning and design of the Cardington Frame fire tests and were the first to model the tests using the finite element code VULCAN (previously INSTAF[210]). El-Rimawi[69] describes numerical studies conducted prior to the tests to determine the important test parameters at Cardington.

Bailey describes an early, simple model of the British Steel Test 1.[21] The beam was modelled using 2-noded beam elements and the slab using 4-noded slab elements. The authors acknowledged the shortcomings of their slab model. Material degradation was not modelled at high temperatures, identical properties were assumed in tension and compression and no through depth thermal gradients were applied. This test was driven by highly restrained thermal expansion causing large compressions in the beam and composite. Therefore the assumptions were less important for modelling of this test. Predicted and measured deflections showed good agreement. Other tests are reported using the same simplified slab model.[18, 206] A major shortcoming of these early models is that they do not include geometrically non-linear behaviour in the slab although they do in the beams. In 1999 this was changed when a non-linear slab element was developed.[109] The Cardington tests were modelled again showing good agreement with the measured deflections until the end of the test.[111]

Huang *et al*[110] reports on a further development of the VULCAN slab model of a modified layered slab element. This new element enables the orthotropic slab at Cardington to be modelled. A nominal thickness of element is assumed and an effective stiffness parameter is introduced to modify the material stiffness matrices of plain concrete to take account of the ribs in the slab. A maximum strain failure criterion is also introduced to the concrete model. Comparisons are made with the Cardington test data.

In earlier work at Sheffield[20] strain reversal in the steel during cooling has also been investigated. This is important for modelling cooling fires and spreading fires (where parts of the structure may be cooling).[71] This is a shortcoming of Edinburgh's work where modelling of cooling has not been achieved to date.

4.6 Developments in Europe

4.6.1 ECSC Project[246]

A major ECSC project, *"Design tools for the behaviour of multi-storey steel framed buildings exposed to natural fires"* is close to completion in Europe. The project partners include TNO, ARBED, CTICM, CORUS and sub-contracted to CORUS BRE and SCI, UK. The aim of the project is to develop design guidance for multi-storey composite steel structures in fire based on the results of several parametric studies on a generic steel frame similar in size and construction to the 8-storey Cardington Frame. After considering a number of finite element codes DIANA and ABAQUS were chosen to carry out any further studies because they had been sufficiently validated against the Cardington tests[6,187] for further parametric studies to be meaningful. Initial studies involved testing DIANA and ABAQUS against experimental data from single beams and small steel frames. The results from the numerical models were also cross checked. The floor plan of the generic building is illustrated in Figure 4.20. The fire compartment is confined to this one floor and is always rectangular in plan.

The width (x), depth (y) and location (x_0) of the compartment can be altered to enable office fire scenarios of various size and location over the building. However it is always assumed that one wall of the compartment is on the outside of the building because severe post-flashover fires need ventilation. OZone[50] was used to calculate the natural fires and CEFICOSS and the heat transfer Equations in EC3/4[77,79] were used to calculate the thermal response.[246] The temperature development of the steel beams and columns were taken as a fixed fraction of the temperatures achieved by the unprotected beams. Other Parameters studied include investigations of the steel grade, reinforcement ratio, load level of the steel beams and 2 types of steel decking. The live load applied was 7.5kN/m^2. Results of the work have not been published to date.

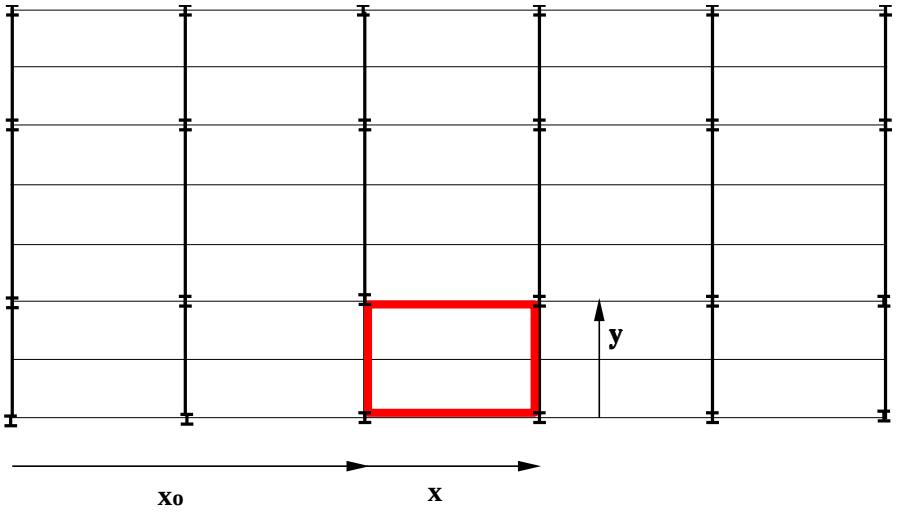

Figure 4.20: The floor plan of the ECSC Building

4.7 Design guidance

4.7.1 SCI design guide

In 2000 SCI produced level 1 design guidance[170] based on work carried out by Bailey,[23] observations of the Cardington frame fire tests and similar tests carried out in Australia and Europe. The guide is designed to allow secondary beams in composite steel framed structures to be left unprotected by capturing the strength enhancement of the slab in tensile membrane action at high deflections in fire. Recommendations given in the new guide are restricted to structures similar to the Cardington 8-storey composite steel frame i.e. non-sway frames with composite steel decks. The slab should comprise steel decking, reinforcing mesh and normal weight or light weight concrete. The profile can be trapezoidal or re-entrant. The floor beams should act compositely (including the edge beams) and be designed to BS 5950 Part 3 or EC4. This method does not apply to fabricated beams or beams with large openings, pre-cast concrete slabs or slimfloor construction. The design method is simplified into a set of look up tables based on the standard fire exposure. But the BRE full structural model can be implemented with natural fire curves. The maximum fire resistance that can be achieved using the guide is restricted to 60 minutes. Rules and guidelines are based on there being no increased threat to life safety of the occupants or firefighters. Excessive deflections should not cause compartmentation breach and fires should not be able to spread horizontally or vertically as a result of deflections imposed by the heating regime.

The method is designed to capture the enhanced strength of slabs at large deflections as a result of tensile membrane action. It requires the building floor to be split into square or rectangular design zones or panels with each panel incorporating a number of unprotected beams. The spans are restricted to 9m spans whereas in reality most multi-storey buildings incorporate 12-15m spans. The edges of each panel must be vertically supported for the duration of the fire. The size of the panel depends on the strength of the composite slab including the enhancement of membrane action, the strength of the composite beams, the fire resistance period and the allowable vertical displacement. Catenary action of the beams is conservatively ignored. As a result of the slab membrane forces, beams at the boundaries of the floor design zones receive additional loading due to forces transferred from the slab thus increasing the load ratio.

Failure is defined in terms of a maximum allowable vertical displacement. The displacement includes the effects of mechanical and thermal strains. Mechanical strains are limited on a simple basis by assuming a maximum allowable stress for the reinforcement of $0.5f_y$. A geometrical limit of L/30 is also placed on the deflections as a result of mechanical strains. Thermal strains are based on gradients in the slab. A constant temperature difference of 770^oC between the top and bottom of the slab is assumed for all the Cardington tests and is the basis for the deflections as result of thermal effects. This is a shortcoming of the method because the gradient will vary according to the heating regime. The combined deflections are compared with all the Cardington test data and a factor of safety is derived such that the estimated maximum vertical displacements correspond to four of the tests and overestimate two.

The equation for allowable vertical displacements should always give conservative results because of the various assumptions made and the fact that there was no failure observed in any of the Cardington tests. The enhancement as a result of tensile membrane action is restricted by this limit and it is impossible to know how over-conservative this method is because failure has not been observed. Proposals to test to failure have been suggested but this is a matter for great debate in the research community. Structural engineers need to define failure in terms of collapse of the structure (the ultimate limit state). Fire engineers are concerned with compartmentation failure which will inevitably occur before collapse of a composite steel frame.

Figure 4.21 defines the design procedure. The chart also includes options to enhance the strength of the slab if the load capacity is less than the applied load. For instance increasing the mesh size or slab depth. Bailey's approach is overly simple and conservative in its present form but is a considerable improvement on prescriptive design approaches.

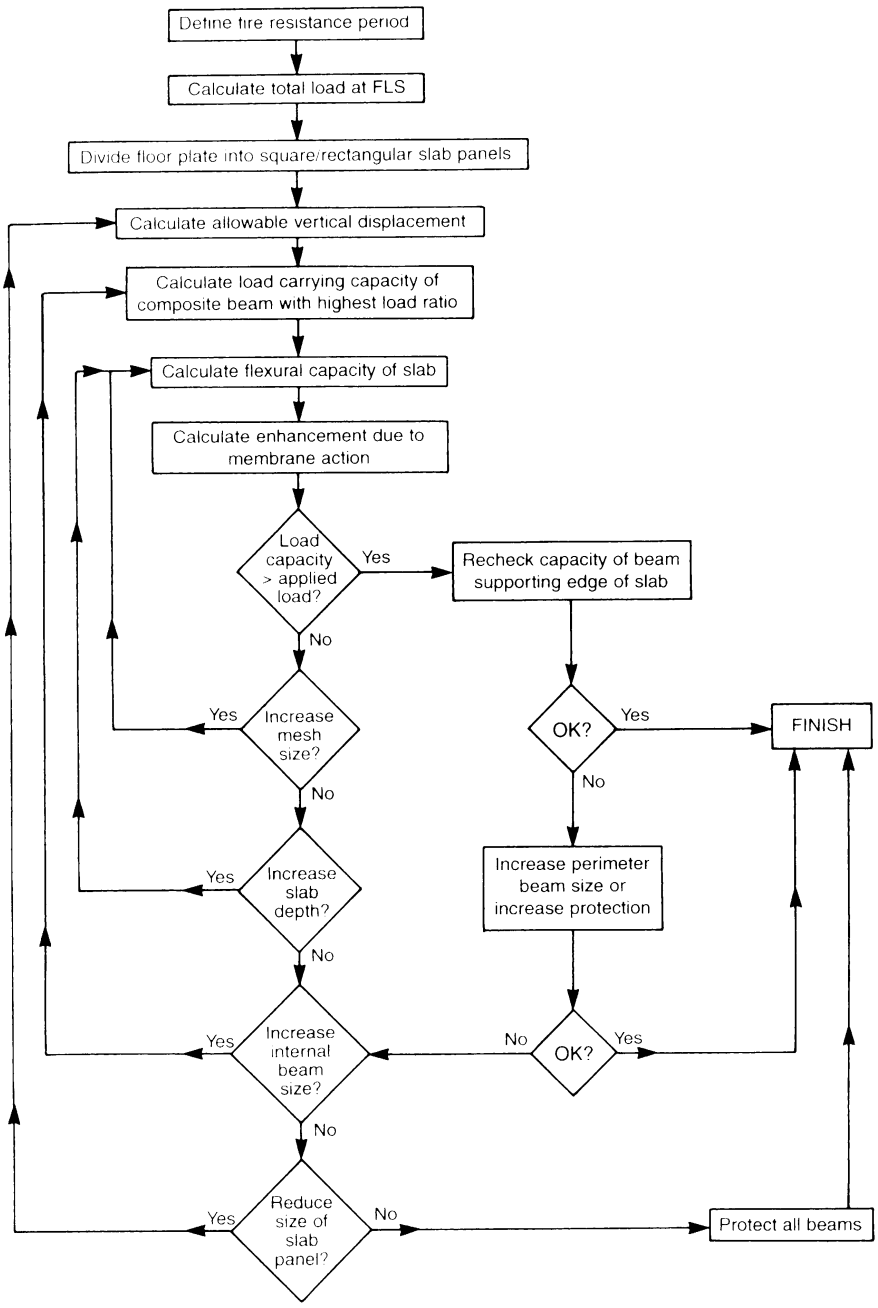

Figure 4.21: The basis of the SCI design procedure[24]

4.7.2 Design guidance developed in New Zealand

In 1998 HERA (Heavy Engineering Research Association) of New Zealand published a Draft for Development: Design procedure for the inelastic floor-system/frame response of multi-storey steel framed buildings in fully developed natural fires.[55] By utilising the realistic fire test data from large scale structural testing at Cardington and in Australia a design procedure has been developed to take into account the inelastic reserve of strength available from the floor and frame of a multi-storey steel framed building with composite floor. The guide assumes beams are unprotected but columns are protected. The draft is planned to be amended and reviewed between 1998-2002. This discussion is based on the original draft although it is near the end of the review period. The challenge was to produce a design which could be used for floor systems under significant deformations but complies with the principles of plastic analysis and predicts a response which is in reasonable agreement with test data (conservatively so). The draft includes guidelines on limits of mechanical strain for the elements of structure. Guidelines are also given on temperatures achieved by elements of structure. For steel temperatures the guide differentiates between natural fires with opening factors greater and less than 0.06. Engineering "guesstimates" are provided for the temperatures of edge beams and columns based on maximum unprotected steel temperatures of internal beams. When the OF $\leq$ 0.06 edge beams within 2m of external walls with openings are assumed to be 100^{o}C cooler than the maximum unprotected temperature. When the OF $\geq$ 0.06 the edge beams are 250^{o}C cooler. These assumptions are up for review. HERA have produced reports on temperature gradients in slabs of various effective thickness for various durations of fire tests and different types of New Zealand aggregate concrete. By using the concept of t-equivalence it is suggested this data can be used for natural fires.

The design approach includes strength re-enhancement as a result of tensile membrane action based on work by Wang.[253] Strength re-enhancement as a result of tensile membrane action is a function of the maximum deflection experienced by the slab. As the extent of strength re-enhancement is known this is used to determine the slab deflection at elevated temperatures associated with the required level of strength re-enhancement. Limits are applied to prevent undesirable failure of the slab and secondary beams e.g. fracture of the reinforcement.

The guide states that the slab must be effectively anchored around the edges. It is assumed that the steel edge beams only provide vertical support and stabilise the edge of the floor slab. The compression ring developed in the edge of the floor slab anchors the tensile membrane forces. The draft guide considers all aspects of the frame including pulling-in of the columns when the slab is at very high deflections in tensile membrane

action.

4.8 Conclusion

This chapter has described various fire tests and case studies in detail with particular attention to the Cardington frame tests. The importance of numerical modelling has been highlighted and the work of various research groups summarised. Detailed analysis of the FEAST model has been given because it has been adopted to study generic composite steel frames in later chapters.

The main conclusions of this type of research is that composite frame structures have enormous reserves of strength in the fire limit state. Large deflections in the heated elements are driven by thermal effects such as restrained thermal expansion and bowing. Material degradation and loading play a secondary role.

Tensile membrane action in the composite slab at high temperatures and deflections, considerably enhances the strength of the slab. This can be captured in new design methods. Bailey has developed a simplified approach which is over conservative but enables practising engineers to harness some of this new research in real design. One of the problems associated with developing design guidance is not being able to quantify structural failure. Cardington showed no collapse. Until failure is defined structural design for fire does not have an ultimate limit to work to. However, in fire design there are many more issues for life safety which will define failure before collapse, including compartment breach.

Chapter 5

Heat transfer analysis of the Cardington frame fire tests using HADAPT

5.1 Introduction

The structural modelling of the Cardington Frame fire tests as part of the DETR/PiT project has highlighted the importance of the temperature evolution both temporally and spatially in determining the structural response. Restrained thermal expansion/contraction and thermal bowing are the main driving force behind almost all the structural phenomena witnessed in the tests.

The four British Steel fire tests carried out on the 8-storey composite steel and concrete building at Cardington have provided a wealth of information about the temperatures in the fire atmosphere and the protected and unprotected steel. Unfortunately there is considerably less information on the temperatures attained in the concrete slab. In tests 1-3 the temperatures through the depth of the slab have been recorded only at a few points and in terms of the structural modelling this has been just about adequate but there are no temperatures recorded in the slab in Test 4 (Office demonstration test).

The finite element program HADAPT developed by Usmani[108] has been used to model the heat transfer to the composite steel and concrete slab and to the protected and unprotected edge beams. HADAPT is a 2D adaptive heat transfer code capable of carrying out a non linear, transient, thermal analysis. The user has full control over the material properties and specification of the boundary conditions according to the fire atmosphere temperature regime, convection coefficient and resultant emissivity.
The measured temperatures in Tests 1-3 have been used to calibrate the models. The slab model was then used to predict the slab temperatures in Test 4.

5.2 Solving Transient Conduction using the Finite Element Method

The program HADAPT[108] allows the user to perform an adaptive heat transfer analysis for 2-D, plane or axisymmetric problems using the finite element method.

5.2.1 The Governing Differential Equations and Finite Element Formulation

The basic equations which describe transient heat conduction for an isotropic material may be written using temperature T as the independent variable as follows,

$$\nabla \cdot k(T)\nabla T - \rho c(T)\dot{T} = \dot{Q} \qquad \text{in} \quad \Omega \tag{5.1}$$

Here Ω is the problem domain ($\Gamma = \Gamma_T + \Gamma_q$ is its boundary), $k(T)$ is a symmetric conductivity tensor, ρ and c are density and specific heat and $\dot{Q}$ is the rate of internal heat generation.

The initial temperature field can be specified as,

$$T(x, y, z, 0) = T_o(x, y, z, 0) \qquad \text{in} \quad \Omega \tag{5.2}$$

The boundary conditions for prescribed temperature are,

$$T(x, y, z, t) = T_\gamma(x, y, z, t) \qquad \text{on} \quad \Gamma_T \tag{5.3}$$

and finally the boundary conditions for prescribed heat flux ($\bar{q}$), convection and radiation may be written as,

$$-k(T)\nabla T \cdot \mathbf{n} = \bar{q}(t) + h(t)(T - T_a) + \epsilon_s(t)\sigma(T^4 - T_a^4) \qquad \text{on} \quad \Gamma_q \tag{5.4}$$

where $h(t)$ is the convective heat transfer coefficient, ϵ_s is the resultant emissivity of the solid under consideration and σ is the Stefan-Boltzmann constant.

Standard Galerkin weighted residual method is used to derive the finite element form of the transient equation resulting in a spatially discretised system of ordinary differential equations in the form,

$$\mathbf{C}\dot{\mathbf{T}} + \mathbf{K}\mathbf{T} = \mathbf{F} \tag{5.5}$$

Here, $\mathbf{C}$ represents the global heat capacity matrix, $\mathbf{K}$ represents the global conductivity matrix and $\mathbf{F}$ represents the global *load* vector all obtained from the summation of the element matrices and vectors. To obtain the final set of algebraic equations (which may be solved using a digital computer) the time domain must also be discretised. This is normally done using a variety of finite difference approximations for the time derivative. Further details can be obtained from Huang and Usmani[108] where the model is also bench marked.

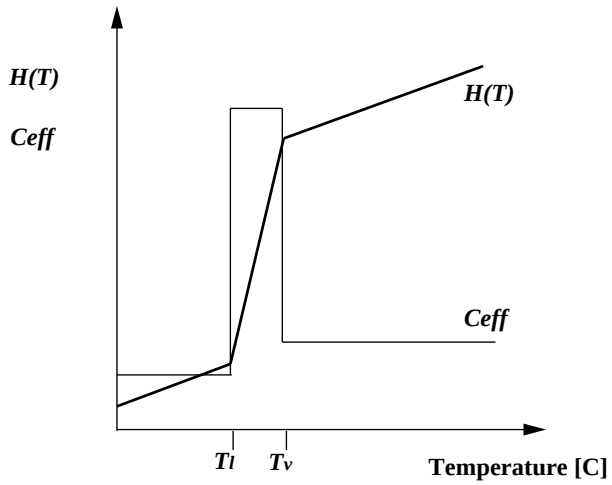

Figure 5.1: Typical variation of enthalpy (H) and c_{eff} with temperature

5.3 Modelling Phase Change

Phase transformations take place in familiar ways such as solidification, melting, vaporisation and condensation etc. The phase change from water to vapour involves latent heat of evaporation. Several methods have been used to take account of latent heat within different thermal analysis programs. The problem can be modelled by an effective heat capacity ($c_{\text{eff}} = \rho c$) for the material but if the phase change occurs over a very narrow range the large increase in heat capacity (as a result of the latent heat) may be missed in a numerical modelling context if the temperature change in one time step at a node or integration point straddles the phase change interval. This imposes severe restrictions on the temporal and spatial step sizes in a numerical analysis. Due to the step like behaviour of c_{eff} around the phase change interval, numerical oscillations may occur, making the achievement of a convergent solution difficult.

The program HADAPT deals with phase change using an enthalpy method. This involves integrating the effective heat capacity, c_{eff}, over the whole temperature range and thus enables the heat capacity to be modelled as a smooth function of temperature. Figure 5.1 illustrates the effective heat capacity (including the step change associated with latent heat of phase change) and the enthalpy method. To avoid numerical difficulties, a small interval of temperature is assumed over which the phase change occurs (although it is known to be isothermal for a constant pressure).

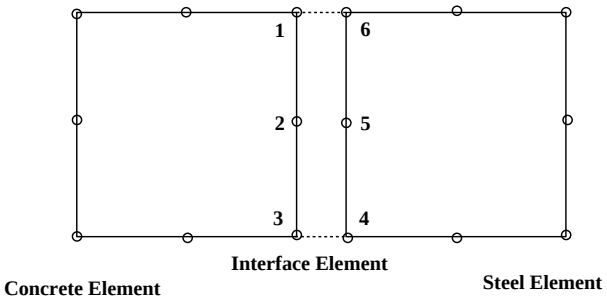

Figure 5.2: Interface element with its nodal connectivity

5.4 Interface Elements for modelling heat transfer between two materials

It is known that the steam pressure generated by evaporating moisture from concrete, separates the steel deck from the concrete quite early on in the fire. The temperature differential between the deck, the concrete slab and the air gaps that arise between the two materials is difficult to model using ordinary elements. This type of problem is best modelled using interface elements. There are a few methods for calculating interface heat transfer between two different materials in this instance an interface element of zero thickness has been used based on the Newtonian heat transfer model described by Equation 5.6.

$$q_f = h_f(T_{\text{steel}} - T_{\text{concrete}}) \tag{5.6}$$

Equation 5.6 can be considered as a constraint for the discretised heat transfer equations. In order to implement the use of interface elements the mesh must be generated in the whole domain so the elements in the steel and the concrete regions have no common nodes. An interface element is generated from the nodes on the coinciding faces of the steel and the concrete elements as shown in Figure 5.2. The stiffness matrix for the element is calculated by integrating over the length of the element as the width is zero.

5.5 The Models

Two models have been developed to model the temperature regime in the slab. The first model excludes the metal deck and enables quick sensitivity analyses of the parameters

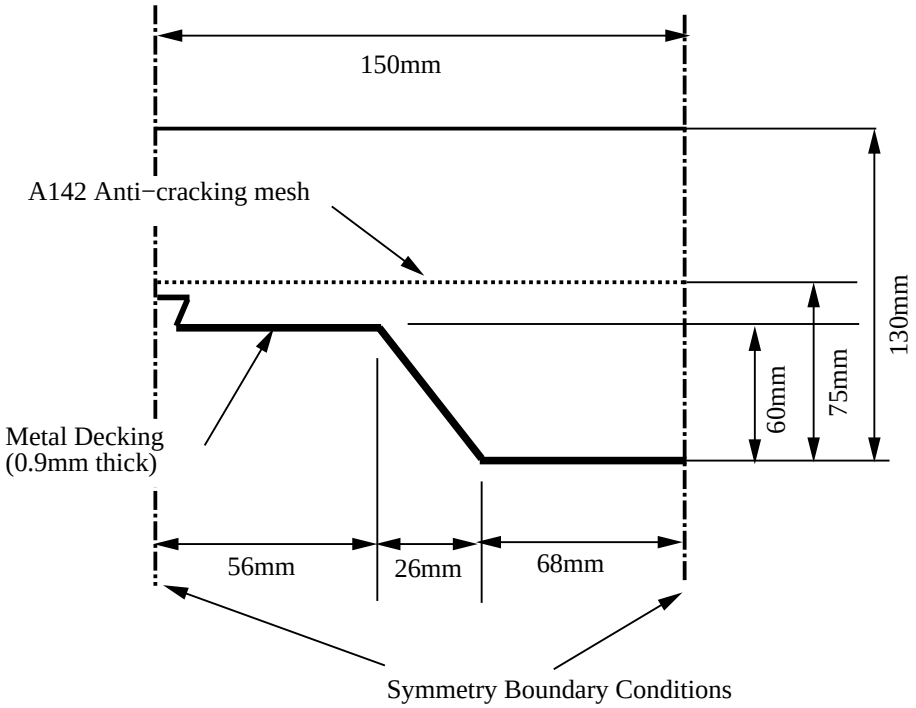

Figure 5.3: The concrete slab model

affecting the heat transfer in the concrete alone. The second and final model is a rigorous approach to the problem including the metal deck. The slab with the metal deck proved difficult to model, firstly because the steel is only 0.9mm thick (considerably thinner than the 130mm of concrete above it) and secondly because there is a high temperature differential between the hot steel and the adjacent cooler concrete. The mesh density in the region of the metal deck would have to be very concentrated. Using interface elements, (section 5.4) with zero thickness enabled the temperature gradient between the concrete and the metal deck to be modelled accurately without requiring excessive mesh refinement. Both models are a simple 2D representation of the whole slab with two symmetry boundary conditions to reduce the processing time. On the underside of the slab the boundary conditions are described by the temperatures achieved in the atmosphere during the compartment fire and a resultant emissivity and convection coefficient. On the top surface or cool side of the slab the boundary conditions are described by 20^{o}C ambient temperature and a convection coefficient. Figure 5.3 describes the model in detail and Figure 5.4 shows the mesh generated in the model including the metal deck.

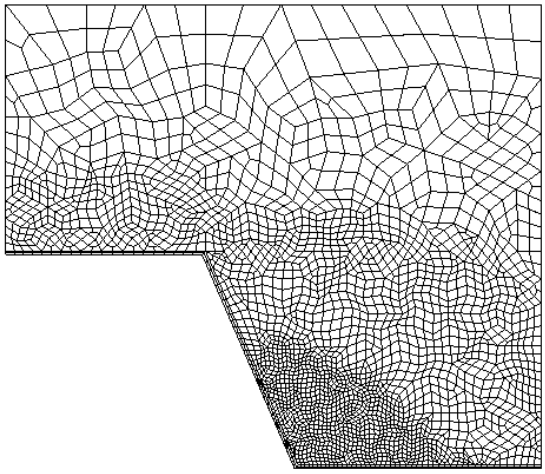

Figure 5.4: The mesh

Property	Concrete	Steel
ρ (kg/m^3)	1850	7850
c (J/kgK)	700	460
k (W/mK)	0.7	45.8
moisture content (%)	5	**
thickness (mm)	130	0.9

Table 5.1: Material Properties

5.5.1 Material Properties

The material properties of the lightweight concrete used in the 8-storey Cardington Frame are reasonably well known. The values for density, specific heat and conductivity are available from British Steel and in the form of technical reports from the producers of Lytag.[152,153] The evaporation of 5% by weight water between temperatures of 100^{o}C and 120^{o}C has been included. The moisture content of the concrete at Cardington was measured, but unfortunately the results are unavailable therefore 5% moisture was assumed. However Moore[164] believes the moisture content may have been between 10-12%. Table 5.1 includes a list of the material properties used in the model for the concrete and the steel metal deck. In the final model the temperature dependence of the conductivities and the specific heat of the steel were included. Temperature dependent properties for steel, including the spike in specific heat at 700^{o}C can be found in the literature.[158]

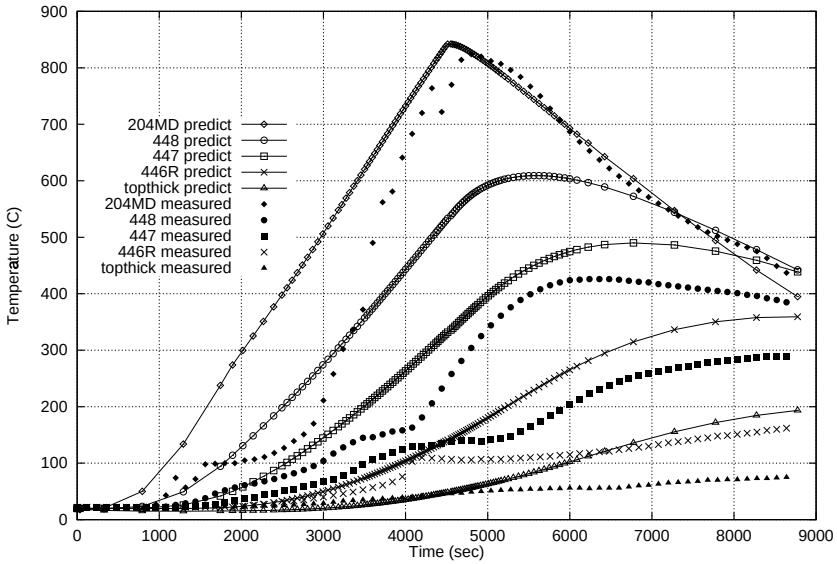

Figure 5.5: Predicted and measured concrete temperatures in Test 3 at CS1: No water evaporation, No metal deck

5.6 Modelling and Analysis

5.6.1 Model 1: No Metal Deck

The initial models analysed represented a concrete section without a metal deck. This was a reasonable approximation because the metal deck is only 0.9mm thick in comparison with a slab thickness of 130mm. This simple model also allowed sensitivity analyses to be carried out with reduced processing time.

The very first attempt at modelling the problem excluded water evaporation. These results were compared with a subsequent model which included the effect of water evaporation as a phase change to establish the full impact of moisture on the temperature evolution in the concrete slab. The second model predicted a lower temperature gradient in the slab at 100^oC but the plateau at 100^oC in the measured test data was not achieved in the predicted data. However, in later analyses when the moisture content in the model has been higher the plateau was observed in the predicted temperatures. This is discussed further in sections 5.6.2 and 5.6.3.3. Figures 5.5 and 5.6 illustrate the first two sets of results respectively compared with the measured temperatures recorded in the rib at cross section CS1, in test 3. The position of the thermocouples corresponding to the legend in these plots are illustrated in Figure 5.7.

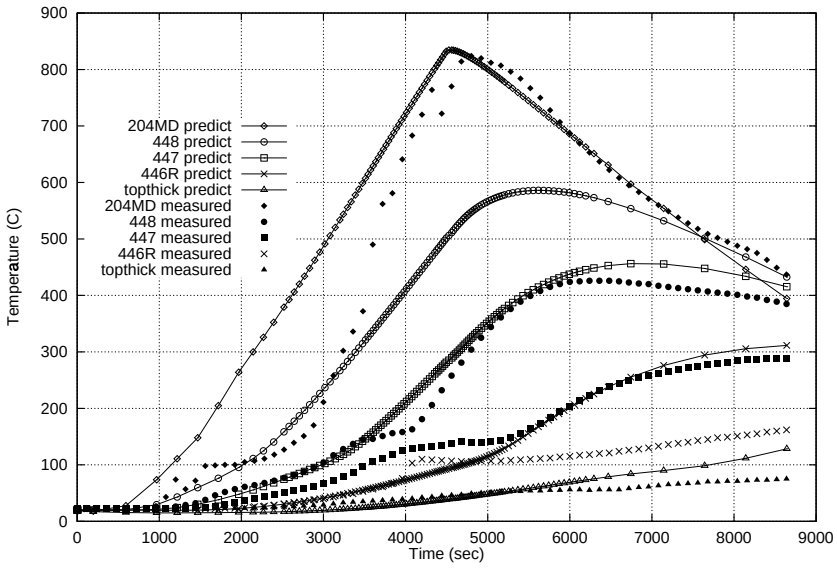

Figure 5.6: Predicted and measured concrete temperatures in Test 3 at CS1: Includes water evaporation, No metal deck

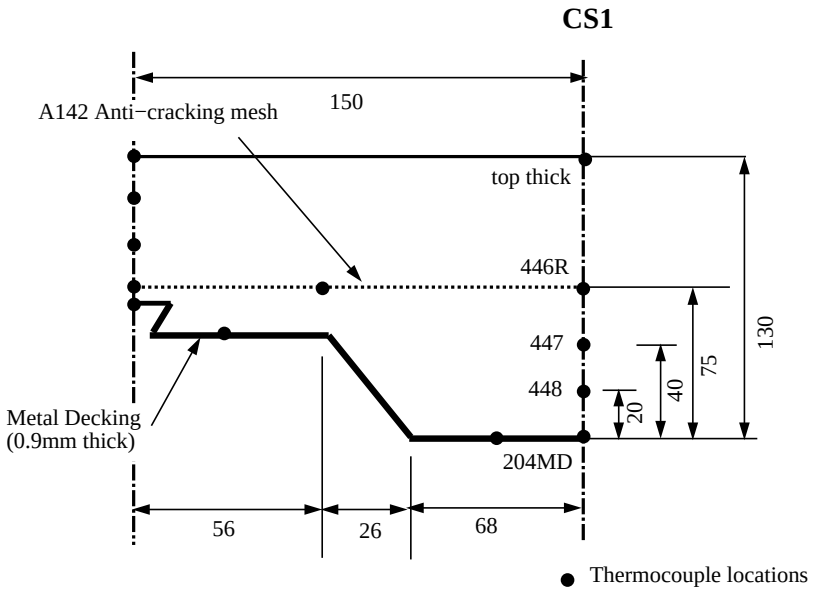

Figure 5.7: Thermocouple locations through the depth of the slab at CS1 in test 3

Variable		Coolest	Hottest	Reference
ρ	(kg/m^3)	2000	1800	1850
c	(J/kgK)	750	700	700
k	(W/mK)	0.3	1.0	0.7
m.c.	(%)	10	3	5
Evaporation Temperature	(^oC)	100-105	100-200	100-120
h (top)	(W/m^2K)	30	10	10
h (bottom)	(W/m^2K)	5	30	5
emissivity		0.4	0.9	0.6
thickness	(mm)	170	130	130

Table 5.2: Variables associated with the hottest and coolest slab

5.6.2 Hottest and Coolest slab

Probable extreme valuables of all relevant parameters were determined so that test results would be bracketed by an upper and lower bound solution of predicted temperatures referred to here as the hottest and coolest slab respectively. The lower bound was defined by subjecting the model to a series of parameters all of which would result in a cooler slab. For instance a low value for conductivity, a high moisture content and a high convection coefficient on the top of the slab with a low convection coefficient on the fire exposed face. The upper bound solution was achieved in a similar manner but with all the parameters affecting the slab temperature resulting in a hotter slab.

The variables, and the values assigned to them in order to obtain these solutions are listed in Table 5.2. The results can be seen in Figures 5.9 and 5.8 and it is clear that the coolest slab is a better representation of the actual slab temperatures during test 3. The results from the coolest slab also show a slight plateau in the concrete temperatures around 100^oC associated with the water being driven off. The plateau at 100^oC has been modelled here because the moisture content in the model is 10% twice that of the 5% assumed to be present in the Cardington slab and a better representation of localised moisture concentrations.
In the real slab the moisture levels at the dry-wet interface will be higher than the 5% applied to every node in the reference model.

5.6.3 Sensitivity Analyses

In order to establish the most influential parameters on the temperatures achieved in the concrete a sensitivity analysis was carried out on all the parameters defining the model and each was analysed separately. Using reference values for all other parameters.

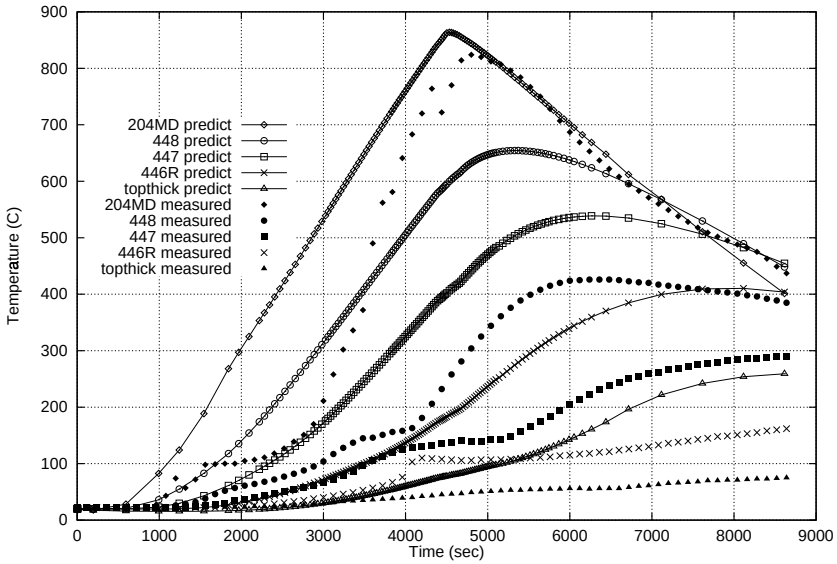

Figure 5.8: Predicted and measured concrete temperatures in Test 3 at CS1: Upper bound solution (HOTTEST SLAB), No metal deck

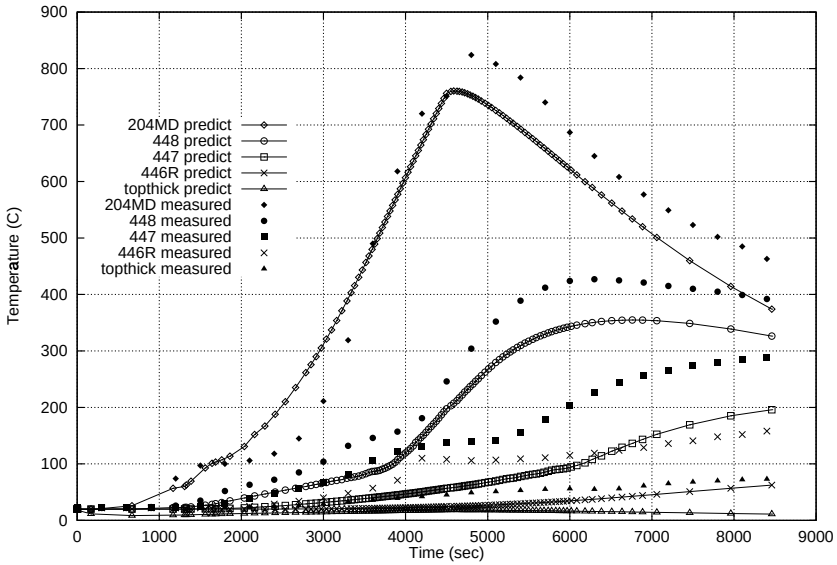

Figure 5.9: Predicted and measured concrete temperatures in Test 3 at CS1: Lower bound solution (COOLEST SLAB), No metal deck

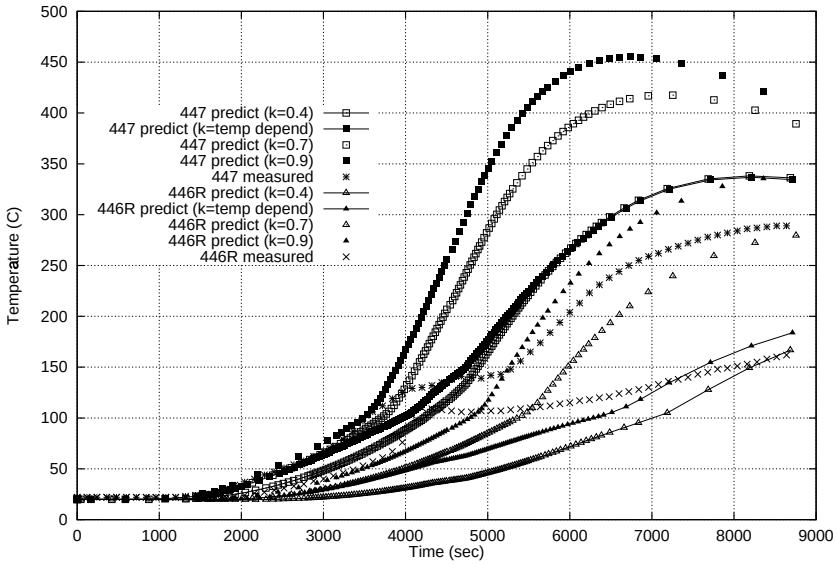

Figure 5.10: Predicted and measured concrete temperatures in Test 3 at CS1: Sensitivity of the predicted concrete temperatures to changes in conductivity

5.6.3.1 Varying Conductivity

The conductivity of the concrete has a significant impact on the predicted temperatures (Figure 5.10). As the conductivity applied is increased the predicted temperatures increase as expected. However, the temperature dependent conductivity gives very similar results to those predicted by k=0.4 W/mK and a better representation of the real temperatures.

5.6.3.2 Varying ρc

The material properties of the concrete used in the Cardington Frame are reasonably well known but there is still a range of values for density and specific heat over which the sensitivity of the model should be tested.

Figure 5.11 shows there is very little dependence on the values of ρc used to model the concrete and as the material values are reasonably well known they will remain at ρ=1850kg/m^2 and c=700kJ/kgK.

5.6.3.3 Varying moisture content

The moisture content in the slab is a key issue. The plateau experienced at 100^{o}C can be seen clearly in the measured concrete temperatures. The dependence of the predicted temperatures to moisture content is plotted in Figure 5.12. As the moisture content

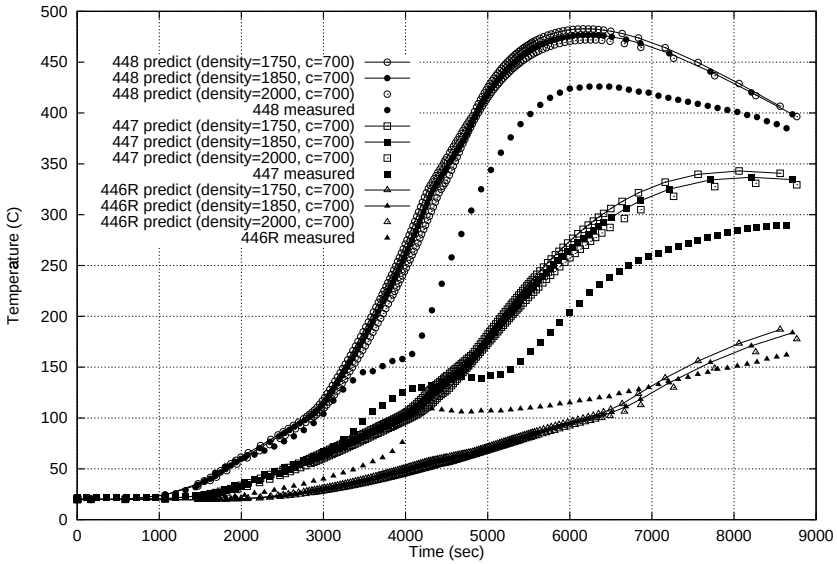

Figure 5.11: Predicted and measured concrete temperatures in Test 3 at CS1: Sensitivity of the predicted concrete temperatures to changes in density and specific heat

increases the predicted concrete temperatures decrease as expected. The temperature range over which the moisture evaporates was also an issue to be investigated because the pore pressure building up in the concrete will increase the temperature range over which the water can evaporate. Indeed, the Eurocode recommends a temperature range between 100-200^{o}C.[76] In this model the dependence on the range for moisture evaporation is insignificant (Figure 5.13).

5.6.3.4 Varying Emissivity

The effective emissivity associated with radiative heat transfer is dependent on many factors including the emissivity of the flames, the compartment walls and the slab itself. The resultant emissivity of steel and concrete is about 0.7 and 0.6 respectively. The emissivity in this sensitivity analysis was varied between 0.4 and 1.0 shown in Figure 5.14. It is clear that changing the resultant emissivity in the model has some effect on the predicted temperature particularly in the concrete near the fire. The temperature in the atmosphere (measured during the tests) will have a bigger impact on the radiative heat transfer because of the T^4 dependence (Equation 5.4).

5.6.3.5 Varying Convection Coefficients

Heat Transfer by radiation dominates the temperature regime in the later stages of the fire but the convection coefficient can not be ignored. The convection coefficient

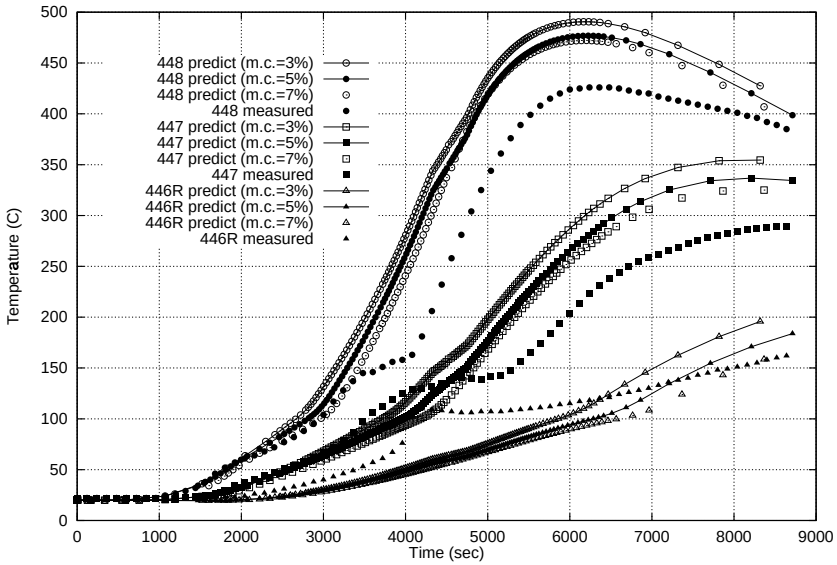

Figure 5.12: Predicted and measured concrete temperatures in Test 3 at CS1: Sensitivity of the predicted concrete temperatures to changes in moisture content

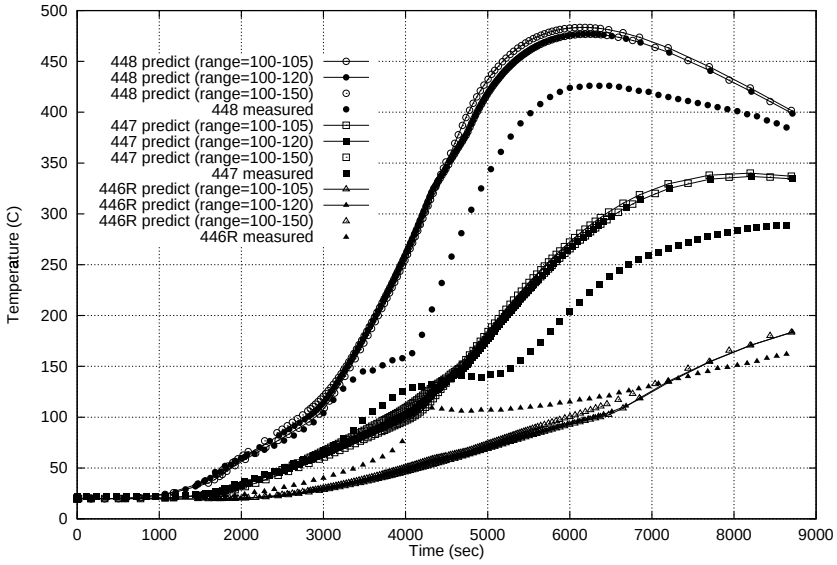

Figure 5.13: Predicted and measured concrete temperatures in Test 3 at CS1: Sensitivity of the predicted concrete temperatures to changes in the temperature range for water evaporation (5% moisture content)

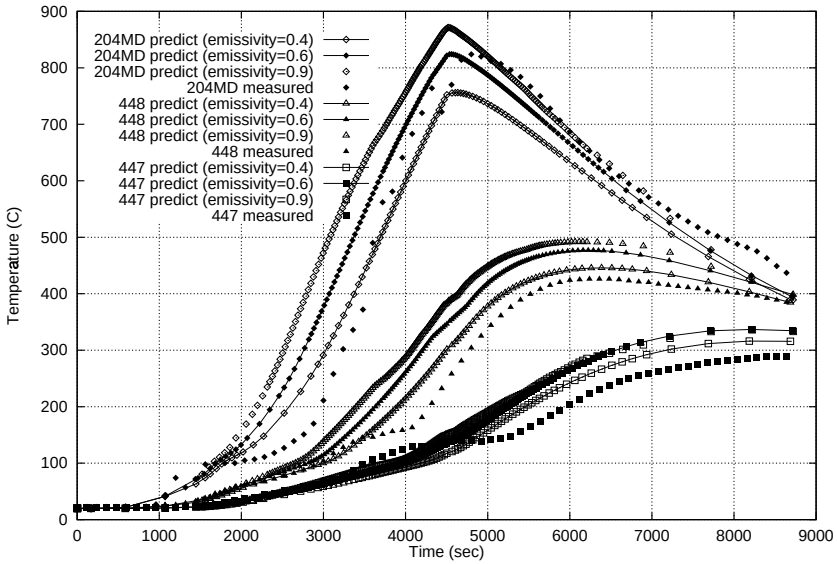

Figure 5.14: Predicted and measured concrete temperatures in Test 3 at CS1: Sensitivity of the predicted concrete temperatures to changes in resultant emissivity

on the fire exposed face of the slab was taken as $23 W/m^2K$[195] and $10 W/m^2K$ on the top surface. However, the convection coefficients applied to the model to obtain the lower bound solution or coolest slab were $5 W/m^2K$ and $30 W/m^2K$ on the bottom and top respectively. The sensitivity analysis of these parameters indicate a stronger dependence on convection than initially thought. Changing the convection coefficient on the unexposed face made little difference to the slab temperatures (compare Figures 5.15 and 5.16). However, increasing the convection coefficient to the exposed face made a significant difference. This is shown in both Figure 5.15 and 5.16. A convection coefficient of $5 W/m^2K$ applied to the fire exposed face of the slab model is very low but it may be compensating for the metal deck missing in this model. As the fire tests progress the metal deck is known to separate from the rest of the slab creating a layer of air which will act like an insulator thus maintaining the slab at a much cooler temperature than the concrete only model. The metal deck itself will also have an impact as a heat sink but any effect would be very small.

5.6.3.6 Varying Slab Thickness

The slab thickness was considered because the Cardington frame slab varies in depth by up to 40mm. The design value is 130mm from the base of the ribs to the top of the slab but in some places it can be up to 170mm thick. This increase in concrete may have been maintaining the slab at a lower temperature than the model would predict. Figure 5.17 shows the thickness of the concrete has very little or no impact on the

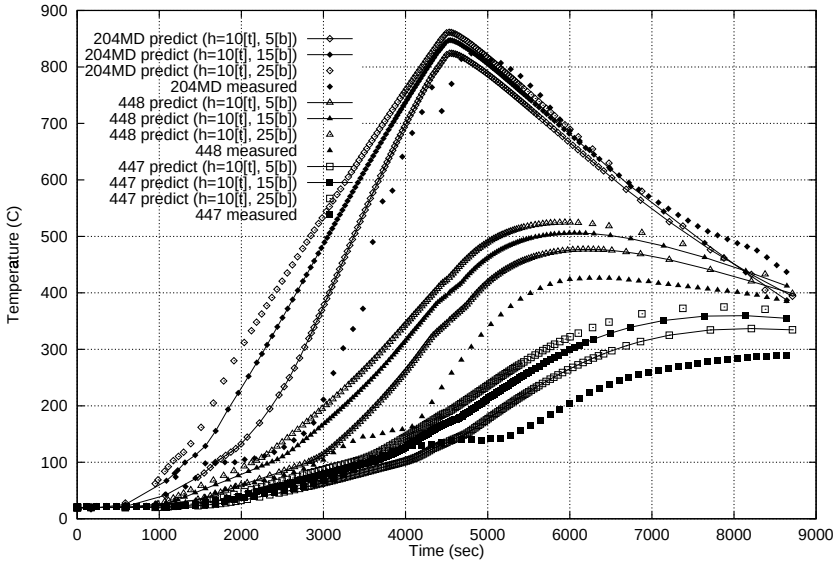

Figure 5.15: Predicted and measured concrete temperatures in Test 3 at CS1: Sensitivity of the predicted concrete temperatures to changes in convection coefficient

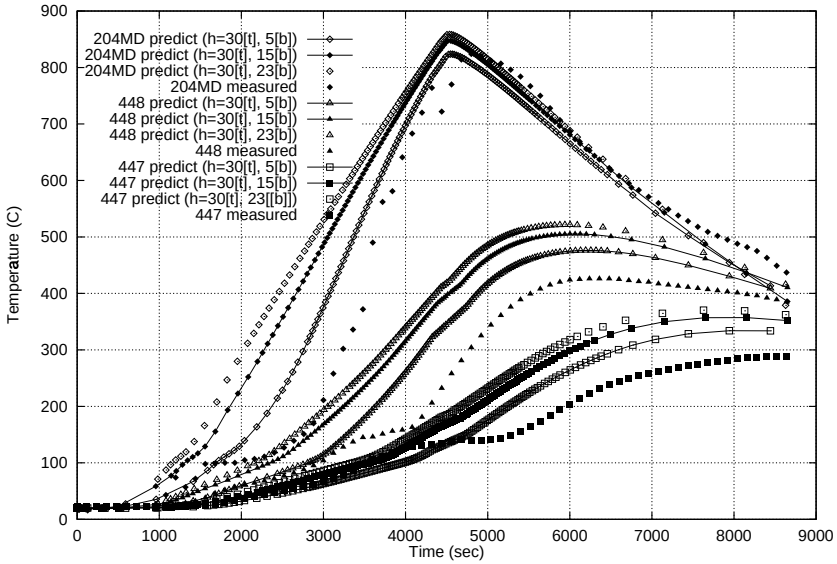

Figure 5.16: Predicted and measured concrete temperatures in Test 3 at CS1: Sensitivity of the predicted concrete temperatures to changes in convection coefficient

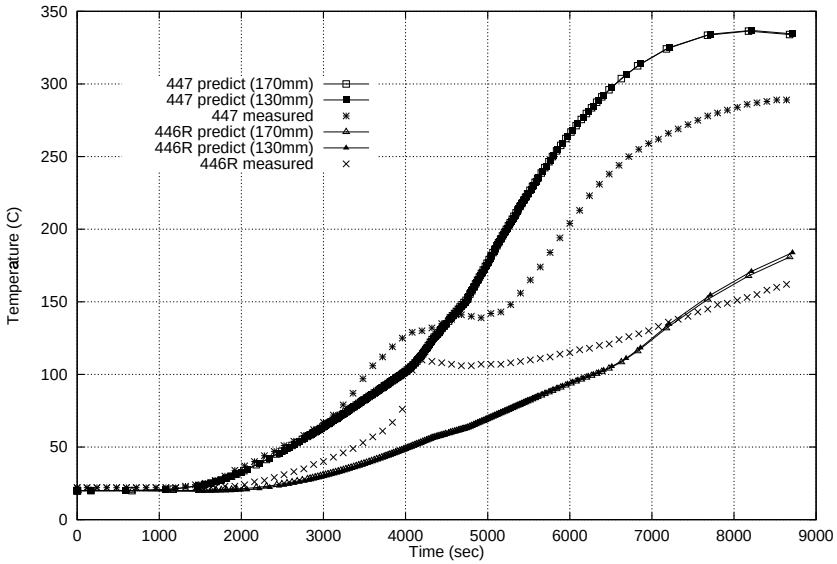

Figure 5.17: Predicted and measured concrete temperatures in Test 3 at CS1: Sensitivity of the predicted concrete temperatures to changes in slab thickness

predicted temperatures of concrete.

5.6.4 Summary

The key factors affecting the predicted temperatures are undoubtedly conduction, moisture content and convection coefficient applied to the fire exposed face of the slab although the latter may be due to the absence of the metal deck.

5.6.5 Correlation with measured temperatures

The results of the final model excluding metal deck included temperature dependent conductivity, ρ=1850kg/m^3, c=700J/kgK, 5% moisture over 100-120^{o}C, resultant emissivity of 0.6 and convection coefficients of 5W/m^{2}K and 10W/m^{2}K on the fire exposed surface and top of the slab respectively and are shown in Figure 5.18. The correlation is very good although the model slightly over predicts the actual temperatures. The concrete alone with a low convection coefficient on the fire exposed surface is a very good representation of the metal deck.

5.7 Model 2: Including the Metal Deck

A rigorous model of the heat transfer to the Cardington frame slab should include the metal deck. The conductivity and specific heat of the steel are included as temperature

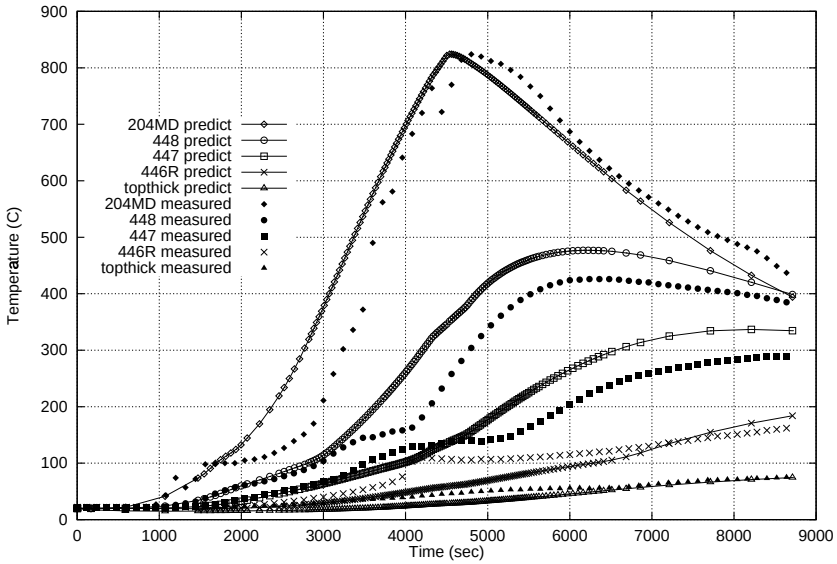

Figure 5.18: Test 3 Predicted and measured temperatures at CS1, No metal deck

dependent properties and the phase change at 700^{o}C is also modelled. The methodology used in the model with concrete alone is applied to the concrete in this model but the resultant emissivity is raised to 0.7 and the convection coefficient on the fire exposed face raised to 15W/m^{2}K. The results for test 3 are shown in Figure 5.24. The correlation with the measured temperatures is very good in terms of the concrete temperatures, especially near the top surface where the temperatures never reach 100^{o}C although the metal deck temperatures seem to be over predicted in the earlier stages of the fire.

Figures 5.19-5.23 show the model results at various atmosphere temperatures throughout the analysis. The distinction between the highly conductive metal deck temperatures and the low conductivity is clearly evident. The area of concrete at the lower corner of the rib reaches higher temperatures because heat is transferred to the rib through both boundaries. Temperatures on the unexposed side are higher above the trough than the rib as expected. Figures 5.22-5.23 show the temperature contours towards the end of the analysis. Although the fire is in decay and atmosphere temperatures are decreasing, concrete temperatures are still rising. The metal deck and the region of concrete near the metal deck are cooler at the end of the analysis than the concrete at the centre of the model. This is because the steel deck responds very quickly to the change in atmosphere temperature and heat is still dissipating through the concrete.

By applying the atmosphere temperatures of test 1 and test 2 as boundary conditions to

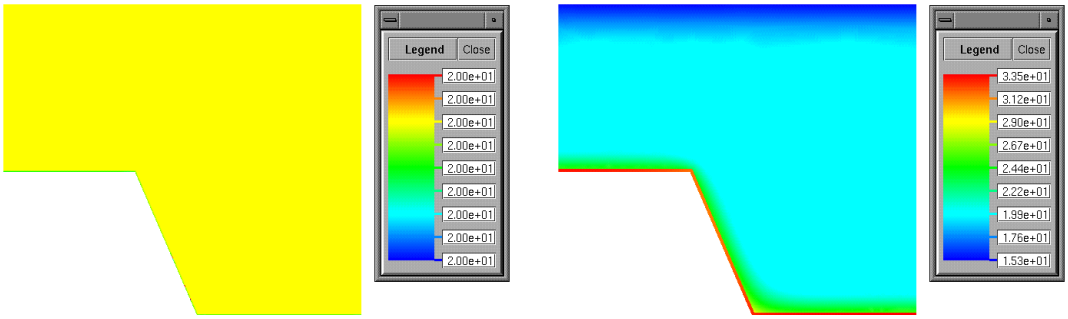

(a) atm. T=20^{o}C (b) atm. T=187^{o}C

Figure 5.19: Test 3 Predicted temperature profile (heating)

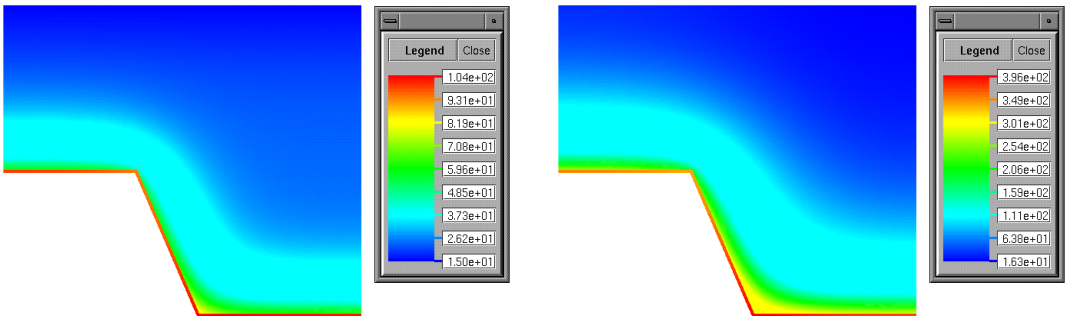

(a) atm. T=327^{o}C (b) atm. T=610^{o}C

Figure 5.20: Test 3 Predicted temperature profile (heating)

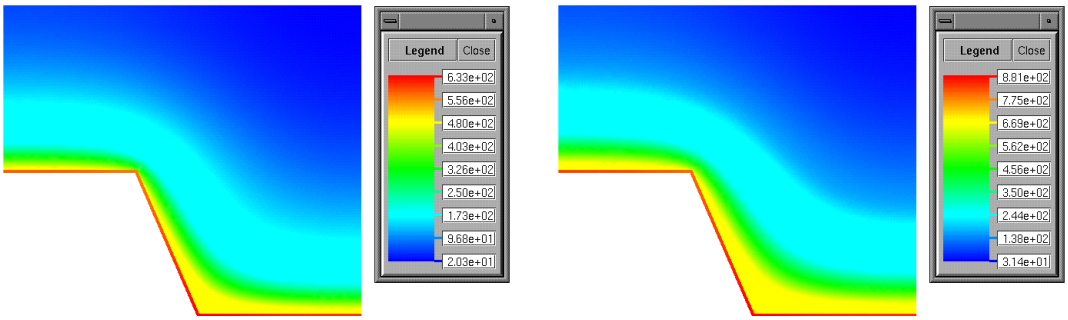

(a) atm. T=771^{o}C (b) atm. T=932^{o}C

Figure 5.21: Test 3 Predicted temperature profile (heating)

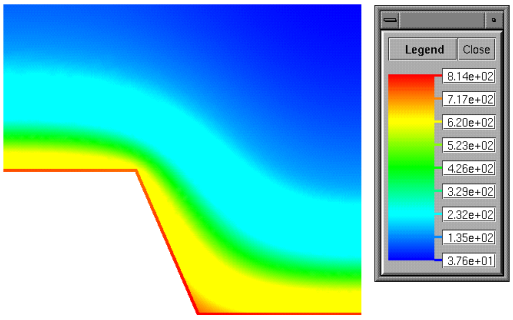

(a) atm. T=848^{o}C

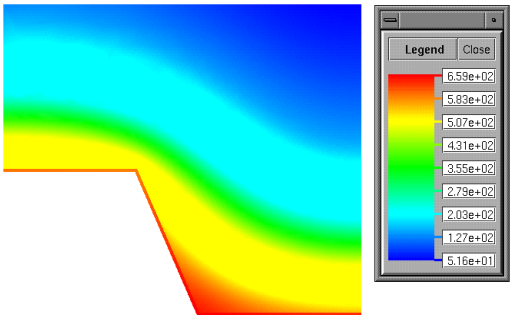

(b) atm. T=667^{o}C

Figure 5.22: Test 3 Predicted temperature profile (cooling)

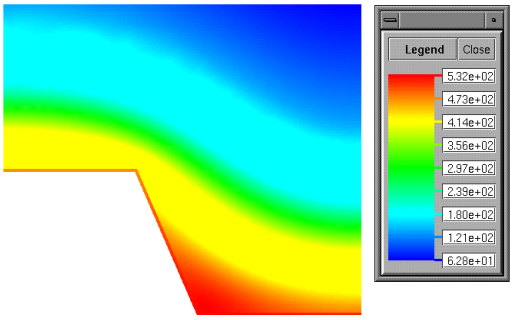

(a) atm. T=505^{o}C

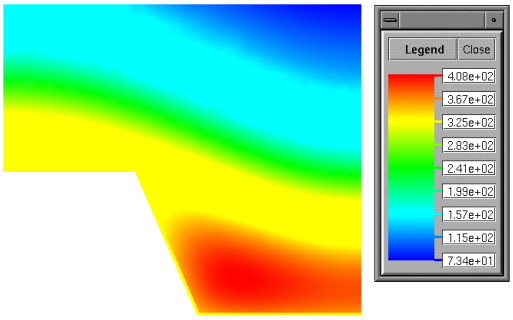

(b) atm. T=305^{o}C

Figure 5.23: Test 3 Predicted temperature profile (cooling)

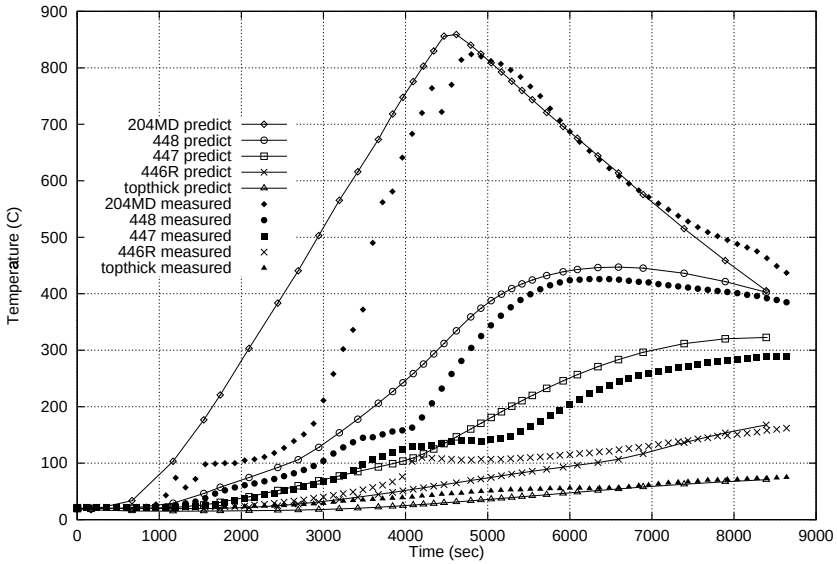

Figure 5.24: Test 3 Predicted and measured temperatures at CS1, includes metal deck

the model, the concrete temperatures in these tests were also predicted and compared with the appropriate measured temperatures. These results can be seen in Figures 5.26 and 5.27 and the locations of the relevant thermocouples are illustrated in Figure 5.25. Once again the metal deck temperatures are over predicted but the correlation with the temperatures in the depth of the slab is very good. The lack of correlation with steel temperatures in the earlier stages of the fires can be explained by the poor representation of high localised moisture concentrations. In the real slab the local moisture levels at the dry-wet interface will be higher than the 5% applied to every node in the model.

5.7.1 Prediction of Test 4 Temperatures

During British Steel test 4 the concrete temperatures were not recorded hindering accurate structural modelling. The model calibrated against the temperature data measured in Tests 1-3 has been used to predict the temperatures in Test 4. The measured atmosphere temperatures in test 4 were applied as a boundary condition. The predicted concrete temperatures have enabled an accurate structural analysis to be made of test 4.[175]

5.8 Modelling Edge beams

Edge beams in a compartment fire invariably experience heat on one side and ambient conditions on the other. This results in a large temperature gradient over the cross

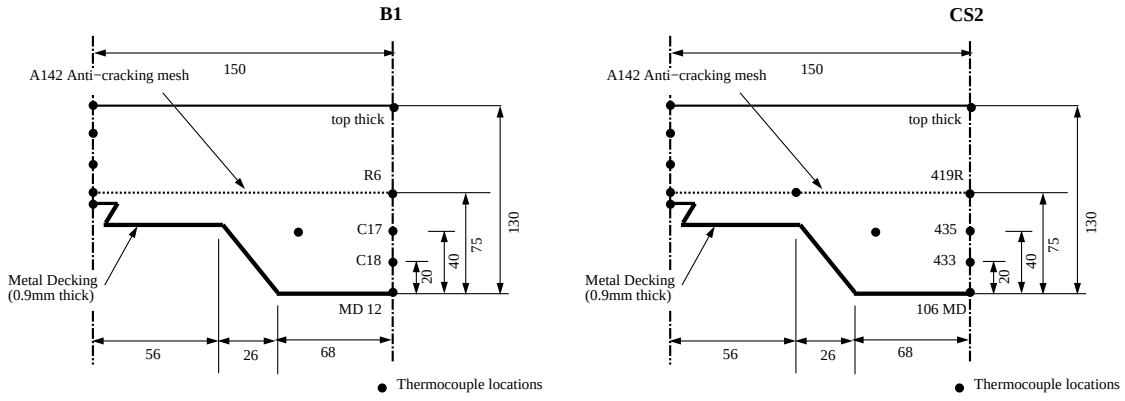

(a) Test 1 (b) Test 2

Figure 5.25: Thermocouple locations in the depth of the slab in Test 1 and Test 2

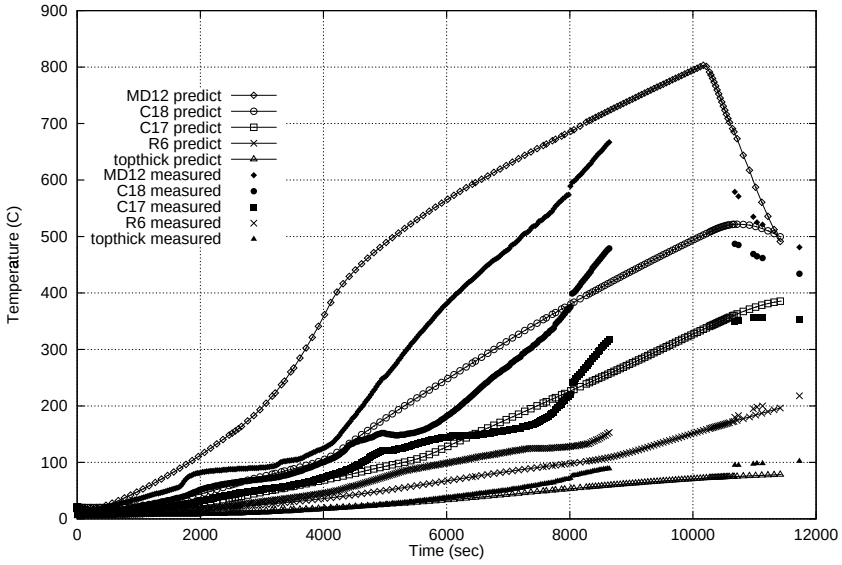

Figure 5.26: Test 1 Predicted and measured temperatures at B1, includes metal deck

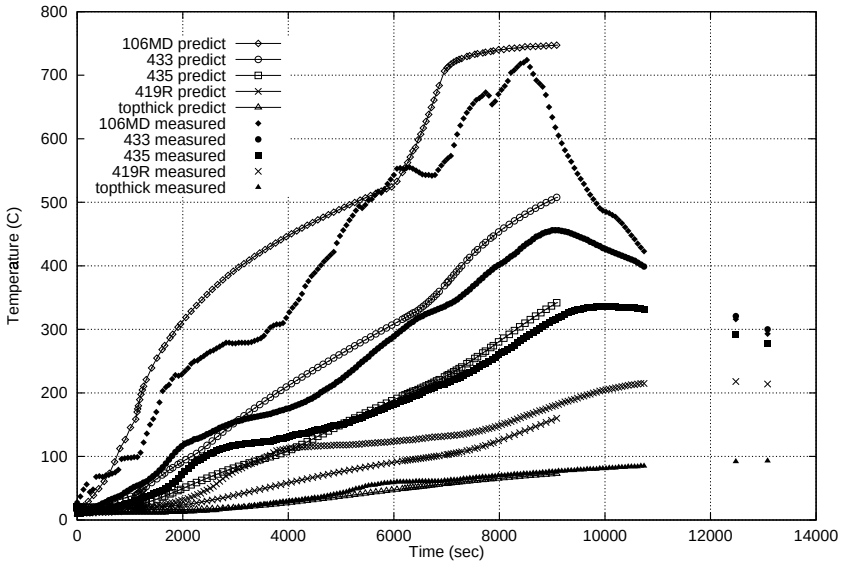

Figure 5.27: Test 2 Predicted and measured temperatures at CS2, includes metal deck

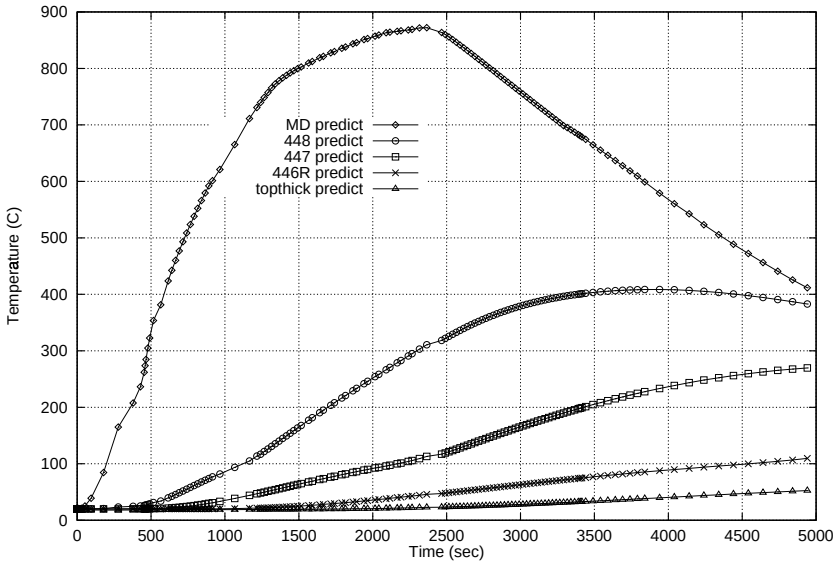

Figure 5.28: Test 4 Predicted temperatures at CS1, includes metal deck

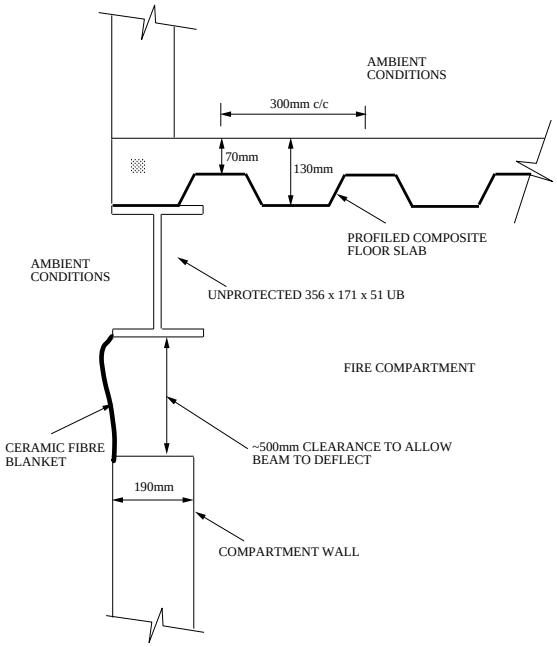

Figure 5.29: Cross section through an unprotected edge beam in Test 4

section which cannot be modelled by simple lumped mass heat transfer equations, such as those in EC 3 part 1.2. HADAPT has been adopted to carry out a 2D analysis of the protected and unprotected edge beams at Cardington.

Figures 5.29 and 5.30 illustrate the 2D scenarios which exist. During test 4 the edge beams were unprotected. This scenario is drawn in Figure 5.29. In test 3 the edge beams had applied fire protection (Figure 5.30). In both tests courses of blockwork were removed from immediately below the edge beams to allow the beams to deflect downwards.

5.8.1 Edge beams in British Steel Test 3

The edge beams in British Steel test 3 were protected with Vicuclad protection. The thermal characteristics of which are detailed in Table 5.4. Vicuclad has a moisture content of about 2-3% although this depends on ambient conditions. Unlike gypsum and other similar products Vicuclad only contains free water not chemically bound water.[64] The heat transfer model assumes a convection coefficient of $15 W/m^2$ on the fire exposed surfaces and $10 W/m^2$ on the unexposed. The resultant emissivity to the exposed surfaces is 0.7. The thermal properties of all the materials making up the slab, beam and fire protection are listed in Table 5.3.

The mesh and a sample contour plot of the temperatures are given in Figures 5.31 and 5.32 respectively. The profiled slab was simplified to a uniform depth of 130mm. This

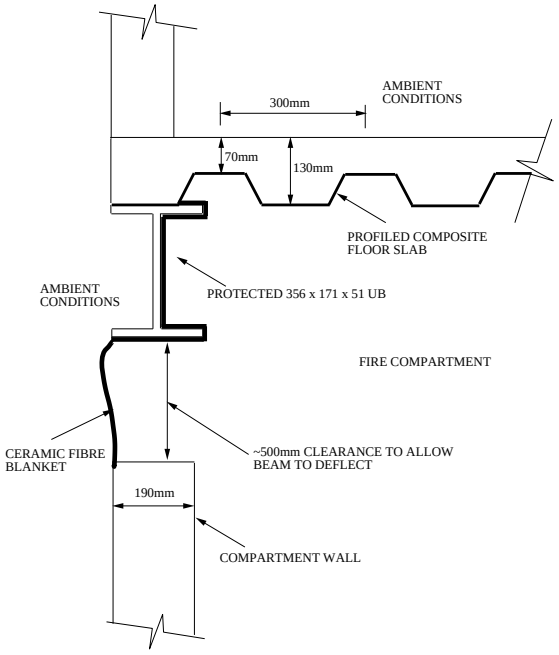

Figure 5.30: Cross section through a protected edge beam in Test 3

Property	Concrete slab	Steel beam	Vicuclad protection
ρ (kg/m^3)	1850	7850	400
c (J/kgK)	700	460	1150
k (W/mK)	0.7	45.8	0.14
moisture content (%)	5	**	3
thickness (mm)	130	**	25

Table 5.3: Material Properties in the Edge beam and Column models

Temperature (C)	k (W/mK)	ρ (kg/m^3)	c (J/kgK)
20	0.14	400 (350-455)	1150
200	0.16		
400	0.19		
600	0.22		
700	0.24 (extrapolated value)		

Table 5.4: Properties of Vicuclad at elevated temperatures. Provided by Promat Technical Department 7/6/2000[64]

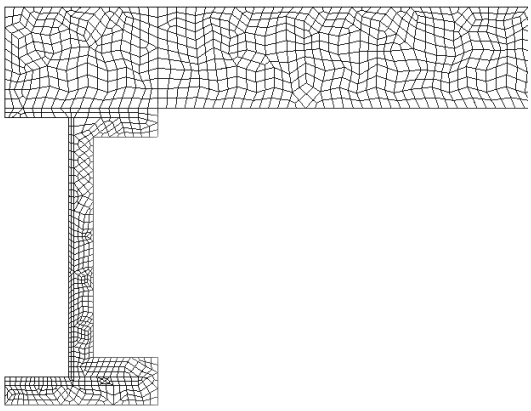

Figure 5.31: Test 3: The mesh used to model protected edge beam

was assumed because the heat sink effect of the slab is still accurately modelled and the geometry of the model is simpler. Figure 5.33 shows the position of the thermocouples along the steel beams in test 3. Two sets of measured data, at locations G and K on gridline F, are compared with the predicted results. The location of the thermocouples at positions G and K are shown in Figure 5.34. The numbering of the thermocouples was adopted in the legend of the results shown in Figures 5.35 and 5.36. At location F the predicted and measured temperatures of the lower flange are in reasonable agreement (Figure 5.35). The upper flange temperatures are also in good agreement (Figure 5.36) although the web temperatures are under predicted. At location K the web temperatures correlate well with measured data and the lower flange is under predicted (Figure 5.37). The model over-predicts temperatures in the early stages this may be due to higher moisture concentrations in the Vicuclad protection than represented in the model. The lower flange temperatures are also over predicted at temperatures around 100^{o}C (Figure 5.38).

5.8.2 Edge beams in British Steel Test 4

A plan of the test 4 compartment is illustrated in Figure 5.39 showing the locations of the test thermocouples. Positions B3 and B11 were chosen for comparison with the model. Ventilation was provided along gridline 4 and position B3 is directly above an opening. The thermocouple labels (Figure 5.40) are adopted in the legends of the plotted results. The measured and predicted results at B3 are plotted in Figure 5.41 and the correlation is good. Discrepancies are as a result of local atmosphere temperatures. Atmosphere temperatures in the model were taken as close to the beam as possible but temperatures at the edge of the compartment near the ventilation could have been

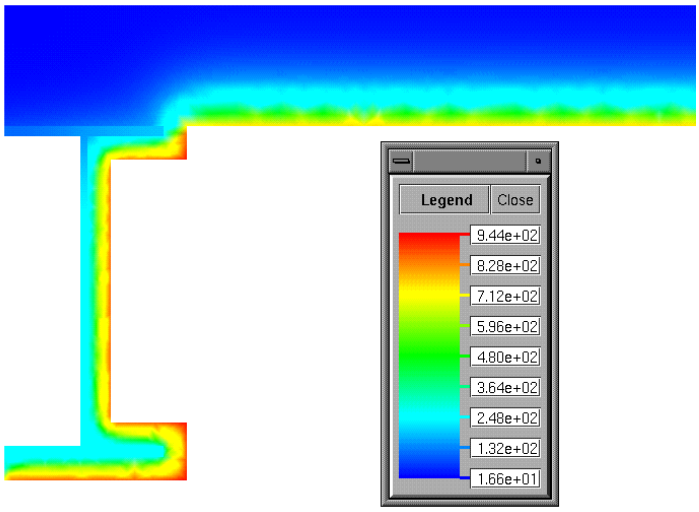

Figure 5.32: Test 3: 2D HADAPT contour plot of the protected edge beam

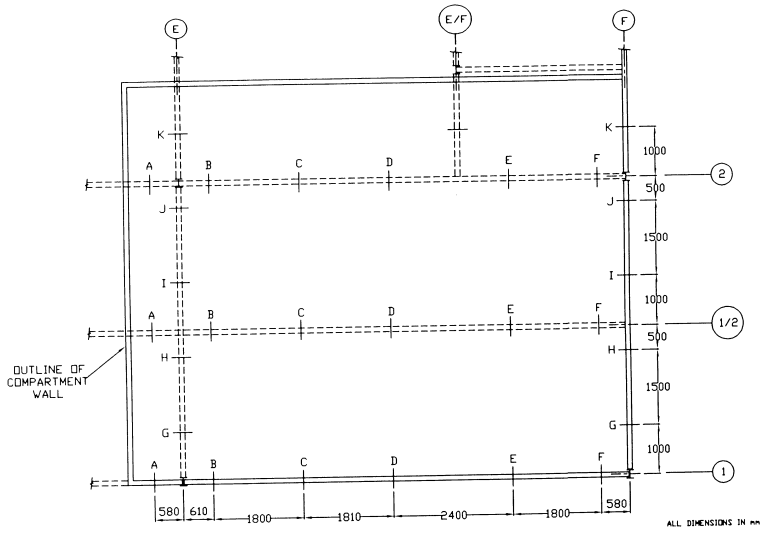

Figure 5.33: Test 3: Plan of test compartment showing location of thermocouples for measuring beam temperature profiles

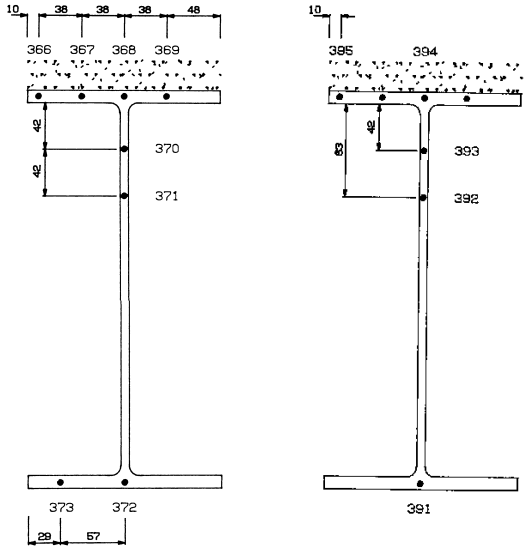

(a) Location G (b) Location K

Figure 5.34: Test 3: Location of thermocouples in protected edge beam on gridline F

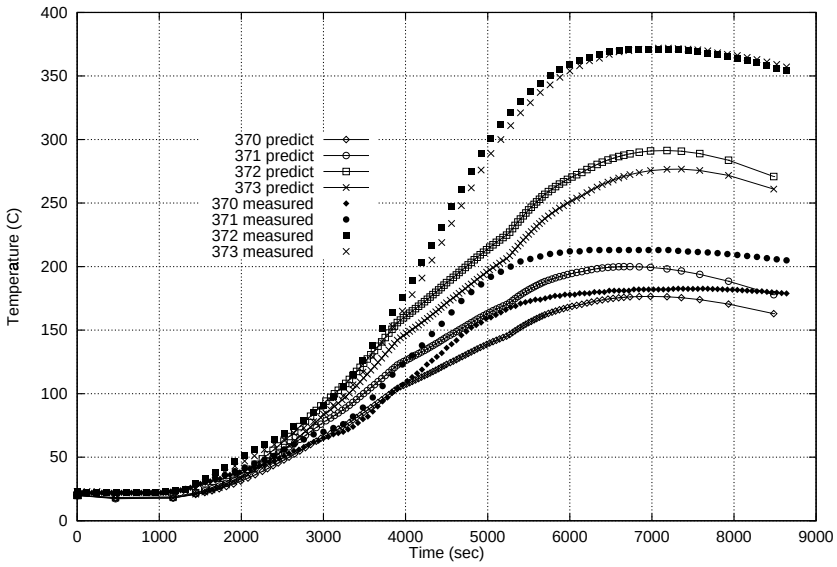

Figure 5.35: Test 3: comparison between predicted and measured steel temperatures in the web and lower flange of the edge beam on gridline F at location G

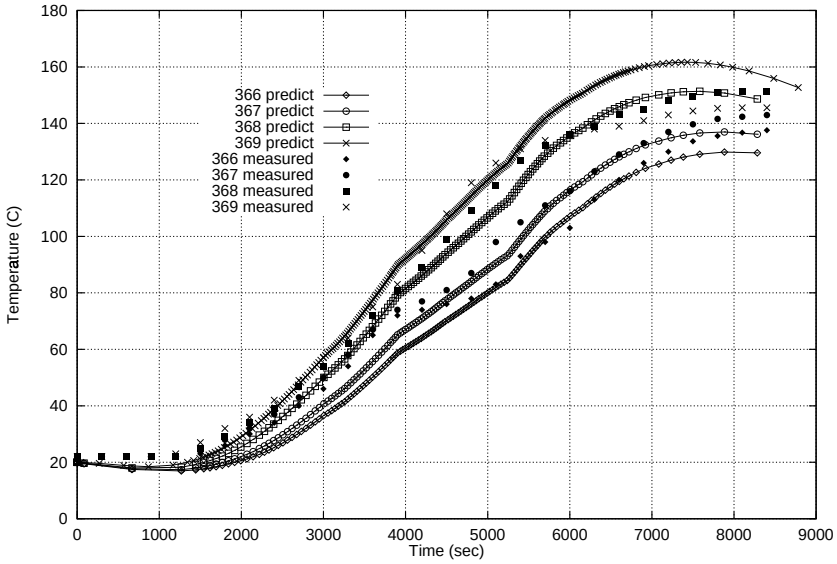

Figure 5.36: Test 3 comparison between predicted and measured steel temperatures in the top flange of the edge beam on gridline F at location G

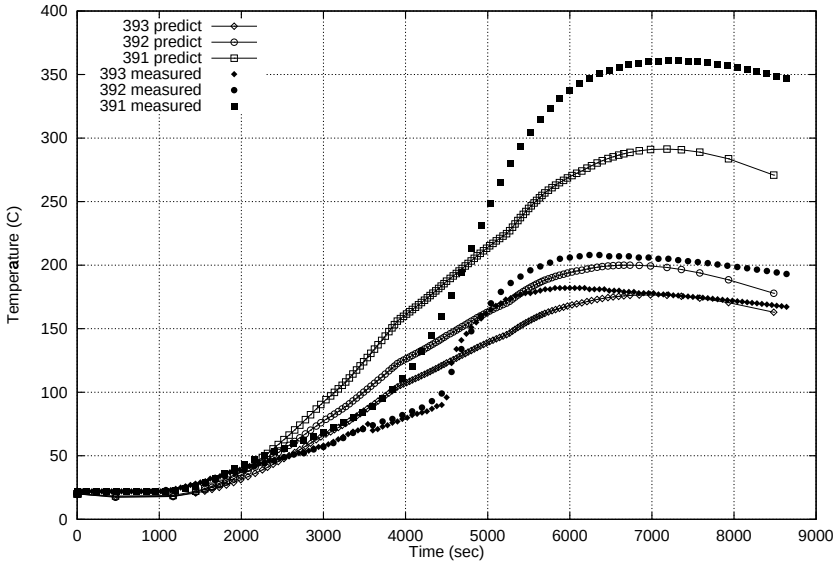

Figure 5.37: Test 3: comparison between predicted and measured steel temperatures in the web and lower flange of the edge beam on gridline F at location K

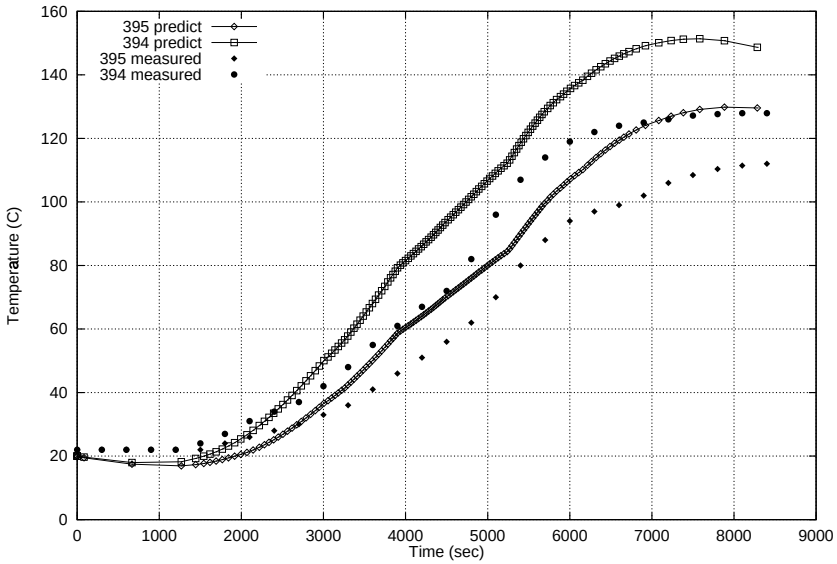

Figure 5.38: Test 3 comparison between predicted and measured steel temperatures in the top flange of the edge beam on gridline F at location K

very variable. At B11 (Figure 5.42) the measured and predicted temperatures are also in reasonable agreement.

5.9 Conclusions

In general this relatively simple model has predicted the measured temperatures in the slab in the first three British Steel fire tests. The predicted temperatures do not show a pronounced plateau at 100^oC. This is because localised moisture concentrations may be considerably higher than the 5% included uniformly distributed in the model. The model including the metal deck over-predicts the steel temperatures but predicts the concrete temperatures very well. Again the over-prediction of the steel temperatures is obviously due to the inadequacies inherent in the model when modelling moisture evaporation. In terms of obtaining reliable slab temperatures for a structural analysis this type of heat transfer model is more than adequate. It also has the advantage of being very efficient and quick to use. The slab temperatures in tests 1-3 have been modelled satisfactorily and the predicted temperatures for test 4 where there was no such data can be assumed to be reliable. Moreover, these temperatures will be invaluable to any group attempting to model and analyse the structural behaviour in British Steel test 4.

The protected and unprotected edge beam temperatures were also predicted with reasonable accuracy. Discrepancies were probably a direct result of local heating effects.

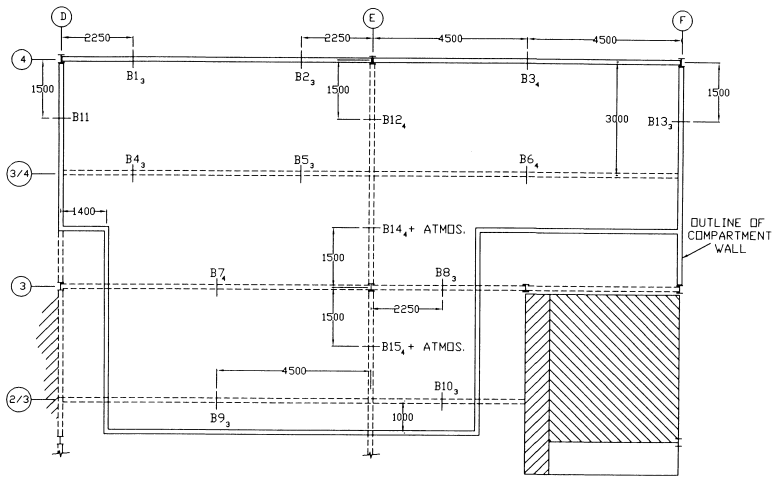

Figure 5.39: Test 4: Plan of test compartment showing location of thermocouples for measuring beam temperature profiles

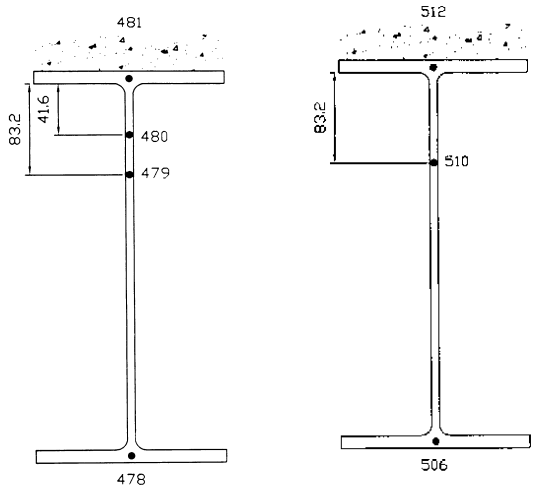

(a) Gridline 4 location b3

(b) Gridline D location b11

Figure 5.40: Test 4: Location of thermocouples in the unprotected edge beams

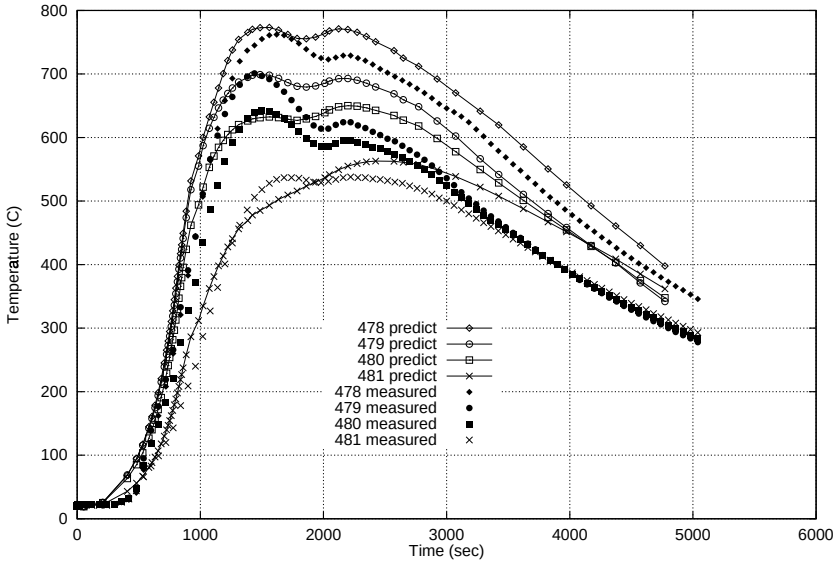

Figure 5.41: Test 4 comparison between predicted and measured temperatures in edge beam on gridline 4 position B3

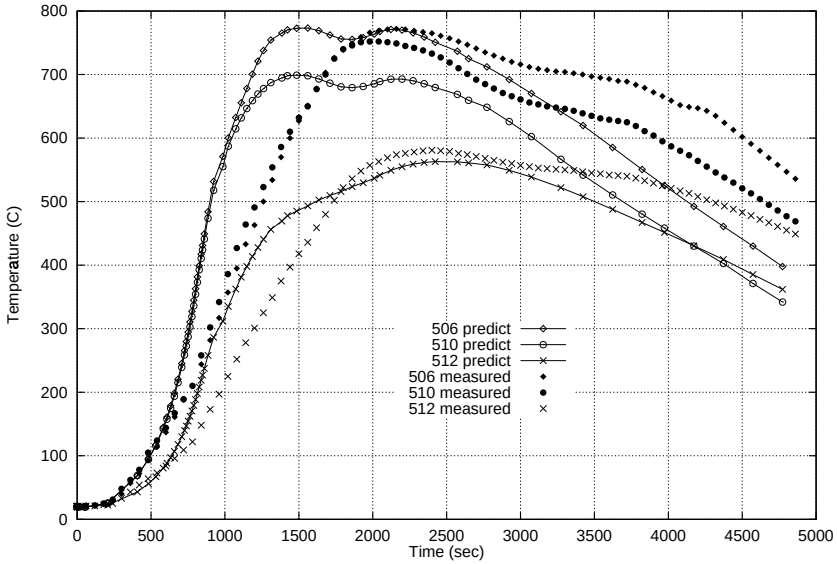

Figure 5.42: Test 4 comparison between predicted and measured temperatures in edge beam on gridline D position B11

Chapter 6

Analytical and numerical analysis of simple beam models in fire

6.1 Introduction

In all the Cardington Frame tests and in accidental compartment fires in redundant, multi-storey, steel framed composite buildings, very large deflections can be observed in the beam and slab elements in the region of the fire. This chapter describes early work carried out as part of the PiT project *"Behaviour of steel framed structures under fire conditions"*[187] to understand these deflections.

Analytical and numerical models of simple beams were analysed to explain the structural behaviour in response to increasing temperature and growing thermal gradient through the depth of the beam. The temperature and gradient along the beam were uniform at all times. Several end restraint conditions were analysed from fully fixed to simply supported (axially unrestrained).

"Runaway" failures in axially unrestrained beams occur at relatively low temperatures. The reasons for this are explained by analysing displacements and forces which show different load carrying mechanisms in restrained and unrestrained beams.

These simple studies made the complex behaviour observed in the numerical models of the Cardington Frame fire tests much easier to interpret.

6.2 Thermal expansion and thermal bowing Interaction

There are two main effects of heating on structural members, thermal expansion caused by an increase in mean temperature and thermal bowing caused by a non-uniform distribution of temperature over the depth of the member. In real structures in fire these two effects act together. Both effects result in thermal strains. If these thermal strains are restrained mechanical strains develop. The most fundamental relationship that governs this behaviour in structures is:

$$\epsilon_{\text{total}} = \epsilon_{\text{thermal}} + \epsilon_{\text{mechanical}} \tag{6.1}$$

with

$$\sigma = f(\epsilon_{\text{mechanical}}) \qquad \delta = f(\epsilon_{\text{total}})$$

The total strains govern the deformed shape of the structure δ, through kinematic or compatibility considerations. The stress state in the structure σ (elastic or plastic) depends only on the mechanical strains. Where the thermal strains are free to develop

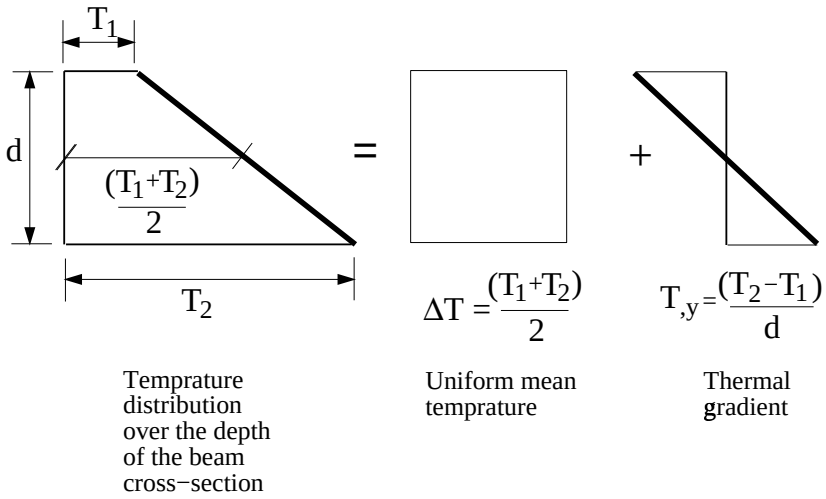

Figure 6.1: Uniform mean temperature and through depth thermal gradient over the cross-section of a beam.

in an unrestricted manner and there are no external loads, axial expansion or thermal bowing results from,

$$\epsilon_{\text{total}} = \epsilon_{\text{thermal}} \qquad \text{and} \qquad \epsilon_{\text{total}} \rightarrow \delta \tag{6.2}$$

By contrast, where thermal expansion strains are fully restrained without external loads, thermal stresses and plastification result from

$$0 = \epsilon_{\text{thermal}} + \epsilon_{\text{mechanical}} \qquad \epsilon_{\text{mechanical}} \rightarrow \sigma \tag{6.3}$$

6.2.1 The heating regime

Figure 6.1 illustrates the temperature regime in a beam heated from underneath. The actual temperature distribution through the depth of the beam can be split into two components consisting of a uniform mean temperature rise (ΔT) and a gradient ($T_{,\text{y}}$).

6.2.2 Thermal expansion

Figure 6.2 illustrates the response of three beams with different support conditions to a uniform mean temperature rise with zero thermal gradient through the depth. Figure 6.2(a) illustrates a simply supported, axially unrestrained beam typical of the type of

arrangement often tested in standard fire resistance tests. The mean temperature rise results in a thermal expansion strain ($\epsilon_{\mathrm{T}} = \alpha\Delta T$) and a simple longitudinal extension ($\epsilon_{\mathrm{T}} l$) of the unrestrained beam. All thermal strains are absorbed in displacements with no mechanical strains (as described by Equation 6.4).

$$\epsilon_{\mathrm{total}} = \epsilon_{\mathrm{t}} = \epsilon_{\mathrm{T}} = \alpha\Delta T \qquad \epsilon_{\mathrm{mechanical}} = \epsilon_{\mathrm{m}} = 0 \tag{6.4}$$

In an axially restrained pin ended beam thermal expansion is restrained (Figure 6.2(b)) initially there is a build up of compressions, P, with no deflections (assuming no transverse load). The mechanical strains are equal and opposite to the induced thermal strains and the total strains (ϵ_{t}) equal zero.

$$\epsilon_{\mathrm{t}} = \epsilon_{\mathrm{T}} + \epsilon_{\mathrm{m}} = 0 \tag{6.5}$$

$$\epsilon_{\mathrm{m}} = -\epsilon_{\mathrm{T}}$$

The forces P equate to:

$$P = EA\epsilon_{\mathrm{m}} = -EA\epsilon_{\mathrm{T}} = -EA\alpha\Delta T \tag{6.6}$$

where,
E =The Young's modulus of the material (N/mm^2)
A =Cross-sectional area of the beam (mm^2)

If the beam is stocky an indefinite increase in temperature will lead to yielding as described by Equation 6.7. Assuming a steel beam $\Delta T_{,\mathrm{y}}$ equals 140^oC.

$$\Delta T_y = \frac{\sigma_y}{E\alpha} \tag{6.7}$$

σ_y =Yield stress of the material (N/mm^2)

However beams are generally slender and an increase in temperature will lead to buckling. The Euler buckling load is described by Equation 6.8. By equating this load to

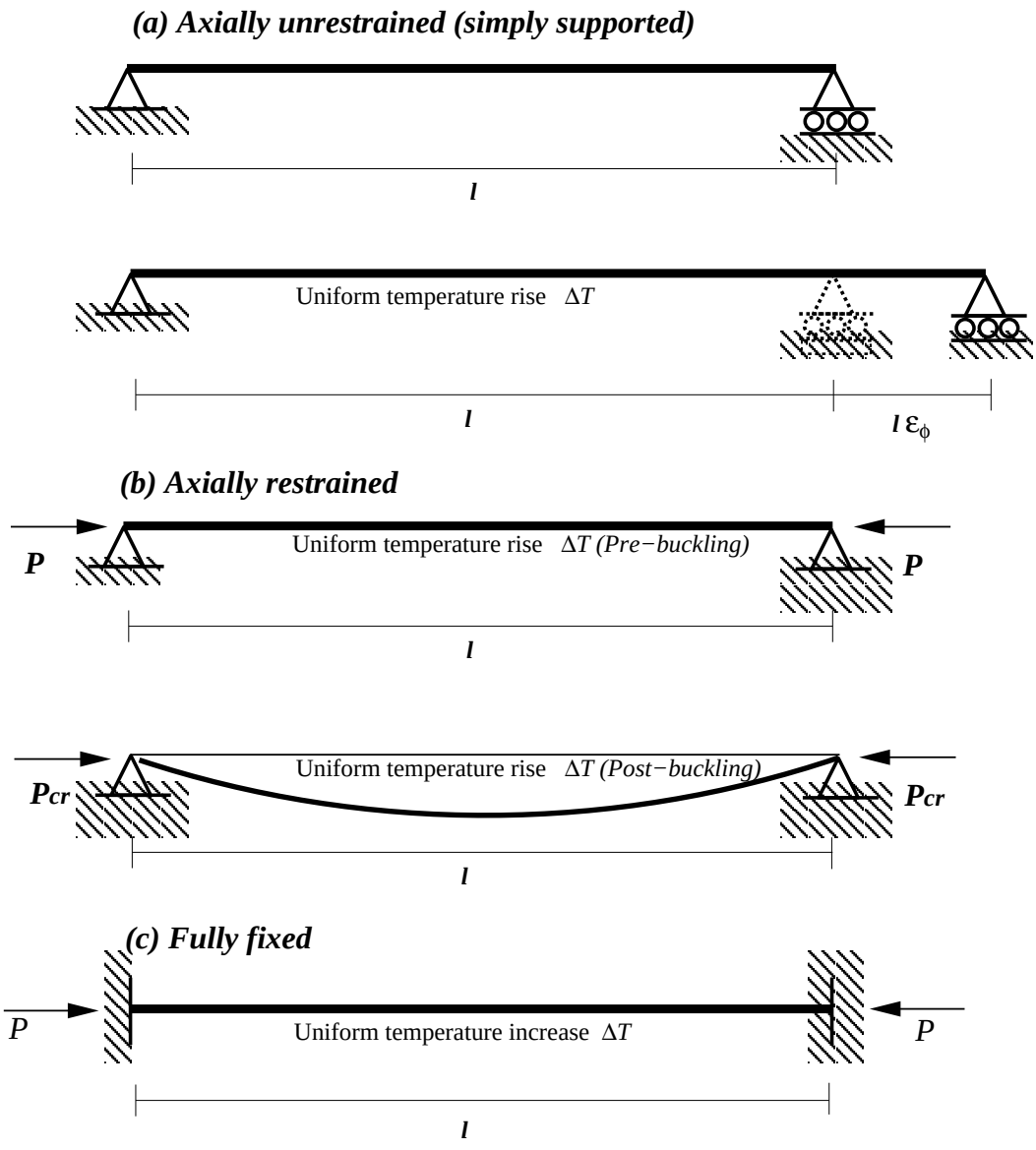

Figure 6.2: Thermal expansion in simple beams with different restraint conditions

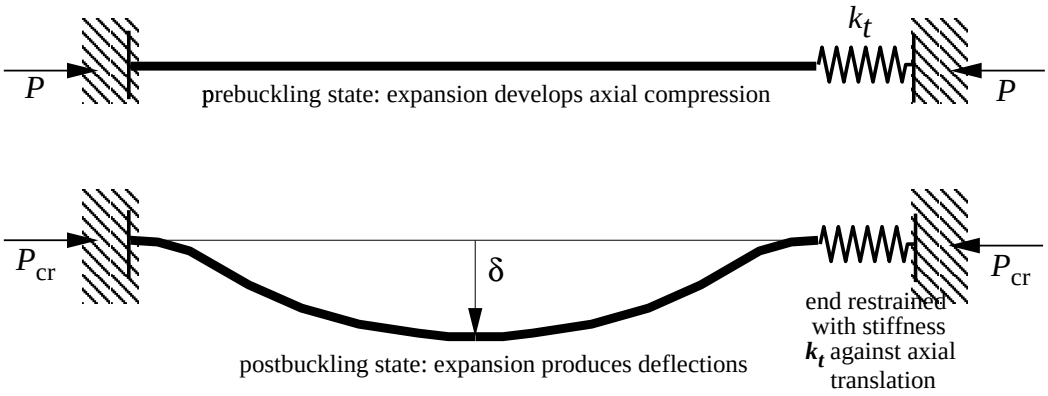

Figure 6.3: Thermal expansion against finite lateral restraints

the restraining force P a critical buckling temperature ΔT_{cr} can be derived (Equations 6.8-6.10). In the post-buckling regime the thermal strains are absorbed by deflections with less need for mechanical straining.

$$P_{\text{cr}} = \frac{\pi^2 EI}{l^2} \tag{6.8}$$

$$EA\alpha\Delta T = \frac{\pi^2 EI}{l^2} \tag{6.9}$$

$$\Delta T_{\text{cr}} = \frac{\pi^2}{\alpha}\left(\frac{r}{l}\right)^2 \Longrightarrow \Delta T_{\text{cr}} = \frac{\pi^2}{\alpha\lambda^2} \tag{6.10}$$

I =Second moment of area of the beam cross section (mm^4)
$\frac{l}{r} = \lambda$ =slenderness ratio of the beam
l =effective length of the beam (mm)
r =radius of gyration of the beam (mm)

Figure 6.2(c) illustrates a fully fixed beam. The force necessary for this beam to buckle is four times that of the pinned case.
In real structures the level of restraint against axial translation will be between pinned and fully fixed. If the ends are restrained with stiffness k_t against axial translation (Figure 6.3) the compressive axial stress and critical buckling temperature can also be derived.

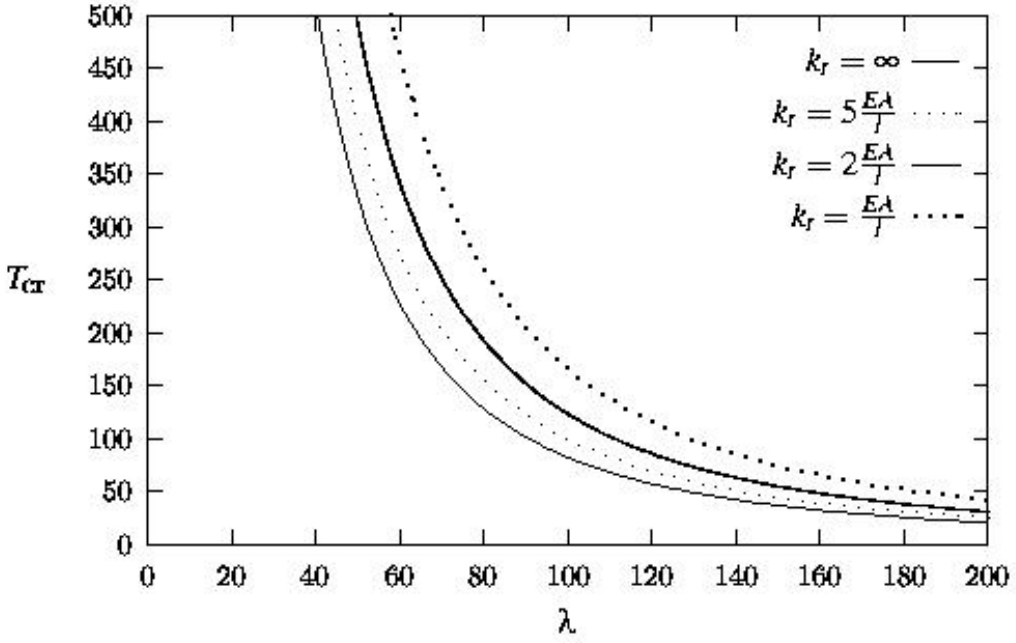

Figure 6.4: Buckling temperatures for thermal expansion against finite lateral restraints (Usmani *et al*[249])

$$\sigma = \frac{E\alpha\Delta T}{(1 + \frac{EA}{k_t l})} \tag{6.11}$$

$$\Delta T_{\rm cr} = \frac{\pi^2}{\alpha\lambda^2}\left(1 + \frac{EA}{k_t l}\right) \tag{6.12}$$

Figure 6.4 plots critical buckling temperature against slenderness ratio, λ, for various translational stiffnesses. There is only a factor of two difference between the critical buckling temperature with infinite restraint ($k_t = \infty$) and a restraint stiffness equal to that of the beam axial stiffness itself ($k_t = \frac{EA}{L}$). Moreover, during heating the stiffness properties of the beam are decreasing thus the level of restraint required is also decreasing. The level of restraint required to cause buckling in a real structure in fire is relatively small. This is illustrated in the Cardington tests where internal beams restrained only by hot edge beams buckled allowing large deflections to develop relieving mechanical strains.

6.2.3 Thermal Bowing

Beams and slabs subjected to fire inevitably develop thermal gradients over their depth. This gradient can be represented by Equation 6.13,

$$T_{,\mathrm{y}} = \frac{T_2 - T_1}{d} \tag{6.13}$$

where,
T_2 =Temperature of the exposed face
T_1 =Temperature of the unexposed face
d =depth of the section

Figure 6.5 shows the same three restraint conditions as before but this time in response to a uniform temperature gradient $T_{,\mathrm{y}}$ with no mean temperature rise. In all cases a uniform curvature is induced along the length of the beam $\phi = \alpha T_{,\mathrm{y}}$. When the beam is axially unrestrained this reduces the distance between the ends of the beam (Figure 6.5(a)). This can be interpreted as a contraction strain ϵ_ϕ described by Equation 6.14. When the ends are pinned (axially restrained but rotationally free) the contraction strain ϵ_ϕ generates a tensile force P causing a P-Δ moment over the length of the beam. In the fully fixed case rotations cannot happen therefore a uniform moment, $M = EI\phi$, develops along the length of the beam (Figure 6.5(c)). In many real structures the rotational stiffness (k_r) will fall between fully fixed and pinned conditions (Figure 6.6). The restraining moment in the rotational springs can be described by equation 6.15.

$$\epsilon_\phi = 1 - \frac{\frac{sinl\phi}{2}}{\frac{l\phi}{2}} \tag{6.14}$$

$$M = \frac{EI\alpha T_{,\mathrm{y}}}{(1 + \frac{2EI}{k_r l})} \tag{6.15}$$

6.2.4 Combined thermal expansion and thermal bowing

In this discussion so far, thermal bowing and thermal expansion effects have been treated separately but in reality they act together. The concept of effective strain described by Equation 6.16 allows the combined effects of thermal expansion and thermal bowing to be analysed.

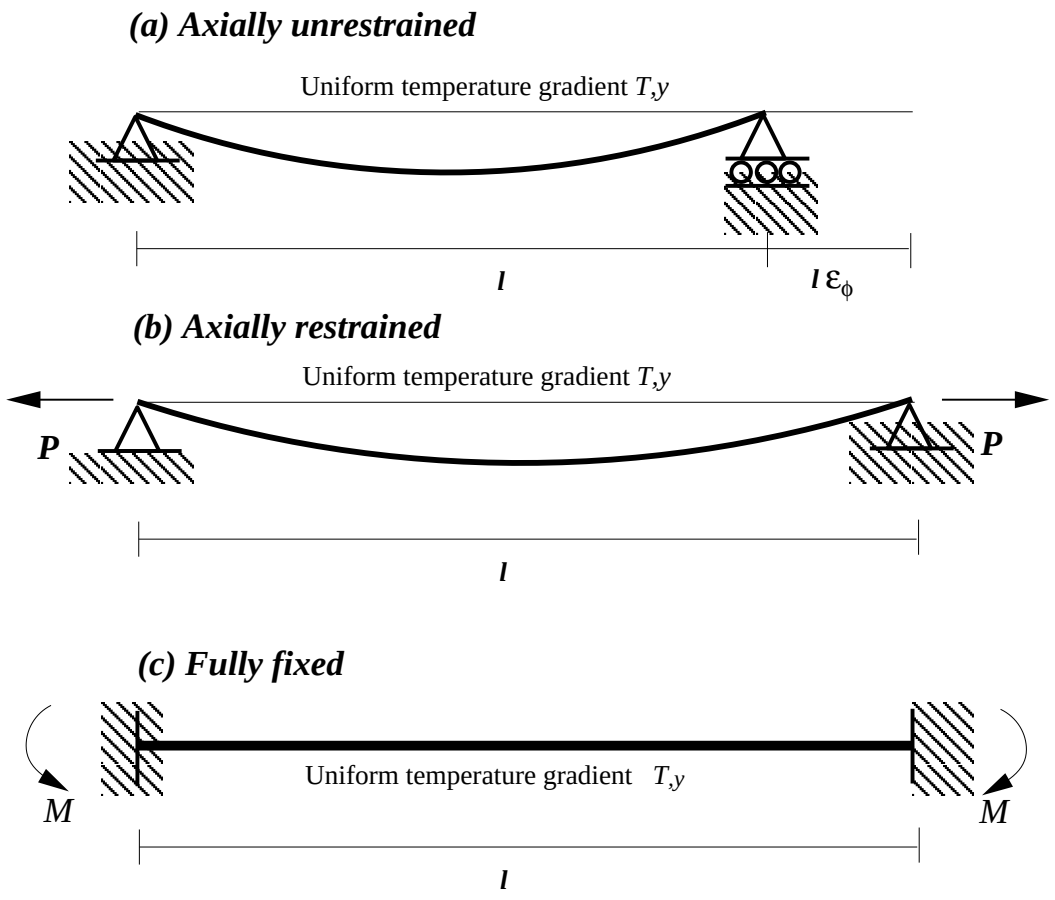

Figure 6.5: Thermal bowing in simple beams with different restraint conditions

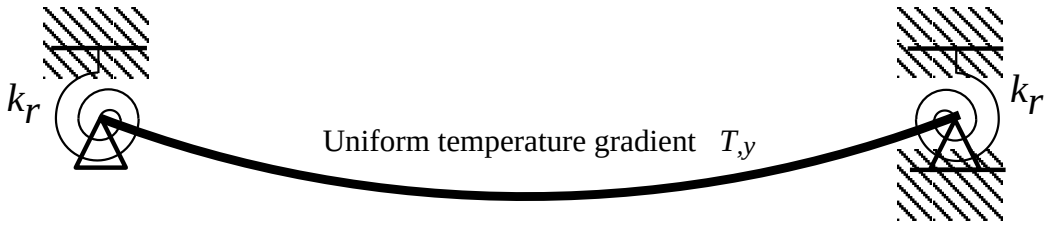

Figure 6.6: Thermal bowing in a beam with rotational stiffness k_r at its ends

$$\epsilon_{\text{eff}} = \epsilon_{\text{T}} - \epsilon_{\phi} \tag{6.16}$$

Figure 6.7 shows the effects of combined thermal expansion and thermal bowing on all three beam models. Axially unrestrained the thermal expansion causes a longitudinal extension which is partially or totally absorbed by thermal curvature pulling the beam ends back. In a pin ended beam axial tension or compression may exist depending on the relative magnitudes of the gradient and mean temperature. If the expansion strain and contraction strain cancel each other out a zero stress state could exist. In a fixed ended member the mean temperature rise leads to compression and the uniform gradient causes a uniform moment over the length of the beam. The combined compressions induced by restrained thermal expansion and moment result in high compressions on the exposed face of the beam and tensions (or small compressions) on the unexposed side (Figure 6.7(c)).

Many variations of mean temperature and gradient exist in structural elements under different heating regimes thus many displacement and force patterns will also exist. Figure 6.8 is a schematic representation of the various displacement configurations which could occur in an axially restrained pin ended beam. When there is only a mean temperature applied there are compressive forces in the beam and the deflection response is that of the pre-buckling, post-buckled shape. As a thermal gradient is incorporated the deflected shape becomes smoother and the magnitude of the deflections increase. Compressions are also absorbed resulting in a possible zero stress case. Where large thermal gradients exist the beam is in tension.

The first part of this chapter has summarised theoretical work conducted at Edinburgh. For a more detailed description see reports TM1[208] and TM2[248] and Usmani *et al.*[249]

6.2.5 Numerical analysis of thermal expansion and thermal bowing in a restrained beam

This study is extracted from report TM3 of the PiT project.[134] It describes a series of analyses carried out on a simple ABAQUS beam model to investigate and understand the behaviour of the beam when the deflection response is governed primarily by restrained thermal expansion and thermal bowing. The study was developed as part of this PhD research to calibrate and test the results of the theoretical analysis summarised above.

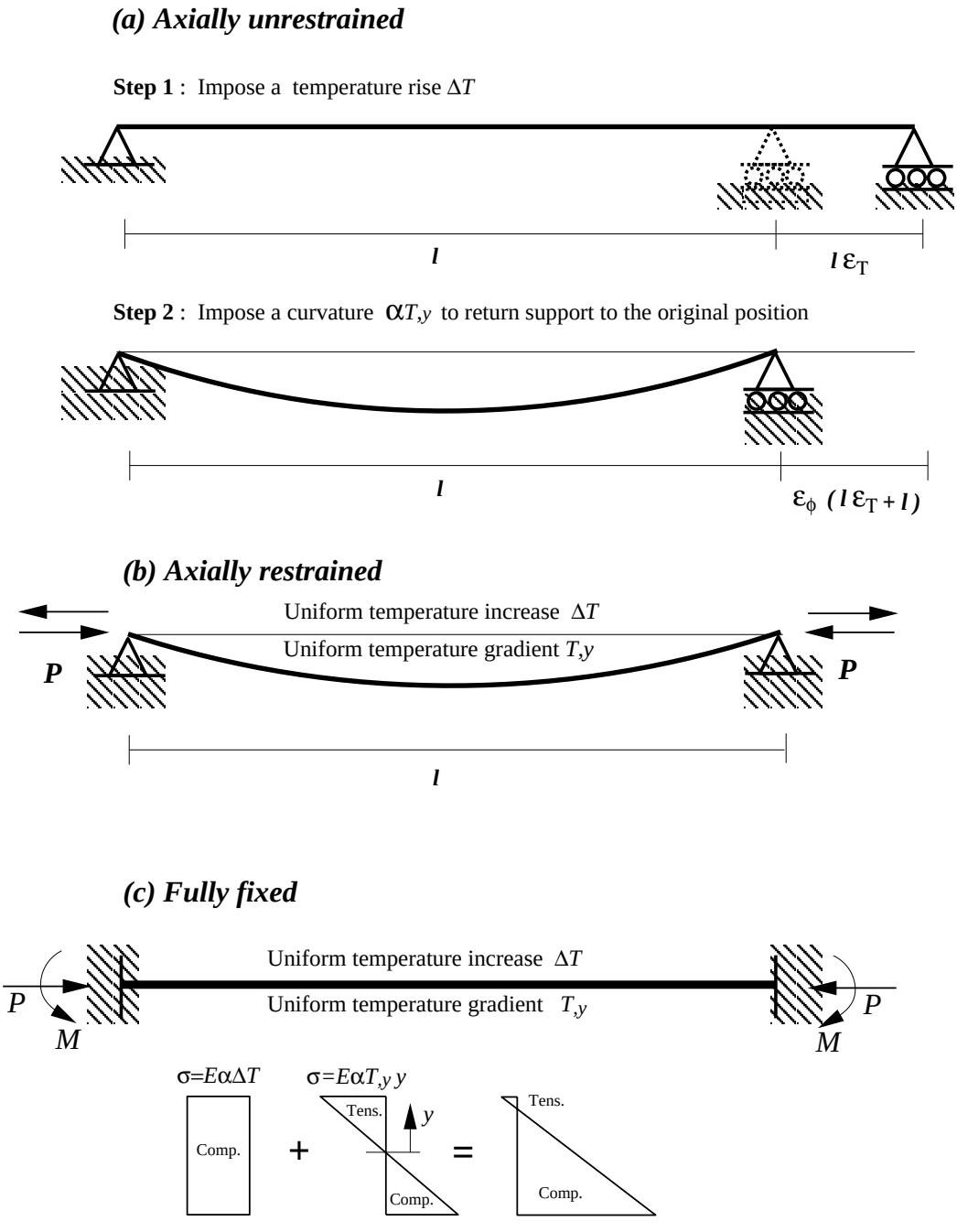

Figure 6.7: Thermal expansion and thermal bowing interaction in simple beam models

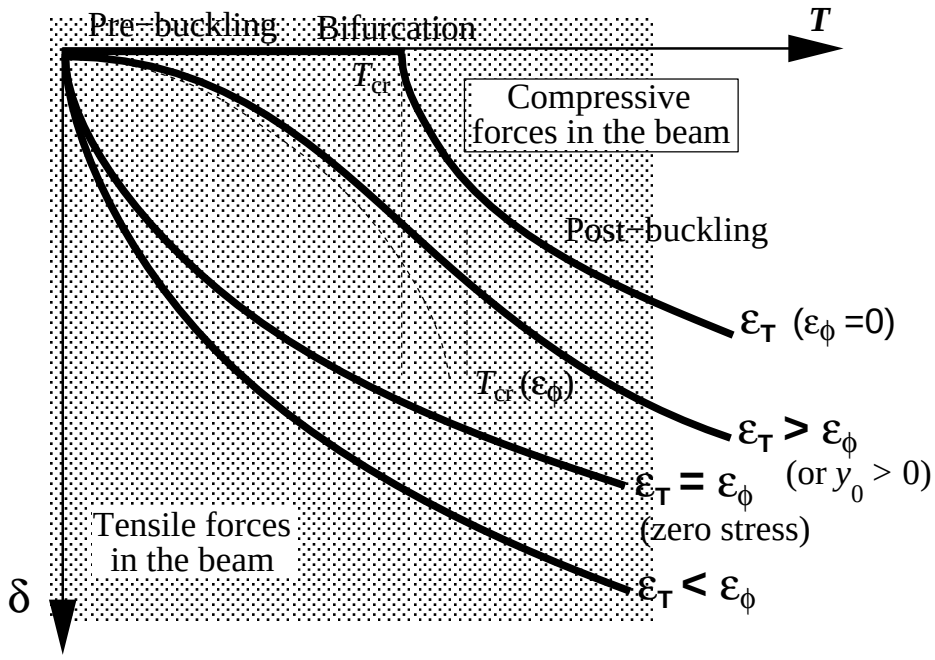

Figure 6.8: Temperature deflection responses for combinations of ΔT and $T_{,y}$

6.2.5.1 The simple ABAQUS beam models

The ABAQUS beam models studied included a fully fixed beam and a pinned beam (axially restrained but rotationally free). Exactly the same end conditions as figure 6.7(b) and 6.7(c) respectively.
The model characteristics are as follows,

- Length=l
- slenderness ratio (fixed ends), $l/r = 35$
- slenderness ratio (pinned ends), $l/r = 70$
- Area, A=5160mm^2
- Thermal expansion coefficient, $\alpha = 8 \times 10^{-6}$mm/^{o}C
- Uniformly Distributed Load, UDL=0.1N/mm
- E=constant N/mm^2

The Young's modulus, E, was assumed to be constant with increasing temperature to be easily compared with the theory. However, the analysis is fully geometrically non-linear.

The heating regime applied to the model included,

- A mean temperature rise (uniform over the length)= ΔT
- An effective thermal gradient through the depth= $T_{,\mathrm{y}} = \frac{T_2 - T_1}{d}$

and is described in Figure 6.1.

The temperature increase, ΔT and thermal gradient, $T_{,\mathrm{y}}$ are applied to the simple beam model at a constant rate from zero to their maximum values.

6.2.5.2 Summary of the structural response

For a uniform temperature increase with no gradient,

- the thermal expansion strain= $\epsilon_T = \alpha \Delta T$
- therefore the thermal expansion = $\epsilon_T l$

and for an effective thermal gradient through the depth of the model with no mean temperature rise

- thermal bowing induced curvature = $\phi = \alpha T_{,\mathrm{y}}$
- thermal bowing induced contraction strain= $\epsilon_\phi = 1 - \frac{\sin \frac{l\phi}{2}}{\frac{l\phi}{2}}$
- thermal bowing induced contraction= $\epsilon_\phi l$

Combinations of ϵ_T and ϵ_ϕ are applied and the response is interpreted based upon the fundamental relationships for thermal stress as described by Equations 6.1.

6.2.5.3 Studies on Model 1 (Fixed ends)

In the fully fixed beam the restraint causes compressive axial forces as it tries to expand. The thermal gradient induces a uniform curvature $\phi = \alpha T_{,\mathrm{y}}$ which is cancelled out by the equal and opposite curvature induced by the support moments. Thus the beam remains straight with a constant moment, $M = EI\phi$, along its length. The analyses carried out on the fully fixed beam are listed in Table 6.1.

The results of these analyses were as expected. Plots of deflection, axial force and moment at mid-span, against temperature, are given in Figures 6.9-6.11. The results of two scenarios are plotted, a uniform mean temperature rise up to 400^oC and a

Boundary conditions	Mean temperature rise ΔT (^oC)	Gradient $T_{,y}$ (^{o}C/mm)
Fixed ends	400	
Fixed ends	100	1
Fixed ends	200	1
Fixed ends	400	1
Fixed ends	100	5
Fixed ends	200	5
Fixed ends	400	5

Table 6.1: Conditions in each run on Model 1

combination of mean temperature and gradient. In both cases the deflections are almost zero, while the axial forces due to thermal expansion are in compression. There is no difference between the axial force in each case because the beam cannot rotate at its ends and so can not bow in response to the gradient to produce axial tensions. The moments are zero for pure thermal expansion and increasing uniformly in hogging when there is an increase in gradient.

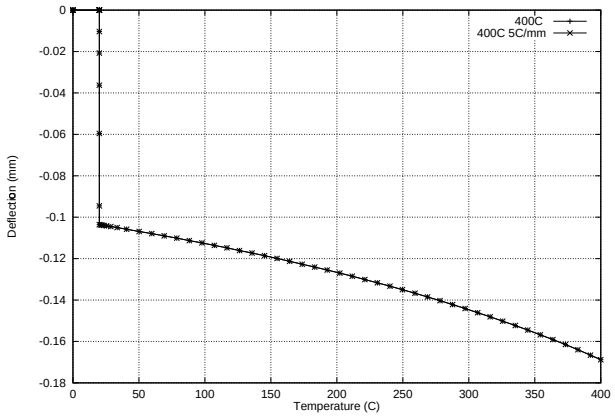

Figure 6.9: Numerical Model: Deflection at mid-span of the fully fixed beam

6.2.5.4 Studies on Model 2 (Pinned ends)

Table 6.2 lists the initial studies on the pinned beam (laterally restrained but free to rotate at its ends). In the first three analyses the effect of thermal expansion and thermal bowing were studied separately.

Based on the theory outlined at the start of this chapter if there is no thermal gradient in the beam but a uniform temperature rise is applied the only response will be restrained thermal expansion of which there are two distinct stages. A pre-buckling phase and a post-buckling phase. In the pre-buckling phase the thermal expansion is

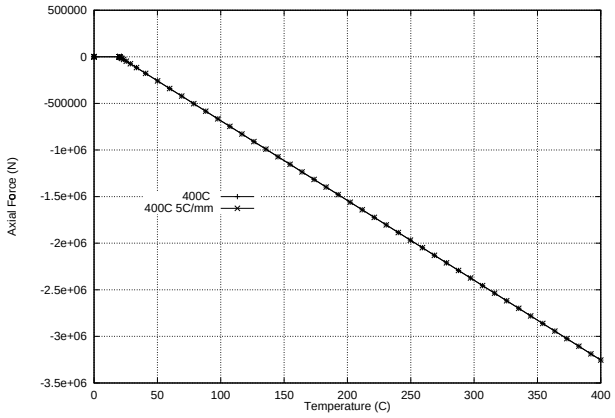

Figure 6.10: Numerical Model: Axial force at mid-span of the fully fixed beam

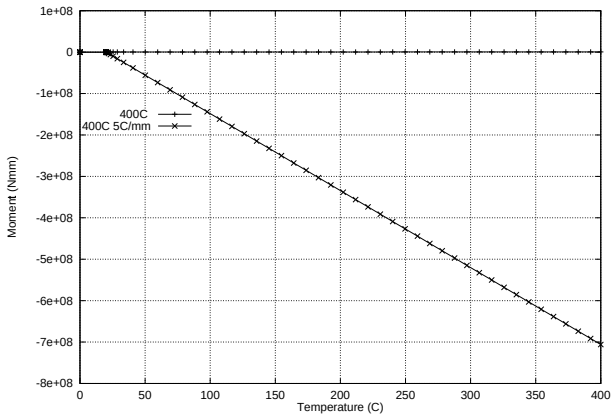

Figure 6.11: Numerical Model: Moment at mid-span of the fully fixed beam

absorbed in elastic (or plastic) strains and very little displacement is produced. The thermal and mechanical strains are equal. High stresses are generated until the beam reaches its limit and buckles. Once buckling occurs all further thermal strains produce large deflections. If there is no mean temperature rise applied to the beam, only a thermal gradient, the axial forces are caused by tensile "contraction" strains as a result of the thermal curvature imposed on the beam trying to pull the beam ends in.

Figures 6.12-6.20 show the deflections, axial forces and moments from the three ABAQUS analyses listed in Table 6.2. When there is only a mean temperature rise the double curvature of the pre-buckling post buckling phase is clear in the deflected shape of Figure 6.12. The axial force is in pure compression (Figure 6.15). In contrast where there is only a gradient applied deflected shapes are very smooth, axial forces are in tension and moments are in hogging. When the gradient is small deflections can be very linear (Figure 6.13)

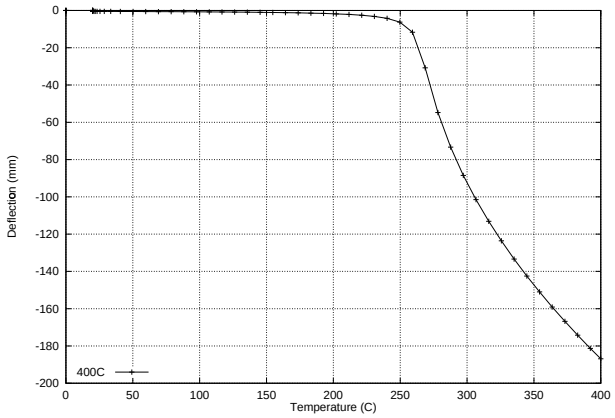

Figure 6.12: Numerical Model: Deflections at mid-span of the pinned beam, $\Delta T = 400^o$C

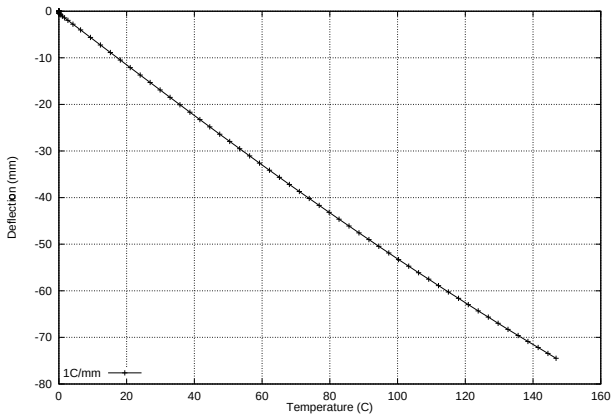

Figure 6.13: Numerical Model: Deflections at mid-span of the pinned beam, $T_{,\mathrm{y}}$=1^{o}C/mm

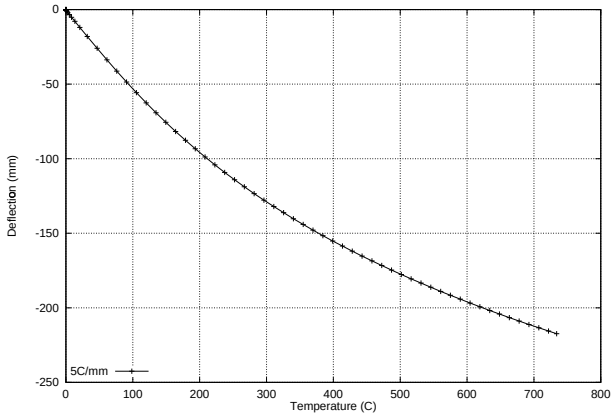

Figure 6.14: Numerical Model: Deflections at mid-span of the pinned beam, $T_{,\mathrm{y}}$=5^{o}C/mm

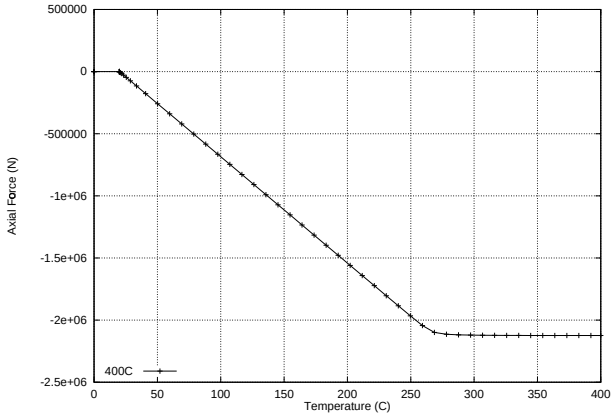

Figure 6.15: Numerical Model: Axial force at mid-span of the pinned beam, $\Delta T = 400^o$C

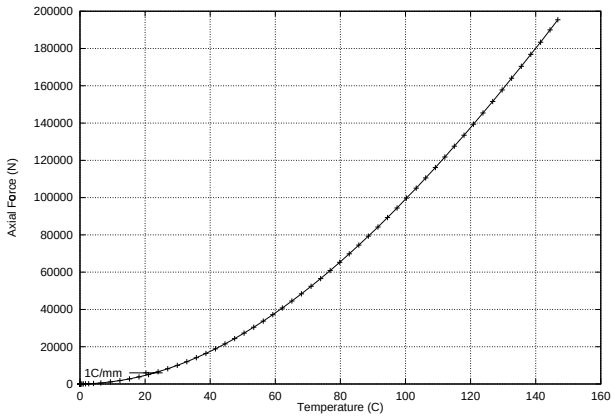

Figure 6.16: Numerical Model: Axial force at mid-span of the pinned beam, $T_{,\mathrm{y}}$=1^{o}C/mm

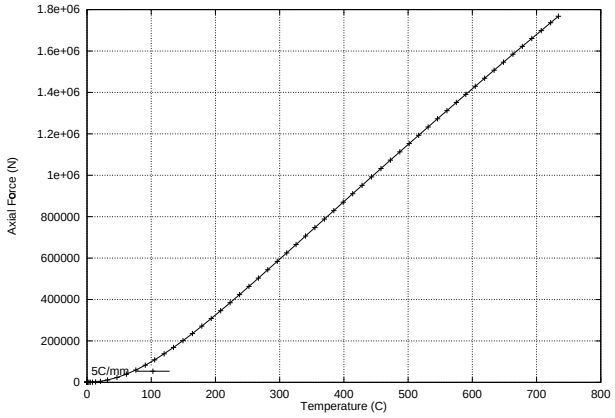

Figure 6.17: Numerical Model: Axial force at mid-span of the pinned beam, $T_{,\mathrm{y}}$=5^{o}C/mm

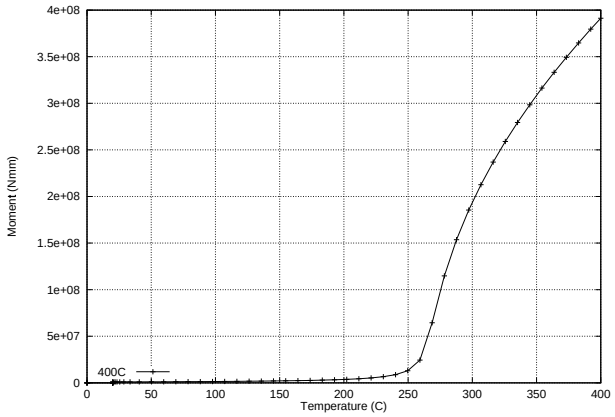

Figure 6.18: Numerical Model: Moment at mid-span of the pinned beam, $\Delta T = 400^o$C

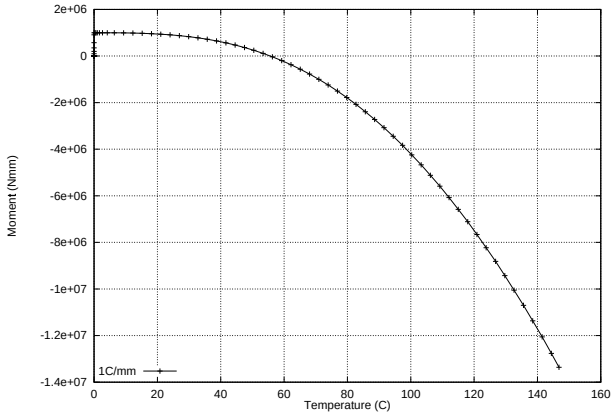

Figure 6.19: Numerical Model: Moment at mid-span of the pinned beam, $T_{,\mathrm{y}}$=1^{o}C/mm

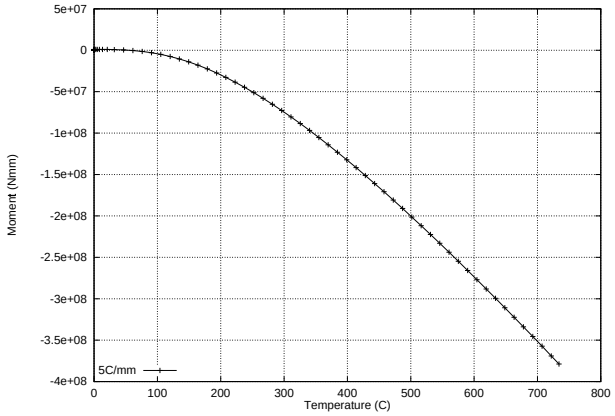

Figure 6.20: Numerical Model: Moment at mid-span of the pinned beam, $T_{,\mathrm{y}}$=5^{o}C/mm

Boundary conditions	Mean temperature rise ΔT (^{o}C)	Gradient $T_{,y}$ (^{o}C/mm)
Pinned ends	400	
Pinned ends		1
Pinned ends		5

Table 6.2: Conditions in each run on Model 2

Boundary conditions	Mean temperature rise ΔT (^{o}C)	Gradient $T_{,y}$ (^{o}C/mm)
Pinned ends	100	1
Pinned ends	200	1
Pinned ends	400	1
Pinned ends	100	5
Pinned ends	200	5
Pinned ends	400	3
Pinned ends	400	5
Pinned ends	400	10

Table 6.3: Conditions in each run on Model 2

6.2.5.4.1 Combined thermal expansion and thermal bowing In the numerical study discussed here the temperature increase ΔT and the thermal gradients $T_{,y}$ are applied to the model at a constant rate from zero to their maximum value. The strains induced in the beam by the two effects are in opposition to each other.

The final set of analyses carried out on the pinned end model are listed in Table 6.3.

Depending on the magnitude of the mean temperature rise in relation to the magnitude of the thermal gradient there are a range of responses in terms of deflections, axial forces and moments as a result of thermal expansion and thermal bowing interaction. The thermal expansion produced is partly used up in generating mechanical strains and partly in generating deflections. This is governed by Equation 6.16. ϵ_{eff} is the component that generates stresses to push the beam towards buckling. The ϵ_ϕ component takes part of the expansion and produces deflections by imposing curvature with the available excess length.

Figures 6.21, 6.22 and 6.23 show the results from a selection of the analyses listed in Table 6.3. In terms of deflection for a pure thermal expansion with no thermal gradient applied to the model the response is the double curvature of the pre-buckled/post-buckled form. As a thermal gradient is incorporated into the analyses the deflections increase and the overall shape becomes smoother. The axial forces (Figure 6.22) gradually decrease in compression (near zero in some cases) and move into high tension as the thermal gradient applied increases. Finally in terms of the moments as the gradients increase the beam moves into hogging bending.

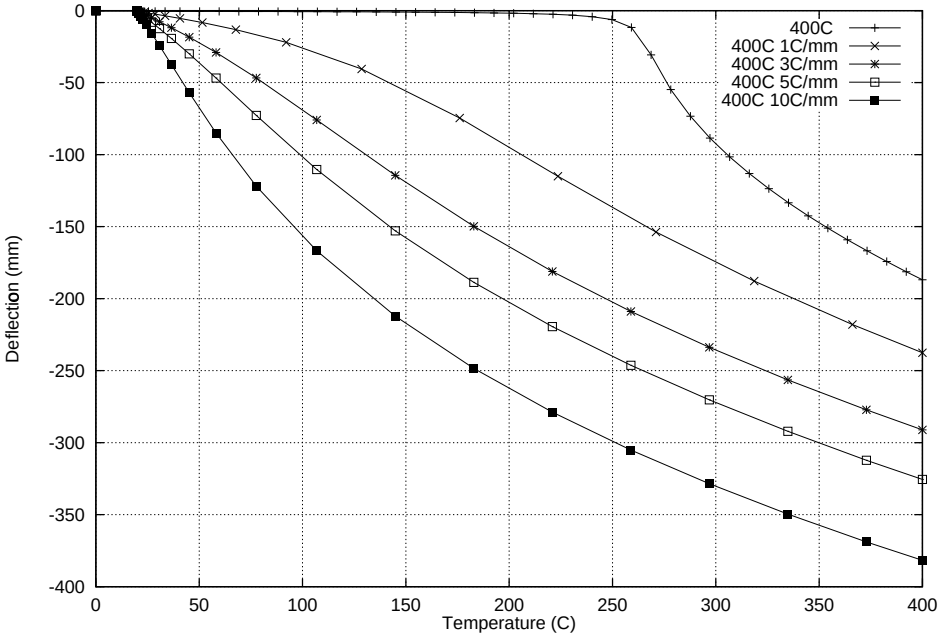

Figure 6.21: Deflections of the pinned beam at mid-span in response to thermal expansion and thermal bowing

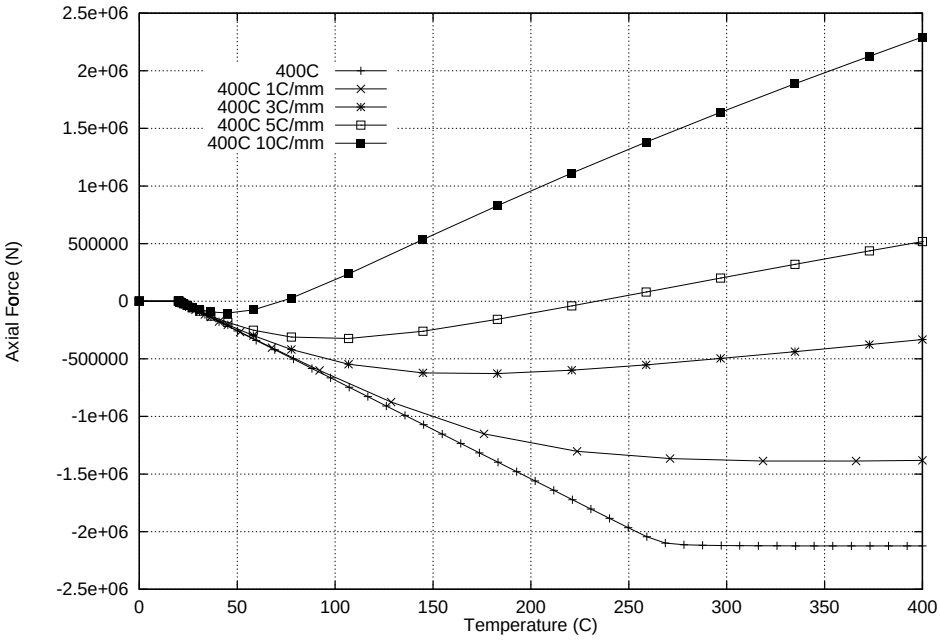

Figure 6.22: Axial forces in the pinned beam in response to thermal expansion and thermal bowing

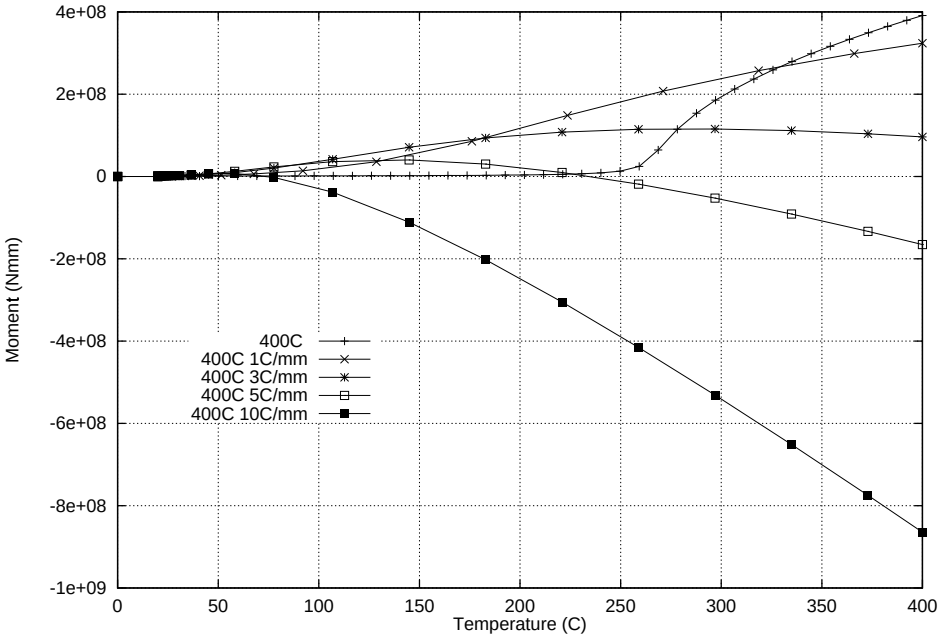

Figure 6.23: Moments in the pinned beam in response to thermal expansion and thermal bowing

6.2.6 Summary

- The numerical analysis supports the analytical studies
- The results from the simple beam models highlight the key responses to restrained thermal expansion and thermal bowing
- Fully restrained beams respond to thermal expansion with very small deflections but high compressive axial forces and to thermal bowing with no deflections but a uniform moment along the beams length.
- A beam which is free to rotate at its ends will buckle under restrained thermal expansion at a critical load. Any further expansions will be absorbed in large downward deflections.
- A pinned beam will rotate in response to a thermal gradient resulting in deflections and tensions
- Thermal expansion and thermal bowing act in opposition to each other. Tensions caused by gradients absorb compressions as a result of restrained thermal expansion and a low stress state may exist.
- Thermal expansion and thermal bowing interaction produces a large number of responses in terms of deflections, axial forces and moments.

6.3 Runaway in axially unrestrained and axially restrained beams

This next study analyses the load carrying mechanisms in a simple beam model when the ends are axially restrained but rotationally free and fully unrestrained. The purpose of this exercise is to explain why axially unrestrained beams in the fire resistance test reach runaway failure at much lower temperatures than restrained beams in real buildings. The analysis is reported by Lamont *et al.*[136]

Standard fire resistance tests in the USA (E 119) allow beams or slabs to be tested in a restrained test. The level of end restraint equals the level of restraint likely to be experienced in the life of the structural element. Also in the UK BS 476 provides provision for beams and slabs to be tested restrained in accordance with their expected use. However, very often beams and slabs are tested unrestrained because the end conditions in use are unknown. The "yellow book"[7] data is based entirely on results from unrestrained tests.

This is a geometrically and materially non-linear analysis of a simply supported universal beam with a slenderness ratio, $l/r = 70$ subjected to heating. The beam has a small through depth thermal gradient increasing linearly throughout the analysis from 0-0.5^{o}C/mm. It is heated linearly from 0-1200^{o}C uniformly, along its entire length. The beam is studied under axially unrestrained conditions and axially restrained conditions typical of the arrangement in a fire resistance test and a multi-storey frame structure respectively. The two models are illustrated in Figure 6.7 parts (a) and (b). In the British Standard fire resistance test the beam is allowed to translate laterally as shown in Figure 6.7(a). Therefore, the increase in length as a result of thermal expansion is accommodated by simply expanding. Any downward displacement is entirely due to the gravity loading applied. In a real indeterminate structure the beam would experience some degree of restraint against thermal expansion as shown in Figure 6.7(b), and initially the increase in length would cause strains as the beam is pushed up against the supports. However, if the beam is sufficiently slender, according to Equation 6.8 the beam will buckle and move into a large displacement non-linear mode of behaviour with no further increase in stress. The temperature at which this may happen is given by Equation 6.10 (for rigid axial restraint).

Figure 6.24 shows the deflection response of the two beam models. First consider the results of the axially unrestrained beam. Initially there is very little downward deflection because the supports are allowed to translate outwards upon expansion until around 450^{o}C when "runaway" occurs. This happens as a result of the supports being pulled in when the material properties degrade with increasing temperature and the beam stiffness can no longer support the gravity loading. In stark contrast is the

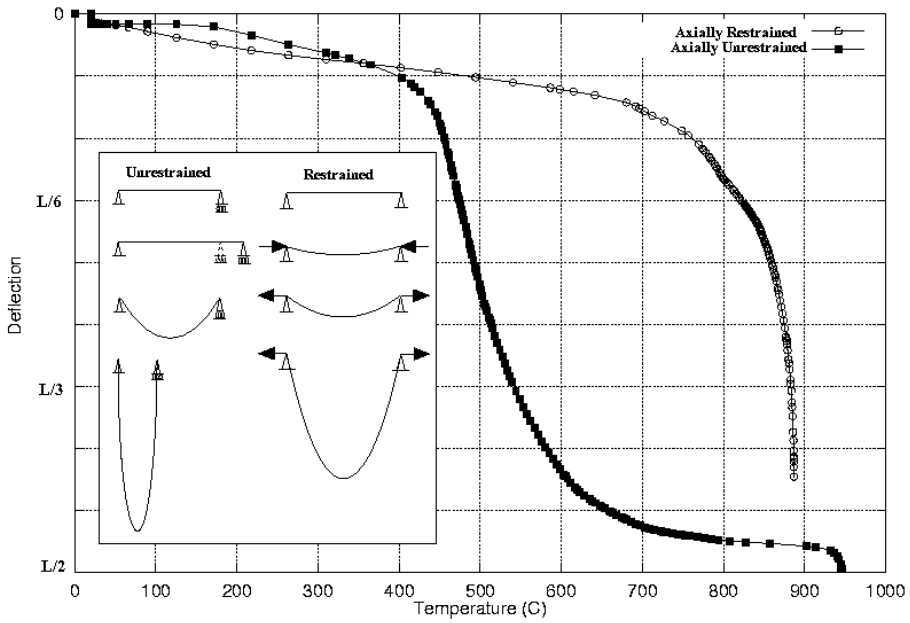

Figure 6.24: Runaway in an axially restrained and unrestrained beam

deflection history of the axially restrained beam. It buckles at around 70^oC and as a result has higher initial vertical displacements. "Runaway" is not reached until much later at temperatures around 750^oC when the steel properties are highly degraded. This illustrates that the presence of restraints to end translation delays "runaway" to much higher temperatures because of the development of catenary action to replace the highly depleted flexural stiffness.

The magnitude of the deflections plotted here are very high but they are only meant to illustrate the difference between failure temperatures of the unrestrained and restrained beam. In a composite structure where the steel beams are acting compositely with the slab such high deflections would not be achieved. The second beam is a better representation of beams in large redundant steel frame structures. In real composite frame structures, restraint to thermal expansion is available and the steel beam is in composite action with the slab which produces a much stronger structure. Large deflections seen in real structures are often misinterpreted as impending "runaway" failure. Figure 6.24 shows that for temperatures below 300^oC the deflections for the restrained beam are much higher than for the laterally unrestrained beam but they are not indicative of "runaway". These deflections are caused entirely by the increased length of the beam in a post-buckled state as a result of thermal expansion. In a real structural element in

a large structure the large displacements are due to a combination of thermal expansion and thermal bowing effects.

6.3.1 The impact of loading on "runaway" in a pinned beam

Next the effect of loading on the simple beam is studied. The moment experienced by the beam can be described by, $M = \frac{wL^2}{8}$. A load w, equivalent to achieving the maximum plastic moment Mp at the mid-span of the beam was applied to the model before introducing the heating regime. This process was repeated varying the UDL's (uniformly distributed loads) to obtain a spread of results corresponding to moments lesser and greater than Mp. The results of this analysis are given in Figure 6.25 where it is shown that the response of the restrained beam with a loading w causing Mp does not achieve "runaway" until 700^{o}C. The beams with UDL's causing less than Mp, typical of designed structures are not achieving "runaway" until very high temperatures are reached (typically greater than 800^{o}C).
By differentiating the results plotted in Figure 6.25 a much clearer picture of runaway failure can be drawn. Figure 6.26 is a plot of dy/dT (rate of deflection change with change in temperature) against increasing temperature, showing the points of "runaway" failure in each load case as a distinct change in gradient.
Deflections before impending structural failure are dominated by thermal effects. The failure temperature is reached when any further deflections are dominated by loading. Initially in Figure 6.25 the load-deflection curves are parallel to each other for all loads, which indicates that deflections are dominated by temperature rise until a temperature is reached where the beam has weakened to an extent that the loads begin to dominate, leading to "runaway" failure.

As well as looking at the deflection response of the simple beam model to changing loads, the axial forces and moments experienced by the beam were also investigated. From equilibrium, at all times the beam must carry the applied moment. Initially flexural resistance of the beam achieves equilibrium with the applied moment. However as the material properties degrade, as a result of increasing temperatures, the moment capacity of the beam reduces and the applied moment is carried by a combination of the remaining flexural capacity and the P-Δ tensile membrane resistance or catenary action. The equilibrium of the problem is illustrated in Figure 6.27. The applied moment is $\frac{wL^2}{8}$ and the tensile membrane or catenary resistance is Hd where H is the axial force and d the displacement of the beam at mid-span.

Figures 6.28-6.33 show the bending moments and axial forces generated in the beams

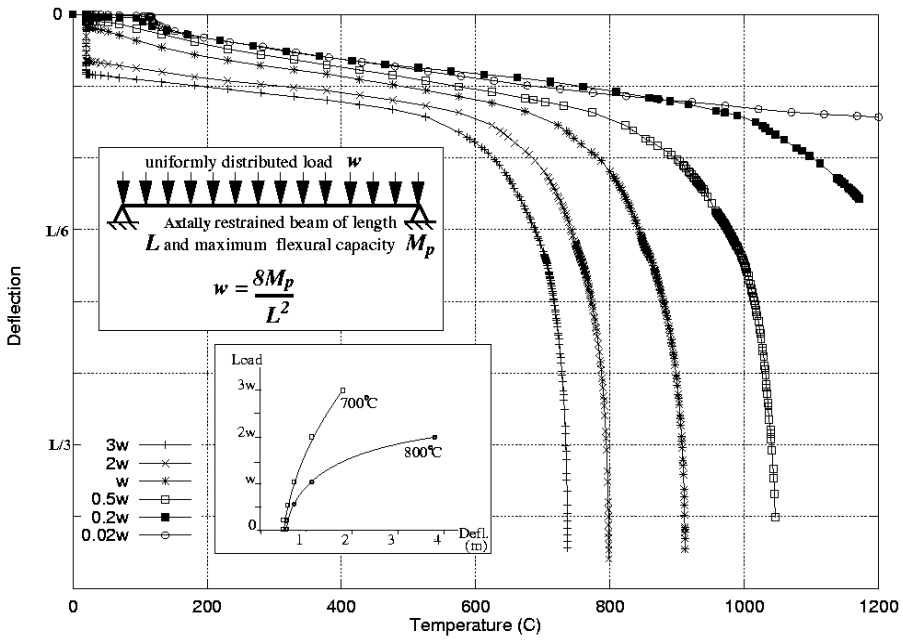

Figure 6.25: The effect of loading on a simple restrained beam subject to heating

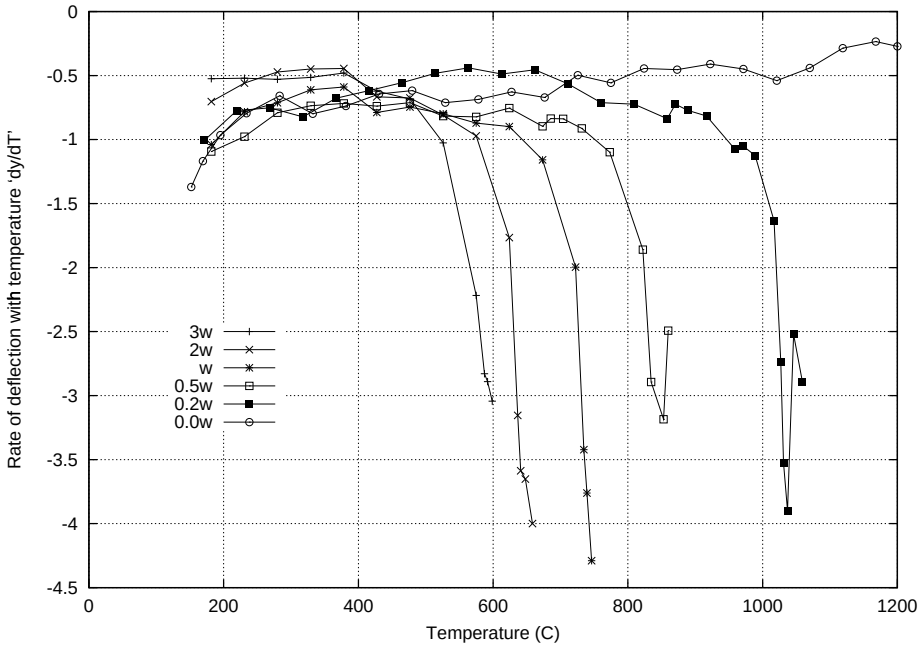

Figure 6.26: Rates of deflection at mid-span against temperature for all load cases

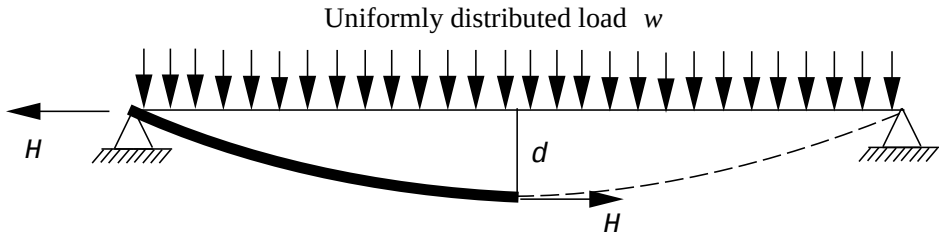

$$\text{Applied moment} = \frac{wL^2}{8}$$

Tensile membrane or catenary resistance =Hd

Residual moment capacity =Mp(T,H)

Figure 6.27: Catenary action coupled with flexural resistance

for three of the load cases studied ($0.5w$, $1.0w$, $2.0w$). In each case, when plotting the moments, the plastic moment capacity of the beam, the P-Δ (tensile membrane resistance), the flexural resistance and the total moment applied to the beam are shown. The plots of axial force show the axial force at the support and at mid-span and the axial (tensile) capacity. These figures highlight the change in load carrying mechanism as the material properties degrade.

For the load case $0.5w$ the moments and axial forces are plotted in Figure 6.28 and Figure 6.29 respectively. In the early stages of the heating regime, up to 400^oC, the total moment (from both loading and additional "compressive" P-Δ moments) is carried by the flexural resistance of the beam. As the moment capacity and the flexural resistance decrease, "compressive" moments decrease to zero (with increasing deflection), with the entire load being resisted by the residual flexural capacity. Beyond this point the "tensile" P-Δ moments assist the flexural mechanism in supporting the applied moment. Runaway occurs when both load carrying mechanisms are exhausted. The axial forces consist of a small tension in the beginning, then they increase in compression as the temperature of the beam increases and the beam starts to expand against the rigid supports. After the beam buckles at around 70^oC and begins to deflect, the axial force reduces in compression and moves into tension. Towards the end of the analysis, just before impending runaway, the axial tension and the tensile capacity converge.

The explanation is very similar for $1.0w$ and $2.0w$. Figure 6.30 and Figure 6.31 illustrate the results of the analysis for a UDL of 1.0w. Initially the plastic moment capacity is equal to the total moment as a result of the load applied. The moment is carried by a combination of flexural resistance and P-Δ tensile membrane resistance from the start. At 20^oC there is tensile membrane resistance as a direct result of the gravity loading. The flexural resistance increases up to Mp at 80^oC as the tensile mem-

brane resistance drops back to zero. Beyond 100^oC the flexure resistance decreases and the tensile membrane resistance increases to maintain equilibrium and carry the applied moment. After 400^oC the moment capacity begins to decrease as the material properties of the steel degrade leading to an increased reduction in flexural resistance. Runaway occurs at about 900^oC. Figure 6.31 shows the beam to be in axial tension throughout the analysis because the gravity loading causes catenary action from the very beginning of the analysis. The axial tension decreases a little as thermal expansion causes compression. Above a steel temperature of 500^oC the forces increase in tension (to maintain equilibrium by substituting for the declining flexural resistance) and then decrease as the stiffness properties decrease to converge with the tensile capacity of the beam. A UDL of $2.0w$ results in a total moment equal to double the moment capacity of the beam. Therefore the total moment is carried by a combination of flexural resistance and tensile membrane capacity or catenary action from ambient conditions to the end of the analysis. The high catenary action at ambient is a direct result of the high gravity loading causing large deflections initially see Figure 6.25. Once again as the deflections increase as a result of thermal expansion and thermal bowing and the beam loses its stiffness as a result of material degradation the tensile membrane resistance increases and the flexural resistance drops off. Figure 6.33 shows the high axial tension in the beam at 20^oC resulting from the high gravity loading and the decrease in tensile forces as the thermal expansion effects cause compression with increasing temperature. The axial forces and axial capacity converge at "runaway".

6.3.2 Implications

The simple studies discussed have highlighted the differences in behaviour between an unrestrained beam commonly tested in a standard fire resistance test and an axially restrained beam typical of a beam in a highly redundant composite frame structure. It has been shown that "runaway" in an unrestrained beam will occur at much lower temperatures than in the same beam restrained axially. It has also been shown that the load carrying mechanisms of a restrained beam will change to accommodate the loss of stiffness of the beam as a result of material degradation with temperature. Catenary action develops in the beam as a result of the deflected shape caused by thermal expansion and thermal bowing (and loading at high loads). Thus the moment applied to the beam is carried by a combination of flexural resistance and tensile membrane resistance. The tensile membrane resistance compensates for the reduction in flexural resistance. Now that the shortcomings of the fire resistance test have been formally stated. What are the implications? Despite deficiencies it is a universally recognised method of determining the fire resistance of elements of construction. Present fire resistance gradings of buildings are based on a very simplistic methodology which cannot

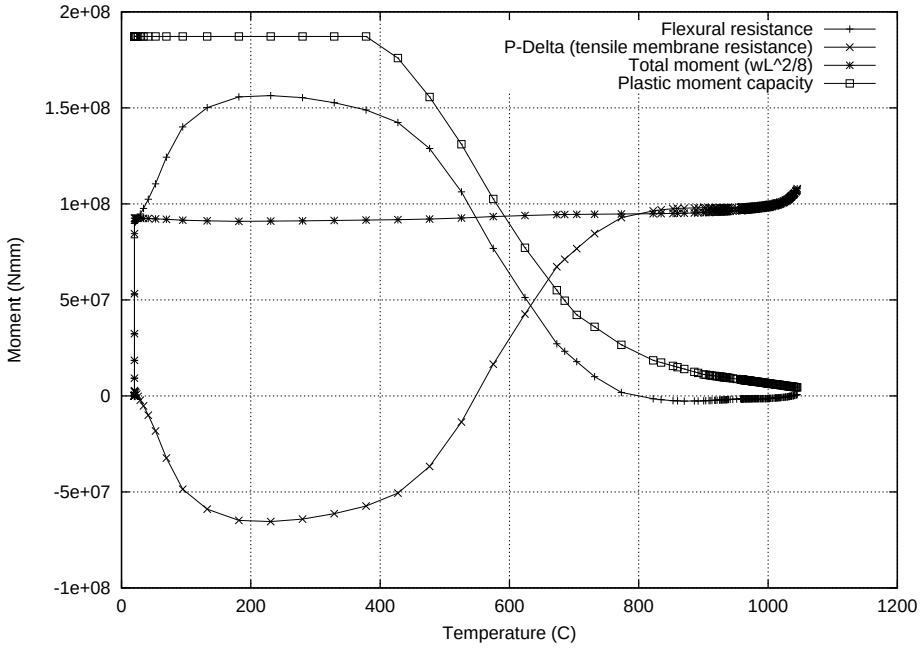

Figure 6.28: Moment equilibrium for udl 0.5w

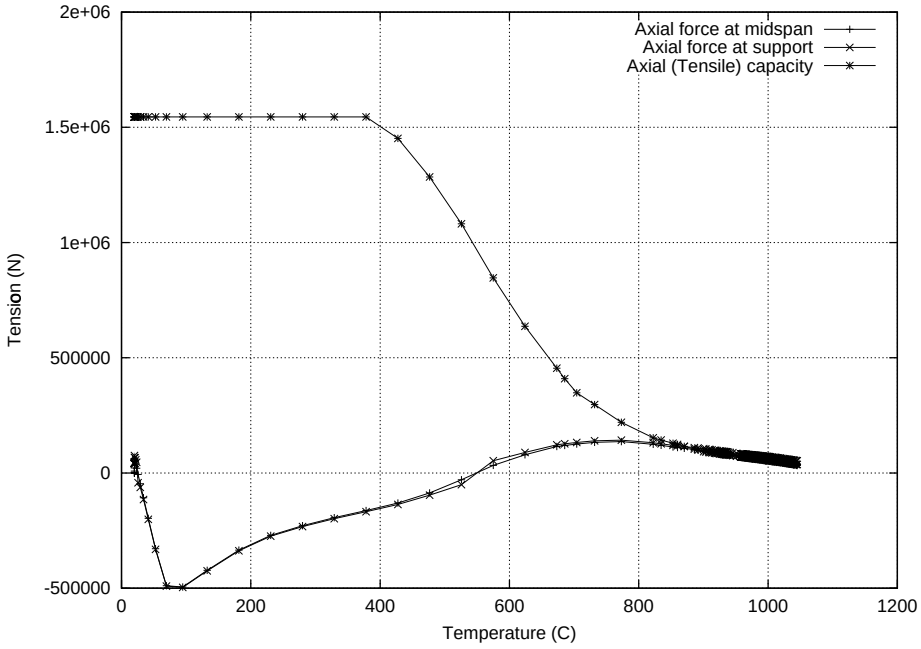

Figure 6.29: Axial force for udl 0.5w

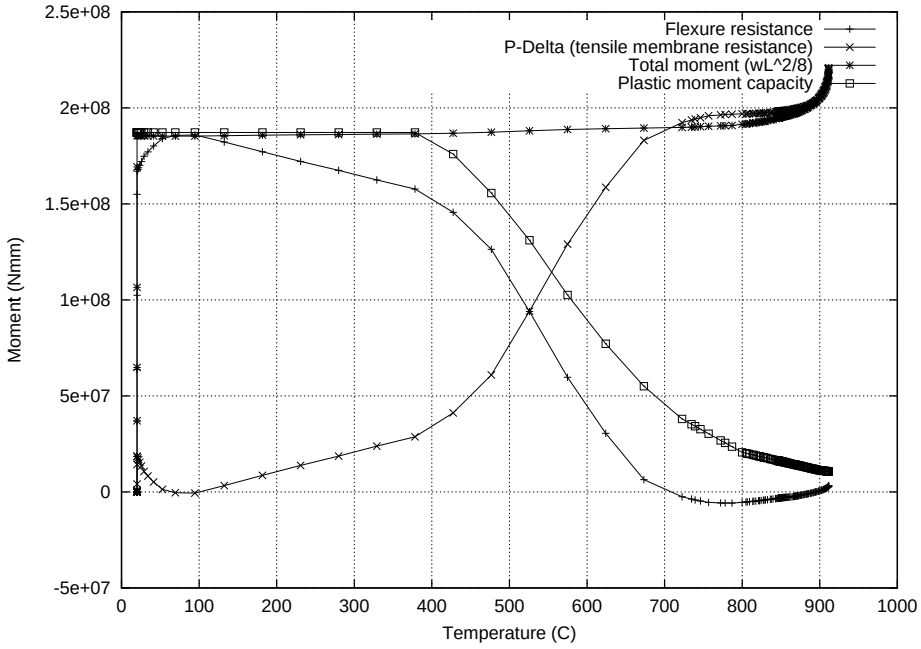

Figure 6.30: Moment equilibrium for udl 1.0w

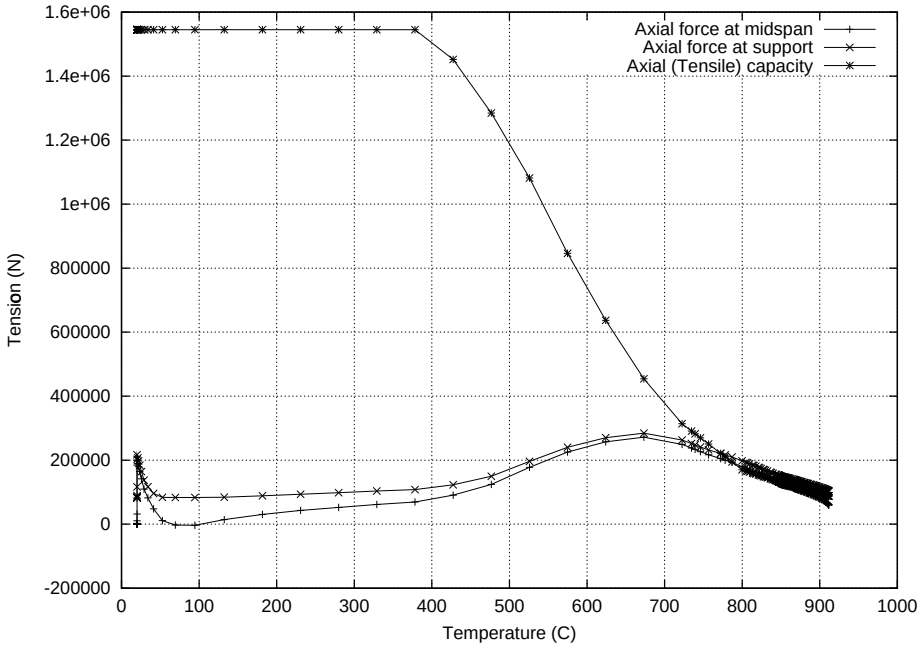

Figure 6.31: Axial force for udl 1.0w

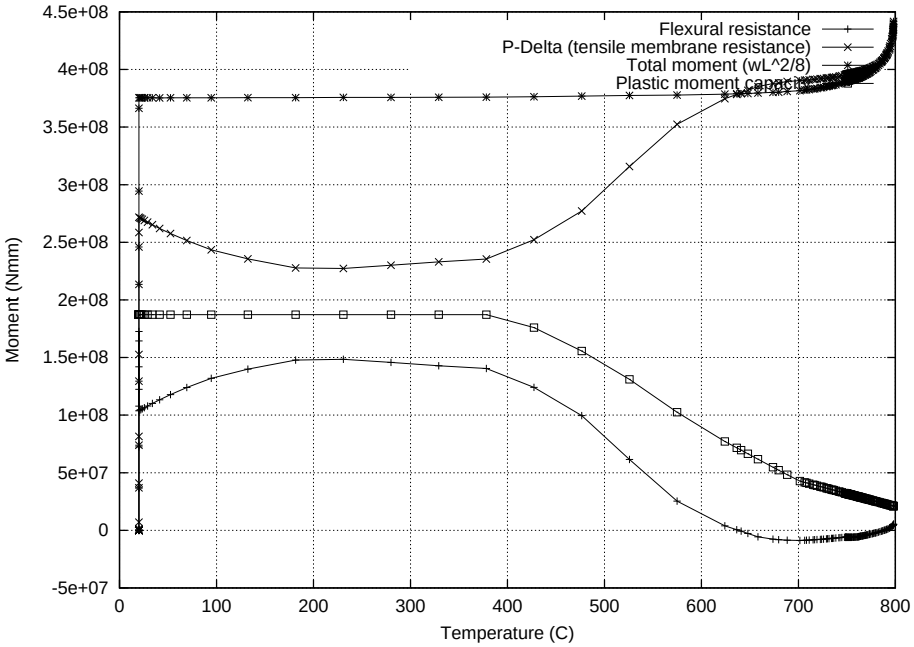

Figure 6.32: Moment equlibrium for udl 2.0w

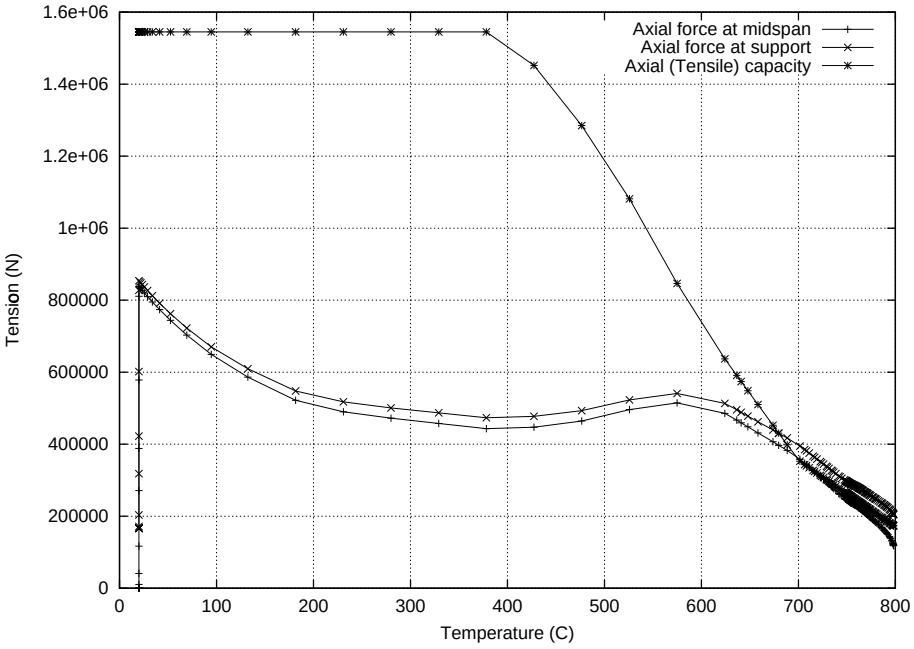

Figure 6.33: Axial force for udl 2.0w

represent the effects of temperature on a restrained structural element in a highly redundant structure. A thorough scientific understanding of the behaviour of the whole structure in fire is needed. Only then can this understanding be incorporated into design codes. Admittedly the above discussion concerns a very simple system and does not consider all the complexity in a real composite frame structure such as the compatibility of deflections in the two directions of a composite floor slab, but nevertheless it highlights the inadequacy of the fire resistance test quite clearly.

6.4 Conclusions

The beam models have highlighted the effects of thermal expansion and thermal bowing under different restraint conditions. The numerical models agree well with the analytical studies thus provide confidence. The cause of large deflections in structures subject to thermal loading are,

- Thermal expansion is the primary cause.
- Thermal gradients play a supporting role.
- Thermal expansion can only produce large downward deflections if the ends are restrained from expanding.
- Thermal gradients can only produce deflections if the ends are free to rotate (by imposing curvature).
- The variation of ϵ_{eff} (for various thermal regimes) can produce a large variety of responses from thermal expansion dominant to thermal bowing dominant.

In summary, the development of internal forces and moments in the beam is governed by the interaction of mean temperature increase, through depth thermal gradients and the end restraints to translation and rotation. Therefore any state from high compression to high tension can (theoretically) exist in heated structural members. However, in all these cases large deflections will be present albeit having developed through different mechanisms.

The second simple beam analysis has shown that the unrestrained fire resistance test bears little relevance to the behaviour of structural elements as part of highly indeterminate structures typical of modern, composite steel frame buildings. The test methods are inadequate when the end conditions during service are unknown and the beam is tested as simply supported i.e. no consideration of restraint is made. By including the

effect of restraint in a simple beam model the temperature at which "runaway" occurs is greatly increased. The reasons for this i.e. the changing load carrying mechanisms involved as catenary action develops as a result of the deflected shape have also been explained.

Chapter 7

Structural behaviour in British Steel Test 1 under different heating regimes

7.1 Introduction

Chapter 6 highlighted the two main effects of heating in a structural member, thermal expansion caused by an average rise in temperature, and thermal bowing caused by a non-uniform distribution of temperature over the depth of the member. Both of these actions impose thermal strains (longitudinal extension in case of expansion and curvature as a result of thermal bowing). However if these thermal strains are restrained, the result is the development of mechanical strains in the opposite sense of the thermal strains thus reducing the total strains (and therefore displacements), giving rise to large forces. This chapter describes a series of parametric studies on the effect of changing the thermal gradient and the mean temperature in the Cardington slab. The analyses were conducted on the grillage model of British Steel test 1, the restrained beam test. The analysis was carried out in two parts first different thermal gradients were applied to the concrete slab while maintaining the average temperature increase over the slab depth equal to a fixed reference value. The second part presents the results and interpretations of applying different average temperature increases and maintaining the gradients at reference value.

7.2 Effect of varying the slab thermal gradients in British Steel test 1

ABAQUS[102] finite element models developed to simulate the behaviour of the structure in the Cardington fire tests[214, 215] reproduce the phenomena occurring during a fire. The grillage models provide a description of the complex behaviour in a relatively simplified manner by representing the slab with a grid of 1D elements.

7.2.1 Description of the fire compartment

The compartment studied is identical to the one constructed for the first British Steel test, which is the reference case. This test was designed to study the behaviour of a secondary beam spanning between two columns. The dimensions of the compartment were $8m \times 3m$ and the tested beam had a span of 9m (Figure 7.1).[38] Full details were given in Chapter 4.

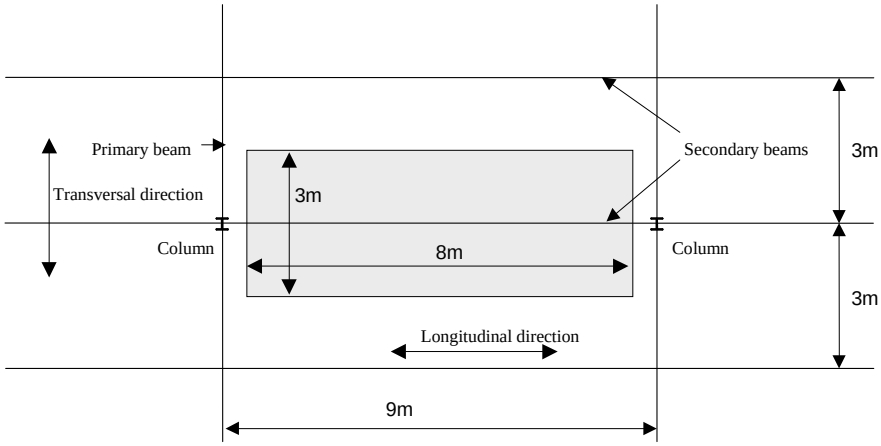

Figure 7.1: Layout of the Cardington frame fire test

7.2.2 The finite element model

The ABAQUS grillage model developed by Sanad[223] and validated against the results of British Steel test 1 is used for this study. The ABAQUS model was developed to illustrate the structural behaviour in British Steel Test 1 in a relatively simple manner. Exploiting symmetry, only half the compartment was modelled and the effect of the surrounding floor was also represented by symmetry boundary conditions (Figure 7.2). In the model, the slab was represented by a grillage of cross beams running in two directions, parallel to the secondary beams (longitudinal direction) and parallel to the primary beam in the direction of the ribs (transverse direction).

In the transverse direction, each rib of the slab is represented by a discrete beam connected to the secondary beams. In the longitudinal direction, the composite slab is represented by a concrete beam rigidly connected to the secondary steel joist below it. The beam elements representing the ribs and the composite slab are also rigidly connected. The effective width of the composite slab and the material properties used for concrete were deduced from Eurocode.[76–79] Each secondary steel joist is connected to either a column or a primary beam using a pinned connection. The primary joist also has a slab rigidly connected to it to model the composite behaviour. The temperature regime applied to the slab was represented by a mean temperature (calculated using the measured test temperatures and an assumed weighted area of concrete over which the temperature would act) acting at the geometric centroid and a mean gradient acting through its depth as illustrated in Figure 7.3 for the ribs, and in Figure 7.4 for the composite longitudinal slab. The temperature applied to each member was increased

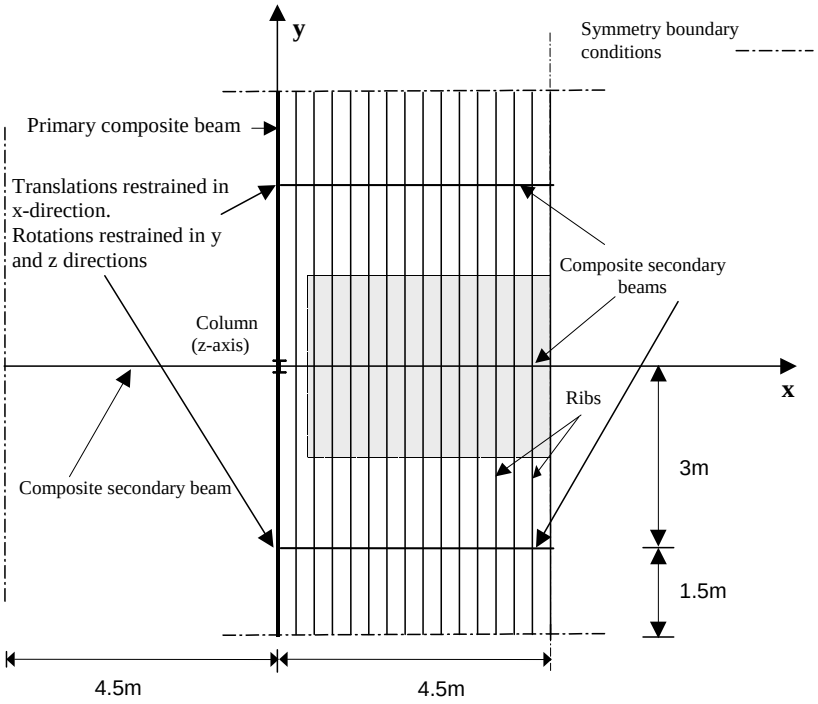

Figure 7.2: Layout of the Cardington frame fire test

Structural member	**Reference final temperature**	**Reference final gradient**
	(^{o}C)	(^{o}C/mm)
Heated Joist	800	0.26
Composite slab	265	4
Ribs	360	5

Table 7.1: Reference thermal loading on the structure

linearly from ambient to the maximum temperature. The gradient in the slab and the joist was also increased linearly from zero to the final value. The actual variation of temperature and gradient in the tests was not linear, however this idealisation of linear evolution allows an easier interpretation of the structural behaviour. This is because in a detailed examination of model results the events related to structural phenomena are separated from variations caused by changes in the temperature history. The temperatures and gradients over the structural elements were applied separately for the steel joists, the longitudinal composite slab and the transverse ribs. Table 7.1 gives the values used in the reference calculation for the test derived from the experimental data.

An increase of the temperature at the geometric centroid of the slab implies an increase in the slab length. When the slab is restrained against axial expansion, axial thrusts

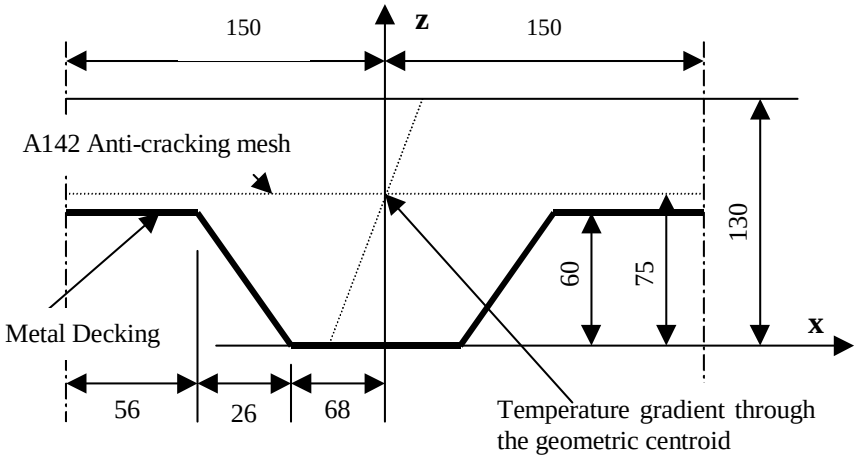

Figure 7.3: Cross section of one rib showing the location of the geometric centroid and the temperature gradient through its depth

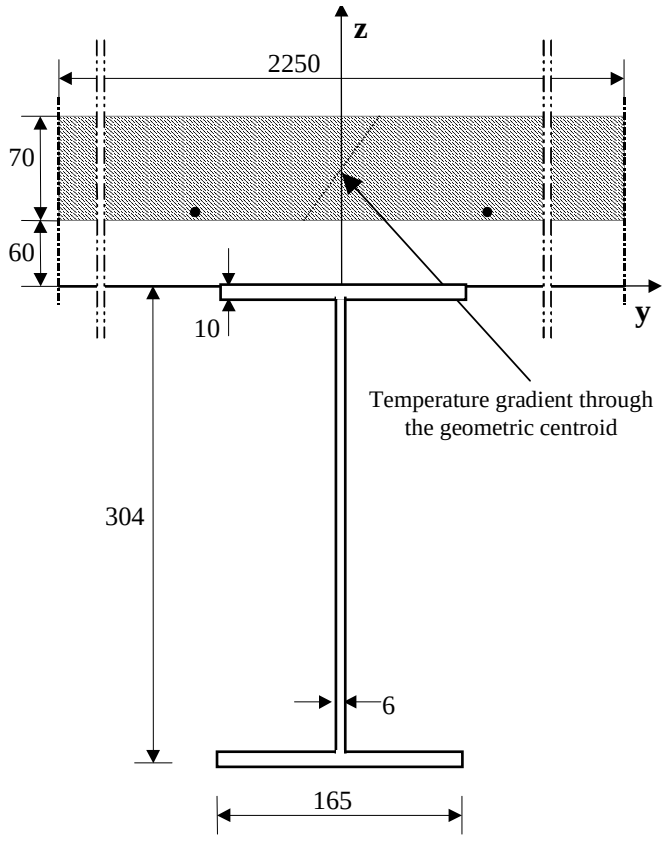

Figure 7.4: Cross section of the composite beam showing the location of the slab geometric centroid and the temperature gradient through it

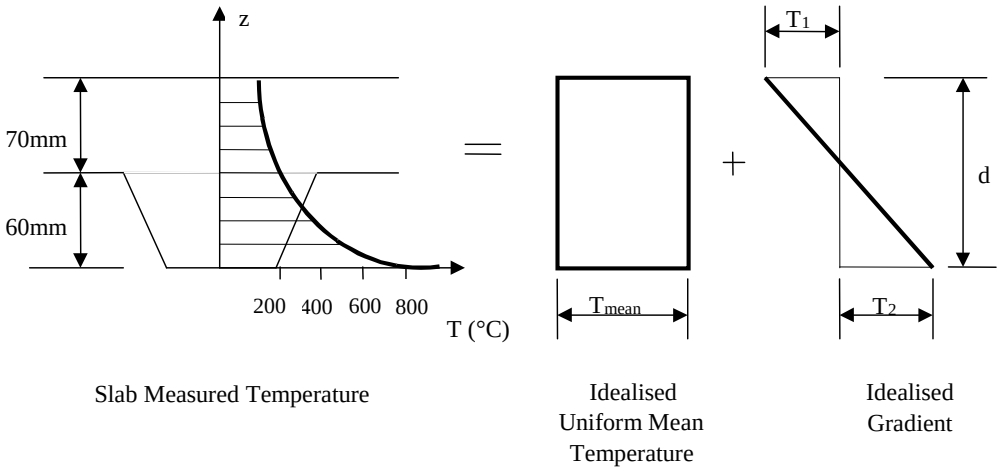

Figure 7.5: Idealisation of the temperature regime acting on the slab

are induced. In the real structure the restraint to thermal expansion is provided by the surrounding cold structure. A temperature difference between the top and bottom surface of the slab imposes a thermal curvature on the slab cross section. When the slab is restrained against end rotation, a hogging moment over the slab is produced over the whole length without deflections, with the bottom surface of the slab in compression and the top surface in tension. If the slab has a relatively small rotational restraint and its ultimate hogging moment capacity is reached early on, further increase in thermal gradients (thereby increasing the imposed curvature) leads to thermal bowing and deflections.

Another important effect on the behaviour of a slab is the geometry of the compartment. Heating of the slab induces thermal expansion and curvature which depend on the coefficient of thermal expansion of the slab and the length or dimension of the compartment. In the case of a rectangular compartment like the one studied here (8m x 3m) the expansion related displacement in the longitudinal direction is higher than in the transverse direction. Compatibility imposes the same deflection in the 2 directions so the structural response in each direction will depend on, both the thermal loading and the response in the orthogonal direction.

To analyse the effect of thermal loading on the structural response in the 2 directions, the effect of varying the temperature gradient and the mean uniform temperature through the depth is studied as described in Table 2. All other parameters remained unchanged except for the thermal action being studied. Separation of thermal loads into components influencing only one direction is unrealistic, but it reveals key features

Part	Parameter investigated	Location in the compartment
1	Temperature Gradient	Transverse direction
2	Temperature Gradient	Longitudinal direction
3	Mean centroidal temperature	Transverse direction
4	Mean centroidal temperature	Longitudinal direction

Table 7.2: Four Parts to the parametric analysis

of the structural behaviour.

The results of the studies on the effect of varying thermal gradients or mean temperature are presented below and will be interpreted in the context of the fundamental behaviour patterns identified in chapter 6.

7.2.3 Slab gradient variation in longitudinal direction

7.2.3.1 Response of the composite beam

The compartment considered here is characterised by the presence of a highly restraining cold structure around it. It can be argued that the restraint to translation is considerably more severe than the restraint to rotation around the compartment. Although the slab is continuous in all directions and therefore considerable rotational restraint can materialise, there will be a limit imposed on the magnitude of this restraint based on the hogging capacity of the slab. The results show that altering the temperature gradient in the longitudinal direction has very little or no effect on the maximum deflection obtained at mid-span of the beam (Figure 7.6). This is expected as in the longitudinal direction the slab thermal gradients are a very small proportion of the total gradient. A much larger gradient comes from the temperature differential over the composite section (slab and joist) which is not varied in this study. This effect declines at higher temperatures however there still is no appreciable change in deflections with varying thermal gradients. This is because the effect of the high translational restraints at the beam ends and the restraints imposed by orthogonal compatibility are too dominant. This remains the message for all significant outputs from this exercise. The moments and forces in the slab joist are also not sensitive to the variation of the slab gradient. The response of the composite beam is also not affected by the slab gradient as can be seen from Figure 7.7 to Figure 7.9, where the thermally induced (P-Δ) moment and the total moment in the beam remain unchanged for different gradient regimes.

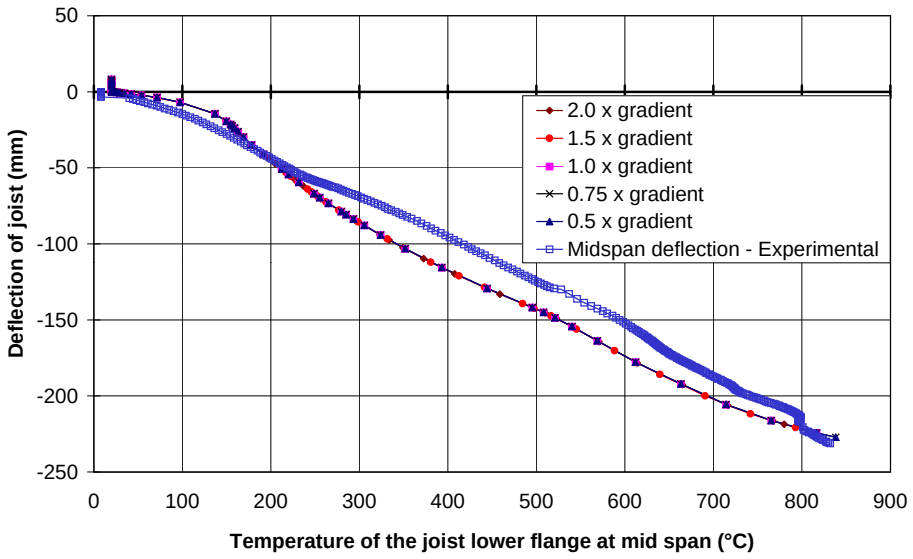

Figure 7.6: Joist deflection: Varying the temperature gradient in the longitudinal slab

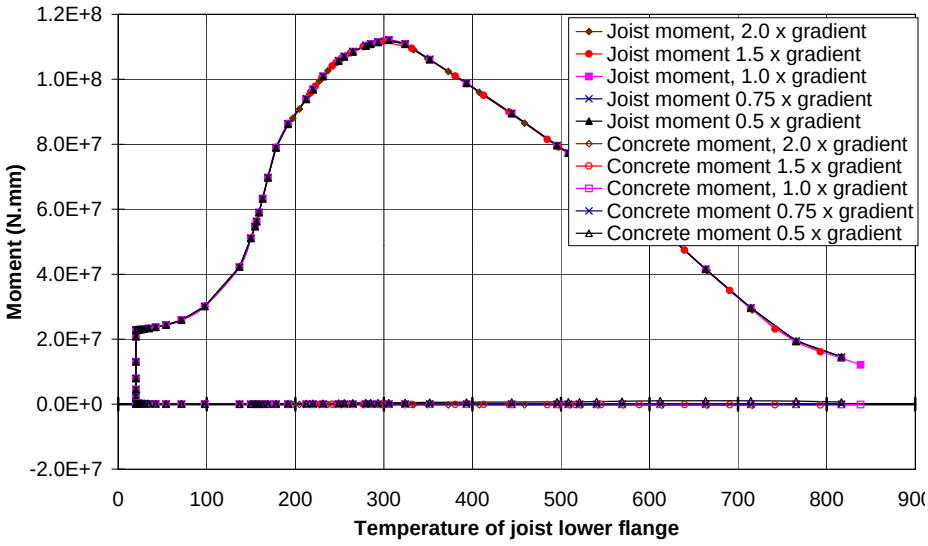

Figure 7.7: Moments at mid-span: Varying the temperature gradient in the longitudinal slab

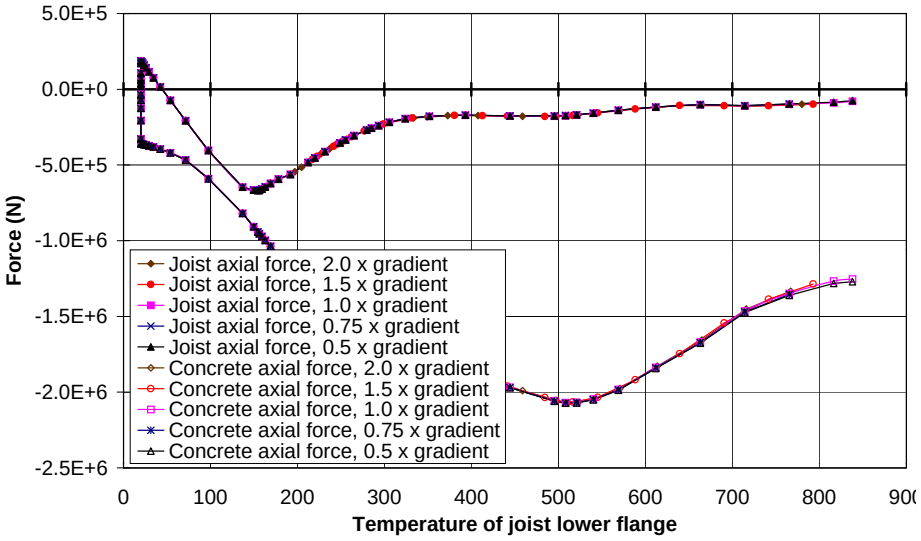

Figure 7.8: Axial forces at mid-span: Varying the temperature gradient in the longitudinal slab

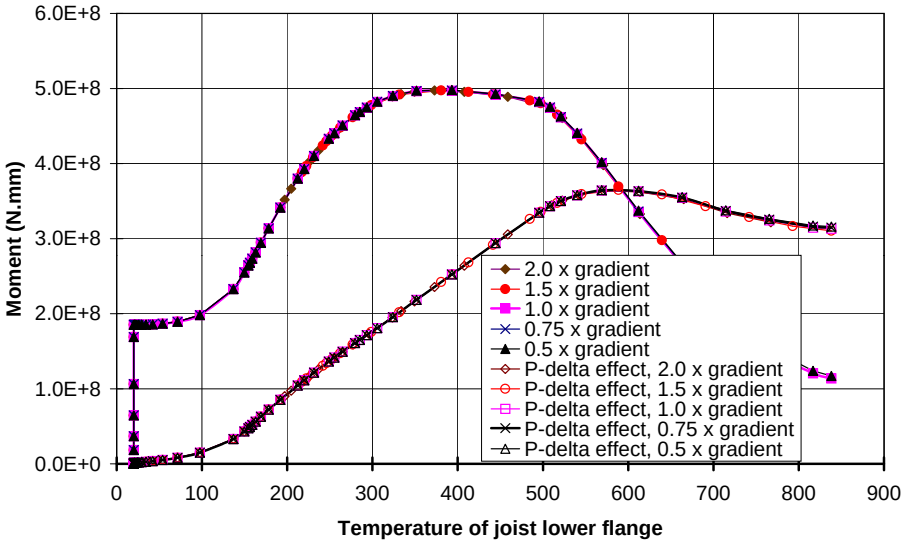

Figure 7.9: Moment Differences: Varying the temperature gradient in the longitudinal slab

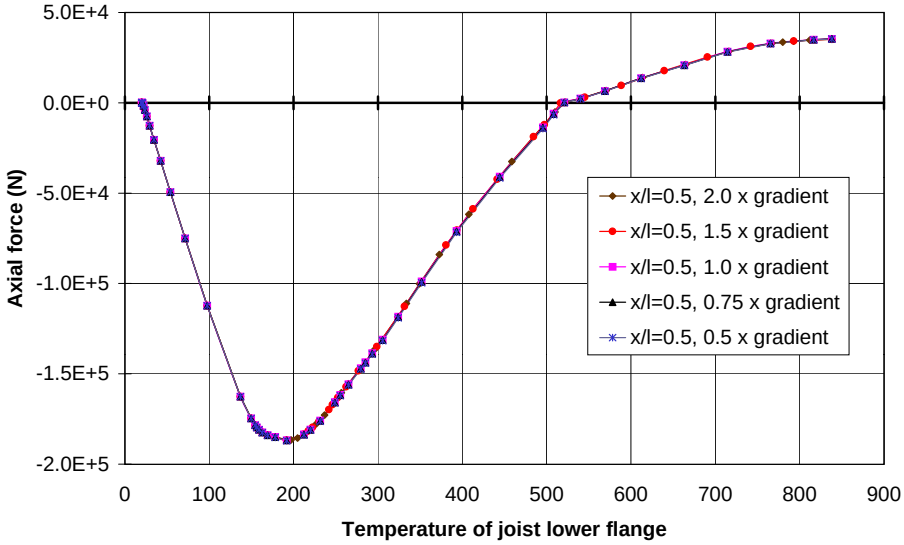

Figure 7.10: Ribs axial force: Varying the temperature gradient in the longitudinal slab

7.2.3.2 Response of the Ribs

Figure 7.10 and Figure 7.11 show the axial force and moment (at the section over the joist) respectively, in the transverse rib located at the mid-span of the composite beam. Again very little difference is seen. The behaviour of the ribs is dominated by the compatibility of displacements with the composite beam and varying the slab gradient has little effect on the displacements as described above.

From Figure 7.10 it can be seen that the compressive axial force in the rib increases because of restrained thermal expansion reaching a peak at approximately 200^oC. Beyond this point the increasing deflections of the composite beam cause the compression in the transverse direction to decline (predominantly in the central ribs). This is because the thermal expansion in the longitudinal direction is greater that in the transverse direction (length of 8m against 3m) and therefore to maintain compatibility of deflection in the two directions mechanical strains compensate for the lack of thermal strain in the transverse direction. This results in a reduction of compression (caused by the initial thermal expansion) up to 550^oC after which the central rib goes into tension. This is a clear evidence of the tensile membrane action creating an alternative load path to redistribute the forces imposed by thermal actions.

As mentioned earlier, the varying of slab thermal gradients in the longitudinal direction

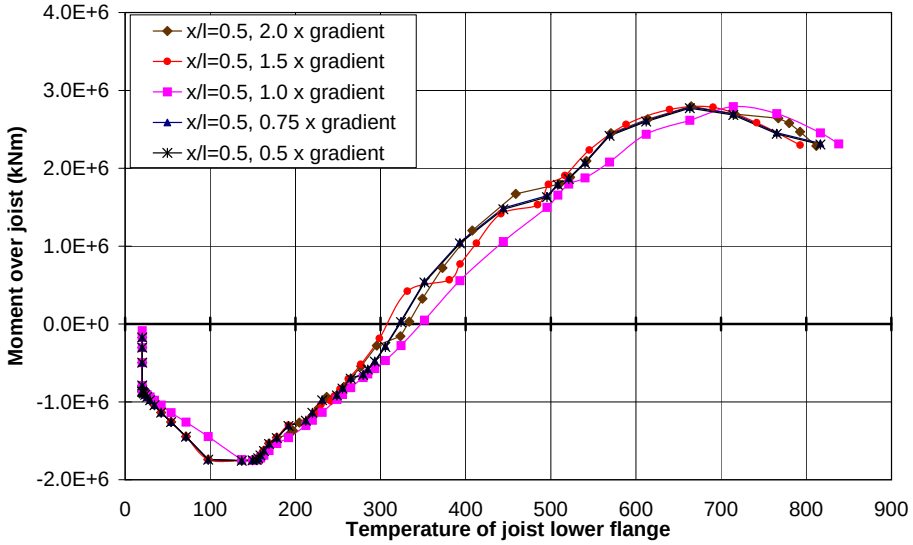

Figure 7.11: Ribs moment over the joist: Varying the temperature gradient in the longitudinal slab

does not produce a significant difference in behaviour. The moments in the central rib shown in Figure 7.11 are initially in hogging as the rib spans over the composite beam at this location. The increasing thermal gradients in the rib (with the fire) initially produce an increase in the hogging moments along its length because of the end rotational restraints (from continuity of the slab), which peaks at approximately 150^oC. The hogging moment reduces beyond this point because of the imposed deflection caused by the composite beam, which (whilst initially acting as a support) begins to act as a point load at the midspan of the central rib producing sagging moments from 350^oC onwards.

7.2.4 Slab gradient variation in transverse direction

This study varies the slab gradient in the transverse (rib) direction from 80% to 200% of the reference gradient. An overview of the full set of results reported here shows that changes in gradient in the transverse slab has a small effect on the deflection where the increase of gradient causes a slight decrease in mid-span deflection (Figure 7.12). This is explained by considering compatibility and total strains leading to deflections. Initially the ribs are in high compression up to 150^oC (Figure 7.17). Compressive strains as a result of restrained thermal expansion dominate. Simultaneously the longitudinal slab and beam are pulling down on the ribs because of compatibility resulting in tensile strains. Any increase in length of the ribs as a result of expansion is absorbed by downward deflections. The total strains producing deflections remain compressive. By

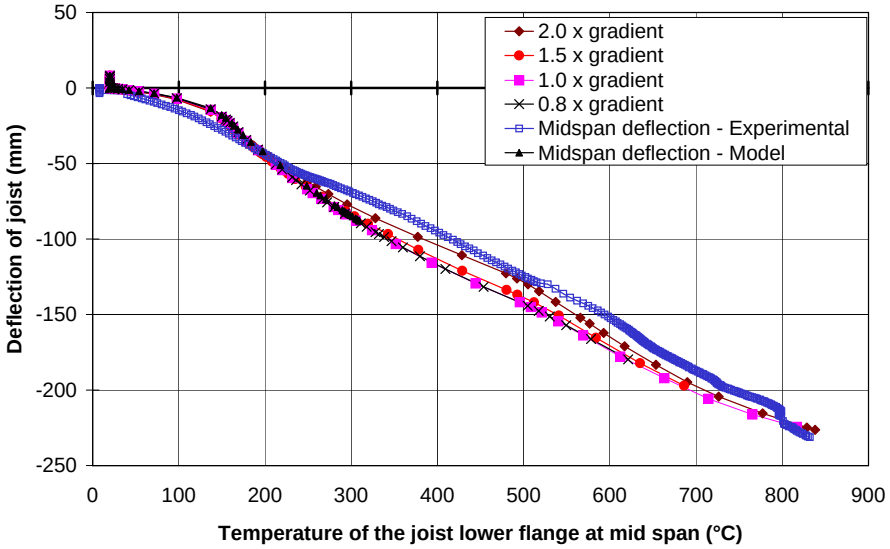

Figure 7.12: Joist Deflection: Varying the temperature gradient in the transverse slab

increasing the rib gradient the total compressive strains in the ribs are reduced and deflections decrease after a reference temperature of 200^{o}C. Beyond 500^{o}C the ribs are in tension (Figure 7.17) so deflections increase because total (tensile) strains are increasing.

7.2.4.1 Response of the composite beam

For both the mid-span and the ends (Figure 7.13 and Figure 7.14) the compressive force in the concrete increases with an increase in the gradient applied to the ribs. This agrees with the fundamental patterns of behaviour discussed earlier, i.e. the increased hogging moments in the ribs caused by increased thermal gradients will offer greater resistance to the deflecting composite beam resulting in increased axial compressions in the composite. Figure 7.15 shows the moments in the joist at the mid-span and the ends. Both moments decrease slightly with increased transverse gradients midway through the fire, reflecting the drop in the composite beam moment arising from a reduced deflection. Figure 7.16 shows the P-Δ moment increasing through the fire and exceeding the initial moment ($\frac{wL^2}{8}$) due to the distributed load at nearly 350^{o}C and finally rising above the increasing total moment in the beam (end to centre difference) at 580^{o}C to the end of fire.

The composite moment difference between the support and mid-span is a measure of a notional uniformly distributed load, w, on the composite beam and is also shown in

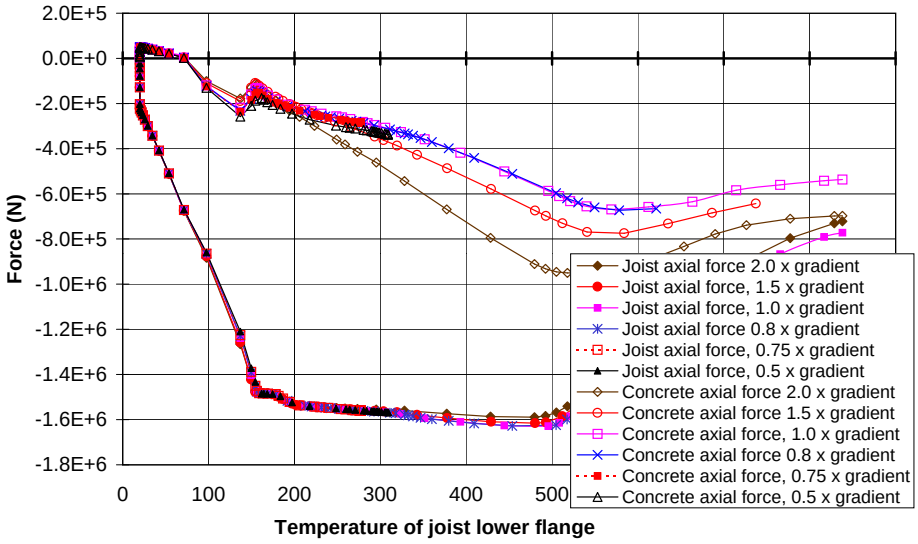

Figure 7.13: Axial force at x/l=0.0: Varying the temperature gradient in the transverse slab

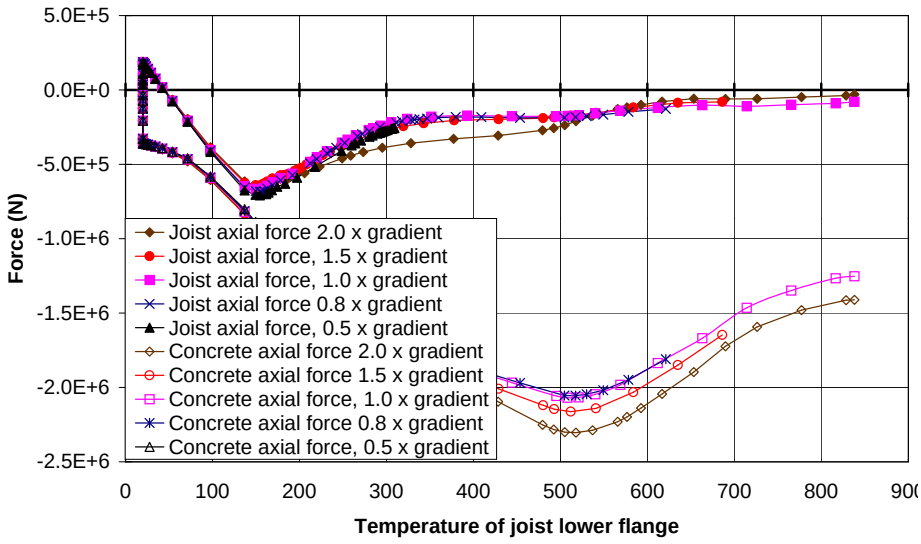

Figure 7.14: Axial force at x/l=0.5: Varying the temperature gradient in the transverse slab

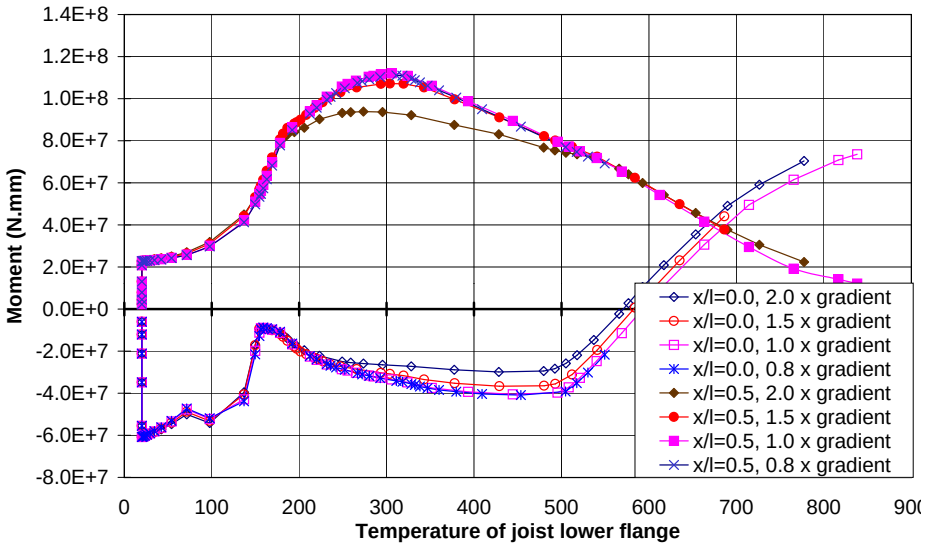

Figure 7.15: Joist Moment at x/l=0.0 and 0.5: Varying the temperature gradient in the transverse slab

Figure 7.16. This moment tends to decrease for the higher gradient regime leading to a lower total moment carried between 200^{o}C and 500^{o}C for the same reasons (reduced deflection). From 580^{o}C onward the beam applies more thermal induced load on the structure than it carries and at this stage the stability of the floor system is ensured by the tensile membrane forces developed in the transverse direction as shown in Figure 7.17.

7.2.4.2 Response of the ribs

Figure 7.18 shows clearly that much larger hogging moments are imposed on the central rib at higher gradients through its depth (due to ends being rotationally restrained), the same is true for other ribs. The imposed moments increase with the fire (increasing thermal gradients) and then reduce in general as explained previously (through deflection compatibility). For double the reference gradient, there is a significant hogging moment in the rib for the whole duration of the fire. This is despite the axial tension in the rib at high temperatures caused by its geometrically non-linear response to the imposed displacement from the composite beam, and the sagging moments caused by the linear response (clearly seen in Figure 7.18 by the deviation in the moment curve at nearly the same point from where the composite beam begins to act as a point load on the central rib).

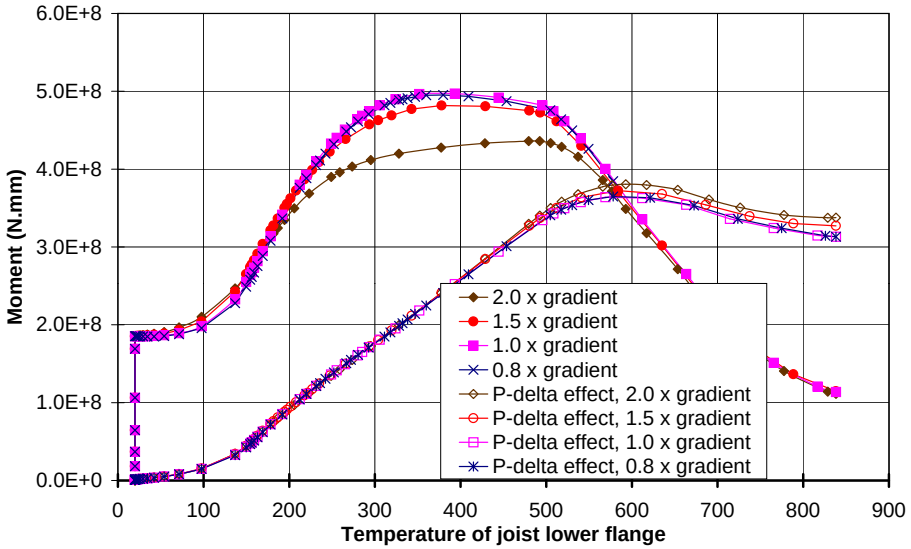

Figure 7.16: Moment Differences: Varying the temperature gradient in the transverse slab

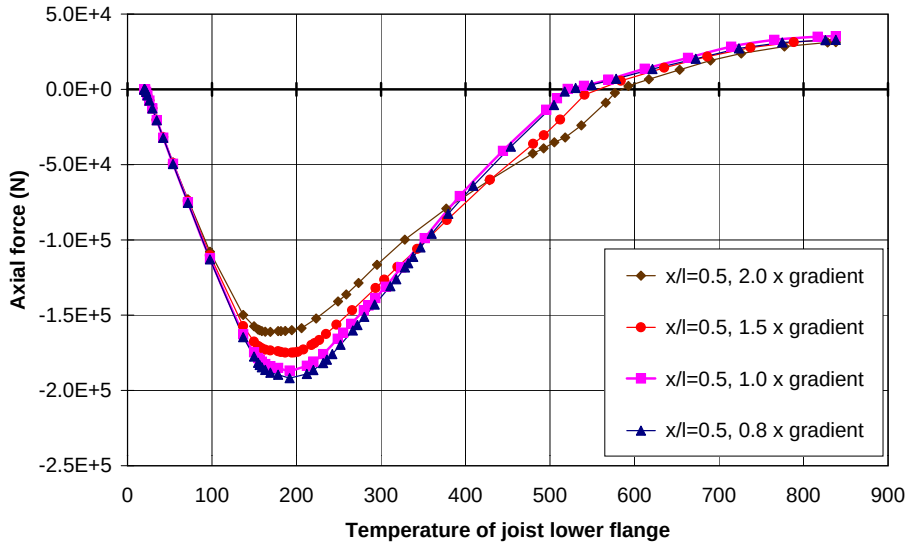

Figure 7.17: Ribs Axial force: Varying the temperature gradient in the transverse slab

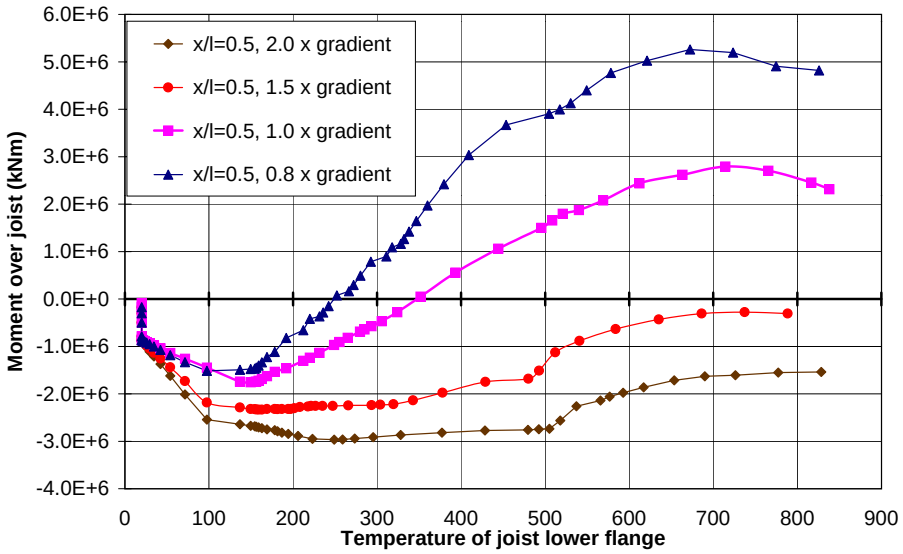

Figure 7.18: Ribs Moment over the joist: Varying the temperature gradient in the transverse slab

7.3 Effect of varying the slab mean temperature in British Steel test 1

In this second part the results obtained from varying the mean temperature rise in the slab in both directions (parallel and perpendicular to the composite beam), while maintaining the thermal gradients to the reference values, are reported. The joist temperature is also kept unchanged increasing to 850^{o}C by the end of the analysis.

7.3.1 Slab mean temperature variation in longitudinal direction

In the first study the temperature at the geometric centroid of the composite slab in the longitudinal direction is varied while the temperatures of the joist and the ribs are maintained as in the reference calculation. The effects of this variation are examined in terms of the deflections of the composite beam and by analysing different quantities that contribute to the equilibrium of the whole compartment in order to determine the impact of such variation on the stability of the structure and its response. The mean temperature in the longitudinal direction is varied from 50% to 200% of the reference value obtained from the reference calculation.[220]

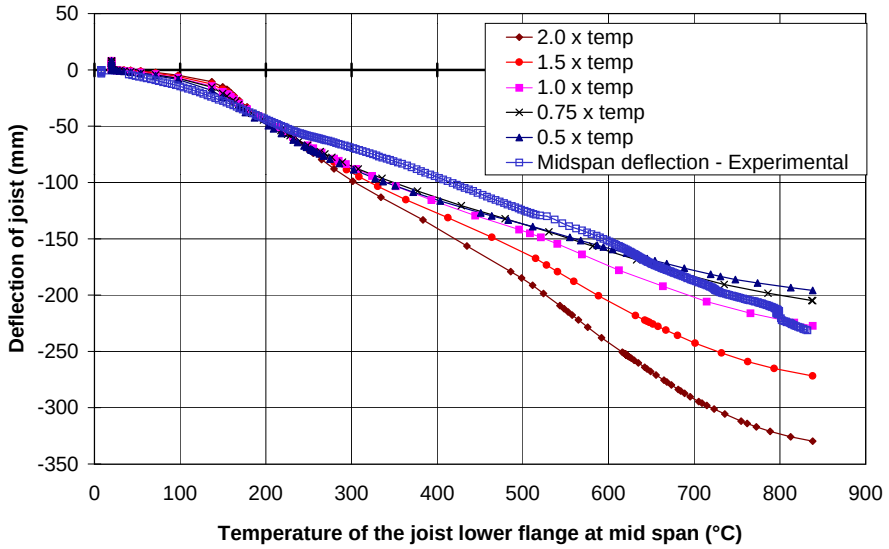

Figure 7.19: Joist Deflection: Varying the temperature at the centroid of the longitudinal slab

7.3.1.1 Response of the composite beam

As the temperature applied to the slab is increased the mid-span deflection gradually increases. At the end of the heating regime the deflection calculated for 1.5 and 2 times the reference temperature is respectively 20% and 40% greater than the reference case (Figure 7.19). This is clearly what is expected as the considerable excess thermal expansions generated by the increased temperatures must be accommodated in deflections. This calculation shows that the effect of slab mean temperature on the structural response is considerable. For temperatures lower than the reference case the final deflection decreases and tends towards a limit of the order of 200mm. The final deflection depends upon the mean temperature of the composite section (slab and joist) but here only the slab temperature has been changed. Reducing the slab temperature reduces the mean temperature (therefore reduces deflections), however another effect of this is an increase of thermal gradient which tends to increase deflection. This combined with the expansion of the transverse ribs (maintained here at the reference value) leads to a limiting deflection. Further explanations of this limiting deflection will appear in the discussion of the response of the ribs below.

To understand the forces driving the deflection the internal forces inside the joist and the concrete slab are studied at 2 main locations, at the end of the beam where the joist is connected to the column and at mid-span where the maximum moments occur.

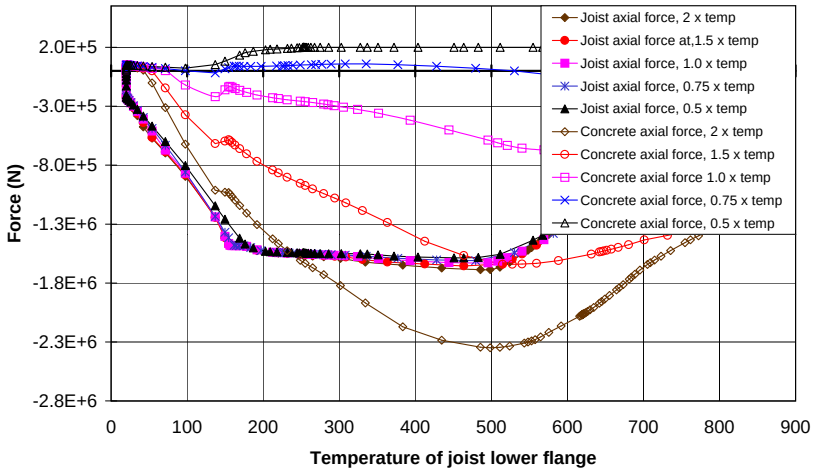

Figure 7.20: Axial force at x/l=0.0: Varying the temperature at the centroid of the longitudinal slab

At both locations the increase of the slab temperature leads to an increase in the slab axial thrust due to the axial restraint provided by the columns and the surrounding structure (Figure 7.20 and Figure 7.21). The large increase in the slab thrust at both sections increases the total thrust acting on the composite beam, which is defined by the sum of the thrust in both individual elements. The development of large axial thrust together with the deflection of the beam produces a P-Δ moment (P is the composite axial force and Δ is the deflection). This new moment can be seen as a thermal load applied to the structure. The magnitude of this moment can reach several times the value of the moments at ambient due to the distributed load carried by the composite beam. Therefore the beam resists both the moments caused by the loads and the P-Δ moments as illustrated in Figure 7.22 which also shows the plot of the difference between the end moment and midspan moment which is a measure of the "equivalent" uniformly distributed load on the beam. At the later stages of the fire (600^{o}C of the reference case, 1.0 x temperature) the P-Δ moment exceeds the difference between the end moment and midspan moment (Figure 7.22) and it is at this point that the composite beam begins to apply a load on the central rib.

At $x/l = 0$ the axial force developed in the joist is insensitive to changes in the temperature applied to the slab (Figure 7.20). This is because the joist at this location

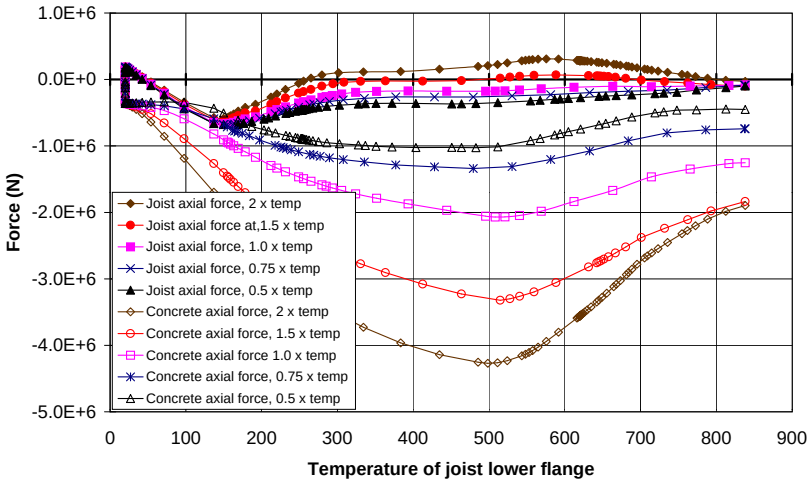

Figure 7.21: Axial force at x/l=0.5: Varying the temperature at the centroid of the longitudinal slab

reaches its yield capacity in compression[222] and the magnitude of the axial force is constrained to remain at the maximum possible value based on the joist temperature. At $x/l = 0.5$ the axial compression in the joist decreases when the slab temperature increases (Figure 7.21). The joist acting compositely with the slab at mid-span experiences positive (sagging) moment, mainly from the P-Δ moments which are affected very strongly by the slab temperature variation (P-Δ moment increases by more than double the reference value upon doubling the slab temperature as shown in Figure 7.22). When the composite beam is in sagging bending, the joist is expected to be in tension (or lesser compression) and the slab in high compression. The moment at this location depends mainly on the difference of thrusts developed in each member of the composite beam and the moment on each element separately. Decreasing the joist thrust leads to a larger moment carried by the beam at this location. Therefore the total moment carried by the beam (difference between the sagging moment at mid-span and the hogging moment at the supports) increases under fire to carry the extra implied moment. Figure 7.22 illustrates this and also shows how the moment carried by the beam increases with increasing the temperature of the slab.

The total composite moment at each location depends also on the moment carried by the joist and the slab individually, however the slab moment is far smaller than the joist

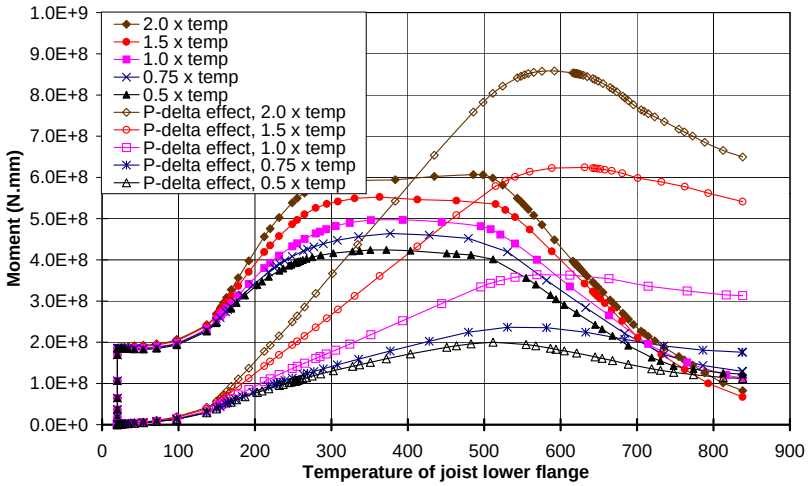

Figure 7.22: Moment differences: Varying the temperature at the centroid of the longitudinal slab

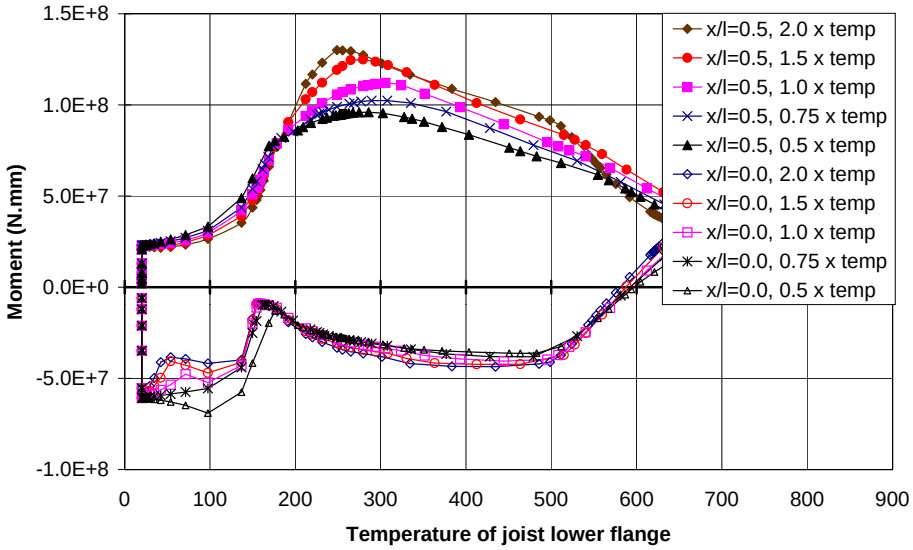

Figure 7.23: Joist Moment at x/l=0.0 and 0.5: Varying the temperature at the centroid of the longitudinal slab

moment and thus is not discussed here. At $x/l = 0$ the hogging moment carried by the joist increases if the temperature applied is reduced but only until the reference lower flange temperature reaches 150^{o}C. This effect is due to the increased thermal gradient (for lower slab temperatures) causing a greater hogging moment along the composite beam.[220] Beyond this, the moment at $x/l = 0$ is insensitive to the applied temperature until 500^{o}C then decreases non-linearly and moves into sagging bending till the end of the fire. At mid-span the sagging moment in the joist increases with an increase in temperature applied to the concrete in the direction of the joist to contribute to the total moment carried by the beam. This is illustrated in Figure 7.23.

7.3.1.2 Response of the Ribs

The following discussion concerns mainly the ribs crossing the heated joist at mid-span to identify the interaction between the ribs and the beam at the most deflected location, where membrane action can be identified clearly. Figure 7.24 shows the axial force in the central rib, which shows an initial increase in the rib compression due to the restrained thermal expansion in the transverse direction. This linear increase reaches a limit before the reference temperature reaches 200^{o}C for all cases, then decreases to zero near 500^{o}C for the reference case. Beyond this point the rib goes into tension to the end of the test. Here the compatibility of deflections in the plane of the slab plays a major role. The initial compressive strains in the ribs are relaxed gradually as the slab deflects and eventually turn into tensile strains at the later stages of the fire to support the extra implied load of the expanding longitudinal slab. This illustrates the development of tensile membrane action in the transverse slab. The magnitude of the tensile membrane forces (or rib axial tensions) determines the restraint provided by the transverse slab to the deflection of the longitudinal slab. This restraint is limited by the tensile capacity of the ribs and therefore for larger longitudinal slab temperatures relatively greater deflections are obtained (see Figure 7.19).

At ambient the central rib is supported over the beam thus the moment in the central rib over the joist is a hogging moment. This support reduces from 150^{o}C and at higher temperatures the central rib moment (over the joist) goes into sagging (see Figure 7.25). This effect is magnified when the longitudinal slab temperatures are increased suggesting that even higher loads are imposed by the longitudinal slab on the central ribs. The decrease in longitudinal slab temperatures shows the reverse.

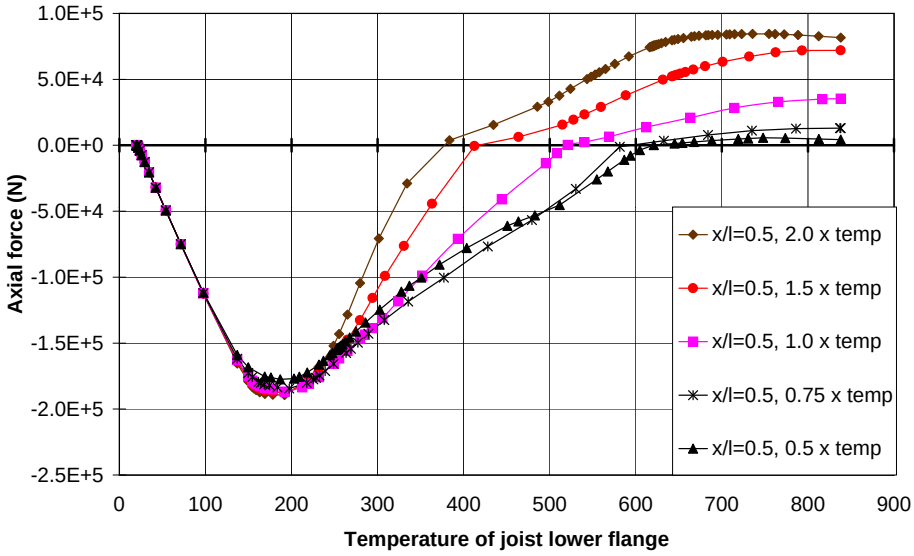

Figure 7.24: Ribs axial force : Varying the temperature at the centroid of the longitudinal slab

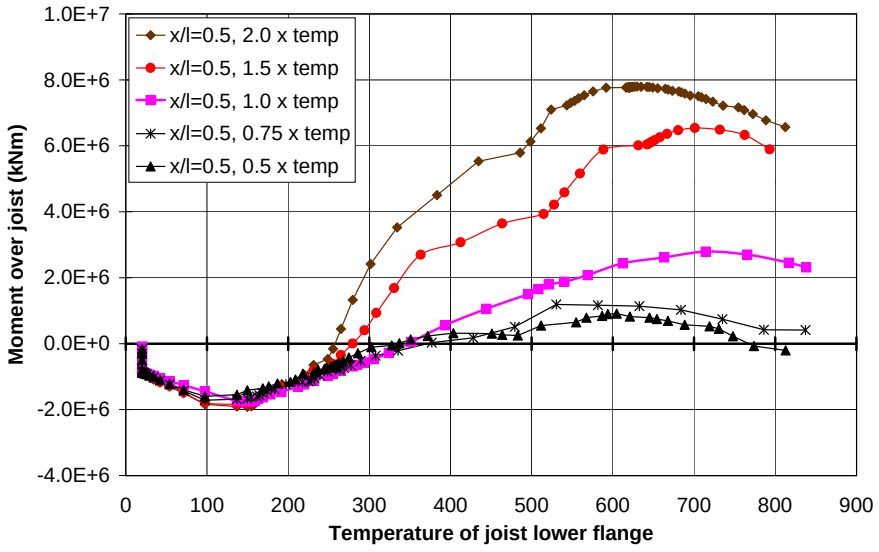

Figure 7.25: Ribs Moment over the joist: Varying the temperature at the centroid of the longitudinal slab

7.3.2 Mean temperature variation in transverse direction

In this section the effect of varying the mean slab temperature in the transverse direction is examined. The mean temperature is varied from 50% to 150% of the reference while maintaining the composite beam (joist and longitudinal slab) at its reference values.

7.3.2.1 Response of the composite beam

The first observation concerns the deflection at mid-span of the composite beam. A 50% increase in temperature of the transverse slab produces nearly 10% (25mm) greater deflection throughout the compartment as shown on Figure 7.26. This is the result of larger thermal expansions in the transverse direction.

The axial forces in the longitudinal slab at the column ($x/L = 0$) decrease significantly with higher transverse slab temperatures (Figure 7.27). However the joist is insensitive to changes in the temperature regime as the axial force in the joist at this location coincides with its yield limit in compression. The increased thermal expansion of the transverse slab (for the higher temperature regime) delays the development of tensile membrane action in the ribs. Therefore the composite beam must continue to carry the thermally imposed loads by a substantial increase (doubling) in the total moment (end to midspan difference) as shown in Figure 7.29. This increase comes mainly from the increase in hogging at the column end through large reductions in the axial compression in the longitudinal slab, as shown in Figure 7.27.

The increased deflections must be compensated by the development of tensile strains in the longitudinal direction (as the temperature in the longitudinal slab is maintained at the reference values), thereby decreasing the axial compressions in it. This effect is clearly observed as the compressive forces in both the longitudinal slab and steel joist tend to decrease with increasing transverse slab temperatures (Figure 7.28), leading to smaller total compressive forces acting in the composite beam. This reduction in the beam axial force reduces the P-Δ moment (Figure 7.29) and reduces the total thermally imposed load redistributed to the transverse direction.

Figure 7.30 shows that the sagging moment in the joist at mid-span and the hogging moment at the column end increases with increasing temperatures in the transverse slab. Together with the changes in the axial forces, this variation of joist moment provides a larger difference in moment between mid-span and column end, which increases the thermally imposed load carried by the composite beam because of the reduction in

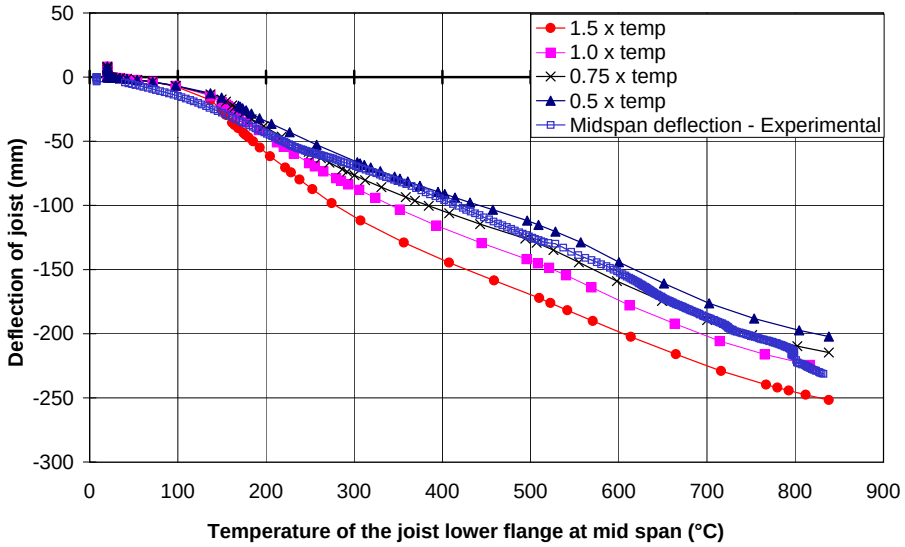

Figure 7.26: Joist deflection: Varying the temperature at the centroid of the transverse slab

support from the ribs.

7.3.2.2 Response of the Ribs

Figure 7.31 highlights the response of the ribs in terms of the development of axial forces. The axial compressions in the ribs increase significantly with increasing temperature as expected because of the effect of restrained thermal expansion. This is consistent with the conclusions made above regarding the delay in load redistribution to the ribs by tensile membrane action.

Figure 7.32 shows that the moments in ribs over the joist are relatively unaffected by the change in temperature until 200^{o}C, beyond this point the moment decreases and goes to sagging bending in the central ribs and increases thereafter. This pattern of behaviour does not change fundamentally for varying transverse slab temperatures, however the differences in magnitude are quite large. The fundamental behaviour remains that of initial hogging moment at ambient, increasing due to thermal gradients and then reducing due to progressive loss of support from the composite beam, leading, initially to sagging moments and finally to tensile membrane action when the composite beam begins to impose load, arising from deflection compatibility.

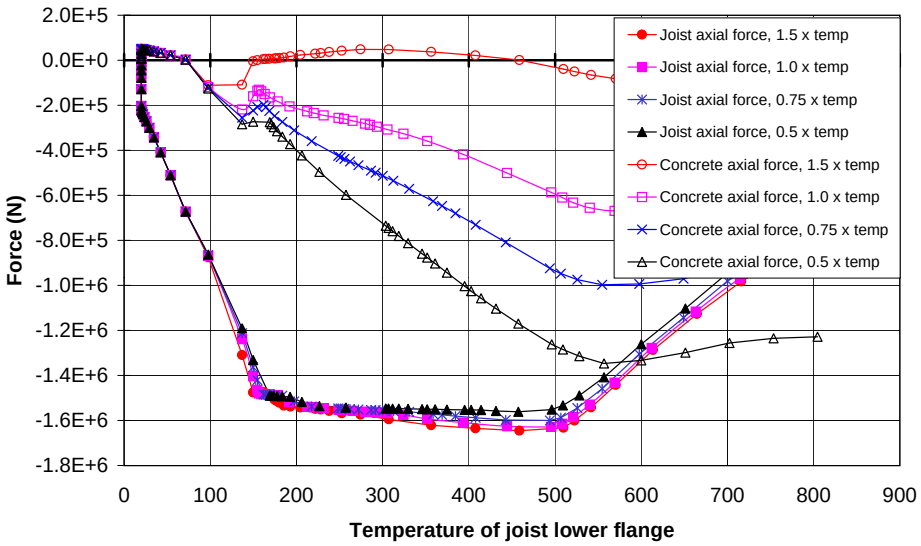

Figure 7.27: Axial force at x/l=0.0: Varying the temperature at the centroid of the transverse slab

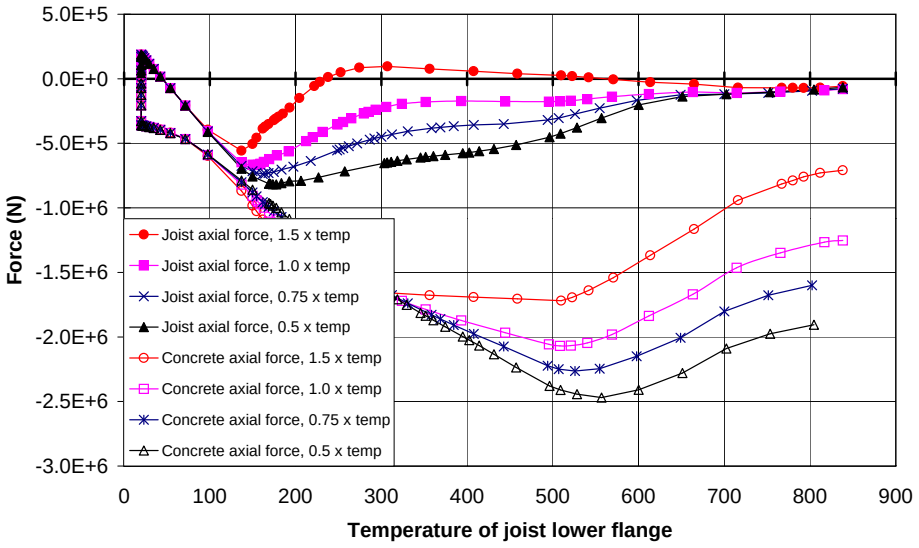

Figure 7.28: Axial force at x/l=0.5: Varying the temperature at the centroid of the transverse slab

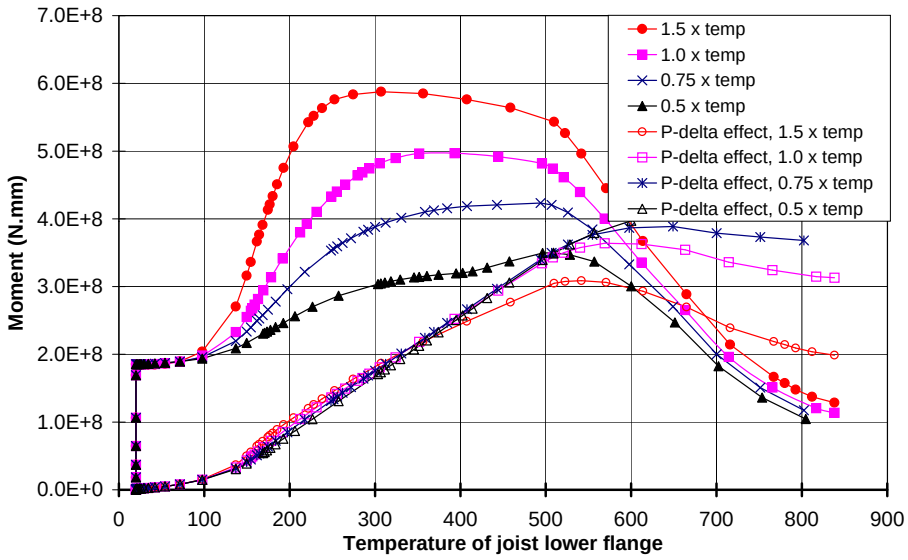

Figure 7.29: Moment Differences: Varying the temperature at the centroid of the transverse slab

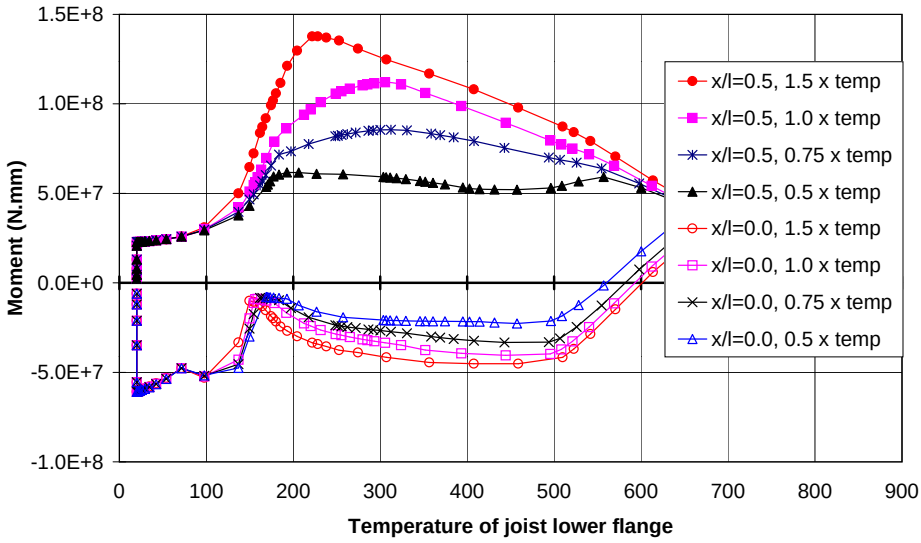

Figure 7.30: Joist Moment at x/l=0.0 and 0.5: Varying the temperature at the centroid of the transverse slab

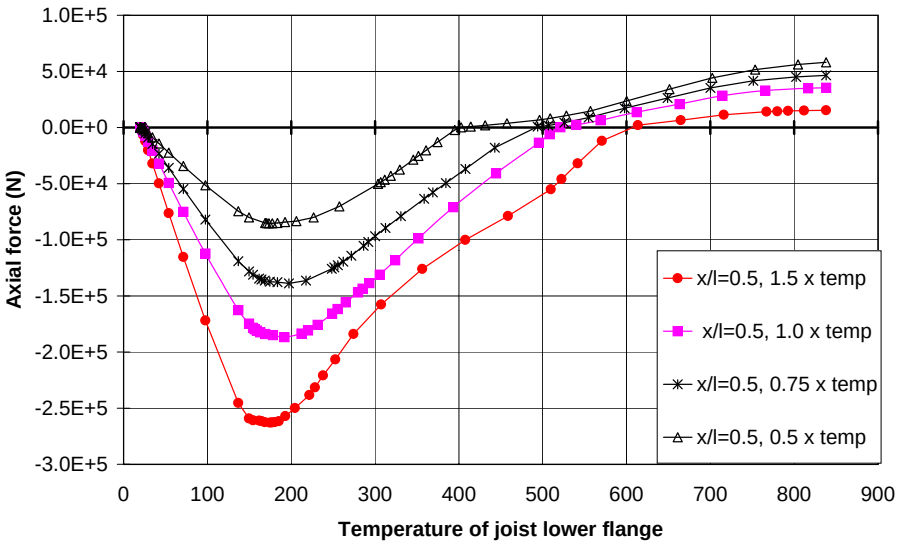

Figure 7.31: Ribs Axial force: Varying the temperature at the centroid of the transverse slab

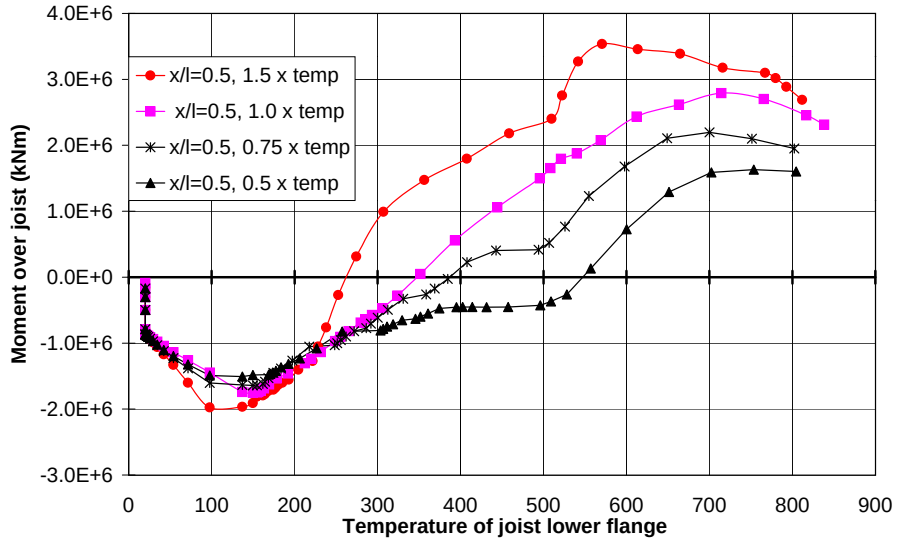

Figure 7.32: Ribs moment over the joist: Varying the temperature at the centroid of the transverse slab

7.4 Conclusions

This exercise has shown that all of the structural responses observed in the models studied above are consistent with the expected patterns of behaviour. In terms of the effect of varying through depth gradients, the general conclusion is that there are no real changes in the pattern of behaviour from the reference case.[222]

In general varying mean temperatures also produces the same patterns of behaviour as identified in the reference calculation.[222] The structural response is manifested more significantly in the variation of internal forces and deflections than when the gradient was changed. The larger deflection variations seen here are because mean temperature changes cause changes in length which have a much stronger effect on deflections relative to the changes in through depth gradients (which impose curvatures which can more easily be restrained by a stiff structure).

The studies described here show that mean temperature increases result in large increases in deflection (through thermal expansion) and large increases in internal forces (P-Δ forces) because of the high lateral restraint in the structure modelled. The equivalent mean temperature variation also has a significant effect on the timing of the development of the redistribution mechanism of tensile membrane action in the transverse slab direction, which occurs between the reference temperatures of 400^{o}C to 600^{o}C depending upon the temperature regime applied.

From the investigations carried out it can be concluded that the response of composite frame structures subjected to local fires in small internal compartments is governed to a large extent by the interaction of the following key phenomena:

1. Thermal expansion caused by a rise in mean temperature
2. Restraint to lateral translation from surrounding structure
3. Thermal bowing caused by the through depth thermal gradient
4. Restraint to end rotation
5. Compatibility of displacements in compartments with orthogonal stiffness distribution

Chapter 8

Parametric studies on a small generic composite steel frame

8.1 Introduction

During the Cardington frame fire tests the structure survived a number of compartment fires ranging in location and geometry, from a highly restrained internal compartment test on a single beam, to a large compartment test over half of a whole floor. The fire temperature-time histories were different in each test and in all but one of the large compartment tests all the steel beams were left unprotected. Undoubtedly the work at Cardington has provided a greater understanding of whole composite frame behaviour in fire. But the new knowledge is based on 6 tests on one structure.

The aim of this chapter and Chapter 9 is to further understand the effects of variables such as fire severity, compartment fire size and compartment fire location on the structural behaviour of generic composite steel frames. The ability of the structure to survive without applied fire protection to the steel beams is also investigated.

Two generic composite steel frames have been designed in accordance with EC4 Part 1.1. Their shape and size in plan were chosen to be significantly different from the Cardington frame. The behaviour of a 2x2 bay frame in a series of parametric studies is discussed in this chapter and the behaviour of a 9x9 bay frame in a similar set of scenarios is reported in Chapter 9.

The small generic frame was subjected to a series of whole floor fire scenarios. Two natural fires based on Pettersson's[195] temperature-time curves were adopted to describe fires with the same fire load but different ventilation. One fire had an opening factor of $0.08m^{1/2}$ and is characterised by high temperatures but short duration. The other fire has a smaller opening factor of $0.02m^{1/2}$. By reducing the opening factor thus the available ventilation the fire achieved lower maximum temperatures but the duration of the post-flashover phase was notably longer.

The structure responded to these two heating regimes in two distinct ways both thermally and structurally. During the "short-hot" fire the unprotected steel achieved temperatures close to the fire atmosphere. The lightweight concrete because of its much lower thermal conductivity and the short fire exposure reached temperatures only marginally higher than at ambient. Thus a high gradient was established over the depth of the composite section. In contrast the "long-cool" fire allowed the concrete slab much longer to respond to the heating regime. In this second scenario the steel temperatures were relatively lower and the mean temperature of the composite section was higher. There were two distinct situations, one of a high gradient leading to structural performance influenced by thermal bowing and a second scenario where the mean temperature of the composite section was high and the behaviour of the structure was dominated by thermal expansion effects.

The effect of maintaining or removing fire protection on the steel beams was also tested

on the small generic frame. Three situations were investigated 1) protecting the primary and edge beams, 2) protecting the edge beams only and 3) leaving all beams unprotected. It was assumed that the columns should always be protected.

8.2 Analysis

The generic frame studies were in three parts. First the design fires were established then heat transfer calculations were carried out to obtain the temperature-time histories of the structural elements. The steel and concrete temperature data was then included in the ABAQUS structural model.

8.2.1 The generic frame

A schematic plan view of the 2x2 bay generic frame designed for the purposes of this research is shown in Figure 8.1. The layout of the 2x2 frame is asymmetric about the x-axis. The location of the bracing adds to this asymmetry. The structure is 5 storeys high (20m) similar in construction to the Cardington 8-storey frame. It comprises a 130mm trapezoidal composite steel and lightweight concrete deck and a frame of steel columns and composite beams. Composite action is achieved with shear studs welded to the top flange of the beams.
Based on the height of the building and an office occupancy the required fire resistance period of the 2x2 bay structure is 60 minutes.[62] When fire protection was applied to the steel members it was prescribed in accordance with the yellow book.[7]
In both cases the beams and columns were designed to a Load ratio[39] between 0.5-0.7.
A grid system has been devised for naming the structural members. For instance when referring to secondary beam AB2 this lies between gridlines A and B and along gridline 2.

8.2.2 Design fires

Using the natural fire curves described by Pettersson[195] and assuming a constant fire load but different opening factors two design fires were derived (See Figure 8.2). With an opening factor of $0.08m^{1/2}$ the post-flashover fire is short in duration reaching high maximum compartment temperatures. The fire with an opening factor of $0.02m^{1/2}$ is characterised by lower maximum compartment temperatures but relatively longer duration. For the purposes of this discussion the fires will be referred to as the "*short-hot*" fire and the "*long-cool*" fire respectively. In both cases the fire load is equal to

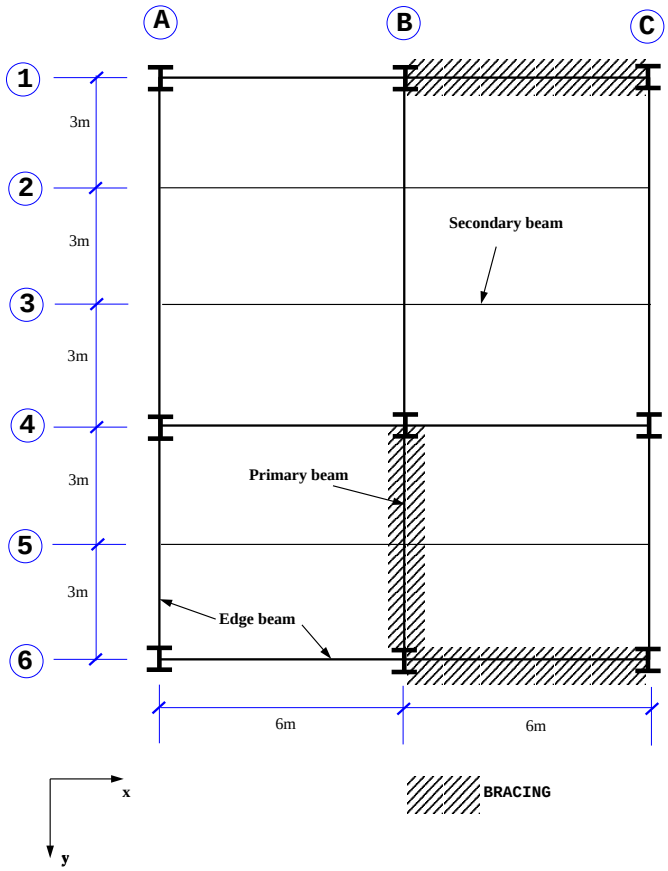

Figure 8.1: Schematic plan view of the 2x2 bay generic frame

215MJ/m^2. Pettersson expresses fire load in terms of the surface area of the whole compartment less the area of the openings. Nowadays fire loads are expressed in terms of the floor area,[115] therefore the equivalent load is about 700MJ/m^2. The Pettersson model ignores the growth phase of the fire. To aid convergence of the structural solution a small delay was incorporated in both fire curves before flashover. These were based on a "fast" t^2 fire assuming an office occupancy.[115] The growth phase in both fires is identical up to 450^{o}C until the natural fires begin (Figure 8.2).

8.2.3 Heat transfer

Heat transfer to protected and unprotected internal steel beams was calculated using the equations in Eurocode 3 Design of steel structures, Part 1.2: General rules (structural fire design).[77] Using the heat transfer model HADAPT[108,137] the temperatures of the composite slab and the protected edge beams were modelled. This modelling has already been discussed in Chapter 5 when analysing the Cardington frame fire tests.

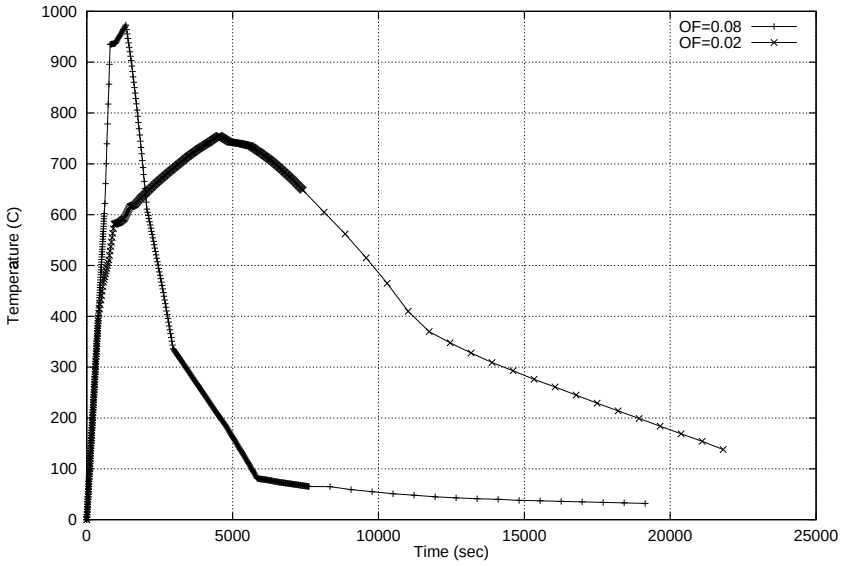

Figure 8.2: Compartment fire Temperature-time curves developed by Pettersson[195]

8.2.4 Temperature loading

The atmosphere temperatures have been modelled using Pettersson's approach which assumes the compartment after flashover is a well-mixed environment of uniform temperature. Therefore any differences in the temperatures of the structural elements are attributed to their material properties, dimensions or location(e.g the edge beams have a considerable gradient across their section whereas the internal beams have a small gradient over their depth). This assumption leads to hotter edge beams because in a real compartment fire the atmosphere temperatures near the walls or windows will be slightly cooler. In the Cardington frame tests the edge beams were found to be 25% cooler than the hottest internal beam.[176,197]

8.2.4.1 Beam and column temperatures

The mean temperatures of the protected and unprotected steel sections of the 2x2 bay frame are shown in Figure 8.3 against time. However, the results of these analyses are plotted against unprotected secondary beam temperature. This method of presenting the results is more useful than data against time because the temperatures at which forces and deflections occur are shown directly. The mean temperature histories of the protected and unprotected steel sections of the 2x2 bay frame are shown in Figure 8.4 against secondary beam temperature. The gradient over the cross-section of the edge beams was predicted using HADAPT. To model the temperature of the steel beams or

columns in the structural model, ABAQUS reads 5 temperatures over their cross section (2 in each flange and 1 in the web) as shown in Figure 8.5. ABAQUS interpolates between these data points. The temperature histories of the steel beams in ABAQUS are defined by an amplitude curve thus the actual fire history can be modelled.

The column temperatures were calculated using the heat transfer equations in EC3 Part 1.2. The mean temperature histories of an edge column, corner column and internal column for both fires are shown in Figure 8.6. Corner columns achieve very low temperatures because they are shielded by the walls spanning into them. It was assumed that the columns were slightly cooler near the floor of the compartment than near the ceiling although at best these were "guesstimates" based on Cardington test data.

8.2.4.2 Slab temperatures

Two sets of temperature data are given for the slab:

1. a mean temperature and linear through depth gradient in the ABAQUS input file for the thermal loading.
2. a set of non-linear through depth gradients for the ribs and troughs of the profiled floor slab in SRAS of FEAST for the temperature dependent section properties.

The linear gradient and mean temperature given in the ABAQUS input file act at the centroid of the section (Figure 8.7) and are an idealisation of the real temperature regime through the depth of the slab. The actual temperature distribution through the depth of the slab was calculated using HADAPT. By calculating the stresses and strains as a result of the actual temperature distribution, the equivalent mean temperatures and linear gradients to give an equivalent stress state can be calculated.[247] Table 8.1 lists the mean temperature and through depth linear gradient used in ABAQUS for both fire scenarios.
The slab mean temperature follows the course of the heating regime but the slab gradient in the ABAQUS input file must increase linearly over time. The history of the slab gradients are described in Figure 8.8. This has important implications because the gradients are very different from the start of the analysis and not just after flashover. Thus although the atmosphere temperatures are identical in both heating regimes up to flashover the slab gradients differ, exaggerating the difference between the two fires in the early stages.

Opening factor	ΔT	$T_{,y}$
($m^{1/2}$)	(^{o}C)	(^{o}C/mm)
0.08	100	8
0.02	190	4

Table 8.1: Mean temperature ΔT and gradient $T_{,y}$ in the concrete slab

SRAS reads non-linear gradients, described by polynomials, to calculate the behaviour of the shells at high temperatures used to represent the slab in the ABAQUS model. The actual gradient calculated by HADAPT and the best-fit polynomials are shown in Figures 8.9-8.10 for both fires in the ribs and troughs of the slab.

The structural analysis continues until the unprotected steel temperatures peak because FEAST cannot model unloading during cooling. The slab and protected steel temperatures are considerably lower at this stage and would continue to rise after the end of the analysis.

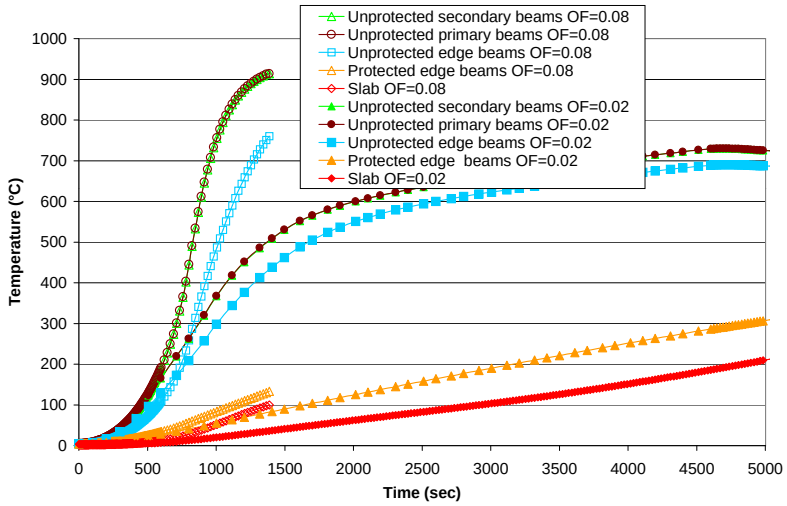

Figure 8.3: Mean steel and concrete temperatures against time used in the ABAQUS model

8.2.5 The structural model

The beams and columns are modelled using 2-noded beam elements and the slab is represented by a mesh of 8-noded reduced integration shell elements. The columns are modelled on two floors, that of the fire compartment and the floor above. The bases of all the columns are fixed (no translations or rotations) vertical translations only are allowed at the top.

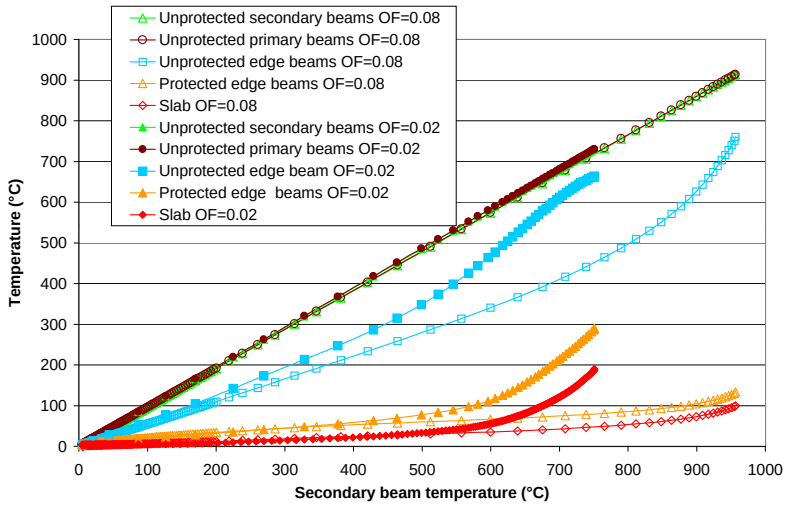

Figure 8.4: Mean steel and concrete temperatures against secondary beam temperature used in the ABAQUS model

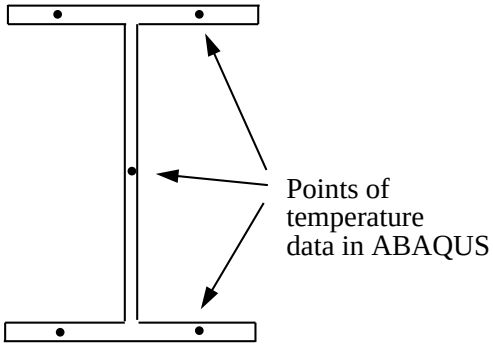

Figure 8.5: Points of beam temperature data in ABAQUS

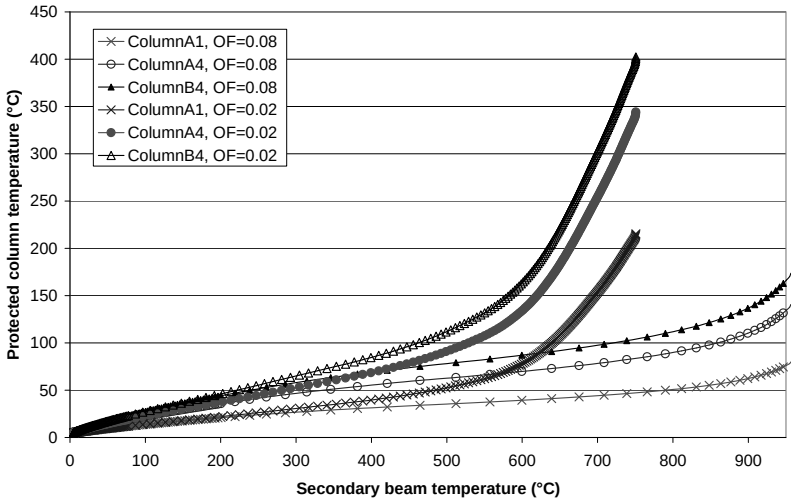

Figure 8.6: Column temperature histories

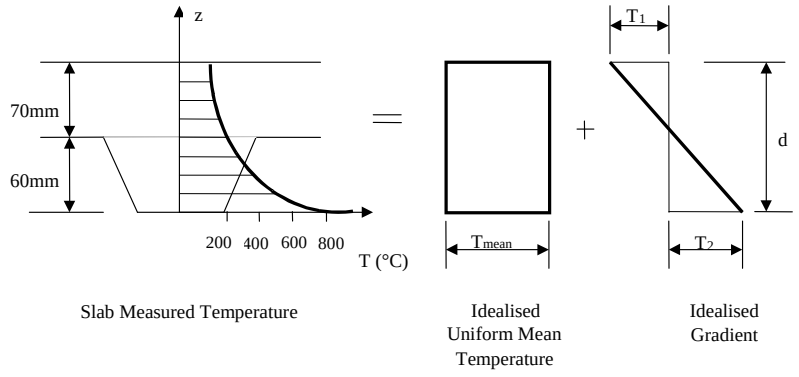

Figure 8.7: Idealisation of the temperature regime acting over the slab

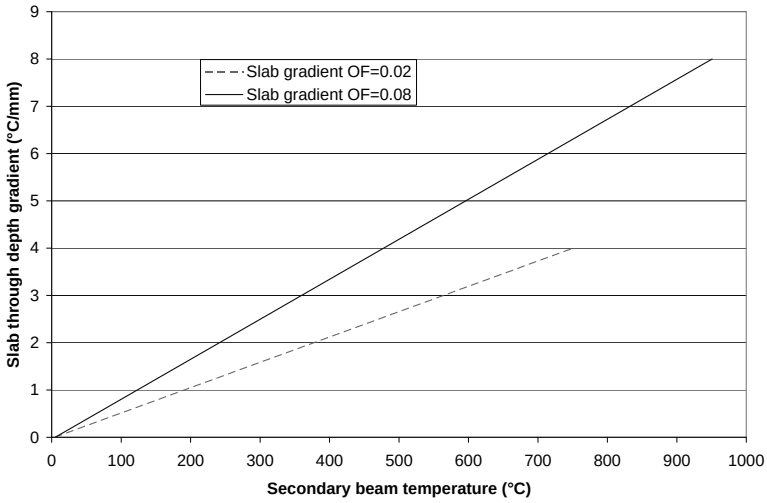

Figure 8.8: Linear gradient history of the concrete slab

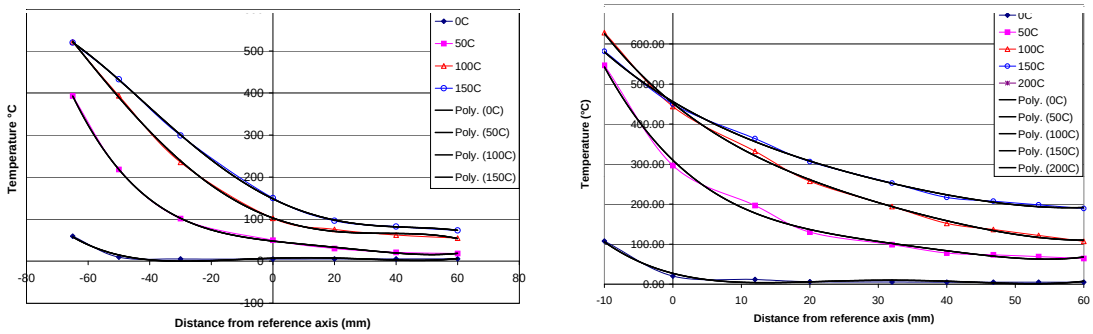

(a) Ribs

(b) Trough

Figure 8.9: Non-linear gradients through the depth of the slab for the "short-hot" fire, OF=0.02

The structure was designed for a dead plus imposed load of 9.25kN/m^2 (a factored design load of 13.4kN/m^2). The imposed load applied to the ABAQUS structural model is 7.25kN/m^2 distributed over the whole floor slab. An imposed load of 7.25kN/m^2 is high but it is in agreement with similar work ongoing in Europe.[246] Initially the analyses were to be conducted with an imposed load of 5kN/m^2, increasing the load caused an increase in the design load ratio of the beams. The secondary and edge beams in the 2x2 frame remained within the 0.5-0.7 limits of load ratio. However the load ratio of the primary beams increased to 0.75. This load ratio is outwith those specified in BS 5950 Part 8 of up to 0.7 but the worst case scenario provided interesting results. Tables 8.2-8.4 list the loading conditions, and load ratios in these studies and at Cardington.

Type of load	**Design characteristic load** (kN/m^2)	**Load applied during fire tests** (kN/m^2)
Raised floor	0.4	0.4
Services	0.25	0.25
Ceiling	0.15	0.15
Partitions	1	1
Imposed	2.5	0.83
Dead	2.85	2.85
Total	**7.15**	**5.48**

Table 8.2: Loads on the Cardington frame[6]

Type of load	**Design characteristic load** (kN/m^2)	**Design factored load** (kN/m^2)	**Load applied to the ABAQUS model** (kN/m^2)
Ceiling and services	0.4	0.54	0.4
Partitions	1	1.5	1
Imposed	5	7.5	7.25
Dead	2.85	3.85	2.85
Total	**9.25**	**13.4**	**11.5**

Table 8.3: Loads applied to the generic frames

Frame	**Section size (grade S275)**	**Location**	**Load Ratio**	**Limiting Temperature to BS 5950 Part 8** (^oC)
Cardington	305x165x40 UB	9.0m Secondary beam	0.4	680
Cardington	356x171x51 UB	6.0m Primary beam	0.39	685
Cardington	610x229x101 UB	9.0m Primary beam	0.26	747
2x2 bay frame	254x146x43 UB	6.0m Secondary beam	0.55	635
2x2 bay frame	457x191x74 UB	9.0m Primary beam	0.75	< 590
2x2 bay frame	305x127x48 UB	6.0m Primary beam	0.75	< 590
9x9 bay frame	356x171x67 UB	9.0m Secondary beam	0.47	659
9x9 bay frame	610x229x125 UB	9.0m Primary beam	0.65	605

Table 8.4: Load ratio

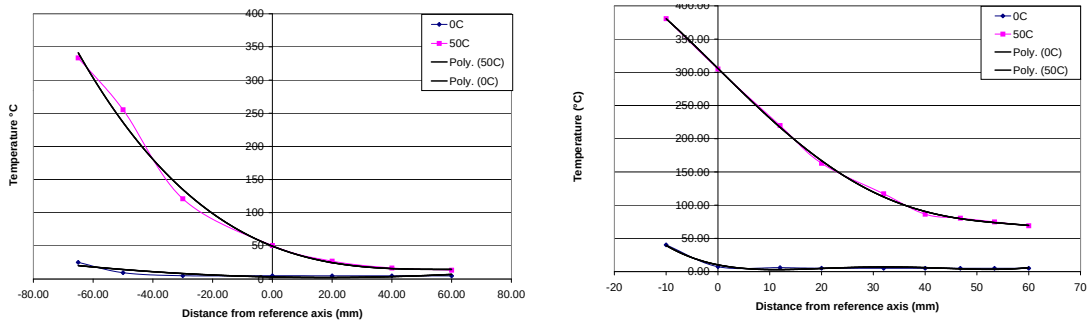

(a) Ribs (b) Trough

Figure 8.10: Non-linear gradients through the depth of the slab for the "short-hot" fire, OF=0.08

8.2.6 The numerical model

The shell model FEAST (Finite Element Analysis of Shells at High Temperatures) developed by Gillie[88] to analyse slabs under fire conditions with the finite element package ABAQUS has been used in these studies. The model has already been checked against the test data from the Cardington frame fire tests[90] and validated by Gillie.[88, 89] A review of this information has been presented in Chapter 4 including the assumptions made during the development of the model and any shortcomings or limitations. The assumptions in the Cardington frame modelling (Section 4.4.1.2.2) have also been applied to the generic frames. The mesh for the 2x2 frame is shown in Figure 8.11.

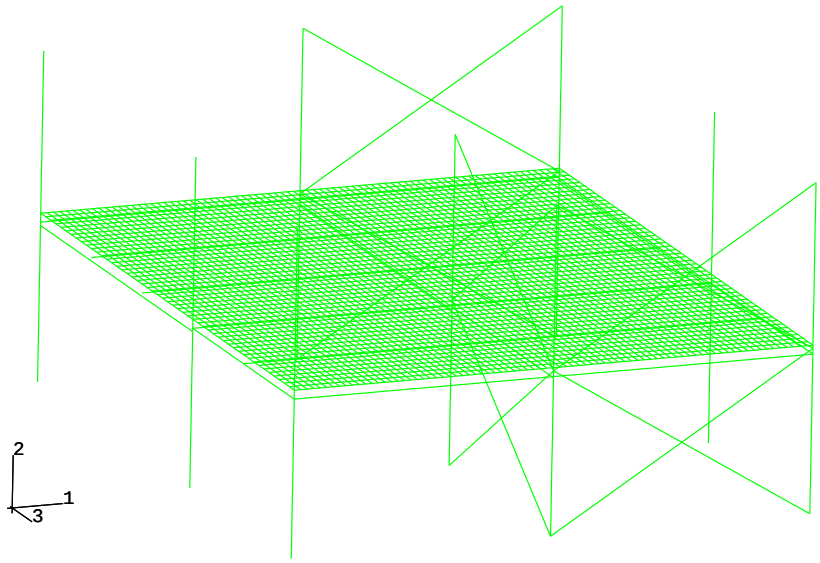

Figure 8.11: ABAQUS mesh of the 2x2 frame

Scenario	Frame	Opening factor ($m^{1/2}$)	Compartment	Protected beams	Imposed + Dead Loading (kN/m^2)
1	2x2	0.02	Whole floor	Primary and Edge	11.5
2	2x2	0.02	Whole floor	Edge	11.5
3	2x2	0.08	Whole floor	Edge	11.5
4	2x2	0.02	Whole floor	None	11.5
5	2x2	0.08	Whole floor	None	11.5
6	2x2	0.08	Whole floor	Edge	5.5
7*	2x2	0.08	Whole floor	Edge	11.5

Table 8.5: Scenarios conducted on the generic frames (*No secondary beams in the frame of scenario 7)

8.3 Parametric Studies

Seven studies were conducted on the 2x2 bay generic frame. Table 8.5 describes the various parameters. The fire in each case is characterised by the opening factor and the compartment. For instance scenario 3 describes a fire in the 2x2 bay frame with an opening factor of $0.08m^{1/2}$ ("short-hot" fire) acting over one whole floor of the building. The fire scenario in each case is realistic because for a given floor area and opening factor (Equation 8.1), the required area and height of ventilation was calculated. This was checked against the available ventilation from generic windows in the external walls. The scenarios also vary whether there is protection on the edge or primary beams. In all cases the columns are protected to their full height.

$$OF = \frac{A_w\sqrt{H}}{A_T} \tag{8.1}$$

where,
A_w =area of ventilation (m^2)
H =height of opening m
A_T =surface area of walls, floor and ceiling less area of ventilation (m^2)

8.4 Results

8.4.1 Short versus long post-flashover fires in the 2x2 bay frame with edge beams protected

Scenarios 2 and 3 of Table 8.5 are compared in this section.

8.4.1.1 Deflection response

Figures 8.12 shows the mid-span deflection of the secondary beams between gridlines A and B, for both fires, against secondary beam temperature. Figure 8.13 shows the mid-span deflections of the primary beams. The deflections of the unprotected steel beams are very similar in both studies. The greatest deflection (360mm) is recorded in the 9m primary beam in response to the "short-hot" fire. In both fires secondary beam AB4 experiences the lowest deflections, due to the stiffness of the structure around column B4. Column B4 also expands vertically upwards pulling the beams with it. Secondary beams AB2 and AB3 deflect the most because the beams are present in a 6m x 9m bay which because of its basic geometry will expand and deflect more than the 6m x 6m bays.

Figure 8.14 shows the same secondary beam deflections against time. This figure highlights that high deflections are achieved very quickly in response to the "short-hot" fire. During the "long-cool" fire there is a rapid increase in the rate of deflection at 450^{o}C in all the primary beams and the secondary beams. The rate of deflection decreases again after a few degrees rise in temperature. This can be seen in Figures 8.12 and 8.13. This bifurcation is shown in other results and will be discussed again throughout the description of the models behaviour. A similar bifurcation exists in the "short-hot" fire at about 90^{o}C.

The protected edge beam deflections are given in Figures 8.15 and 8.16. The temperatures achieved by the protected members exposed to the "long-cool" fire far exceed the temperatures in response to the "short-hot" fire (See Figures 8.3 and 8.4). This is expected because of the longer fire exposure and results in greater deflections. Beyond a secondary beam temperature of 450^{o}C the rate of deflection of the edge beams exposed to the "long-cool" fire increases considerably.

The 6m edge beams spanning along gridlines 1 and 6 are influenced by the bracing in the same direction. Edge beams BC1 and BC6 are highly restrained thus deflect to a greater extent than beams AB1 or AB6 respectively (see Figure 8.16).

Figures 8.17 and 8.18 plot the rate of mid-span deflection against secondary beam temperature of the beams along gridlines A, B and C. There is a rapid increase in the rate of deflection at the bifurcation event in each fire. However the rate becomes stable again very quickly. In the "long-cool" fire the rate of deflection begins to oscillate towards the end of the test. This type of oscillation behaviour was shown to coincide with runaway failure in a simple beam in Chapter 6. In the "short-hot" fire the rate of deflection remains steady (after the bifurcation event) at the mid-span of all beams.

Figures 8.19(a) and 8.19(b) show the deflection contours of the slab at the end of both heating regimes. These highlight the very smooth patterns of displacement which

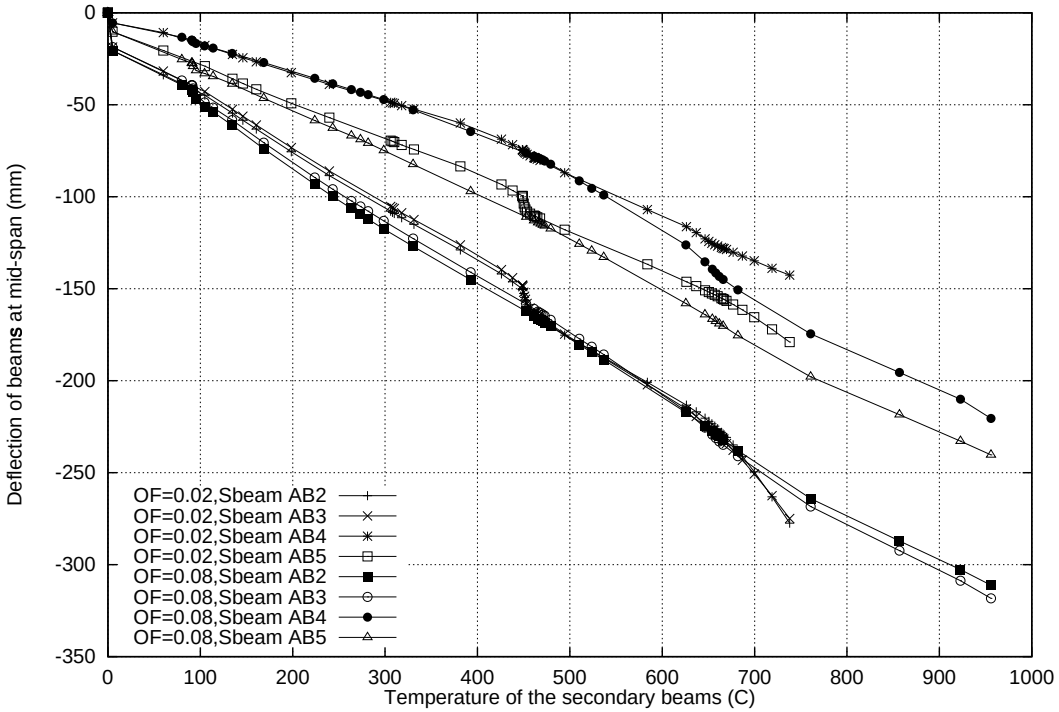

Figure 8.12: Deflection history of the unprotected secondary beams against secondary beam temperature

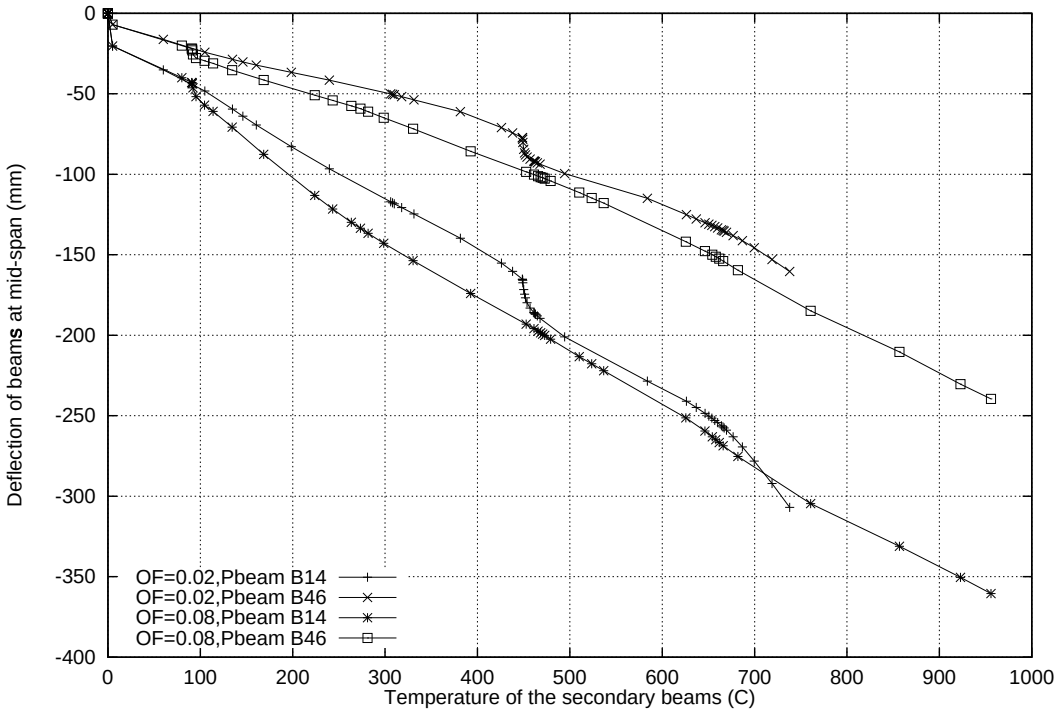

Figure 8.13: Deflection history of the unprotected primary beams against secondary beam temperature

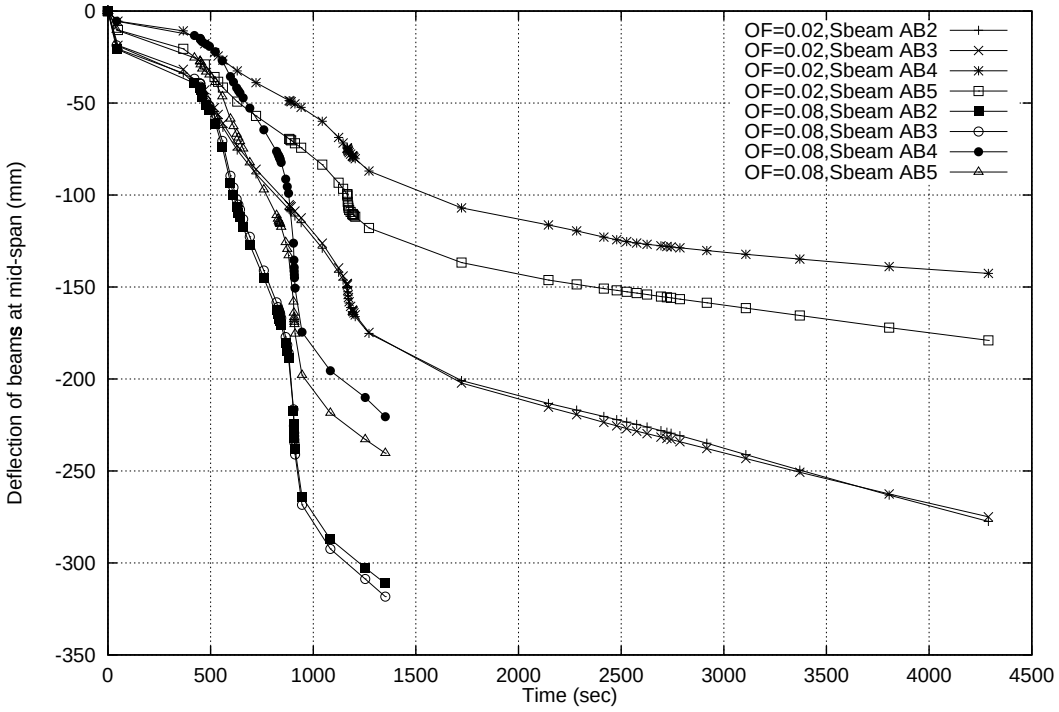

Figure 8.14: Deflection history of the unprotected secondary beams against time

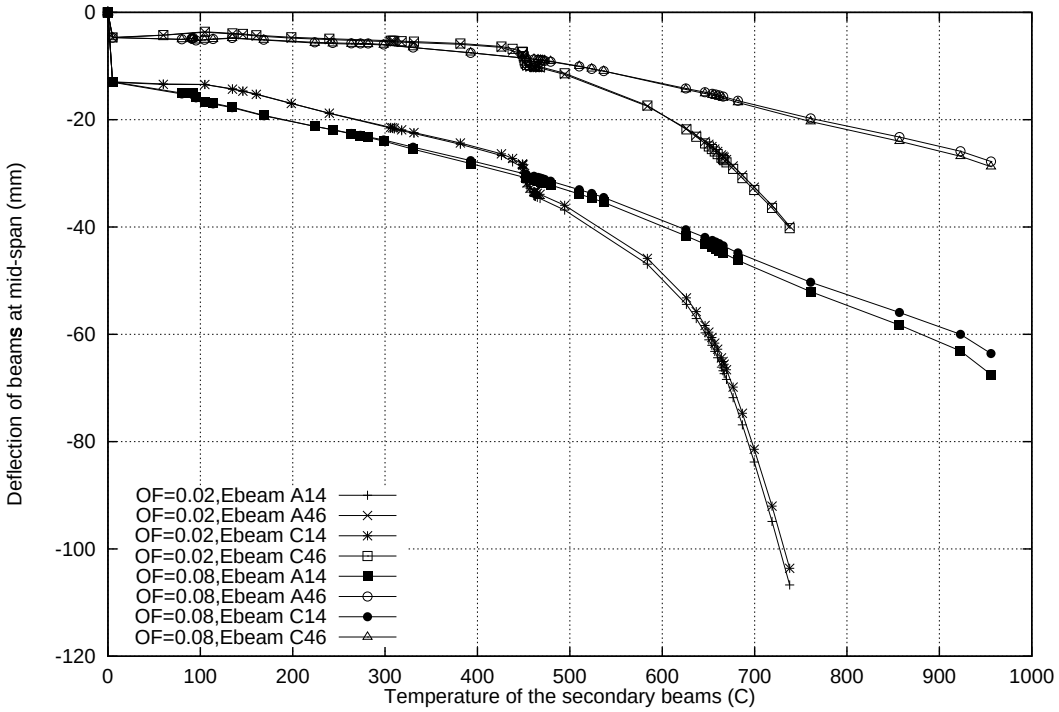

Figure 8.15: Deflection history of the protected edge beams parallel to the primary beams against secondary beam temperature

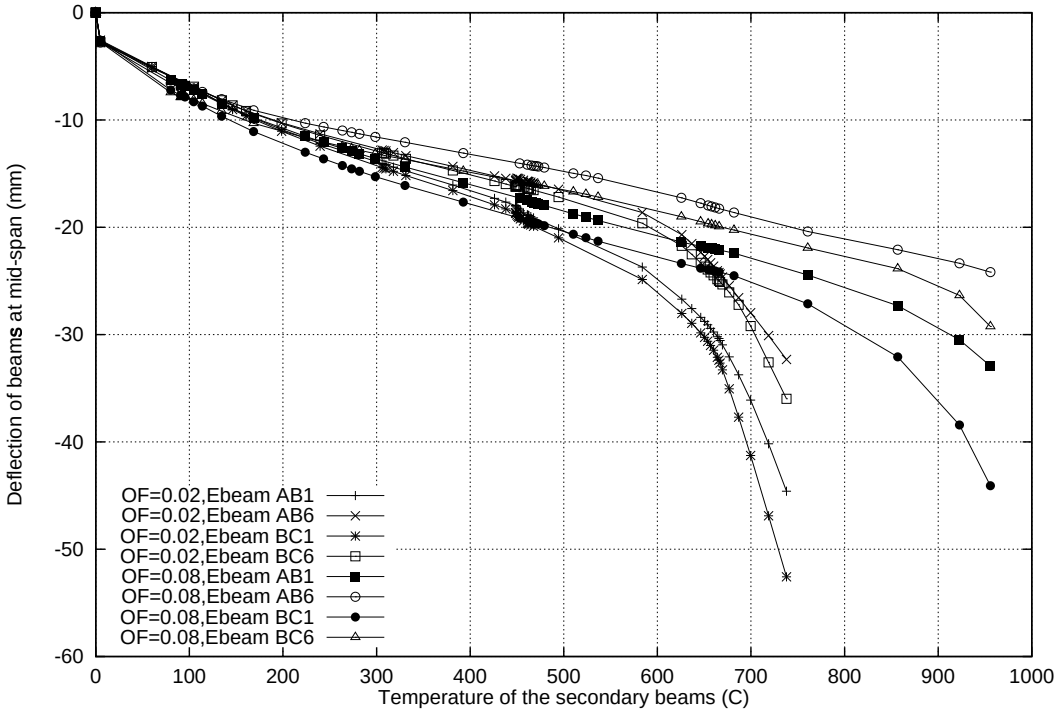

Figure 8.16: Deflection history of the protected edge beams parallel to the secondary beams against secondary beam temperature

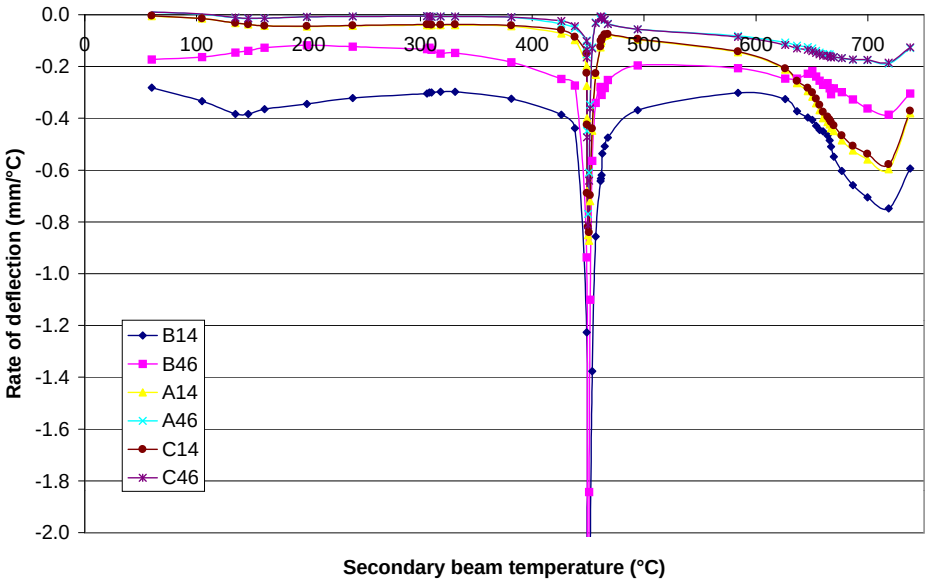

Figure 8.17: Rates of deflection at mid-span of the edge and primary beams against secondary beam temperature, OF=0.02

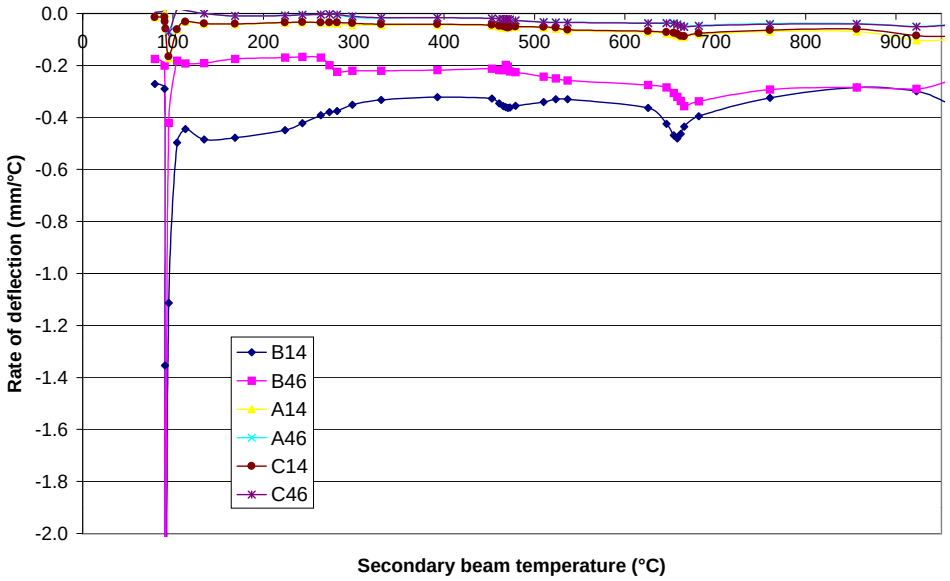

Figure 8.18: Rates of deflection at mid-span of the edge and primary beams against secondary beam temperature, OF=0.08

develop during heating and expansion of the composite slab. They also highlight the peak areas of deflection in the 9m bay and the considerably lower displacements adjacent to the columns on gridline 4. The red zones in both figures highlight positive upwards displacement of the slab in the region of the columns. The dark blue colour highlights the region of maximum downward deflection. In the "'long-cool" fire the maximum displacement is 310mm and in the "short-hot" scenario deflections reach 360mm.

8.4.1.2 Behaviour of the steel beams

8.4.1.2.1 Secondary beams The steel secondary beams on gridlines 2, 3 and 5 are in axial tension at ambient along their entire length except at the connections to the primary beam (Figures 8.20 and 8.21 show axial force against distance along the secondary beams on gridline 2 for both fire scenarios). By 200^{o}C the beams are in high axial compression except for a small region at the edge of the compartment. As the temperature increases the steel remains in compression but decreases with increasing temperature (and material degradation). At the end of the "short-hot" fire (950^{o}C) the axial force in the secondary steel beams is very close to zero. The axial compressions generated in the beams exposed to the "long-cool" fire are always greater because the gradient over the composite is smaller.

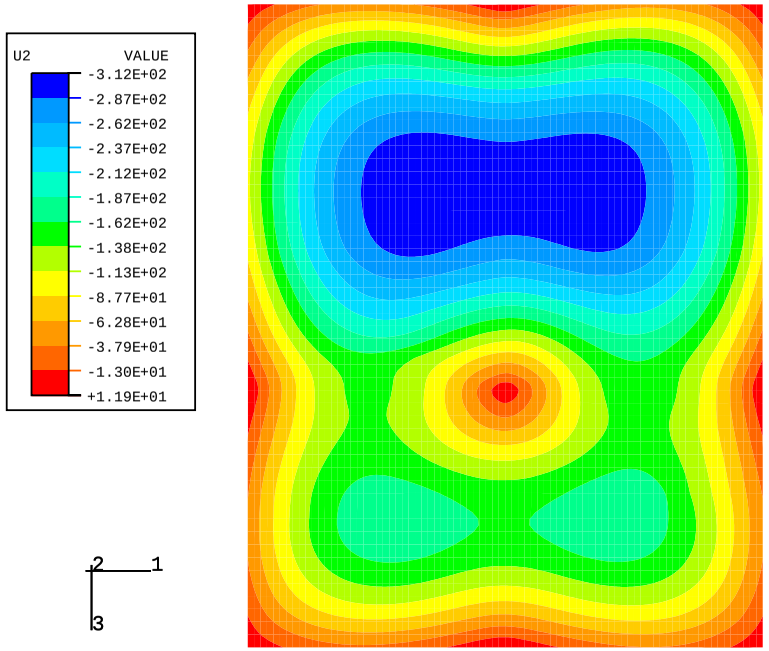

(a) OF=0.02

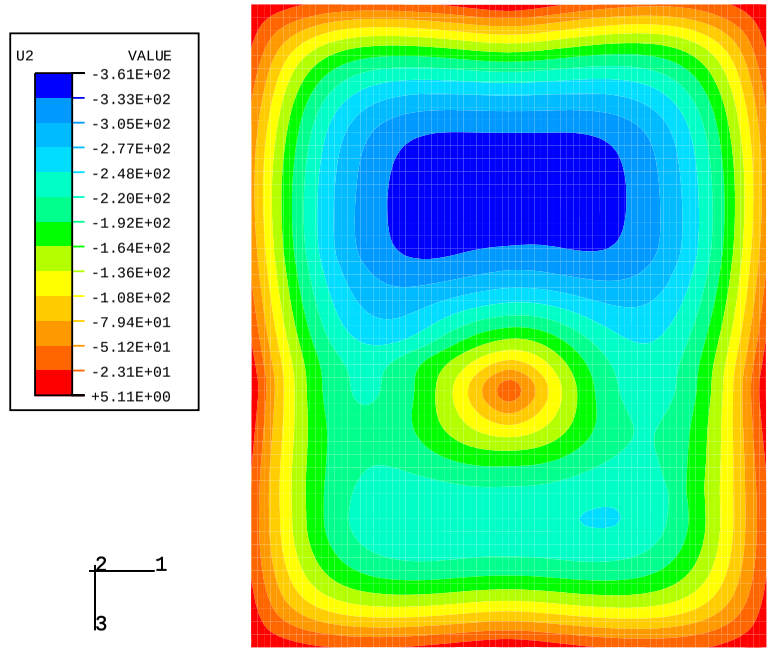

(b) OF=0.08

Figure 8.19: Deflection contours in the slab at the end of heating

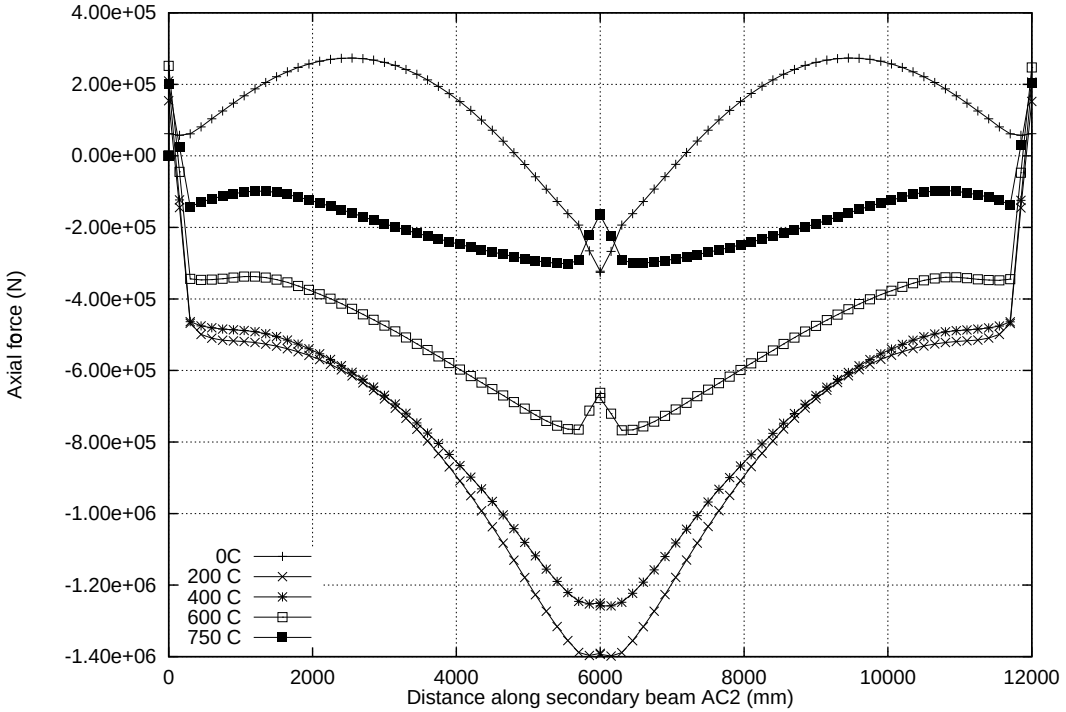

Figure 8.20: Variation of axial force along secondary beam AC2 at various secondary beam temperatures, OF=0.02

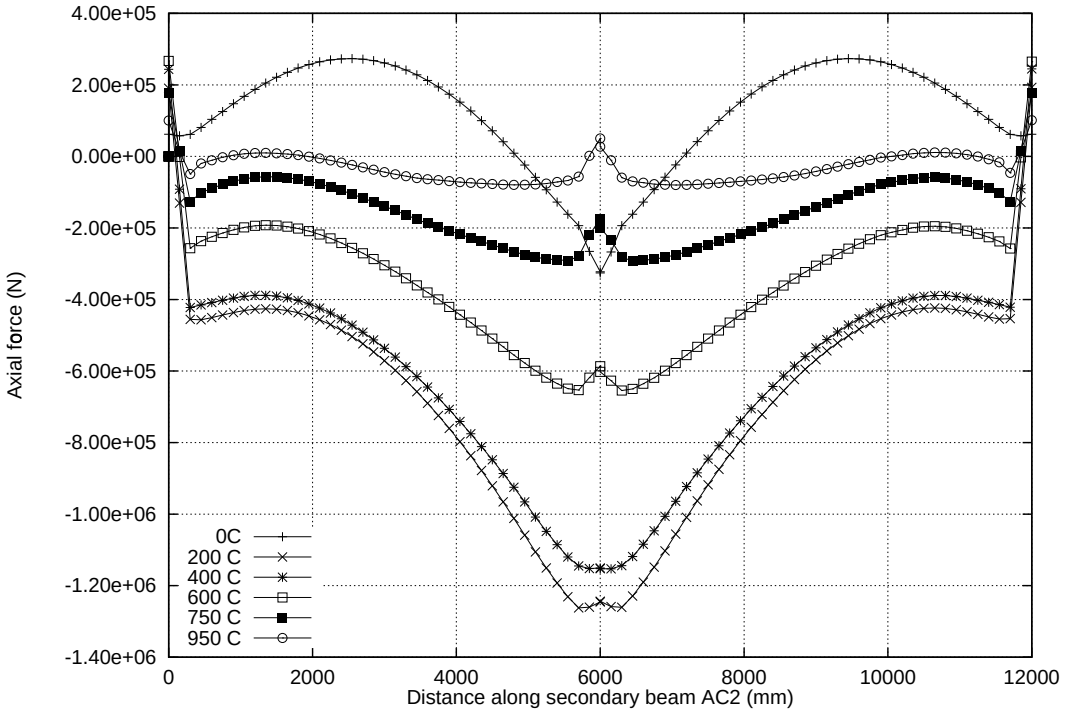

Figure 8.21: Variation of axial force along secondary beam AC2 at various secondary beam temperatures, OF=0.08

Figures 8.22 and 8.23 also show the axial force in secondary beam AB2 but against secondary beam temperature at various equally spaced locations along the beam. x/L=0.125 corresponds to a location just inside the compartment to the right of gridline A. x/L=1.0 is adjacent to gridline B. These types of plots were discussed in detail when the models of the British Steel Cardington tests were being analysed by Edinburgh University and British Steel.[187, 223] At all locations along the beam there is a rapid increase in compression at the beginning of the analysis up to 150^{o}C. At this temperature the steel has reached its first yield and the beam can no longer carry increasing compressions. The force experienced by the beam plateaus or decreases slightly. At the ultimate yield of steel around 450^{o}C, the compressions decrease with increasing temperature until at the end of the analysis the whole beam experiences very similar but small compressions. The greatest compressions are closest to the primary beam connection because of the restraint from the expanding secondary beam BC2. Both fire scenarios initiate the same response but the magnitude of the compressions during the "long-cool" fire are slightly greater (Figures 8.22 and 8.23).

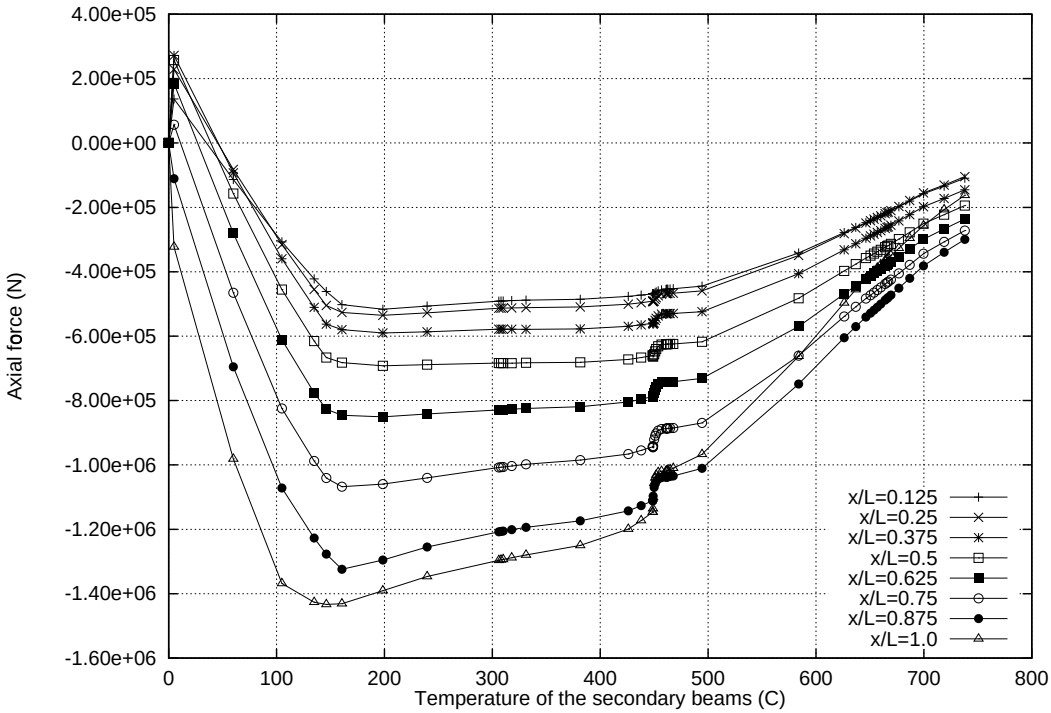

Figure 8.22: Secondary beam AB2: Axial force against secondary beam temperature, OF=0.02

Secondary beams AB4 and BC4 abutting column B4 gain larger compressions along the beam because they deflect less (Figures 8.24 and 8.25).

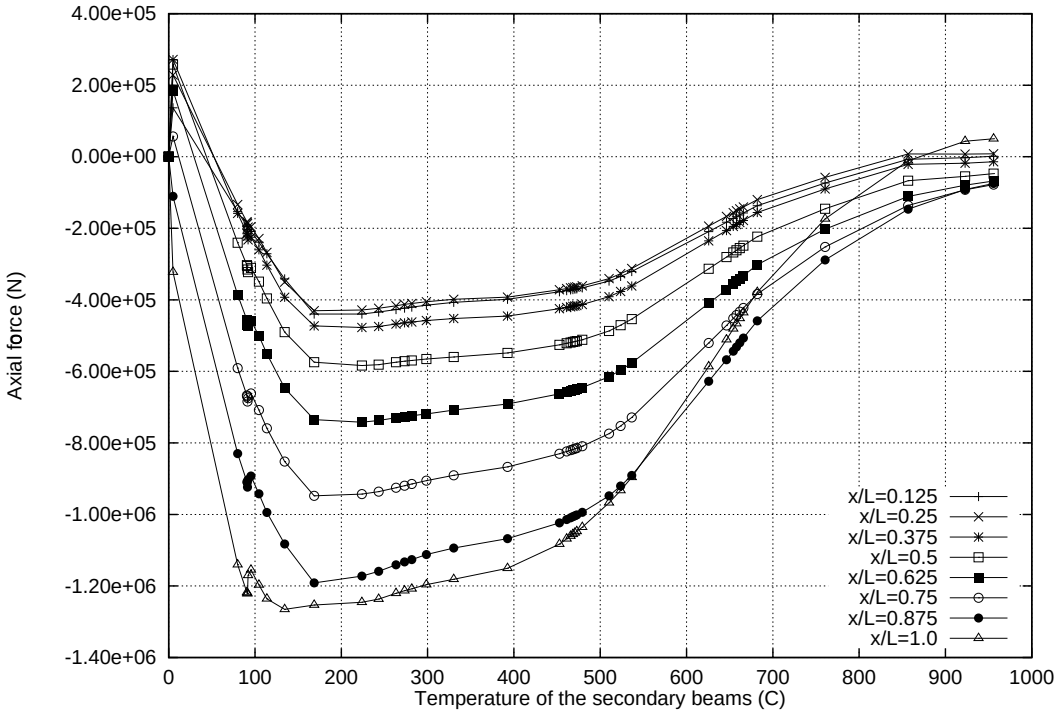

Figure 8.23: Secondary beam AB2: Axial force against secondary beam temperature, OF=0.08

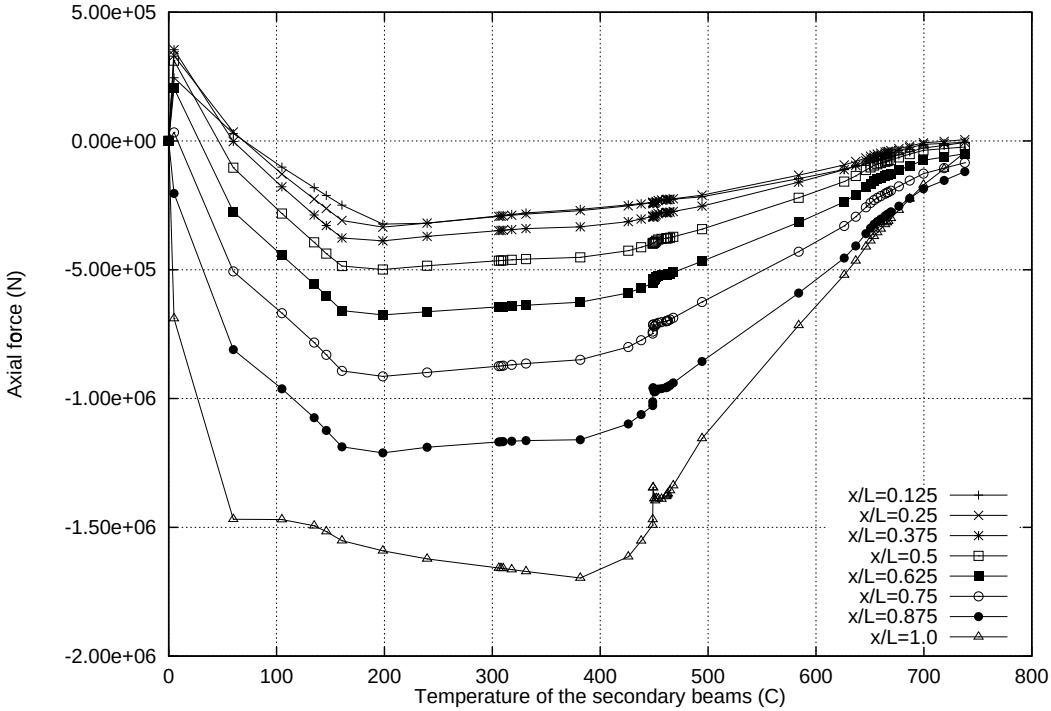

Figure 8.24: Secondary beam AB4: Axial force against secondary beam temperature, OF=0.02

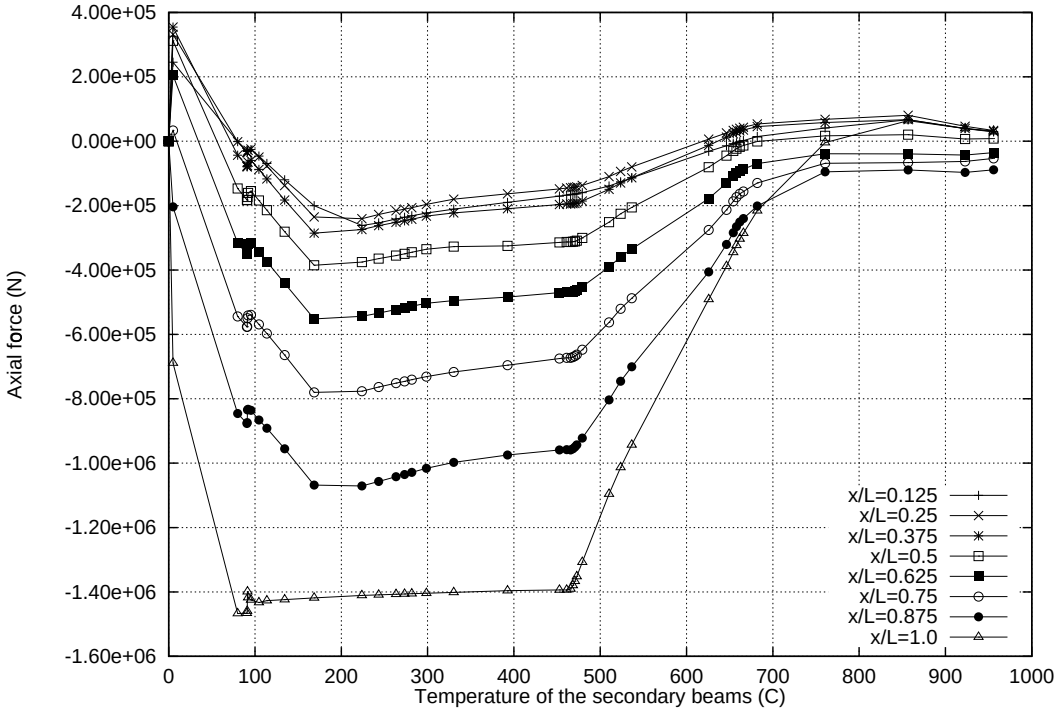

Figure 8.25: Secondary beam AB4: Axial force against secondary beam temperature, OF=0.08

8.4.1.2.2 Primary Beams The 2x2 frame is considerably smaller than the Cardington frame and the primary beam is a key element in the load carrying ability of the structure. In BS test 3 the primary beam was just inside the boundary of the fire compartment and in test 1 the adjacent primary beams formed part of the cold restraining structure. In this study the primary beam is in the middle of the structure surrounded by fire.

Figures 8.26 and 8.27 show the axial force in primary beam B14 against secondary beam temperature. The greatest axial force in primary beam B14 is next to column B4 where the restraint to thermal expansion is highest due to the bracing along gridline B (between gridlines 4 and 6). Primary beam B14 tends to be in small tension or compression near mid-span and increases in compression again towards column B1. A steep drop in compressive axial force occurs at reference temperatures of 450^oC in the "long-cool" fire and at 90^oC in the "short-hot" fire. This also occurs in the 6m primary beam , see Figures 8.28 and 8.29. This bifurcation is mirrored in the secondary beams where a small drop in compression occurs in response to the primary beam. Looking back at the deflection plots (Figure 8.13) there is also an increase in the rate of deflection of the primary beams at the two critical temperatures. All the beams experience a change in axial force and greater deflections as a result of an event occurring in the

primary beam. This event can be explained by considering thermal bowing effects, the yield and ultimate strength of the primary beam and compatibility of deflections over the composite floor.

High gradients in the composite result in large hogging moments. Figure 8.30(a) shows the stress state in the composite at the end of the primary beam as a result of imposed load (M_{load}), mean temperature rise ($EA\alpha\Delta T$) and gradient ($EI\alpha T_{,\mathrm{y}}$). There are high compressions in the steel and tensions (or small compressions) in the slab. Figure 8.30(b) is a picture of the connection detail between the primary beam and column in the building. Although these are designed as simple connections the composite action between slab and beam results in a moment resisting connection. In terms of compatibility of deflections over the floor slab the composite secondary beams expand and bow as the heating regime progresses thus they push down on the primary beam. The moment resisting connection at the end of the primary beam prevents the secondary beams from forcing it down beyond a certain point thus the primary beam carries increasing load. When the moment capacity (steel joist compression capacity in the model, which manifests itself as local buckling in the tests) of the primary beam is reached there is a sudden increase in rotation at the ends of the beam as the end restraint condition changes from moment resisting to pinned and the secondary beams are free to pull the primary beam down. This change in behaviour is dramatic and results in reduced compressions in the primary beam as well as increased deflections. A sudden increase in the rate of rotation is observed in the primary beam at these temperatures in both cases. Figures 8.31(a) and 8.31(b) show the rotations near the ends of primary beam B14 against the reference temperature for both fires.

Figure 8.32 plots the yield and ultimate strength based on the steel material data in the structural model. This shows there is a reduction in the maximum attainable axial force at around 100^oC and 500^oC. In both scenarios on the 2x2 frame the primary beam instability occurs at $2.5 - 3.0 \times 10^6 N$ and a temperature of 100^oC or 450^oC. The sudden increase in rotations as the end restraint conditions change are triggered by the steel properties although the composite as a whole must rotate. At 100^oC (first yield) the primary beam could form a hinge. This happens in the "short-hot" fire because the gradient in the slab is higher (see Figure 8.8). The phenomena is delayed until a reference temperature of 450^oC during the "long-cool" fire.

8.4.1.2.3 Column displacement Figure 8.33 and 8.34 plot the outward lateral displacement of column B1 (in the y direction see Figure 8.1). This is a key feature of behaviour with the expanding primary beam pushing out the columns and edge beams of gridlines 1 and 6. Initially the primary beam expands, pushing out the columns and edge beams thus reducing the thermally induced compressions in the edge beams

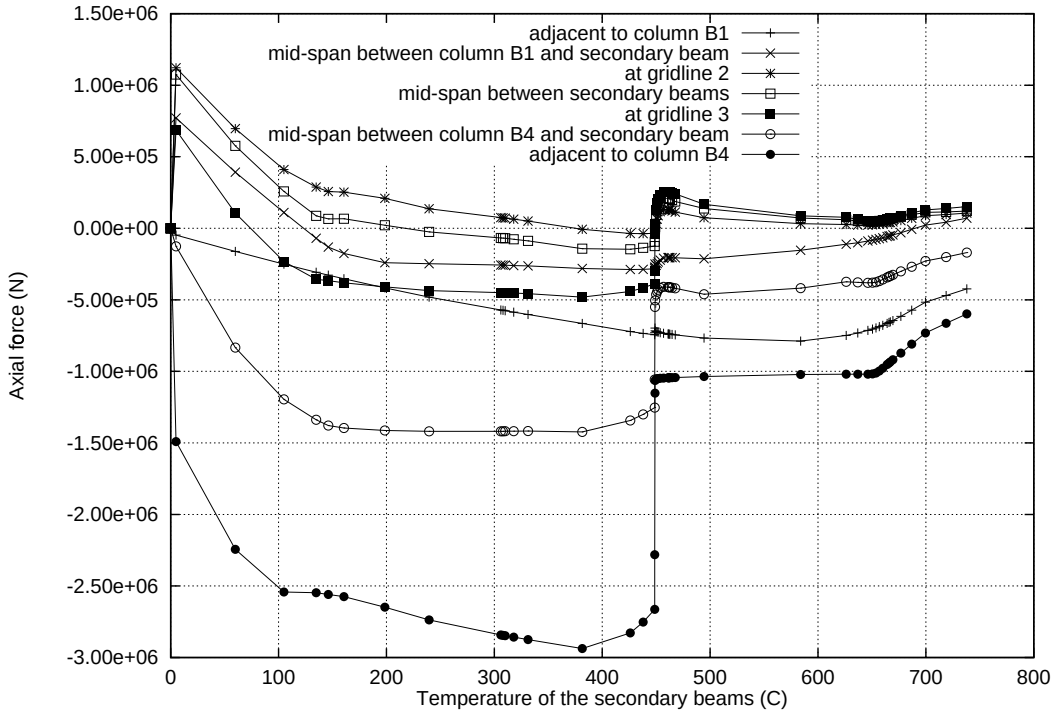

Figure 8.26: Primary beam B14: Axial force against secondary beam temperatures, OF=0.02

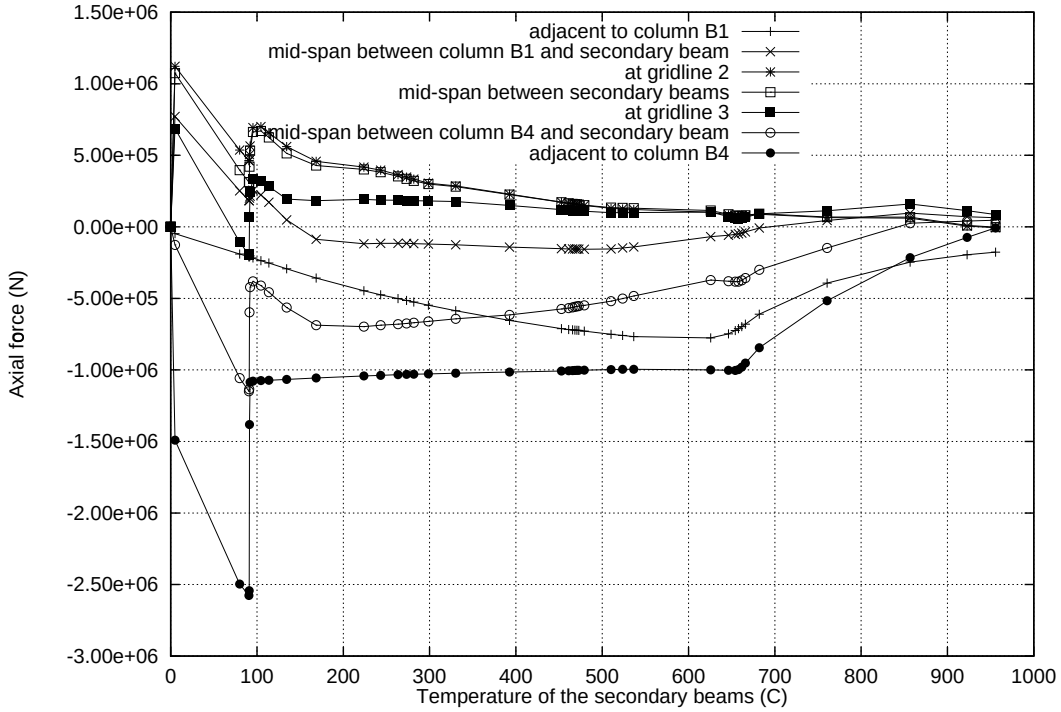

Figure 8.27: Primary beam B14: Axial force against secondary beam temperatures, OF=0.08

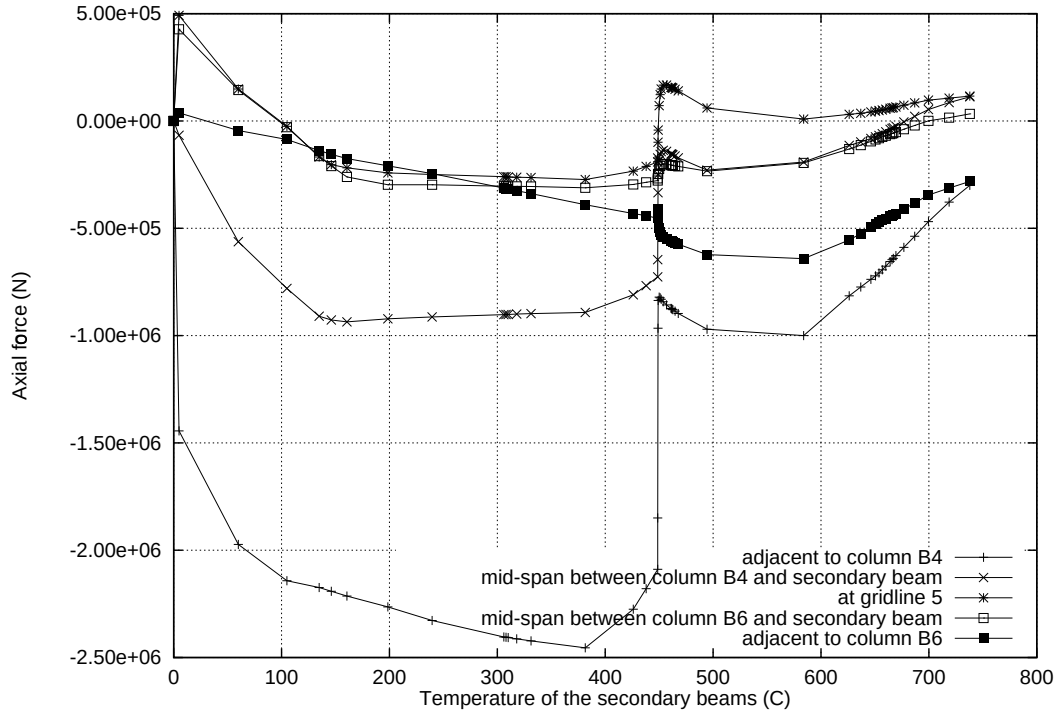

Figure 8.28: Primary beam B46: Axial force against secondary beam temperatures, OF=0.02

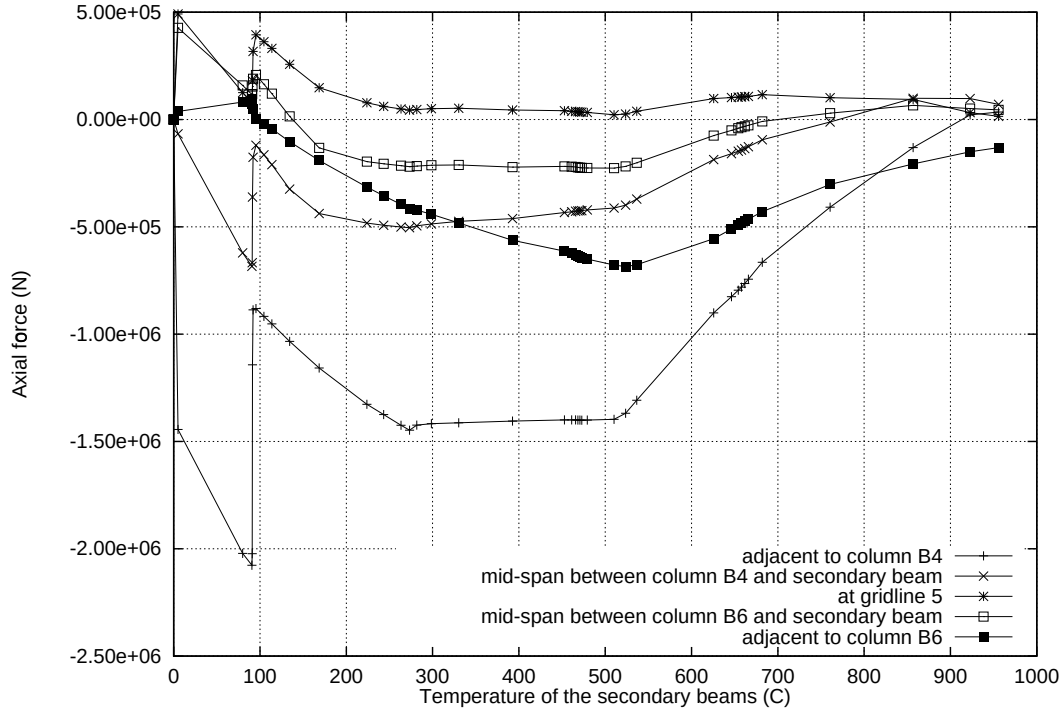

Figure 8.29: Primary beam B46: Axial force against secondary beam temperatures, OF=0.08

(absorbing them in displacements). After the primary beam instability the columns and edge beams retract. This is shown in both figures where the deflected shape of the column is plotted at 200^{o}C intervals and reference temperatures corresponding to the instability event in the primary beam. In the "long-cool" fire at 448^{o}C the instability has not occurred but at 449^{o}C it has.

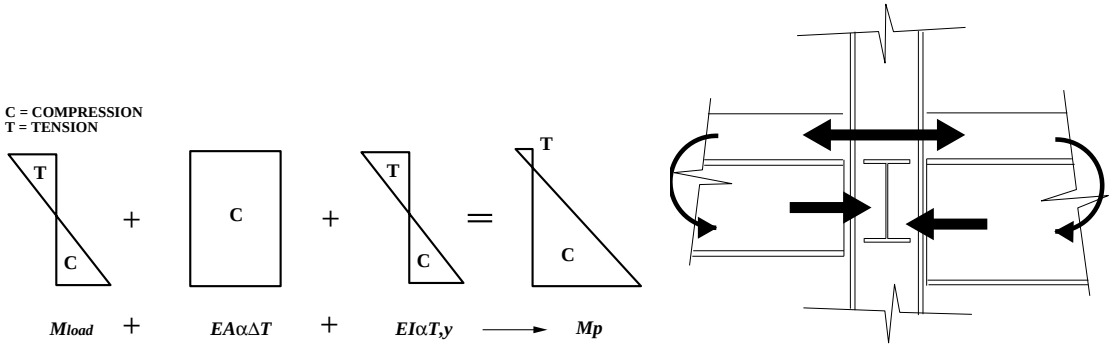

(a) Schematic stress state in the composite at the end of the primary beam

(b) Connection detail

Figure 8.30: Moment resisting connection

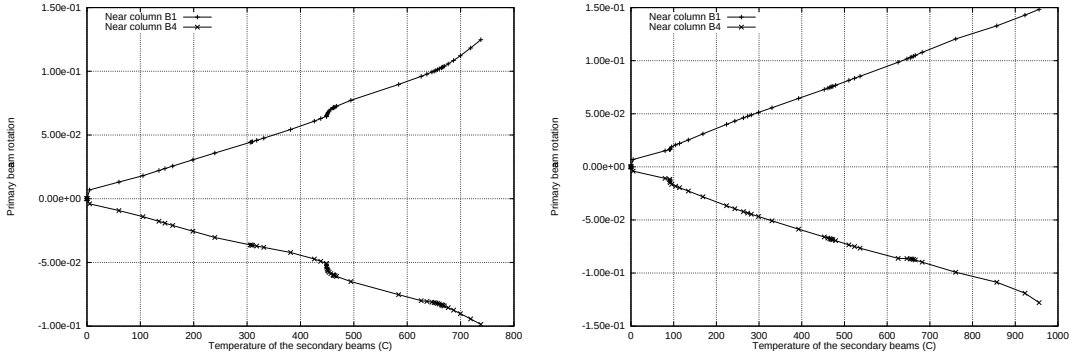

(a) OF=0,02

(b) OF=0.08

Figure 8.31: Rotations near the ends of the primary beam B14

The vertical displacement of column B4 at slab level is shown in Figure 8.35. The column in response to the "long-cool" fire achieves a maximum vertical deflection of 16mm at the end of the analysis. In contrast the column exposed to the "short-hot" fire only moves upwards by 5mm. This difference is due to the duration of the "long-cool" fire exposure leading to higher temperatures in the protected column.

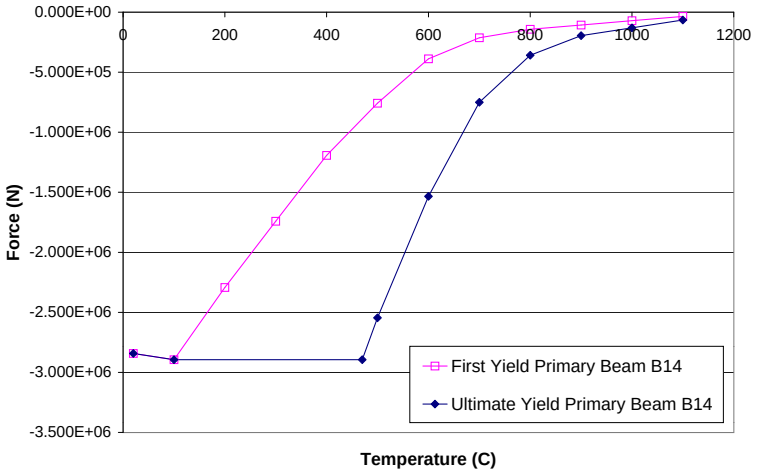

Figure 8.32: Material yield limits of the primary beam

8.4.1.2.4 Column Reactions The instability phenomena in the primary beam leads to a redistribution of the loading from column B4 to columns B1 and B6 at the edges of the building. These column reaction forces are plotted in Figure 8.36(a) and 8.36(b).

Figures 8.37 and 8.38 show the shear forces experienced by primary beam B14 against secondary beam temperature. At the temperature of the instability the shear forces drop between mid-span and column B4 and increase between mid-span and column B1 which coincides with an increase in the reactions of column B1 as expected.

8.4.1.2.5 Edge beams Figures 8.39-8.42 show the compressive forces in edge beams AB1 and BC1 for both scenarios.

There is an increase in compressions in each scenario corresponding to the primary beam instability. Figures 8.33 and 8.34 have shown that when the primary beam is expanding the edge beams and the columns are pushed outwards and after the primary beam instability the columns and edge beams retract. Thus the compression forces in the edge beams must increase. The compressions experienced by the beams between gridlines B and C are smaller because the restraint is higher and the vertical deflections were greater.

The edge beams in the "short-hot" fire achieve low temperatures when compared with those in the "long-cool" fire, therefore material degradation is less. In Figure 8.39 the maximum axial force equals $1.4 \times 10^6 N$ at 650^oC but starts to decrease beyond this reference temperature. In Figure 8.41 at the same reference temperature the axial force is lower because the edge beam is cooler. However, the cooler beam continues to support increasing compressions because material degradation is lower.

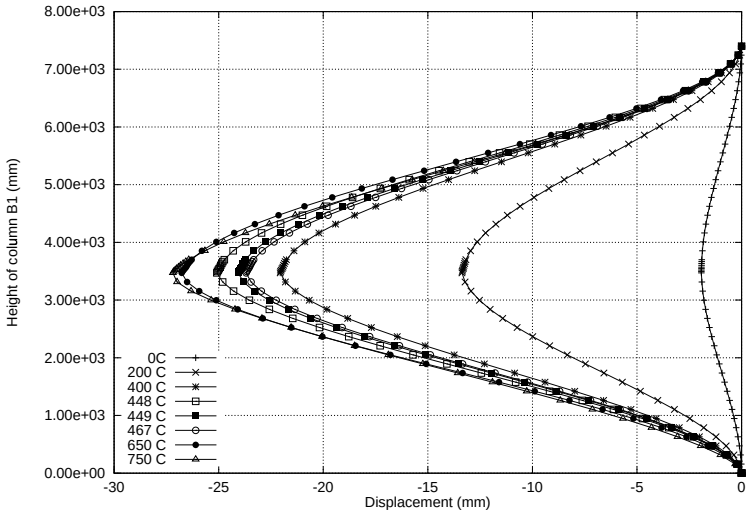

Figure 8.33: Movement of column B1, OF-0.02

8.4.1.3 Behaviour of the frame

The horizontal displacement of the columns in the plane of the slab are described by Figure 8.43 for the "short-hot" fire. The grid represents the beams. The movement of the columns is exaggerated by a factor of 1×10^3 for clarity. The restraint provided by the bracing has a strong influence on the deflected shape of the heated frame. Edge beams along gridlines 1 and 6 push the columns out to a lesser extent because they are protected. This is also true of the edge beams parallel to the primary beams. Column A4 has the highest displacement because it is pushed out by an unprotected steel secondary beam reaching very high temperatures. In addition to the high thermal expansion there is also no bracing on that side of the frame. Primary beam B46 is restricted by the bracing above and below the beam thus reducing the movement of columns B4 and B6 in the direction of the primary beams expansion.

The overall movement of the 9m bays to the left and the 6m bays to the right can be explained by the moments induced as a result of the reaction forces caused by the bracing (assuming the slab acts as a rigid body).

This figure highlights the importance of understanding whole structure behaviour in response to a fire.

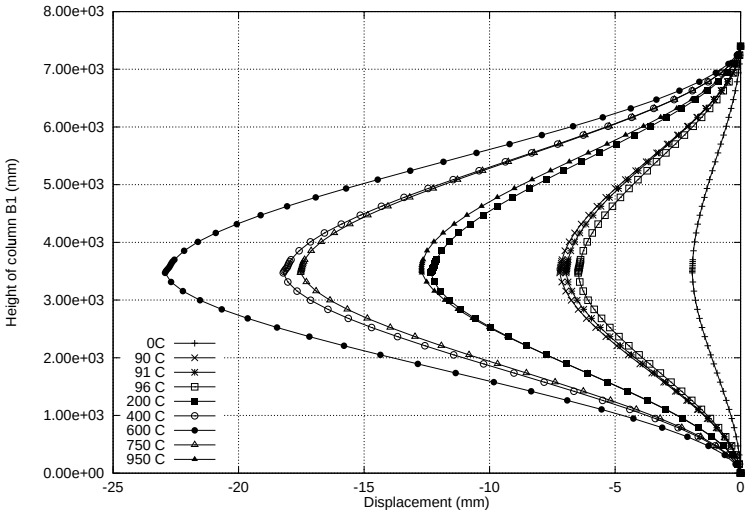

Figure 8.34: Movement of column B1, OF=0.08

8.4.1.4 Behaviour of the composite slab

As expected the "short-hot" fire caused high temperature differentials within the composite sections resulting in a predominantly bowing response. In all cases the composite beams are either in tension or lower compression when the results of the two fires are compared directly. Figure 8.44 shows the axial forces in the composite for the "short-hot" and the "long-cool" regime. At a secondary beam temperature of 200^0C both fires cause overall compressions in the composite. The "short-hot" fire causes lower compressions in the composite because the slab is cooler. The slab also has a higher gradient pushing the steel beams down into a bowed shape. At 400^0C the whole composite is in slightly less compression. At 600^0C the response of the composite to both fires is the same. In both instances the composite is in tension. At 750^0C (the end of the "long-cool" fire) the beam exposed to the "short-hot" fire is in greater tension. At the end of the "short-hot" fire (950^0C) the composite is in considerably increased tension.

A similar trend can be seen in any of the secondary beams. Secondary beam AC4 displays slightly different behaviour as a direct result of being attached to the columns along gridline 4. Tensions in the region of column B4 are significantly greater than the axial forces in the other secondary beams. This is illustrated in Figure 8.45.

Composite moments in secondary beam AC2 are shown in Figure 8.46. At beyond 200^oC the composite is in hogging bending as expected. However the "short-hot" fire produces less hogging than the "long-cool" fire despite higher gradients in the composite as a result of the "short-hot" fire. This is because large deflections are dissipating the moments in the "short-hot" fire.

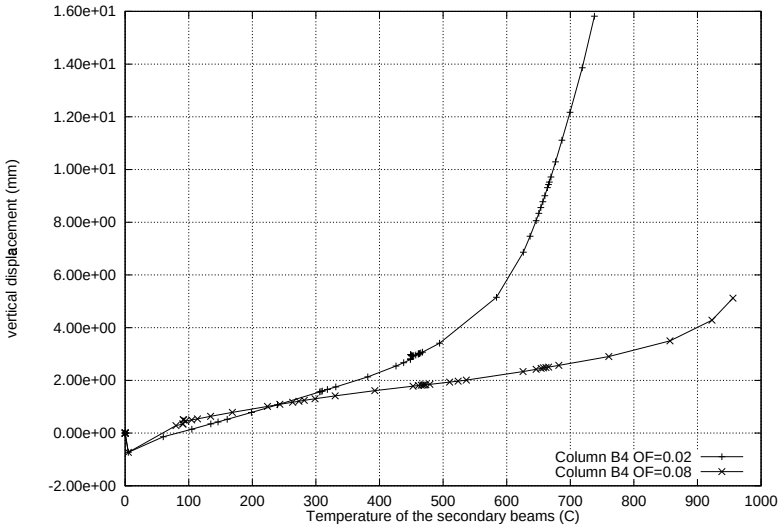

Figure 8.35: Vertical displacement history of column B4 at slab level

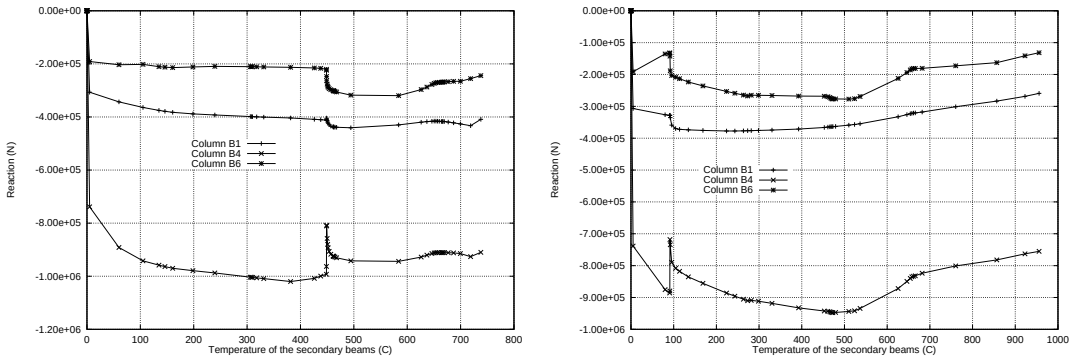

(a) OF=0.02 (b) OF=0.08

Figure 8.36: Reaction forces recorded in the columns against secondary beam temperature

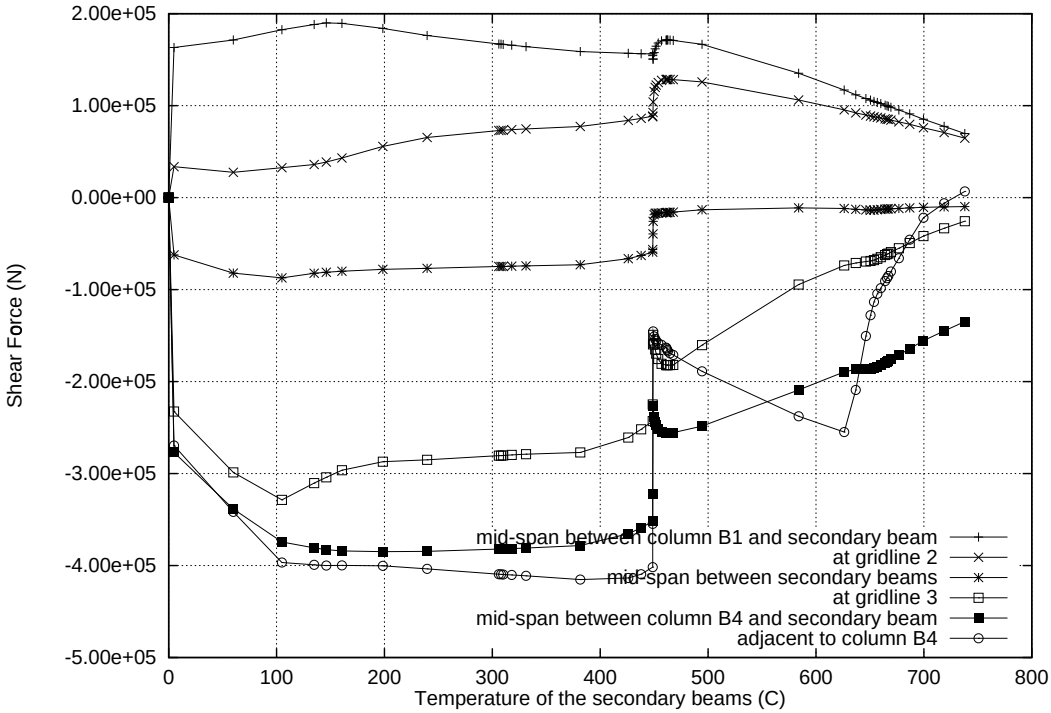

Figure 8.37: Primary beam B14: Shear force against secondary beam temperatures, OF=0.02

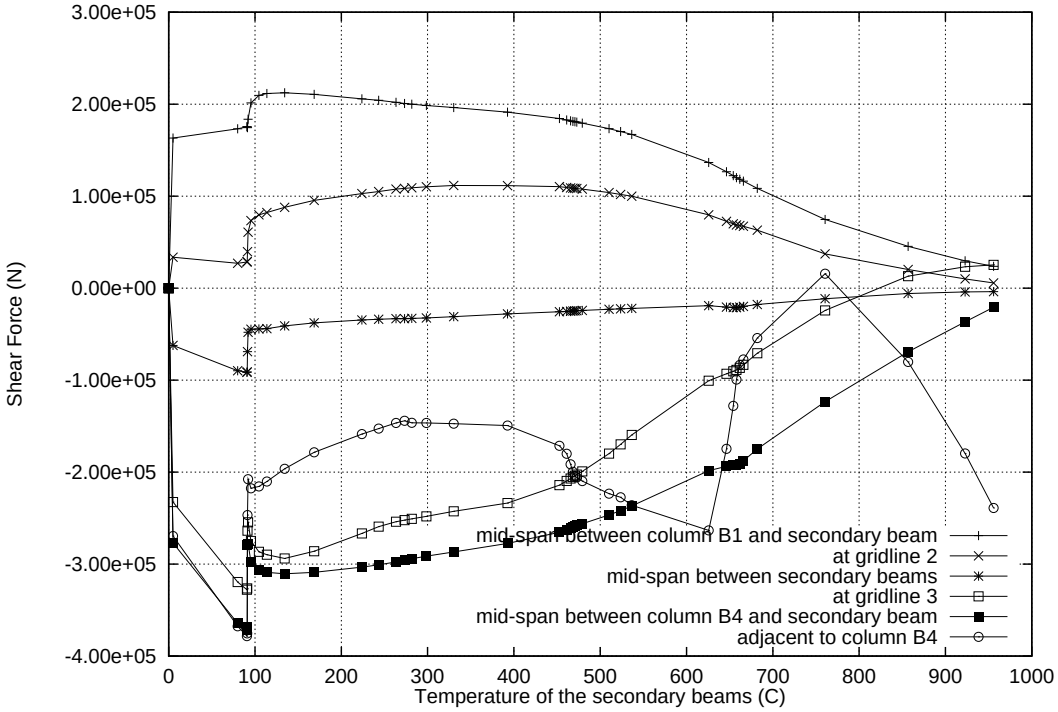

Figure 8.38: Primary beam B14: Shear force against secondary beam temperatures, OF=0.08

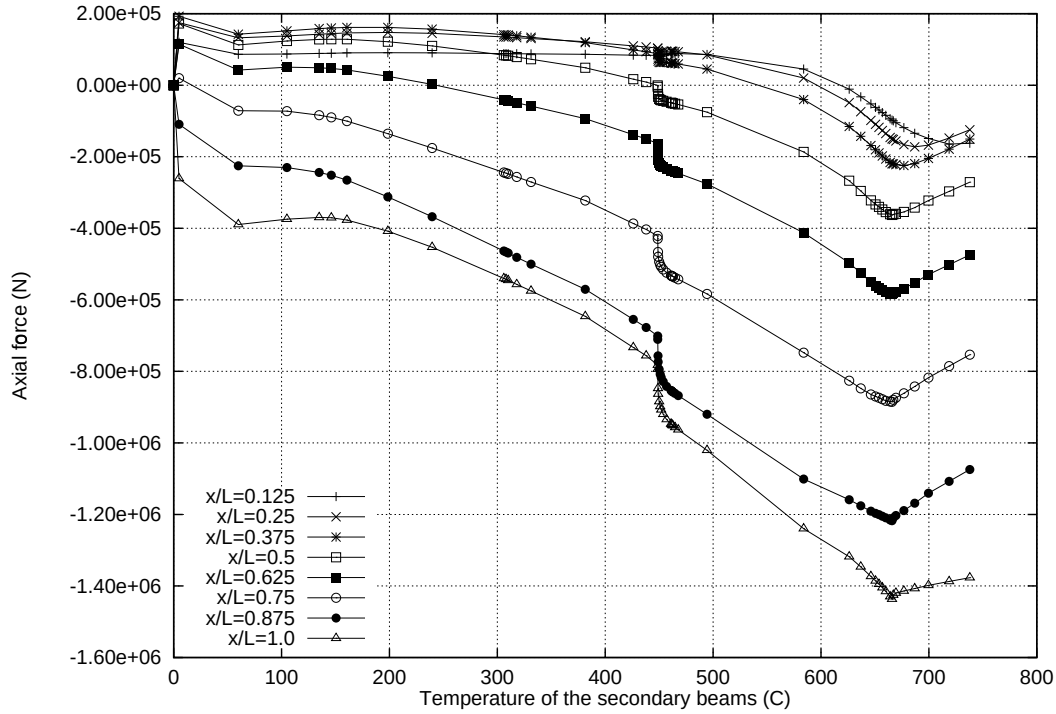

Figure 8.39: Edge beam AB1: Axial force against secondary beam temperature, OF=0.02

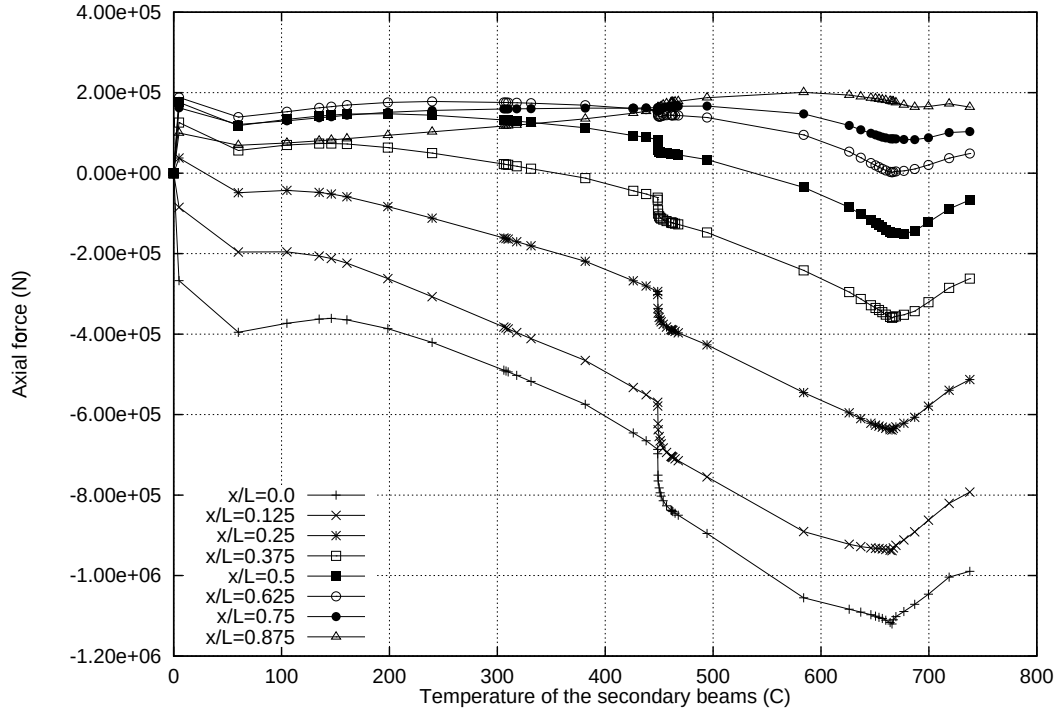

Figure 8.40: Edge beam BC1: Axial force against secondary beam temperature, OF=0.02

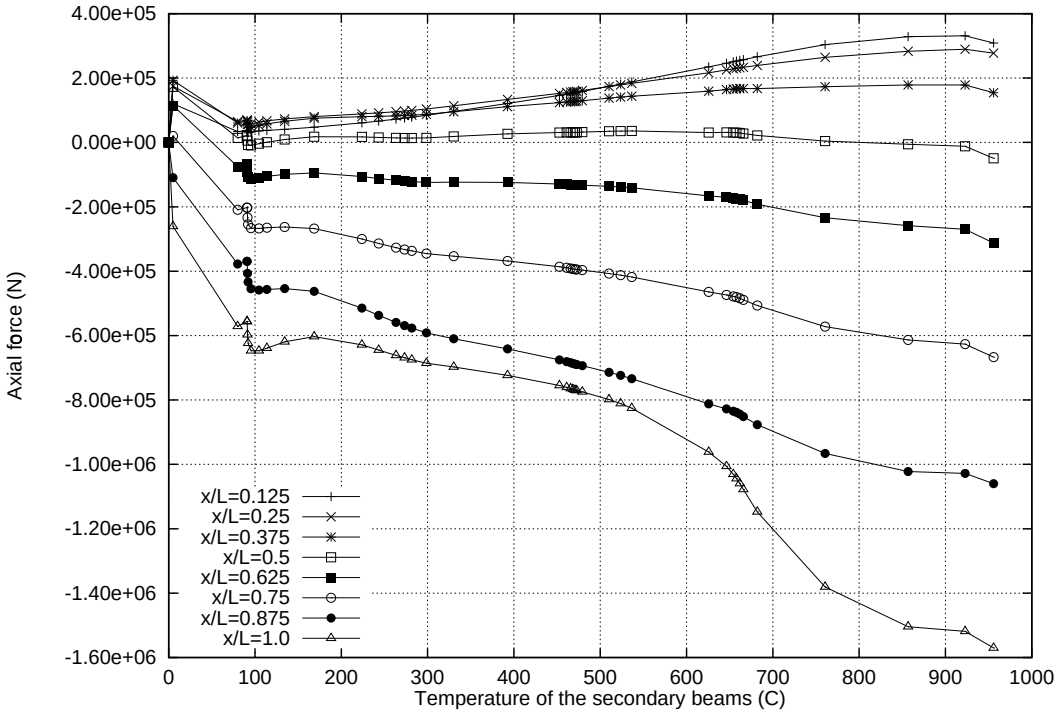

Figure 8.41: Edge beam AB1: Axial force against secondary beam temperature, OF=0.08

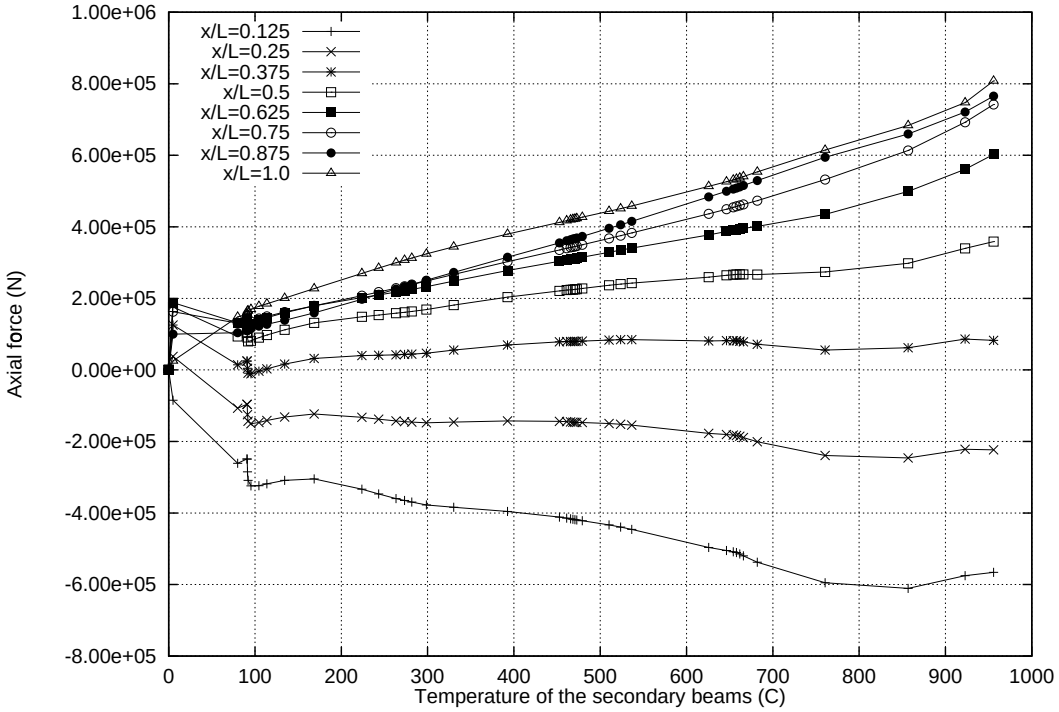

Figure 8.42: Edge beam BC1: Axial force against secondary beam temperature, OF=0.08

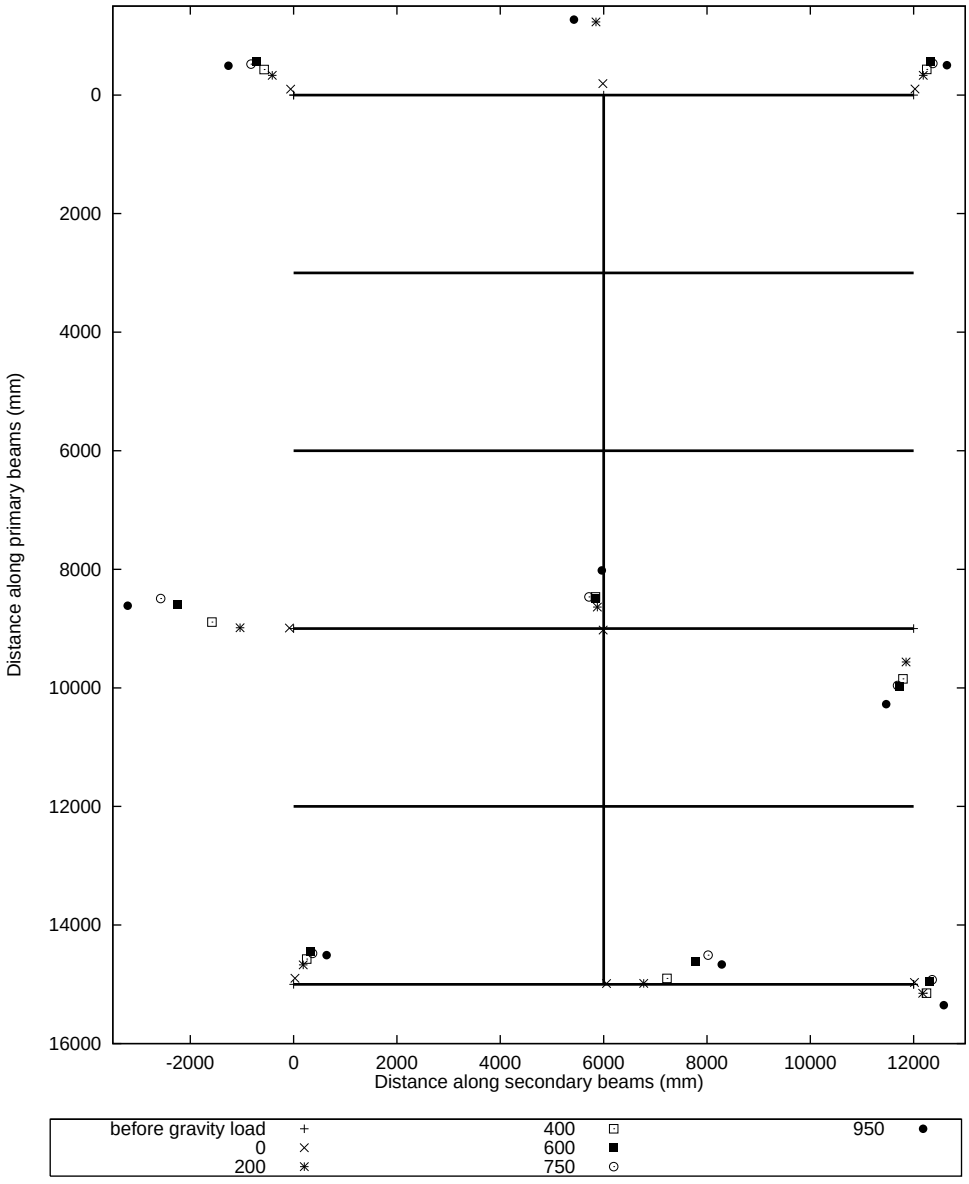

Figure 8.43: Horizontal displacement of all the columns at slab level, OF=0.08

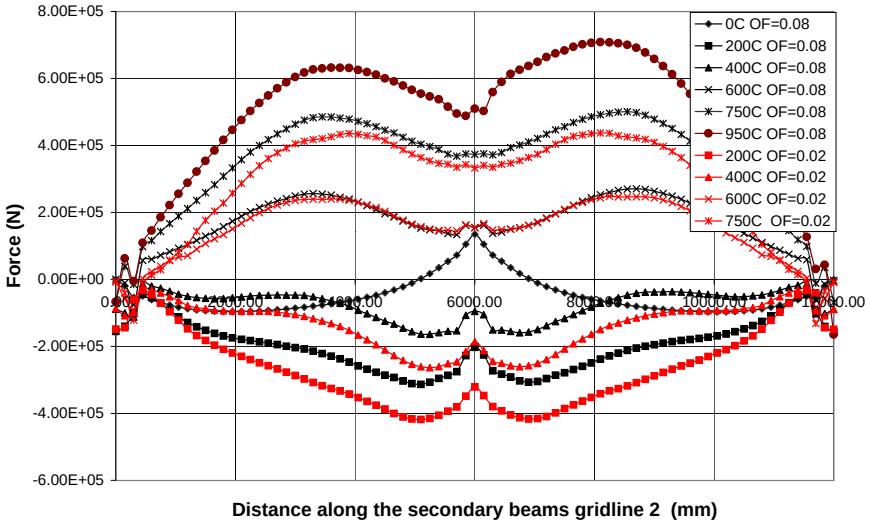

Figure 8.44: Composite axial forces along secondary beam AC2

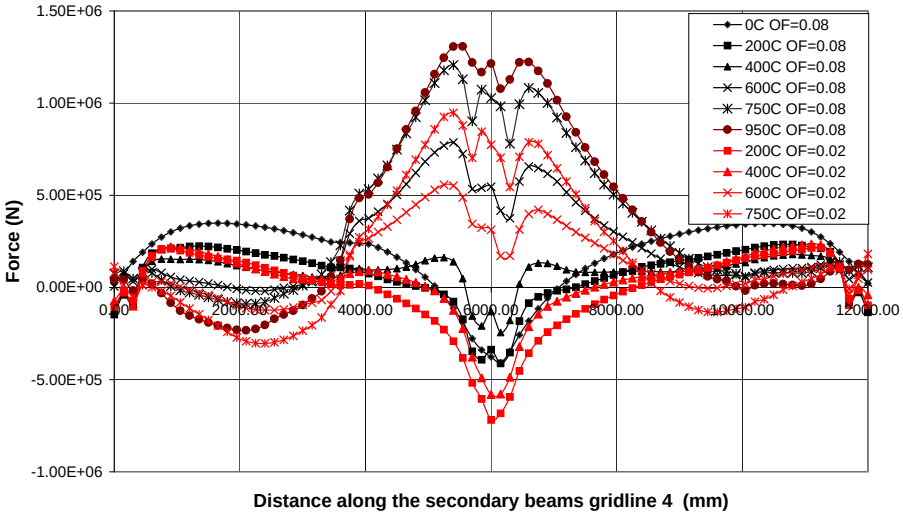

Figure 8.45: Composite axial forces along secondary beam AC4

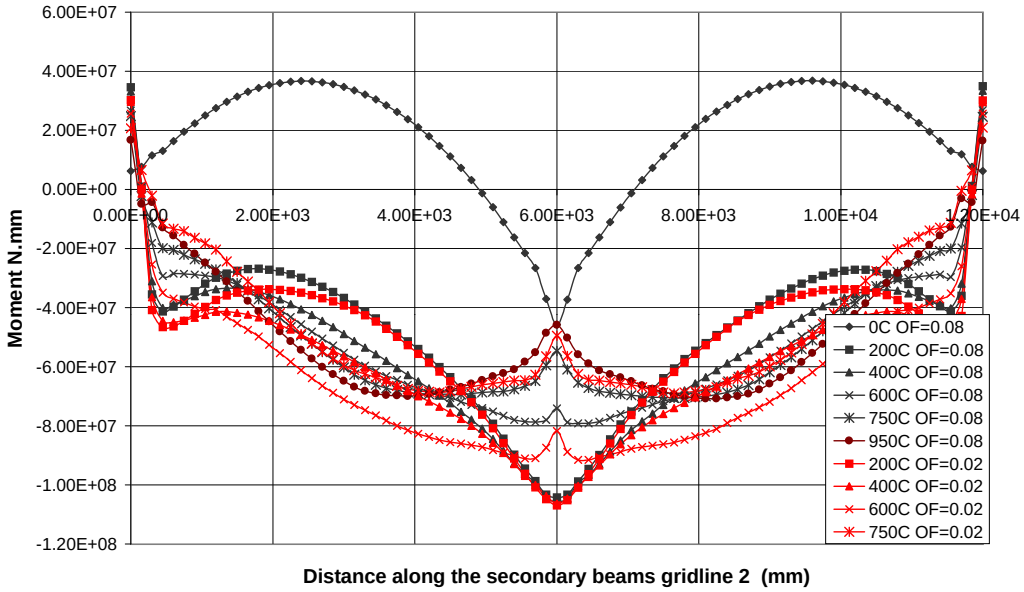

Figure 8.46: Composite moments along secondary beam AC2

8.4.1.5 Behaviour of the slab

The slab rib axial force is plotted along a line 1.2 m from gridline A, parallel to gridline A, in Figures 8.47 and 8.48. The rib forces are always in tension over secondary beam AB4 except at the very end of the "short-hot" fire. In the "short-hot" fire there are high compression at the edges of the building and smaller compressions or tensions near the middle of the bays. The high compressions at the edges are the compression ring forming in the slab to support tensile membrane action. In the "long-cool" fire compressions at the edge are lower because maximum central deflections are lower.

Figures 8.49 and 8.50 show the membrane forces in the slab along a line 600mm from gridline 1. The compressive axial forces are a consequence of the compressive ring effect (combined with the rib behaviours shown in Figures 8.47 and 8.48). The "short-hot" fire produces greater compressions at the edge because the slab deflects more and tensile membrane forces are higher. These figures also show the effect of the bracing. The compressions are lower between gridlines B and C than gridlines A and B.

Figures 8.51 and 8.52 show the membrane force in the slab at another location, along a line 4.2m from gridline 1. At all times during heating the slab is in tension. Tensions are slightly greater in response to the "short-hot" fire because of larger deflections and compatibility of deflections with the perpendicular direction. There is a reduction of tensile axial force at higher temperatures. This is because of reduced imposed loading and P-Δ moments from the primary beam through degradation of steel properties.

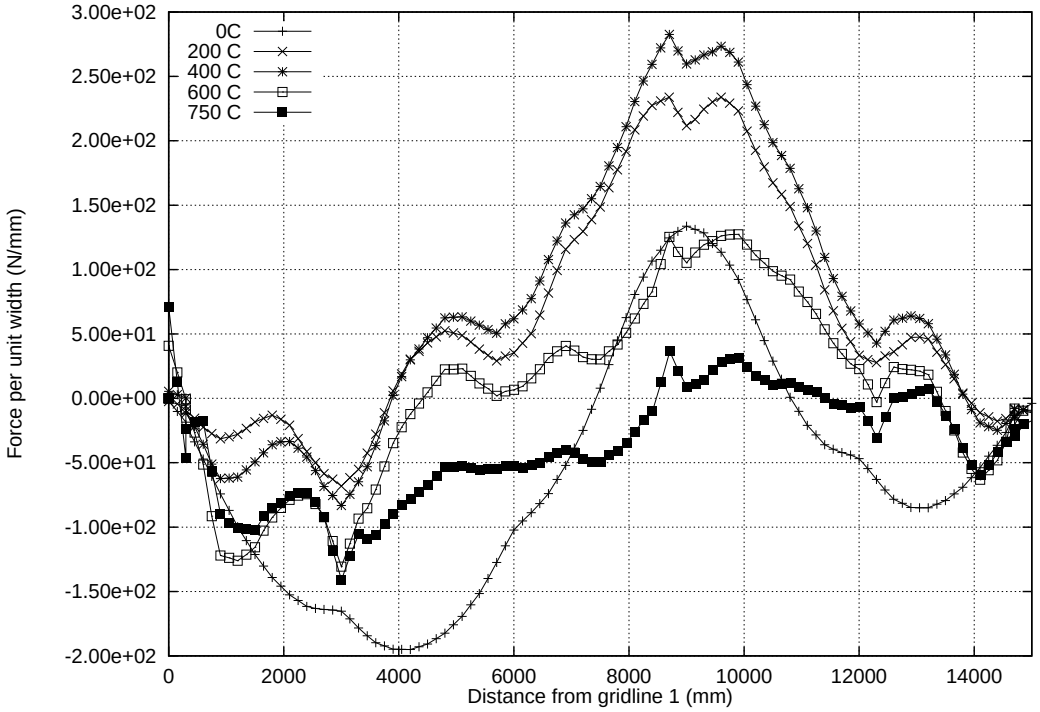

Figure 8.47: Axial force in the ribs of the slab, 1200mm from gridline A, OF=0.02

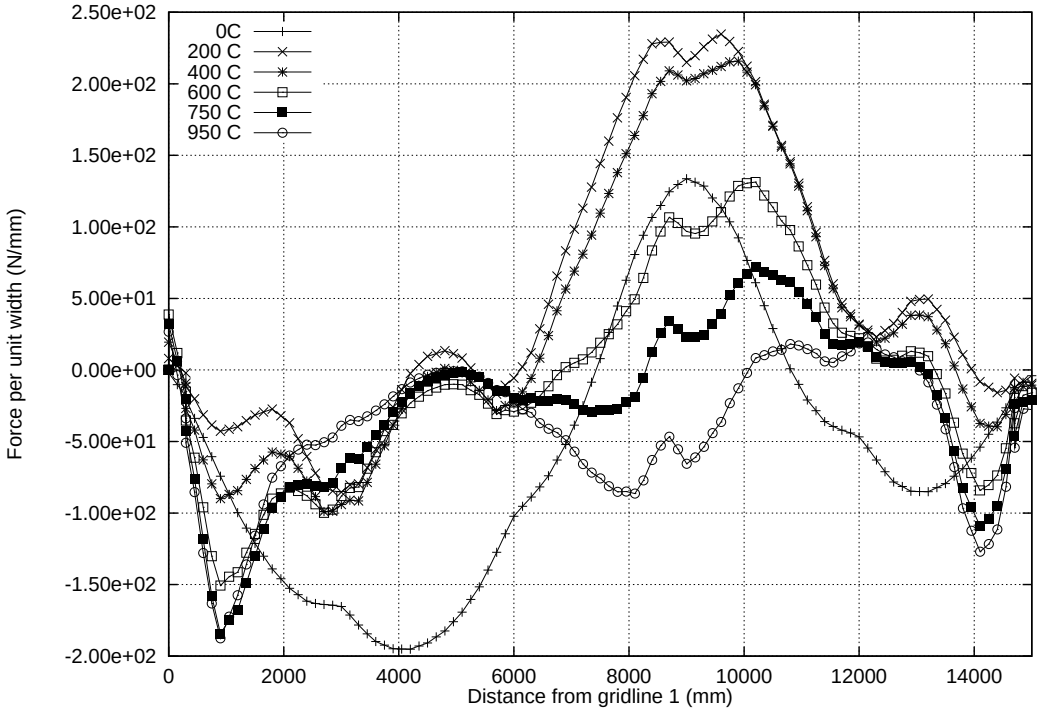

Figure 8.48: Axial force in the ribs of the slab, 1200mm from gridline A, OF=0.08

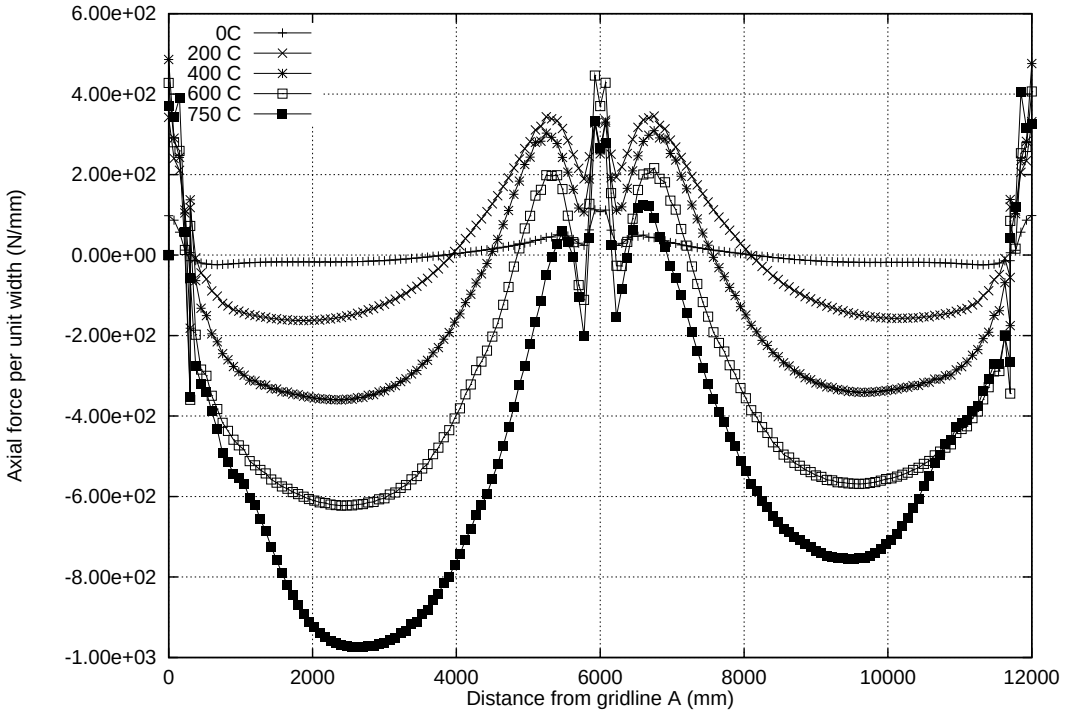

Figure 8.49: Axial force in the thin direction of the slab 600mm from gridline 1, OF=0.02

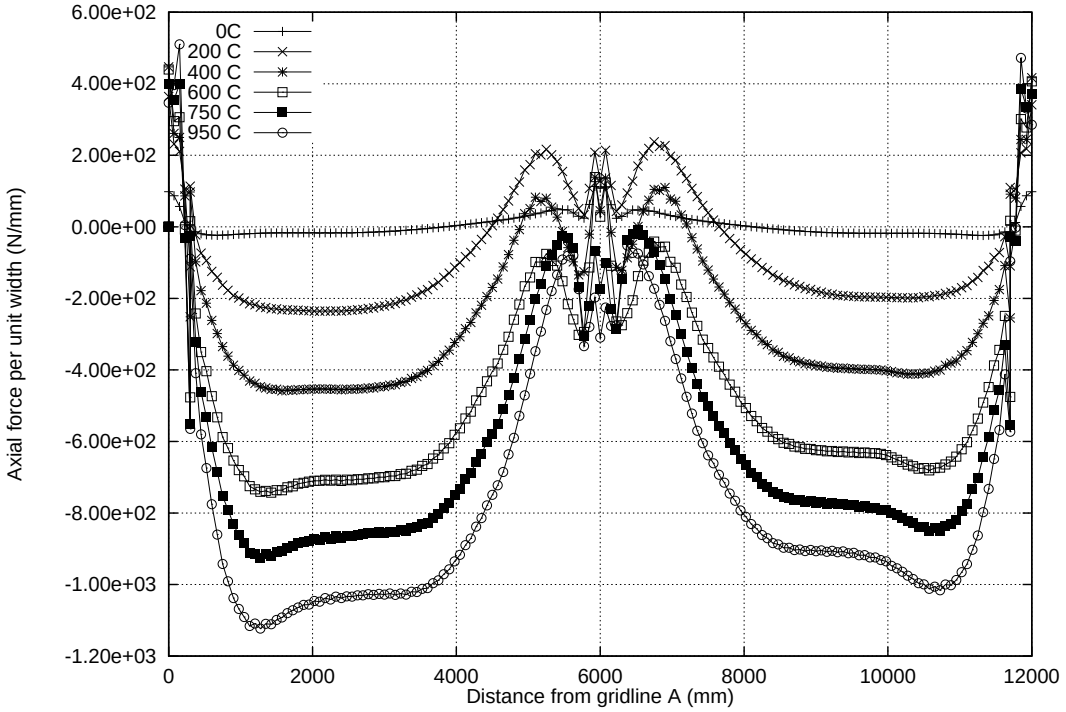

Figure 8.50: Axial force in the thin direction of the slab 600mm from gridline 1, OF=0.08

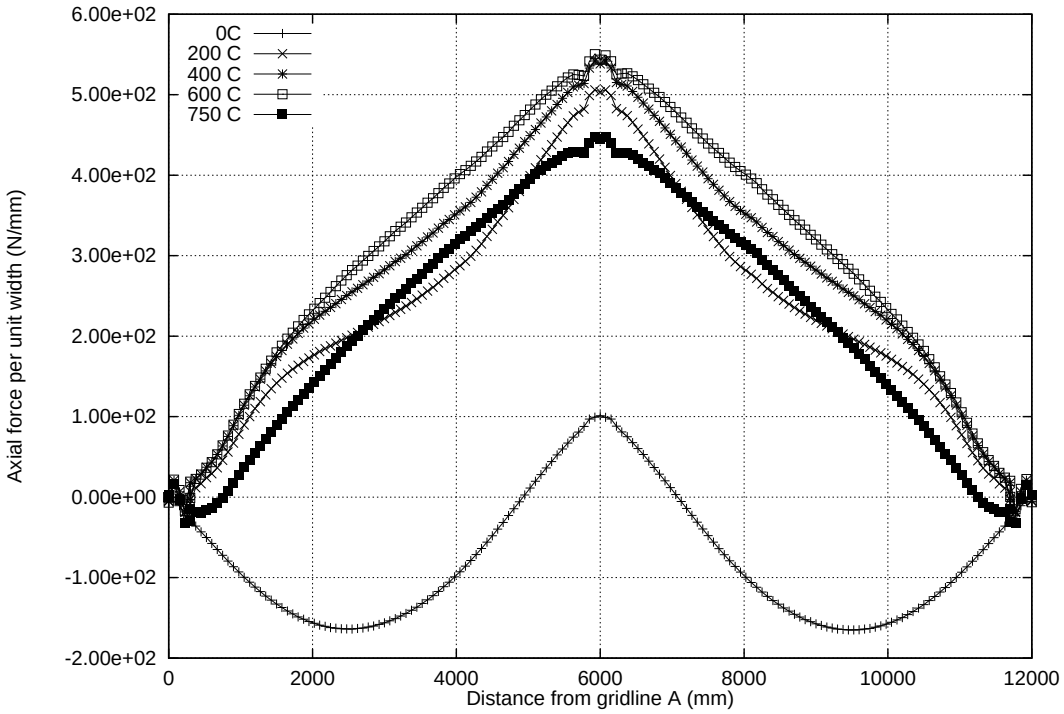

Figure 8.51: Axial force in the thin direction of the slab 4200mm from gridline 1, OF=0.02

Contour plots of the axial forces in the slab are shown in Figures 8.53 and 8.54 in the x and y directions for both fire scenarios. In both fire scenarios there are compressions around the edges of the slab and over the secondary beams on gridline 4. Tensions exist around the middle of all four bays and over deflected primary beam B14. The area covered by tensions is greater in response to the "short-hot" fire.

Plots of the mechanical strains at the level of the slabs reinforcing mesh are given in Figures 8.55-8.59. The plots are a plan of the building in the same orientation as Figure 8.1. The figures are drawn at different reference temperatures and the strains are plotted in either the x-direction (parallel to the secondary beams) or in the y-direction (parallel to the primary beam and the ribs of the slab).

During the "long-cool" fire the slab reaches a maximum temperature of 190^{o}C and a gradient of 4^{o}C/mm. The temperature of the slab increases more rapidly beyond a reference temperature of 450^{o}C. Compressive strains are increasing throughout the "long-cool" fire, see Figures 8.55 and 8.56. During the "short-hot" fire the mechanical strains are growing in tension as the slab heats up to a maximum of 100^{o}C but a high gradient of 8^{o}C/mm (at a reference temperature of 950^{o}C). This is illustrated by the series of figures plotting mechanical strains in the x and y direction at secondary beam

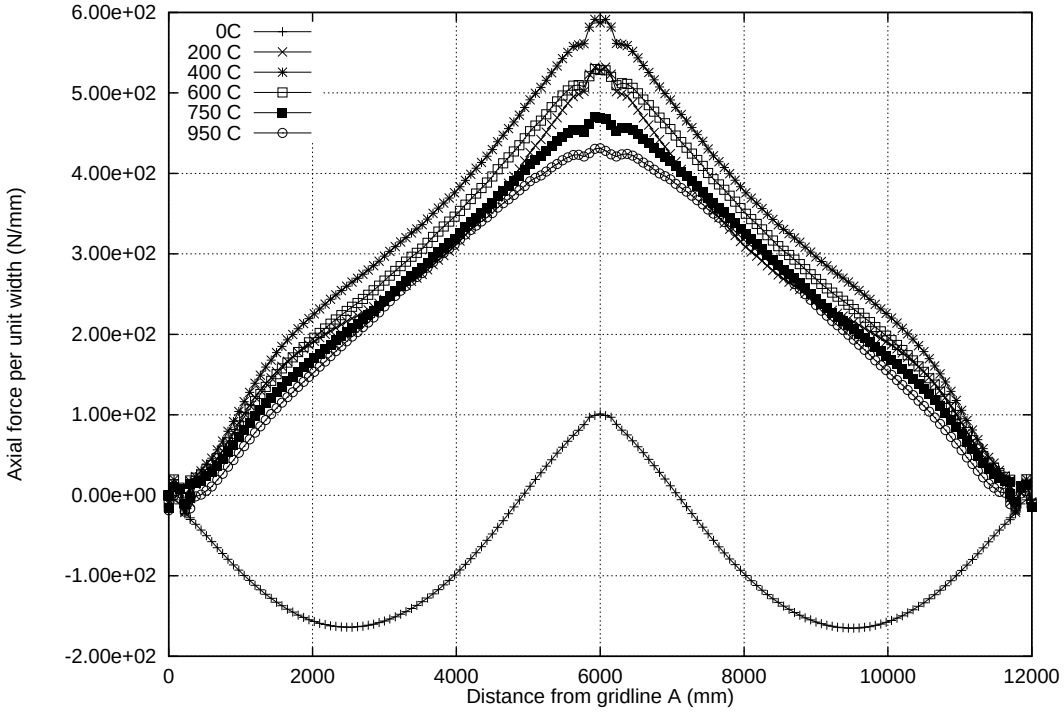

Figure 8.52: Axial force in the thin direction of the slab 4200mm from gridline 1, OF=0.08

temperatures of 600^{o}C, 750^{o}C and 950^{o}C (Figures 8.57, 8.58 and 8.59).

8.4.1.6 Summary

- The "short-hot" fire causes high deflections very quickly in terms of real time
- The "short-hot" fire causes lower maximum deflections in the protected edge beams than the "long-cool' fire because of the differences in duration of the heating regimes.
- There is a major drop in axial compression in the primary beam in both fire scenarios. This bifurcation or instability event occurs at a reference temperature of 90^{o}C in the "short-hot" fire and 450^{o}C in the "long-cool" fire.
- The event in the primary beam has been shown to coincide with a change in the end conditions of the primary beam from moment resisting to pinned.
- The moment at the end of the primary beam depends upon the imposed load, composite gradient and restrained thermal expansion.
- The secondary beams spanning into the primary beam also play an important role in the behaviour of the primary beam. As they expand and bow in response

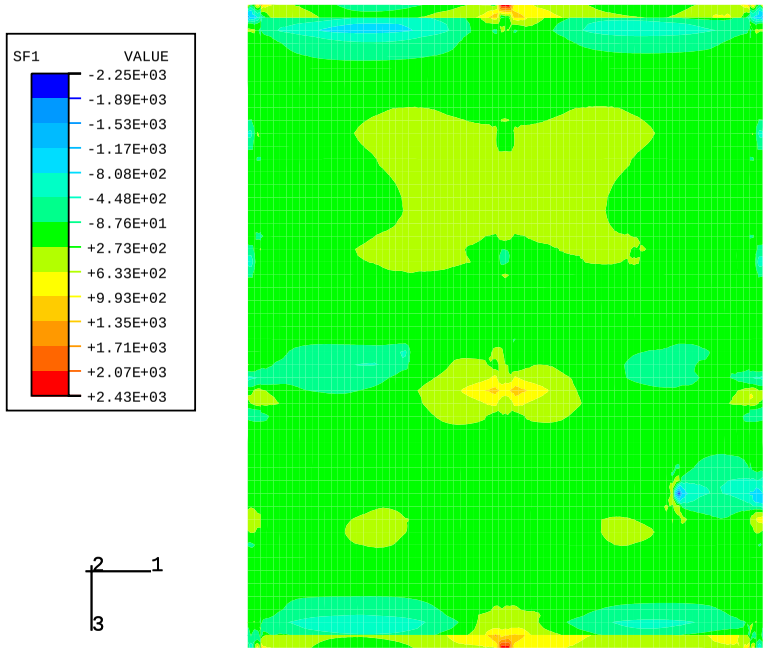

(a) OF=0.02

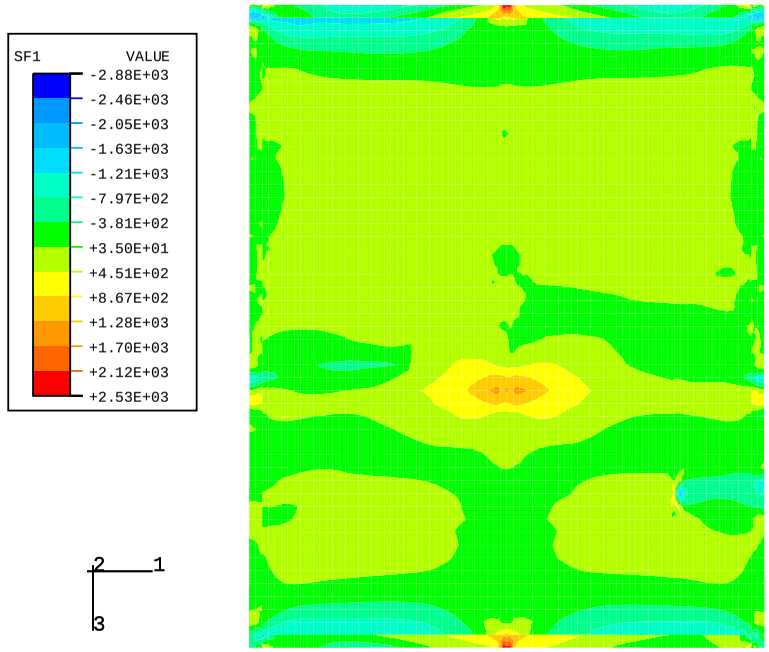

(b) OF=0.08

Figure 8.53: Axial force contours in the slabs x (1) direction at the end of heating

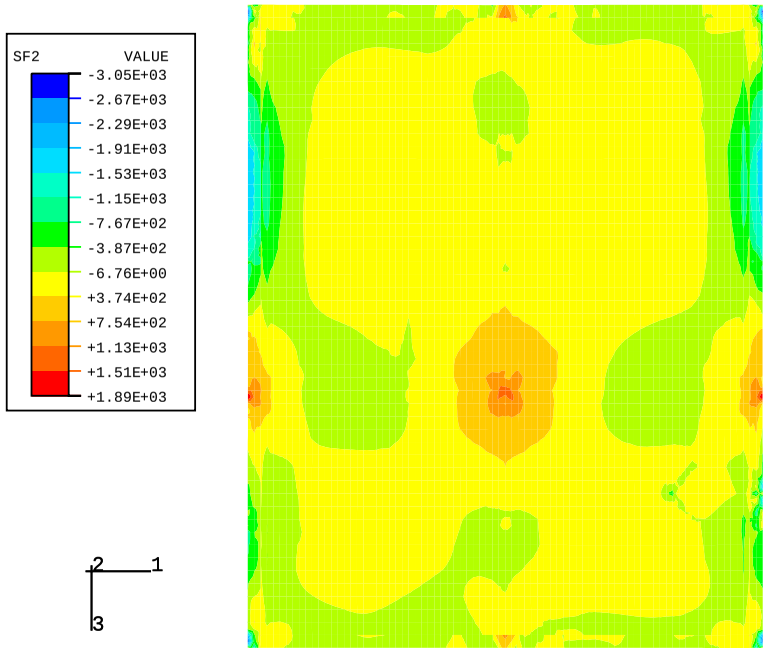

(a) OF=0.02

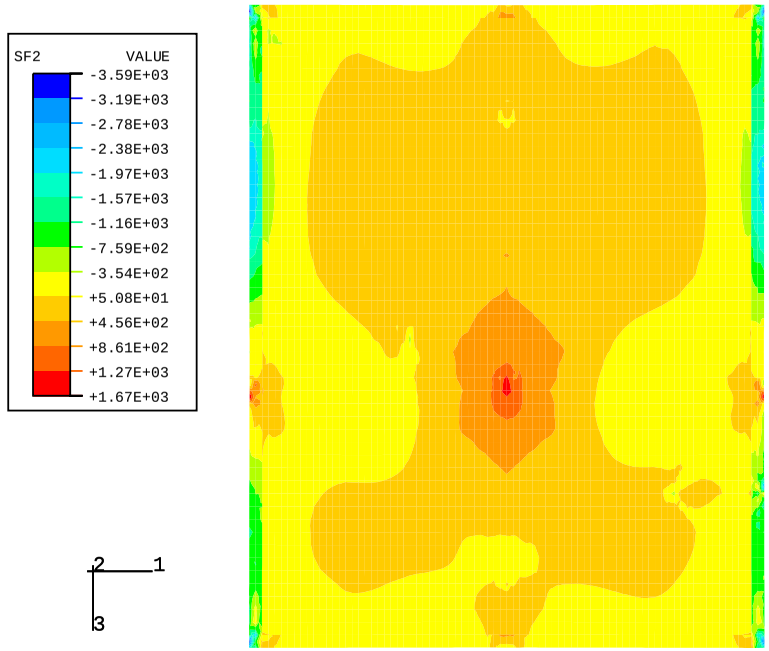

(b) OF=0.08

Figure 8.54: Axial force contours in the slabs y (3) direction at the end of heating

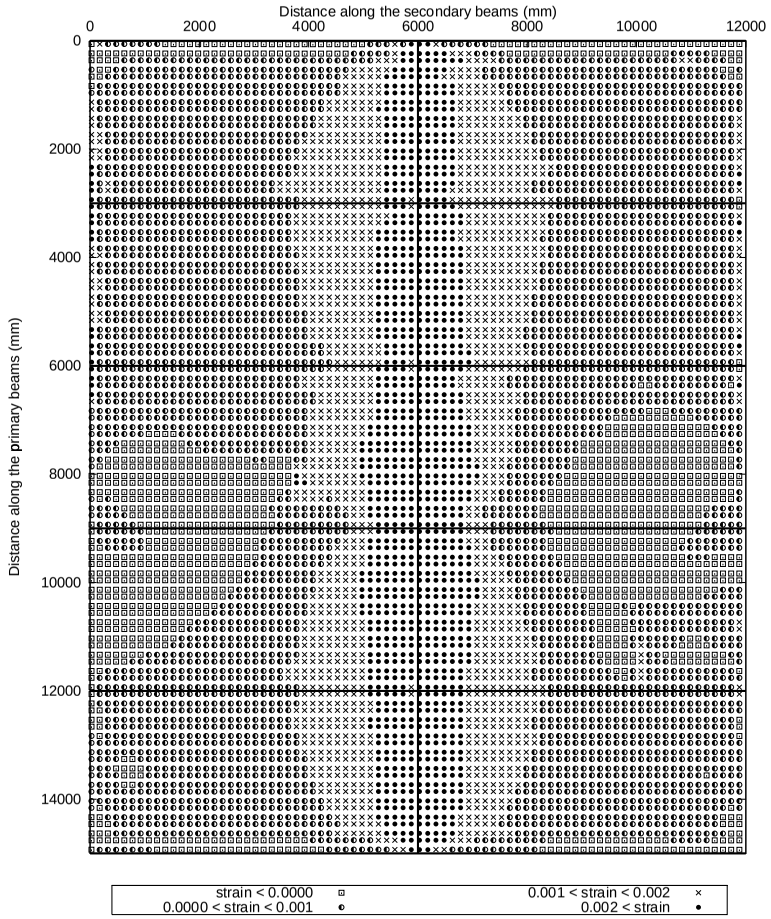

(a) x-direction (parallel to the secondary beams)

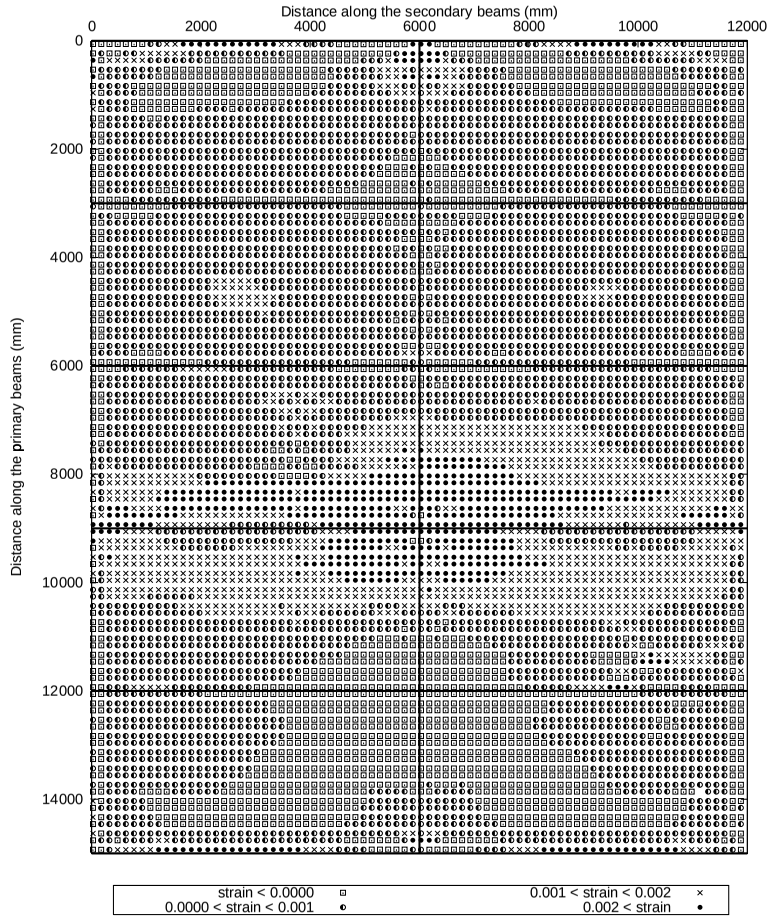

(b) y-direction (parallel to the primary beams)

Figure 8.55: Mechanical strains in the reinforcement OF=0.02, whole floor fire at 600^oC

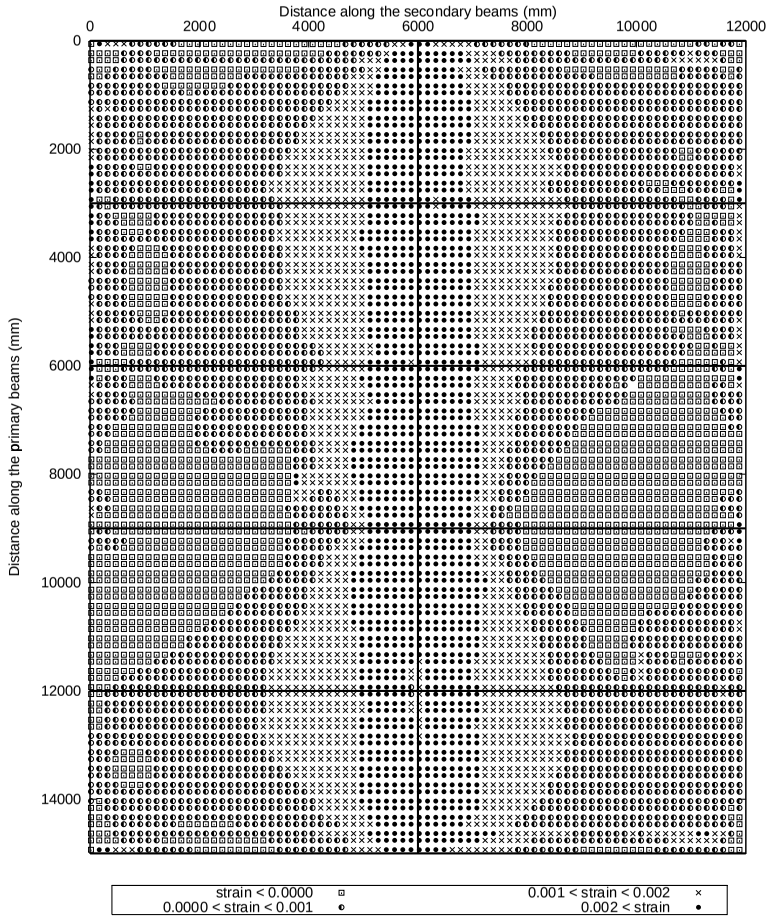

(a) x-direction (parallel to the secondary beams)

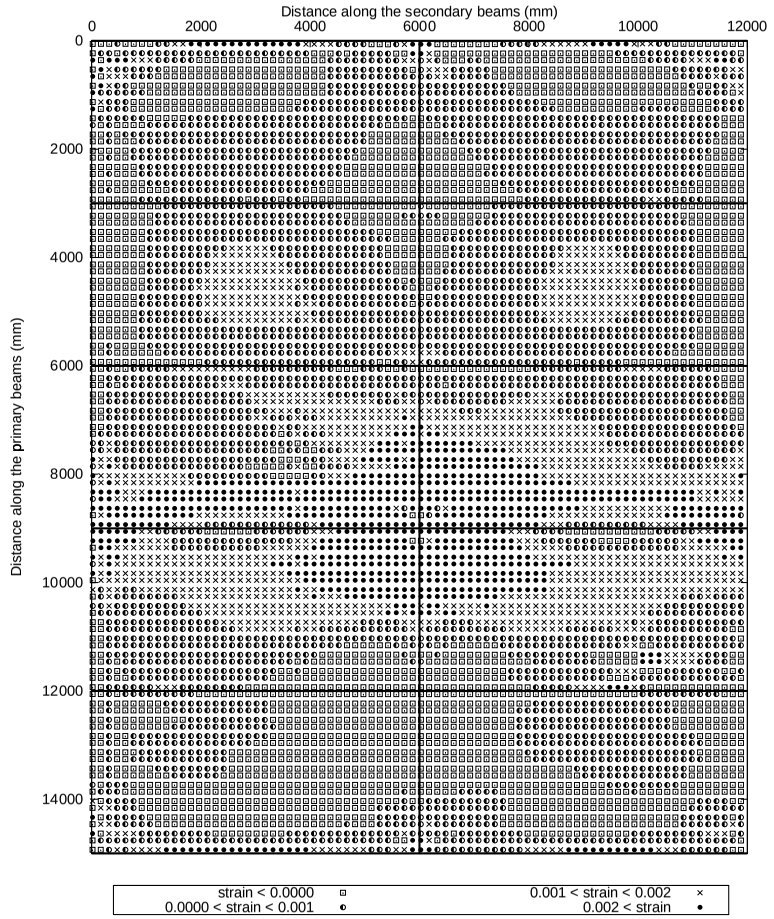

(b) y-direction (parallel to the primary beams)

Figure 8.56: Mechanical strains in the reinforcement OF=0.02, whole floor fire at 750^{o}C

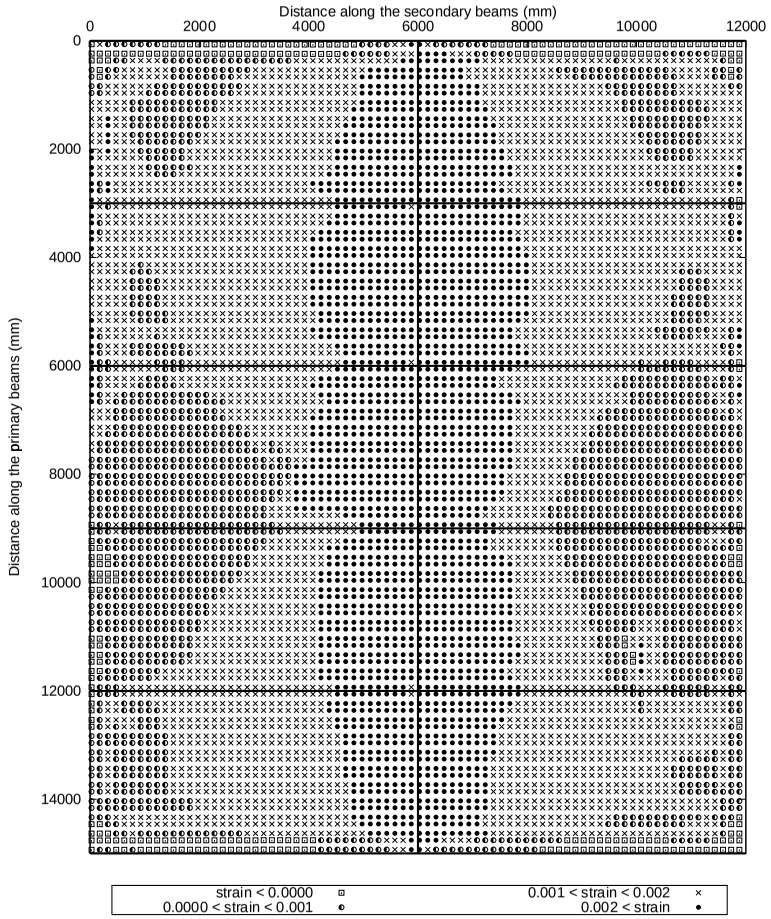

(a) x-direction (parallel to the secondary beams)

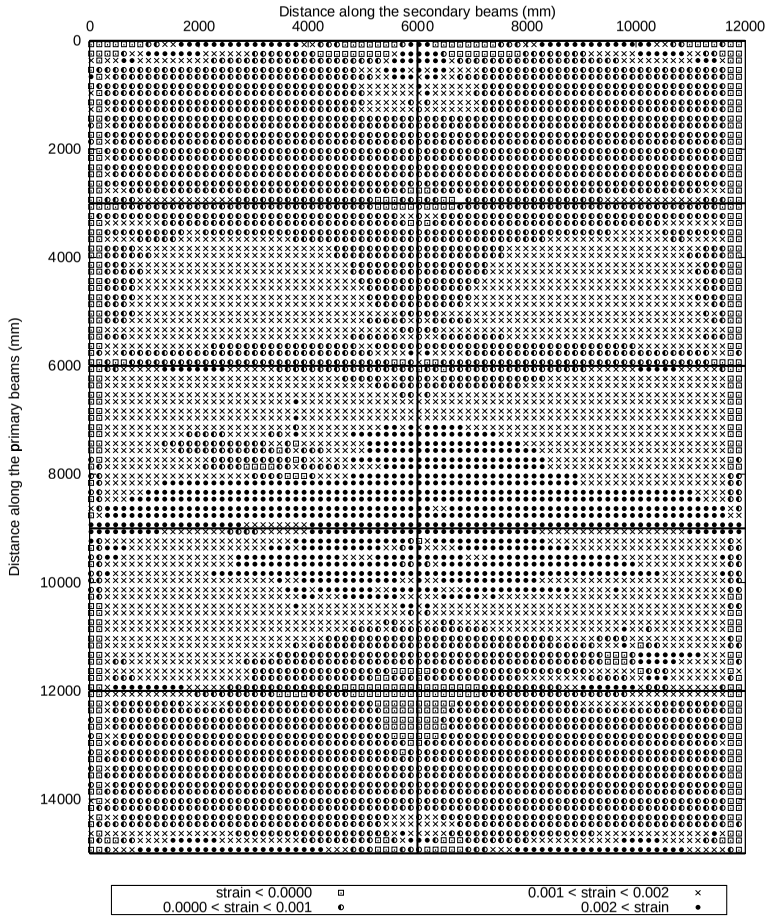

(b) y-direction (parallel to the primary beams)

Figure 8.57: Mechanical strains in the reinforcement OF=0.08, whole floor fire, at 600°C

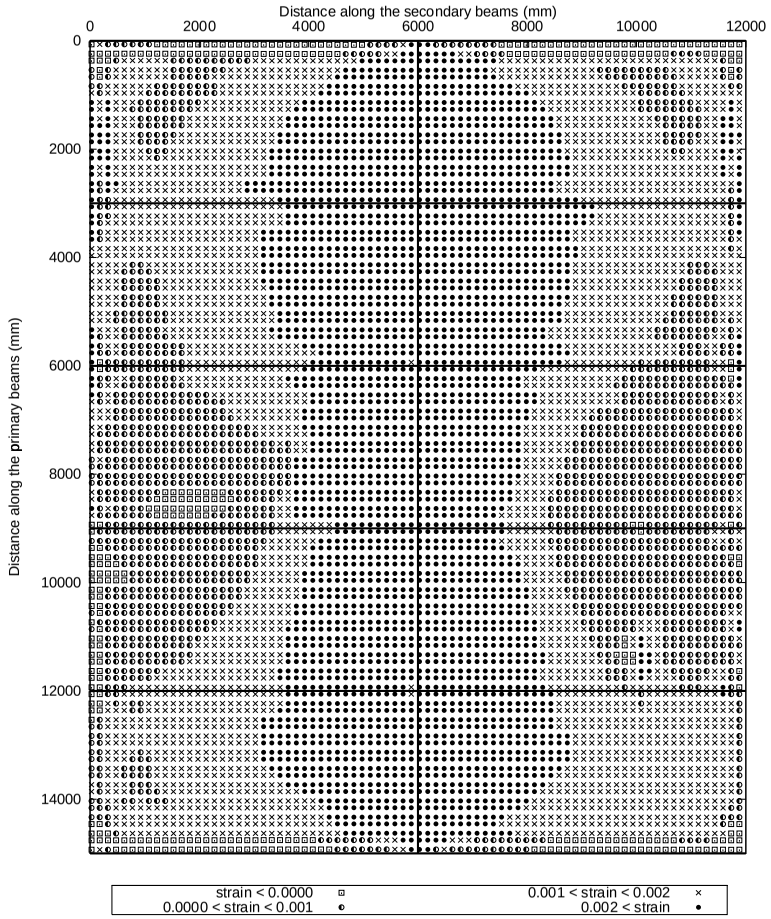

(a) x-direction (parallel to the secondary beams)

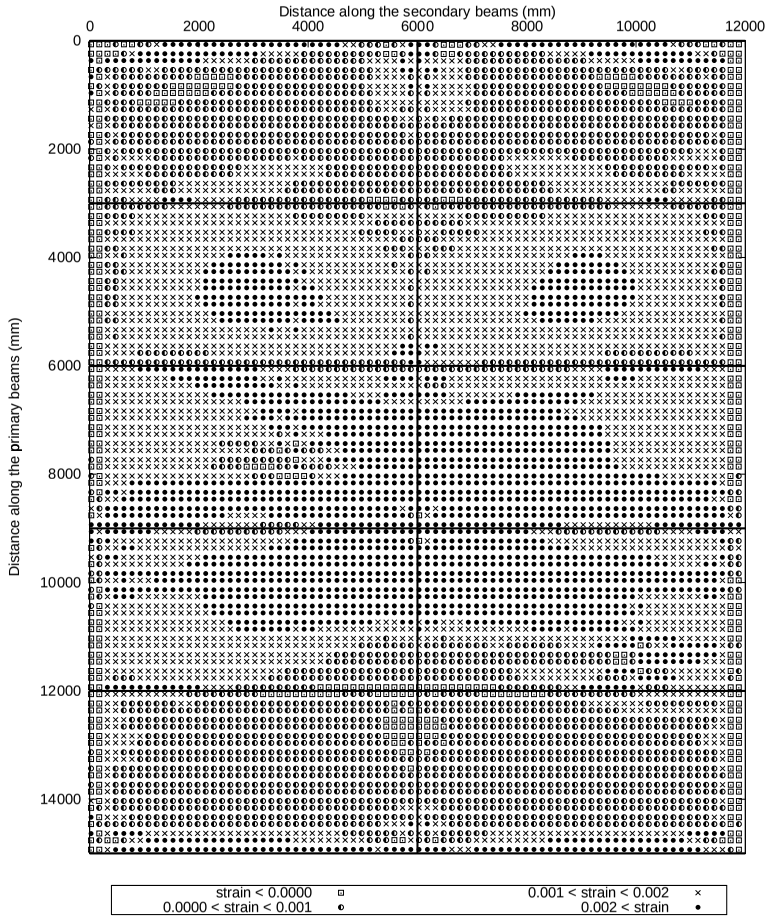

(b) y-direction (parallel to the primary beams)

Figure 8.58: Mechanical strains in the reinforcement OF=0.08, whole floor fire at 750^{o}C

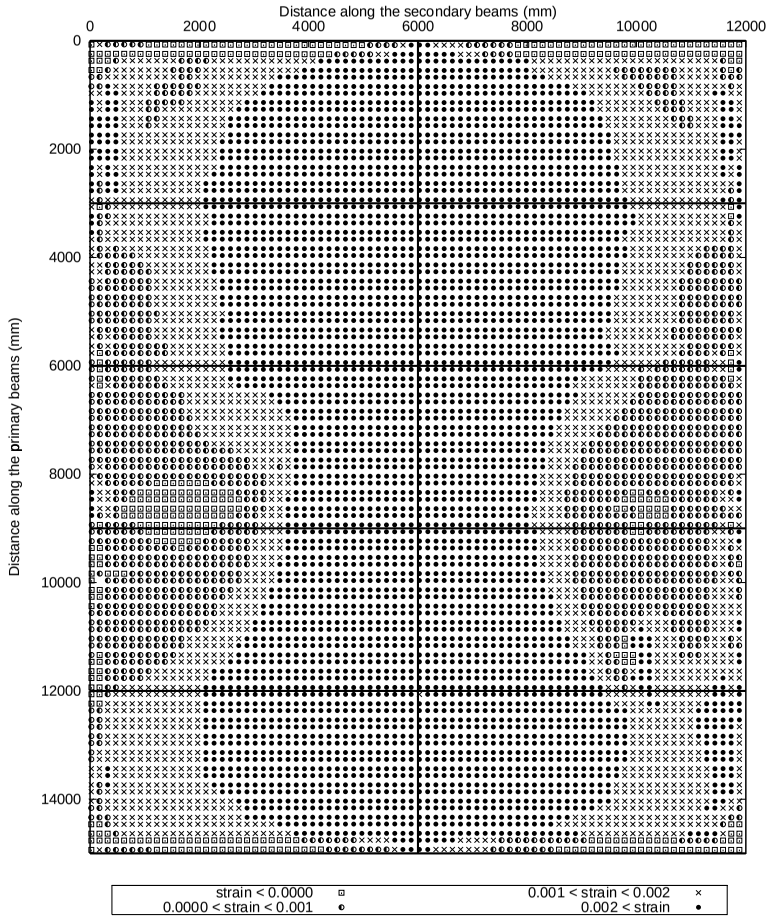

(a) x-direction (parallel to the secondary beams)

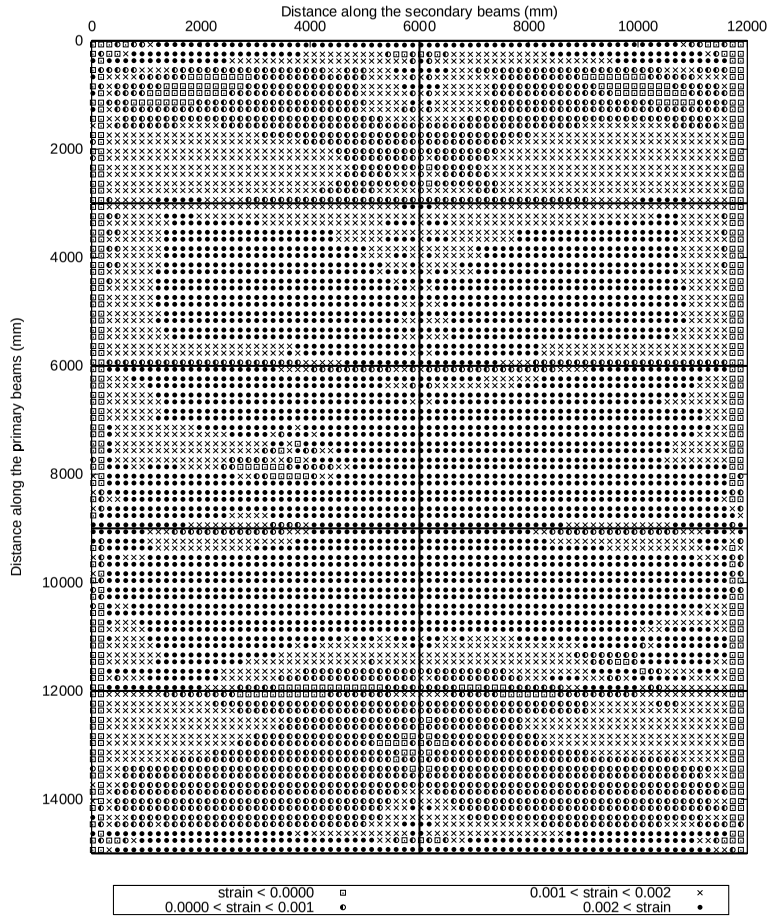

(b) y-direction (parallel to the primary beams)

Figure 8.59: Mechanical strains in the reinforcement OF=0.08, whole floor fire at 950^{o}C

to the heating regime they push down on the primary beam. The moment resisting connection at the end of the primary beam restricts the secondary beam deflections through compatibility. When the moment capacity at the end of the primary beam is reached the secondary beams are relieved and the effect on the structure in terms of increasing deflections and decreasing axial compressions is dramatic and almost instantaneous.

- The instability event coincides with the first yield or ultimate yield of the steel beam thus the moment capacity of the composite primary beam is achieved at the axial compressive capacity of the steel beam but the whole composite rotates.
- The instability event occurs at 90^oC in the "short-hot" fire because the gradient in the slab is high.
- There are larger tensions (or smaller compressions) in the composite of the "short-hot" fire because the composite gradient is high
- Composite moments are strongly influenced by P-Δ moments.
- Mechanical strains in the slab at reinforcement level increase in compression as the "long-cool" fire progresses because the mean temperature of the slab increases considerably beyond a reference temperature of 450^oC.
- In the "short-hot" fire tensions develop over the whole slab due to the build up of high gradients.

8.4.2 Impact of imposed loading on primary beam instability

In parametric studies conducted on finite element models of BS test 1[187,218] doubling the live load in the model made little impact to the mid-span deflection response of the beam. This study was restricted to one highly restrained beam. To test the impact of imposed loading on the 2x2 frame the low imposed load applied to the Cardington frame was applied to the generic frame. Figure 8.60 compares the mid-span deflections of the secondary beams from cases 3 and 6 in Table 8.5. The greatest final deflection with Cardington loading is 25% less than the reference case. In both cases secondary beam deflections are increasing linearly with temperature. Runaway does not occur in either case, however the impact of loading is clearly much greater than calculated for the British Steel restrained beam test.
The axial force in the primary beam is plotted in Figure 8.61 for the lower loading. The sharp drop in axial force associated with changing end conditions is not present. Therefore the effect of loading increases the likelihood of this phenomena. The maximum axial forces in Figure 8.61 do not reach the same level as in case 3 (Figure 8.27)

and are closer to the first yield of steel than the ultimate yield.

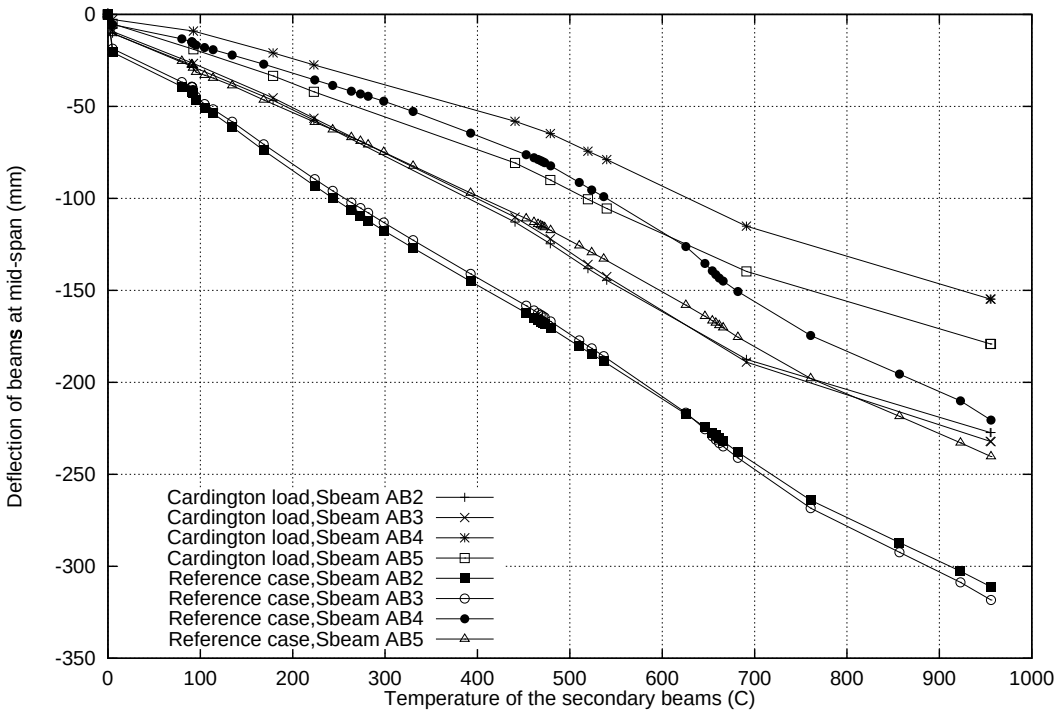

Figure 8.60: Deflection history of the secondary beams at mid-span. A comparison between Cardington live load and the reference case

8.4.3 Impact of secondary beams on primary beam instability

To understand the primary beam instability further scenario 7 in Table 8.5 was conducted. This involved removing the secondary beams from the frame (Figure 8.62). Ordinarily as the heating regime progresses the secondary beams expand and bow pulling down on the primary beam, effectively increasing the point loads on the primary beam. By removing the secondary beams the primary beam instability was delayed. In the same scenario, with secondary beams (scenario 3), the instability occurred at a reference temperature of 90^oC. This can be observed by comparing Figure 8.64 and 8.27. The primary beams mid-span deflections are plotted for scenarios 3 and 7 in Figure 8.63. Initially the deflections are identical until the instability in the reference case after which, in the frame with no secondary beams, the deflections are lower. After 450^oC the deflections are closer again because both scenarios have experienced the primary beam instability (which in this case is precipitated by the downward push on the primary beam from the slab, when the beam reaches its ultimate strength). Final primary beam deflections are greater in the frame with no secondary beams because

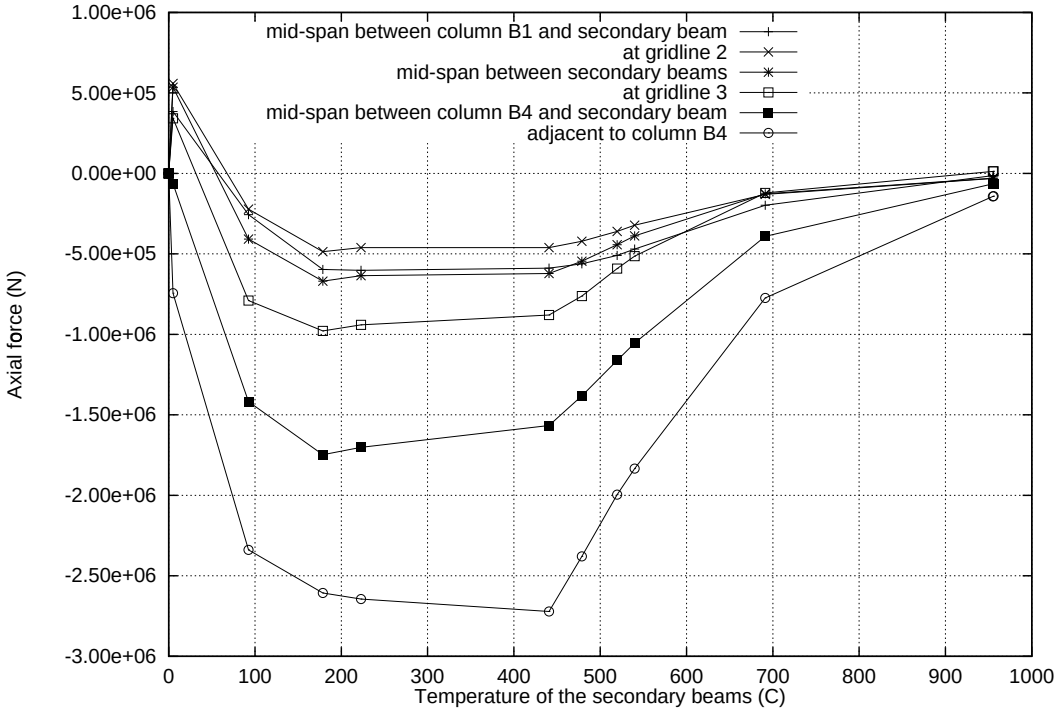

Figure 8.61: Primary beam B14: Axial force in response to the Cardington live load against secondary beam temperature

there are no secondary beams to support and distribute the load. Runaway deflections occur in the primary beam beyond a reference temperature of 850^oC when there are no secondary beams in the frame.

The slab deflection contours for the scenarios with and without secondary beams are plotted in Figure 8.65. The deflection contours highlight that the presence of secondary beams spreads the greatest deflections over a wider floor area.

8.4.4 Simple beam study

The primary beam instability was not observed until the analyses on the 2x2 generic frame thus the phenomena needed to be understood and hopefully reproduced in a simple beam model. The model is shown in Figure 8.66. The composite beams are represented by single steel beams. The secondary beams perpendicular to the primary beam are represented by one beam. The rotational stiffness of the beam to beam and beam to column connections are represented by springs. The springs on the ends of the primary beam (representing a beam to column connection) are stiffer and stronger than those at the ends of the secondary beam (representing a beam to beam connection). The moment capacity of the springs are considerably less than the capacity of

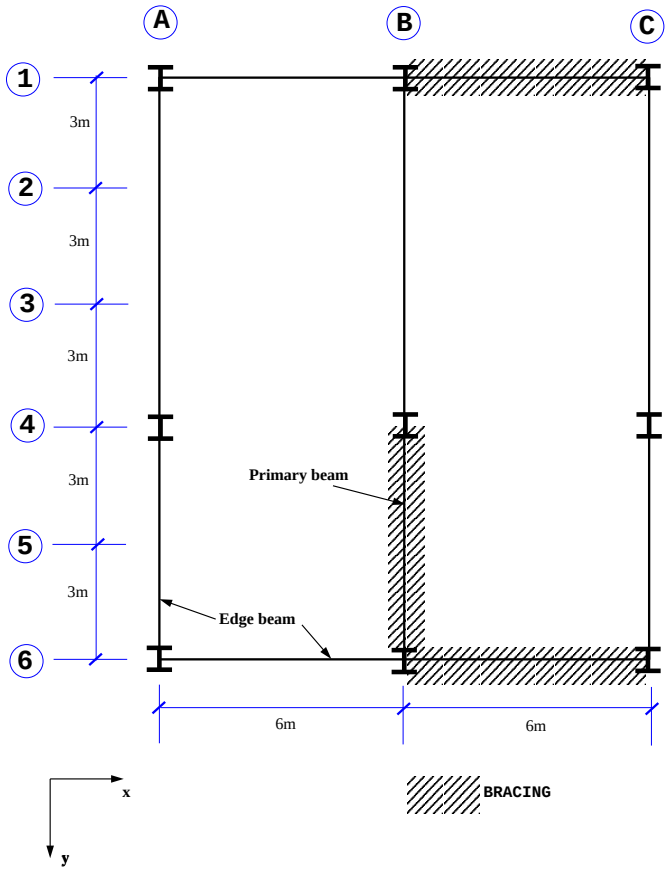

Figure 8.62: Schematic plan view of the 2x2 bay generic frame with all the secondary beams removed

the beams to allow the springs to fail first. The springs will fail on the indicated envelope of the interaction diagram (Figure 8.66). A short parametric study is described in Table 8.6. In each case a mean temperature and a through depth gradient were applied to both beams to increase linearly from zero over time. The results are shown in Figure 8.67. The primary beam instability (characterised by a rapid drop in compression) is present in three of the five simple cases studied. A larger gradient ($8^oC/mm$) reduces the initial peak axial compressions and smoothes the behaviour. This is because bowing induced by gradients absorbs the effects of the restrained thermal expansions. Increasing the mean temperature causes high initial compressions and delays the instability event. This agrees with the comparisons made between the "short-hot" fire and the "long-cool" fire where the larger compressions (or lower gradients) in the composite of the "long-cool" fire delayed the instability event in the primary beam to 450^oC. Increasing the imposed load also reduces the peak axial compressions and the rapid drop in compressive force at the primary beam instability is smaller.

The simple "cross" beams model will not reproduce all the phenomena in the complex

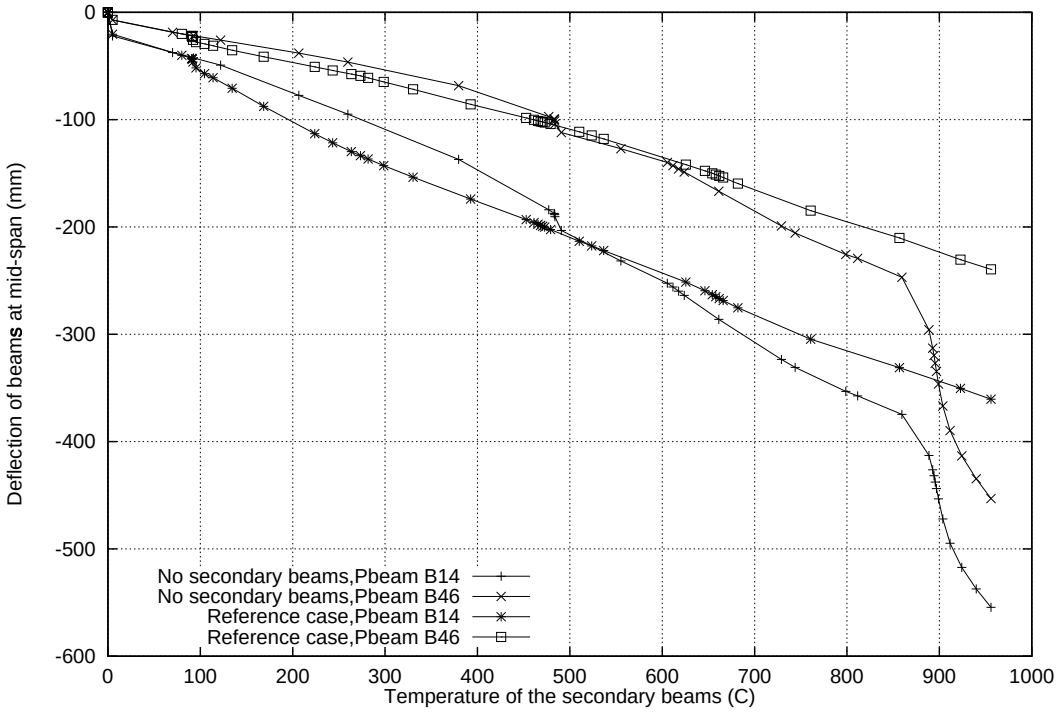

Figure 8.63: Deflection history of the primary beams at mid-span with no secondary beams in the frame

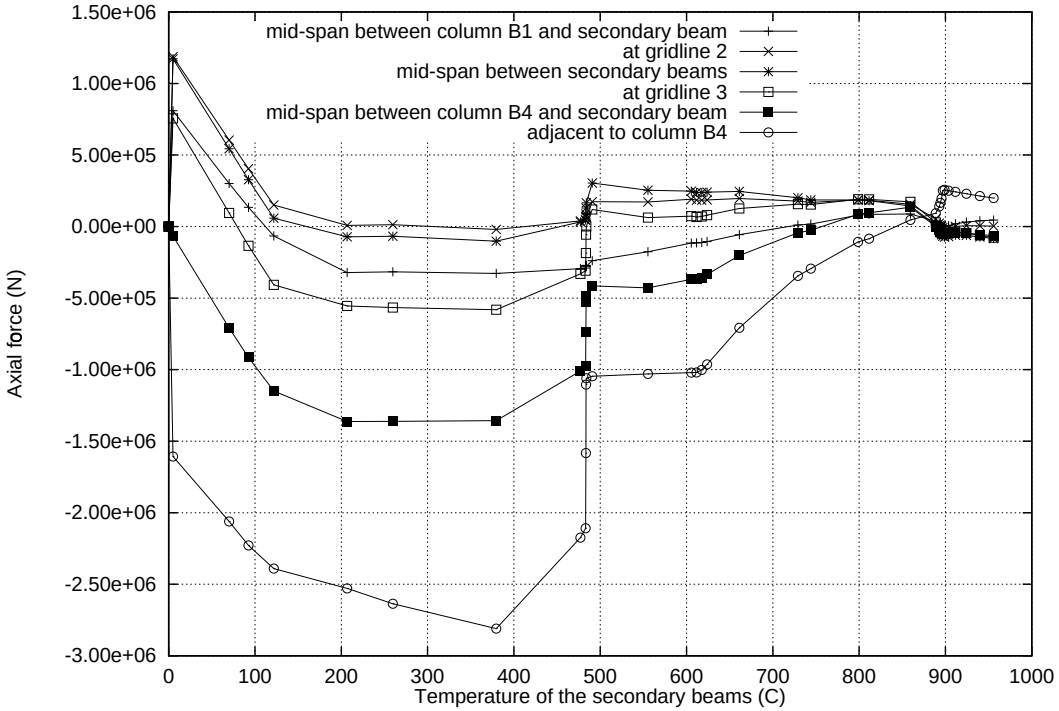

Figure 8.64: Axial force in Primary beam B14 with no secondary beams in the frame

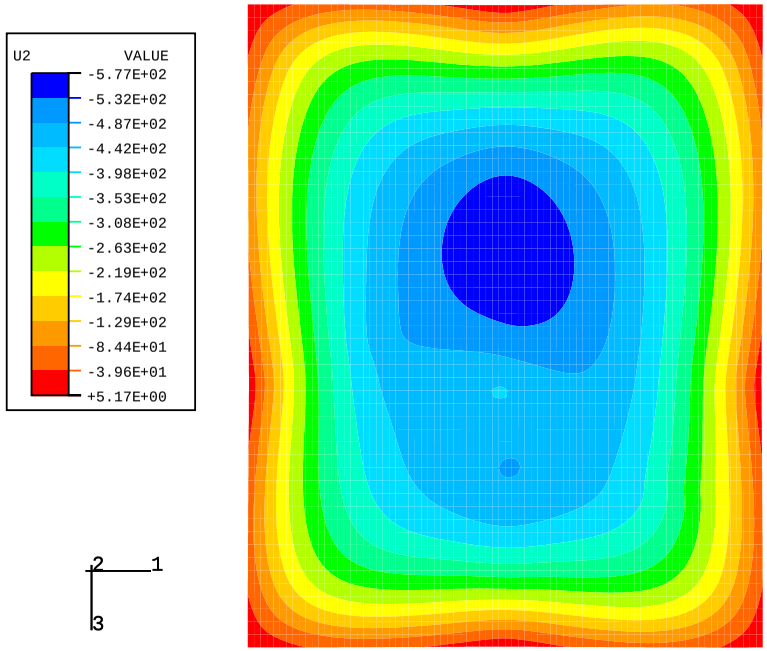

(a) No secondary beams

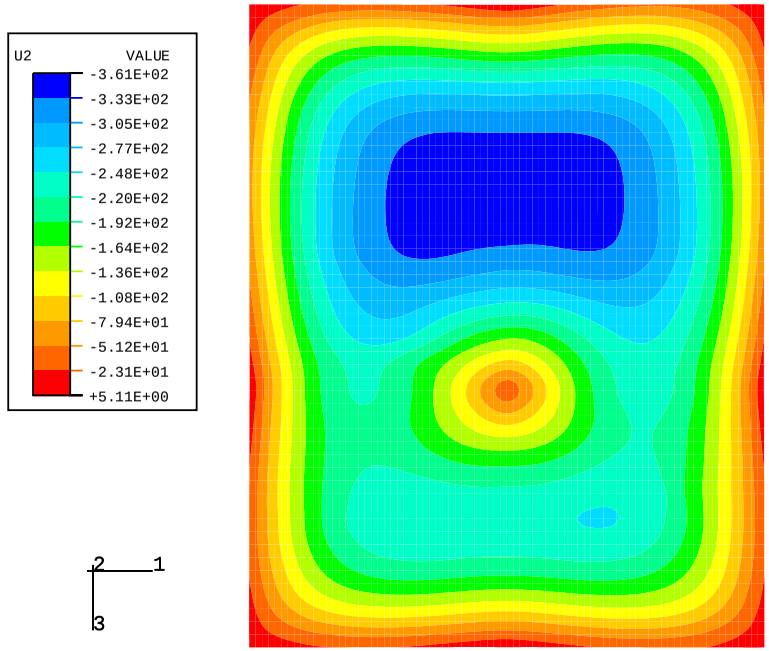

(b) Reference case

Figure 8.65: Deflection contours in the slab at 950^{o}C

Case	ΔT (C)	$T_{,y}$ (C/mm)	Load (N/mm)
1	800	5	8
2	800	5	16
3	800	8	8
4	800	8	16
5	1200	5	8

Table 8.6: Cases studied on the simple ABAQUS "cross" beam model

composite frame. The slab and beam layers are not represented separately in the simple model. However the primary beam instability phenomena is reproduceable.

8.4.5 Effect of applied fire protection in a "long" post-flashover fire

Scenarios 1,2 and 4 of Table 8.5 are compared in this section. The three studies were designed to highlight the differences in structural behaviour of a composite steel frame when the steel beams were protected or not. The only differences between the three scenarios studied were the number of beams with applied fire protection. In one instance the edge and primary beams were protected, in the second scenario only the edge beams were protected and in the third scenario all the beams were left unprotected. The fire scenario is a whole floor fire assuming the Pettersson natural fire with an opening factor of $0.02m^{1/2}$ ("long-cool" fire). The duration of the "long-cool" fire allows the protected edge beams to achieve higher temperatures than the "short-hot" fire thus is a worst case for protected beams. The degree of restraint provided by protected or unprotected edge beams has a strong influence on the structural behaviour.

8.4.5.1 Deflection Response

Figure 8.68 shows the displacement of the slab in contour plots at the end of the analysis. Blue indicates large -ve displacement and red +ve displacement. The first figure includes protection to the edge beams only, whilst the second figure is the response of the structure when all the beams are unprotected. Once again these illustrate the global response of the structure. There are large downward displacements near the centre of the bays and some upward movement of the columns. In both cases maximum displacements occur near the centre of the largest bays (9m x 6m). When the edge beams are protected the displacements are much lower and the slab moves into a large deflected shape anchored on all sides of the building. When the edge beams are unprotected the deflections are greater and the 9m x 6m bays seem to act like a single one way spanning slab. In the latter example the load carrying mechanism developed

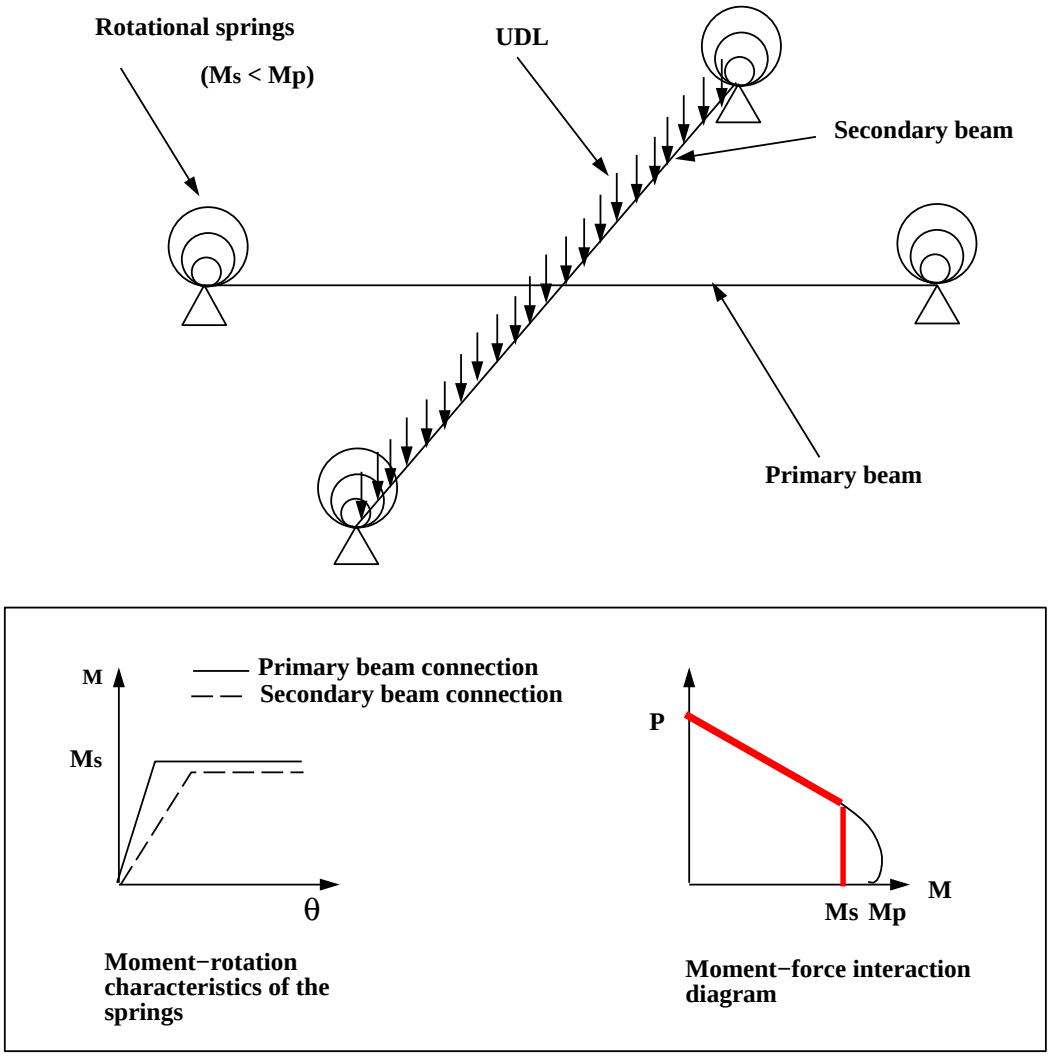

Figure 8.66: The simple ABAQUS "cross" beams model

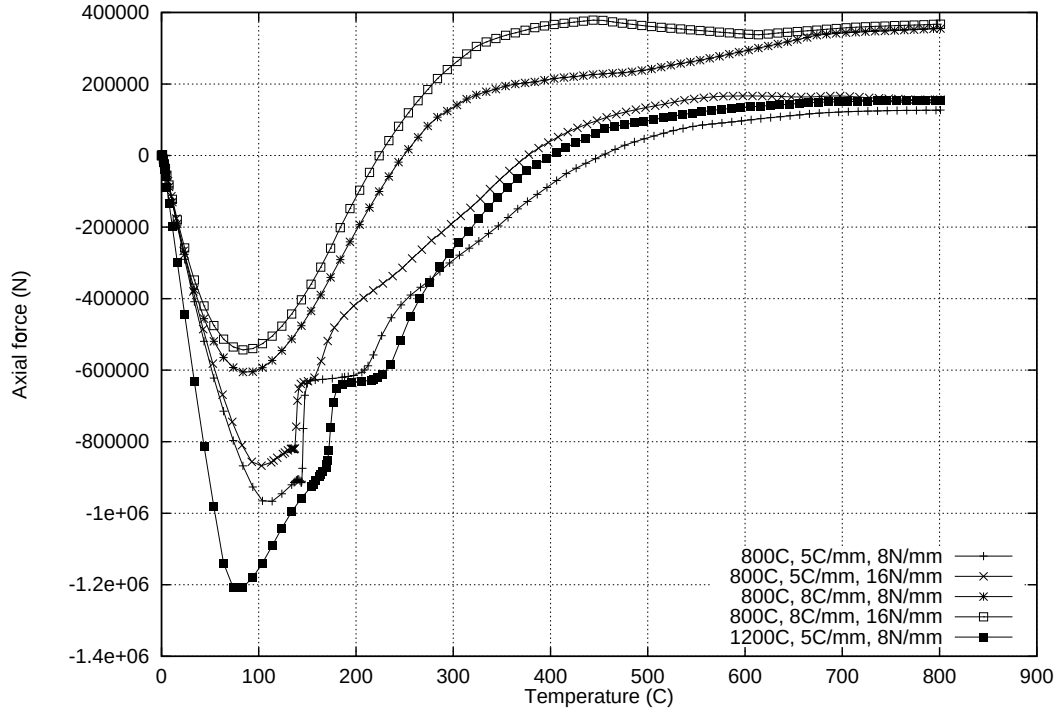

Figure 8.67: Axial force in the primary beam of the simple ABAQUS "cross" beams model

in the slab (at large deflections) is likely to be similar to 1D catenary action rather than 2D tensile membrane action.

Figures 8.69-8.72 show the deflection response at mid-span of most of the beams in all three scenarios. The beams deflect in a relatively linear manner with increasing temperature up to 650^{o}C. As the protection is removed from first the primary beams then all the beams the deflections increase considerably. However, secondary beams AB4 (Figure 8.69) reach very similar deflections in all three scenarios. This indicates that their deflection response is greatly influenced by the stiff structure around column B4.

The response of the edge beams is shown in the plots of Figure 8.71 and 8.72. Edge beams are cooler than internal beams therefore deflect less. In this instance the edge beams parallel to the secondary beams (Figure 8.71) reach maximum deflections of about 100-120mm if the beams are unprotected and 50mm if protected. In contrast the 9m edge beams, when not protected, achieve very similar displacements to the primary beam.

The influence of the wind bracing on the deflection response of the edge beams can be observed by comparing the relative displacements of edge beams AB1 and BC1 or AB6 and BC6. The beams in the same bay as the bracing deflect more as expected (Figure

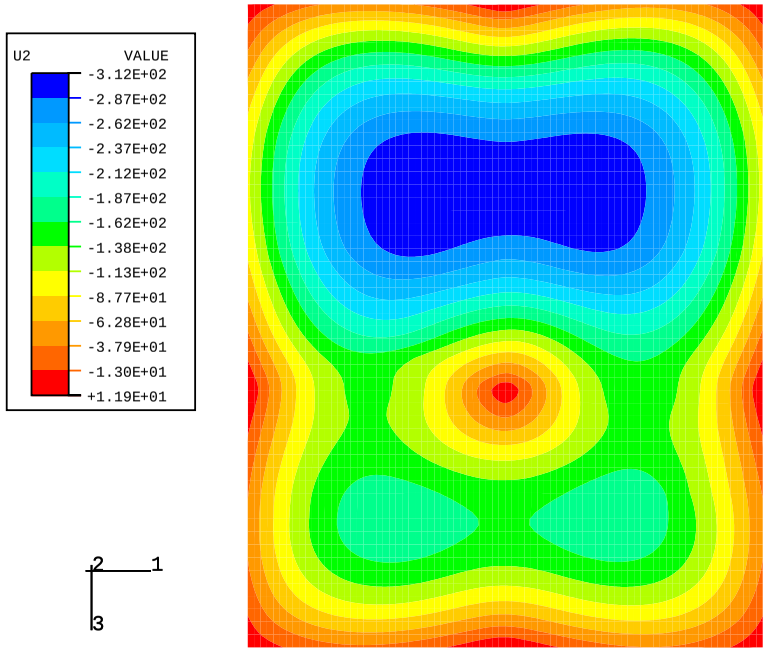

(a) Edge beams protected

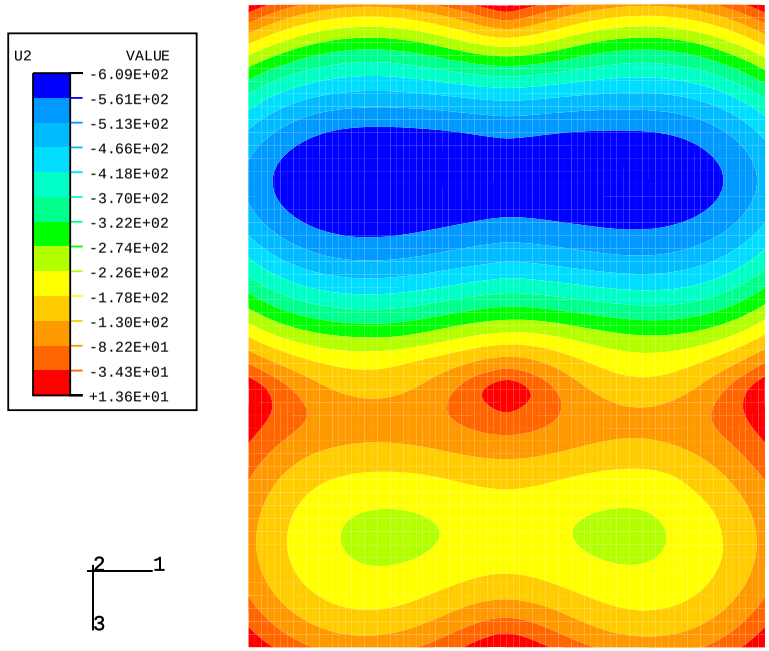

(b) All beams unprotected

Figure 8.68: Deflection contours in the slab at 750^{o}C

8.71).

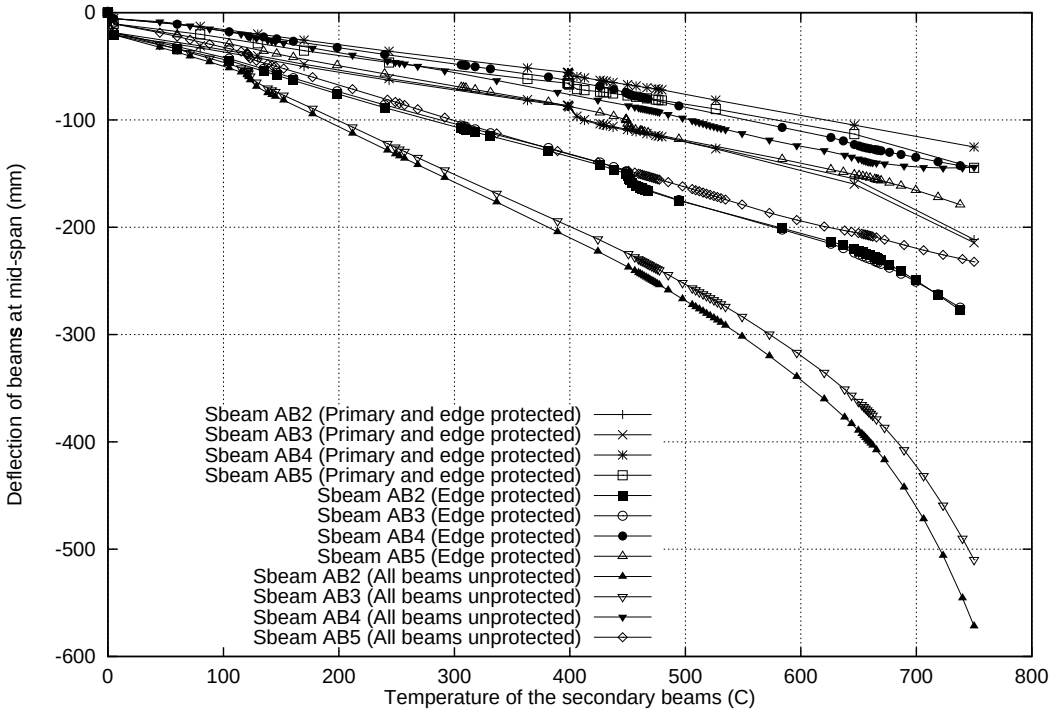

Figure 8.69: Deflections of the secondary beams, OF=0.02

The rates of deflection at mid-span of the beams along gridlines A, B and C are shown in Figures 8.73-8.75. With both the primary and edge beams protected the rate of deflection near the end of the analysis is stable (Figure 8.73). When the edge beams alone are protected the rate of deflection becomes less stable but the magnitudes are very small (Figure 8.74). When all the beams are unprotected the change in rate of deflection of the 9m beams, near the end of the analysis, is considerable (Figure 8.75), suggesting runaway at 650^{o}C.

8.4.5.2 Response of the steel beams

Figures 8.76-8.78 show the axial forces in secondary beam AB2 and primary beam B14 against secondary beam temperature for all three scenarios. The axial force is plotted at various locations along the length of the beams. When the edge beams are unprotected the axial forces experienced by the secondary beams are slightly lower than when the edge beams are protected, clearly due to lower restraint.

The timing of the instability event in the primary beam changes as the level of fire protection applied to the model changes. There is a marked drop in compressive axial force corresponding to a reference temperature of 400^{o}C when the primary and edge

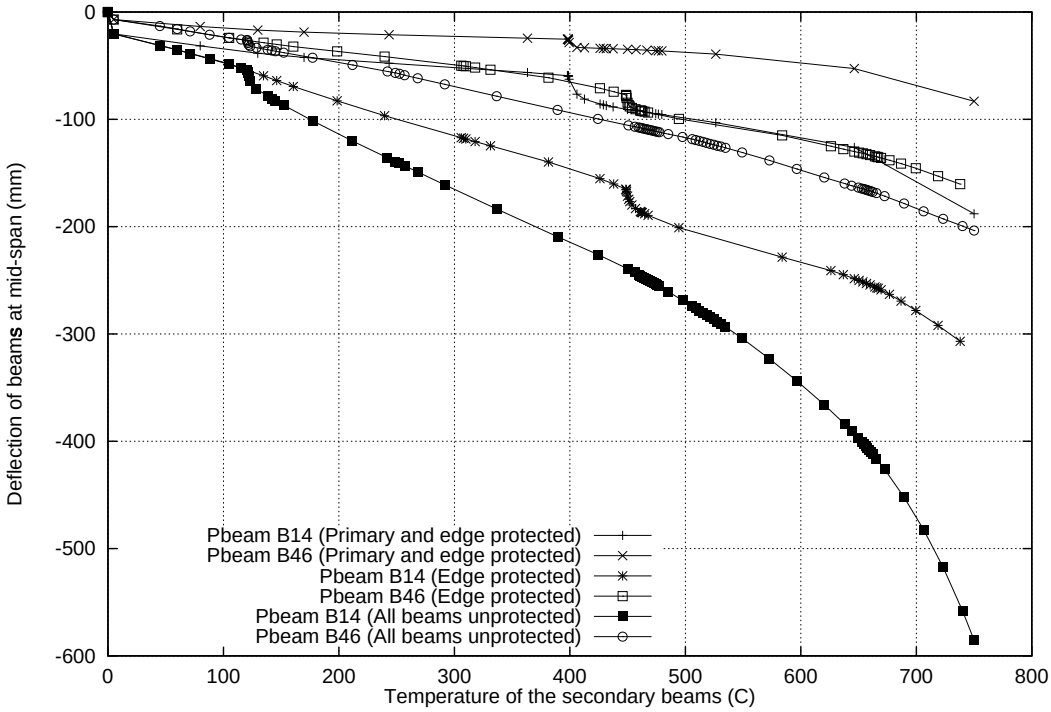

Figure 8.70: Deflections of the primary beams, OF=0.02

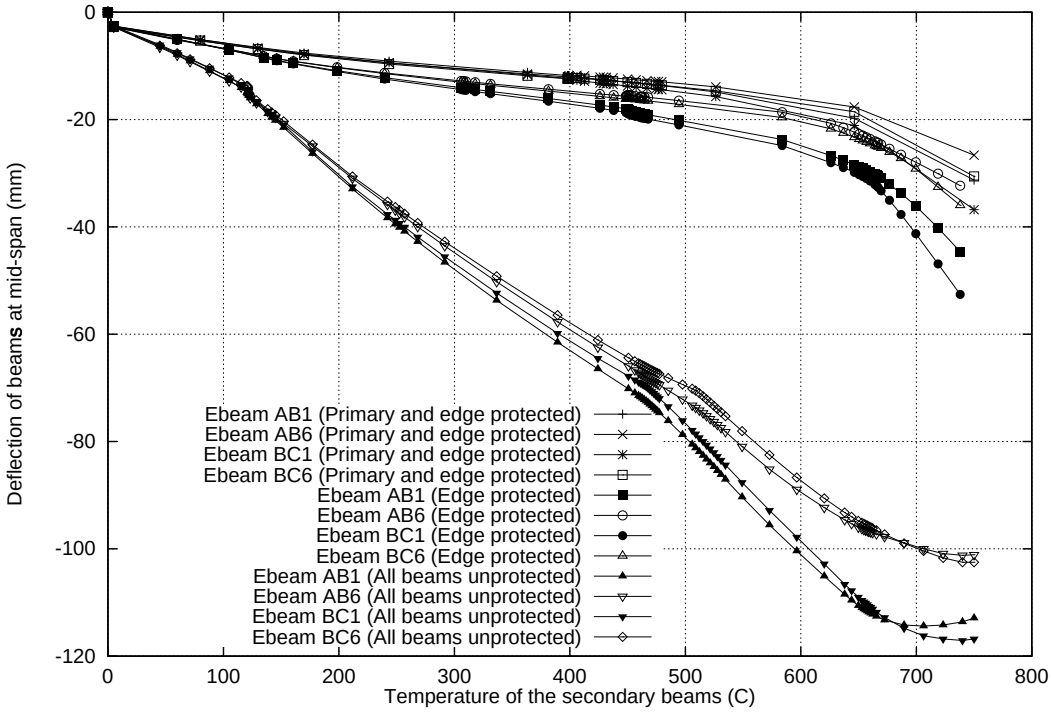

Figure 8.71: Deflections of the edge beams parallel to the secondary beams, OF=0.02

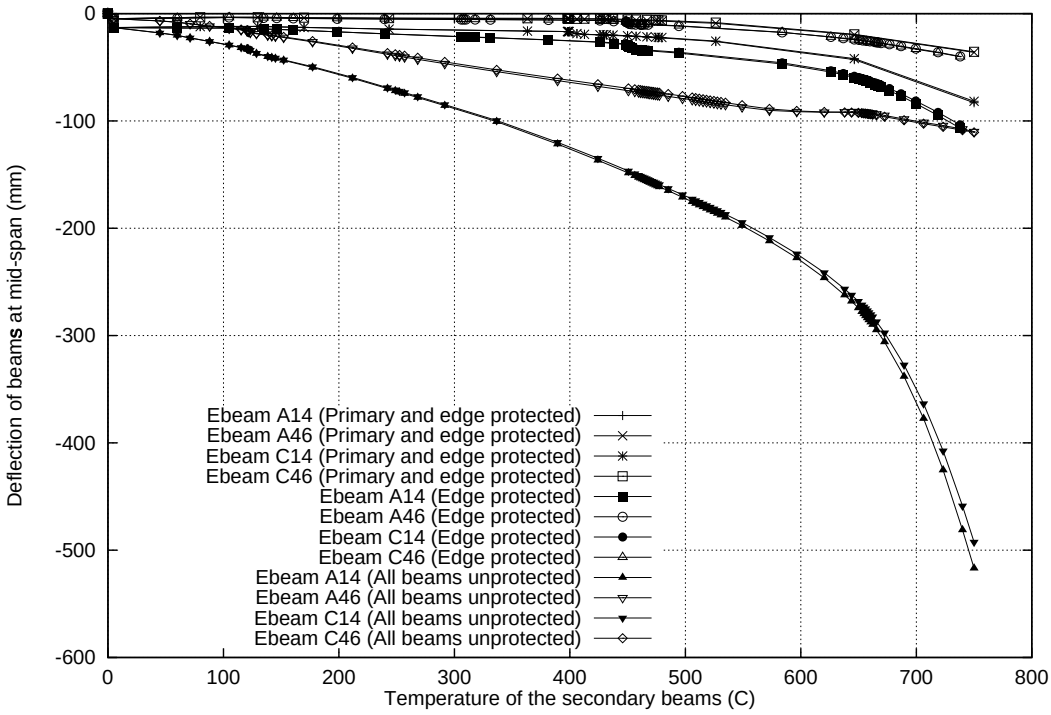

Figure 8.72: Deflections of the edge beams parallel to the primary beams, OF=0.02

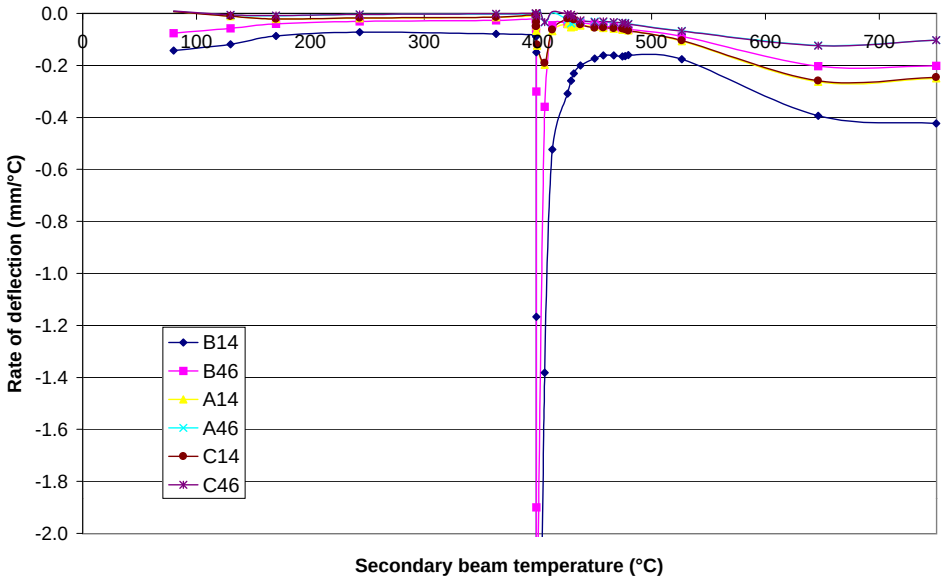

Figure 8.73: Rates of deflection at mid-span of the edge and primary beams against secondary beam temperature, OF=0.02, primary and edge beams protected

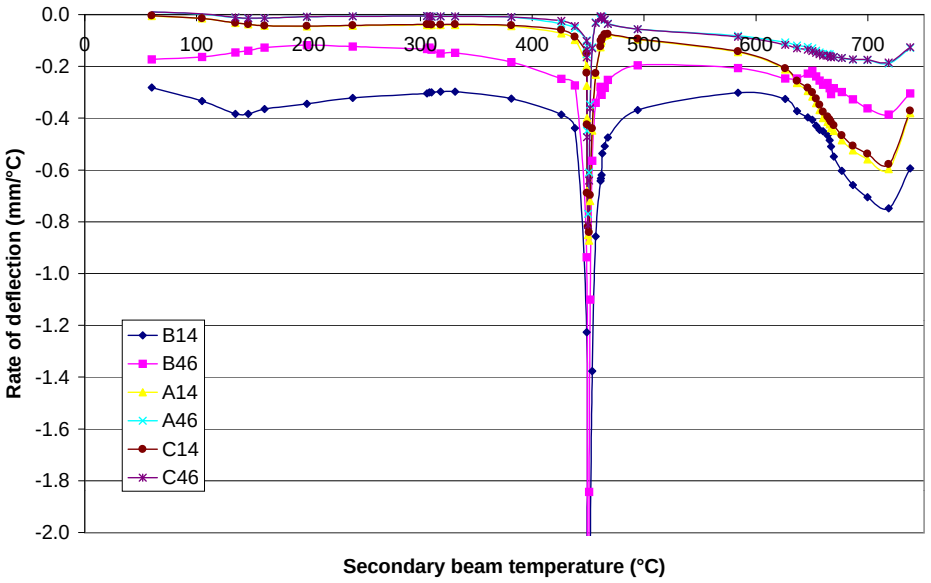

Figure 8.74: Rates of deflection at mid-span of the edge and primary beams against secondary beam temperature, OF=0.02, edge beams protected

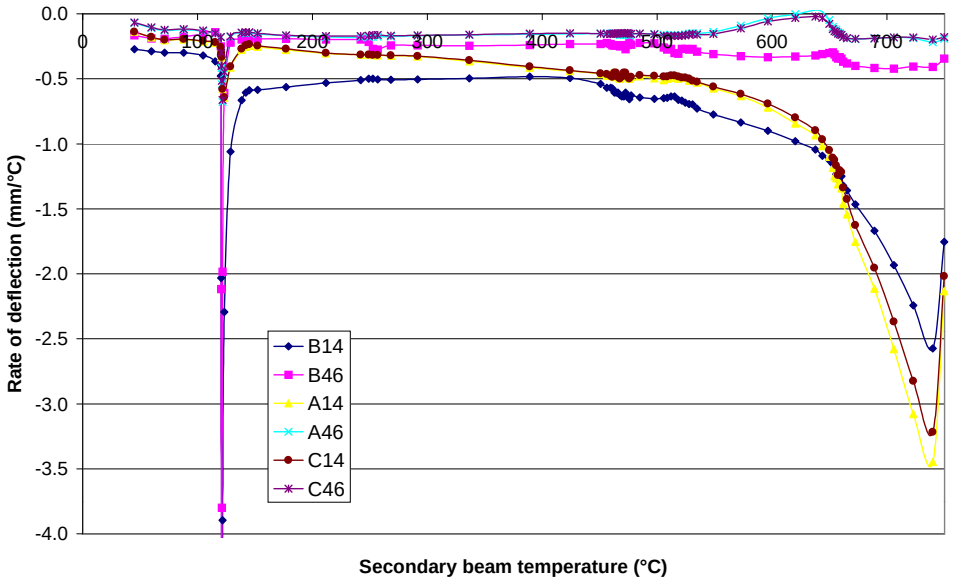

Figure 8.75: Rates of deflection at mid-span of the edge and primary beams against secondary beam temperature, OF=0.02, all beams unprotected

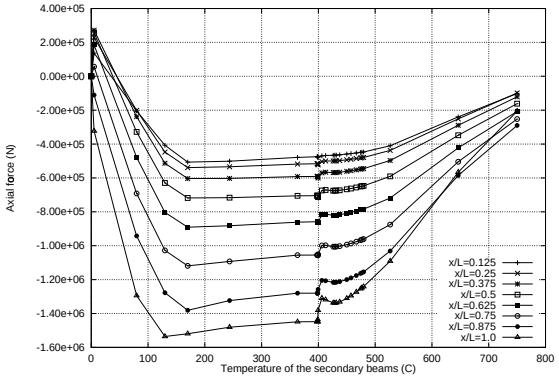

(a) Secondary beam AB2

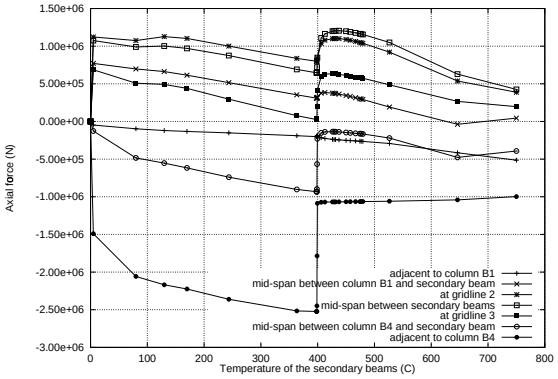

(b) Primary beam B14

Figure 8.76: Variation of axial force against secondary beam temperatures, primary and edge beams protected

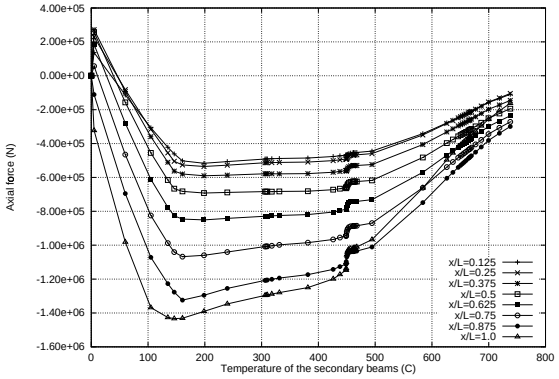

(a) Secondary beam AB2

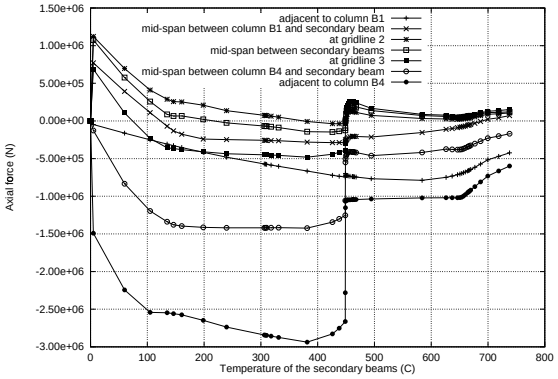

(b) Primary beam B14

Figure 8.77: Variation of axial force against secondary beam temperatures, only edge beams protected

beams are protected. A similar loss in compression occurs at 450^{o}C when the edge beams alone are protected and also at 120^{o}C when all beams are unprotected. When all the beams are unprotected there is reduced restraint so the slab will rotate with the primary beam at 100^{o}C. When the primary beam is protected the loss of moment capacity occurs when the reference temperature is at 400^{o}C (slab and edge beams are hotter so slab will rotate) and the primary beam is at 100^{o}C (first yield). When the edge beams alone are protected there is enough restraint in the cooler edge beams and slab to prevent the slab rotation thus delaying the primary beam instability until much later.

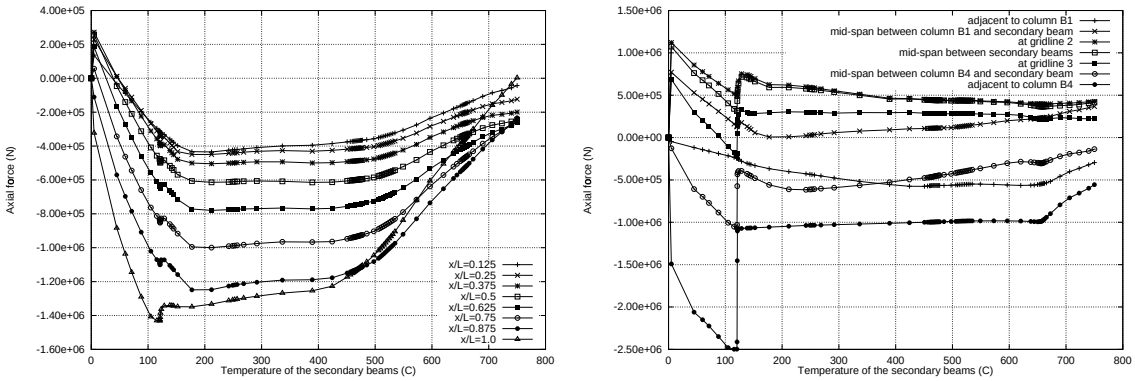

(a) Secondary beam AB2

(b) Primary beam B14

Figure 8.78: Variation of axial force against secondary beam temperatures, all beams unprotected

8.4.5.2.1 Column displacements The horizontal column displacements of column B1 for each protection scenario are shown in Figures 8.79-8.81. When the edge beams are protected the column continues to deflect outwards until the end of the analysis. When all the steel beams are unprotected the highly deflected composite slab pulls the column back near the end of the analysis.

8.4.5.2.2 Edge beams Figures 8.82-8.84 show the compressive forces in edge beams AB1 and BC1 for all three scenarios.

There is an increase in compressive axial force in each scenario corresponding to the primary beam instability. When the edge beams are protected (thus always in growing compression) they anchor the slab allowing tensile membrane action to develop. If the edge beams are unprotected towards the end of the analysis the compressions are small and decreasing. They have very little load carrying ability.

The axial forces experienced by the edge beams depends on the temperature they achieve. The protected edge beams continue to increase in axial compression throughout the analyses. In contrast the unprotected edge beam behaves in a similar manner to the unprotected secondary beams.

8.4.5.3 Behaviour of the slab

The mechanical strains at a reference temperature of 750^{o}C are plotted in Figures 8.85 and 8.86 for the case where the edge beams alone are protected and for the case where all beams are unprotected respectively. The patterns of behaviour a very similar but there is a greater area of compressive strains in the case where the edge beams are unprotected (Figure 8.86).

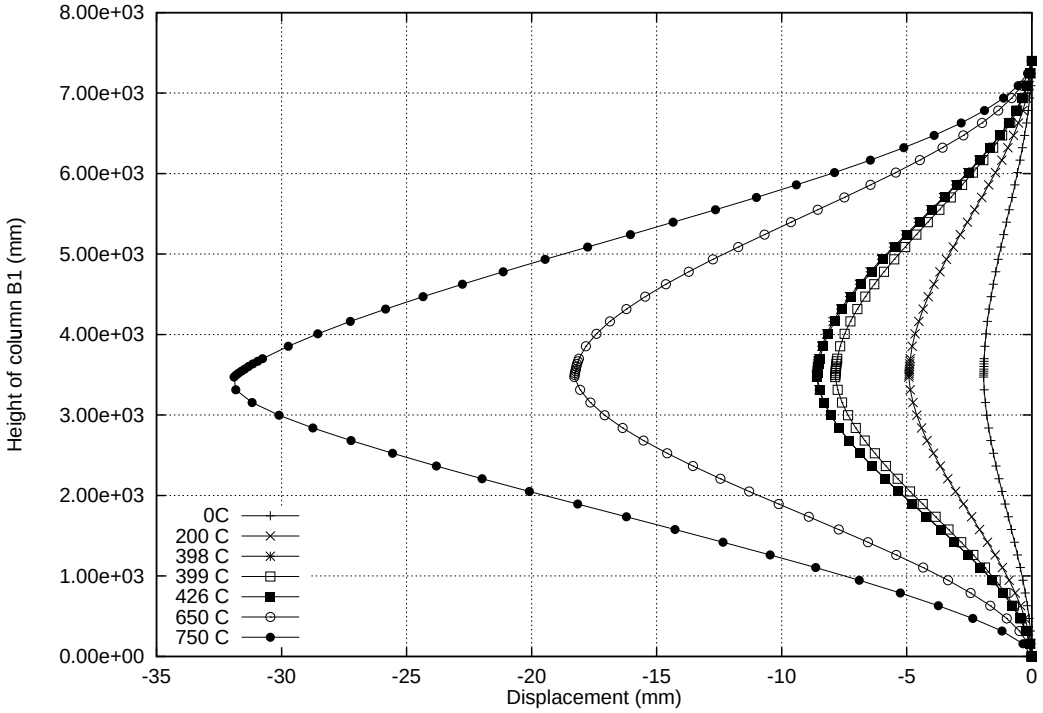

Figure 8.79: Horizontal movement of column B1, OF=0.02, primary and edge beams protected

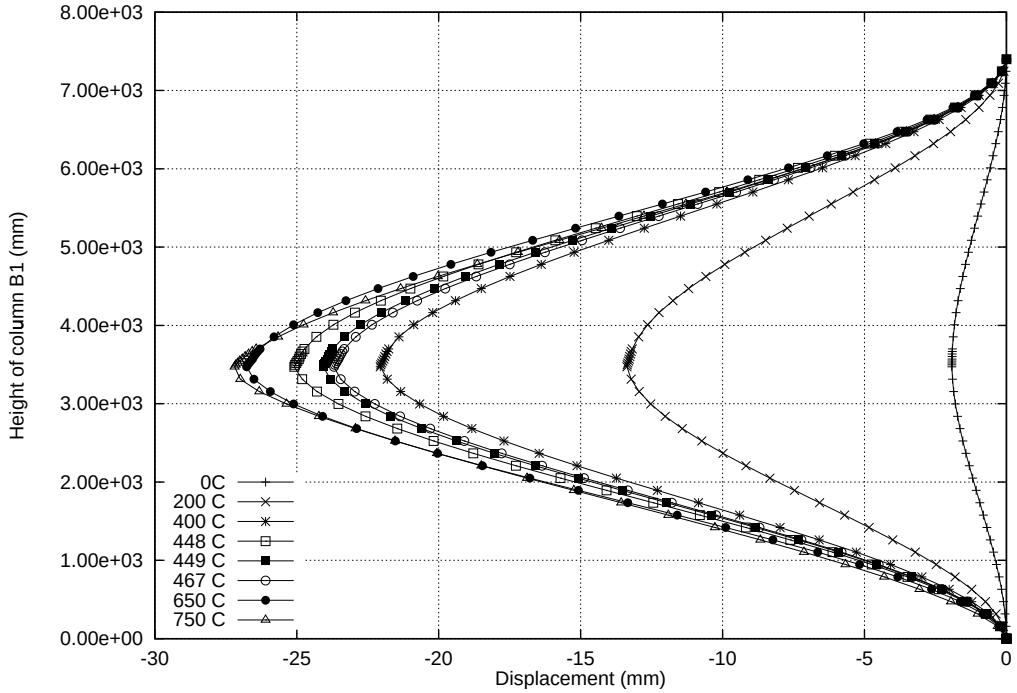

Figure 8.80: Horizontal movement of column B1, OF=0.02, edge beams protected

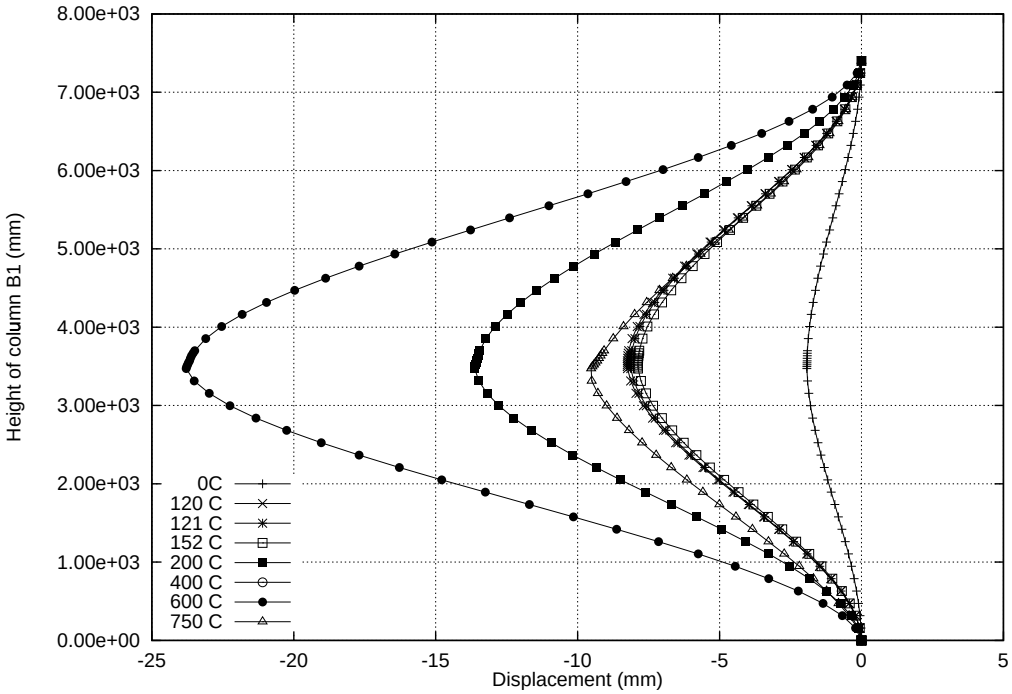

Figure 8.81: Horizontal movement of column B1, OF=0.02, all beams unprotected

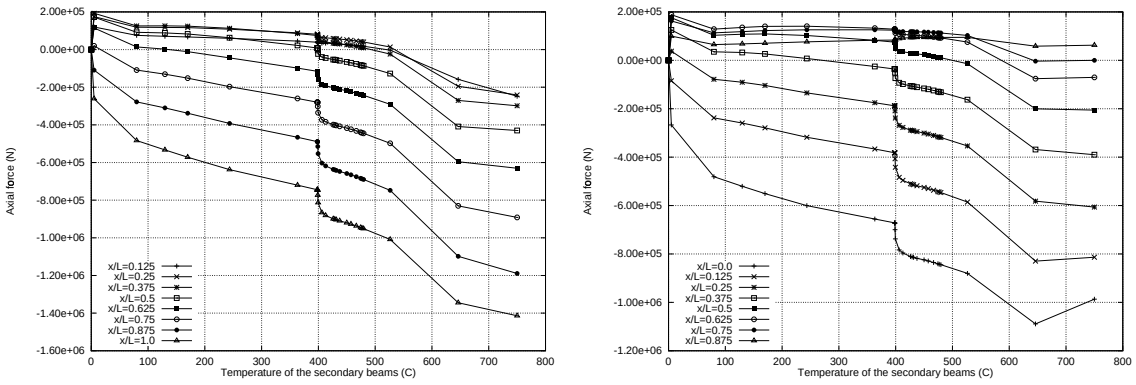

(a) AB1

(b) BC1

Figure 8.82: Variation of axial force at the mid-span of edge beam AB1 and BC1 against temperature, primary and edge beams protected

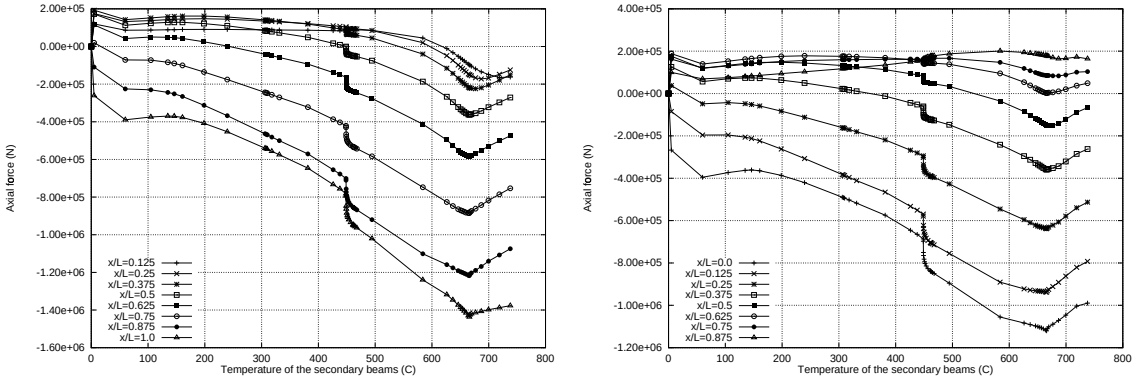

(a) AB1 (b) BC1

Figure 8.83: Variation of axial force at the mid-span of edge beam AB1 and BC1 against temperature, edge beams protected only

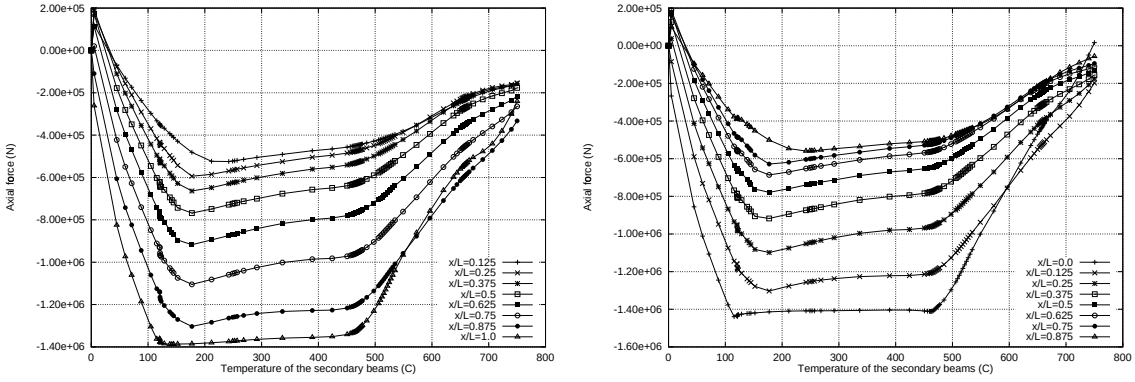

(a) AB1 (b) BC1

Figure 8.84: Variation of axial force at the mid-span of edge beam AB1 and BC1 against temperature, all beams unprotected

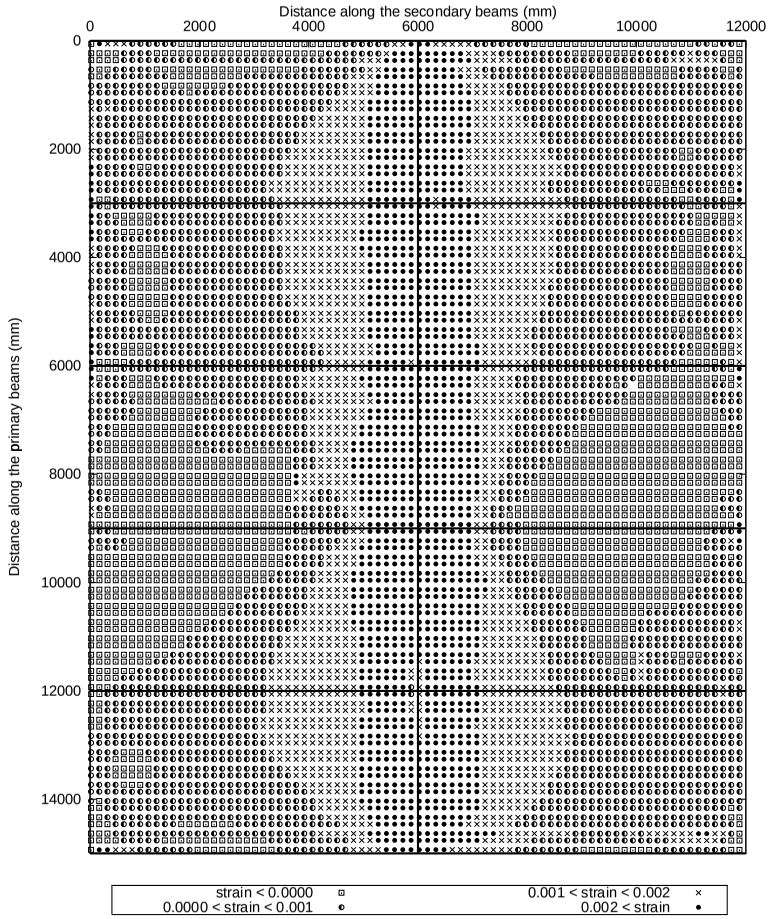

(a) x-direction (parallel to the secondary beams)

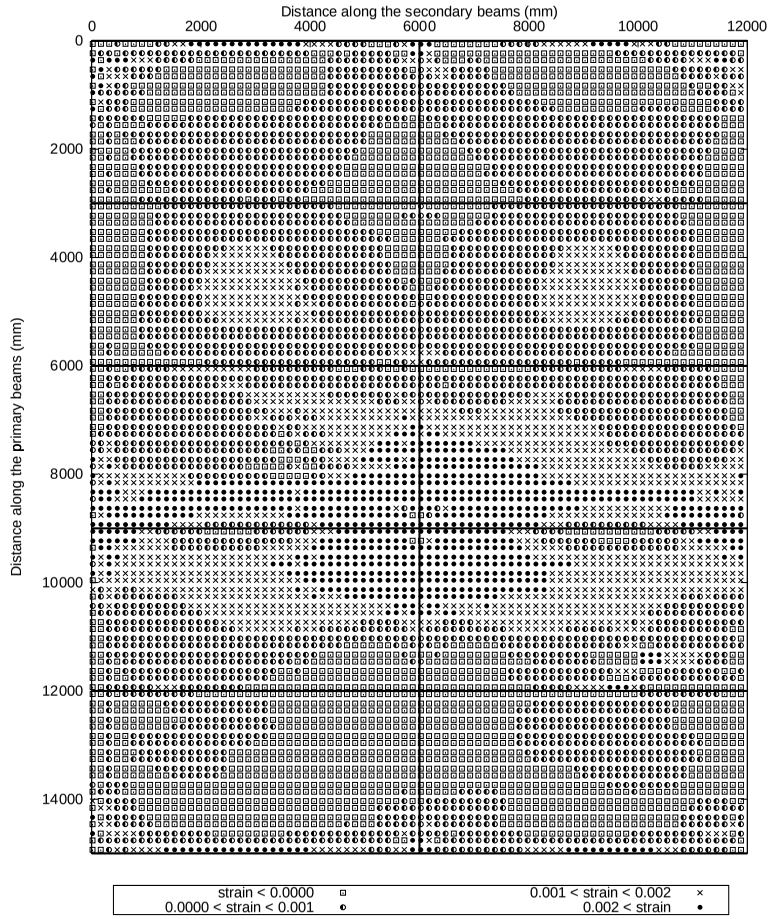

(b) y-direction (parallel to the primary beams)

Figure 8.85: Mechanical strains in the reinforcement OF=0.02, whole floor fire at 750^{o}C, edge beams protected

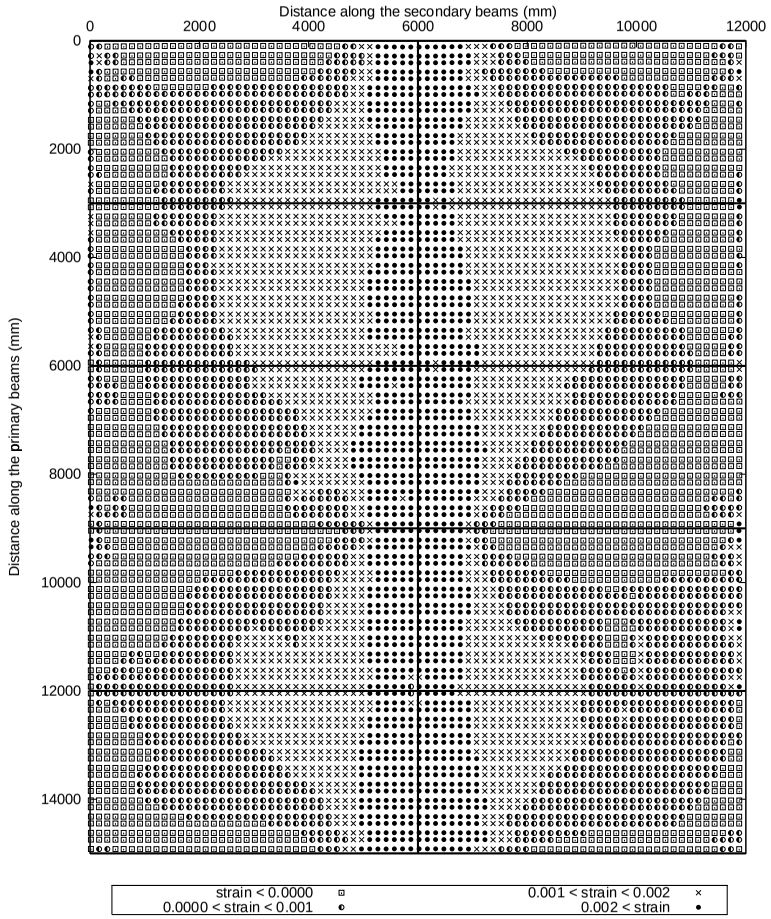

(a) x-direction (parallel to the secondary beams)

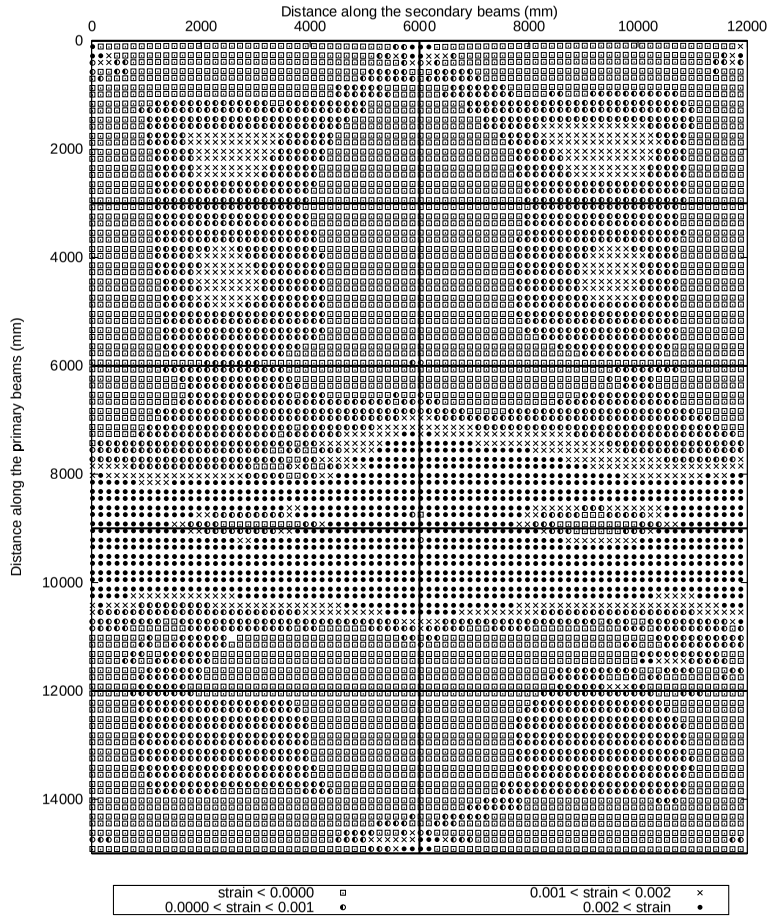

(b) y-direction (parallel to the primary beams)

Figure 8.86: Mechanical strains in the reinforcement OF=0.02, whole floor fire at 750^{o}C, all beams unprotected

8.4.5.4 Summary

- By leaving all the beams unprotected the deflection response of the composite slab is much greater.
- The deflections achieved by the unprotected 9m edge beams are almost the same as the primary beam which results in the 9m x 6m bays to act like a single one-way spanning slab. The load carrying mechanism developed in the slab (at large deflections) is likely to be similar to 1D catenary action rather than 2D tensile membrane action.
- The timing of the primary beam instability is dependent on the restraint from the edge beams (i.e. whether they are protected or not.)
- When the edge beams are unprotected column B1 is pulled in towards the centre of the frame
- The slab compensates for weak unprotected edge beams by forming larger membrane compression rings around areas of high deflection

8.4.6 Effect of applied fire protection in a "short" post-flashover fire

In this section the structural behaviour of the small frame to a "short-hot" fire is compared when the edge beams are protected or unprotected (scenarios 4 and 5 in Table 8.5). This is the same study as described in Section 8.4.5 but the fire severity has changed. With a "short-hot" fire, protected beams do not reach high temperatures but unprotected beams react very quickly to changes in the fire atmosphere. This is in contrast to the "long-cool" fire where the protected edge beams can reach considerable temperatures.

8.4.6.1 Deflection response

As in the "long-cool" fire when the protection from the edge beams is removed the large deflections at the centre of the floor slab, thus the tensile membrane forces, are anchored on two edges rather than all four. This is similar to catenary action in a beam and cannot be as strong as the support provided by all four sides when the edge beams are protected. See Figure 8.87.

Secondary and primary beams deflect more when the edge beams are unprotected as expected. See Figures 8.88 and 8.89. The edge beams along gridlines 1 and 6 (Figure 8.90) deflect very little when they are protected (maximum mid-span deflection of 45mm on the braced side of the structure). When unprotected the maximum mid-span

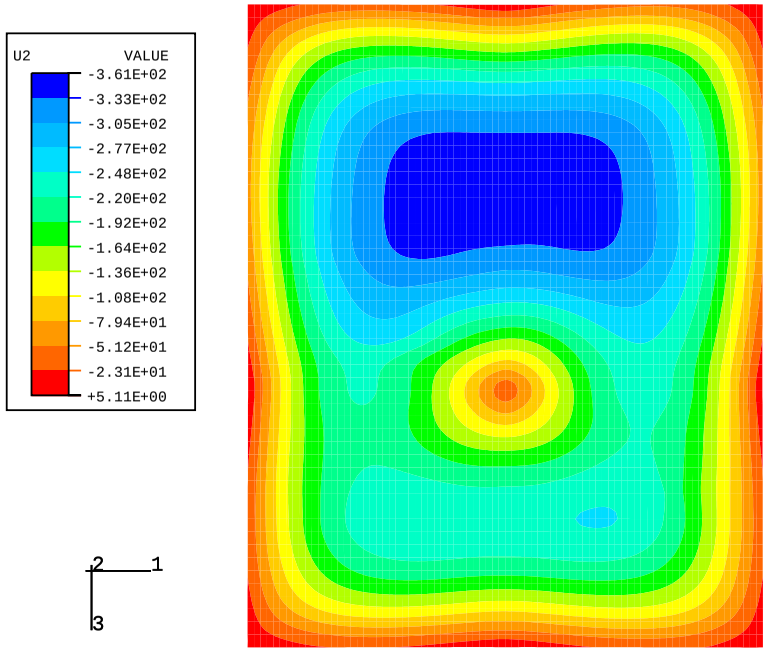

(a) Edge beams protected

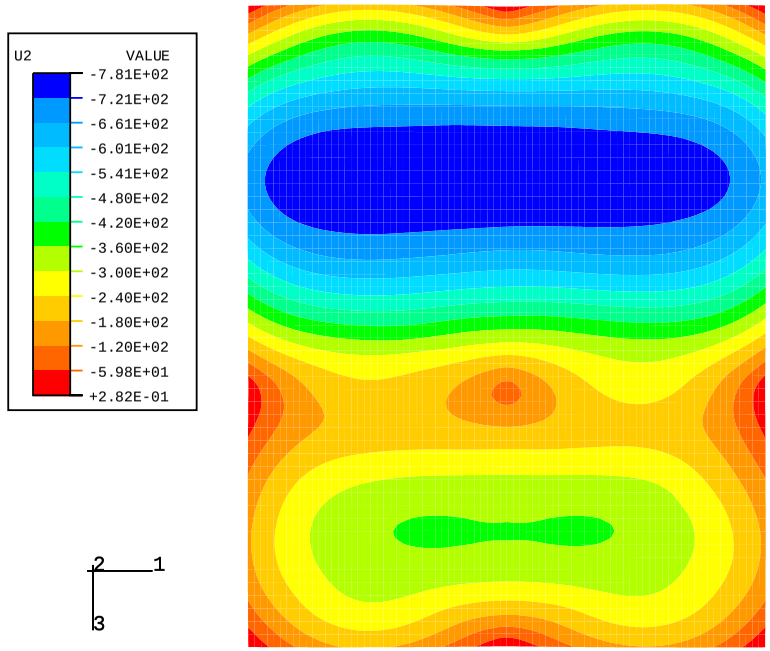

(b) All beams unprotected

Figure 8.87: Deflection contours in the slab at 950^{o}C

deflections are five times greater.

Figure 8.91 shows the mid-span deflection histories of the edge beams parallel to the primary beams. The 9m edge beams show a considerable increase in deflection when unprotected compared with the protected case.

In the "long-cool" fire with all beams unprotected maximum primary beam deflections were 600mm (see Figure 8.70) whereas in the "short-hot' fire they reach 780mm. The edge beams in response to the "short-hot" fire deflect more because the unprotected steel responds very quickly to changes in atmosphere temperature.

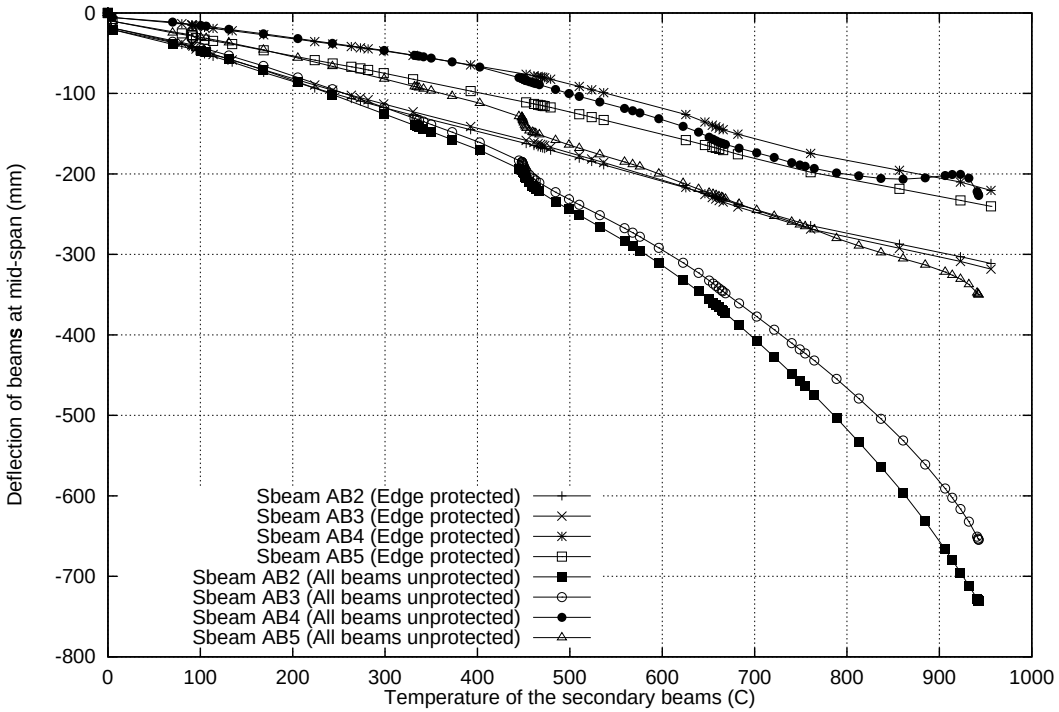

Figure 8.88: Deflections of the secondary beams, OF=0.08

The rates of deflection are plotted in Figures 8.92 and 8.93. Once again without applied fire protection on the edge beams the rate of mid-span displacement towards the end of the analysis is very unstable, suggesting runaway.

8.4.6.2 Response of the steel beams

The axial forces in secondary beam AB2 and primary beam B14 are plotted in Figures 8.94-8.97 for both scenarios. When the edge beams are protected the secondary beams carry lower axial compressions. This is due to the relative displacement between the edge beams and the mid-span of the secondary beams. When edge beams are protected the relative displacement is considerable but when they are unprotected the relative

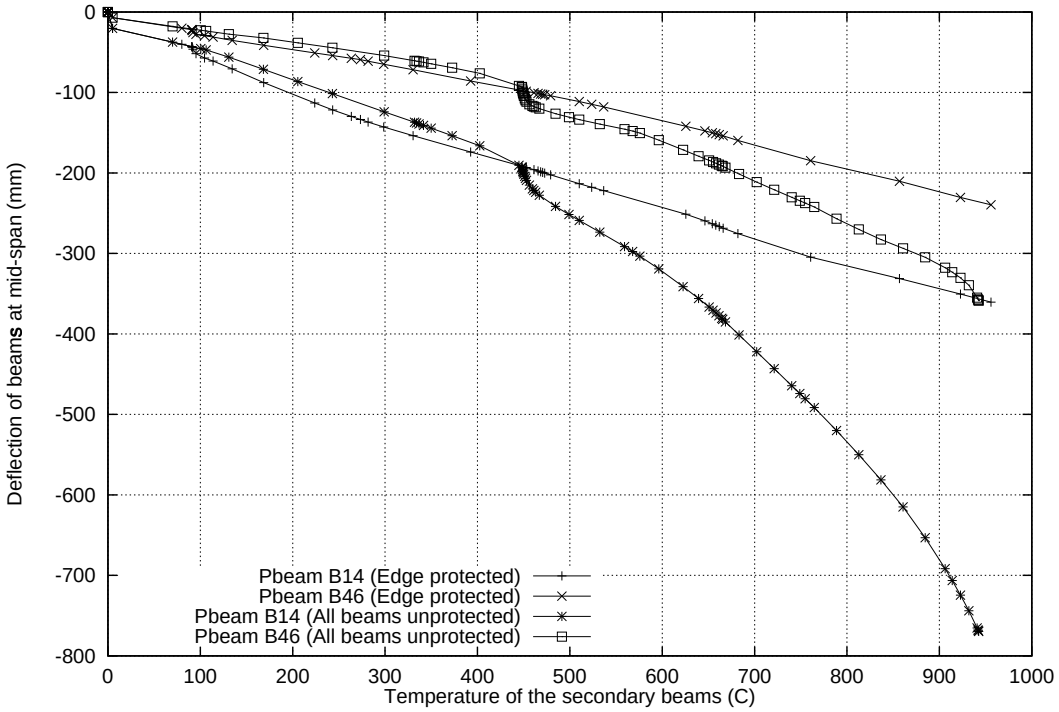

Figure 8.89: Deflections of the primary beams, OF=0.08

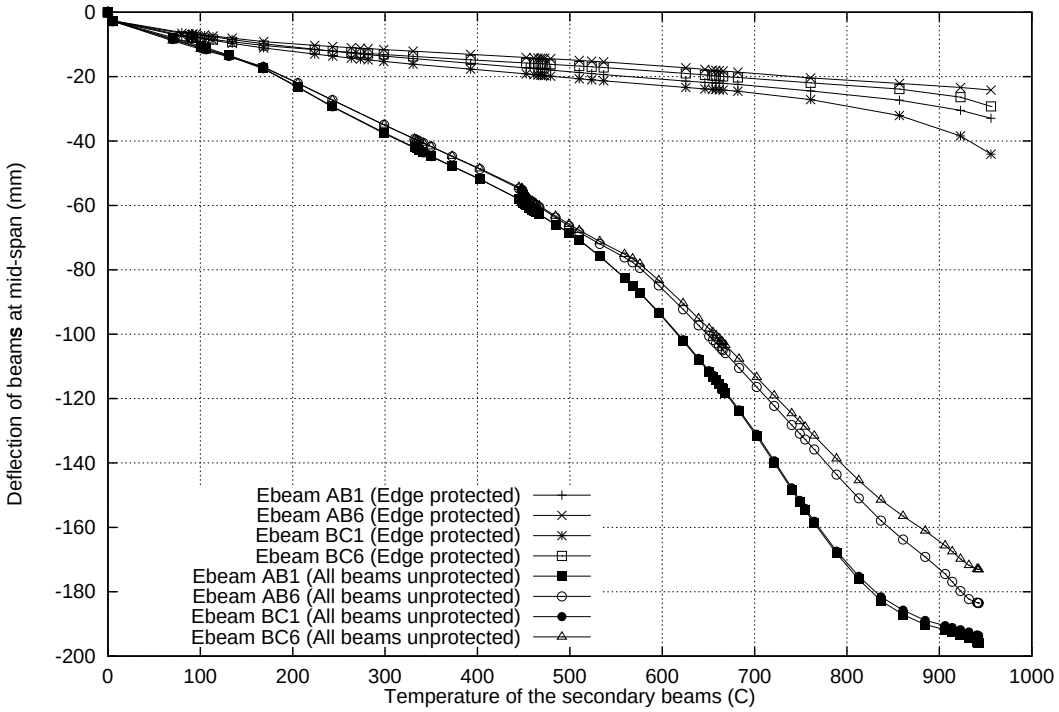

Figure 8.90: Deflections of the edge beams parallel to the secondary beams, OF=0.08

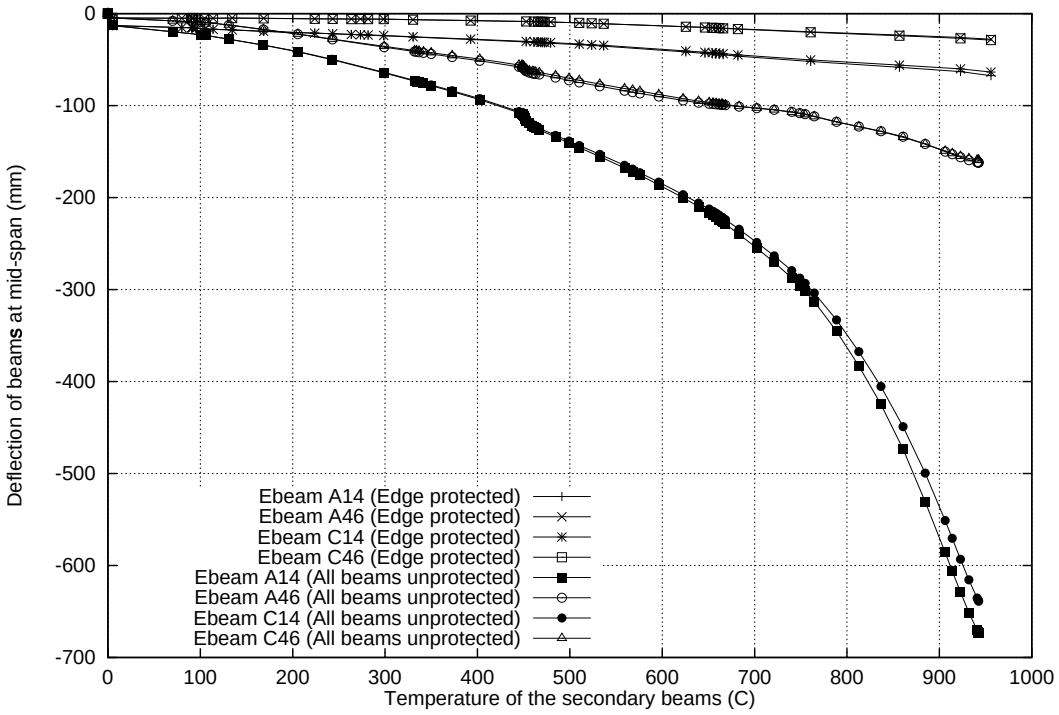

Figure 8.91: Deflections of the edge beams parallel to the primary beams, OF=0.08

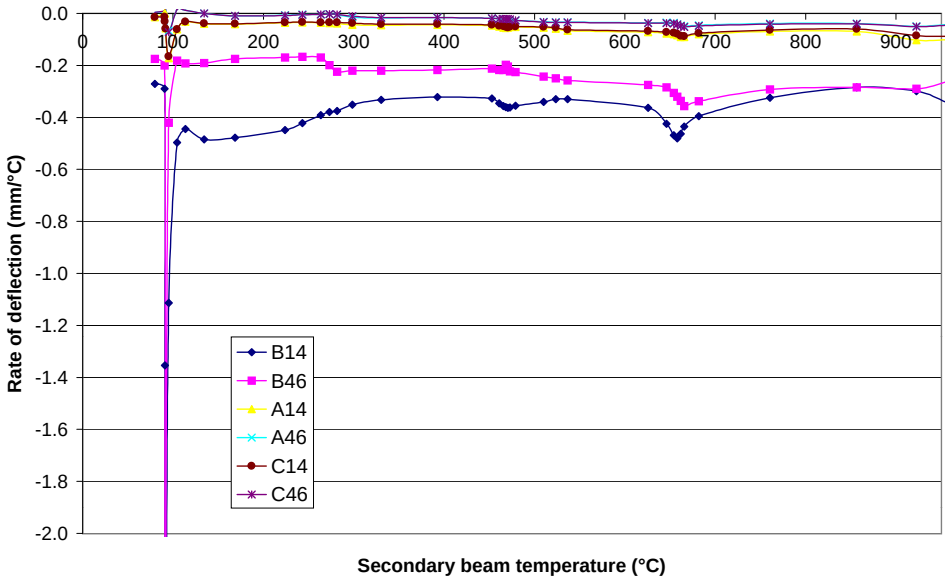

Figure 8.92: Rates of deflection at mid-span of the edge and primary beams against secondary beam temperature, OF=0.08

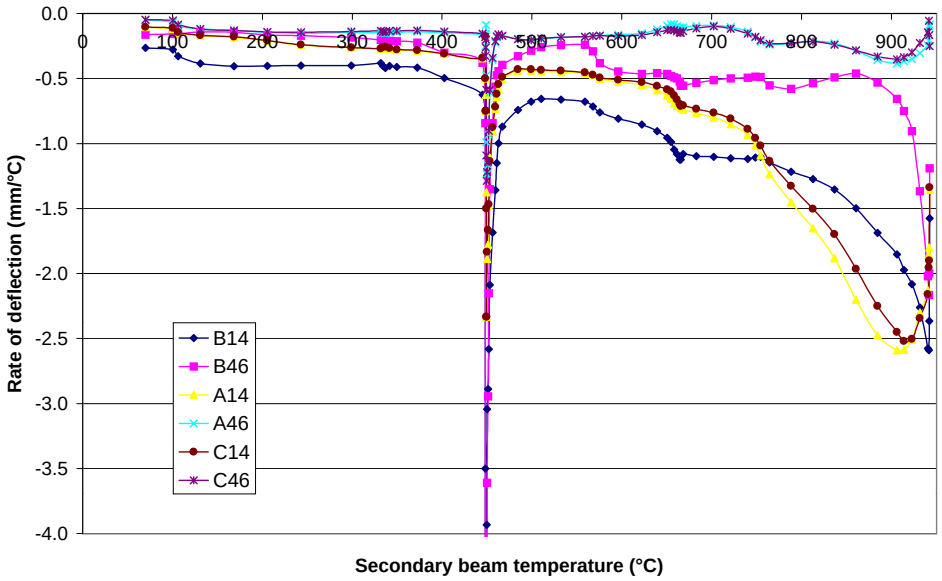

Figure 8.93: Rates of deflection at mid-span of the edge and primary beams against secondary beam temperature, OF=0.08

displacement is low thus the compressions are not absorbed by deflections.
The rapid drop in compression in the primary beam is present in both cases (Figures 8.96 and 8.97). It occurs much earlier in the case with protected edge beams because of high gradients and higher relative displacements (higher P-Δ moments). When the edge beams are unprotected although the gradients in the composite steel secondary beams are still large, the relative displacement between the edge and primary beam is low, reducing the P-Δ moment leading to a delay in the instability event of the primary beam.

8.4.6.2.1 Column displacements The outward displacement of column B1 over the height of the column is shown in Figures 8.98 and 8.99. When the edge beams are protected the column is pushed out initially, retracts after the primary beam instability and then is pushed out again as the heating regime progresses. Without protection on the edge beams the column does not expand outwards again after the primary beam instability, it is pulled in by the deflecting composite (Figure 8.99) until it is in positive displacement at the end of the analysis. In the"long-cool" fire the column was pulled back but it did not go into positive displacement (Figure 8.81).

8.4.6.2.2 Edge beams The axial forces in edge beams A14 and A46 are shown in Figures 8.100 and 8.101. In the protected case the axial compressions continue

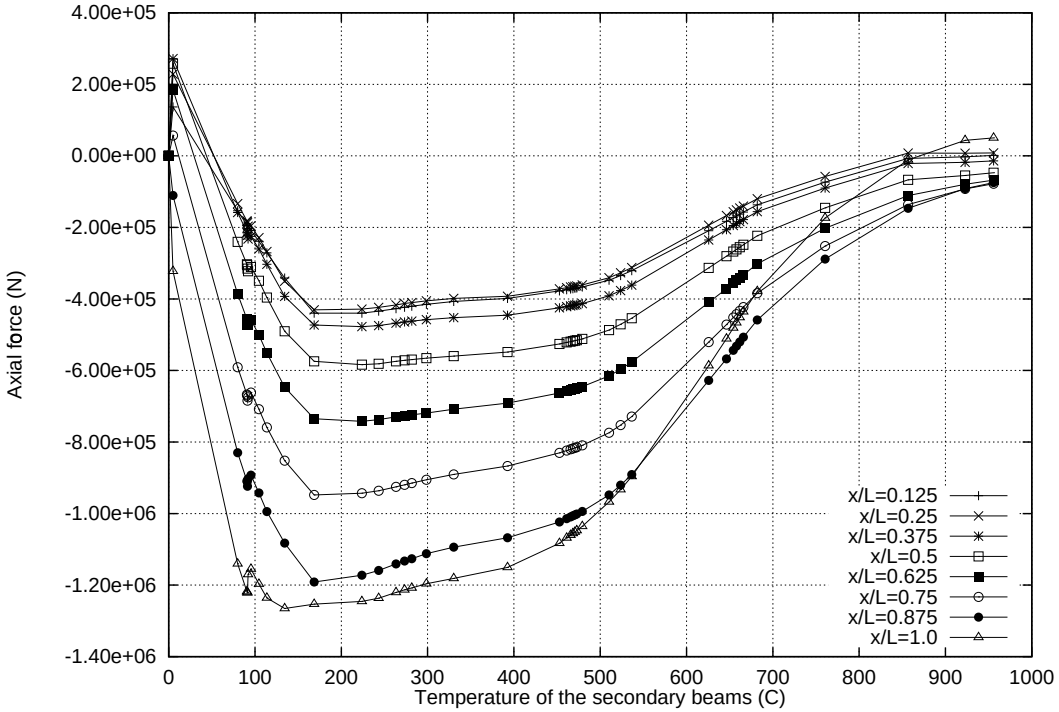

Figure 8.94: Secondary beam AB2: Axial force against secondary beam temperatures, OF=0.08, edge beams protected

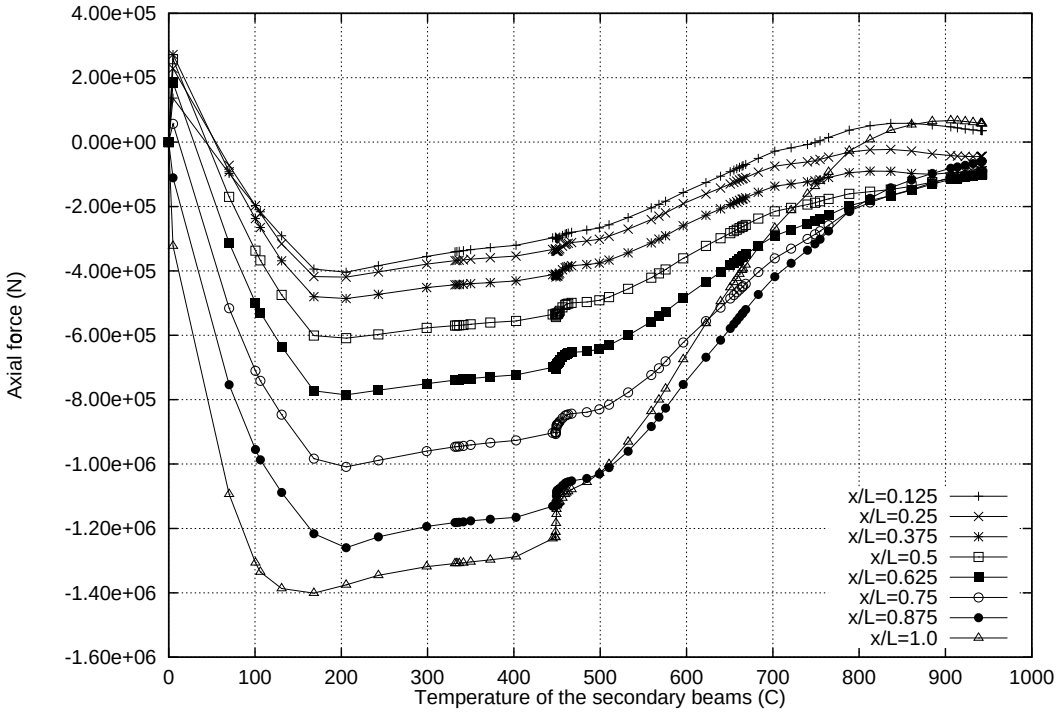

Figure 8.95: Secondary beam AB2: Axial force against secondary beam temperatures, OF=0.08, all beams unprotected

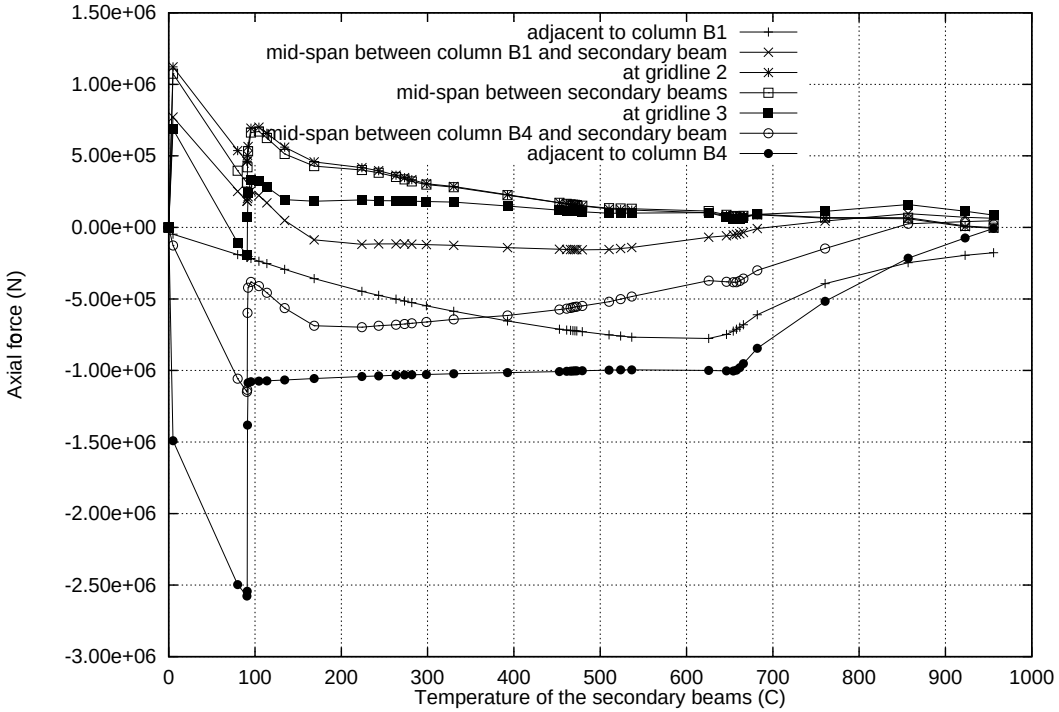

Figure 8.96: Primary beam B14: Axial force against secondary beam temperatures, OF=0.08, edge beams protected

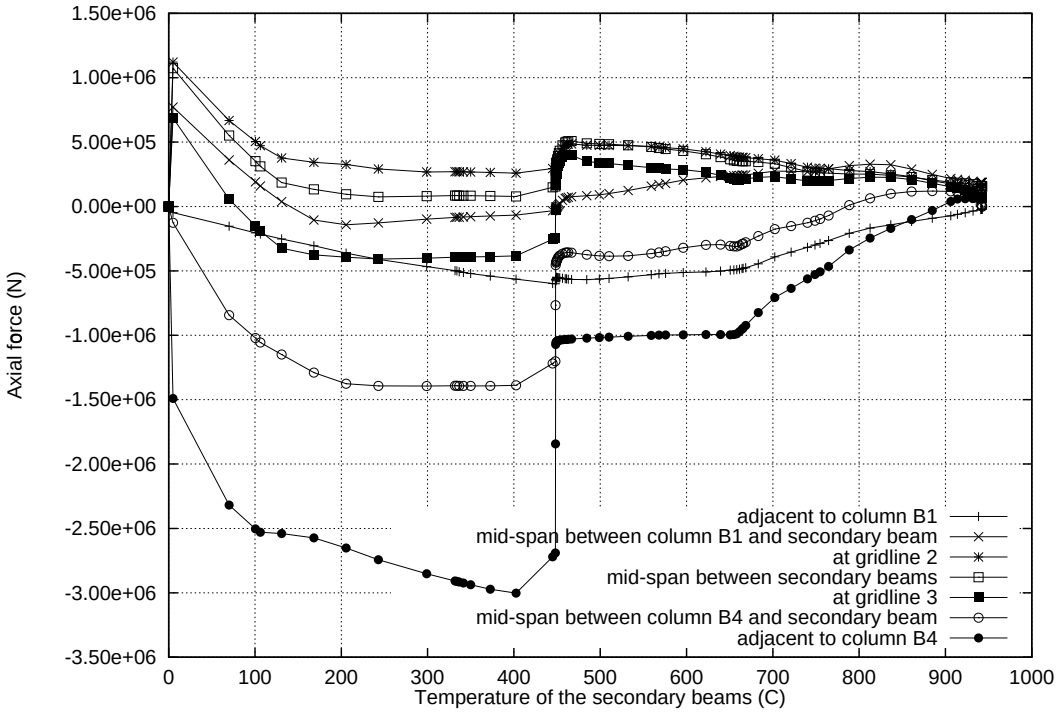

Figure 8.97: Primary beam B14: Axial force against secondary beam temperatures, OF=0.08, all beams unprotected

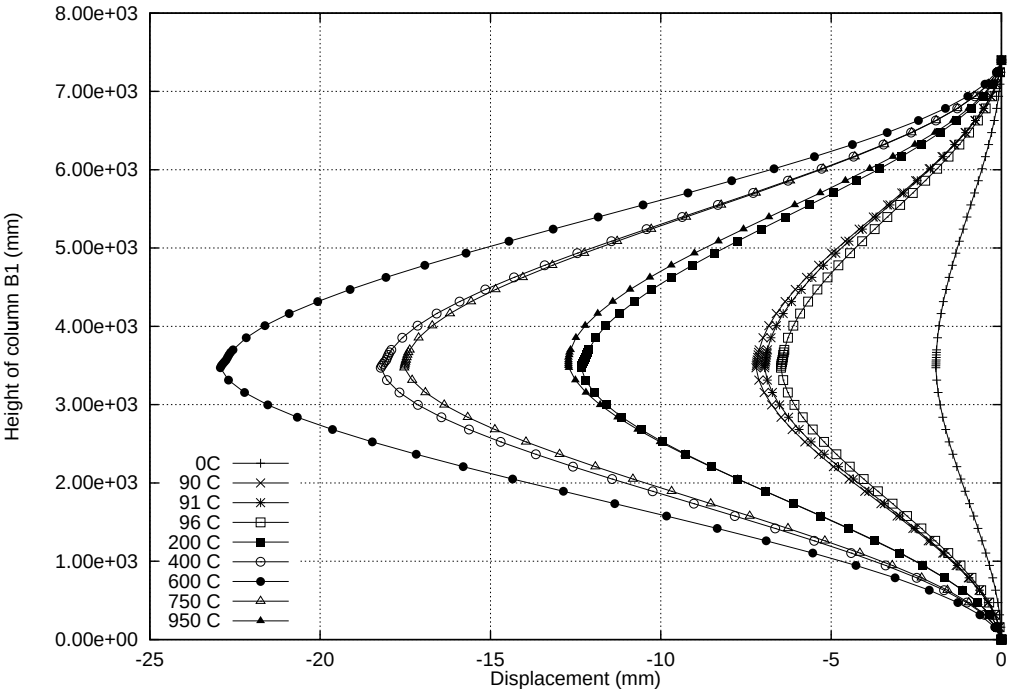

Figure 8.98: Movement of column B1, edge beams protected

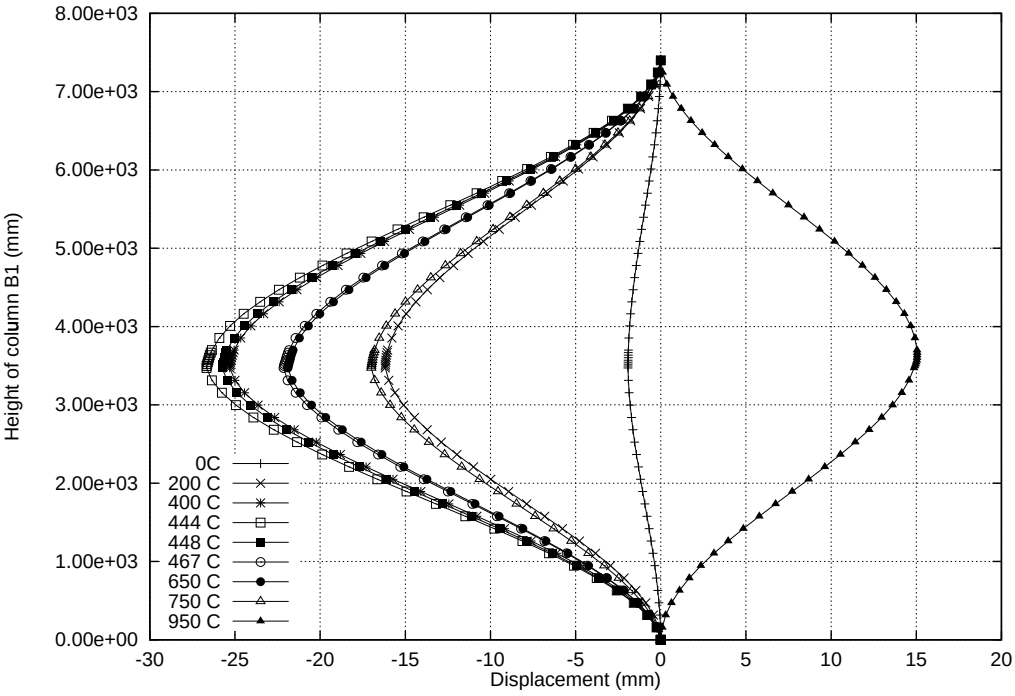

Figure 8.99: Movement of column B1, all beams unprotected

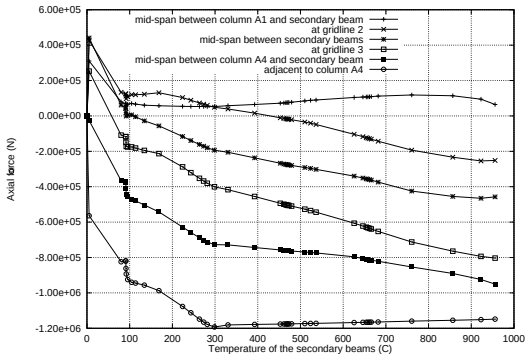

(a) Edge beam A14

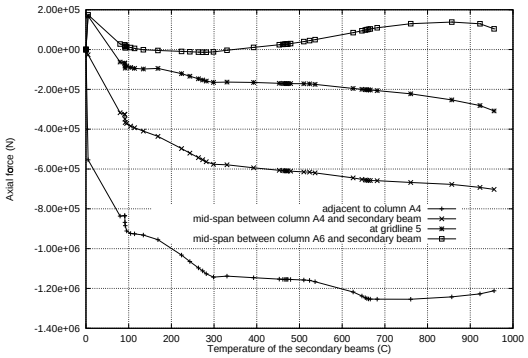

(b) Edge beam A46

Figure 8.100: Variation of axial force against secondary beam temperatures, only edge beams protected

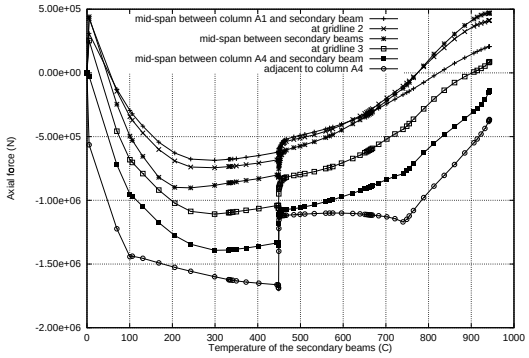

(a) Edge beam A14

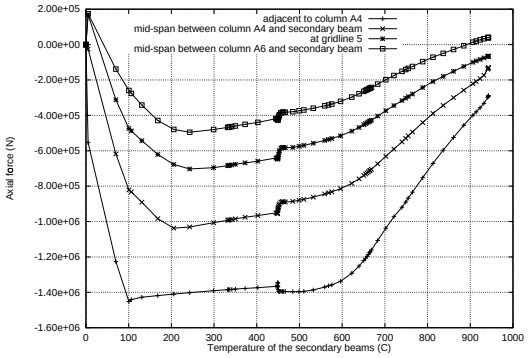

(b) Edge beam A46

Figure 8.101: Variation of axial force against secondary beam temperatures, all beams unprotected

to increase or remain constant throughout the analysis. When the edge beams are unprotected the 9m edge beam exhibits a similar rapid drop in compression to the primary beam. This is the only scenario in which this occurs and makes it the worst case scenario for the steel beams. All the unprotected beams, including the edge beams, achieve very high temperatures.

Axial forces in the edge beams along gridlines 1 and 6 are shown in Figures 8.102 and 8.103. When the beams are protected they carry increasing compressions or tensions throughout the analysis. The unprotected edge beams behave like secondary beams.

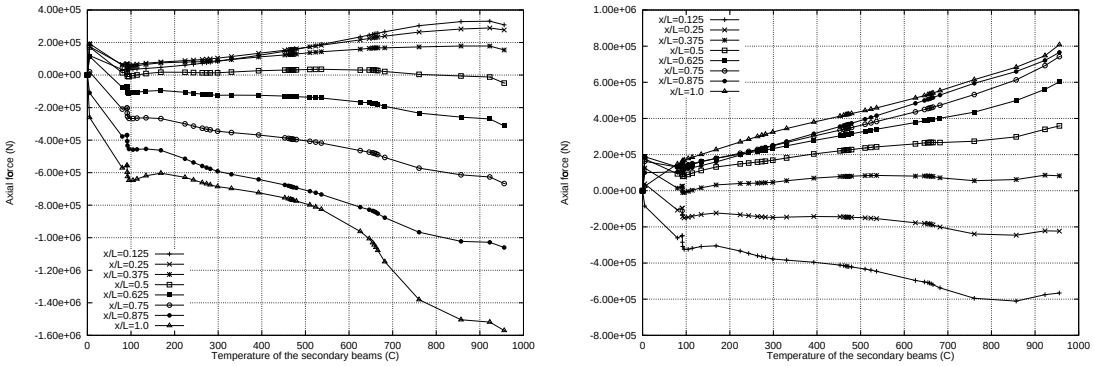

(a) AB1 (b) BC1

Figure 8.102: Variation of axial force at the mid-span of edge beam AB1 and BC1 against temperature, edge beams protected only

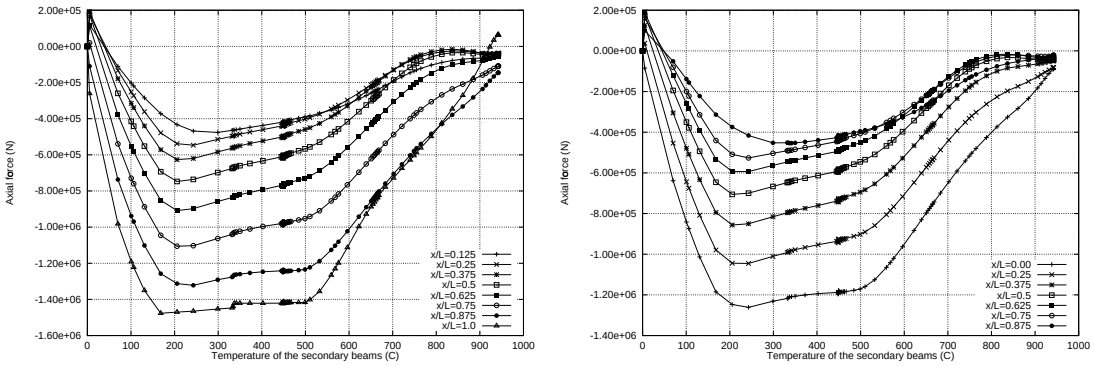

(a) AB1 (b) BC1

Figure 8.103: Variation of axial force at the mid-span of edge beam AB1 and BC1 against temperature, all beams unprotected

8.4.7 Behaviour of the slab

The slab membrane forces are plotted along a line 600mm from gridline 1 for both scenarios in Figures 8.104 and 8.105. When the edge beams are protected this area of slab very close to the edge beams is in compression, increasing throughout the test. There are slightly smaller compressions on the braced side of the structure. when the edge beams are unprotected the slab is in tension initially moving into compression as the fire progresses.

The same plots are drawn at a distance 4.2m from gridline 1 in Figures 8.106 and 8.107. The forces are very similar in both cases.

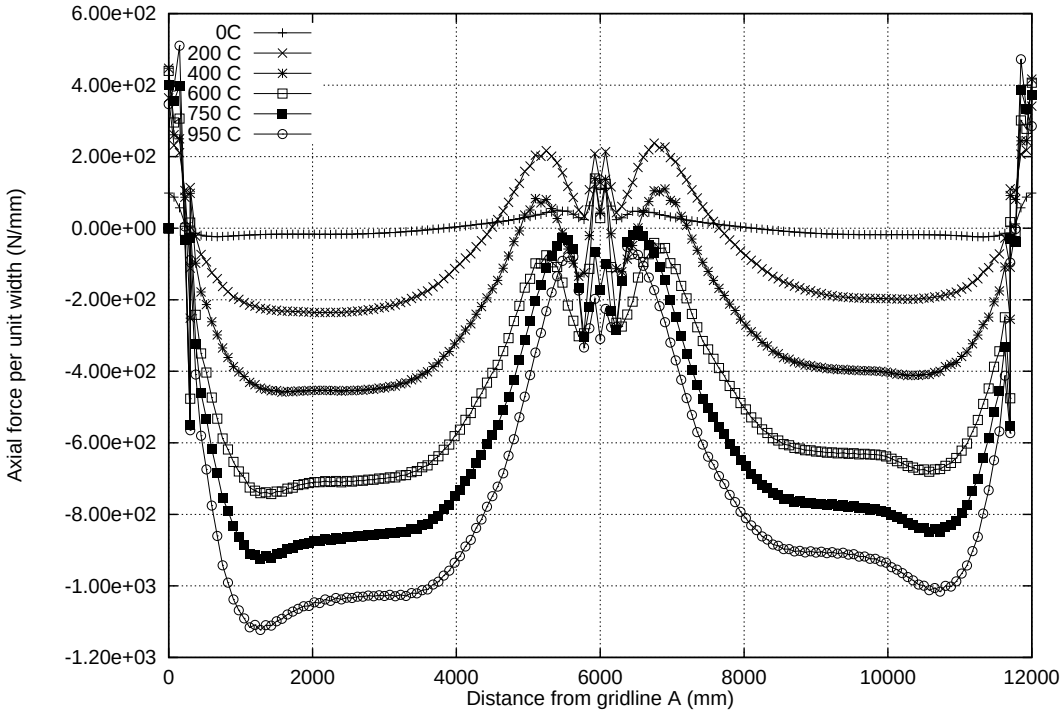

Figure 8.104: Axial force in the thin direction of the slab 600mm from gridline 1, edge beams protected

The mechanical strains at the end of each analysis are plotted in Figures 8.108 and 8.109. Both scenarios create large areas of high tensile strains. Where the edge beams are unprotected there are considerably more areas of compression. Considerable compressions develop in the y-direction over the primary beams. These exist for two reasons. First they compensate for the weak, hot edge beams. Secondly because the relative displacement between the periphery of the compartment and the middle of the compartment is low thus tensile membrane action is limited.

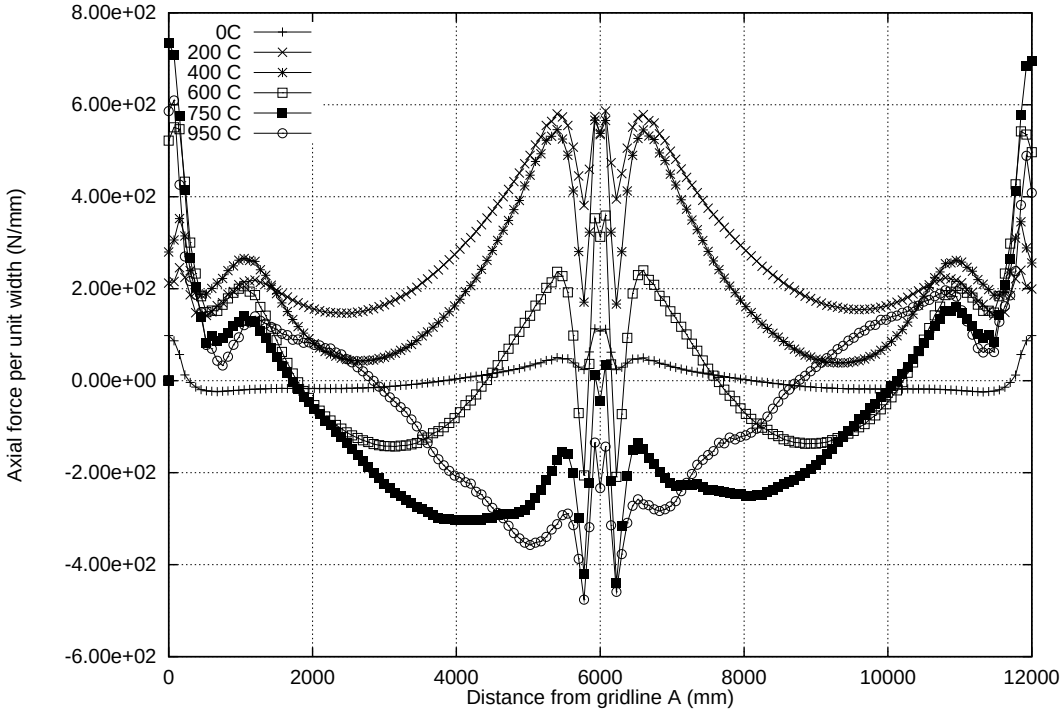

Figure 8.105: Axial force in the thin direction of the slab 600mm from gridline 1, edge beams unprotected

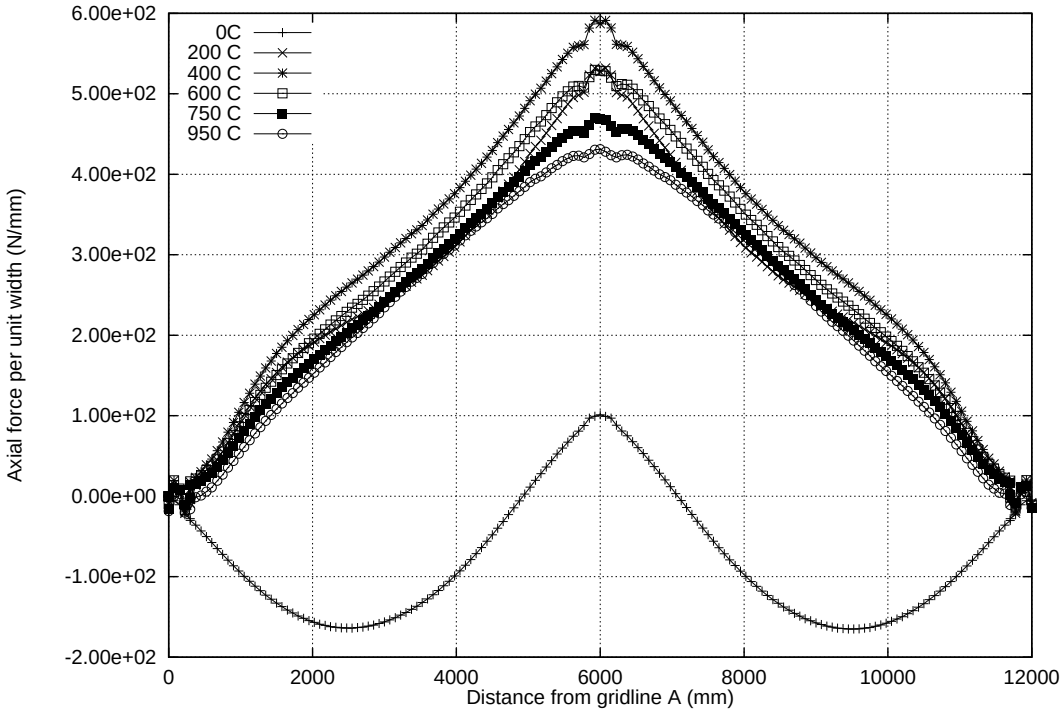

Figure 8.106: Force in the thin direction of the slab 4200mm from gridline 1, edge beams protected

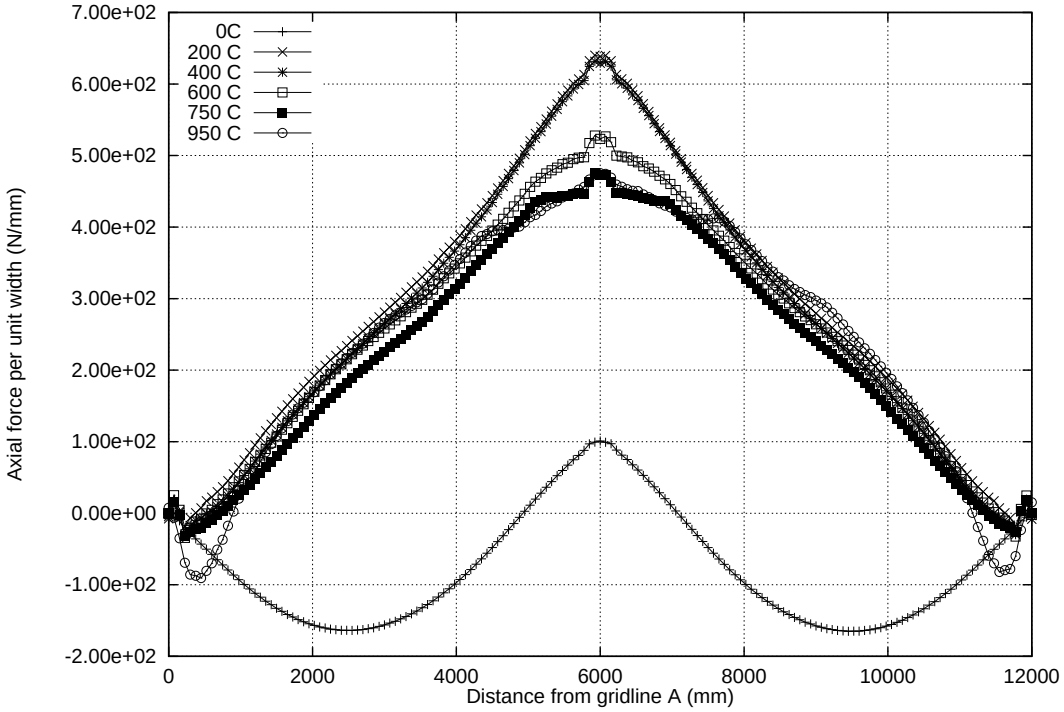

Figure 8.107: Force in the thin direction of the slab 4200mm from gridline 1, edge beams unprotected

8.4.7.1 Summary

- By leaving all the beams unprotected the deflection response of the composite slab is much greater.
- The deflections achieved by the unprotected 9m edge beams are almost the same as the primary beam which results in the 9m x 6m bays to act like a single one-way spanning slab. The load carrying mechanism developed in the slab (at large deflections) is likely to be similar to 1D catenary action rather than 2D tensile membrane action.
- The very large deflections of the frame when the edge beams were unprotected caused the columns to be pulled in towards the centre of the building near the end of the heating regime
- The instability event in the primary beam also occurred in the 9m edge beams when the edge beams were unprotected
- The "short-hot" fire is a worst case scenario for the frame when all the beams are unprotected because of the lack of restraint to tensile membrane action, leading to a one-way mode of deflection.

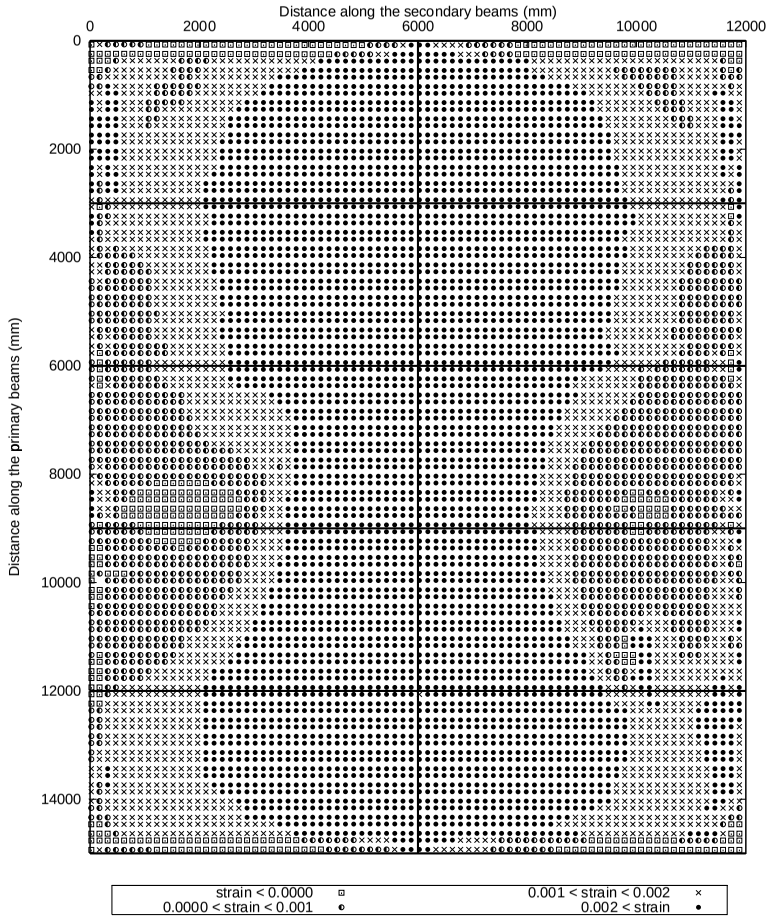

(a) x-direction (parallel to the secondary beams)

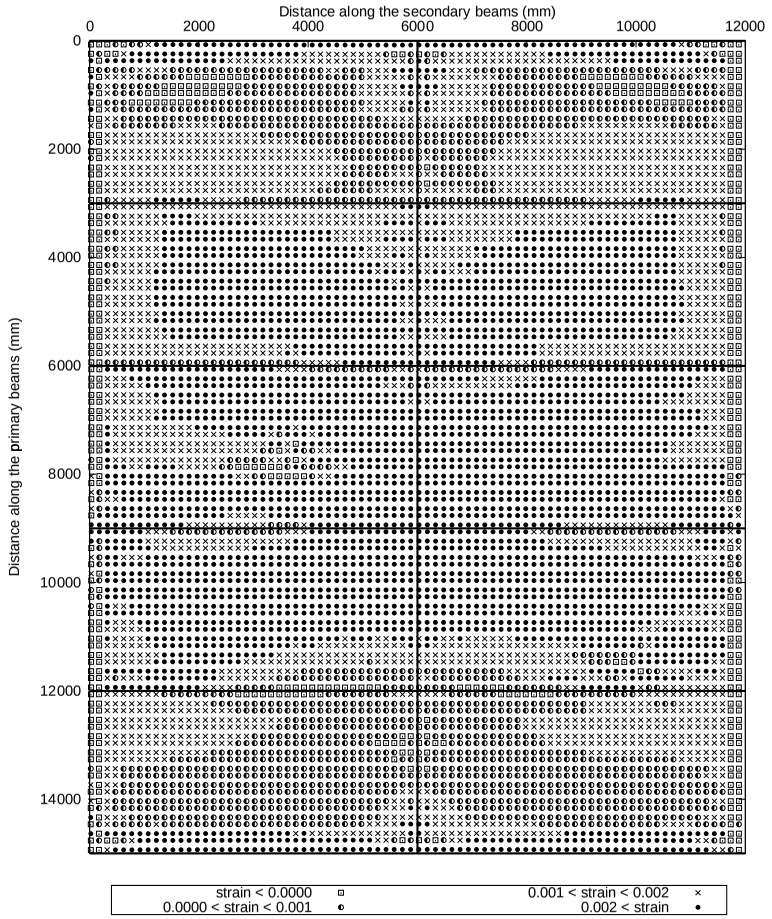

(b) y-direction (parallel to the primary beams)

Figure 8.108: Mechanical strains in the reinforcement OF=0.08, whole floor fire at 950^oC, edge beams protected

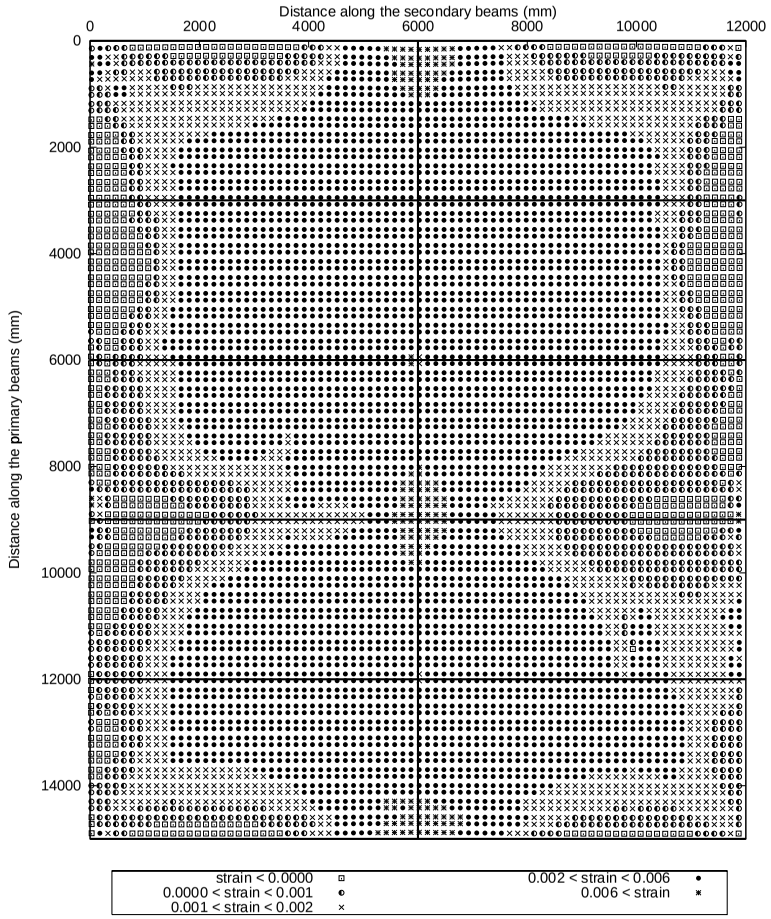

(a) x-direction (parallel to the secondary beams)

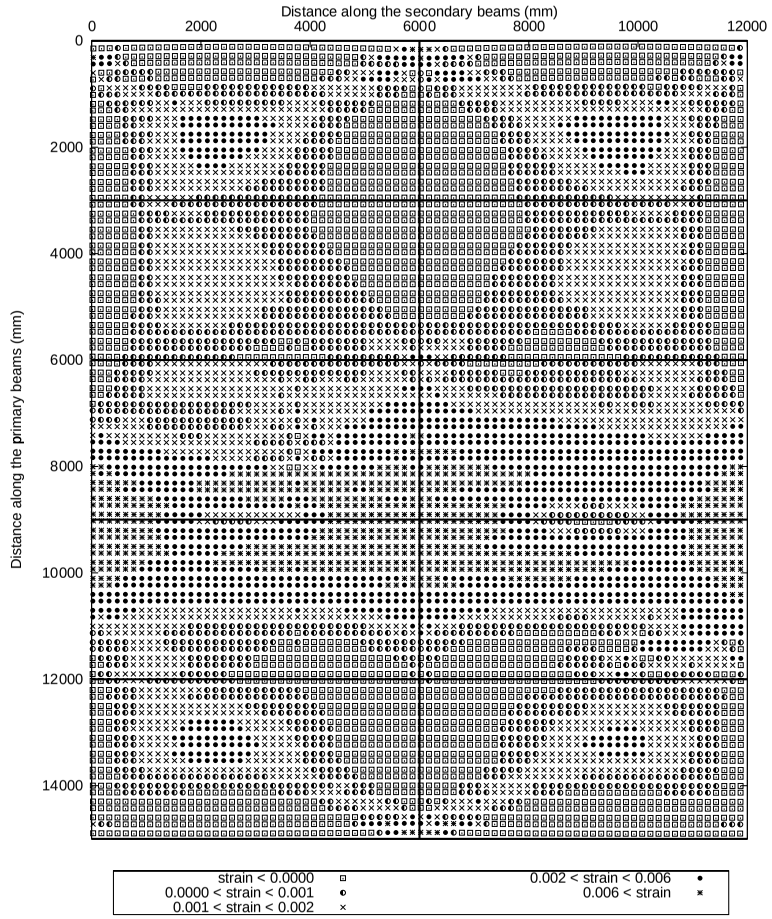

(b) y-direction (parallel to the primary beams)

Figure 8.109: Mechanical strains in the reinforcement OF=0.08, whole floor fire at 950^{o}C, edge beams unprotected

Opening factor ($m^{1/2}$)	**Primary and edge beams protected**	**Edge beams protected**	**All beams unprotected**
0.02	400^oC (Primary beam is at 100^oC)	450^oC	120^oC
0.08	N/A	90^oC	450^oC

Table 8.7: Reference temperature at the primary beam instability in each scenario

- Table 8.7 summarises the temperatures of the primary beam instability in each scenario.
- If the edge beams are protected the high gradient in the slab in the "short-hot" fire causes the primary beam instability at the first yield of the steel (90^oC). The instability in the corresponding "long-cool" fire scenario is delayed until 450^oC
- If the primary and edge beams are protected the instability occurs at a protected primary beam temperature of 100^oC when the unprotected steel is at 400^oC
- When the edge beams are unprotected the deflections at the edge and the centre of the compartment are very similar. This is especially true in the "short-hot" fire because the unprotected beams are all very hot. The primary beam instability occurs at 120^oC in the "long-cool" fire and 450^oC in the "short-hot" fire. The high gradient in the composite slab is no longer dominating as in the scenarios where the edge beams were protected. Now the relative displacement between the edge beams and primary (or secondary) beams dominates and determines the P-Δ moments (with the composite axial force) of the composite secondary beams . At 100^oC in the "short-hot" fire the secondary beam composite axial force is low and the relative displacements are small thus P-Δ moments are low. In the "long-cool" fire at 100^oC the composite axial force in the secondary beams is higher thus P-Δ moments are higher and push the primary beam down.
- The phenomena leading to the primary beam instability have been identified however predicting the occurrence of the event at either the first yield of steel or at the ultimate yield in each scenario is incredibly complex and further investigation is necessary to understand the event completely.

8.5 Conclusions

- The most detrimental fire in terms of the structural response is the "short-hot" fire. Large deflections develop in a very short time. This may result in early compartmentation failure. If edge beams are protected large tensile strains are present in the slab throughout the analysis.

- The "long-cool" fire results in higher temperatures in the concrete and the protected steel. This results in greater displacements in the protected structural elements but much later in terms of real time. However because the concrete slab achieves higher temperatures there is much less tension in the slab with growing compressions towards the end of heating.

- The instability event in the primary beam has been shown to coincide with a change in the end conditions from moment resisting to pinned.

- In the small 2x2 frame the events in the primary beam are a catalyst for events in the rest of the frame.

- There is redistribution of the loads to the outer parts of the frame after the primary beam instability.

- The change in the end restraint condition causing the relief of axial forces in the primary beam is attributed to large compressions because of restrained expansion, moments due to gradients, moment due to imposed loading and increased loading on the primary beam as a result of expanding and bowing secondary beams pushing it down.

- These conclusions have been confirmed by decreasing the imposed loading, removing secondary beams from the frame and a numerical analysis on a simple beam model.

- This type of behaviour was not observed at Cardington probably because the loading was too small, or the structure too large.

- When the edge beams are unprotected the whole composite floor slab reaches similar deflections.

- Unprotected edge beams result in the columns being pulled in as the slab moves into greater deflections and tensile membrane action.

- The slab exhibits greater areas of compression rings when the edge beams are unprotected because the edge beams are weak and because relative displacements are lower so smaller tensile membrane forces develop.

- The structure survives the various scenarios tested although rate of deflection plots show runaway may be close or occurring in some cases.

- Protected edge beams allow the slab to be anchored on all four sides of the frame throughout the heating regime. When the edge beams are unprotected the slab is anchored more fully on the short sides of the frame.

- Protected edge beams will allow this type of structure (relatively low redundancy) to survive for a longer period of time.

Chapter 9

Parametric studies on a relatively large generic composite steel frame

9.1 Introduction

This chapter summarises the results of a series of studies on a relatively large (9x9 bay) generic composite steel frame. The structural design follows EC4 Part 1.1. Typically in a large frame a fully flashed over whole floor fire is unlikely therefore two smaller compartments were analysed. A corner compartment (18m x 18m in plan) and a compartment on the edge of the building (18m x 27m long). The natural fires studied are exactly the same as in Chapter 8. The locations provided two very different boundary restraint conditions which caused different deflection and internal force patterns in each compartment.
A similar set of parametric studies to those in chapter 8 were undertaken.

9.2 The generic frame

The 9x9 generic frame is drawn in plan in Figure 9.1. The frame is perfectly symmetrical about both x and y axes thus one quarter of the frame was modelled in ABAQUS (Figure 9.2). The finite element mesh developed in ABAQUS is illustrated in Figure 9.3.

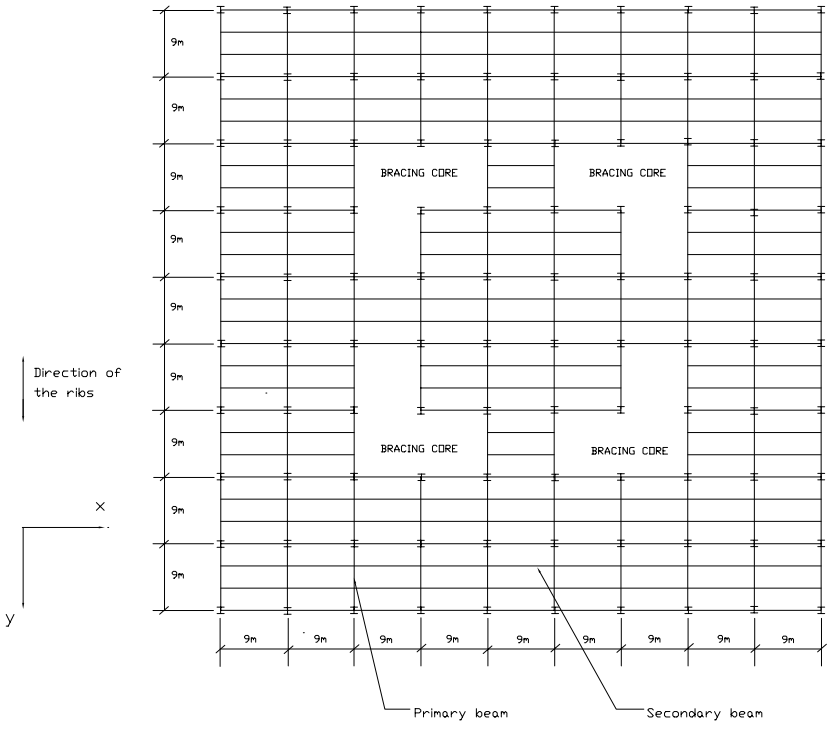

Figure 9.1: Schematic plan view of the 9x9 bay generic frame

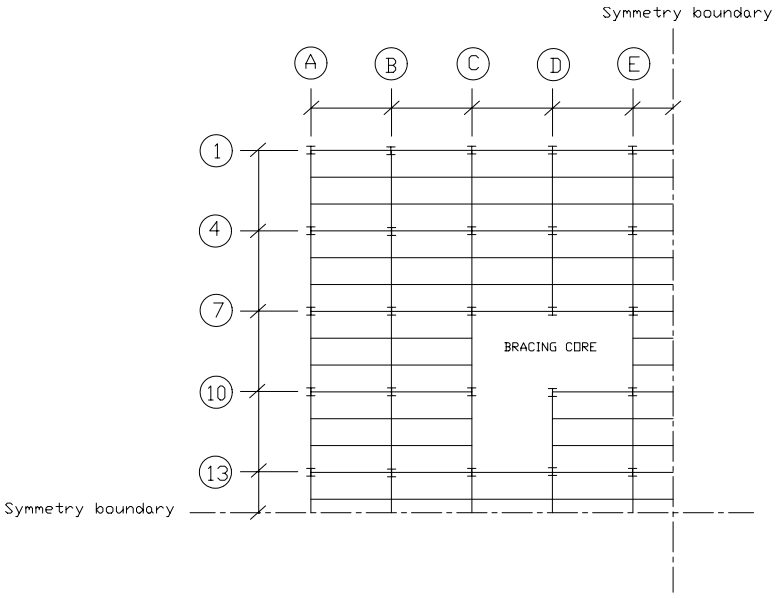

Figure 9.2: Schematic plan view of the 9x9 bay generic frame numerical model

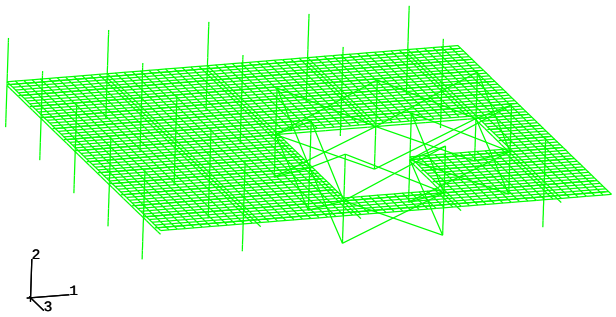

Figure 9.3: The finite element mesh of the 9x9 frame created in ABAQUS

9.3 Compartment fires

The 9x9 generic frame measures 81m square in plan and a fully flashed over fire is unlikely to occur over a whole floor although a whole floor fire, at various stages of growth and decay, could occur. For the purposes of this research two smaller compartment fire scenarios were assumed. These are illustrated in Figure 9.4. The walls of the fire compartment are directly underneath the periphery beams. The natural fire curves assumed in Chapter 8 were also used in these studies. However, the edge compartment could not experience a fire with an opening factor of $0.08\text{m}^{1/2}$ because there is insufficient ventilation so only a "long-cool" (OF=$0.02\text{m}^{1/2}$) fire was tested.

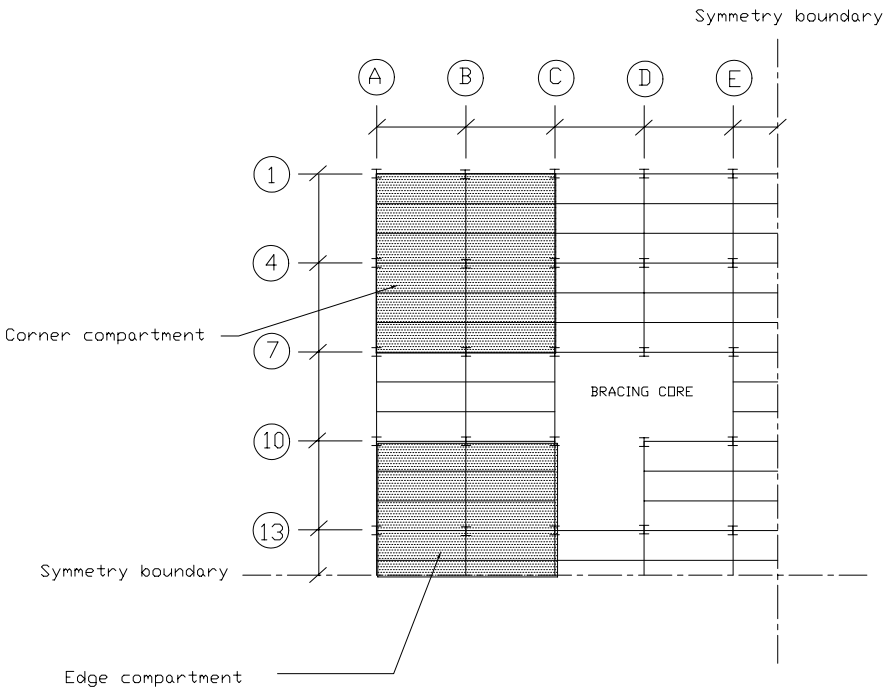

Figure 9.4: Schematic plan view of the 9x9 bay generic frame showing the location of the compartment fires

9.4 Temperature loading

The heat transfer calculations for the 9x9 frame were carried out in the same manner as for the 2x2 frame. The temperatures of the steel members in the 9x9 frame are very similar to those in the 2x2 frame. Small variations exist because the steel beams are heavier in the larger frame. Protected elements are cooler because the protection provided 90 minutes fire resistance[62] where only 60 minutes was provided in the 2x2 frame. The temperature histories of the beams are shown in Figure 9.5 against unprotected secondary beam temperature. The slab is exactly the same in both designs thus the temperature and gradients calculated through the depth of the slab for the 2x2 frame are also applicable to the large frame.

9.5 Scenarios tested

The various parametric studies conducted on the 9x9 frame are listed in Table 9.1. Fewer studies were undertaken on this frame. However the 4 cases enable three comparisons to be made. Scenarios 1 and 2 provided a comparison between the structural behaviour in response to the two natural fires. Scenarios 3 and 4 allowed a direct comparison between compartment fire location (all other parameters are constant) and

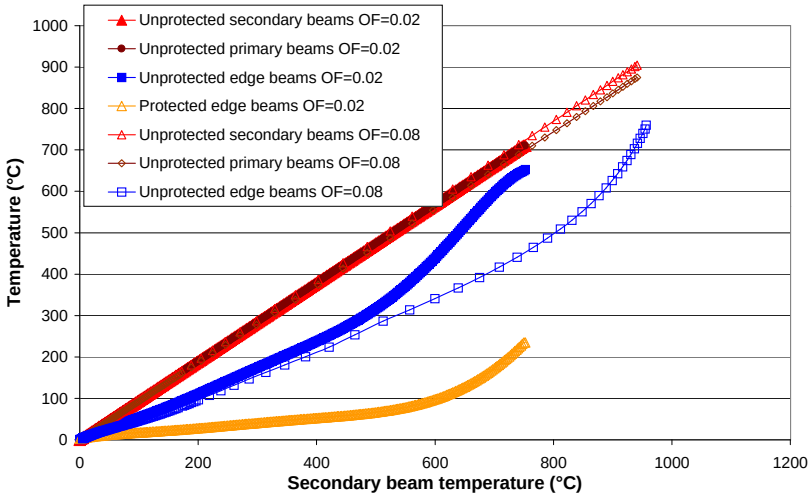

Figure 9.5: Mean steel and concrete temperatures against secondary beam temperature used in the ABAQUS model

Scenario	**Frame**	**Opening factor** ($m^{1/2}$)	**Compartment**	**Protected beams**	**Imposed + Dead Loading** (kN/m^2)
1	9x9	0.02	Corner	None	11.5
2	9x9	0.08	Corner	None	11.5
3	9x9	0.02	Corner	Edge	11.5
4	9x9	0.02	Edge	Edge	11.5

Table 9.1: Scenarios conducted on the generic frames

scenarios 1 and 3 have enabled a comparison between a structure with and without protected edge beams.

9.6 Results

9.6.1 Short versus long post-flashover fires in the 9x9 bay frame with the Edge beams unprotected

The results of scenarios 1 and 2 of Table 9.1 are discussed in this section. The compartment fires were situated in the corner of the building in a square 18 m x 18m in plan. The edge beams were unprotected.

Figure 9.6 shows the mid-span deflection histories of the secondary beams. Maximum deflections are greater than in the small frame because all of the beams are 9m long. Secondary beam deflections at the end of the "long-cool" fire are 60% less than at the end of the "short-hot" fire.

Primary beam deflections are plotted in Figure 9.7. Primary beam B47 deflects less because of continuity of the slab over gridline 7 (resulting in reduced rotations at this compartment boundary).

Mid-span deflections of the edge beams are shown in Figures 9.8 and 9.9. Edge beam AB1 in the "short-hot" fire achieves higher deflections because it is a smaller steel section than edge beam A14 and the slab is hotter and weaker in the direction perpendicular to the ribs . In the "short-hot" fire edge beam AB1 is deflecting to the same extent as an internal secondary beam causing the slab to tend towards 1D catenary action rather than 2D tensile membrane action. This runaway behaviour would also occur in the "long-cool" fire if the temperatures had continued to rise (Figure 9.8). This type of behaviour was also observed in the small frame when the edge beams were unprotected.

The primary beams along gridline C are highly restrained by the bracing core and reach higher deflections than the edge beams along gridline A (Figure 9.9).

Figures 9.10 and 9.11 show deflection contours of the composite slab at reference temperatures of 600^oC and at the end of heating respectively. They show a change in the pattern of deflections between 600^oC and the end of heating towards larger deflections in the least supported bay (the outside corner bay). Figure 9.11 also highlights the deflected shape of the slab in double curvature in the "long-cool" fire and tending towards single curvature in the "short-hot" fire.

9.6.1.1 Behaviour of the steel beams

Axial forces along the length of the secondary beams on gridline 2 are plotted in Figures 9.12 and 9.13 for both fires. Forces are very similar and compressions are lower in the cold adjacent structure. At 950^oC in the "short-hot" fire the beam is carrying very little axial force.

The axial forces experienced by secondary beam AB2 in each fire are plotted in Figures 9.14 and 9.15 against secondary beam temperature (x/L=0.167 is close to gridline A and x/L=1.0 is close to gridline B). Secondary beam AB2 is influenced by an instability event in primary beam B14 at 180^oC in the "short-hot" fire.

The axial forces at various locations along primary beam B14 are plotted in Figures 9.16 and 9.17. In common with the small 2x2 frame there is a rapid drop in compressive axial force at 180^oC in the "short-hot" fire. A smaller event has also occurred in the primary beam (adjacent to column B4) in the "long-cool" fire at 40^oC. This could be a numerical effect because the mesh is coarser than that used to model the Cardington tests and the 2x2 frame. A finer mesh would have been computationally expensive. It is unlikely to be a thermal effect at 40^oC. In both fire scenarios the primary beam axial

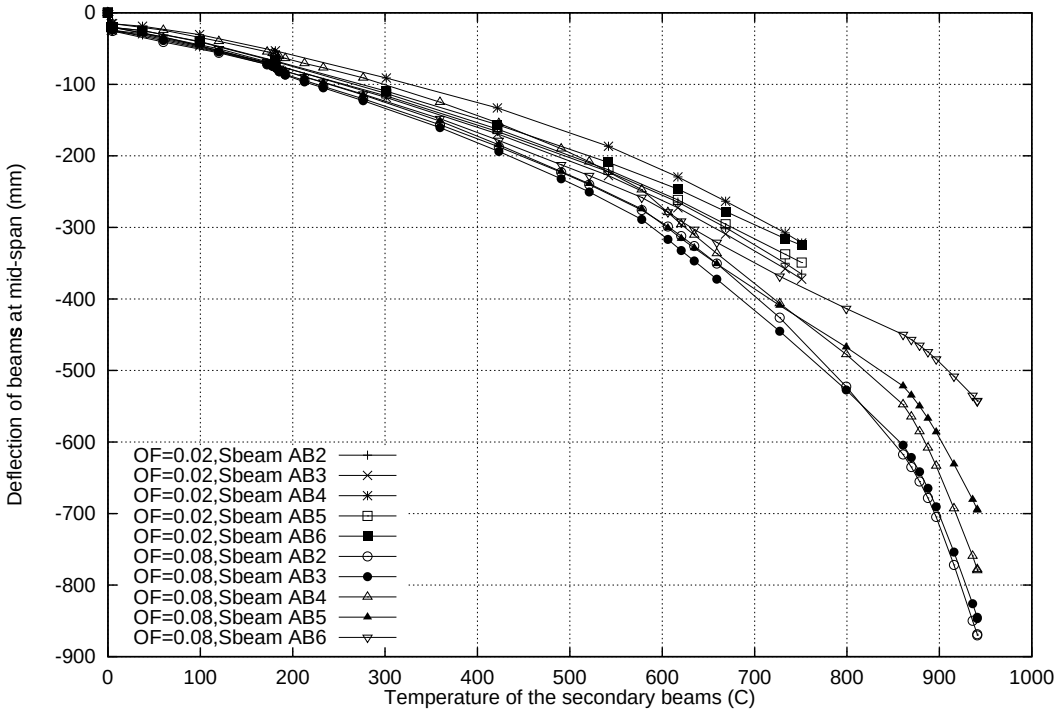

Figure 9.6: Deflection history of the unprotected secondary beams against secondary beam temperature

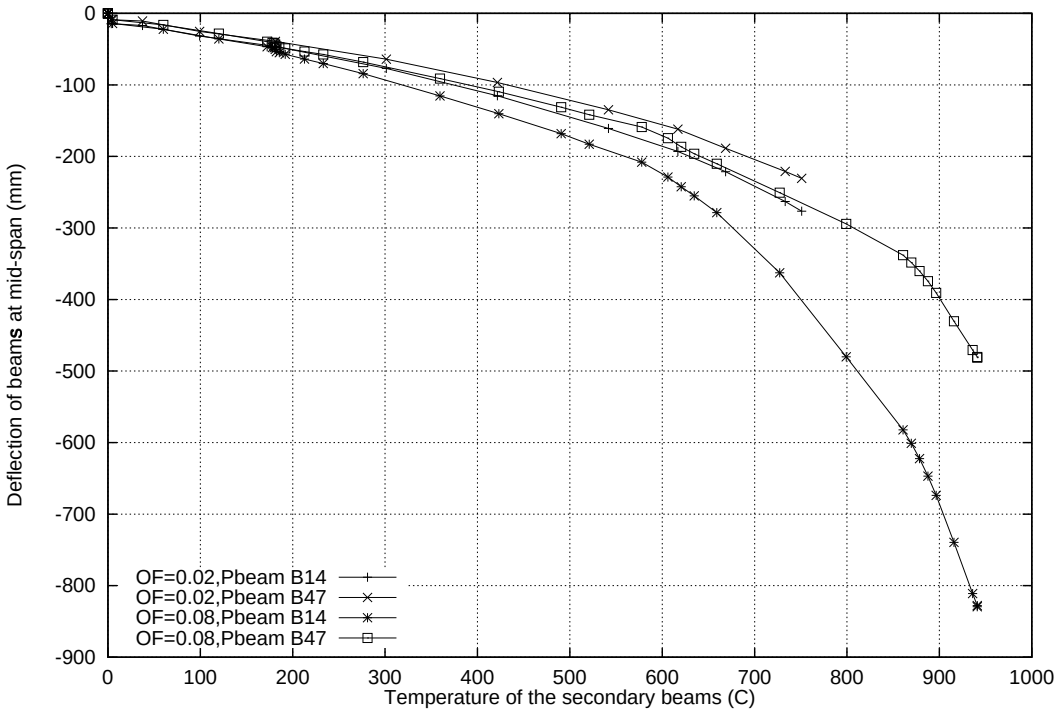

Figure 9.7: Deflection history of the unprotected primary beams against secondary beam temperature

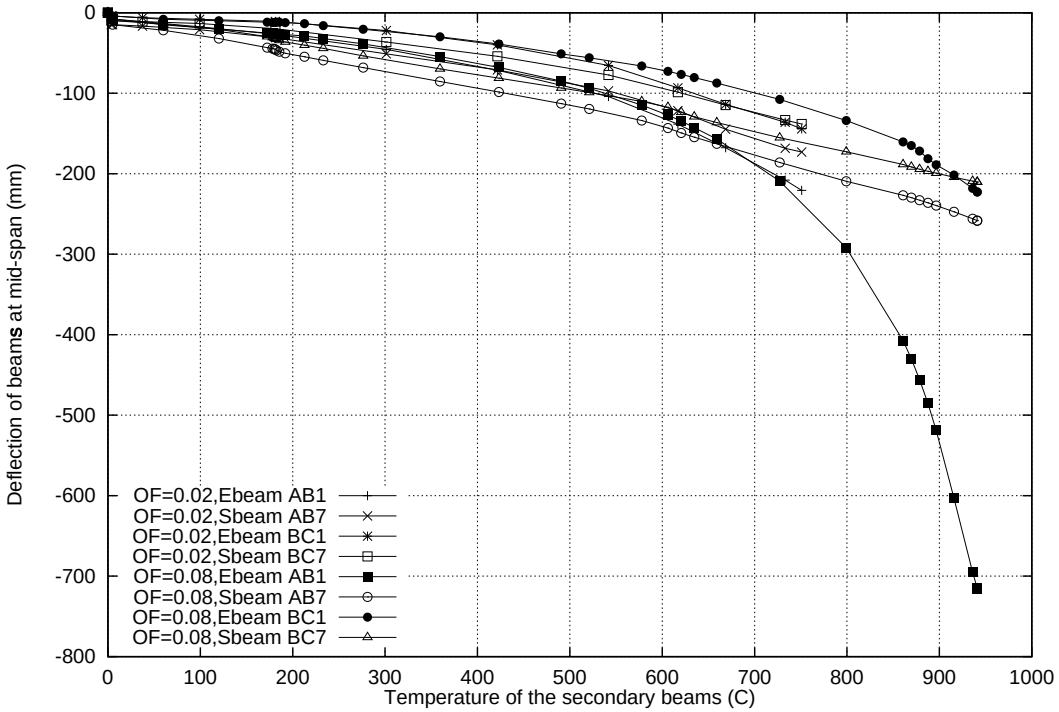

Figure 9.8: Deflection history of the protected edge beams parallel to the secondary beams against secondary beam temperature

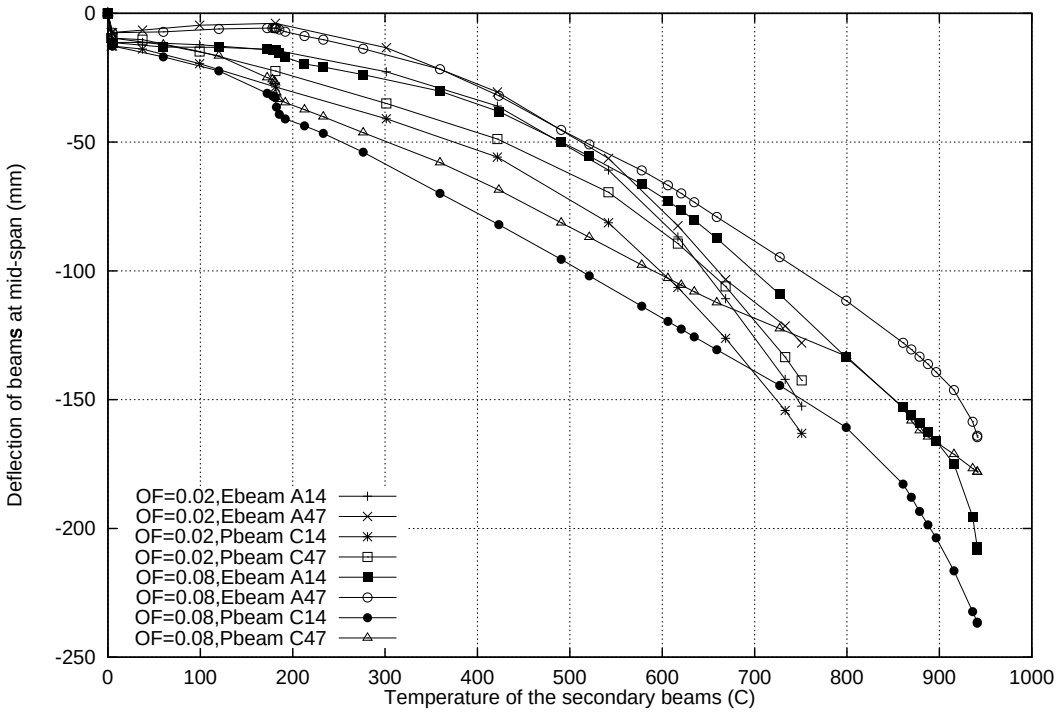

Figure 9.9: Deflection history of the protected edge beams parallel to the primary beams against secondary beam temperature

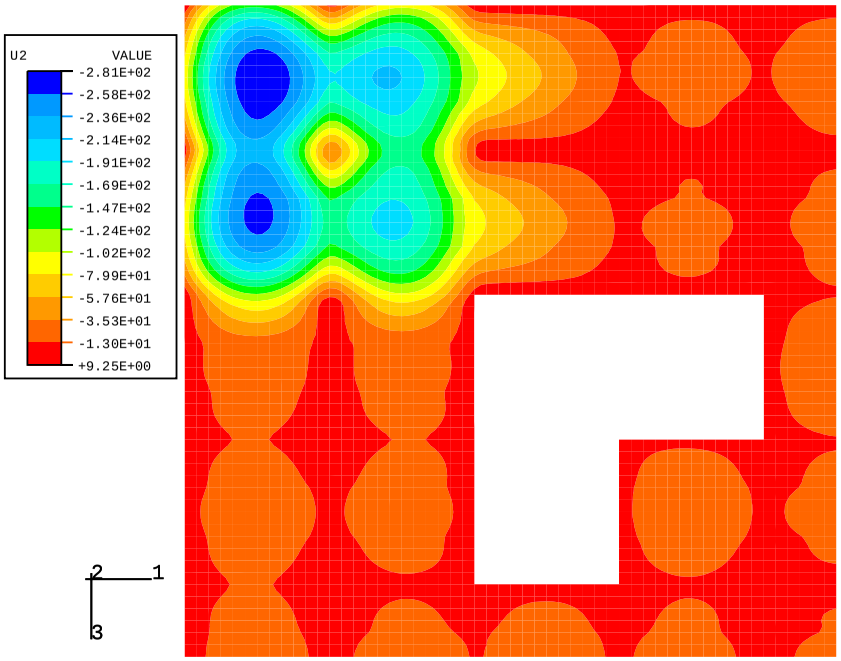

(a) OF=0.02

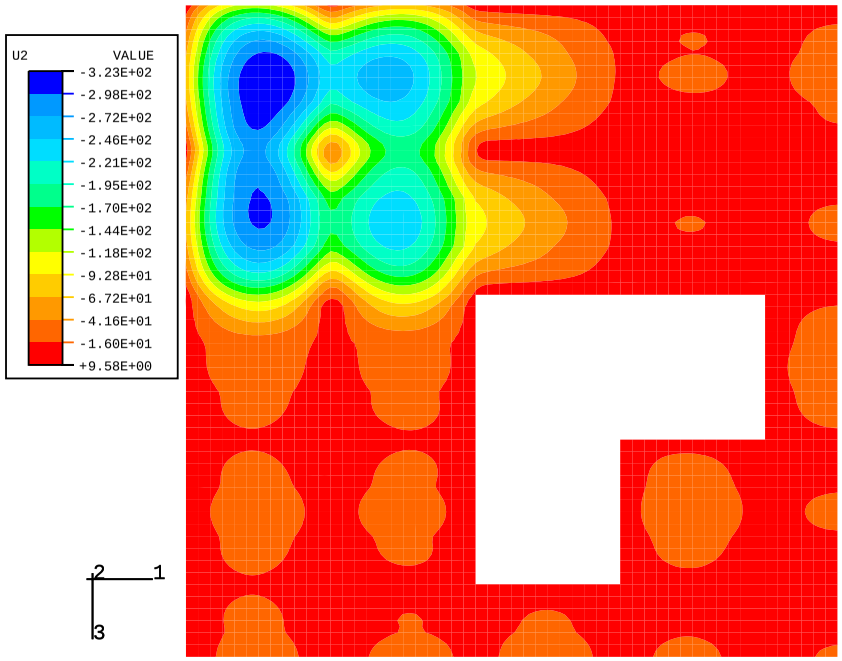

(b) OF=0.08

Figure 9.10: Deflection contours in the slab at a reference temperature of 600^{o}C

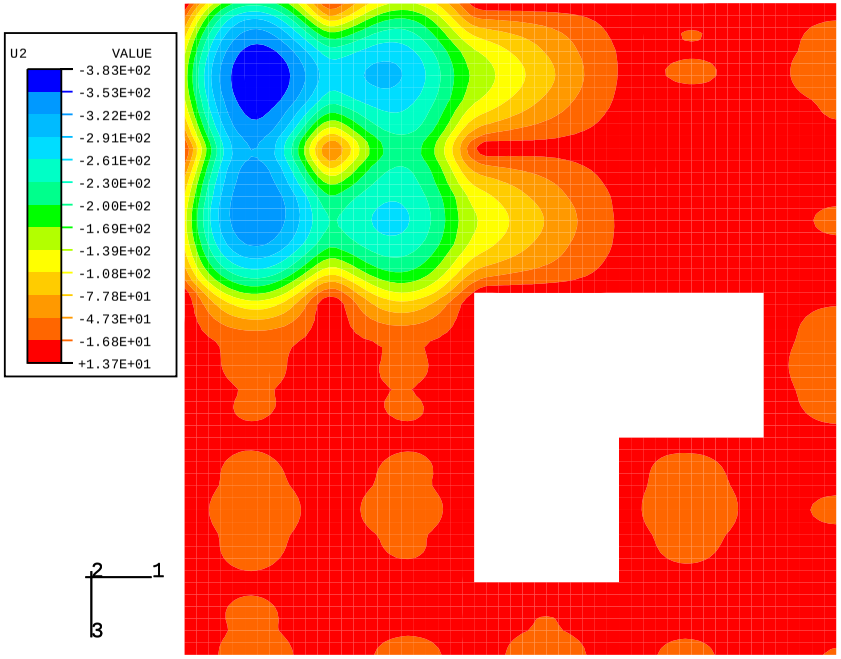

(a) OF=0.02 (750^{o}C)

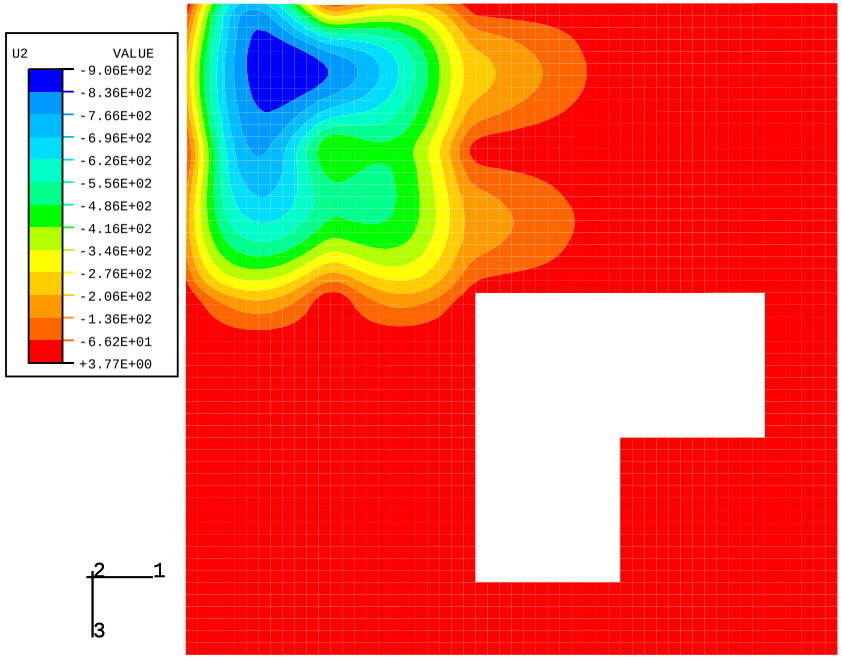

(b) OF=0.08 (950^{o}C)

Figure 9.11: Deflection contours in the slab at the end of heating

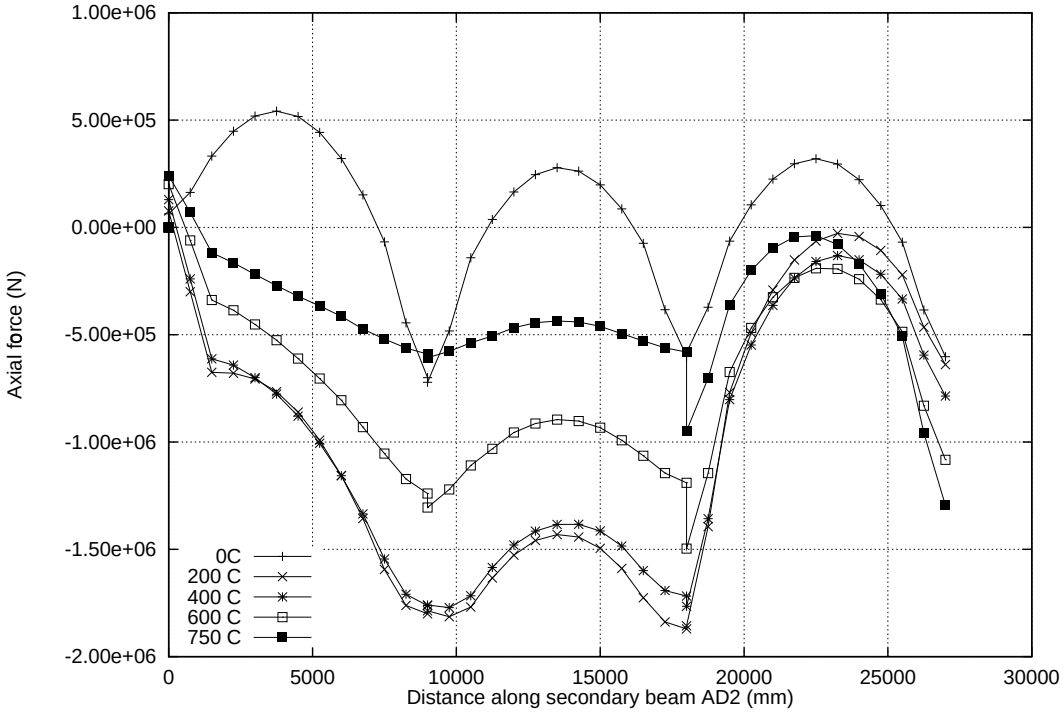

Figure 9.12: Variation of axial force along secondary beam AD2 at various secondary beam temperatures, OF=0.02

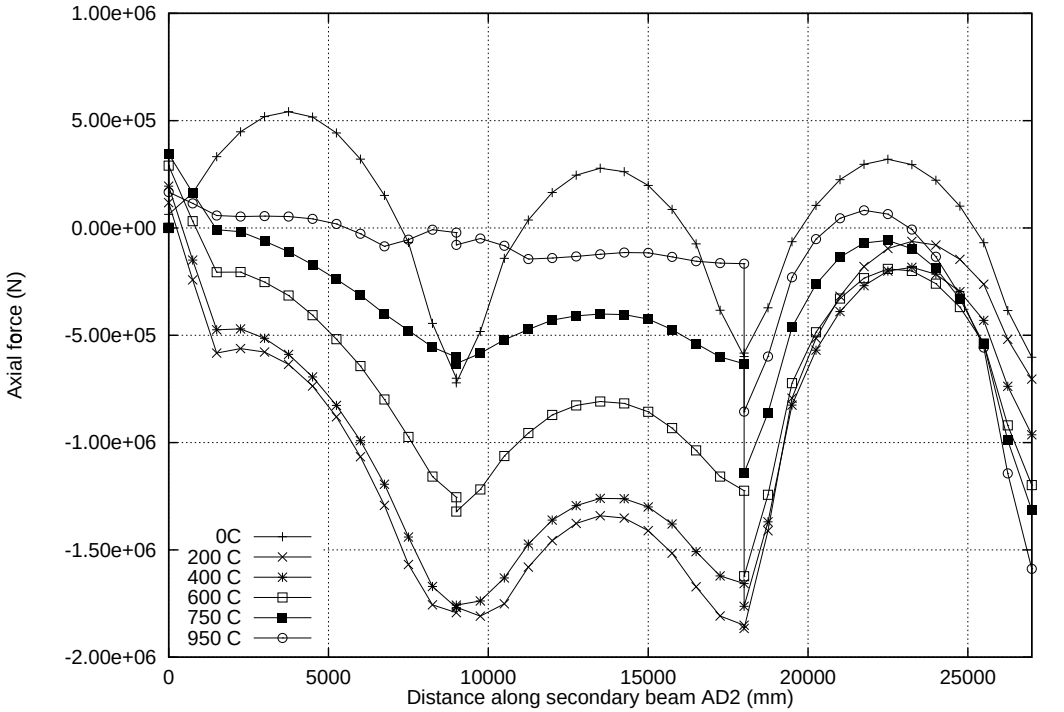

Figure 9.13: Variation of axial force along secondary beam AD2 at various secondary beam temperatures, OF=0.08

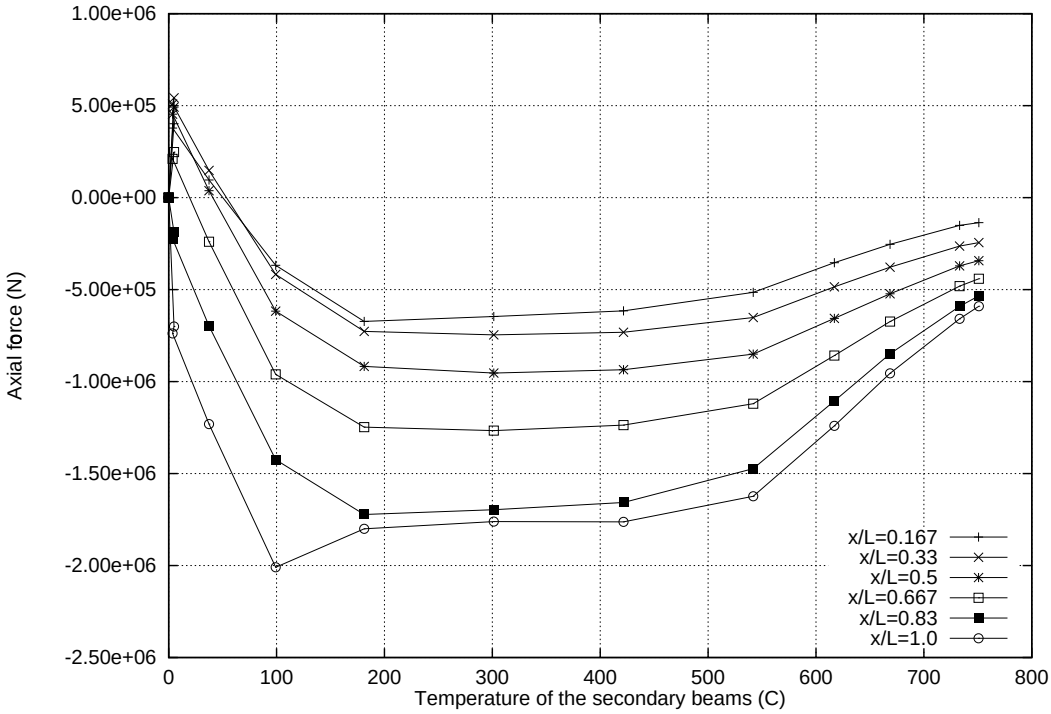

Figure 9.14: Secondary beam AB2: Axial force against secondary beam temperature, OF=0.02

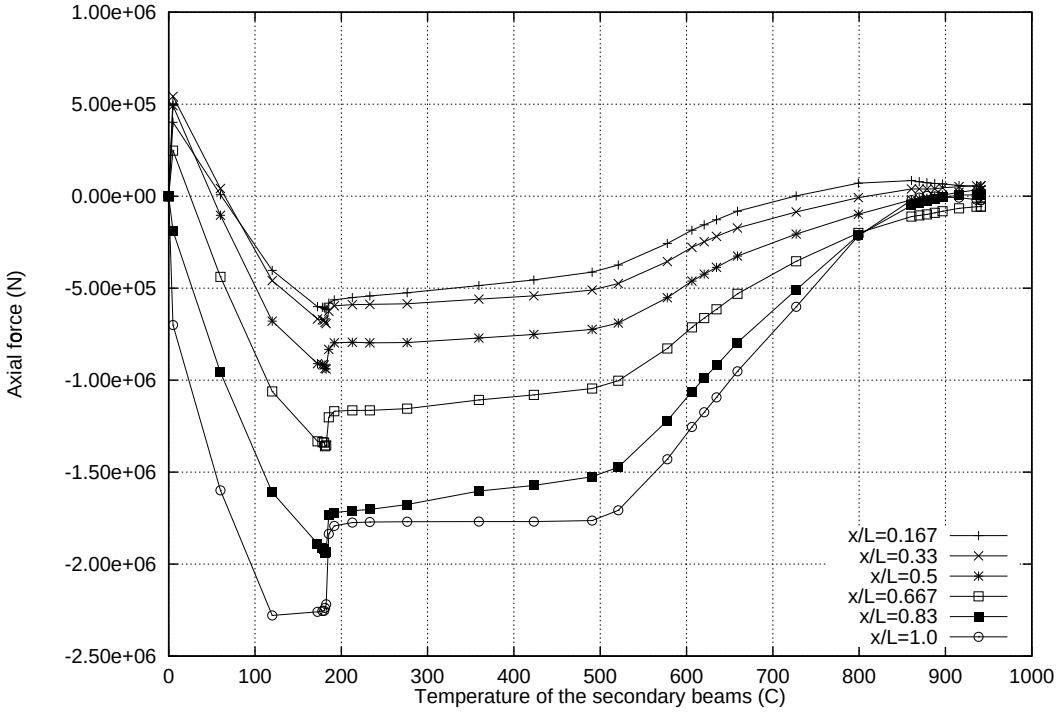

Figure 9.15: Secondary beam AB2: Axial force against secondary beam temperature, OF=0.08

forces are very similar beyond 200^oC.

The rotations at the ends of primary beam B14 are plotted for the "short-hot" fire in Figure 9.18. There is a rapid increase in the rate of rotation at a reference temperature of 180^oC associated with the rapid loss in axial compression in the primary beam as expected. The axial force capacity of the primary beam is plotted in Figure 9.19. For the maximum level of axial force experienced by the primary beam in the analysis ($4 \times 10^6 N$) the first yield would occur at 180^oC. This confirms that the instability event in the 9x9 frame is the same as that in the small frame.

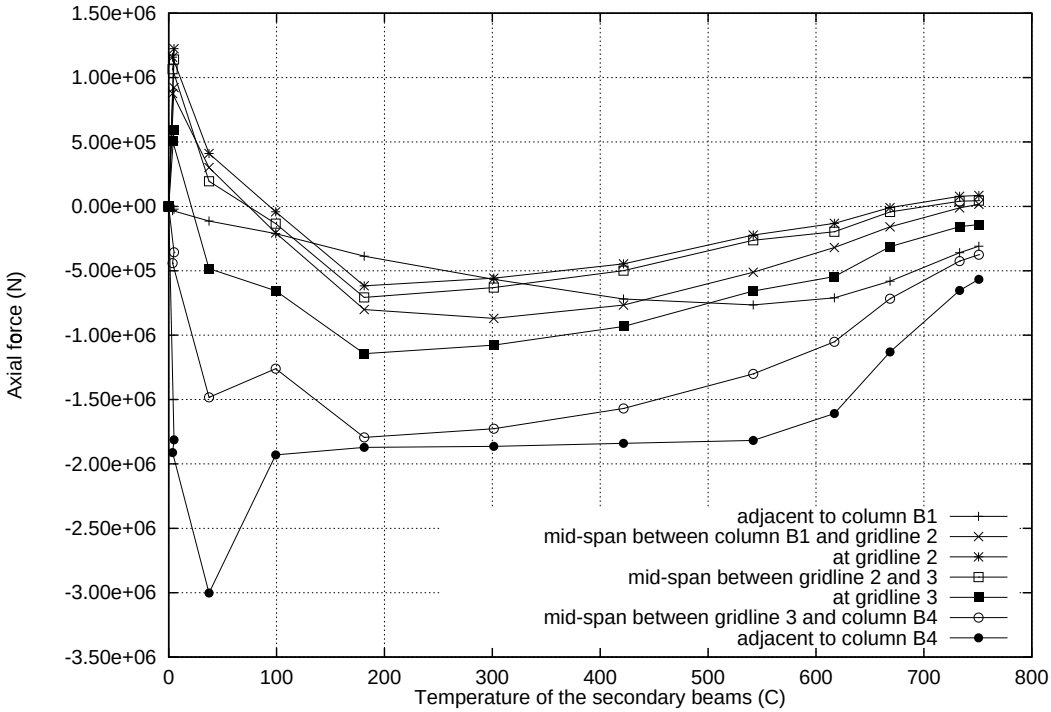

Figure 9.16: Primary beam B14: Axial force against secondary beam temperature, OF=0.02

The axial forces in edge beams AB1 and BC1 against secondary beam temperature are given in Figures 9.20-9.23. The instability event in the primary beam during the "short-hot" fire is mirrored in these axial forces. As in the small frame there is an increase in axial compression in the edge beams (Figures 9.21 and 9.23) when the primary beam rapidly loses compression. There is also a significant decrease in axial compressions of the edge beam prior to the instability event as the primary beam pushes out column B1.

In the "short-hot" fire edge beam AB1 deflects to a greater extent (after 600^oC) than any other edge beam . The compressions in this beam are lower than edge beam AB1 in the "long-cool" fire after 600^oC and the axial tensions at the end of the analysis

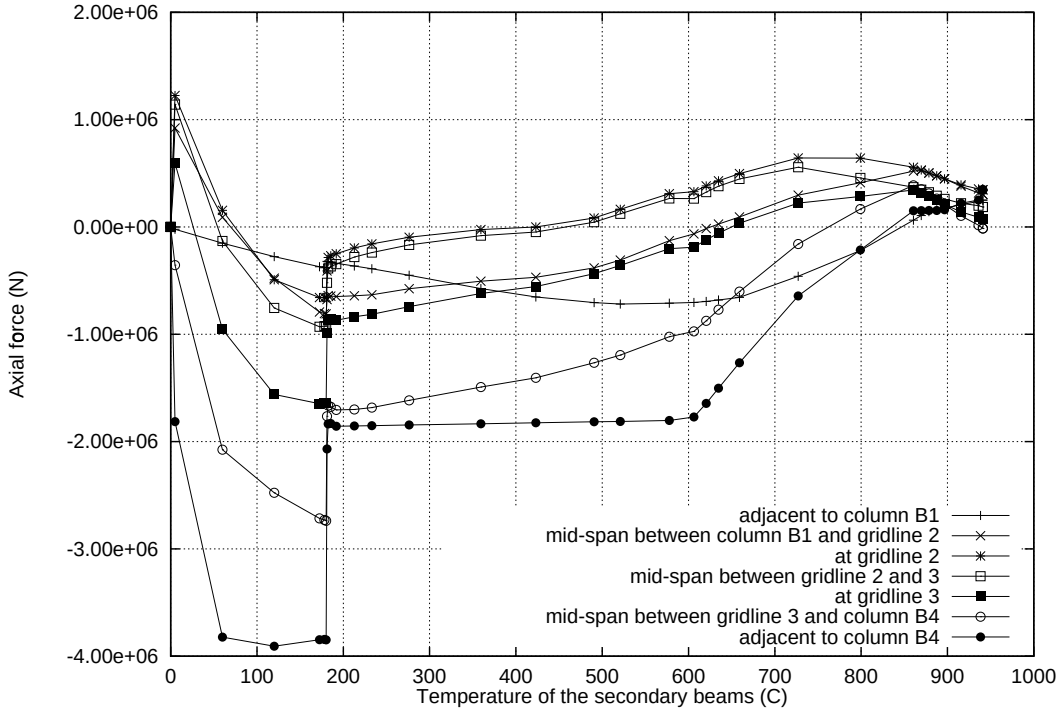

Figure 9.17: Primary beam B14: Axial force against secondary beam temperature, OF=0.08

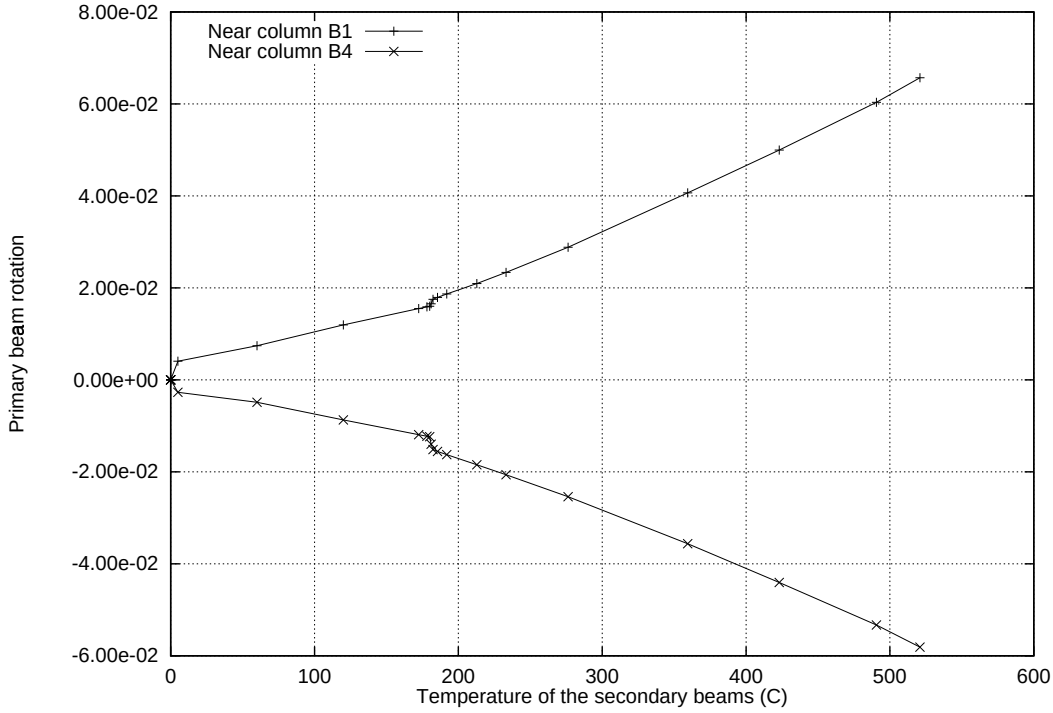

Figure 9.18: Rotations near the ends of the primary beam B14, OF=0.08

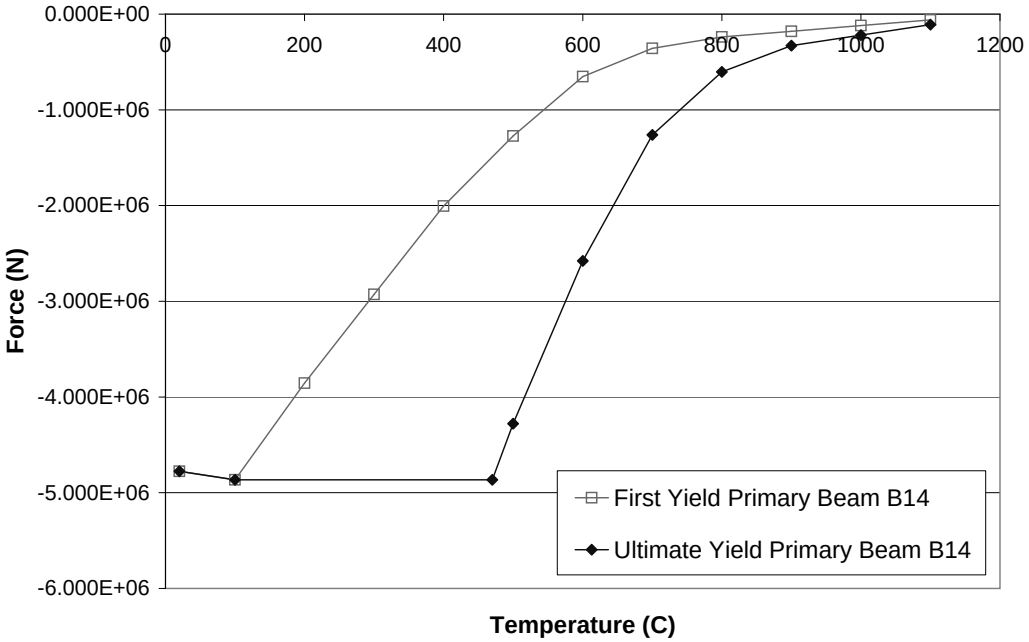

Figure 9.19: Material yield limits of the primary beam

are much higher. The axial forces in the edge beams along gridline A (parallel to the primary beam) are shown in Figures 9.24-9.27. The axial force along the length of edge beam A47 is very uniform because the beam is heavily restrained at both ends (by expanding beam A14 at one end and the cold structure at the other).

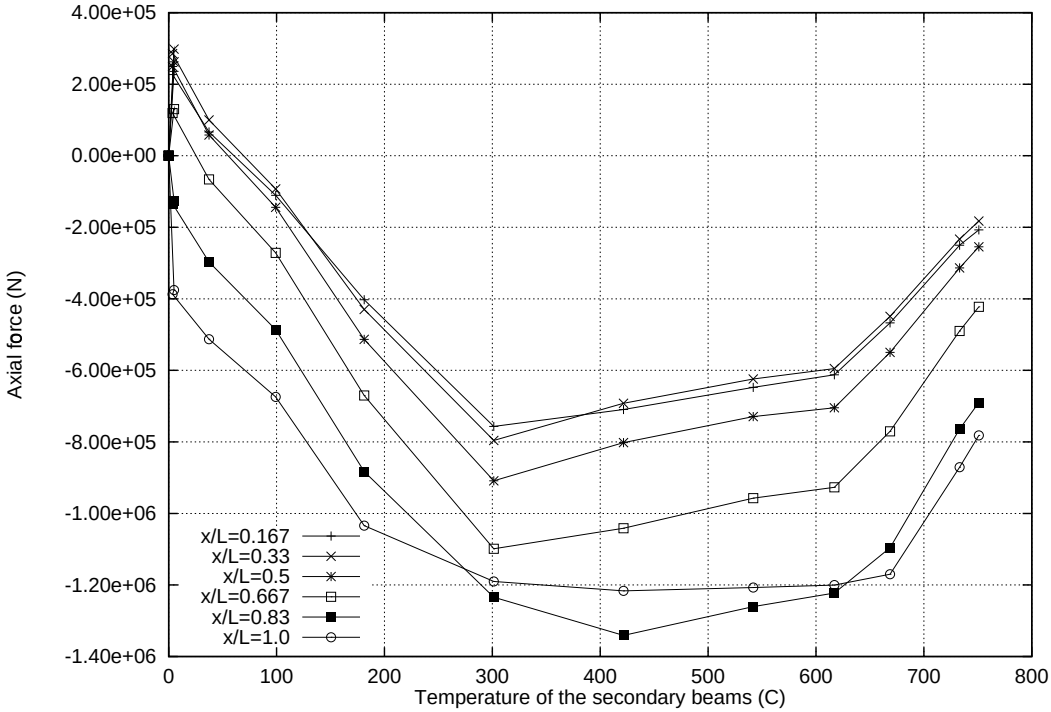

Figure 9.20: Edge beam AB1: Axial force against secondary beam temperature, OF=0.02

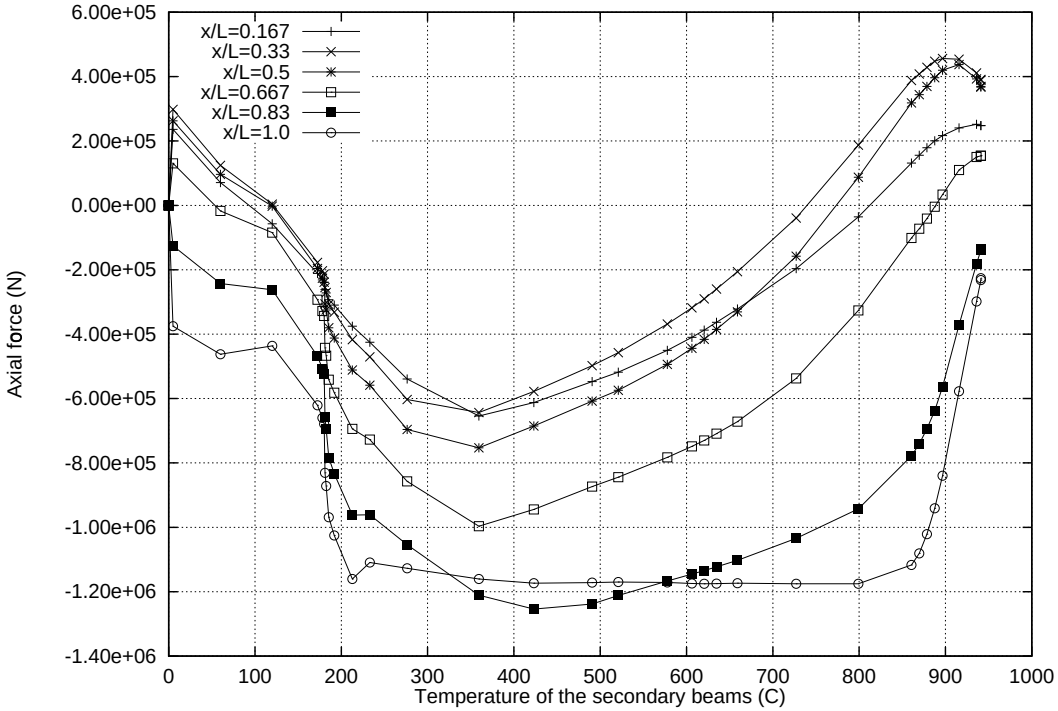

Figure 9.21: Edge beam AB1: Axial force against secondary beam temperature, OF=0.08

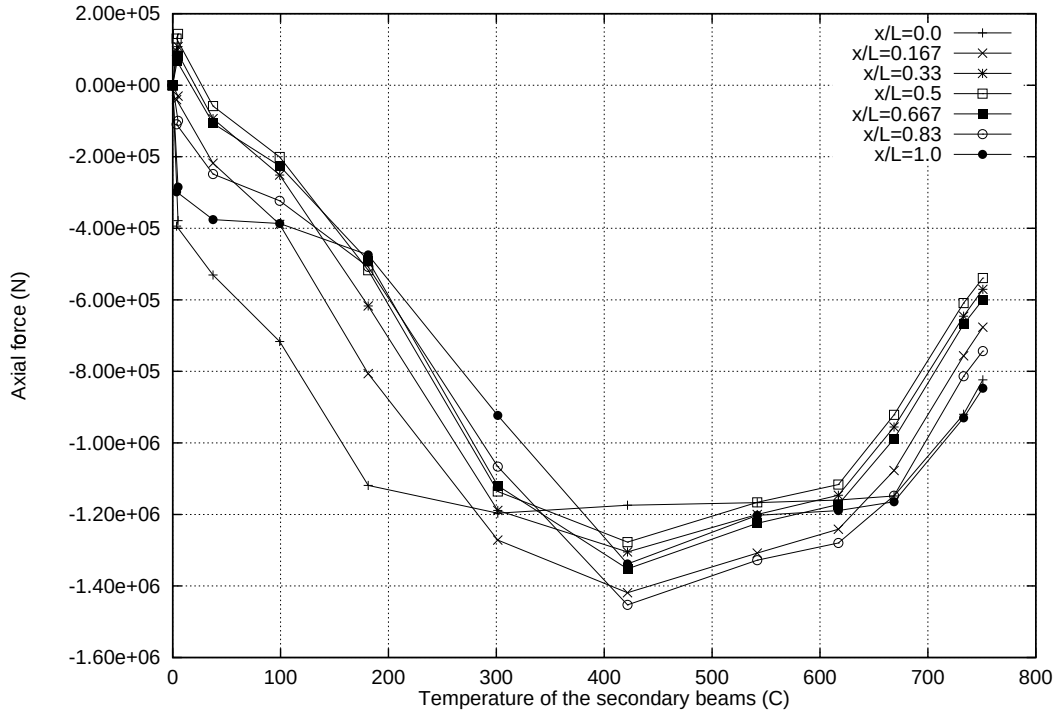

Figure 9.22: Edge beam BC1: Axial force against secondary beam temperature, OF=0.02

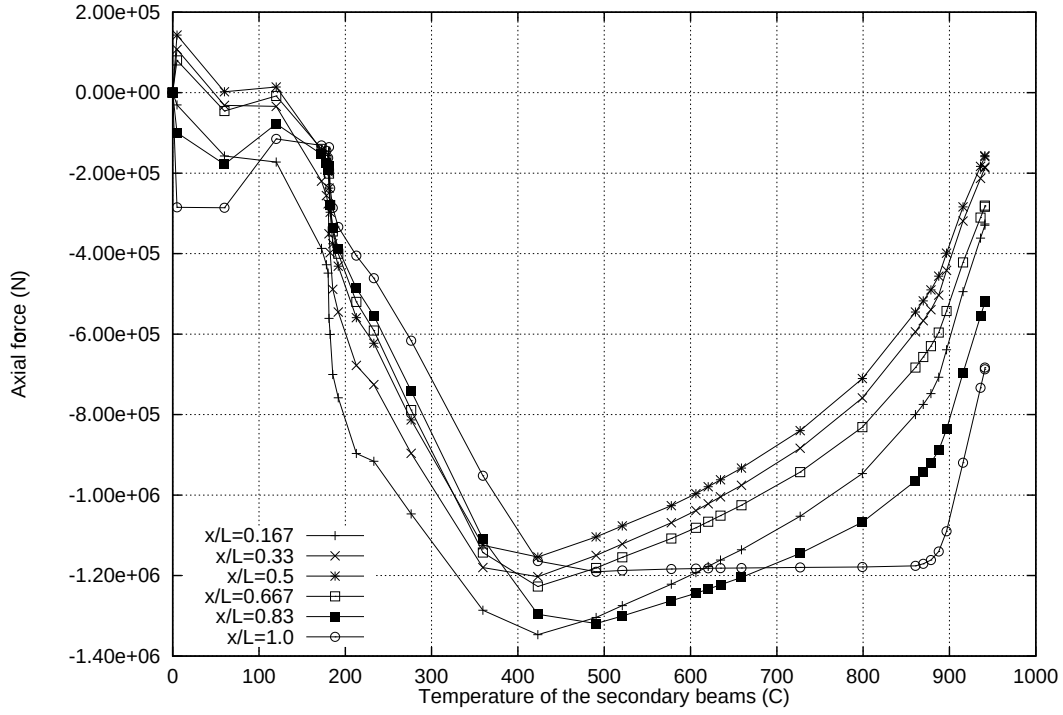

Figure 9.23: Edge beam BC1: Axial force against secondary beam temperature, OF=0.08

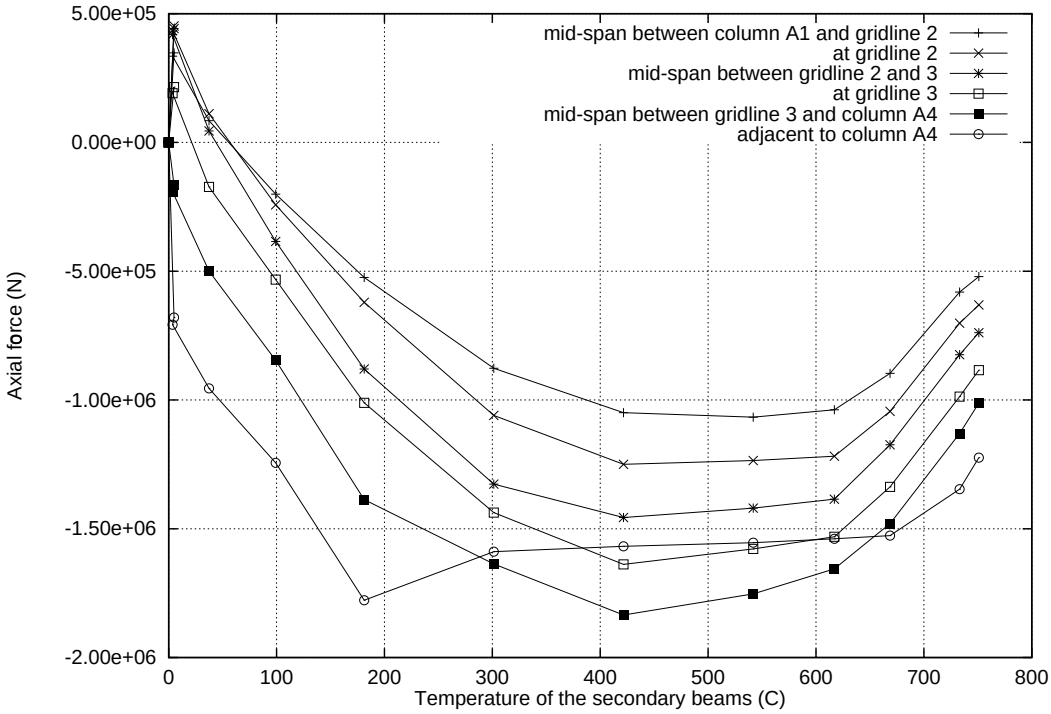

Figure 9.24: Edge beam A14: Axial force against secondary beam temperature, OF=0.02

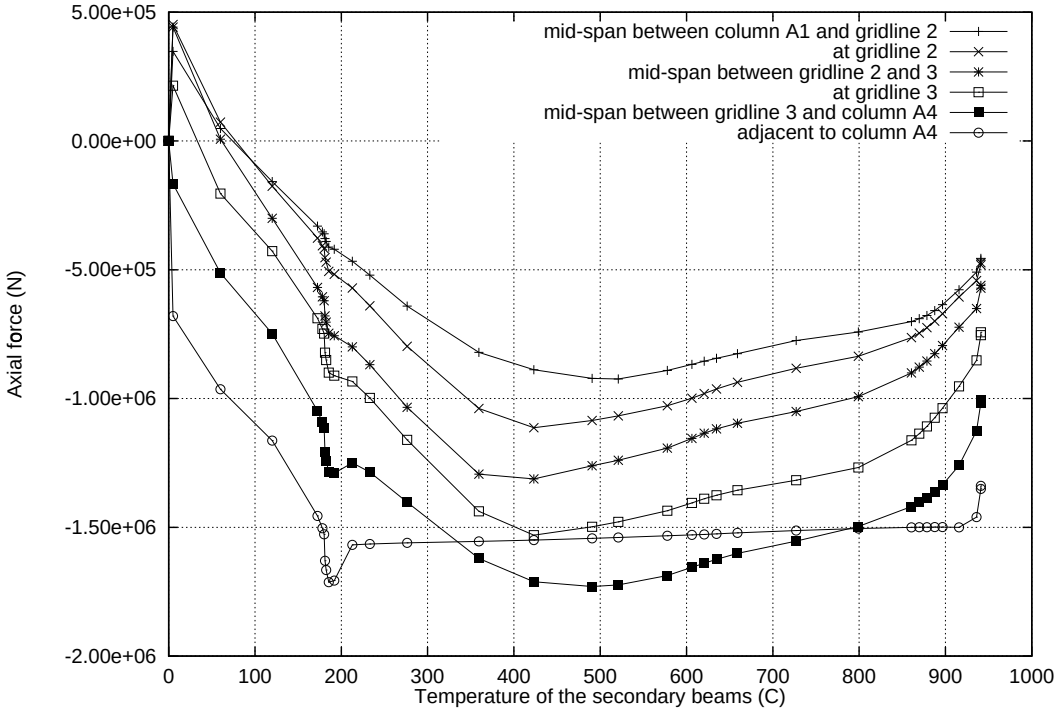

Figure 9.25: Edge beam A14: Axial force against secondary beam temperature, OF=0.08

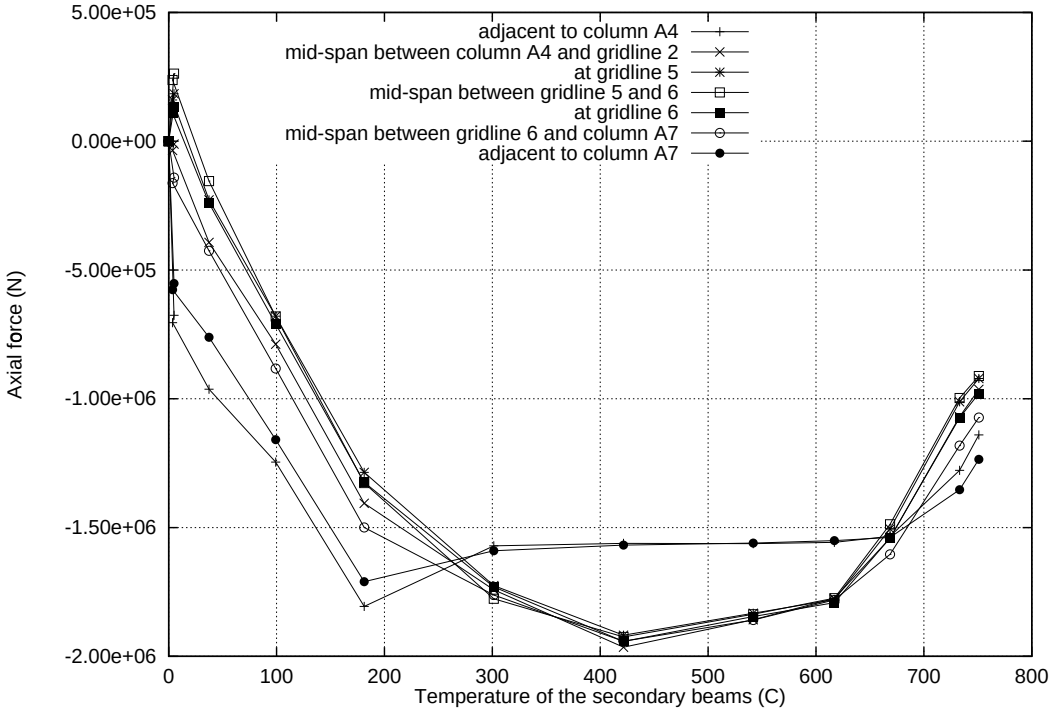

Figure 9.26: Edge beam A47: Axial force against secondary beam temperature, OF=0.02

9.6.1.2 Behaviour of the slab

The mechanical strains in the slab at the level of the reinforcement are plotted in Figures 9.28 and 9.29 in the x and y-direction at the end of heating in both fires. The mechanical tensions are much higher in the "short-hot" fire although the pattern of strains is similar in both scenarios.

9.6.1.3 Summary

- The "Short-hot" fire caused greater deflections of unprotected steel members.
- The primary beam instability event also occurred in the 9x9 frame and was associated with the steel beam reaching its compression capacity and sudden rotations near the connection confirming that it was the same mechanism as in the small frame.
- In the "short-hot" fire edge beam AB1 deflections were considerable towards the end of the analysis. This caused the slab to tend towards 1D catenary action.

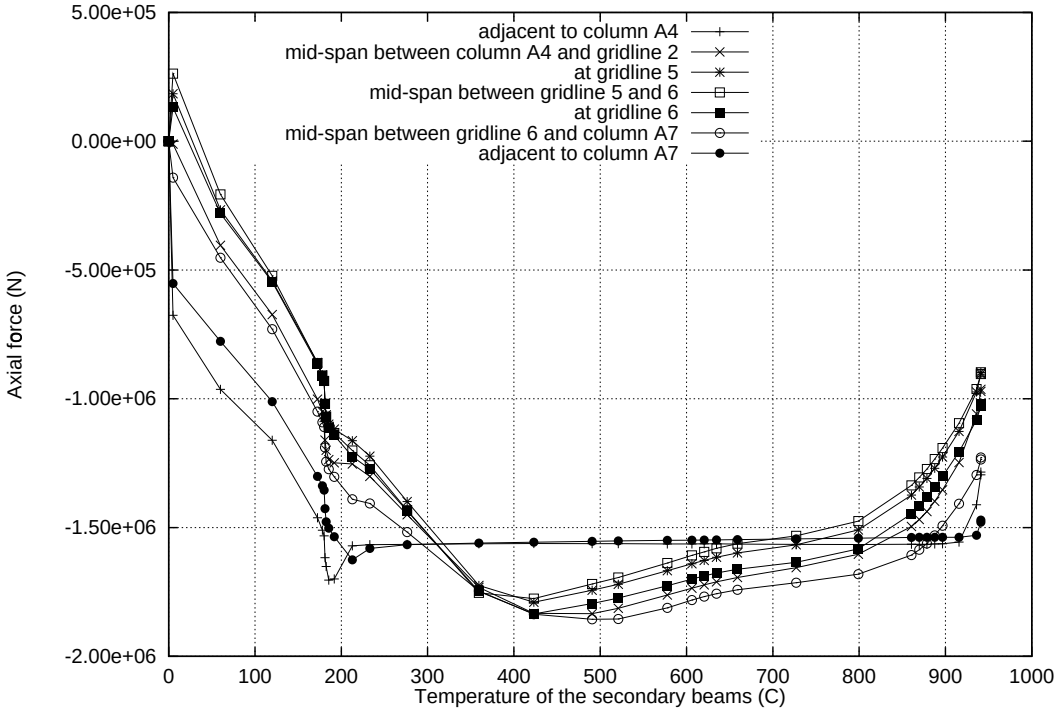

Figure 9.27: Edge beam A47: Axial force against secondary beam temperature, OF=0.08

- The slab exhibits greater membrane tensions in response to the "short-hot" fire as expected.

9.6.2 Corner and Edge compartment fires in the 9 x 9 frame

Studying scenarios 3 and 4 of Table 9.1 allowed a comparison between an edge compartment and a corner compartment. The edge compartment is highly restrained by the surrounding cold structure on 3 sides and the nearby bracing bay.
The two fire compartments were illustrated in Figure 9.4.

9.6.2.1 Deflections

Secondary beam displacements are plotted in Figure 9.30 and 9.31. The maximum displacement occurs in the corner compartment at the mid-span of secondary beam AB3 (Figure 9.30) because the beam is in the middle of the least supported outside bay. Between gridlines B and C (Figure 9.31) the secondary beams in the highly restrained edge compartment (secondary beams BC11 and BC12) deflect the most.
Overall the pattern of displacements can be seen in the contour plots of Figure 9.32.

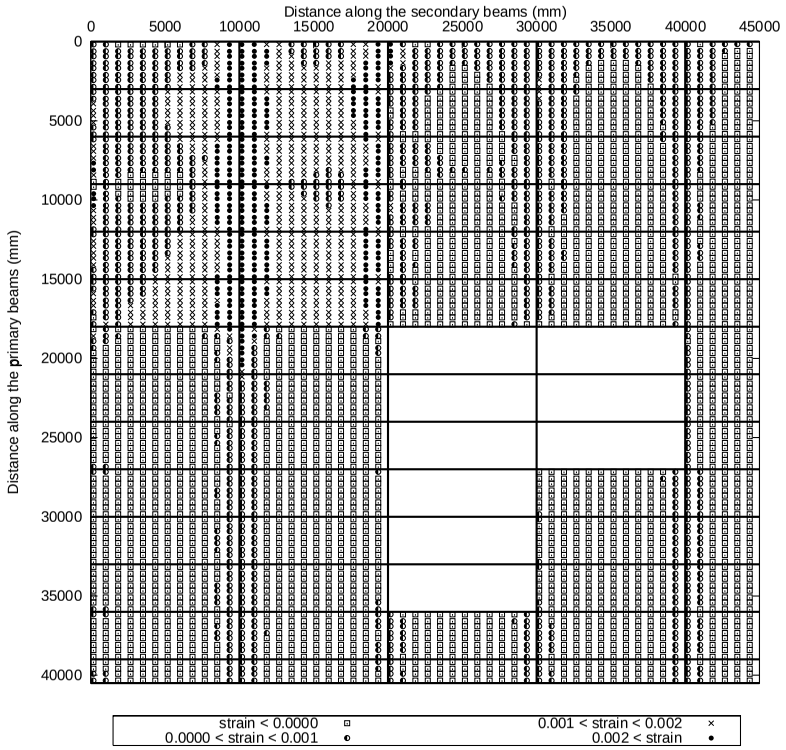

(a) x-direction (parallel to secondary beams)

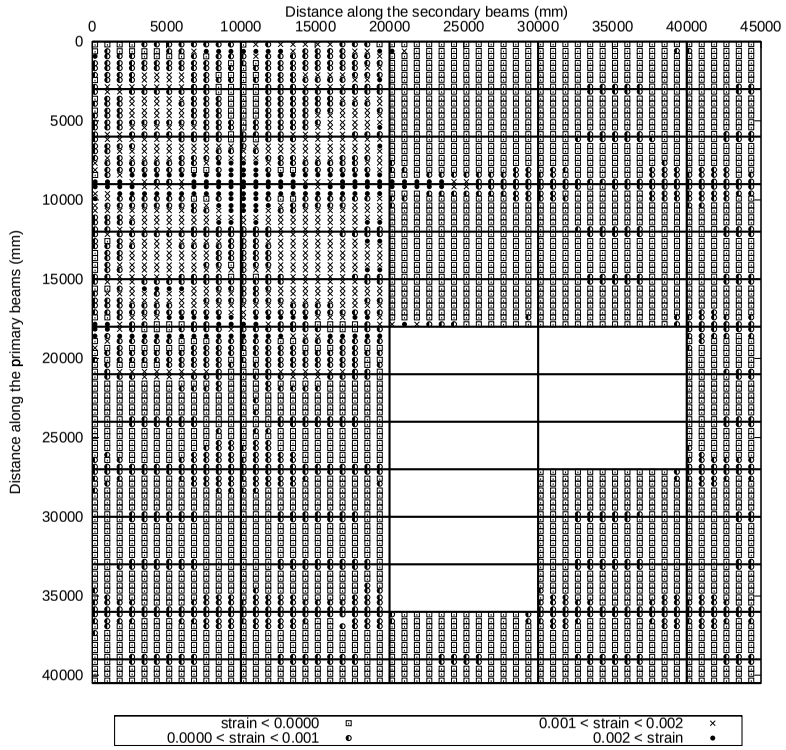

(b) y-direction (parallel to primary beams)

Figure 9.28: Mechanical strains in the reinforcement OF=0.02, corner compartment fire at 750^{o}C

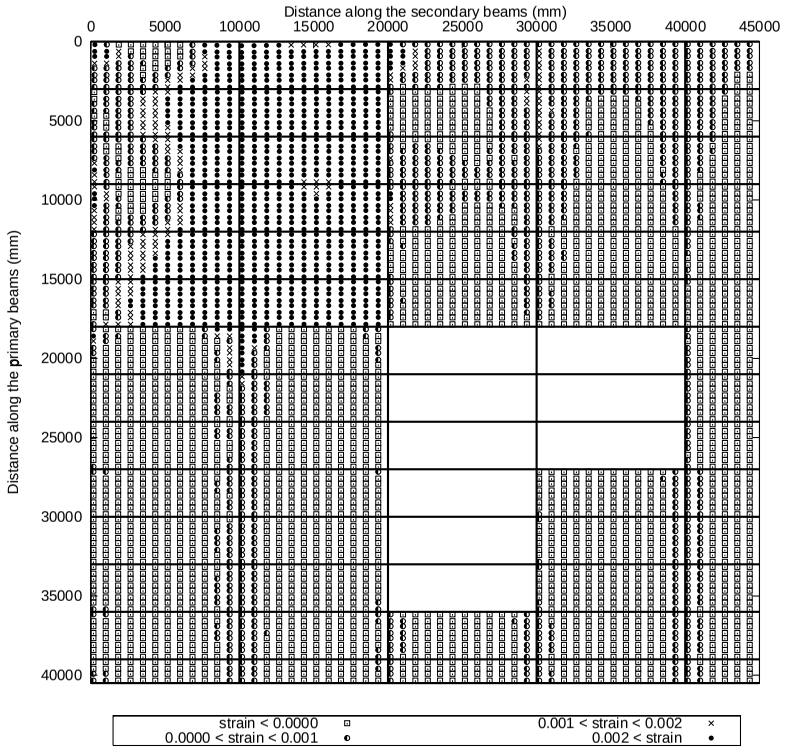

(a) x-direction (parallel to the secondary beams)

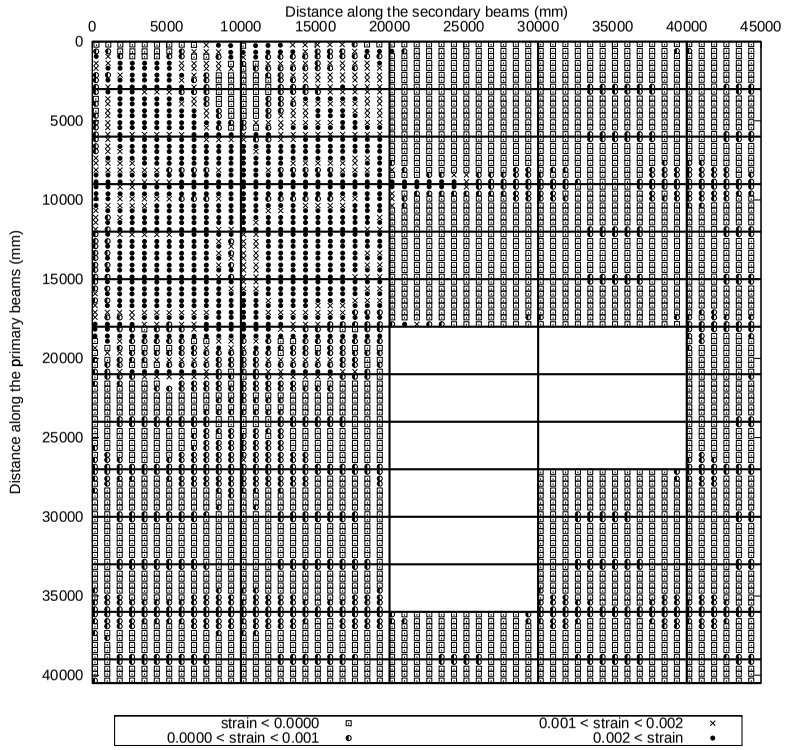

(b) y-direction (parallel to the primary beams)

Figure 9.29: Mechanical strains in the reinforcement OF=0.08, corner compartment fire at 950^{o}C

Deflections are largest in the least supported bay of the corner compartment. In the edge compartment between gridlines 13 and 15 there is continuity of the slab (rotational restraint) between the fire compartment and the cold structure (there is no such continuity next to the bracing), so the maximum deflections are lower.

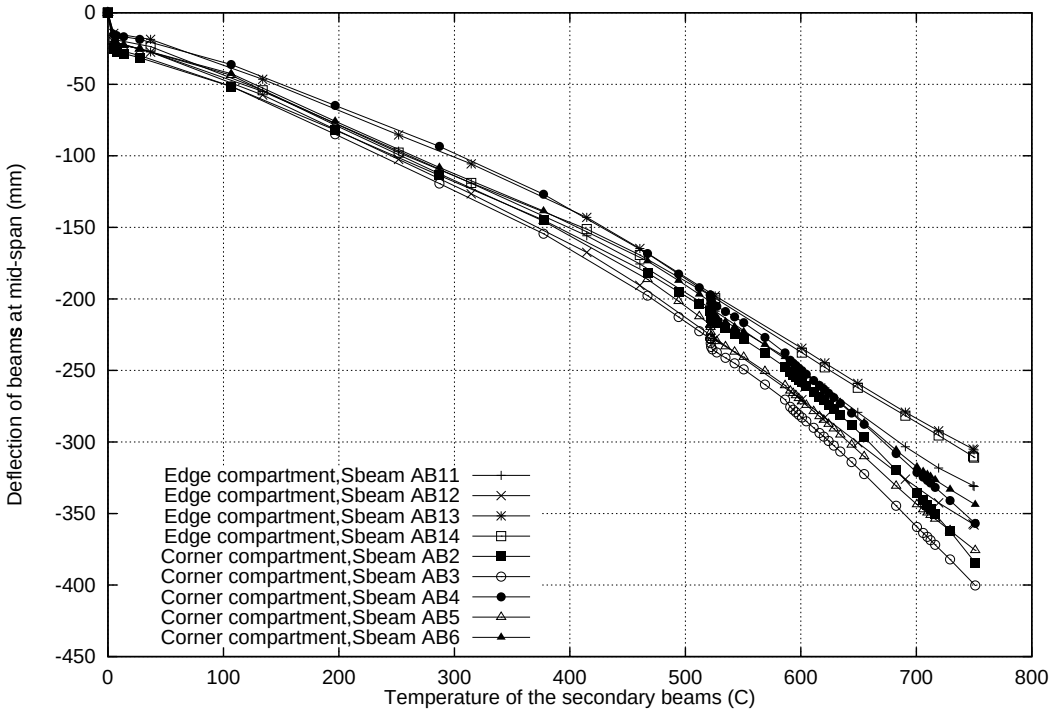

Figure 9.30: Deflection history of the unprotected secondary beams against secondary beam temperature

9.6.2.2 Behaviour of the steel beams

The axial force in secondary beams AB11 and AB2 are shown in Figures 9.33 and 9.34 at various locations along the beam. The forces are very similar. However in secondary beams BC11 and BC2 the forces are lower in secondary beam BC11 because of higher deflections (Figures 9.35 and 9.36).

The axial forces in primary beam B1013 and B14 are shown in Figures 9.37 and 9.38 respectively. There is a rapid loss of compression in the primary beam in the corner compartment at 520°C (at the ultimate yield of the primary beam, see Figure 9.19. Before this instability the compressive forces in both members are similar.

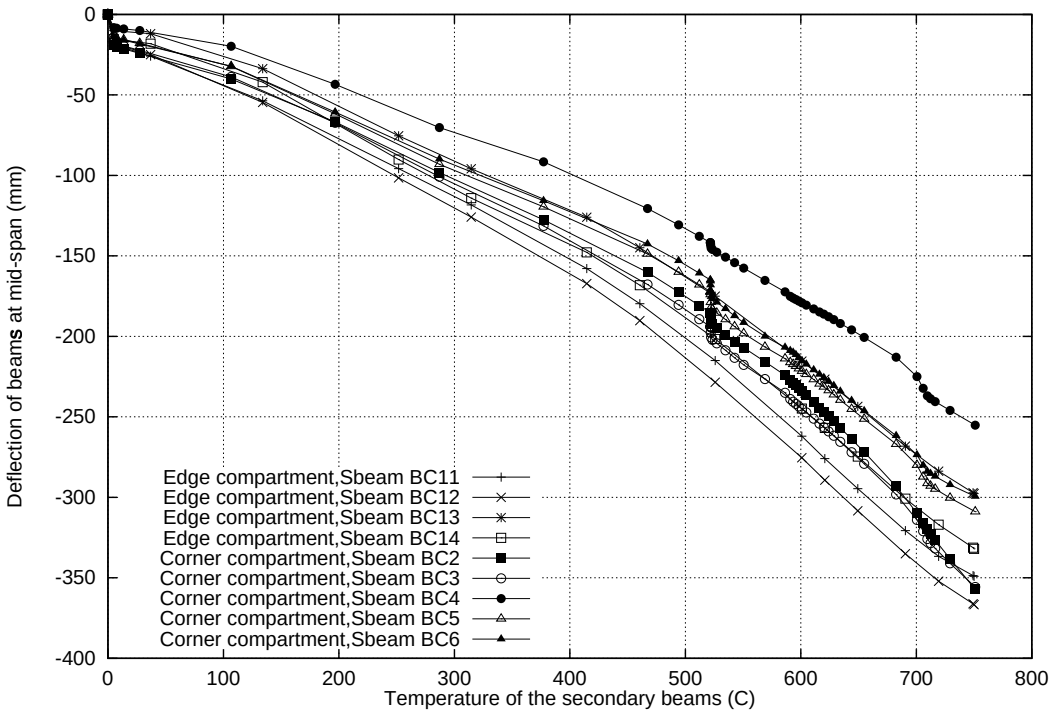

Figure 9.31: Deflection history of the unprotected secondary beams against secondary beam temperature

9.6.2.3 Behaviour of the slab

The membrane forces are illustrated in Figures 9.39 and 9.40 at the end of heating. The strains are quite low and there is very little difference in the stress state of the two scenarios other than in the y-direction (parallel to the primary beams) in the edge compartment where there are increased areas of high tension (>0.002) because of high restraint. The bracing parallel to the primary beams is providing more restraint to the edge compartment than the bracing parallel to the secondary beams which only significantly affects gridline 13.

9.6.2.4 Summary

- Secondary beams deflected to a greater extent in the corner compartment.
- The bracing core has a major influence on the behaviour of the edge compartment in terms of displacements and axial forces in the beams immediately adjacent to the bracing core.
- Forces and deflections in beams remote from the bracing are very similar in both the corner and the edge compartment.

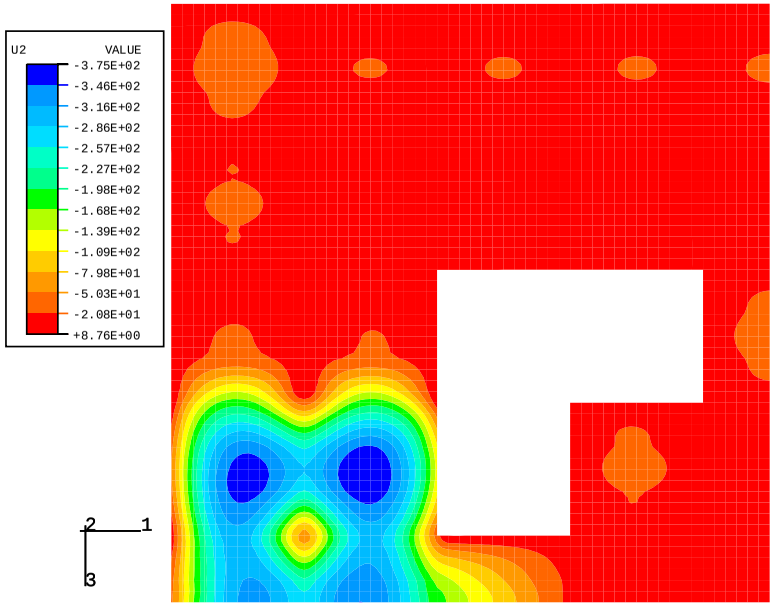

(a) Edge compartment

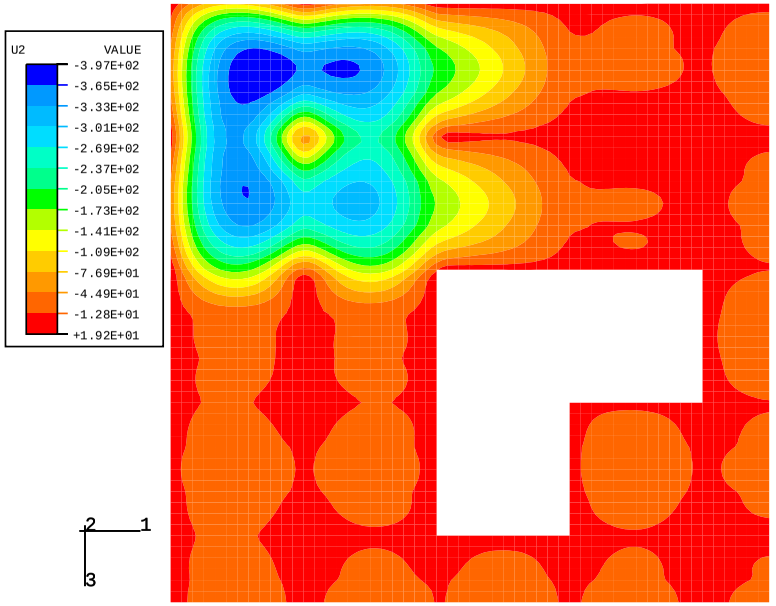

(b) Corner compartment

Figure 9.32: Deflection contours in the slab at the end of heating

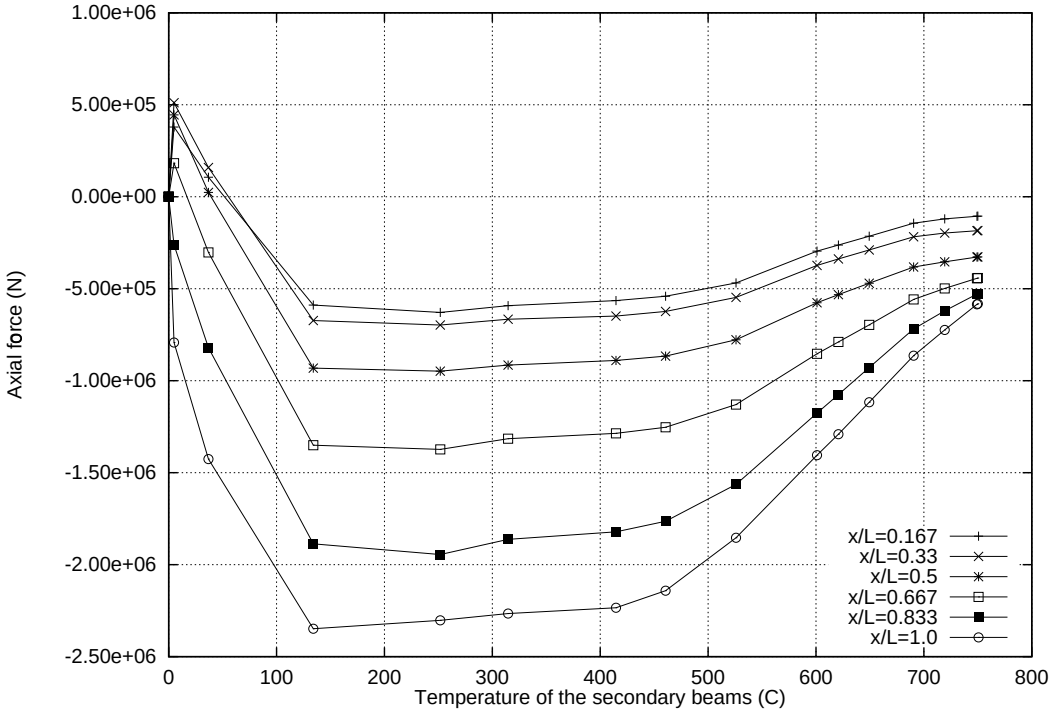

Figure 9.33: Secondary beam AB11: Axial force against secondary beam temperature, Edge compartment

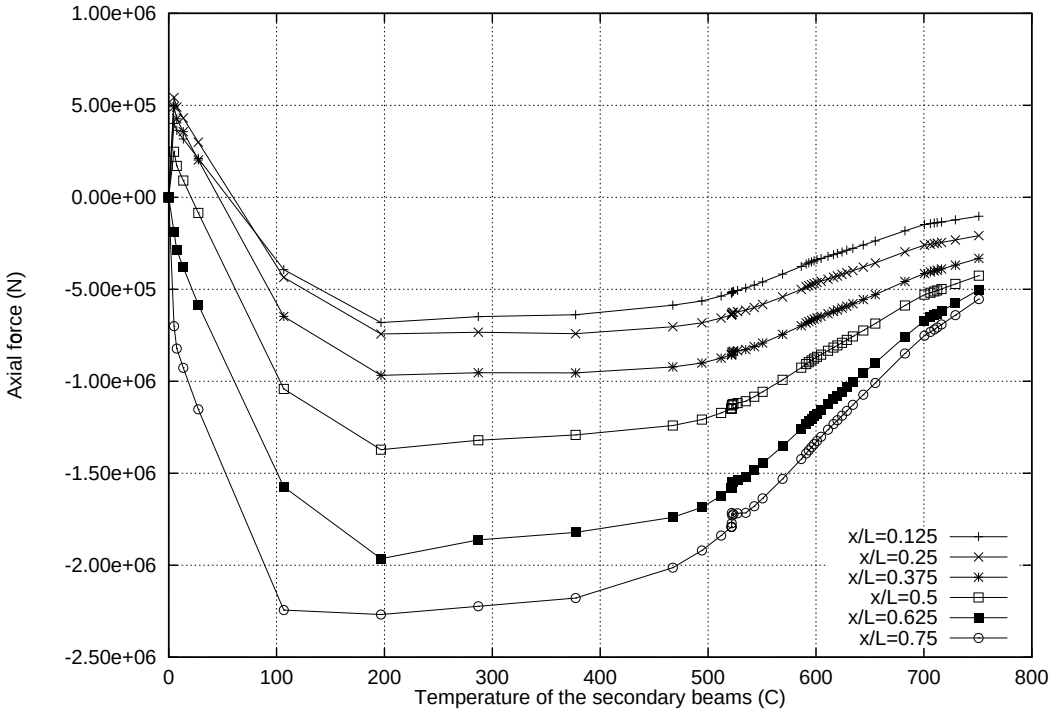

Figure 9.34: Secondary beam AB2: Axial force against secondary beam temperature, Corner compartment

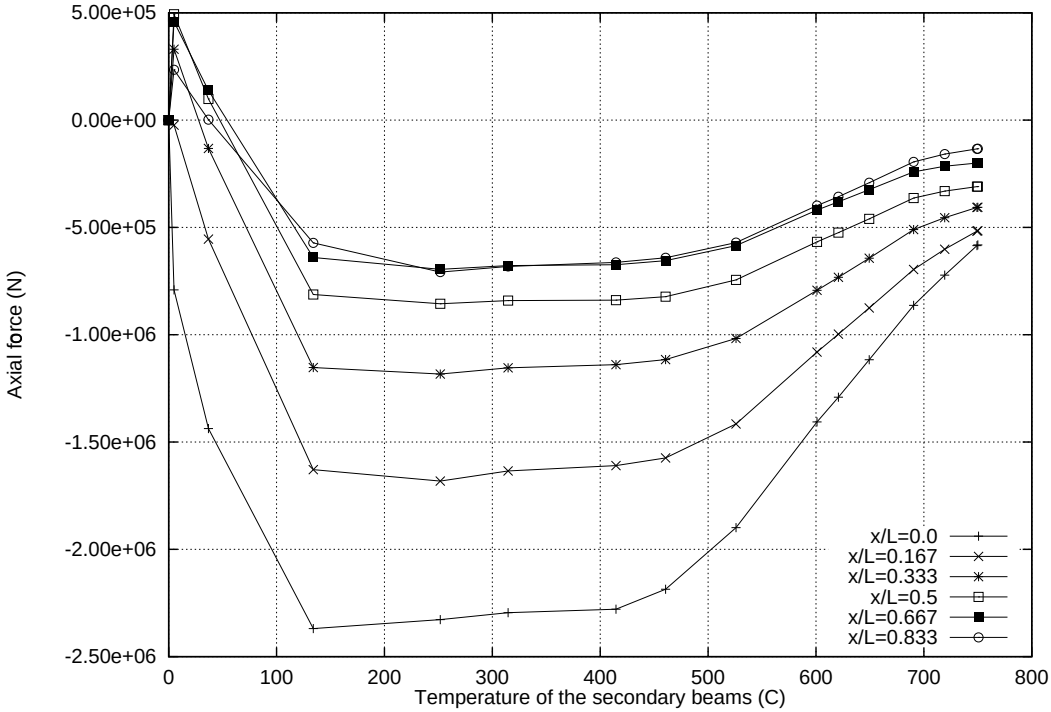

Figure 9.35: Secondary beam BC11: Axial force against secondary beam temperature, Edge compartment

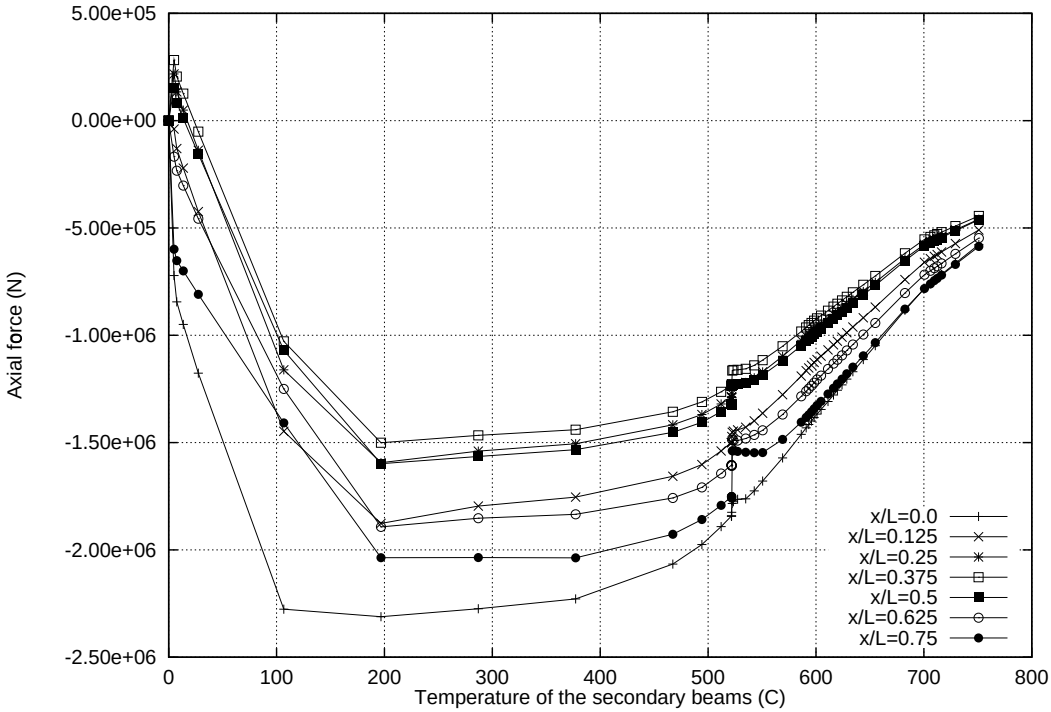

Figure 9.36: Secondary beam BC2: Axial force against secondary beam temperature, Corner compartment

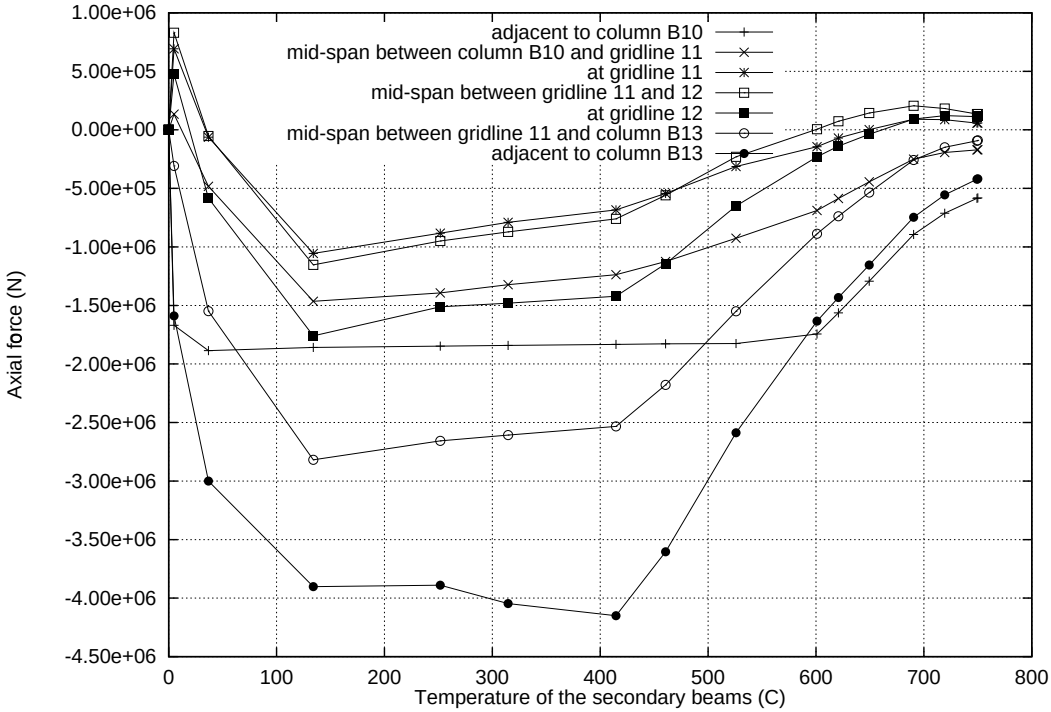

Figure 9.37: Primary beam B1013: Axial force against secondary beam temperature, Edge compartment

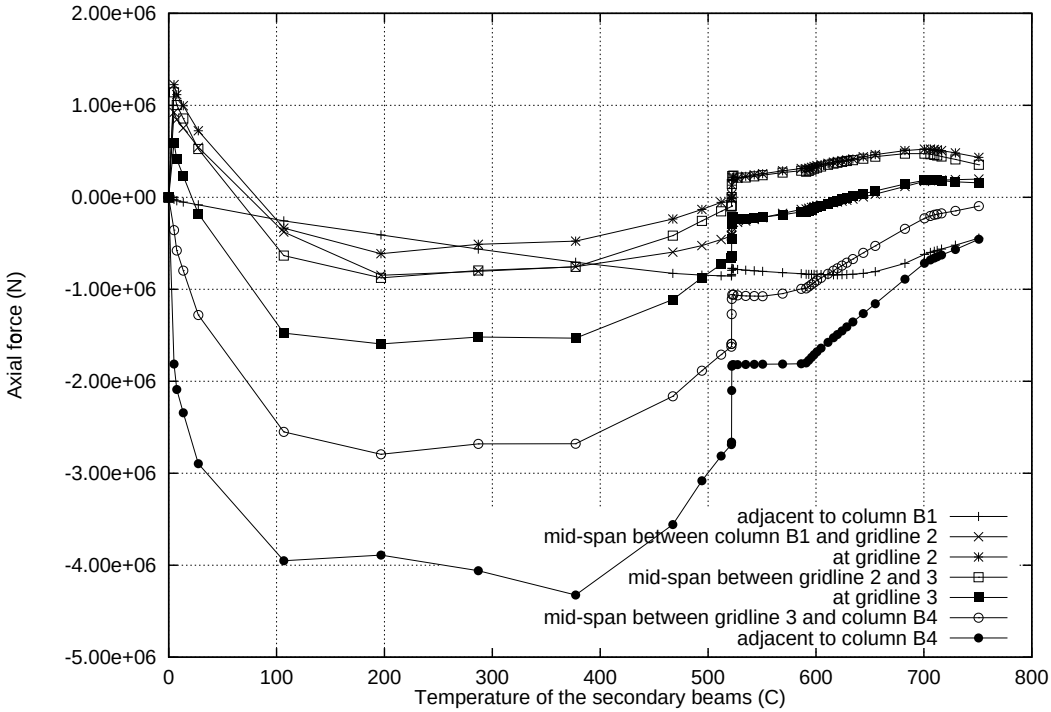

Figure 9.38: Primary beam B14: Axial force against secondary beam temperature, Corner compartment

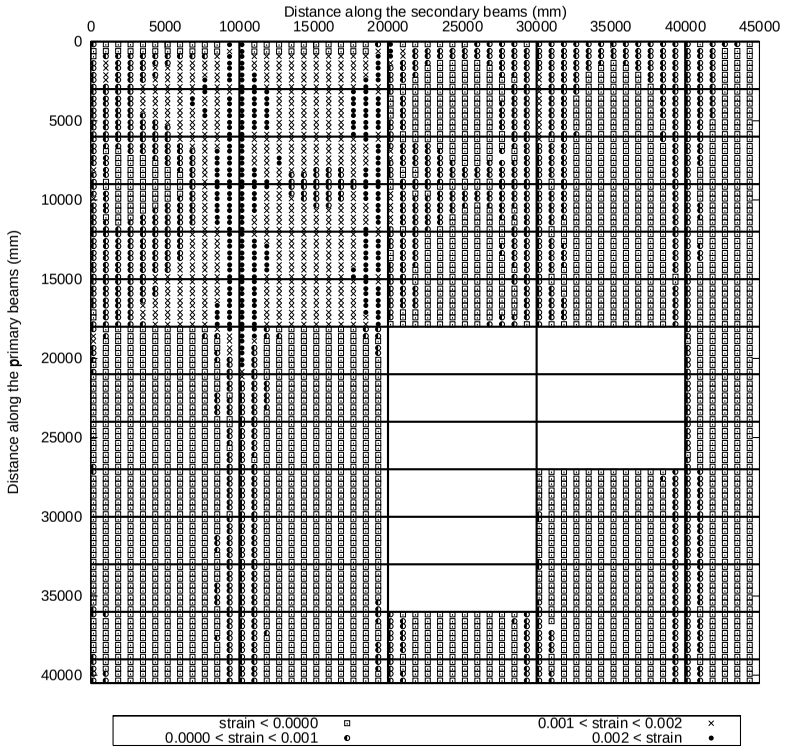

(a) x-direction (parallel to the secondary beams)

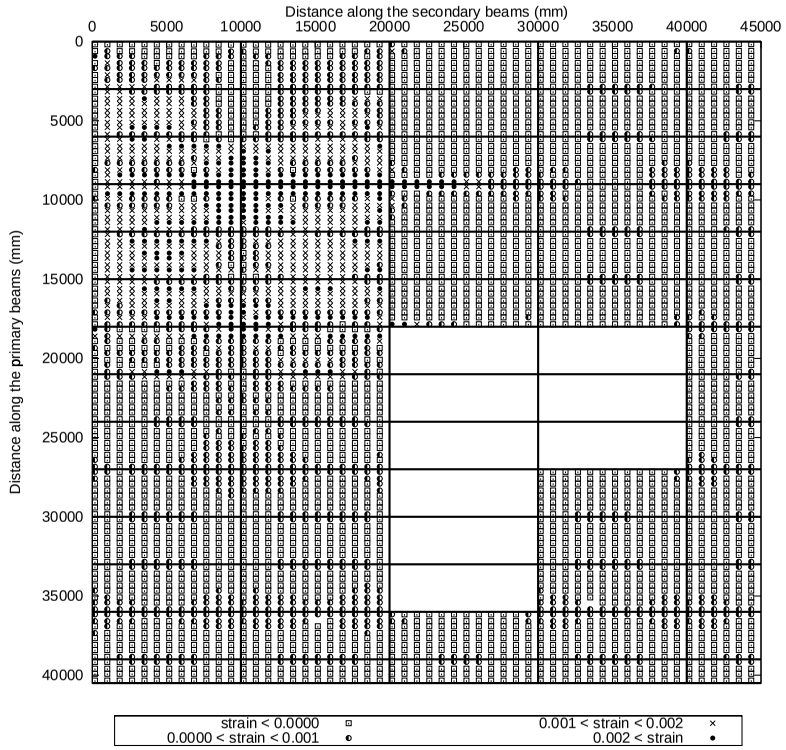

(b) y-direction (parallel to the primary beams)

Figure 9.39: Mechanical strains in the reinforcement OF=0.02, corner compartment fire at 750^{o}C

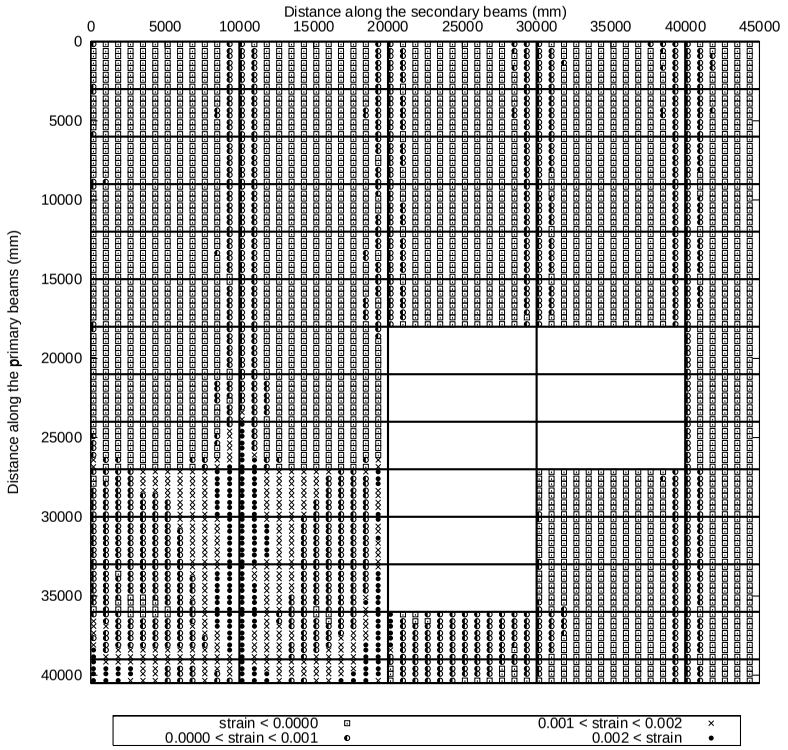

(a) x-direction (parallel to the secondary beams)

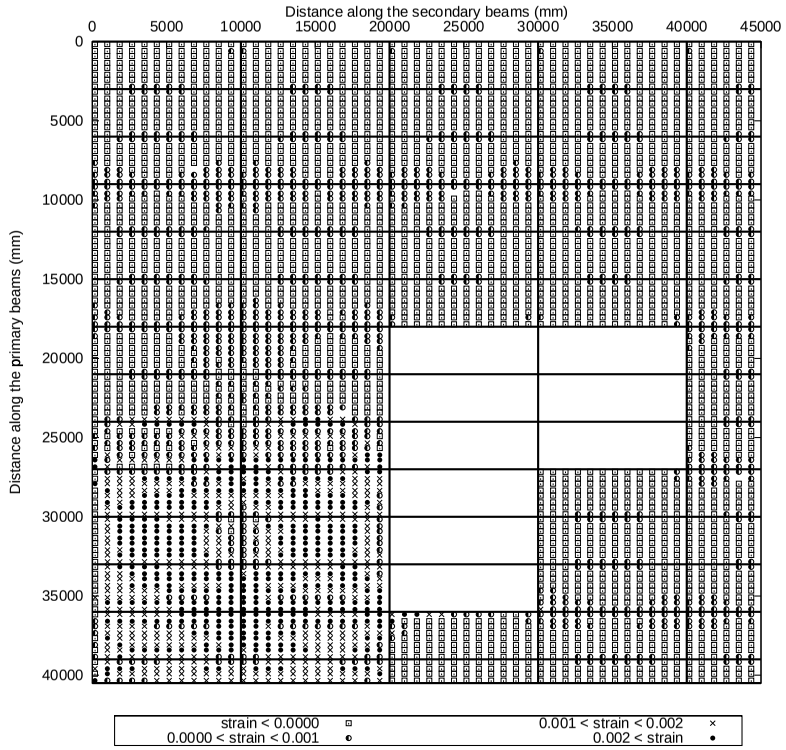

(b) y-direction (parallel to the primary beams)

Figure 9.40: Mechanical strains in the reinforcement OF=0.02, edge compartment fire at 750°C

- The mechanical strains at reinforcement level in the slab were low in both scenarios.

9.6.3 Effect of protection level under a "long" post-flashover fire in a large frame

Scenarios 1 and 3 of Table 9.1 are compared in this section. Based on the knowledge gained from the same comparison in the small frame the relative displacement between the outside edges of the compartment and the inside edges should be small when the edge beams are unprotected. This is the case because unprotected edge beam deflections are of the same magnitude as the primary and secondary beams. See Figures 9.41and 9.42 for secondary and primary beam deflections and Figures 9.43 and 9.44 for edge beam deflections.

In the small frame primary and secondary beam mid-span deflections were greatest when the edge beams were unprotected. In this instance the mid-span deflection of the primary and secondary beams are greatest where the edge beams are protected as a result of higher restraint in the large frame.

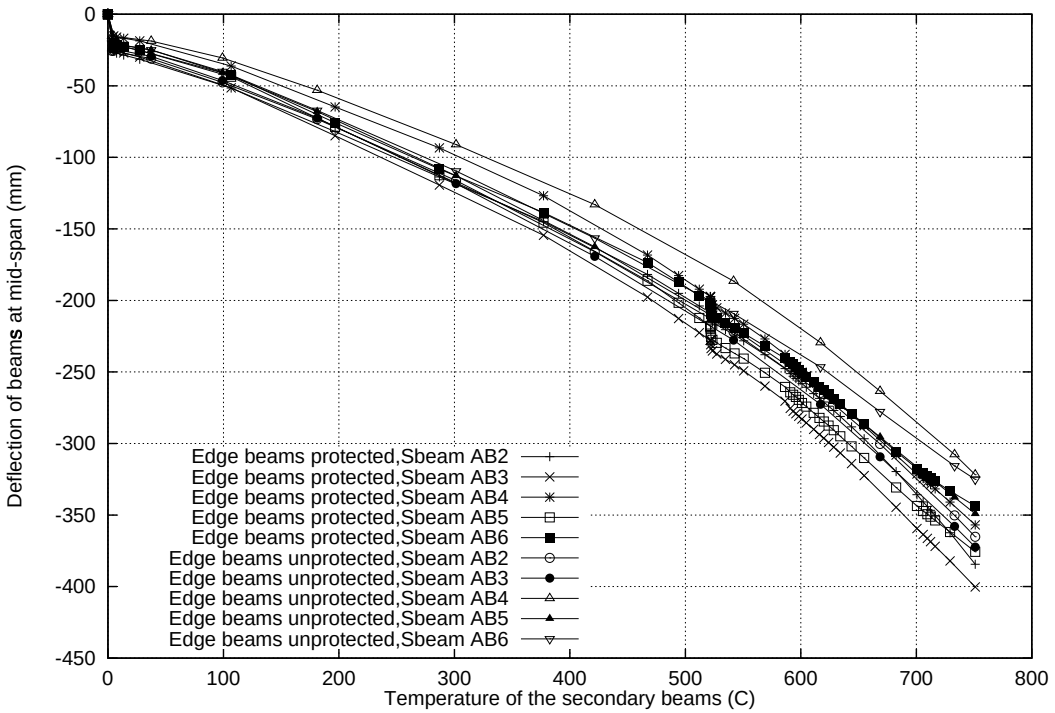

Figure 9.41: Mid-span deflection of the secondary beams

The slab deflections are shown in contour plots at the end of heating in Figure 9.45.

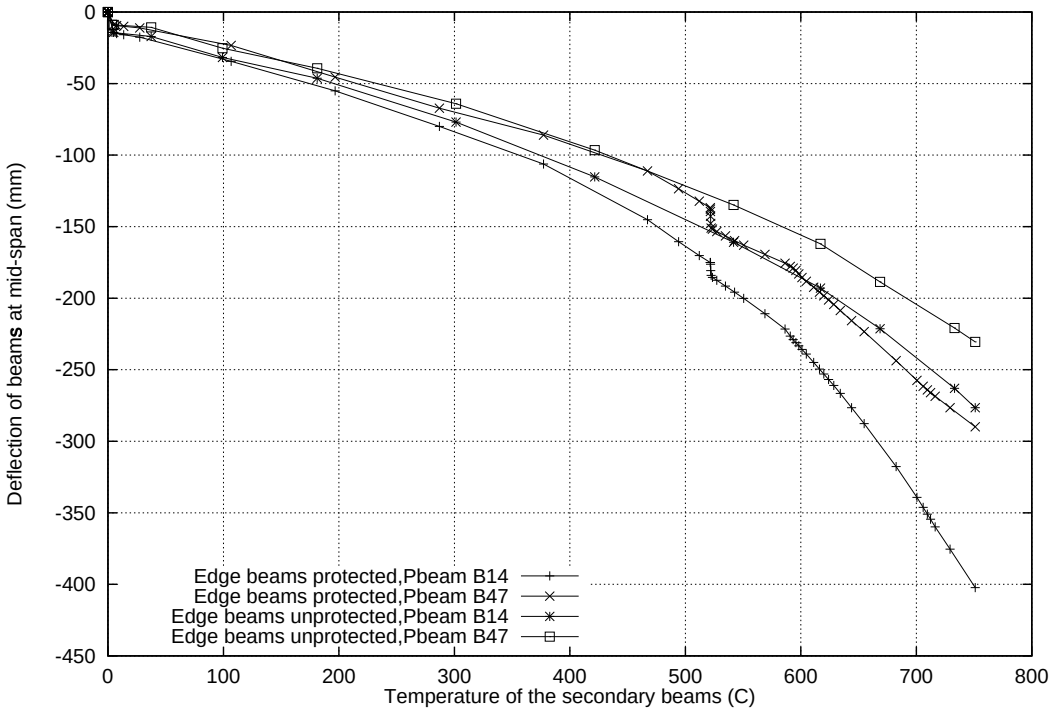

Figure 9.42: Mid-span deflection of the primary beams

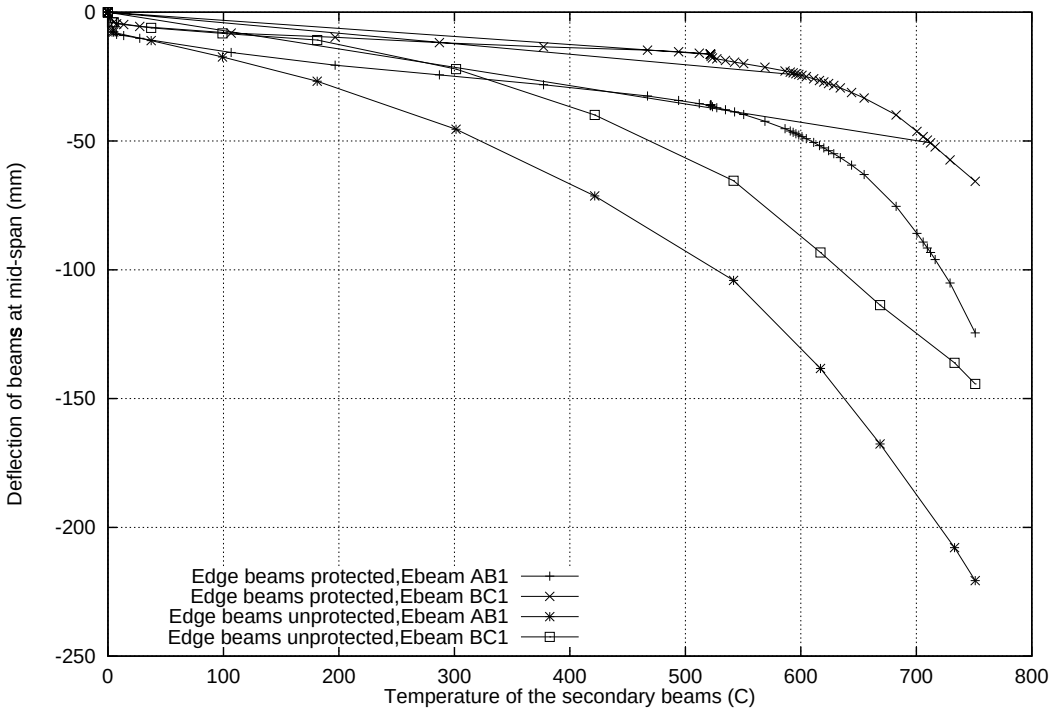

Figure 9.43: Mid-span deflection of the edge beams along gridline 1

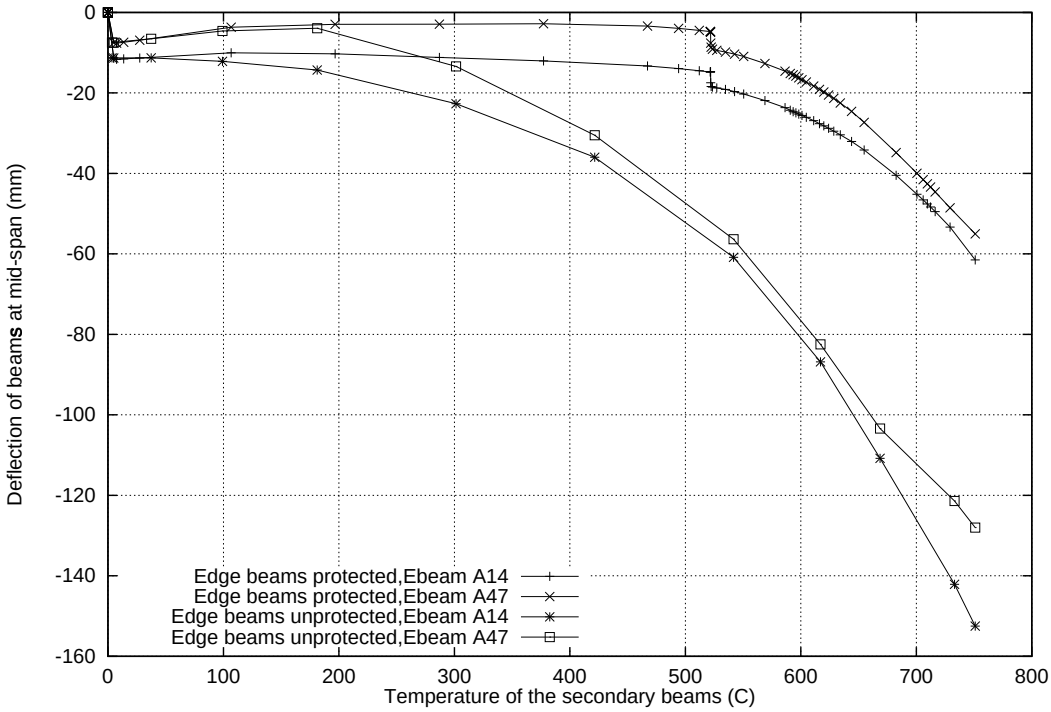

Figure 9.44: Mid-span deflection of the edge beams along gridline A

Large slab deflections in the centre of the compartment bays are supported on all sides when the edge beams are protected. When the edge beams are unprotected the slab is beginning to move into 1D behaviour especially in the corner bay where edge beam AB1 is deflecting considerably.

9.6.4 Response of the beams

Axial forces in edge beam AB1 are plotted for both scenarios in Figures 9.46 and 9.47. When the edge beams are protected edge beam AB1 is in axial tension along its length between reference temperatures of $100 - 300^{o}$C. In the 2x2 frame in the same scenario edge beam AB1 remained in compression between mid-span and gridline B. However edge beam AB1 in the small frame was only 6m long. Unprotected edge beam AB1 (Figure 9.47) behaves like a secondary beam.

9.6.5 Slab behaviour

The mechanical strains at the end of heating are shown in Figures 9.48 and 9.49. There is very little difference between the two scenarios. In the y-direction there is a larger area of compression strains along gridline 1 when the edge beams are protected because of greater restraint to expansion from the protected edge beam.

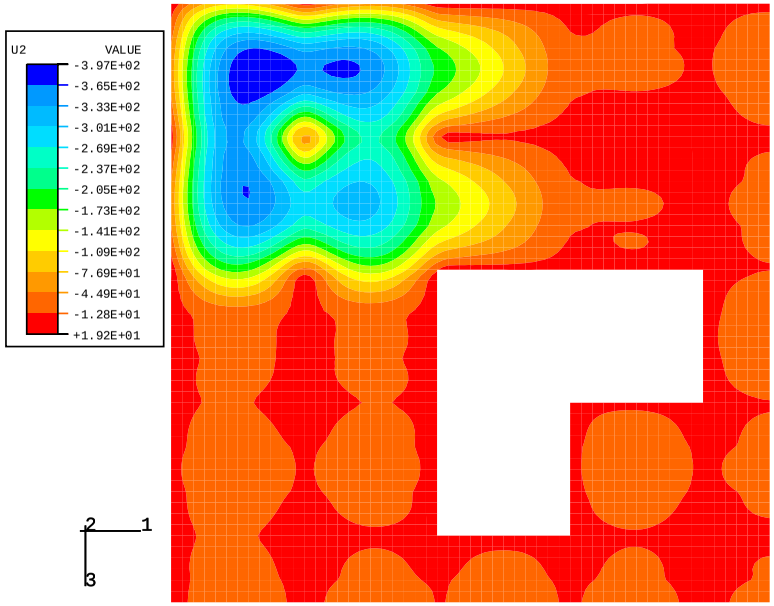

(a) Edge beams protected

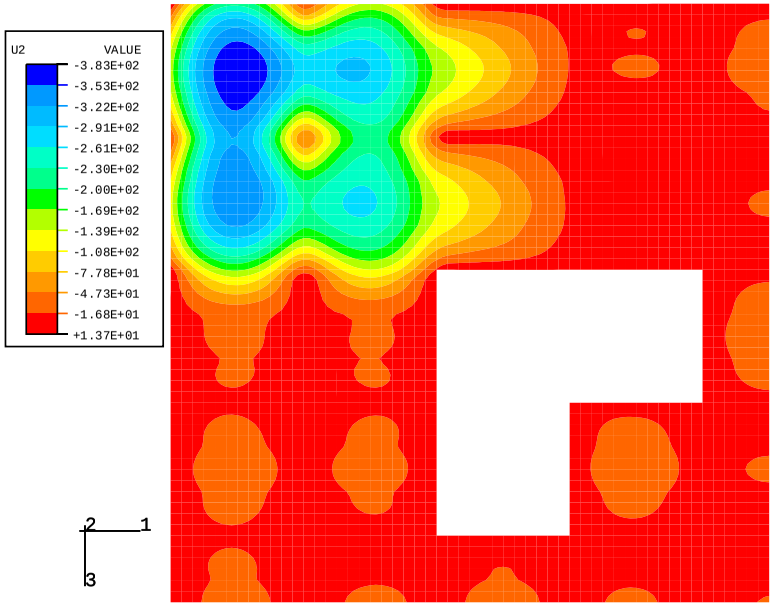

(b) All beams unprotected

Figure 9.45: Deflection contours in the slab at 750^{o}C

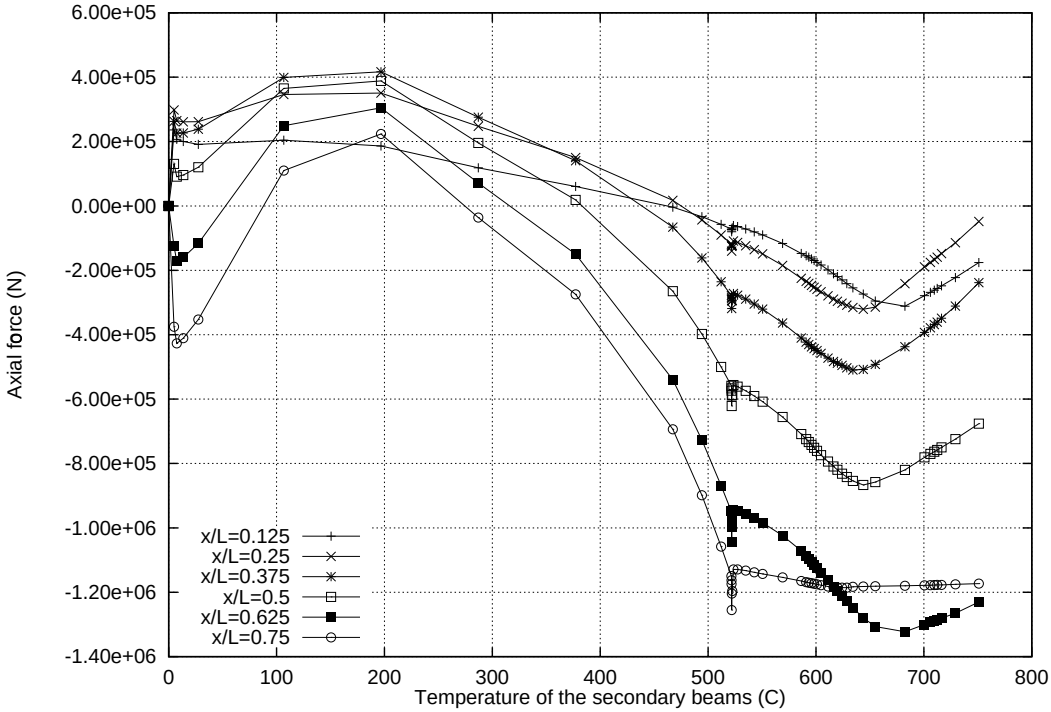

Figure 9.46: Edge beam AB1: Variation of axial force against secondary beam temperature, edge beams protected

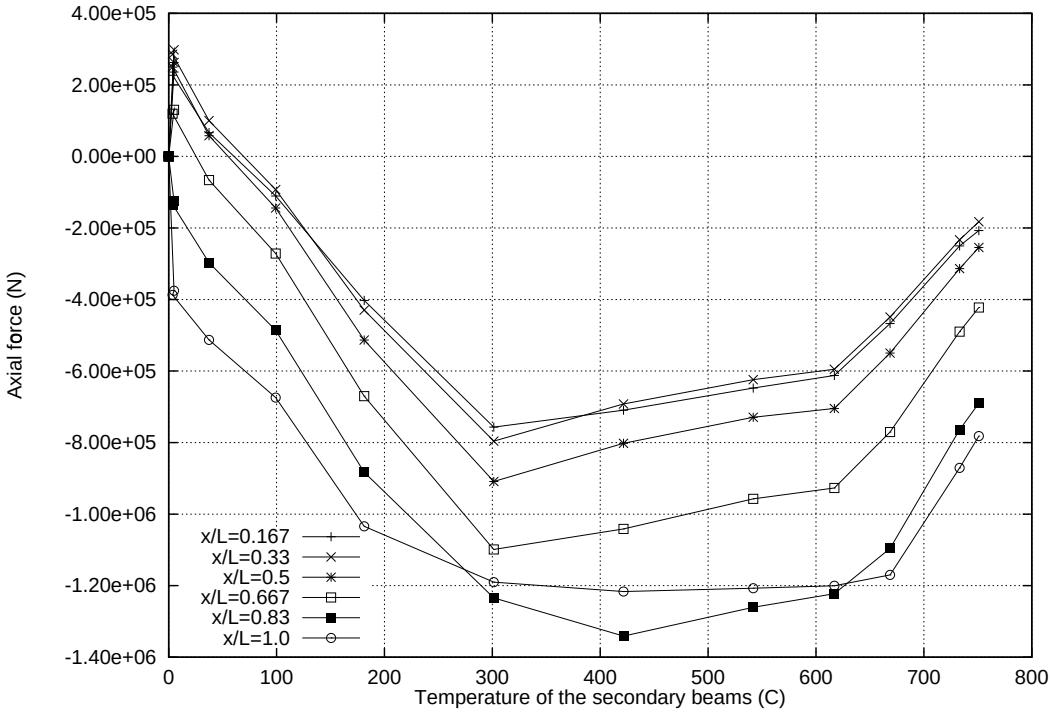

Figure 9.47: Edge beam AB1: Variation of axial force against secondary beam temperature, edge beams unprotected

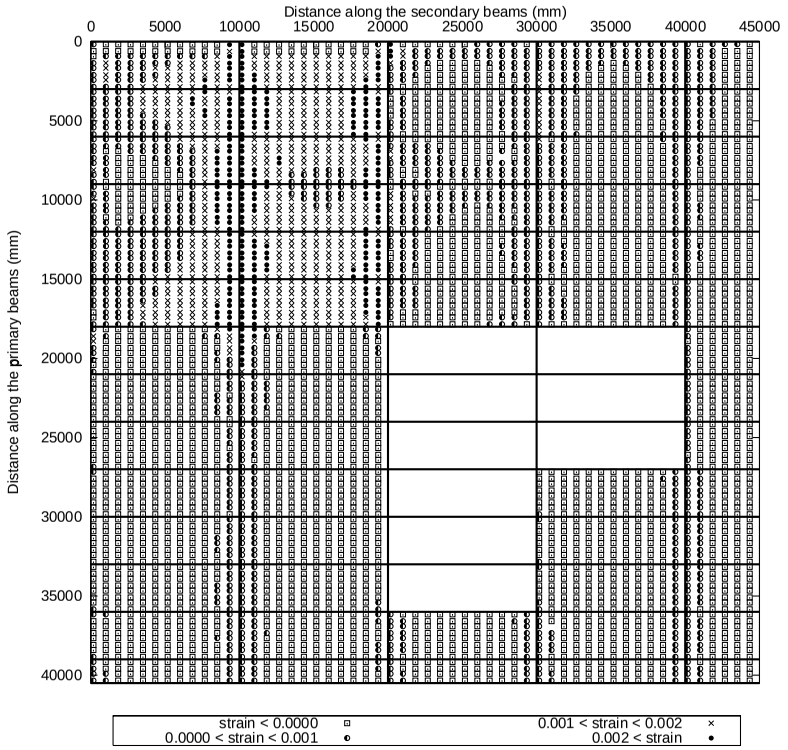

(a) x-direction (parallel to the secondary beams)

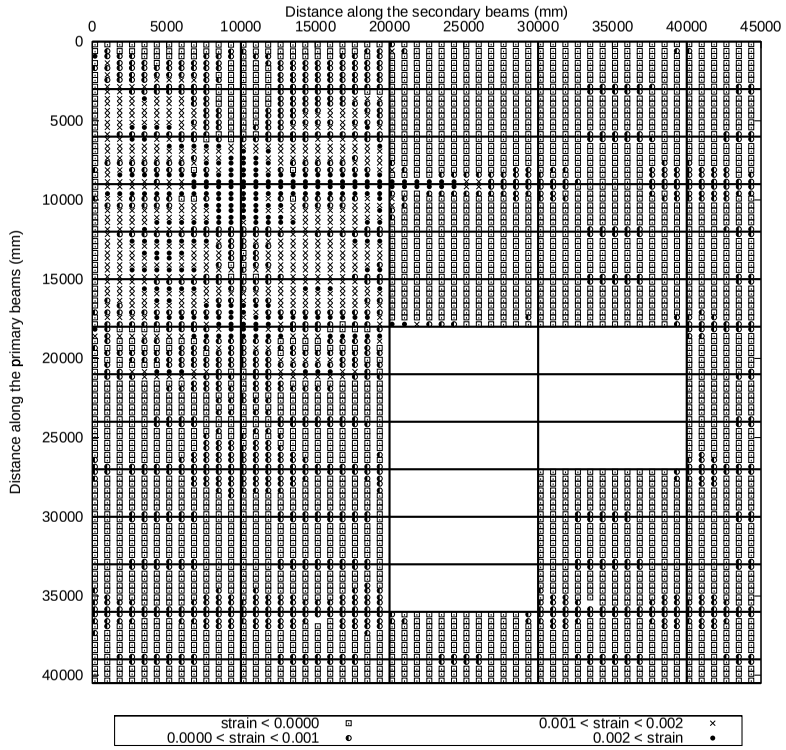

(b) y-direction (parallel to the primary beams)

Figure 9.48: Mechanical strains in the reinforcement OF=0.02, edge beams protected at 750^{o}C

9.6.6 Summary

- Mid-span deflections of the various beams are influenced by the fact that two sides of the compartment provide greater rotational restraint through continuity of the slab into the cold surrounding structure.
- Mechanical strains in the slab at reinforcement level were very similar in both cases.

9.7 Large versus small frames

Very similar parametric studies have been conducted on the small 2x2 frame and the large 9x9 frame. In some respects the models behaved in the same way. Both frames behaved in a similar manner to the "short-hot" fire and the "long-cool" fire. Also both frames experienced instabilities in their primary beams associated with the steel beam reaching its capacity in compression causing the whole composite slab to rotate as the end restraint conditions changed from moment resisting to pinned.
Compatibility was an issue in the small frame between the 9m primary beam and the 6m secondary beams spanning into it. In the large frame all the beams were of equal length so compatibility had a lesser role.
When the edge beams were unprotected the slab of the small frame moved into 1D catenary action because of very high deflections in the 9m edge beams. This load carrying mechanism is much weaker than 2D tensile membrane action which was allowed to develop when all the edge beams were protected. In the large frame in response to the "short-hot" corner fire the outside corner bay of the compartment also experienced very large deflections in one edge beam resulting in a similar 1D response in the slab. The large 9x9 frame has considerably more redundancy than the small frame because the frame is larger and made up of more members but also because the large frame was only subjected to compartment fires acting over a relatively small area of the whole floor. Yet, the small frame was very robust surviving large instabilities in the primary beam. Runaway was only observed when the edge beams were unprotected.
Mechanical strains plotted at reinforcement level in the slab were considerably higher in the small frame than the large frame. This was partly due to compatibility of deflections. In the small frame compatibility played a major role whereas in the large frame all the bays were 9m square and compatibility was insignificant.

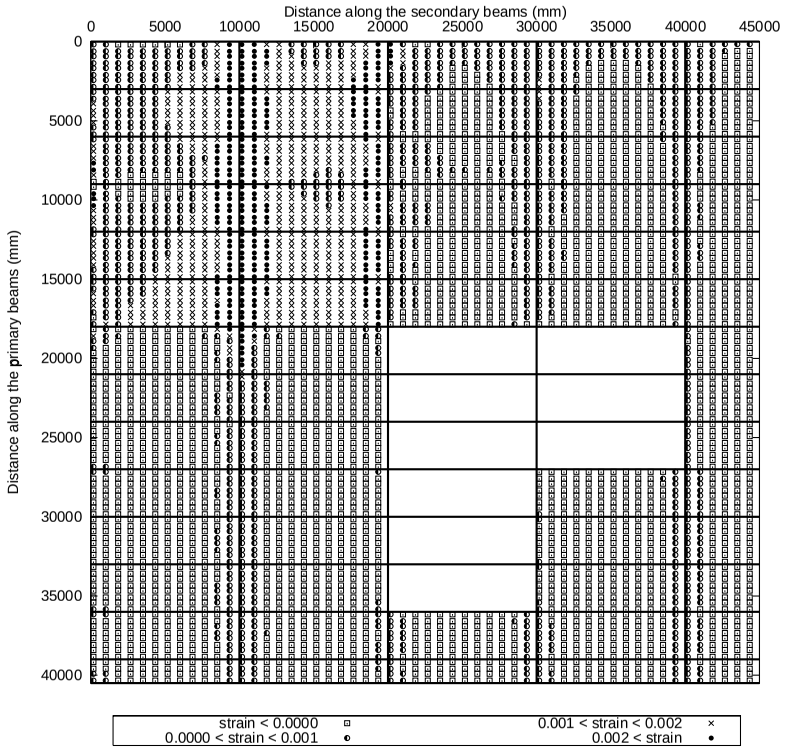

(a) x-direction (parallel to the secondary beams)

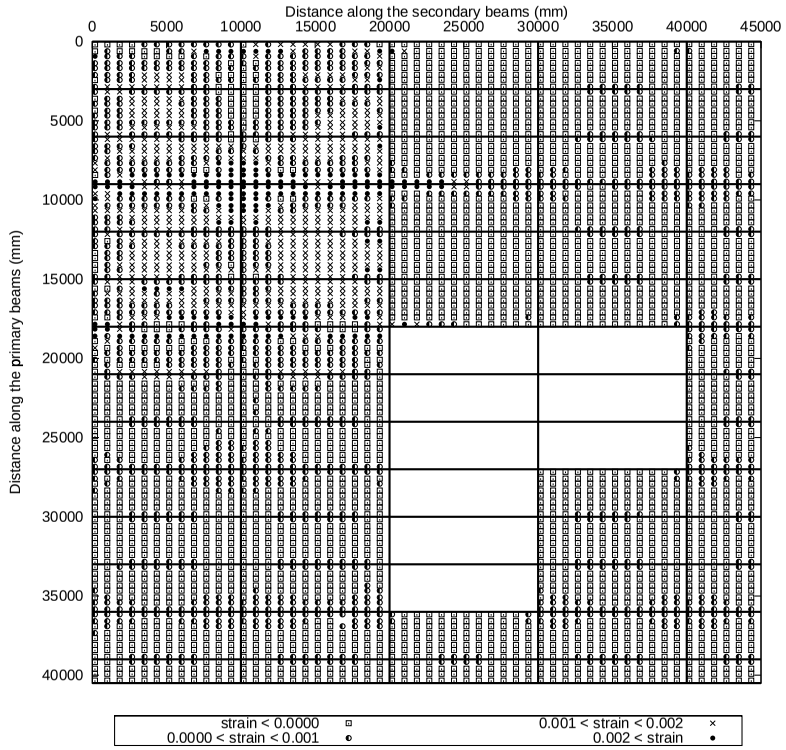

(b) y-direction (parallel to the primary beams)

Figure 9.49: Mechanical strains in the reinforcement OF=0.02, edge beams unprotected at 750^{o}C

9.8 Conclusions

- The most detrimental fire in terms of the structural response in the large frame is the "short-hot" fire. Large deflections developed in the unprotected edge beam AB1 causing the slab to effectively act in one direction. There were also larger mechanical strains in the slab in the "short-hot" corner fire scenario.

- The "long-cool" fire results in higher temperatures in the concrete which results in much less tension in the slab.

- The instability event in the primary beam viewed in the small frame also occurred in the large frame in the "short-hot" corner fire with edge beams unprotected (at 180^oC) and in the "long-cool" corner fire with edge beams protected (at 520^oC).

- The corner and edge compartment fires caused differences in behaviour of the members which were exaggerated by the bracing core immediately adjacent to the edge compartment.

- Secondary beams between gridlines A and B deflected to a greater extent in the corner compartment than the edge compartment for the same fire scenario. However, secondary beams between gridlines B and C achieved larger deflections in the edge compartment because of the restraint from the bracing core.

- The primary beam instability occurred in the corner compartment fire but not in the edge compartment.

- When comparing the effect of edge beam protection on the behaviour of the structure in the corner compartment fire, mid-span deflections of the various beams are influenced by the fact that two sides of the compartment have continuity with the cold surrounding structure. Deflections are governed by high restraint from the protected edge beams, the surrounding cold structure and the rotational restraint from the continuity of the slab.

- Mechanical strains in the slab at reinforcement level were very similar whether the edge beams were protected or not.

- Protected edge beams allow the slab to be anchored on all four sides of the frame throughout the heating regime.

- Protected edge beams will allow the structure to survive for a longer period of time.

- The 2x2 frame with a whole floor fire was more sensitive to changes in parameters such as fire severity and protected or unprotected edge beams than the large frame with corner and edge compartment fires.

Chapter 10

Conclusions and Further work

10.1 Introduction

This research has been diverse and wide reaching. It has covered in some detail all areas necessary for structural analysis of composite steel frame structures in fire. The most recent methods of computing compartment fire histories have been reviewed. Heat transfer analysis of protected and unprotected steel as well as composite slabs has been performed. In early work, alongside the PIT project, analytical studies and simple numerical models were developed to understand the response of simple beams to changes in mean temperature and thermal gradients. The influence of restraint was also analysed enabling a detailed explanation of the behaviour of beams in fire to be developed, including an analysis of single member tests. Parametric studies on the existing grillage model of British Steel test 1 (the restrained beam test) tested the effect of changing the gradient and the mean temperature in the slab so testing the theories developed for thermal expansion and thermal bowing on simple models. Extensive parametric studies on generic frame models then followed. The purpose of this chapter is to summarise and appraise the conclusions of this research. Suggestions for possible further work are also made.

10.2 Summary and Conclusions

- Design of steel structures against fire has traditionally been based upon testing of single determinate elements in a standard furnace. Failure or runaway of an axially unrestrained beam in a standard fire resistance test is a direct result of material degradation at high temperatures. This response cannot hope to model the failure of a restrained beam in a highly redundant multi-storey structure.

- A detailed description of fire resistance design was outlined in Chapter 2. The fire resistance test is inadequate in a number of respects not least because the fire exposure is not representative of real fires or that single elements are tested to failure and the results used in the design of whole frames.

- Methods of calculating the fire resistance of structural elements have also been outlined such as the limiting temperature method in BS 5950 Part 8. These are still based on single element behaviour and do not consider the interaction of the connected structure. This approach to steel design has led to extensive use of applied fire protection, to limit the temperature of the steel in fire, at considerable cost.

- The Broadgate phase 8 fire, in the late 80s, initiated the beginnings of change. The Broadgate building was under construction at the time of the fire. There were no sprinklers in operation and most of the steelwork was unprotected. Despite large deflections in the composite floor slab the structure survived the fire. It cost £25 million to reinstate the building but only £2 million represented structural repairs.

- The Broadgate fire provided real evidence that composite steel frame structures can survive fire without applied fire protection. To understand the behaviour of composite frame structures in fire BRE built an 8-storey composite steel frame structure in their large scale test facility at Cardington. Six full-scale fire tests were conducted on the frame (four by British Steel and two by BRE) ranging from a furnace test on a highly restrained single beam to a half floor compartment fire test. The frame survived all six tests.

- Finite element modelling of the structural behaviour in the Cardington frame fire tests followed. Work at Edinburgh University as part of the PiT project *"The behaviour of steel framed structures under fire conditions"*[187] highlighted that the structural behaviour was dominated by the thermal regime and that material degradation and loading play a secondary role. Thermal expansion and thermal bowing of the composite floor caused large thermal strains which when absorbed in deflections, instead of mechanical straining, were not detrimental to the structure. Axially restrained steel beams buckled at very low temperatures (100^{o}C) allowing longitudinal thermal expansions to be absorbed in downward deflections. The survival of the composite frame relied on these large deflections to allow tensile membrane action to develop in the floor slab. In general highly redundant composite framed structures possess large reserves of strength by adopting large deflection configurations.

- Despite extensive dissemination of the output from the Cardington tests limited progress has been made in the form of new design guidance. This is partly because the new knowledge was from only six tests on one structure.

- Factors influencing the behaviour of steel and composite structures in fire such as material degradation, axial and rotational restraint, thermal bowing and thermal expansion were highlighted in Chapter 2 of this thesis. Each factor was discussed separately although in a real structure they would interact to define the behaviour.

- During the Cardington frame tests steel and concrete temperatures were measured at many locations. In performance based design, natural design fires are assumed

based on the geometry of the compartment, thermal properties of the compartment boundaries, available ventilation and fire load. Heat transfer calculations are then undertaken to estimate the temperature of the connected structure.

- There are a whole range of design tools available to the engineer to calculate first the compartment fire history and secondly the heat transfer to the elements of construction.

- The advent of reliable and powerful computers has enabled very sophisticated modelling of fires and heat transfer. The level of sophistication necessary depends on the fire engineering design. In most cases a simple parametric calculation of the post-flashover fire is all that is required. Detailed examination of the parametric temperature-time curve in EC1 and the one zone computer fire model OZone have highlighted the shortcomings of these tools however in general, they over predict compartment fire temperatures leading to safe designs.

- Heat transfer to steel beams and columns can be calculated by simple lumped mass heat transfer relationships because the high conductivity and homogeneity of steel make simple calculations accurate. Concrete temperatures are more difficult to predict and require finite element models to get accurate data.

- Heat transfer analysis of the composite floor slab in the Cardington frame was conducted using an in-house 2D adaptive finite element code HADAPT. Phase change of moisture to vapour in the concrete was represented by the enthalpy method. The relatively simple 2D model predicted the measured temperatures in the slab in the first three British Steel fire tests.

- The protected and unprotected edge beam temperatures were also predicted with reasonable accuracy. Discrepancies were as a result of local heating effects. During a compartment fire convective flow near an edge beam may be very different from the convection currents underneath the ceiling in the middle of the compartment.

- The results from complex finite element models of whole frames are difficult to interpret. Also design rules need to be based on a theoretical understanding of structural behaviour. Thus simple theoretical analyses of single beams in response to different heating regimes were carried out as part of the PIT project. The theory was validated against simple numerical models in Chapter 6. The simple analyses resulted in a clear understanding of large deflections in structures subject to thermal loading:

  - Thermal expansion and thermal gradients are the primary cause.

- Thermal expansion can only produce large downward deflections if the ends are restrained from expanding.
- Thermal gradients can only produce deflections if the ends are free to rotate (by imposing curvature).
- The development of deflections and internal forces in the beam is governed by the interaction of mean temperature increase, through depth thermal gradients and the end restraints governing translation and rotation. The variation of mean temperature and thermal gradients (for various thermal regimes) can produce a large variety of responses from largely compression when thermal expansion is dominant to mainly tension when thermal bowing is dominant. Therefore any state from high compression to high tension can (theoretically) exist in heated structural members. However, in all these cases large deflections will be present albeit having developed through different mechanisms.

- The simple beam analyses also showed that an axially unrestrained beam tested in a standard furnace bears little relevance to the behaviour of structural elements as part of highly indeterminate structures typical of modern, composite steel frame buildings. The test methods are inadequate when the beam is tested as simply supported i.e. no consideration of restraint is made. By including the effect of restraint in a simple beam model the temperature at which "runaway" occurred was greatly increased. The reasons for this i.e. the changing load carrying mechanisms involved as catenary action develops at large deflections were explained.

- A detailed parametric study on the grillage model of British Steel restrained beam test further enforced the importance of the thermal regime in defining the structural behaviour. The structural response was dominated by restrained thermal expansion and compatibility of deflections. The studies showed that increasing the mean temperature of the slab results in large increases in deflection (through thermal expansion) and large increases in internal forces (P-Δ forces) because of the high lateral restraint to the beam. Thermal gradients had considerably less influence in this test because curvatures can more easily be restrained by a stiff structure.

- Chapters 8 and 9 presented the behaviour of two generic steel frames to different fire scenarios and fire protection configurations.

- The most detrimental fire in terms of the structural response was the "short-hot" fire. Large deflections developed in a very short time. This may result in early

compartmentation failure. The slab experienced high mechanical tensile strains at reinforcement level because of the high gradient in the composite.

- The "long-cool" fire resulted in higher temperatures in the concrete and the protected steel. This caused greater displacements in the protected structural elements but much later in terms of real time. However, because the concrete slab achieved higher temperatures there was much less tension in the slab with growing compressions towards the end of heating.

- Compatibility played a significant role in the behaviour of the rectangular 2x2 frame but less of a role in the large square frame. Compatibility in the 2x2 frame caused greater mechanical strains (tensions) in the slab.

- Both the small frame and the large frame experienced an instability event in the primary beam causing a rapid loss in axial compression. This was shown to coincide with a change in the end conditions of the primary beam from moment resisting to pinned at the compression capacity of the steel joist.

- The mechanism which caused a sudden reduction of axial forces along the primary beam was a change in the end restraint conditions of the primary beam from fixed to pinned because of increasing moment at the connection. The primary beam to column connection is designed as simple but the composite action between the beam and slab result in a fixed connection. The fixity prevents the secondary beams from deflecting (compatibility) to the extent that the thermal regime would allow and the primary beam carries increased loading from the expanding and bowing secondary beams pushing it down. When the compression capacity at the end of the primary beam is reached the whole composite rotates and there is a rapid increase in the rate of deflection of the composite floor. The end conditions of the primary beam are influenced by large compressions in the steel beam because of restrained thermal expansion, moments due to thermal gradients, moment due to imposed loading and increased loading on the primary beam from the secondary beams.

- This type of behaviour in the primary beams was not observed at Cardington because the loading was too small. The primary beams in both frames had a high load ratio relative to the primary beams in the Cardington frame.

- When the edge beams were unprotected the composite floor reached similar deflections over the whole fire compartment. The relative displacement between the outside edges and the middle of the compartment was small reducing the development of tensile membrane action.

- Protected edge beams allowed the slab to be anchored on all four sides of the frame throughout the heating regime. When the edge beams were unprotected the slab would tend towards 1D catenary action which is a much weaker load carrying mechanism than 2D tensile membrane action.
- Protected edge beams will allow the structure to survive for a longer period of time.
- The 2x2 frame with a whole floor fire was more sensitive to changes in parameters such as fire severity and protected or unprotected edge beams than the large frame with corner and edge compartment fires because the former is a small low redundancy frame and the latter is a large highly redundant frame.

10.3 Further work

The last 10 years has seen new understanding of the behaviour of steel frame structures in fire. The research described in this thesis has taken this understanding further but inevitably there is still many issues unresolved.

10.3.1 Further development of FEAST

The FEAST suite of programs is probably the most comprehensive model arising out of the PiT project. Further improvements could include,

- Modelling the true unloading path, especially to enable the modelling of cooling.
- Inclusion of non-linear gradients in the ABAQUS input file to match the accuracy in SRAS

10.3.2 Further parametric studies

Chapters 8 and 9 describe the response of two generic frame structures to various compartment fire scenarios. The need for fire protection on the primary and edge beams was also investigated in detail. However there are many other parametric studies which could be carried out. The effect of the fire exposure has been covered in some detail with less emphasis on the structural layout, material properties and dimensions of the structural members. The overall size of the buildings has been investigated. The 2x2 bay frame and the 9x9 bay frame are sufficiently different from the Cardington frame (3x5 bay) and were chosen for this reason. However the construction of the frames do

not differ. No studies were conducted on analysing the strength of steel used or the type of concrete. The depth of the slab and the reinforcing mesh were also identical to the Cardington frame. Figure 10.1 shows the matrix of possible scenarios considered during this research. The red dots highlight the scenarios which were finally tested.
An interesting structure to investigate would be a column free space (columns restricted to the outer edges of the building). In this situation the spans would be much longer resulting in higher thermal expansion effects.
The steel reinforcing mesh in the LWC slab plays a critical role in the later stages of the fire. It is very likely that by increasing the mesh thickness an increased level of fire resistance would be achieved. Indeed Bailey[24] proposes this in his design method for composite frame structures in fire. This needs to be investigated in detail. In particular quantifying failure of the reinforcing mesh during the fire (or cooling) is very important.

10.3.3 Spreading fires

In very large spaces of varying fire load it is unlikely that the whole compartment will achieve flashover at the same time. Spreading fires have not been addressed in this research. However they provide an interesting scenario both thermally and structurally. During a spreading fire the fire will grow and decay in different parts of the space at different times. This scenario should be investigated after a reliable model is developed to include unloading of the material curves under cooling.

10.3.4 Cardington Frame Fire Test Data

The six Cardington Frame Fire tests, described in detail in Chapter 4 and discussed throughout this thesis have also been reported and analysed in the research literature and engineering forums for many years. However there is still a wealth of well documented data from these tests which has not been exploited. CORUS have gone some way towards analysing all available data from their 4 tests but it is a huge task. Now reliable numerical models are available and there is a greater understanding of the structural behaviour of the Cardington Frame Structure in fire analysing the test data available could be a much more useful task. Heat transfer models could also provide much more detailed information about the spatial and temporal heating regime in all the structural elements.

	Building			Fire compartment					Fire type			Protected elements				
	2x2	9x9	Load	corner	internal	edge	half	whole	Low vent.	High vent	spreading	Columns only	Eb+C	Pb+Eb + C	ignore Sb	mesh size
2x2			•					•	•	•		•	•	•	•	
9x9				•		•			•	•		•	•			
Load	•							•		•			•			
Corner		•							•	•		•	•			
Internal																
Edge		•							•				•			
Half																
Whole	•		•						•	•		•	•	•	•	
Low vent.	•	•		•		•		•				•	•	•		
High vent.	•	•	•	•				•				•	•		•	
Spreading																
Columns only	•	•		•				•	•	•						
Eb+C	•	•	•	•		•		•	•	•					•	
Pb+Eb+ C	•							•	•					•		
Ignore Sb	•							•		•			•			
Mesh size																

Key: Eb Edgte beam
Sb Secondary beam
Pb Primary beam
C Column

Figure 10.1: Matrix of possible parametric studies

10.3.5 Future fire tests

The most important future fire test is that which will define structural failure of a composite frame in fire.

10.3.5.1 Ultimate limit state for fire design

Structural failure of the Cardington Frame fire tests did not happen. Ambient structural design has been driven by the limit state philosophy for many decades and there are growing efforts to define failure of composite structures in fire. However there is controversy about this research because there are many factors to consider in fire safety engineering design and failure is defined at many levels. Integrity failure of a compartment boundary is much more likely to occur before the structure will collapse.
There are also many issues surrounding the maximum allowable deflections in structural members during a fire. Large displacements in composite floor slabs enable tensile membrane action to develop and carry the load. They also absorb thermal expansions and reduce thermally induced mechanical strains. However highly deflected beams may not be acceptable to the owner of the building if they have to be replaced after a fire. This may delay the start of business operations. Large deflections in floors could also be dangerous for the fire service if they are walking through a building.

10.3.6 Development of design codes

In chapter 6 the understanding of structural behaviour in fire was greatly enhanced by simple beam models. The obvious next step is to carry out similar analyses with slabs or plates. This work is already on going at Edinburgh University. This is particularly important because the tests and numerical models have highlighted the benefits of tensile membrane action in carrying the structure during the post-flashover and decay phase of the fire. By developing simple analytical expressions the design of slabs and whole frames in fires should become a reality.

There are two possible approaches to simple design in fire. The first has been highlighted by developing expressions for slabs in highly deflected shapes. The other is to reduce the complexity of finite element grillage models so designers can carry out simple, fast numerical studies.

The SCI publication "Fire safe design: A new approach to multi-storey steel framed buildings" developed as a direct result of theoretical work carried out by Bailey[23] is a considerable step towards designing composite frame structures in fire. The rules

regarding maximum bay sizes may be conservative although protected edge beams considerably enhance the load carrying capacity of the frame at large deflections. The generic frame studies showed that the slab could behave like a beam in catenary action rather than a slab in tensile membrane action when the edge beams were unprotected.

Performance based fire design is essential in slightly extraordinary structures. Large spaces (like airports) or very high spaces (like atria) provide much more scope to apply some engineering logic to the fire strategy. In these cases applying fire protection in accordance with the code would be onerous and result in inefficient design. By simply proving that wide open spaces with low fire loads will not result in fires which will allow structural steel temperatures to exceed 550^{o}C the steel can be left unprotected. Buildings like the Cardington frame which in reality would be filled with office space resulting in moderately high fire loads in relatively confined spaces do not allow such freedom of engineering initiative. The new SCI guide[170] is the only method of reducing applied fire protection in composite frame structures. An understanding of structural behaviour in fire will lead to less fire protection in steel frame buildings where fully-flashed over fires in compartments are more likely to occur.

Bibliography

[1] G.N. Ahmed and J.P. Hurst. Modelling pore pressure, moisture and temperature in high-strength concrete columns exposed to fire. *Fire Technology*, 35:232–261, 1999.

[2] F.A. Ali, I.W. Simms, and D.J. O'Conner. Behaviour of axially restrained steel columns during fire. In *5th International Symposium of Fire Safety Science*, 1997.

[3] R.L. Alpert. Calculation of response times of ceiling mounted fire detectors. *Fire Technology*, 8:181–195, 1972.

[4] Y. Anderberg. Modelling steel behaviour. *Fire Safety Journal*, 13:17–26, 1988.

[5] Y. Anderberg, N.E. Forsen, and B. Assen. Measured and predicted behaviour of steel beams and columns in fire. In *1st International Symposium of Fire Safety Science*, 1985.

[6] G.S.T. Armer and T. O'Dell, editors. *Fire Static and Dynamic Tests of Building Structures*. E and FN SPON, Chapman and Hall, 1999.

[7] Association for Specialist Fire Protection, Steel Construction Institute, Fire Test Study Group. *Fire protection for structural steel in buildings*, 2nd edition, 2000.

[8] ASTM. *E 119-95a: Standard test methods for fire tests of building construction materials*, 1995.

[9] V. Babrauskas. A closed-form approximation for post-flashover compartment fire temperatures. *Fire Safety Journal*, 4:63–73, 1981.

[10] V. Babrauskas. *Burning rates*, chapter 1 section 3. The SFPE Handbook of Fire Protection Engineering, 2nd edition, 1995.

[11] V. Babrauskas and S.J. Grayson, editors. *Heat release in fires*, chapter 6, Room fire models, pages 113–171. 1992.

[12] V. Babrauskas and U. Wickstrom. Thermoplastic pool compartment fires. *Combustion and flame*, 34:195–202, 1979.

[13] V. Babrauskas and B. Williamson. Post-flashover compartment fires: Basis of a theoretical model. *Journal of Fire and Materials*, 2:39–53, 1978.

[14] V. Babrauskas and B. Williamson. Post-flashover compartment fires: Application of a theoretical model. *Journal of Fire and Materials*, 3:1–7, 1979.

[15] V. Babrauskas and R.B. Williamson. Post-flashover compartment fires: Basis of a theoretical model. *Fire and Materials*, 2(2):39–53, 1978.

[16] V. Babrauskas and R.B. Williamson. The historical basis of fire resistance testing-Part I. *Fire Technology*, 14:185–194, 1978.

[17] V. Babrauskas and R.B. Williamson. The historical basis of fire resistance testing-Part II. *Fire Technology*, 14:304–316, 1978.

[18] C. Bailey. Computer Modelling of the corner compartment fire test on the large-scale Cardington test frame. *Journal of Constructional Steel Research*, pages 27–45, 1998.

[19] C.G. Bailey. The influence of the thermal expansion of beams on the structural behaviour of columns in steel-framed structures during a fire. *Engineering Structures*, 22:755–768, 2000.

[20] C.G. Bailey, I.W. Burgess, and R.J. Plank. Analyses of the effects of cooling and fire spread on steel framed buildings. *Fire Safety Journal*, 26:273–293, 1996.

[21] C.G. Bailey, I.W. Burgess, and R.J. Plank. Computer simulation of a full-scale structural fire test. *Structural Engineer*, 74(6):93–100, 1996.

[22] C.G. Bailey, I.W. Burgess, and R.J. Plank. The lateral-torsional buckling of unrestrained steel beams in fire. *Journal of Constructional Steel Research*, 36:101–119, 1996.

[23] C.G. Bailey, T. Lennon, and D.B. Moore. The structural behaviour of steel frames with composite floor slabs subject to fire: Part 1: Theory and part 2: Design. *The structural engineer*, 78(11):19–33, 2000.

[24] C.G. Bailey and D.B. Moore. The behaviour of full-scale steel framed buildings subjected to compartment fires. *The Structural Engineer*, 77(8):15–21, 1999.

[25] C.G. Bailey, D.S. White, and D.B. Moore. The tensile membrane action of unrestrained composite slabs simulated under fire conditions. *Engineering Structures*, 22:1583–1595, 2000.

[26] D.J. Baker and Y.M. Xie. Elasto-plastic creep analysis of restrained steel columns exposed to fire. In *4th International Symposium of Fire Safety Science*, 1994.

[27] D.J. Baker, Y.M. Xie, and P.H. Daywansa. Numerical predictions and experimental observations of the structural response of steel columns to high temperatures. In *5th International Symposium of Fire Safety Science*, 1997.

[28] Z.P. Bazant, J-C. Chern, and W. Thonguthai. Finite element program for moisture and heat transfer in heated concrete. *Nuclear Engineering and Design*, 68:61–70, 1981.

[29] Z.P. Bazant and W. Thonguthai. Pore Pressure in Heated Concrete Walls: Theoretical Prediction. *Magazine of Concrete Research*, 31(107):61–76, 1979.

[30] V. Beck. Rational Design Methods for Fire Safety: The Warren Centre Project. In *Fire Safety and Engineering, International Symposium Papers*, pages 5–14. The University of Sydney, The Warren Centre, The University of Sydney, Australia, 1989.

[31] V. Beck. Performance based fire engineering design and its application in Australia. In *5th International Symposium of Fire Safety Science*, pages 23–40, 1997.

[32] V.R. Beck and D. Yung. The development of a risk cost assessment model for the evaluation of fire safety in buildings. In *Proceedings of the Fourth International Conference on Fire Safety Science*, pages 817–828, 1994.

[33] J. Becker and B. Bresler. Fires-RC A Computer Program for the Response of Structures- Reinforced Concrete frames. Technical Report Report No. UCB FRG 74-3, University of California Berkeley, 1074.

[34] J.M. Becker, H. Bizri, and B. Bresler. FIRES-T - A computer program for the FIre REsposnse of STructures-Thermal. Technical Report Report No. UCB FRG 74-1, University of California, Berkeley, 1974.

[35] R. Becker. Thermal and structural behaviour of continuous steel construction under fire conditions. In *First International workshop, Structures in Fire*, Copenhagen, 2000.

[36] C.L. Beyler. Fire plumes and ceiling jets. *Fire Safety Journal*, 11:53–75, 1986.

[37] B. Bohm and S. Hadvig. Non-conventional fully developed polyethylene and wood compartment fires. *Combustion and flame*, 44:201–221, 1982.

[38] P.N.R. Bravery. Cardington large building test facility, construction details for the first building. Technical report, British Steel plc (now CORUS), 1993.

[39] British Standard Institution. *BS 5950: Structural Use of Steelwork in Building: Part 8*, 1990.

[40] British Standards Institution. *BS 476: Parts 20-23: 1987 Fire tests on building materials and structures*, 1987.

[41] British Standards Institution. *BS 5950: Part 8: 1990 Structural use of steelwork in building Part 8. Code of practise for fire resistant design*, 1990.

[42] A.H. Buchanan. Fire engineering for a performance based code. *Fire Safety Journal*, 23:1–16, 1994.

[43] A.H. Buchanan. *Structural design for fire safety.* Wiley, 2001.

[44] R.W. Bukowski. International activities for developing performance based fire codes. In *Fire safety design of buildings and fire safety engineering, mini symposium*, Japan, 1995.

[45] M.L. Bullen and P.H. Thomas. Compartment fires with non-cellulsoic fuels. In *17th Symposium (International) on Combustion*, pages 1139–1148. The Combustion Institute, Pittsburgh, 1979.

[46] I.R. Burgess, J.A. El-Rimawi, and R.J. Plank. Analysis of beams with non-uniform temperature profile due to fire exposure. *Journal of Constructional Steel Research*, 16:169–192, 1990.

[47] I.R. Burgess, J.A. El-Rimawi, and R.J. Plank. Studies of the behaviour of steel beams in fire. *Journal of Constructional Steel Research*, 19:285–312, 1991.

[48] I.W. Burgess, J.A. El-Rimawi, and R.J. Plank. A secant stiffness approach to the fire analysis of steel beams. *Journal of Constructional Steel Research*, 11:105–120, 1988.

[49] I.W. Burgess and S.R. Najjar. A simple approach to the behaviour of steel columns in fire. *Journal of Constructional Steel Research*, 31:115–134, 1994.

[50] J-F. Cadorin and J-M. Franssen. The one zone model OZone-Description and validation based on 54 experimental fire tests. unpublished.

[51] J. Case, Lord Chilver, and C.T.F. Ross. *Strength of materials and structures.* Edward Arnold, 3rd edition, 1992.

[52] V. Chandrasekaran and N.L. Mulcahy. Analysis of time of collapse of steel columns exposed to fire. In *5th International Symposium of Fire Safety Science*, 1997.

[53] D. Charters. Engineering a solution. *Fire Engineers Journal: Fire Prevention*, November 2000.

[54] K.P. Christiansen. The effect of membrane stresses on the ultimate strength of the interior panel in a reinforced concrete slab. *The Structural Engineer*, 41(8):261–265, 1963.

[55] G.C. Clifton. Draft for development: Design procedure for the inelastic floor system/frame response of multi-storey steel framed buildings in fully developed natural fires. Technical Report R4-90-DD, HERA (Heavy Engineering Research Association), Mankau City, New Zealand, 1998.

[56] G.M. Cooke. An introduction to the mechanical properties of structural steel at elevated temperatures. *Fire Safety Journal*, pages 45–54, 1988.

[57] G.M.E. Cooke. Thermal bowing and how it affects the design of fire separating construction. In *Interflam'88*, pages 230–236, 1988.

[58] L. Corradi, C. Poggi, and P. Setti. Interaction domains for steel beam-columns in fire conditions. *Journal of Constructional Steel research*, 17:217–235, 1990.

[59] M. Cross, R.D. Gibson, and R.W. Young. Pressure generation during the drying of a porous half-space. *International Journal of Heat and Mass Transfer*, 22:47–50, 1977.

[60] A. Dayan. Self-similar temperature, pressure and moisture distributions within an intensely heated porous half space. *International Journal of Heat and Mass Transfer*, 25(10):1469–1476, 1982.

[61] A. Dayan and E.L. Gluekler. Heat and mass transfer within an intensely heated concrete slab. *International Journal of Heat and Mass Transfer*, 25(10):1461–1467, 1982.

[62] DETR (Department of the Environment, Transport and Regions). *Approved document to support Part B: Fire safety. Building regulations 1991*, 2000.

[63] P.J. DiNenno, editor. *The SFPE Handbook of Fire Protection Engineering.* National Fire Protection Association and Society of Fire Protection Engineers, Massachusetts, USA, 2nd edition, 1995.

[64] N. Mc Donald. Properties of Vicuclad: Promat Technical Department 7th July 2000. Personal Communication.

[65] J. Dowling and J. Robinson. Fire resistance of steel frame buildings. British Steel Plc, 1998.

[66] D.D. Drysdale. The flashover phenomenon. *Fire Engineers Journal*, pages 18–23, 1996.

[67] D.D. Drysdale. *An Introduction to Fire Dynamics*. John Wiley and Sons, 2nd edition, 1999.

[68] E.R.G. Eckert and M. Faghri. A general analysis of moisture migration caused by temperature differences in an unsaturated porous medium. *International Journal of Heat and Mass Transfer*, 23:1613–1623, 1980.

[69] J.A. El-Rimawi, I.W. Burgess, and R.J. Plank. Model studies of composite building frame behaviour in fire. In *4th International Symposium of Fire Safety Science*, pages 1137–1148, 1994.

[70] J.A. El-Rimawi, I.W. Burgess, and R.J. Plank. The analysis of semi-rigid frames in fire-a secant approach. *Journal of Constructional Steel Research*, 33:125–146, 1995.

[71] J.A. El-Rimawi, I.W. Burgess, and R.J. Plank. The treatment of strain reversal in structural members during the cooling phase of a fire. *Journal of Constructional Steel Research*, 37:115–135, 1996.

[72] J.A. El-Rimawi, I.W. Burgess, and R.J. Plank. The influence of connection stiffness on the behaviour of steel beams in fire. *Journal of Constructional Steel Research*, 43:1–15, 1997.

[73] J.A. El-Rimawi, I.W. Burgess, and R.J. Plank. Studies of the behaviour of steel sub-frames with semi-rigid connections in fire. *Journal of Constructional Steel Research*, 49:83–98, 1999.

[74] A.Y. Elghazoulli, B.A. Izzuddin, and A.J. Richardson. Numerical modelling of the structural fire response of a steel framed building. Technical report, Imperial College, London University, 2000. CESLIC Report CC15, PIT Report MD15/AM7.

[75] *Eurocode 1: Basis of design and structures Part 2.2: Actions on structures exposed to fire*, 1996.

[76] *Eurocode 2: Design of concrete structures Part 1.2: General rules - Structural Fire Design*, 1995.

[77] *Eurocode 3: Design of steel structures Part 1.2: Fire Resistance*, 1995.

[78] *Eurocode 4: Design of composite steel and concrete structures Part 1.1: General rules and rules for buildings*, 1994.

[79] *Eurocode 4: Design of composite steel and concrete structures Part 1.2: Fire resistance*, 1994.

[80] R. Eyre and K.O. Kemp. In-plane stiffness of reinforced concrete slabs under compressive membrane action. *Magazine of Concrete Research*, 46(166):67–77, 1994.

[81] G. Faller. Performance-based design approach to fire resistance grading of buildings. *Fire Engineers Journal*, 60(205):23–27, March 2000.

[82] C. Fleischmann. *Analytical Methods for Determining Fire Resistance of Concrete Members*, chapter 10 section 4. The SFPE Handbook of Fire Protection Engineering, 1988.

[83] J-M. Franssen, J-B. Schleich, and L-G. Cajot. Simple model for the fire resistance of axially loaded members according to Eurocode 3. *Journal of Constructional Steel Research*, 35(1), 1995.

[84] J.M. Franssen. Improvement of the Parametric Fire of Eurocode 1 Based on Experimental Test Results. In *6th International Symposium of Fire Safety Science*, 1999.

[85] J.M. Franssen, J.B. Schleich, L-G. Cajot, D. Talamona, B. Zhao, L. Twilt, and K. Both. A comparison between five structural fire codes applied to steel elements. *4th International Symposium of Fire Safety Science*, pages 1125–1136, 1994.

[86] R. Friedman. An international survey of computer models for fire and smoke. *Journal of Fire Protection Engineering*, 4(3):81–92, 1992.

[87] R.G. Gewain and E.W.J. Troup. Restrained fire resistance ratings in structural steel buildings. Prepared for AISC Engineering Journal, Second Quarter 2001.

[88] M. Gillie. *The behaviour of steel-framed composite structures in fire conditions.* PhD thesis, The University of Edinburgh, 2000.

[89] M. Gillie. Modelling heated composite floor slabs with ABAQUS using a UGENS subroutine. In Karlson Hibbit and Sorrenson, editors, *ABAQUS Users' conference 2000*, pages 335–354, Pawtucket, RI, USA, 2000.

[90] M. Gillie, A.S. Usmani, and J.M. Rotter. Modelling of heated composite floor slabs with reference to the Cardington experiments. *Fire Safety Journal*, 36(8):745–767, 2001.

[91] M. Green. Fire safety engineering-the role of the structural engineer. *The Structural Engineer*, 77(19):18–20, 1999.

[92] M. Green. The recent UK BS9999-Presentation and worked examples. In *First International workshop, Structures in Fire*, Copenhagen, 2000. Abstract only.

[93] M. Green and Y. Wong. Value of the full scale Cardington fire tests to the structural engineer. In *Proceedings of the 2001 Structures Congress and Exposition.* ASCE, SEI, 2001.

[94] L.K. Guice and E.J. Rhomberg. Membrane action in partially restrained slabs. *ACI Structural Journal*, (85):365–373, 1988.

[95] G.V. Hadjisophocleous, N. Benichou, and A.S. Tamim. Literature review of performance-based fire codes and design environment. *Journal of Fire Protection Engineering*, 9(1):12–40, 1998.

[96] T.Z. Harmathy. A new look at compartment fires, Part I. *Fire Technology*, 8:192–217, 1972.

[97] T.Z. Harmathy. A new look at compartment fires, Part II. 8:327–351, 1972.

[98] T.Z. Harmathy. Properties of building materials: basis for fire safety design. In *Design of structures against fire*, pages 87–103, Aston University, Birmingham, April 1986. Elsevier Applied Science.

[99] T.Z. Harmathy. On equivalent fire exposure. *Fire and Materials*, 11, 1987.

[100] T.Z. Harmathy. *Fire Safety Design and Concrete*. Longman Scientific and Technical, 1993.

[101] T.Z. Harmathy. *Properties of Building Materials*, chapter 10 section 1, pages 141–155. The SFPE Handbook of Fire Protection Engineering, 2nd edition, 1995.

[102] Hibbit, Karlsson and Sorensen Inc., Pawtucket, Rhode Island, USA. *ABAQUS Theory and Users manual*, 5.7 edition, 1994.

[103] M. Hirota, K. Shinoda, K. Nakamura, and K. Kawagoe. Experimental study on structural behaviour of steel frames in building fire. *Fire Science and Technology*, 4(2):151–162, 1984.

[104] HMSO. Fire grading of buildings -Part 1. General principles and structural precautions, Post war building studies No. 20, 1946. HMSO, Ministry of Works, London.

[105] C.L.D. Huang. Multi-phase moisture transfer in porous media subjected to temperature gradient. *International Journal of Heat and Mass Transfer*, 22(1295-1307), 1979.

[106] C.L.D. Huang, G.N. Ahmed, and D.L. Fenton. Responses of concrete walls to fire. *International Journal of Heat and Mass Transfer*, 34(3):649–661, 1991.

[107] C.L.D. Huang, H.H. Siang, and C.H. Best. Heat and moisture transfer in concrete slabs. *International Journal of Heat and Mass Transfer*, 22:257–266, 1979.

[108] H-C. Huang and A.S. Usmani. *Finite Element Analysis for Heat Transfer*. Springer-Verlag, London, 1st edition, 1994.

[109] Z. Huang, I.W. Burgess, and R.J. Plank. Nonlinear analysis of reinforced concrete slabs subjected to fire. *ACI Structural Journal*, 96(1), 1999.

[110] Z. Huang, I.W. Burgess, and R.J. Plank. Effective stiffness modelling of composite concrete slabs in fire. *Engineering structures*, 22:1133–1144, 2000.

[111] Z. Huang, I.W. Burgess, and R.J. Plank. Non-linear modelling of three full-scale structural fire tests. In *First International Conference, Structures in Fire*, Copenhagen, June 2000.

[112] Z. Huang, I.W. Burgess, and R.J. Plank. The influence of tensile membrane action in concrete slabs on the behaviour of composite steel-framed buildings in fire. In *Proceedings of the 2001 Structures Congress and Exposition*. ASCE, SEI, 2001.

[113] J.P. Hurst and G.N. Ahmed. Validation and application of a computer model for predicting the thermal response of concrete slabs subjected to fire. *ACI Structural Journal*, 95:480–487, 1998.

[114] S.H. Ingberg. Fire loads. *Quarterly Journal of the National Fire Protection Association*, pages 43–61, 1928.

[115] British Standards Institute. *Fire Safety Engineering in Buildings: DD240: Part 1. Guide to the application of fire safety engineering principles*, 1997.

[116] The Steel Construction Institute. Structural Fire Engineering, Investigation of Broadgate Phase 8 fire. Technical Report, June 1991.

[117] J. Janss. Statistical analysis of fire tests on steel beams and columns to Eurocode 3: Part 1.2. *Journal of Constructional Steel Research*, 33:39–50, 1995.

[118] J. Janss and R. Minne. Buckling of steel columns in fire. *Fire Safety Journal*, 4:227–235, 1981/82.

[119] P.F. Johnson. International developments in fire engineering of steel structures. *Journal of Constructional Steel Research*, 46(415), 1998.

[120] B. Karlsson and J.G. Quintiere. *Enclosure fire dynamics*. CRC Press, 2000.

[121] K. Kawagoe. Fire behaviour in rooms. Technical Report 27, Building research institute, Japan, 1958.

[122] K. Kawagoe and T. Sekine. Estimation of fire temperature-time curve in rooms. Technical Report 11, Building Research Institute, Ministry of Construction, Tokyo, Japan, 1963.

[123] G.A. Khoury, B.N. Grainger, and P.J.E. Sullivan. Strain of concrete during first heating to $600^o c$ under load. *Magazine of concrete research*, 37(133), 1985.

[124] G.A. Khoury, B.N. Grainger, and P.J.E. Sullivan. Transient thermal strain of concrete: literature review, conditions within specimen and behaviour of individual constituents. *Magazine of Concrete Research*, 37(132), 1985.

[125] G.A. Khoury and P.J.E. Sullivan. Research at Imperial College on the Effect of Elevated Temperatures on Concrete. *Fire Safety Journal*, 13:69–72, 1988.

[126] B.R. Kirby. Fire Resistance of Steel Structures: Modern Fire Protection Systems and Design Methods. British Steel Plc.

[127] B.R. Kirby. Recent development and application in structural fire engineering design- a review. *Fire Safety Journal*, 11:141–179, 1986.

[128] B.R. Kirby. Large Scale Fire Tests: the British Steel European Collaborative Research Programme on the BRE 8-Storey Frame. In *5th International Symposium of Fire Safety Science*, 1997.

[129] B.R. Kirby. British Steel data on Cardington fire tests. Technical report, British Steel, 2000. PIT Project Research Report ED1.

[130] B.R. Kirby and L.N. Tomlinson. *The temperatures attained by unprotected steelwork in building fires*. CORUS Research, Development and technology, 2000.

[131] B.R. Kirby and D.E. Wainman. The behaviour of structural steelwork in natural fires: The temperatures attained by unprotected structural steelwork in natural fires. Technical report, British Steel, 1997. reprint of report RSC/7281/10/86.

[132] B.R. Kirby, D.E. Wainman, L.N. Tomlinson, T.R. Kay, and B.N. Peacock. Natural fires in large scale compartments-A British Steel Technical, Fire Research Station collaborative project. Technical report, British Steel Plc, 1994.

[133] K. Kordina. Behaviour of composite columns and girders in fire. In *2nd International Symposium of Fire Safety Science*, pages 681–695, 1989.

[134] S. Lamont. Study of thermal expansion and thermal bowing in a restrained beam. Technical report, The University of Edinburgh, 2000. PIT Project Research Report TM3.

[135] S. Lamont, D.D. Drysdale, W. Robinson, and B.R. Kirby. Evaluation of the Software OZone: Supplementary Final Report to the DETR: Development of the UK and European Design Codes-Natural Fires and the Response of Structural Steel. Technical Report 39/3/489, CORUS, 2000.

[136] S. Lamont, B. Lane, A.S. Usmani, and D.D. Drysdale. Assessment of the fire resistance test with respect to beams in real structures. Submitted to AISC Journal 2001.

[137] S. Lamont, A.S. Usmani, and D.D. Drysdale. Heat transfer analysis of the composite slab in the Cardington frame fire tests. *Fire Safety Journal*, 36(8):815–839, 2001.

[138] B. Lane. *The response of steel frame structures under fire conditions.* PhD thesis, The University of Edinburgh, 1997.

[139] M. Law. A relationship between fire grading and building design and contents. Technical report, 1971.

[140] M. Law. A review of formulae for t-equivalent. In *5th International Symposium of Fire Safety Science*, pages 985–996. International Association for Fire Safety Science, 1997.

[141] M. Law and T. O'Brien. *Fire and steel construction: Fire safety of bare external structural steel.* The Steel Construction Institute, Ascot, Berks, 1986.

[142] R.M. Lawson and G.M. Newman. *Fire resistant design of steel structures-A handbook to BS 5950: Part 8.* The Steel Construction Institute, Ascot, Berkshire, 1990.

[143] R.M. Lawson and G.M. Newman. Structural fire design to EC3 and EC4, and comparison with BS 5950. Technical Report SCI Publication 159, The Steel Construction Institute, 1996.

[144] T.T. Lie. *Fire and Buildings.* Applied Science Publishers, London, 1972.

[145] T.T. Lie. Characteristic temperature curves for various fire severities. *Fire Technology*, 10(4), 1974.

[146] T.T. Lie. *Fire Temperature Time Relations*, chapter 8 section 4. The SFPE Handbook of Fire Protection Engineering, 2nd edition, 1995.

[147] T.T. Lie and M. Chabot. Evaluation of fire resistance of compression members using mathematical models. *Fire Safety Journal*, 20:135–149, 1993.

[148] T.T. Lie and T.D. Lin. *Fire Safety Science and Engineering*, chapter Fire Performance of Reinforced Concrete Columns, pages 176–205. ASTM, 1985.

[149] T.C.H. Liu. Finite element modelling of behaviours of steel beams and connections in fire. *Journal of Constructional Steel Research*, 36(3):181–199, 1996.

[150] CORUS UK Ltd. Final Report to the DETR: Development of the UK and European Design Codes-Natural Fires and the Response of Structural Steel. Technical Report 39/3/489, Swinden Technology Centre, 2000.

[151] P. Luyckx, P. Stienon, J-M. Franssen, J-C. Dotreppe, and M. Hogge. Numerical procedure for calculation of temperature evolution in composite elements with internal cavities. *Communications in Numerical Methods in Engineering*, 10:437–451, 1994.

[152] *LYTAG The Lightweight Aggregate.*

[153] *Lytag Technical Bulletin No.5*, 1961.

[154] Z. Ma and P. Makelainen. Parametric temperature-time curves of medium compartment fires for structural design. *Fire safety journal*, 34(4):361–375, 2000.

[155] S.E. Magnusson and S. Thelandersson. Temperature-time curves of complete process of fire development-theoretical study of wood fuel fires in enclosed spaces. Technical Report 65, 1970.

[156] S.E. Magnusson and S. Thelandersson. A discussion of compartment fires. *Fire Technology*, 10(3), 1974.

[157] H.L. Malhotra. Fire resistance versus fire behaviour. *Fire Prevention*, (134):21–27, 1980.

[158] H.L. Malhotra. *Design of Fire Resisting Structures.* Surrey University Press, Glasgow, 1982.

[159] B.J. Meacham. Concepts of a performance based building regulatory system for the United States. In *5th International Symposium of Fire Safety Science*, pages 701–712, 1997.

[160] S.J. Melinek. Prediction of the fire resistance of insulated steel. *Fire Safety Journal*, 14(127-134), 1989.

[161] J. Milke. *Analytical Methods for Determining Fire Resistance of Steel Members*, chapter 9 section 4, pages 174–201. The SFPE Handbook of Fire Protection Engineering, 2nd edition, 1995.

[162] J.A. Milke. Software review: Temperature analysis of structures exposed to fire. *Fire Technology*, 28:184–189, 1992.

[163] H.E. Mitler. The harvard fire model. *Fire Safety Journal*, 9, 1985.

[164] D. Moore. Personal Communication, 27th April 2000.

[165] F.W. Mowrer. Lag times associated with fire detection and fire suppression. *Fire Technology*, 26, 1990.

[166] S.R. Najjar and I.W. Burgess. A nonlinear analysis for three dimensional steel frames in fire conditions. *Engineering Structures*, 18(1):77–89, 1996.

[167] K. Nakamura, K. Shinoda, M. Hirota, and K. Kawagoe. Structural behaviour of steel frame in building fire. In *1st International Symposium Fire Safety Science*, 1985.

[168] I. Nakaya and K. Akita. A simulation model for compartment fires. *Fire Safety Journal*, 5:157–165, 1983.

[169] A.M. Neville. *Properties of Concrete*. Longman Group Ltd., 1983.

[170] G.M. Newman, J.T. Robinson, and C.G. Bailey. *Fire safe design: A new approach to multi-storey steel framed buildings*. Steel Construction Institute, Ascot, 2000.

[171] NFPA. *NFPA Fire Protection - Handbook*. National Fire Protection Association, Quincy, MA, 18th edition, 1997.

[172] NIST Building and Fire Research Laboratory: Fire Modelling Programs. http://www.bfrl.nist.gov/864/fmabbs.html.

[173] A.J. Ockleston. Load test on a three-storey reinforced concrete building in Johannesburg. *The Structural Engineer*, October 1955.

[174] A.J. Ockleston. Arching action in reinforced concrete slabs. *The Structural Engineer*, June 1958.

[175] M. O'Connor. BS/TEST4 ABAQUS half-floor model using elastic shell with rotational discontinuities. Technical report, The University of Edinburgh, 1999.

[176] M. O'Connor. Analysis of British Steel Cardington test data. Technical report, British Steel, 2000. PIT Project Research Report AE1.

[177] M. O'Connor. British Steel Fire Test 1: ABAQUS half floor model using beam general section for slab. Technical report, CORUS, 2000. PIT Project Research Report MD6.

[178] M. O'Connor. British Steel Fire Test 1: ABAQUS half floor model using elastic shell for slab. Technical report, CORUS, 2000. PIT Project Research Report MD5.

[179] M. O'Connor. British Steel Fire Test 1: ABAQUS Model using shell elements for beam and beam general section for slab. Technical report, CORUS, 2000. PIT Project Research Report MD4.

[180] M. O'Connor. British Steel Fire Test 2: ABAQUS half floor model using elastic shell for slab. Technical report, CORUS, 2000. PIT Project Research Report MD8.

[181] M. O'Connor. British Steel Fire Test 2: ABAQUS model using beam general section for slab. Technical report, CORUS, 2000. PIT Project Research Report MD9.

[182] M. O'Connor. British Steel Fire Test 2: ABAQUS using shell elements for beams and beam general section for slab. Technical report, CORUS, 2000. PIT Project Research Report MD7.

[183] M. O'Connor. British Steel Fire Test 3: ABAQUS half floor model using elastic shell for slab. Technical report, CORUS, 2000. PIT Project Research Report MD12.

[184] M. O'Connor. British Steel Fire Test 3: ABAQUS half floor model using elastic shell with rotational discontinuities for slab. Technical report, CORUS, 2000. PIT Project Research Report MD13.

[185] M. O'Connor. British Steel Fire Test 4: ABAQUS half floor model using elastic shell for slab. Technical report, CORUS, 2000. PIT Project Research Report MD14.

[186] K. Odeen. Theoretical study of fire characteristics in enclosed spaces. In *Bulletin No.10*. Royal Institute of Technology, Stockholm, Sweden, 1963.

[187] The University of Edinburgh. Final report of the DETR-PIT project: Behaviour of steel framed structures under fire conditions. Technical report, The University of Edinburgh, 2000. www.civ.ed.ac.uk/research/fire/project/reports.html.

[188] NIST (National Institute of Standards and technology). Fire dynamics simulator-technical reference guide. on the world wide web, http://fire.nist.gov/fds/.

[189] G.W. Owens and P.R Knowles, editors. *Steel Designers' Manual*. Blackwell Science, fifth edition edition, 1994.

[190] R. Park. Tensile membrane behaviour of uniformly loaded rectangular reinforced concrete slabs with fully restrained edges. *Magazine of Concrete Research*, 16(46), 1964.

[191] R. Park. The ultimate strength and long-term behaviour of uniformly loaded, two-way concrete slabs with partial lateral restraint at all edges. *Magazine of Concrete Research*, 16(48), 1964.

[192] R. Park. The lateral stiffness and strength required to ensure membrane action at the ultimate load of a reinforced concrete slab-and-beam-floor. *Magazine of Concrete Research*, 17(50), 1965.

[193] D.L. Parkinson. Performance based structural design for fire conditions. In *Proceedings of the 2001 Structures Congress and Exposition*. ASCE, SEI, 2001.

[194] O. Pettersson. Practical need of scientific material models for structural fire design. *Fire Safety Journal*, 13:1–8, 1988.

[195] O. Pettersson, S.E. Magnusson, and J. Thor. *Fire Engineering design of Steel Structures*. Swedish Institute of Steel Construction, Publication 50, Stockholm, 1976.

[196] R. Phylaktou. University of Leeds Short courses: Fire dynamics and modelling, January 2000.

[197] British Steel Plc. The behaviour of multi-storey steel framed buildings in fire. British Steel plc, Swinden technology centre, 1999.

[198] R.W. Portier, R.D. Peacock, and P.A. Reneke. Fastlite: Engineering tools for estimating fire growth and smoke transport. http://www.bfrl.nist.gov/864/fmabbs.html.

[199] J.A. Purkiss. *Design of Structures Against Fire*. Elsevier Applied Science, 1986.

[200] J.G. Quintiere. *Compartment fire modelling*, chapter 5 section 3. The SFPE handbook of Fire Protection Engineering, 2nd edition, 1995.

[201] Z. Nizamuddin R.H. Iding and B. Bresler. *FIRES-T3 - Computer program for the FIre REsponse of Structures - Thermal 3-Dimensional Version*. University of California, Berkeley, October 1977.

[202] R.L.P.Custer and B.J.Meacham. *Introduction to performance based fire safety*. Society of Fire Protection Engineers, 1st edition, 1997.

[203] J. Robinson, C. Bailey, G. Newman, M. Green, and J. Dowling. Fire safe design. *New Steel Construction*, 9(1):23–33, January/February 2001.

[204] J.T. Robinson and D.J. Latham. *Design of structures against fire*, chapter Fire resistant steel design-The future challenge. Elsevier Applied Science, London, 1986.

[205] J.P. Correia Rodrigues, I. Cabrita Neves, and J.C. Valente. Experimental research on the critical temperature of compressed steel elements with restrained thermal elongation. *Fire Safety Journal*, 35:77–98, 2000.

[206] P.S. Rose, I.W. Burgess, R.J. Plank, and C.G. Bailey. The influence of floor slabs on the structural behaviour of composite frames. In Lee, editor, *Structures in the New Millennium*, 1997.

[207] J.M. Rotter, A.M. Sanad, A.S. Usmani, and M. Gillie. Structural performance of redundant structures under local fires. In *Interflam'99 8th International Fire Science and Engineering Conference*, pages 1069–1080, 1999.

[208] J.M. Rotter and A.S. Usmani. Behaviour of highly indeterminate composite framed structures in fire. Technical report, The University of Edinburgh, 2000. PIT Project Research Report TM1.

[209] A. Rubert and P. Schaumann. Critical temperatures of steel columns exposed to fire. *Fire Safety Journal*, 13:39–44, 1988.

[210] H.A Saab and D.A. Nethercot. Modelling steel frame behaviour under fire conditions. *Engineering Structures*, 13, 1991.

[211] M.S. Sahota and P.J. Pagni. Heat and mass transfer in porous media subject to fires. *International Journal of Heat and Mass Transfer*, 22:1069–1081, 1979.

[212] H. Saito and N. Seki. Mass transfer and pressure rise in moist porous material subjected to sudden heating. *Journal of Heat Transfer*, 99:105–112, 1977.

[213] H. Saito, H. Uesugi, M. Yamaguchi, and A. Kodaira. Thermal stress and deformation of steel structures of high rise buildings in fire. In *2nd International Symposium of Fire Safety Science*, pages 719–728, 1989.

[214] A.M. Sanad. British Steel Fire Test 1: Reference ABAQUS model using grillage representation for slab. Technical report, The University of Edinburgh, 2000. PIT Project Research Report MD1.

[215] A.M. Sanad. British Steel Fire Test 3: Reference ABAQUS model using grillage representation for slab. Technical report, The University of Edinburgh, 2000. PIT Project Research Report MD10.

[216] A.M. Sanad. Effect of changing boundary restraints on BS/Test 1. Technical report, The University of Edinburgh, 2000. PIT Project Research Report SM3.

[217] A.M. Sanad. Effect of changing steel section in the BS/Test 1 composite beam. Technical report, The University of Edinburgh, 2000. PIT Project Research Report SM2.

[218] A.M. Sanad. Effects of increasing live loads on BS/Test 1. Technical report, The University of Edinburgh, 2000. PIT Project Research Report SM1.

[219] A.M. Sanad and S. Lamont. Effect of changing slab temperature evolution on BS/Test 1. Technical report, The University of Edinburgh, 2000. PIT Project Research Report SM4.

[220] A.M. Sanad, S. Lamont, A.S. Usmani, and J.M. Rotter. Structural behaviour in fire compartment under different heating regimes-part 1 (slab thermal gradients). *Fire Safety Journal*, 35:99–116, 2000.

[221] A.M. Sanad, S. Lamont, A.S. Usmani, and J.M. Rotter. Structural behaviour in fire compartment under different heating regimes-part 2 (slab mean temperatures). *Fire Safety Journal*, 35:117–130, 2000.

[222] A.M. Sanad, J.M. Rotter, A.S. Usamni, and M.A. O'Connor. Composite beams in large buildings under fire-numerical modelling and structural behaviour. *Fire Safety Journal*, 35:165–188, 2000.

[223] A.M. Sanad, J.M. Rotter, A.S. Usmani, and M.A. O'Conner. Finite Element Modelling of Fire Tests on the Cardington Composite Building. In *Interflam'99 8th International Fire Science and Engineering Conference*, volume 2, pages 1045–1056, 1999.

[224] J.B. Schleich, L.G. Cajot, and M. Pierre. Competitive steel buildings through natural fire safety concept. Technical report, PROFIL ARBED, 2000.

[225] J.B. Schleich, J.C. Dotreppe, and J.M. Franssen. Numerical simulations of fire resistance tests on steel and composite structural elements or frames. In *1st International Symposium of Fire Safety Science*, 1985.

[226] J.B. Schleich, J.C. Dotreppe, and J.M. Franssen. Numerical simulations of fire resistance tests on steel and composite structural elements and frames. In *1st International Symposium of Fire Safety Science*, pages 311–323, 1986.

[227] U. Schneider. Behaviour of concrete under thermal steady state and non-steady state conditions. *Fire and Materials*, 1:103–115, 1976.

[228] U. Schneider. Concrete at high temperatures- a general review. *Fire Safety Journal*, 13:55–68, 1988.

[229] J. Selih, A.C.M. Sousa, and T.W. Bremner. Moisture and heat flow in concrete walls exposed to fire. *Journal of Engineering Mechanics*, 120(10):2028–2043, 1994.

[230] D. Smith. Time for a change. *Fire Engineers Journal: Fire Prevention*, November 2000.

[231] L. Song, B.A. Izzuddin, A.S. Elnashai, and P.J. Dowling. An integrated adaptive environment for fire and explosion analysis of steel frames- part 1: Analytical models. *Journal of Constructional Steel Research*, 53(1):63–85, 2000.

[232] E.S. Sterner and U. Wickstrom. *TASEF- Temperature Analysis of Structures Exposed to Fire*. Swedish National Testing and Research Institute, Sweden, 1990.

[233] D.W. Stroup. *Using Field Modelling to Simulate Enclosure Fires*, chapter 8, Section 3. The SFPE Handbook of Fire Protection Engineering, 2nd edition, 1995.

[234] G.C. Thomas, A.H. Buchanan, and C.M. Fleischmann. Structural fire design: The role of t-equivalence. In *5th International Symposium of Fire Safety Science*, pages 607–618, 1997.

[235] I.R. Thomas and I.D. Bennetts. Fires in enclosures with single ventilation openings-comparison of long and wide enclosures. In *6th International symposium of Fire Safety Science*, pages 941–952. International Association for Fire safety Science, 1999.

[236] P. Thomas and L. Nilsson. Fully developed compartment fires: New correlations of burning rates. FR Note No. 979, Fire research station, Borehamwood, Herts, UK, 1973.

[237] P.H. Thomas. Modelling of compartment fires. *Fire Safety Journal*, 5:181–190, 1983.

[238] P.H. Thomas, editor. *Design Guide: Structural Fire Safety*. CIB Workshop W14, Fire Safety Journal, 1986.

[239] P.H. Thomas. Studies of fires in buildings using models. Part 2 Some theoretical and practical considerations. In *P. H. Thomas Fire Research Station 1951-1986. Selected Papers*. Building Research Establishment, 1986.

[240] P.H. Thomas and M.L. Bullen. On the role of $k\rho c$ of room lining materials in the growth of room fires. *Fire and Materials*, 3(2):68–73, 1979.

[241] P.H. Thomas and A.J.M. Heselden. Fully developed Fires in Single Compartments a Co-operative Research Programme of the Conseil International du Batiment (CIB). 1972.

[242] P.H. Thomas and M. Law. The projection of flames from buildings on fire. *Fire Prevention Science and Technology*, (10):19–26, 1974.

[243] Y. Tsuchiya and K. Sumi. Computation of the behaviour of fire in an enclosure. *Combustion and Flame*, 16:131–139, 1971.

[244] B. Tubbs. ICC Performance Code for buildings and facilities-Structural fire protection provisions. In *Proceedings of the 2001 Structures Congress and Exposition*. ASCE, SEI, 2001.

[245] L. Twilt. Strength and deformation properties of steel at elevated temperatures: Some practical implications. *Fire Safety Journal*, 13:9–15, 1988.

[246] L. Twilt and C. Both. Design tools for the behaviour of multi-storey steel framed buildings exposed to natural fires. Technical report, TNO Building and Construction Research, 2000. 3rd Interim report.

[247] A.S. Usmani. Application of fundamental structural mechanics principles in assessing the Cardington fire tests. In *Structures in Fire Proceedings of the First International Workshop*, Copenhagen, June 2000.

[248] A.S. Usmani and J.M. Rotter. Fundamental principles of structural behaviour under thermal effects. Technical report, The University of Edinburgh, 2000. PIT Project Research Report TM2.

[249] A.S. Usmani, J.M. Rotter, S. Lamont, A.M. Sanad, and M. Gillie. Fundamental principles of structural behaviour under thermal effects. *Fire Safety Journal*, 36(8):721–744, 2001.

[250] W.D. Walton. *Zone computer fire models for enclosures*, chapter 3 section 7. The SFPE handbook of Fire Protection Engineering, 2nd edition, 1995.

[251] W.D. Walton and P.H. Thomas. *Estimating temperatures in compartment fires*, chapter 6 section 3. The SFPE handbook of Fire Protection Engineering, 2nd edition, 1995.

[252] Y.C. Wang. Tensile membrane action and fire resistance of steel framed buildings. Technical Report PD59/96, Building Research Establishment, 1996.

[253] Y.C. Wang. Tensile membrane action in slabs and its application to the Cardington fire tests. In *Proceedings of the 2nd Cardington Conference*. BRE, March 1996.

[254] Y.C. Wang. Tensile membrane action and fire resistance of steel framed buildings. In *5th International Symposium of Fire Safety Science*, 1997.

[255] Y.C. Wang, T. Lennon, and D.B. Moore. The behaviour of steel frames subject to fire. *Journal of Constructional Steel Research*, 35:291–322, 1995.

[256] Y.C. Wang and D.B. Moore. Effect of thermal restraint on column behaviour in a frame. In *4th International Symposium of Fire Safety Science*, pages 1055–1066, 1994.

[257] Y.C. Wang and D.B. Moore. Steel frames in fire: analysis. *Engineering Structures*, 17(6):462–472, 1995.

[258] J. M. Watts. Performance based codes. *Fire Technology*, 30, 1994.

[259] U. Wickstrom. An evaluation scheme of computer codes for calculated temperatures in fire exposed structures. In *Interflam'99*, volume 2, pages 1033–1044, 1999.

Appendix A

Review of the Parametric Temperature-time curve in EC 1 Part 2.2

Appendix B

Review of O Zone